Engineering Geology ETH-Zürich / K. Evans Consulting: Publications

Valley, B., Dezayes, C., Genter, A., Maqua, E. and Guillaume, S., 2005, Main fracture zones in GPK3 and GPK4 and crosshole correlations, Soultz Scientific Meeting, Soultz-sous-Forêts, France, 17th March.

Valley, B. and **Evans, K.F.**, 2005. Stress estimates from analysis of breakouts and drilling-induced tension fractures in GPK3 and GPK4. Soultz Scientific Meeting, Soultz-sous-Forêts, France, 17th March.

Dezayes, C., **Valley, B.**, Maqua, E., Guillaume, S. and Genter, A. 2005, Natural fracture system of the Soultz granite based on UBI data in the GPK3 and GPK4 wells, Soultz-sous-Forêts, France, 17th March.

Evans, K.F. and **Valley, B.** 2005, Ein Überblick über "Enhanced Geothermal Systems" (erweiterte geothermale Systeme) / Un aperçu des 'Enhanced Geothermal Systems' ('systèmes géothermiques stimulés'). GEOforum ACTUEL, 4, 17-44, Akademie der Naturwissenschaften Schweiz.

Valley, B. and **Evans, K.F.**, 2006. Stress state at Soultz to 5 km depth from wellbore failure and hydraulic observations. Annual Scientific Meeting of the Soultz Project, Soultz-sous-Forêts, 15-16 June.

Valley, B. and **Evans K.F.**, 2006. Strength and elastic properties of the Soultz granite. Annual Scientific Meeting of the Soultz Project, Soultz-sous-Forêts, 15-16 June.

Valley, B. and **Evans, K.F.**, 2007. Stress heterogeneity in the Soultz granite inferred from analysis of wellbore failure to 5 km depth. Annual Scientific Meeting of the Soultz EGS project, Soultz-sous-Forêts, 28-29 June.

Valley, B. and **Evans, K.F.** 2007. Stress state at Soultz-sous-Forêts to 5 km depth from wellbore failure and hydraulic observations. 32nd Workshop on Geothermal Reservoir Engineering, Stanford, California, 22-24th January, Stanford University.

Valley, B., Dezayes, C. and Genter, A. 2007. Multi-scale fracturing in the Soultz-sous-Forêts basement from borehole images analyses. Annual Scientific Meeting of the Soultz EGS project, Soultz-sous-Forêts, 28-29 June.

Evans, K.F., Baisch, S., Cuenot, N., Dorbath, N. and Jung, R. 2008. Milestone events & key observations in thermics, stress and hydraulics at Soultz (1987-2002), Soultz Scientific Meeting, Soultz-sous-Forêts, France, 24-25 September.

Evans, K.F., Hopkirk, R., Jung, R., Nami, P., Schindler, M., Teza, D., Tischner, T. 2008. Milestone events & key observations in seismics at Soultz (1987-2002), Soultz Scientific Meeting, Soultz-sous-Forêts, France, 24-25 September.

Genter A., Dezayes Ch., Ledesert B., Sausse J. and **Valley B.** 2008, Geological reconnaissance of deep fractured geothermal reservoirs: what we have learnt at

Soultz in 20 years?, Soultz Scientific Meeting, Soultz-sous-Forêts, France, 24-25 September.

Genter, A., **Evans, K.F.**, Cuenot, N., Baticci, F., Dorbath, L., Graff, J.J. and Sanjuan, B., 2009. The EGS Soultz project (France): from reservoir development to electricity production. Annual meeting of the Geothermal Resources Council, Reno, 4-7 October, Geothermal Resources Council.

Dorbath, L., **Evans, K.F.**, Cuenot, N., Valley, B., Charléty, J. and Frogneux, M., 2010. The stress field at Soultz-sous-forêts from focal mechanisms of induced seismic events: cases of the wells GPK2 and GPK3. Geoscience: submitted.

Dezayes, C., Genter, A. and **Valley, B.**, 2010b. Structure of the low permeable naturally fractured geothermal reservoir at Soultz. Geoscience: submitted.

Genter, A., **Evans, K.F.**, Cuenot, N., Fritsch, D. and Sanjuan, B., 2010. The Soultz geothermal adventure: 20 years of research and exploration of deep crystalline fractured rocks for EGS development. Geoscience: submitted.

Dezayes, C., Genter, A. and **Valley, B.**,. Overview of the fracture network at different scales within the granite reservoir of the EGS Soultz site (Alsace, France). World Geothermal Congress, Bali, 25-29 April 2010 of Conference, International Geothermal Association. submitted

Valley, B. and **Evans, K.F.**, 2010. Stress Heterogeneity in the Granite of the Soultz EGS Reservoir Inferred from Analysis of Wellbore Failure. World Geothermal Congress, Bali, 25-29 April 2010, International Geothermal Association. submitted

Engineering Geology ETH-Zürich: Theses

Valley, B., 2007. The relation between natural fracturing and stress heterogeneities in deep-seated crystalline rocks at Soultz-sous-Forêts (France). Ph.D. Thesis, Swiss Federal Institute of Technology (ETH).

Main fracture zones in GPK3 and GPK4 and crosshole correlations

Benoît Valley*, Chrystel Dezayes**, Albert Genter**, Emilien Maqua*** and Guillaume Syren***
**ETH Zürich, Switzerland*
***BRGM Orléans, France*
****Université de Savoie, France*

Presented at the Soultz Scientific Meeting at Soultz-sous-Forêts on 17th March 2005.

EC Contract ENK5-2000-00301

PARTICIPANT ORGANIZATION NAME: ETH Zürich

Synthetic final report

Related with Work Package

MAIN FRACTURE ZONES IN GPK3 AND GPK4 AND CROSSHOLE CORRELATIONS

Benoît Valley*, Chrystel Dezayes**, Albert Genter**, Emilien Maqua*** and Guillaume Syren***
*ETH Zürich
**BRGM Orléans
***Université de Savoie
e-mail: valley@erdw.ethz.ch

ABSTRACT

Some of the fractures in the Soultz granite clustered and then form fracture zones (Genter et al., 1998). Using borehole images, fracture zones can be identified along the boreholes. A non-exhaustive examination of GPK3 permits to highlight 25 fracture zones. 104 fracture zones have been identified along the GPK4 borehole between 1418 and 5260m (borehole depth). Fracture zone mean strike is about N160° while considering all fractures mean strike is more N-S (N174°).

The rich fracture dataset collected on GPK3 and GPK4 borehole and the boreholes proximity are very favorable for fracture correlation between boreholes. Using geometric criteria, fractures crossing both boreholes have been tracked. Statistical analyses of the obtained correlated dataset permit to estimate most probable fractures radius at about 10 to 20 m. Moreover, correlated fractures dip preferentially to the east.

The fracture zones have been correlated between boreholes. A preliminary correlation has been performed from GPK3 to GPK4. It shows that fracture zones are very poorly correlated where borehole horizontal distance is higher than 100 m. A detailed correlation has been performed from GPK4 to GPK3, for GPK4 borehole depth smaller than 3000 m. Shallower than 2000 m 55% of fracture zones can be correlated. Correlated fracture zones preferentially dip to east. This suggests that most persistent features crossing the upper part of the Soultz granite are dipping to the east.

INTRODUCTION

UBI images (Ultrasonic Borehole Imager) permit to describe the general fracturing of Soultz granite (Genter et al, 1997). The preponderant strike direction of fractures is known from previous borehole dataset being about N175°. Previous knowledge on the fracturing of Soultz granite shows that not all fractures have the same importance. Although fractures tend to be distributed in cluster forming fracture zones (Genter et al., 1998). These fracture zones play a pre-eminent role in the hydro-geological behavior of the HDR reservoir (Dezayes et al., 2004). The general strike orientation of these fracture zones is about N160° and seem then to slightly turn to the west in comparison to the entire fracture dataset (Dezayes, 1995; Evans et al., 2005).

This paper present on going work on the description of the fracture zones met in GPK3 and GPK4 and their correlation between both boreholes. While this work is still in progress, the results presented here under shouldn't be taken as definitive, but they give an insight in what will be the development of this work in the future. The borehole wall images recorded in GPK3 and GPK4 have been used to localize fracture zones. The fracture zones have been classified based on there geometrical characteristics. Orientation of fracture zones has been estimated. The obtained results confirm the previous ones presented here over. In addition to this, correlation between GPK3 and GPK4 has been performed. The extension of fractures and fracture zones in Soultz granite being not well known, these correlations using the large amount of fractures data collected in GPK3 (Maqua, 2003, Syren, 2004, Dezayes et al, 2004) and GPK4 (Valley, 2004, Dezayes et al, 2005) have be used to give some constrain on possible fracture sizes. Indeed, the proximity of these two boreholes permits cross-hole correlation of fractures and statistical analyses of the probable fractures extension. Fracture zones have been although correlated between boreholes. A preliminary correlation has been done from GPK3 to GPK4. A more detailed correlation has been performed from GPK4 to GPK3 only for the upper part of the borehole (<3000m). Preliminary results show that fracture zones are poorly correlated where borehole horizontal distance is higher than 100m and fracture zones dipping to the east are preferentially correlated.

DATA SETS

Table 1 summarizes the data sets used in this article. They mainly consist in Ultrasonic Borehole Images (UBI) of GPK4 and GPK3. Without other indications, depth has always to be understood as borehole depth, with the zero depth set at the working platform (9.7m above ground level for GPK4). Fractures data sets have been extracted by analyzing borehole images. In GPK4, useful UBI images were obtain between 1455m and 4730m borehole depth for the 12.25 inch section and 4767m and 5258m for the 8.5 inch section (outer these ranges, logs are run in casing or suffer acquisition problem). Moreover, when borehole inclination exceed 25° (2680 to 4730 in the 12.25 inch section) induced features as breakout

Borehole	*Data type*	*Borehole depth range*
GPK4	UBI 12.25 inch	1431-4733m
GPK4	UBI 8.5 inch	4740-5263m
GPK4	Fractures data set (UBI analyses)	1456-5248m
GPK3	Fractures data set (UBI analyses)	1453-5087m

Table 1. Data sets used in this study

or artifacts as key seat or borehole enlargement at upper oriented wall could mask some natural features.

FRACTURE ZONES LOCATION

In a first step a non exhaustive localization of fracture zones along GPK3 as been performed. Then an exhaustive, detailed localization of fracture zones along GPK4 has been done. For this last, the methodology exposed here under has been used.

Methodology

Fracture zones are isolated along the borehole by careful analysis of the UBI images. They are described by their top and bottom depth and their type. Indeed the fracture zones have been classified in six different types resumed and illustrated in figure 1. The classification criteria are the general geometry of the fracture zone and the presence of visible alteration on the UBI images. Some zones (type 2 and 3) are clearly dominated by a single major fracture while other zones (type 4 and 5) are clusters of major fractures with different orientation without a clear dominating fracture. There are fracture zones accompanied with a clear alteration of the UBI image (type 3 and 5) and other zones where granite between fracture look unaltered. Sometimes only clear alteration is visible without visible fracture (type 1). This doesn't imply that there are no fractures, but fractures are probably masked on UBI images by the strong alteration. Fracture zones of type 6 are heavily damaged borehole section. Such zones of weakness are evidently although highly affected by drilling induced features like breakouts. In these zones, distinguishing clear natural fracture traces become then very difficult.

The orientation of fracture zones is although estimated. If this orientation is quite obvious for fracture zones composed by a single fracture (type 2 and 3) this not at all the case for other types. For alteration zones without clearly visible fractures (type 1) the orientation of their border is chosen as representative orientation. In case of diffuse border this estimation of fracture zones orientation is then very difficult. For fracture clusters (type 4 and 5), the fracture having the stronger trace on the UBI image is chosen to give the orientation of the zone. The choice of this dominating fracture is not obvious. Moreover, there is no proof that this chosen orientation is representative of the fracture zone orientation at a scale larger that the borehole scale. For complex damage zones (type 6), the determination of a representative orientation becomes very hazardous.

Results

The non-exhaustive fracture zones localization along GPK3 borehole reveal 25 fracture zones. They are dispatch along the whole borehole. Figure 2c show their orientation in a stereoplot. Mean strike is N164°. Dip angles are higher than 60°. Looking at all fracture zones, they slightly dip preferentially to the east. Figure 4 shows orientations of fracture zones vs. depth. There is no clear deviation of the mean strike direction in function of depth. In an other hand, the dominant dip directions vary with depth. Shallower than 3400 m dip directions to the east are dominant. Then from 3400 m to 4200 m fracture zone dip exclusively to the west. Deeper than 4200 m dip direction to the west are slightly dominant.

Along GPK4, 104 fracture zones have been isolated. The cumulative fracture zone curve in figure 3 highlights a fracture density of about 6 fractures per 100m for depth smaller than 2000m and higher than 4800m. In between, fracture zone density is smaller, about or even less than 2 fracture zone per 100m (excepted between 4200 m and 4500 m where fracture density is about 4 fractures / 100 m) . There

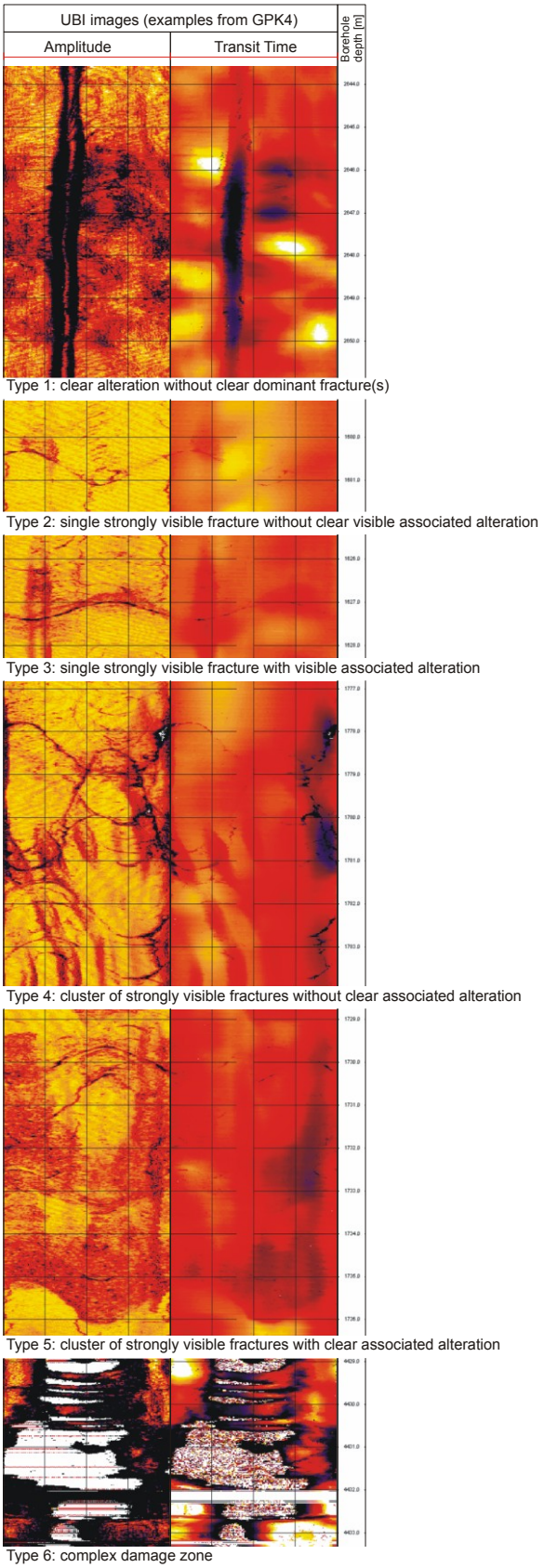

Figure 1: Examples of the 6 types of fracture zones

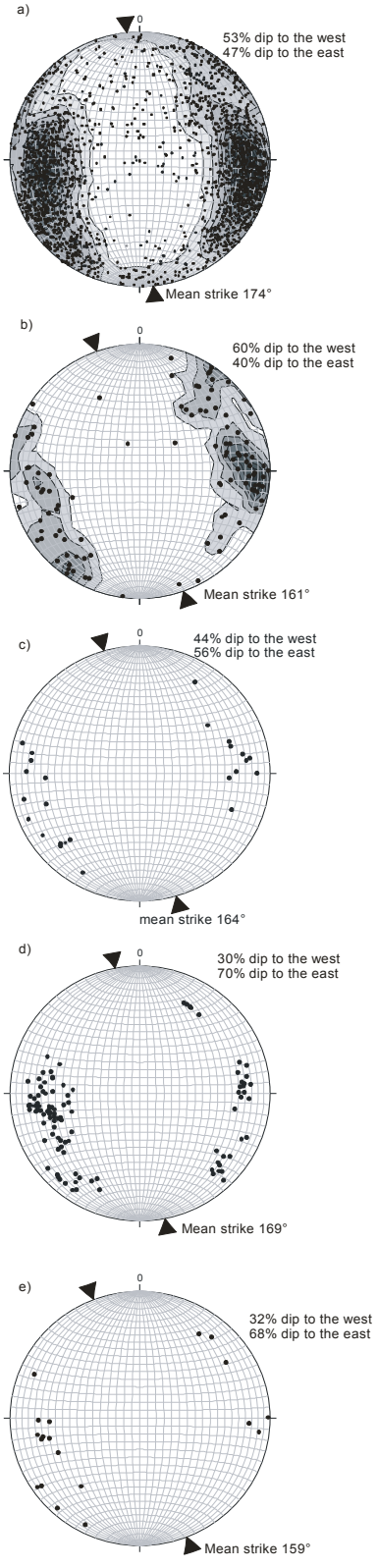

Figure 2: a) orientation of all the fractures in GPK4 (n=2215) b) orientation of all fracture zones in GPK4 (n=104) c) orientation of all fracture zones in GPK3 (n=25) d) fracture of GPK4 correlated with fractures of GPK3 (n=104) e) fracture zones which was successfully correlated between GPK4 and GPK3 (n=19). All stereoplots are lower-hemisphere, equal area projection.

are 12 fractures zones of type 1 (11%), 24 of type 2 (23%), 28 of type 3 (27%), 18 of type 4 (17%), 19 of type 5 (19%) and 3 of type 6 (3%). Different types seem well disseminated along the borehole. Figure 3 don't permit to clearly highlight grouping of type along the borehole. If the fracture zones of type 3 (single strongly visible fracture with visible associated alteration) are the most present they can not be call dominating type of fracture zones, while other types have about the same numbers of invidious excepted for type 6 (complex damage zones) which are quite rare (only 3 occurrences).

All the fracture orientations of GPK4 have been plotted in a stereographic representation in figure 2a for comparison purpose. The mean strike of all fractures in GPK4 is 174° with a broad deviation. The fractures dip about equally to the east (47%) or to the west (53%).This is in agreement to results obtain on previous fracture dataset at Soultz (Genter et al., 1997; Dezayes et al., 2004).

In spite of the difficulties approached above as for the determination of the dominant orientation of the fracture zones, it was possible to determine orientation for all the zones. Fracture zones orientations are plotted in figure 2b. Fracture zones mean strike is N161°. They generally have steep dip angle, 82% of fracture zone being steeper than 60°. Considering all fracture zones, they dip slightly preferentially to the west (60% of the zones). Figure 5 shows orientation of fracture zones vs. depth. There is no clear deviation of the mean strike direction in function of depth. In an other hand, the dominant dip directions vary with depth. Shallower than 3000m dip directions to the east are slightly dominant (63%). Then from 3200m to 4200m fracture zone dip exclusively to the west. Deeper than 4200m dip direction to the west are slightly dominant (65%).

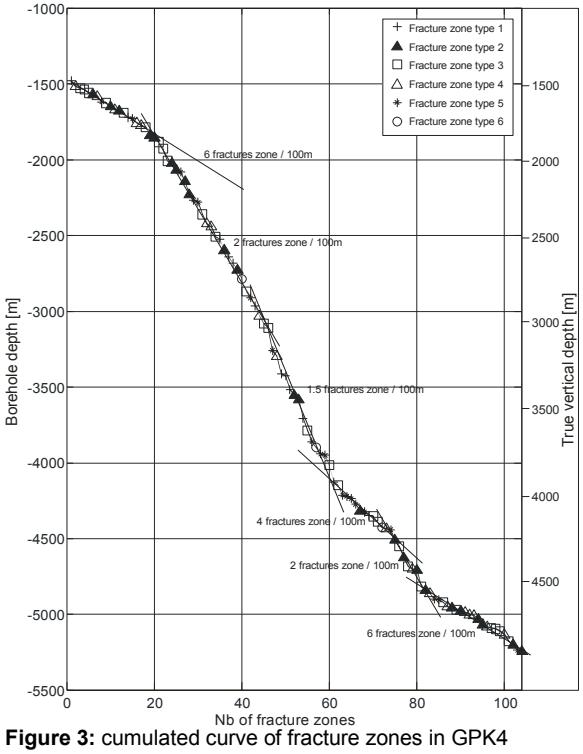

Figure 3: cumulated curve of fracture zones in GPK4

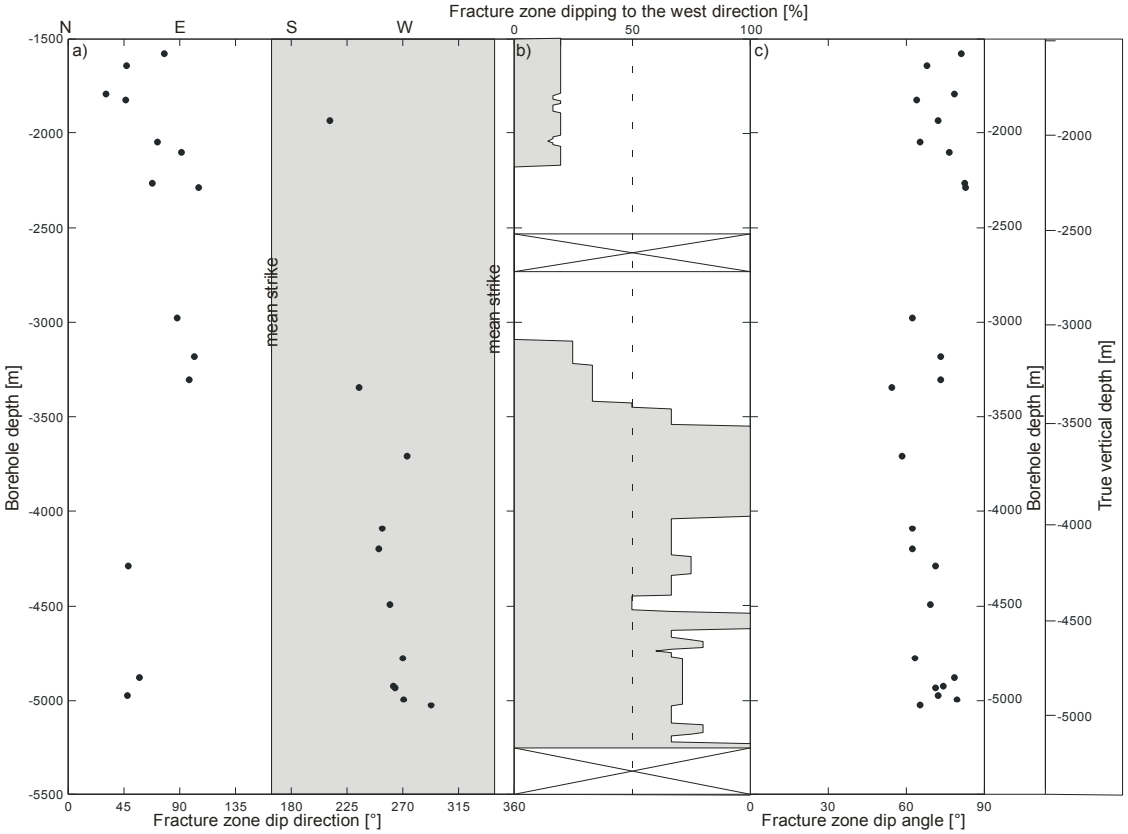

Figure 4: orientation of fracture zones of GPK3 vs. depth. a) fracture zone dip direction b) percentage of fractures zones dipping to the west in a 500 m depth window c) fracture zones dip angle.

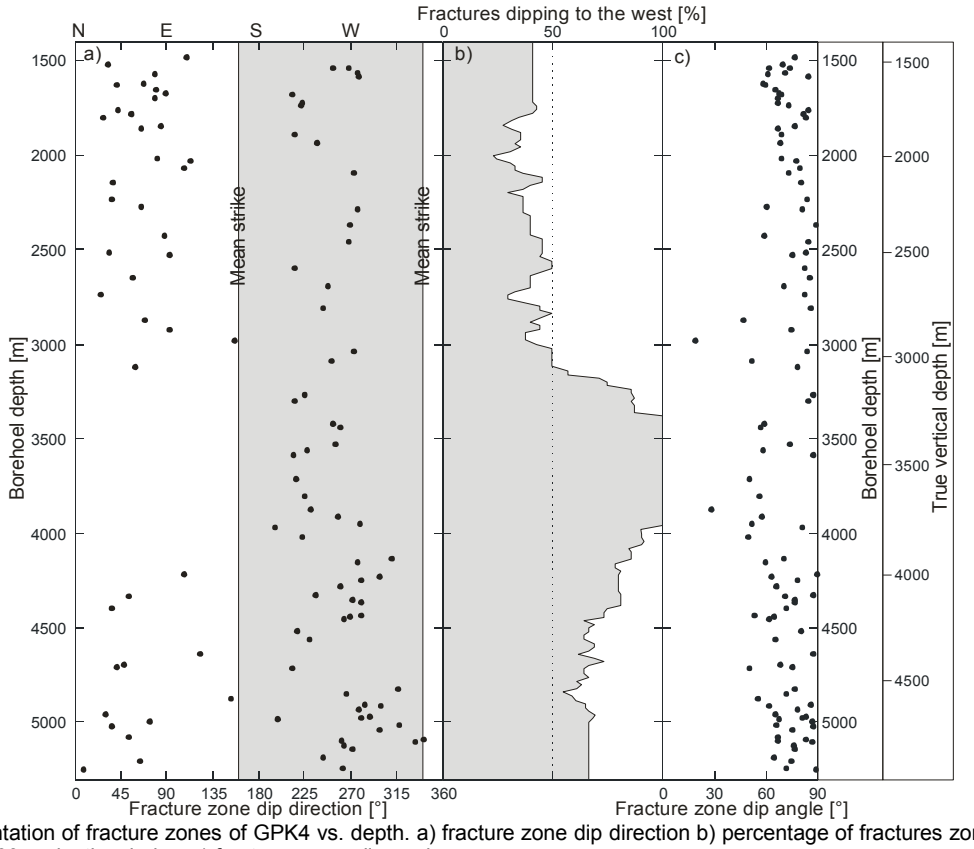

Figure 5: orientation of fracture zones of GPK4 vs. depth. a) fracture zone dip direction b) percentage of fractures zones dipping to the west in a 500 m depth window c) fracture zones dip angle.

Fracture zone density variations with depth are concordant with the variation of the density of all fractures (Syren, 2004, Valley, 2004). To the top of the granite and toward the bottom of the borehole (borehole depth > 4800 m) the fracture and fracture zone density are higher. In comparison with all fractures, fracture zones mean strike turn to the west. This result was although observed looking at fractures and fracture zones in the GPK1 borehole (Dezayes, 1995; Evans et al., 2005). Variation of dip direction versus depth has already been investigated on GPK3 fracture dataset (Syren, 2004). Further investigation will be necessary to explain the geological meaning of such variations.

FRACTURE EXTEND

GPK3 and GPK4 have both about 4km of UBI borehole images permitting the location of fractures. These boreholes are separated with less than 15m between the TVD (True Vertical Depth) 1500 m to 2250 m. Then distance between borehole increases to reach 700 m at bottom hole (figure 6). This rich dataset will be used to estimate fracture length by correlation of fractures between the two boreholes.

Data sets

The data sets used are the fractures data obtain by interpretation of UBI images using the appropriate fracture typology (Maqua, 2003; Syren, 2004; Dezayes et al,2004; Valley 2004). The GPK3 dataset include 1926 fractures. Due to their orientation and their position on the borehole some of them will never meet the trajectory of the opposite borehole. So only 1725 of them are oriented so that they could cross GPK4. The GPK4 borehole dataset include 2213 fractures and for the same raison that the one invoked here over, only 1879 of them could potentially intercept GPK3. For the fracture potentially intercepting both boreholes, the distance between boreholes in the fracture plane, *d,* can be calculated. This distance, further called *d*-value is a basic quantity to know in order to estimate fracture extension. *d* reach a minimum of 14 m for fractures located in the upper part of the imaged boreholes and a maximum of about 4500 m for fractures located close to the bottom depth. The distribution of *d* is highly dissymmetric, the mean being about 350m and the most current value of *d* (the mode) is about 18m (figure 7).

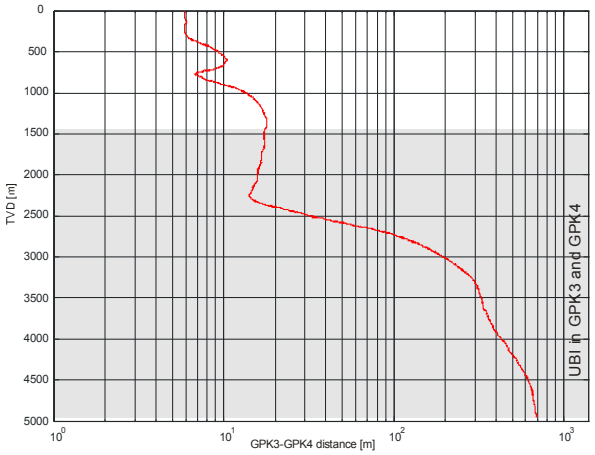

Figure 6: Horizontal distance between GPK3 and GPK4 vs. true vertical depth. Gray depth interval correspond with depth where borehole images are available for both boreholes.

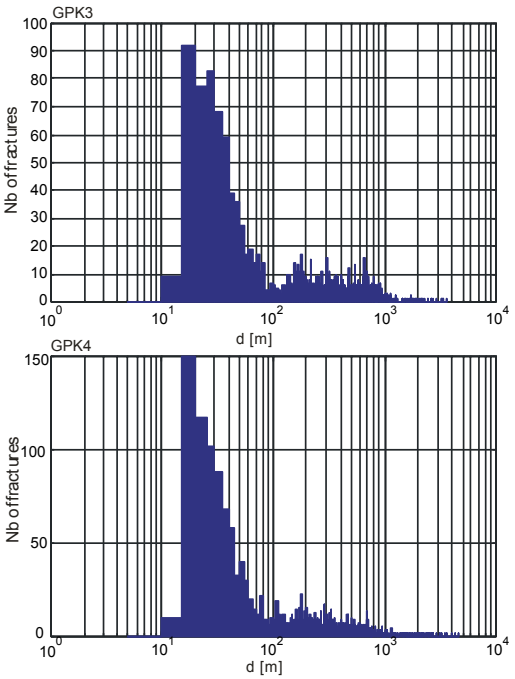

Figure 7: distribution of *d*-values (distance between boreholes within fracture plane) for both boreholes

Methodology

In order to test if a fracture could be geometrically correlated between the two boreholes, the following procedure has been used:

For all fractures an interval is define on the opposite borehole. This interval is the intersection of the fracture with the borehole assuming uncertainty on the dip direction ($\pm\Delta\alpha$), the dip ($\pm\Delta\varphi$) and the depth location ($\pm\Delta$d) of the fracture. For certain geometry (for example fracture sub-parallel to the borehole) this interval can be too wide for sensible correlation. Then if this interval is wider than a chosen threshold value (dmax), the width of the interval is reduced to dmax. For this purpose, the intersection of the fracture with the opposite borehole is considered to be the interval center. The reduced interval is then obtained by adding and subtracting dmax/2 to the intersection depth.

A “mother fracture” on borehole 1 is correlated with a “daughter fracture” on borehole 2 if (figure 8):

1) The “daughter fracture” is in the interval defined by the “mother fracture”

2) The “the mother fracture” is in the interval defined by the “daughter fracture” (reciprocity)

3) The angle between the poles of the two fractures is smaller than a threshold value θ_t.

If after this procedure more than one daughter fracture is candidates to be correlated with a mother fracture, the “daughter fracture” having the lowest angle (between poles) with the mother fracture is selected.

The parameter $\Delta\alpha$, $\Delta\varphi$ and Δd are estimated by summing realistic errors range on borehole trajectories (Walstrom et al., 1969) and errors range on the determination of fracture orientation on borehole images. The following values are retained: $\Delta\alpha$ =5° (uncertainty on dip direction) , $\Delta\varphi$ =0.75° (incertainty on dip angle) and Δd=5 m (incertainty in depth location). dmax has been chosen being as 10m and θ_t as 10°.

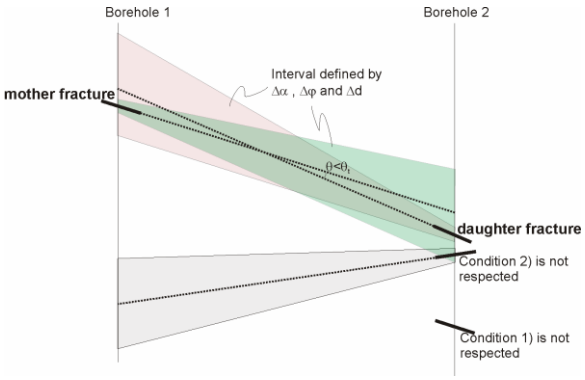

Figure 8: principle of fracture correlation between 2 boreholes.

Results of the borehole correlation

On the 1725 possibly intercepting fractures of GPK3, 90 found a "daughter fracture" on GPK4 and on the 1879 possibly intercepting fractures of GPK4, 104 found a "daughter fracture" on GPK3. So about 5% of the entire fracture population is correlated between the two boreholes. Considering the fracture typology (Maqua, 2003) there isn't any type of fracture preferentially correlated between boreholes. About 70% (figure 2d) of correlated fractures are dipping to the east. So knowing that the whole fracture population is about equally dipping to the west or the east (figure 2a), fractures dipping to the east are really preferentially correlated.

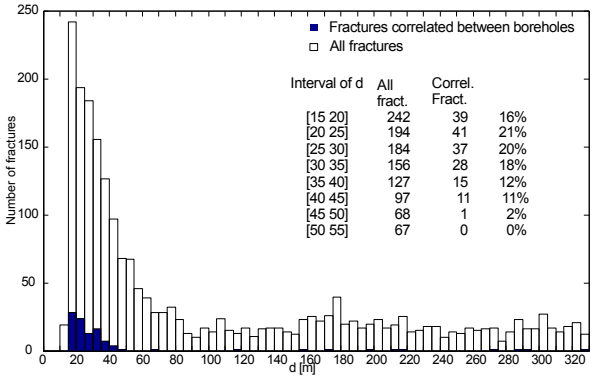

Figure 9: histogram of the d-value for all fractures and for correlated fractures. Only d-value from 0 m to 330 m are displayed.

The *d*-values (distance between the two boreholes in the fracture plane) of the correlated fractures are between 15m and 327 m (figure 9) . For correlated fractures, the mean of *d* is 45 m and the median of *d* is 25 m. For *d* bigger than 45 m correlation is only sporadic. Taking 5m-width class of d, there is never more than one fracture per class when *d* is bigger than 45 m.

Comparing the correlated fractures population with all fractures shows that for *d*-value smaller than 45m about 10-20% of all fractures are correlated (figure 9). The "best" result is for fractures with *d* between 20 m and 25m where 21% of the fractures are correlated between boreholes.

Some reserves have to be emitted concerning the validity of these correlations. Knowing that natural fractures tend to be organized in sets of similar orientation, the probability that two different fractures are aligned "by chance" is not negligible. For this reason, range of *d*-value where only 1 fracture is present (for *d*-value bigger than 45 m) are doubtful and will not be used in the interpretation in terms of fracture size.

Interpretation of the results of correlation in terms of fracture size

Considering penny shape fractures (discs), the simplest way of evaluating the fracture size is to use the *d*-value of correlated fractures as lower bound for fracture diameters. Considering the results of the correlation, the highest lower bound for fracture radii is then 22.5 m. The most part of correlated fractures having *d*-value between 20 m and 30 m, a lower bound for fracture radius between 10 m and 15 m seem to be the more realistic.

A statistical approach to estimate fracture radii is although possible. The fracture radius can be express as function of the *d*-value (figure 10).

$$r = k \cdot d \qquad (1)$$

with

r : fracture radius
d : distance between boreholes in the fracture plane
k : factor of proportionality between *r* and *d, k>0*

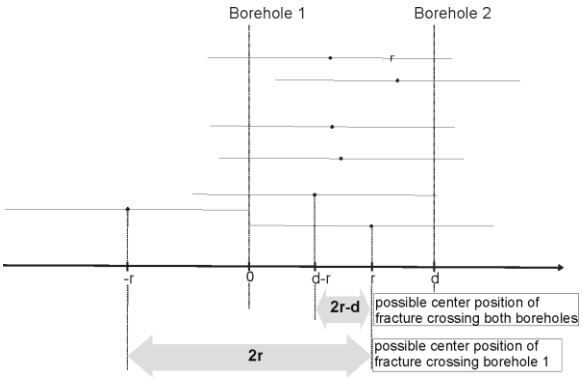

Figure 10: schematic representation of the boreholes and fractures (see text for explanation).

If the fracture radius is smaller than the half of the *d*-value (*k*<0.5) then the probability that this fracture view in one borehole cross the other borehole is zero (the fracture is too short).

$$p = 0 \text{ for } k \leq 0.5 \qquad (2)$$

If a fracture as a radius higher that the half of the *d*-value (k>0.5), this fracture seen in one borehole has some chance to cross the other borehole. It depends of the relative position of the fracture to both boreholes. A fracture visible in borehole 1 will obligatory have its center in a *2r* interval around borehole 1 (figure 10). But a fracture visible in both borehole will have its center in a *2r-d* interval only. Consider-

ing that fracture center repartition is uniform, for a fixed *d*-value, the probability that intersection of both boreholes occurs is given by (figure 10):

$$p = \frac{2r - d}{2r} \quad \text{for } k>0.5 \qquad (3)$$

Combining (1) and (3), the probability that intersection of both boreholes occurs can be express as a function of *k* only (figure 11):

$$p = 1 - \frac{1}{2k} \quad \text{for } k>0.5 \qquad (4)$$

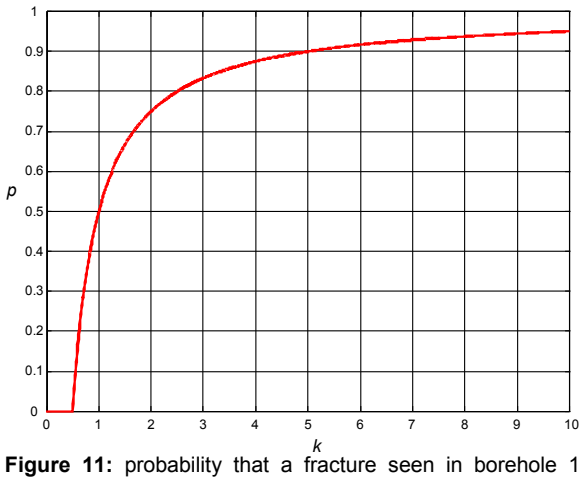

Figure 11: probability that a fracture seen in borehole 1 cross borehole2 as function of *k*.

If the probability of intersection can be estimated then *k* can be calculated:

$$k = \frac{1}{2 - 2p} \qquad (5)$$

Finally, for a given *d*, *r* can then be determined.

The probability that a fracture with a given *d*-value intersect both boreholes can be estimated by the analyses of the fracture correlation between boreholes presented here over and using the following formula:

$$p_e = \frac{N_i}{N_a} \qquad (6)$$

p_e : estimated probability, $p_e \cong p$

N_a : number of fractures with a given *d*-value

N_i : number of fractures with a given *d*-value and correlated between both boreholes.

Formula (5) permit then to calculate the most probable value of *k*. Combining the considered *d*-value and the calculated *k*, formula (1) permit to calculate the most probable fracture radius.

This method applied to our correlated fractures give results presented in table 2. These results suggest that the most probable fracture radius lie between 9 to 26 m. The most reliable value is for fracture having *d*-value between 15 and 20 (biggest sample), for which calculated most probable radius is between 9 and 11m.

d [m]	N_a	N_i	P_e	*k*	*r* [m]
[15 20]	242	39	16%	0.60	[9 11]
[20 25]	194	41	21%	0.63	[13 16]
[25 30]	184	37	20%	0.63	[16 19]
[30 35]	156	28	18%	0.61	[18 21]
[35 40]	127	15	12%	0.57	[20 23]
[40 45]	97	11	11%	0.57	[23 26]

Table 2. estimation of most probable radius value for our correlated fractures.

FRACTURE ZONE CORRELATION IN THE UPPER PART OF GPK4 AND GPK3

The proximity of GPK3 and 4 and the quality of the wall images collected in these boreholes have been although use to better understand the fracture zone geometry.

Fracture zone correlations between GPK3 and GPK4 have been first attempted by Maqua (2003) and Syren (2004). In this work, correlation with GPK4 of the 25 described fracture zones in GPK3 has been evaluated. The validation of the correlation between boreholes was mainly based on the examination of 3D view of the fracture zones between the boreholes. Accepting this low restrictive correlation criteria, 13 of the 25 fractures zones have been correlated between boreholes GPK3 and GPK4 (figure 12). This work shows that where borehole horizontal distance is bigger than 100m fracture zones are very poorly correlated.

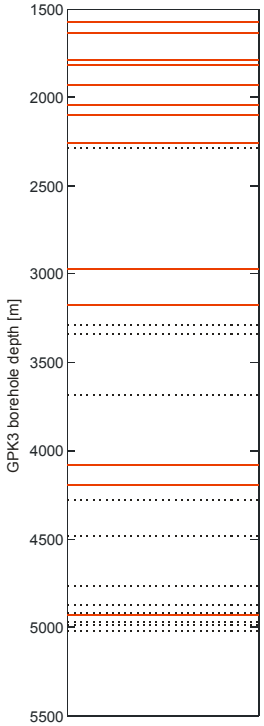

Figure 12: location of non-correlated fracture zones (dotted lines) and correlated fracture zones (plein lines) in the GPK3 well.

The correlation of fracture zones between boreholes have been then refined. The analyses presented here under are preliminary results of this work. This focus only on the correlation of fractures zones with regard to their general orientation as describe in the first part of this paper. For instance, only fracture zones shallower than 3000 m have been investigate. At such depth, borehole horizontal distance is less than 110 m (figure 6).

Methodology

Correlation of fracture zones between GPK4 and GPK3 have been performed manually. From the fracture zone location and orientation on GPK4, the possible intersection depth on GPK3 has been calculated. Then, the concerned section on GPK3 has been investigated in order to see if fracture zones with concordant orientation can be found. For fracture zones with a depth mismatch smaller than 15 m and angle mismatch smaller than 20° the correlation has been validated.

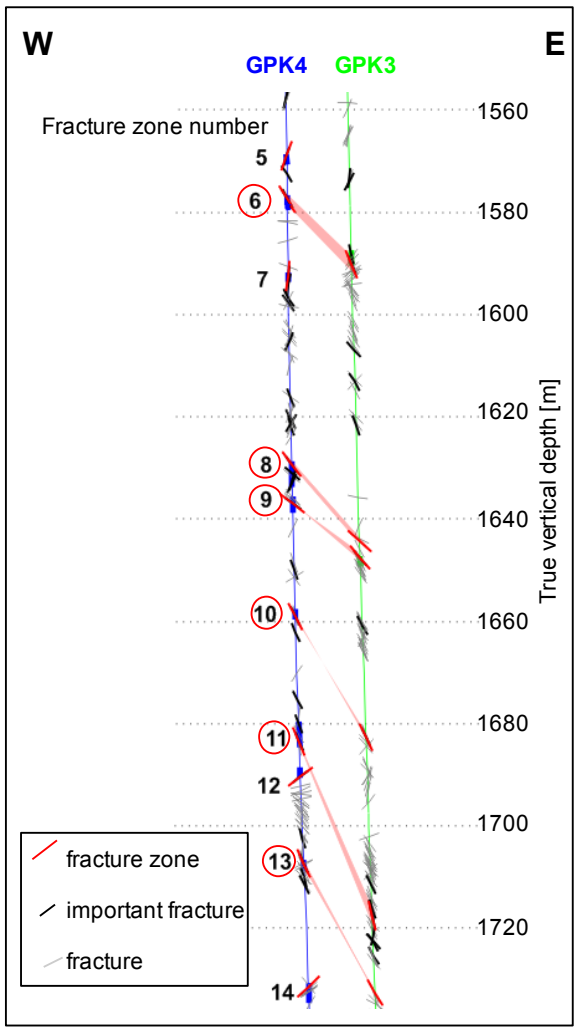

Figure 13: projection of borehole GPK3 and 4 in an W-E plane. Fractures and fracture zones are represented by their apparent dip in an W-E plan. In this section, fracture zones 5 to 14 are visible (bold black numbering). Numbers of fracture zones being correlated between boreholes are circled.

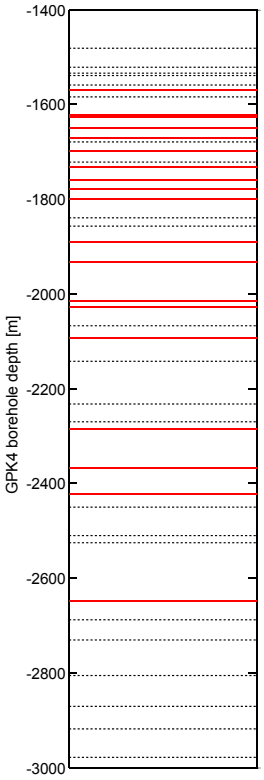

Figure 14: location of non-correlated fracture zones (dotted lines) and correlated fracture zones (plein lines) in the GPK4 well.

Results

In all, 43 fracture zones have been located in the GPK4 section above 3000 m, 16 (37%) of them dipping to the west and 27 dipping to the east (63%) (figure 5). On these fracture zones, 19 (44%) have been correlated between both boreholes. A sample of fracture zones correlated between boreholes is illustrated in an E-W projection in figure 13. On the 19 correlated fracture zones, 6 of them dip to the west and 13 to the east (figure 2e). The mean strike of correlated fracture zone is 159° (figure 2e). 48% of the east dipping fracture zones are correlated for only 38% of the west dipping fracture zones.

Figure 14 shows the depth location on GPK4 of correlated and non-correlated fracture zones. Above 2000 m, not only the fracture zone density is higher (figure 3), but the correlation is although quite high (55%). Deeper than 2000m only 33 % of the zones are correlated, the last correlated zone being at 2650 m.

Correlated fracture zones show a deviation of the strike to the west in comparison with all fractures which is although true regarding all fracture zones (figure 2b and e). But in addition to this, correlated fracture zone tend to mainly dip to the east. This is although the case for correlated fracture (figure 2d). Considering that there is no sampling bias, which should be true while the borehole are subvertical or deviated to the south, fractures and fractures zones striking to about N160° and dipping to the east seem to be the most persistent features in the upper part of the Soultz granite.

CONCLUSION

Some of the fractures embedded within the Soultz granites are clustering forming fracture zones. These fracture zones can be located by detailed analyses of borehole images (UBI). A non-exhaustive examination of the borehole wall image of GPK3 permit to highlights 25 fracture zones. In GPK4, 104 of them have been localized on the Ultrasonic Borehole Images. A typology of fracture zones have been developed in order to classified them. Fracture zones density evolves in function of depth in the same way that considering all fractures. Upper than 2000m and towards the bottom of the borehole, density are higher than in the intermediate section. Mean strike of fracture zones turn slightly to the west in comparison with the whole fracture dataset. This confirms results obtain by others (Dezayes et al, 2004; Evans, 2005). If strike direction stays the same at different depth, the dip direction varies. Further investigations are necessary to geologically explain this last fact.

The very rich fracture data set of GPK3 and GPK4 and the favorable relative position of boreholes permit to find fractures crossing both boreholes. Statistical analyses of these fractures permit to estimate the most probable fracture radius at about 10 to 20 m. Correlated fractures although preferentially dip to the east.

A preliminary fracture zone correlation between GPK3 an GPK4 has been performed and permits to show that where horizontal distance between boreholes is higher than 100 m, correlation is very poor. A finer fracture zones correlation have been done for borehole depth smaller than 3000m. Preliminary results shows that correlated fracture zones mainly strike to N160° (like all other fracture zones) but although preferentially dip to the east. These results suggest that the most persistent feature crossing the top of the Soultz granite dip to the east.

REFERENCES

Dezayes, Ch. (1995), Caractérisation et interprétation d'un volume rocheux fracture à partir de données de forages, les forages géothermiques de Soultz-sous-Forêts. Thèse de doctorat de l'Université de Savoie, Document du BRGM 251.

Dezayes, Ch., Genter, A. & Gentier, S. (2004), Fracture Network of the EGS Geothermal Reservoir at Soultz-sous-Forêts (Rhine Graben, France). *Geothermal Resources Council Transaction,* vol. 28, p.213-218.

Dezayes, Ch., Valley, B., Maqua, E., Syren, G. & Genter, A. (*2005*), Natural fracture system of the Soultz granite based on UBI data in the GPK3 and GPK4 wells. *Proceeding to the march 2005 EHDRA meeting.*

Evans, K.F., Moriya, H., Niitsuma, H., Jones, R.H., Phillips, W.S., Genter, A., Sausse, J., Jung, R., and Baria, R. (2005). Microseismicity and permeability enhancement of hydrogeologic structures during massive fluid injections into granite at 3 km depth at the Soultz HDR site. *Geophys. J. Int.,* 160, p. 388-412.

Genter, A., Castaing, C., Dezayes, Ch., Tenzer, H., Traineau, H. & Villemin, T. (1997), Comparative analysis of direct (core) and indirect (borehole imaging tools) collection of fracture data in the Hot Dry Rock Soultz reservoir (France). *Journal of Geophysical Research,* vol. 102, NO. B7, p. 15,419-15,431.

Genter, A., Dezayes, Ch., Gentier, S., Ledesert, B. & Sausse, J. (1998), Conceptual fracture model at Soultz based on geological data. *Draft proceedings, 4th Int. HDR Forum, Strasbourg, September 28-30, 1998.*

Maqua, E., (2003), Fracturation dans la partie supérieure du forage GPK3 et corrélation avec les autres puits du site de Soultz-sous-Forêts (Alsace, France). *Unpublished report.*

Syren, G. (2004). Analyse de la fracturation utile à l'écoulement dans le forage profond GPK-3 de Soultz-sous-forêts. *Unpublished report.*

Traineau, H., Genter, A., Cautru, J.P., Fabriol, H. & Chevremont, P. (1991), Petrography of the granite massif from drill cuttings analysis and well log interpretation in the geothermal HDR borehole GPK1 (Soultz, Alsace, France).*Geotherm. Sci. & Techn.,* vol. 3(1-4), p.1-29.

Valley, B. (2004), Description of fracturing in GPK4 obtained from UBI-images. *Unpublished report.*

Walstrom, J.E., Brown, A. A: & Harvey, R. P. (1969), An Analysis of Uncertainty in Directional Surveying. *Journal of Petroleum Technology,* April 1969.

Stress estimates from analysis of breakouts and drilling-induced tension fractures in GPK1 AND GPK4

Benoît Valley* & Keith Evans*
**Engineering geology, ETH Zürich, Switzerland*

Presented at the Soultz Scientific Meeting at Soultz-sous-Forêts on 17th March 2005.

EC Contract ENK5-2000-00301

PARTICIPANT ORGANIZATION NAME: ETH Zürich

Synthetic final report

Related with Work Package FP6-WP5

STRESS ESTIMATES FROM ANALYSIS OF BREAKOUTS AND DRILLING-INDUCED TENSION FRACTURES IN GPK1 AND GPK4

Benoît Valley* & Keith Evans*

**Engineering geology, ETH Zürich*

e-mail: valley@erdw.ethz.CH

ABSTRACT

The UBI logs of GPK4 show extensive sections of borehole where breakouts or drilling-induced tension fractures (DITFs) have formed. These features provide a high-quality indication of the orientation of the maximum horizontal principal stress. Results to date indicate that the orientation of the maximum horizontal principal stress in the depth range 4-5 km is approximately North-South, in agreement with the orientation in the depth range 2-3.5 km derived from DITFs and breakouts in GPK1 and GPK2.

INTRODUCTION

The ultrasonic borehole imager (UBI) logs of GPK4 show extensive sections of borehole which are affected by stress-induced failure in the form of either breakouts or drilling-induced tension fractures. Breakouts reflect localised failure of the borehole wall at points where the local value of the circumferential compressive stress at the borehole wall exceeds the rock strength. Thus, they only occur when there is a significant stress difference in the plane normal to the borehole axis, and are typically manifest as pairs of diametrically-opposite spall zones that extend along the borehole axis. In the simple case of a vertical borehole penetrating a rock mass in which one principal stress is vertical, breakouts, if they occur, indicate the orientation of the minimum principal stress (Bell & Gough, 1979). Drilling induced tension fractures (DITFs) form where cooling of the borehole wall by circulation of mud during drilling is sufficiently strong as to produce a tensile circumferential stress at some point around the borehole wall that exceeds the tensile strength of the rock. The tensile stress is the sum of a tensile cooling component, which is axially-symmetric, and the natural wellbore stress concentration arising from the 'far-field' stresses, which is generally not axially-symmetric but may be everywhere compressive (Brudy and Zoback, 1999). In the case of a vertical borehole penetrating a medium in which one principal stress is also vertical, the least compressive value of the circumferential stress variation about the borehole due to the far field stresses occurs in the direction of the maximum principal horizontal stress. Thus it is in this direction that peak tension develops and a pair of diametrically-opposite DITFs form. Since the borehole axis is aligned with a principal stress, they will be axial (Figure 1b). However, in the case where the borehole axis is not aligned with a principal axis, the criterion for tensile fracture might still be met but then DITFs will tend to form as a stack of en-echelon, induced fractures (Figure 1c). The relationship between the induced fracture geometry and the in-situ stress orientations and magnitudes in this case is not so simple as in the aligned case.

Breakouts and DITFs, when they occur, constitute one of the highest quality stress orientation indicators for two reasons. One is the relatively elementary relationship between breakout/DITF orientation and horizontal stress orientation, at least for vertical holes. The second is their tendency to occur over extensive sections of boreholes (if they occur at all), which allows statistical methods to be used to obtain robust estimates of stress orientation.

A number of studies have been conducted of breakouts and DITFs at Soultz, mostly in well GPK1. Tenzer et al. (1992) identified axial tension fractures in ultrasonic televiewer records from GPK1 in the depth range 1450-2000 m (i.e. before the well was extended to 3.6 km). These indicated the maximum principal horizontal stress, S_{Hmax}, in that depth range to be 169° ± 11°. Nagel (1994) picked axial DITFs on an FMI logs run in GPK1 between 2000 and 3590 m and obtained a mean orientation of S_{Hmax} of 181°±22°. Brudy and Zoback (1999) examined en-echelon DITFs on the same logs and remark that that their strikes defined the same orientation distribution as the axial DITFs. Bérard & Cornet, (2003) identified compression-induced breakouts in GPK1 in the depth range 3050-3450 m that implied an S_{Hmax} orientation of N5°E±7°. Genter and Tenzer (1995) identified vertical DITFs in GPK2 in the depth range 1420 - 3880 m and found they indicated an orientation for S_{Hmax} of N175E±17°.

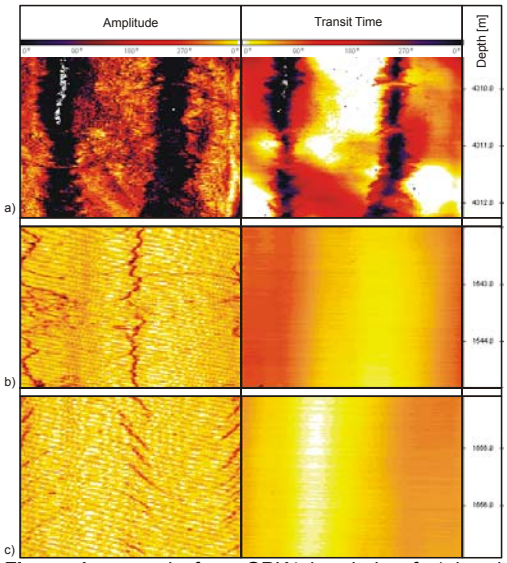

Figure 1: example from GPK4 borehole of a) breakout b) axial drilling induced fracture c) en echelon drilling induced fractures

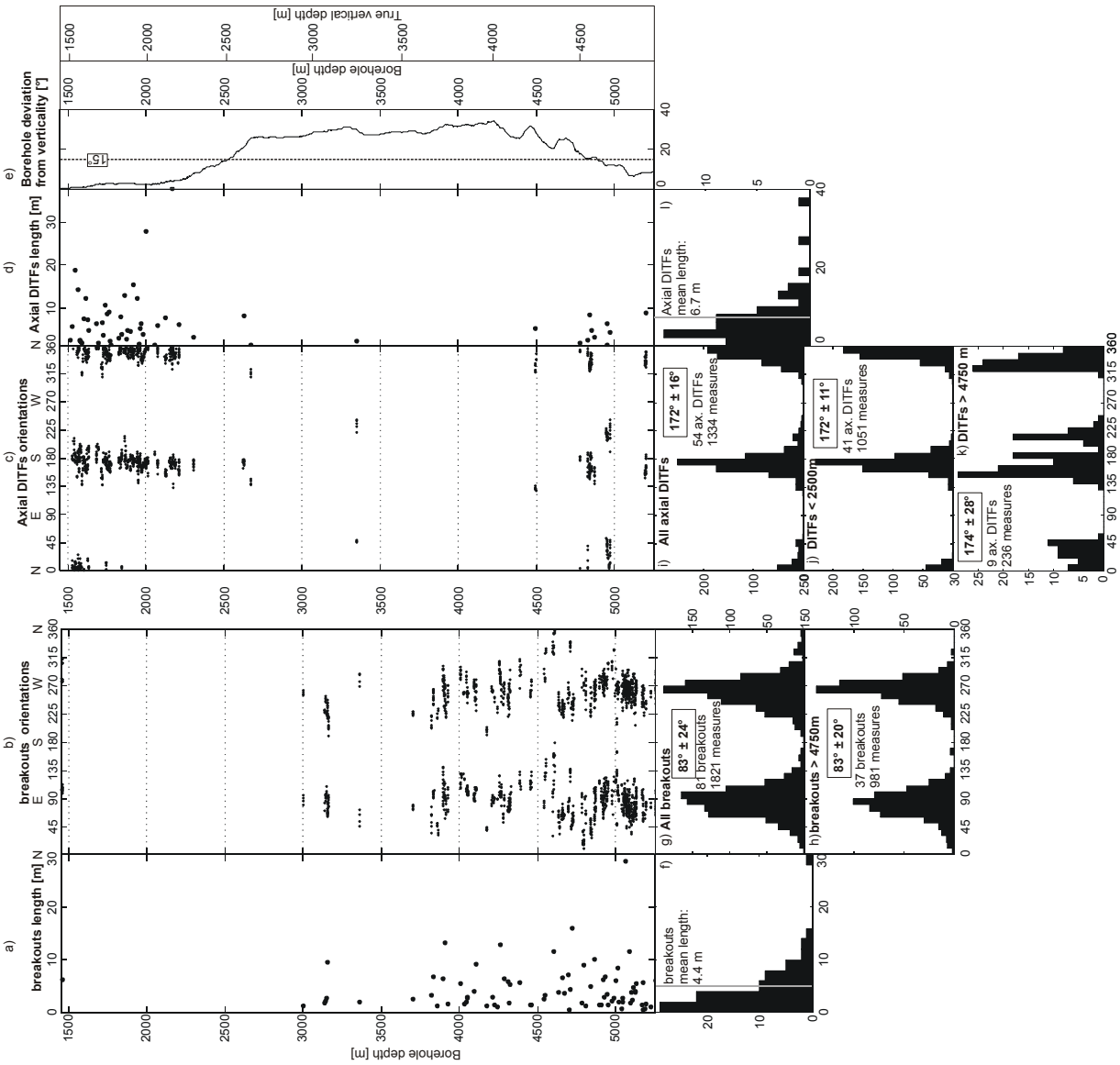

Figure 2: compilation of axial DITFs and breakouts data from GPK4 a) length of breakouts vs. depth b) orientation measurement of breakouts vs. depth c) orientation measurements of axial DITFs vs. depth d) length of axial DIFTs vs. depth e) borehole deviation from verticality f) histogram of breakouts length g) histogram of orientation of all breakouts h) histogram of orientation of breakouts deeper than 4750 m i) histogram of orientation of all axial DITFs j) histogram of orientation of axial DITFs shallower than 2500 m k) histogram of orientation of axial DITFs deeper than 4750 m l) histogram of axial DITFs length

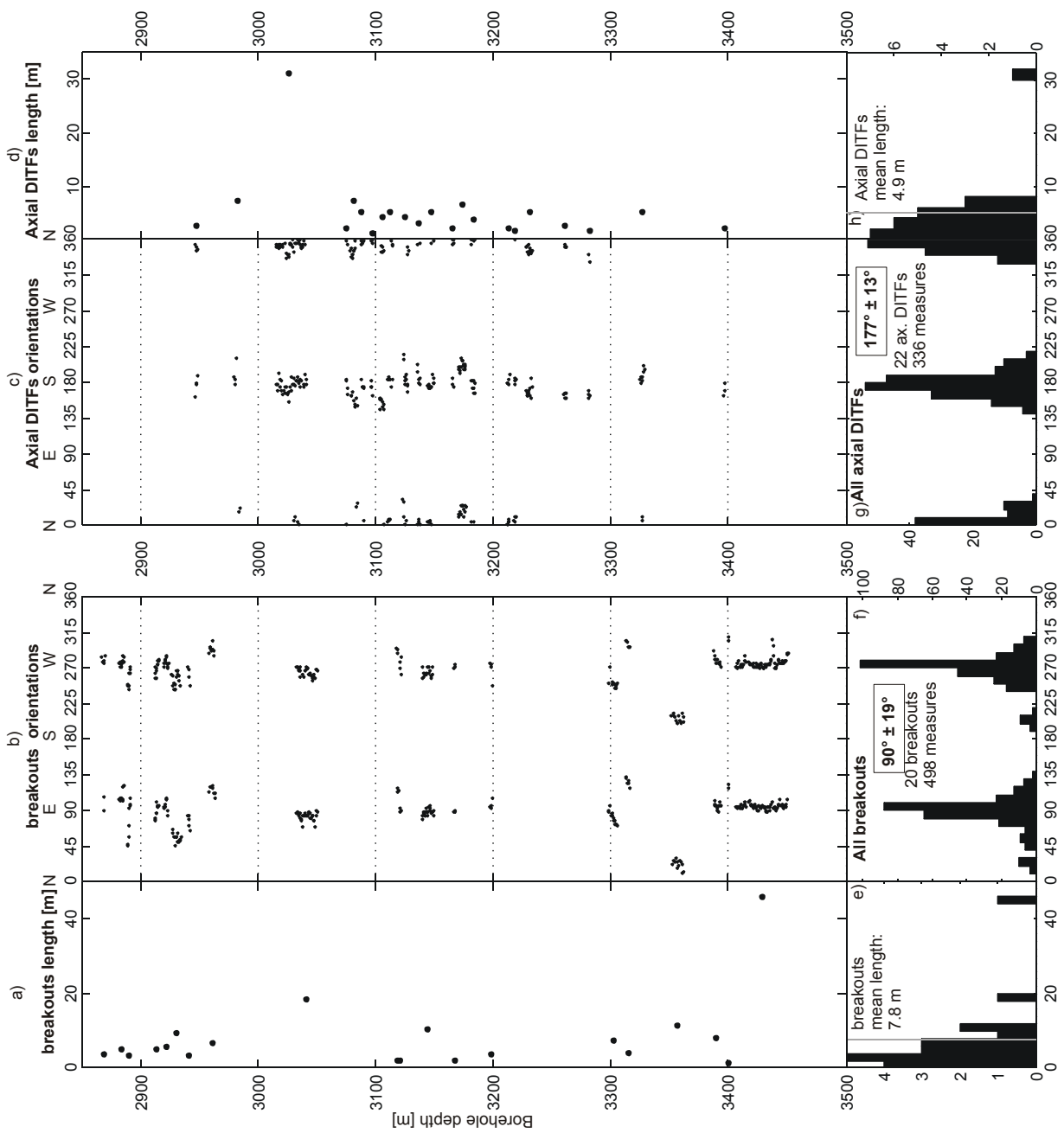

Figure 3: compilation of axial DITFs and breakouts data from GPK1 a) length of breakouts vs. depth b) orientation measurements of breakouts vs. depth c) orientation measurement of axial DIFTs v. depth d) length of axial DIFTs vs. depth e) histogram of breakouts length f) histogram of orientation of breakouts g) histogram of orientation of axial DITFs h) histogram of axial DITFs length.

The above studies provide an unusually well-defined indication that the orientation of S_{Hmax} in the basement above 3800 m is essentially N-S, in accord with other indications derived from the geometry of structures within the induced microseismic cloud (Cornet & Jones, 1994). However, the state of stress at the depth of the 5 km reservoir at Soultz has not yet been established from direct observations. In this paper the measurements of induced fractures in GPK4 are presented. For sub-vertical borehole sections, the orientation of the maximal horizontal stress can be readily obtained from the induced fracture orientation. Thus, we restrict the stress analysis to GPK4 sections where the borehole lies within 15° of vertical (<2500 m and > 4750 m, borehole depth). The analysis of the breakouts/DITFs in other borehole sections will be considered in future work. To ensure consistency with earlier studies, DITFs and breakouts were also identified on UBI and FMI logs from GPK1 using an identical procedure..

DATA SETS

The GPK4 borehole was imaged with a Schlumberger UBI sonde run in the 12.25 inch diameter section from 1431 to 4733 m measured depth (all depth in this report are given as measured depth along borehole unless otherwise indicated), and the 8.5 inch section from 4740 to 5263 m. Images suitable for fracture geometry determination were obtained for 1455-4730 m and for 4767-5258 m. Outside these ranges, the logs are run in casing or suffer from data problems. The borehole trajectory deviates from verticality by less than 15°, and the borehole is then considered sub-vertical, from the surface to 2500 m and again below 4750 m (figure 2e). In between these two depth ranges, the deviation from verticality reaches values as high as 30°.

For the GPK1 borehole, breakouts and axial DITFs were measured from 2840 m to 3510 m using UBI and FMI borehole wall images. Deviation from verticality of the GPK1 trajectory is less than 10°.

DATA ANALYSES

Drilling induced tension fractures and breakouts were determined on the fracture imaging logs using a two-step procedure. First, the depth of the feature was defined by its top and bottom depth. Then the orientation of each breakout or DITF segment was measured at 0.5 m intervals along the length of the feature. Measurements on both traces of the feature, usually separated by about 180°, were taken independently. The entire GPK4 data set was analyzed in this way. Then, the same procedure was applied to the GPK1 logs between 2840 to 2510 m to provide a comparison with existing studies and identify any methodological bias.

Calculations of mean orientation have been done considering measurement as axial data. Mean direction and circular standard deviation have been calculated considering multiply-wrapped distributions as described in Mardia & Jupp (2000).

GPK4

A total of 81 individual breakouts were identified along the entire imaged section of GPK4. The mean length of the individual breakouts was 4.4 m and the longest was 18.7 m (figure 2f). The cumulative length of breakouts amounted to 355 m or 9% of the total borehole length examined. The vast majority of breakouts occur below 3800 m where the cumulative length to 5258 m is 327 m or 22% of borehole length.

From the 81 breakouts, a total of 1821 determinations of breakout orientation were made. Considering all data, the azimuth of the breakouts was determined to be 83°±24° (figure 2g). For the sub-vertical borehole section below 4750 m, the mean azimuth was found to be 83°±20° (figure 2h).

In all, 54 individual axial DITFs were identified along GPK4. The mean and maximum fracture trace lengths were 6.7 m and 37.7 m respectively (figure 2l). Axial DIFTs are generally longer in the upper part of the borehole than in the lower part (figure 2d). The cumulative length of axial DIFTs is 362 m or 10% of the total examined borehole length. Axial DITFs occur primarily above 2250 m and below 4570 m, where the hole is within 15° of vertical. Above 2250 m, the cumulative length of DITFs is 301 m or 38% of the sector length, whereas below 4767 m, the cumulative length of DITFs is 41 m or 9% of the sector length.

A total of 1334 orientations determinations of axial DITFs were made. Considering the whole data set, the induced fractures strike 172°±16° (figure 2i) . For the section where the borehole is sub-vertical and DITFs are well developed (i.e. depth smaller than 2500 m), the mean strike direction is 172°±11° (figure 2j). DITFs located in the deep sub-vertical borehole section (i.e. depth higher than 4750 m), the mean strike direction is 174°±28° (figure 2k).

GPK1

To provide a check on the methodology, breakouts and axial DITFs in GPK1 were analysed using the same procedure as for GPK4.

A total of 20 individual breakouts were identified on GPK1 covering 23% (156 m) of the investigated borehole section. Breakouts mean length is 7.8 m and the maximum breakout length is 46 m (figure 3e). Breakouts are located almost uniformly along the whole investigated section at a mean rate of 3 breakouts per 100 m excepting for a slightly higher breakouts concentration shallower than 2960 m. From the 20 breakouts, 498 orientation determinations were made which indicate an orientation of 90°±19° (figure 3f). The implied orientation of S_{Hmax} is 0°±19°.

In all, 22 axial DITFs have been identified that extend over 16% (108 m) of the investigated borehole section, primarily between 3075 m and 3185 m. In this interval, 12 fractures extend over 19.5 m (18%) of borehole. Mean fracture length is 4.9 m, the longest fracture having a length of 31 m (figure 3h). A total of 336 orientation determinations were made which indicate a mean strike of 177°±13° (figure 3g).

DISCUSSION

The orientation estimates of S_{Hmax} derived from the axial DITFs and breakouts in GPK1 are N0±19° and 177°±13° respectively. These estimates are in accord with the results of previous studies of the data for this well described in the introduction. Thus, the methodology we employ appears to yield consistent results.

The axial DITFs in GPK4 above 2250 m suggest an S_{Hmax} orientation of N172°E±11°, again consistent with the results of earlier studies of the shallow basement at Soultz. Below this depth in GPK4, the axial DITFs largely vanish until near the hole bottom. This is probably a consequence of the deviation of the hole from verticality, which would promote the development of en-echelon fractures, if the conditions of DITF development are met at all. This will be examined in future studies.

In the lower, sub-vertical section of GPK4 below 4750 m, the azimuth of breakouts indicate an S_H direction of 173°±20°, whereas the axial DITFs indicate an S_H direction of 174°±28°. Thus, the results indicate that the orientation of

S_{Hmax} at 5 km depth is the same as in the shallower reservoir.

Future work will focus on extracting stress information (orientation and magnitude) from the non-vertical sections of GPK4, with particular regard to quantifying deviations from uniformity (i.e. the strength of stress heterogeneity) and of relating such deviations to structures in the basement.

CONCLUSION

The orientation of the maximum horizontal principal stress at 5 km depth in GPK4 is 173°±20°, and is not statistically different to the well-determined orientation of S_{Hmax} to 3.8 km from previous studies.

REFERENCES

Bell, J.S., Gough, D.I. 1979. Northeast-southwest compressive stress in Alberta: evidence from oil wells. Earth and planetary Science Letters, vol. 45, n° 2, 1979, p.475-482.

Bérard, T. & Cornet, F.H. 2003. Evidence of thermally induced borehole elongation: a case study at Soultz, France. Int. Journal of Rock Mechanics and Mining Sciences. 40 (2003), p. 1121-1140.

Brudy, M. & Zoback, M.D. 1999. Drilling-induced tensile wall-fractures: implications for determination of *in-situ* stress orientation and magnitude. Int. Journal of Rock Mechanics and Mining Sciences. 36 (1999), p. 191-215.

Cornet, F.H. & Jones, R. 1994. Field evidences on the orientation of forced water flow with respect to the regional principal stress directions. Rock Mechanics. ISBN 90-5410-380-8.

Genter A. and Tenzer, H., 1995. Geological monitoring of GPK2 HDR borehole, 1420-3880 m, BRGM Report No. 38629, BRGM, Orléans, France.

Mardia, K.V. & Jupp, P.E. 2000. Directional Statistics. John Wiley & Sons (Chichester) Ltd. ISBN 0-471-95333-4.

Nagel, R. 1994. Das Spannungsfeld in der Geothermie bohrung Soultz-sous-Forêts abgeleitet aus vertikalen Strukturen in einer Tiefe von 1.9 bis 3.6km.Diplomathesis,Universität Karlsruhe, 1994.

Tenzer, H. ,Mastin L., Heinemann, B., 1992. Determination of planar discontinuities and borehole geometry in the crystalline rock of borehole GPK1 at Soultz-sous-Forêts. Bresee, editor. Geothermal science and technology. Gordon and Breach Publishers, 1992. p. 31-68.

Natural fracture system of the Soultz granite based on UBI data in the GPK3 and GPK4 wells

Chrystel Dezayes*, Benoît Valley**, Emilien Maqua***, Guillaume Syren***, Albert Genter*

**BRGM, F-45060 Orléans*
****ETH Zürich, CH-8093 Zürich*
****University of Savoy, F-73000 Le Bourget du Lac*

Presented at the Soultz Scientific Meeting at Soultz-sous-Forêts on 17th March 2005.

EC Contract ENK5-2000-00301

PARTICIPANT ORGANIZATION NAME: BRGM

Synthetic final report

NATURAL FRACTURE SYSTEM OF THE SOULTZ GRANITE BASED ON UBI DATA IN THE GPK3 AND GPK4 WELLS

Chrystel Dezayes*, Benoît Valley**, Emilien Maqua***, Guillaume Syren***, Albert Genter*

**BRGM, F-45060 Orléans*
****ETH Zürich, CH-8093 Zürich*
****University of Savoy, F-73000 Le Bourget du Lac*
e-mail: c.dezayes@brgm.fr

ABSTRACT

Based on the UBI (Ultrasonic Borehole Imager) data collected in the Soultz EGS site (France), a whole structural analysis has been done in the GPK3 and GPK4 wells, between 1420m and 5100m, and between 1420m and 5260m, respectively. On the whole, more than 7km of borehole images have been analyzed and around 4000 fractures have been measured. A fracture typology has been defined in order to improve our understanding of the deep fractured granite.

Fracture density versus depth alternates with closely spaced fractures and low fracture density zones. A very high density fracture zone occurs in the upper part of a highly altered granite facies.

In the wells, fractures orientations are low scattered and indicate a main N-S direction. That geometry, observed at great depth within the granite basement of the Rhine Graben, is consistent with the extensional regime, which occurred during the rifting at Oligocene time. The vertical evolution of the fracture dip directions with depth shows fractures dipping mainly to the East in the upper part of the granite, nearly equally to East and to West in the intermediate part, and to the West in the lower part of the wells. This tilting of the dip direction of the fractures in the granite massif could be in relation with the main regional structures close to the Soultz site, which constitute the boundary faults of the Rhine Graben. As the fracture geometry is very similar within the deep wells, there is no relationship between fracture geometry (trend, dip) and lithology (standard granite, two-mica granite, biotite rich-granite).

In the open hole sections of the GPK3 and GPK4 wells, the fracture density is moderate with a highly density zone in the boundary of the porphyritic MFK-rich granite and the two-mica granite. The fracture orientations are grouped into a N-S set and mainly dipping to the west. The fracture network intersected by these open hole sections is highly developed and offers a lot of fracture candidates for hydraulic stimulation.

INTRODUCTION

In the framework of the EGS geothermal project at Soultz-sous-Forêts, the natural fracture characterisation of the granite batholith is a primary objective dedicated to structural geologists. As fractures represent the potential fluid pathways, which support the flow, their detailled analysis brings relevant information for a better understanding of the hydraulic stimulation tests and thus, for the deep heat exchanger creation.

The Soultz site is located in France within the Upper Rhine Graben, near its major western boundary fault (Figure 1). Five boreholes have been drilled since 1987: two relatively shallow exploratory wells (GPK1 and EPS1) were drilled to 3600m and 2200m respectively, and three for reservoir development and heat exploitation (GPK2, GPK3 and GPK4). All of which were drilled to depths of approximately 5000 m, where temperatures reach 200°C (Figure 2; Boumgärtner *et al.*, 2004). The future exploitation triplet is formed by GPK2, GPK3 and GPK4, which were drilled from the same well pad and are slightly inclined with depth. The three wells are aligned at 5000 m depth in a N165°E direction and the horizontal distance between adjacent wells is about 700 m (Figure 2).

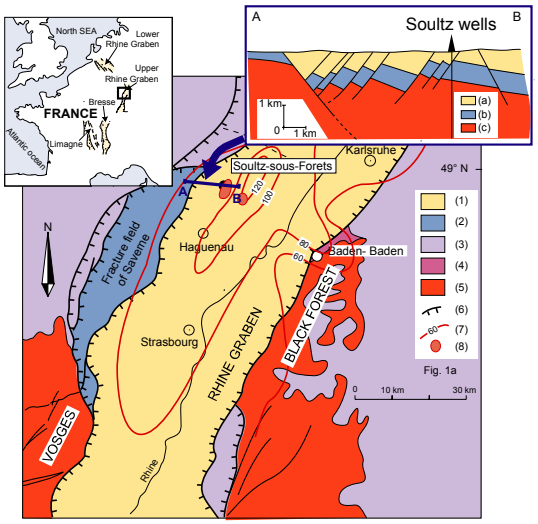

Figure 1: Location of the EGS Soultz site and geology of the Upper Rhine Graben: (1) Cenozoic sediments; (2) Cenozoic volcanism; (3) Jurassic; (4) Trias; (5) Hercynian basement; (6) Border faults; (7) Temperature distribution in °C at 1500m depth (Haenel et al., 1979); (8) Local thermal anomalies (Haenel et al., 1979). Simplified cross-section through the Soultz site: (a) Cenozoic filling sediments; (b) Mesozoic sediments; (c) granite basement.

One of the exploratory wells was cored (EPS1). The others were drilled by destructive mode and partially or totally logged with borehole image logs such as UBI (Ultrasonic Borehole Imager) or FMI (Fullbore Micro Imager).

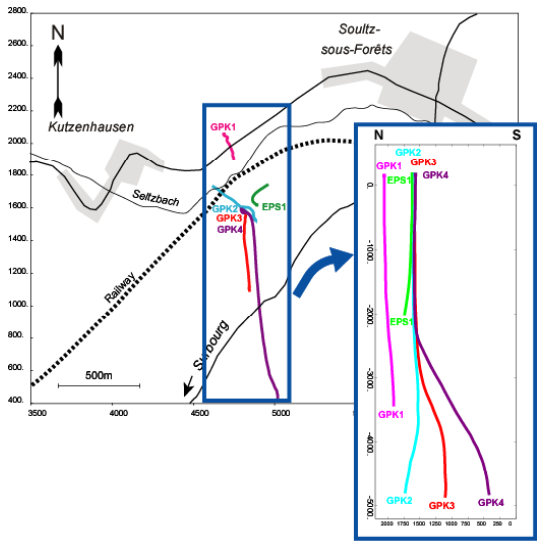

Figure 2: Map view and N-S cross-section of the EGS well trajectories at Soultz.

Cuttings, cores, geophysical logs and borehole image logs acquired in the granite were analysed and interpreted to characterise the fracture network properties as well as the petrographical variations of the granite (Genter *et al.*, 1997; Genter *et al.*, 1999; Dezayes *et al.*, 2004). The deep geology of the Soultz site is mainly composed of two main granites with depth. The upper part (from 1420 to 4700m) is referred to the Mega K-Feldspar granite, with a very altered and fractured intermediate section (between about 2700m and 3900m), and the lower part (from 4700m to 5000m, bottom well) corresponds to a two-mica granite (Dezayes *et al.*, 2005).

This paper presents a detailed fracture analysis of the GPK3 and GPK4 wells based on the interpretation of borehole image logs (UBI). The whole fracture system has been characterised in the granite between 1420m to 5000m depth in terms of fracture typology, fracture orientation (dip direction, dip) and fracture density.

DATA AVAILABLE

Orientation and classification of several thousand fractures were collected from high-resolution acoustic image logs such as BoreHole TeleViewer (BHTV) in GPK1 and EPS1, and Ultrasonic Borehole Imager (UBI) in GPK2, GPK3 and GPK4 (Figure 3). Various electrical image logs (FMS, FMI, ARI) have been run in the GPK1 and GPK2 wells and analysed in previous studies (Genter *et al.*, 1995; Dezayes *et al.*, 1995; Genter *et al.*, 1997).

The method of acoustic imager consists to aiming an ultrasonic beam to the borehole wall. The reflected beam is analysed in terms of amplitude and transit time (Figure 4). The received amplitude depends mainly on the reflectivity of the rock and the transit time on the borehole geometry. The tool produces two complete 360° images (amplitude and transit time), oriented with magnetometer, which gives the orientation of the beam according to the magnetic north.

Anomalies on the images resulting as a sinusoidal feature are interpreted in terms of planar discontinuities (fractures) and their orientation (dip direction and dip) can be measured (Figure 5).

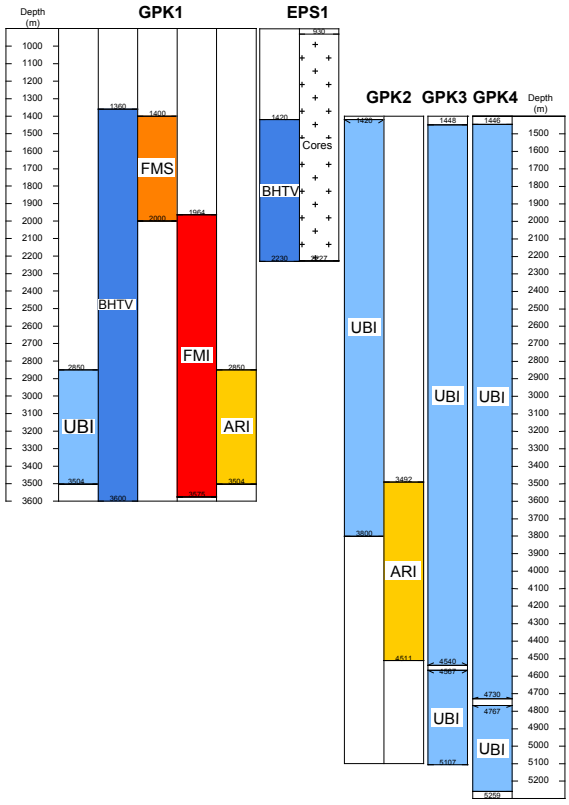

Figure 3 – Core and image data available in the Soultz wells. BHTV: BoreHole Televiewer; UBI: Ultrasonic Borehole Imager; FMS: Formation Micro Scanner; FMI: Fullbore Micro Imager; ARI: Azimuthal Resistivity Imager.

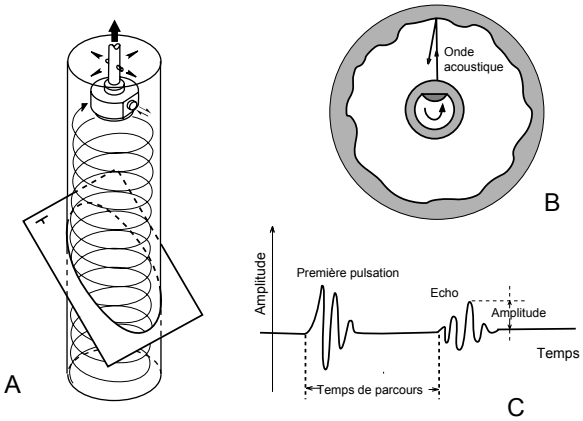

Figure 4 – Principle of the acoustic image tool.

Wells GPK1, GPK3 and GPK4 were fully logged in the granite, whereas in GPK2, due to logging problem, the log stopped at 3800 m and thus no image data were acquired in the bottom part of the well between 3800 and 5100 m. As a whole, about 14000 m of image logs were analysed, and about 7300 natural fractures were measured and their morphology was characterised in relation with the image signature.

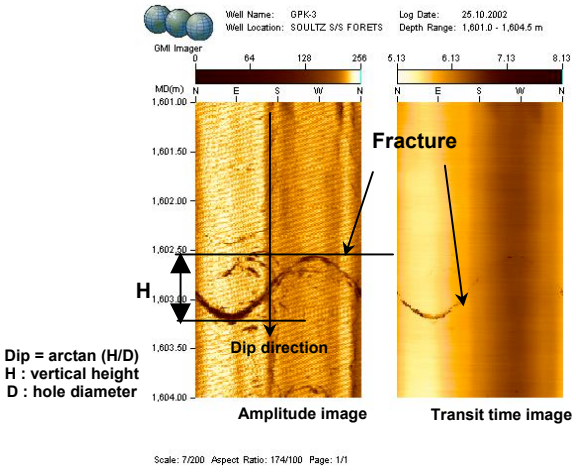

Figure 5 – UBI image from GPK3 well showing a partially open fracture and principle of orientation measurement.

In EPS1, the orientation, location and morphology of about 3000 fractures were determined from 810 m of granite cores (Genter & Traineau, 1992). In the same interval, only 517 fractures were observed on the BHTV images (17%). Despite the better resolution of the more recent acoustic images, the number of fractures is underestimated from the analysis of image logs. However, this does not lead to any biasing relative to the fracture network orientation (Genter *et al.*, 1997).

FRACTURE TYPOLOGY

Two main types of fractures have been defined along the wells based on their origin: the natural fractures, older than the drilling and in relation with the tectonic history of the granite massif, and the induced fractures, formed with the drilling and in relation with the present-day stress field. In this study, only the natural fractures have been take into account. Induced fractures were studied in other papers like Tenzer *et al.* (1991), Genter *et al.* (1995), Dezayes *et al.* (1995), Valley & Evans (1995).

The natural fracture typology has been defined in order to get homogenous fracture datasets in the GPK3 and GPK4 wells. This typology is based on two criteria mainly:

- the comparison between transit time and amplitude image logs permits to determine if the fracture is open (dark traces, Figure 6) or not (no trace, Figure 7).
- the continuity of the sinusoidal trace on the amplitude image to distinguish the scale of fractures (100% to 80% of the sinusoidal trace visible, between 80% and 50%, lower than 50% and uncertain sinusoidal fitting) adding traces with the occurrence of an alteration halo surrounding the fracture.

Open and closed fractures

If a fracture, visible on the amplitude image, shows dark traces on the transit time image, we consider the fracture open at least in the surrounding of the well (Figure 6). In fact, this feature indicates that the distance between the image tool and the fracture is higher than the standard size of the radius borehole. Cores studies at Soultz showed that all the natural fractures are filled or partly filled by hydrothermal secondary minerals (quartz, clays, calcite, hematite,…). The fact that the sinusoidal traces are visible on the transit time image suggests that the hydrothermal filling is uncompleted or that the fractures were washed out by the drilling process. Then, the term “open fracture” does not signify that the fracture is open in its whole surface.

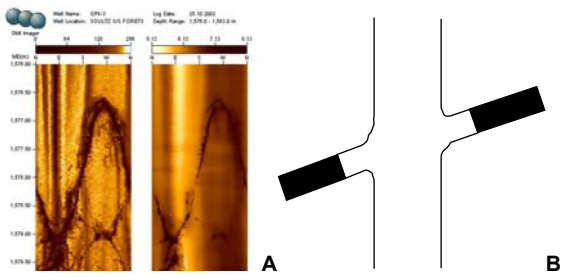

Figure 6 – Open fracture. A: representation on UBI image in the GPK3 well. B: interpretation cross-section of the fracture intersected by the well (in black, hydrothermal filling).

If no trace is present on the transit time image (Figure 7), this indicates that the fracture is filled and there is no difference between the tool-rock distance and the tool-fracture distance.

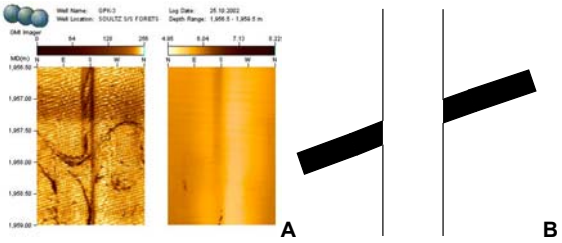

Figure 7 – Closed fracture. A: representation on UBI image in the GPK3 well. B: interpretation cross-section of the fracture intersected by the well (in black, hydrothermal filling).

Alteration zones

Around some major fractures or fractured zones, hydrothermal alteration related to the transformation of the primary granite minerals occurred. Thus, the resulting images correspond to a wide sinusoidal band darker than the surrounding image, i. e. the fresh granite. Generally, a significant fracture trace is clearly visible inside the alteration halo (Figure 8).

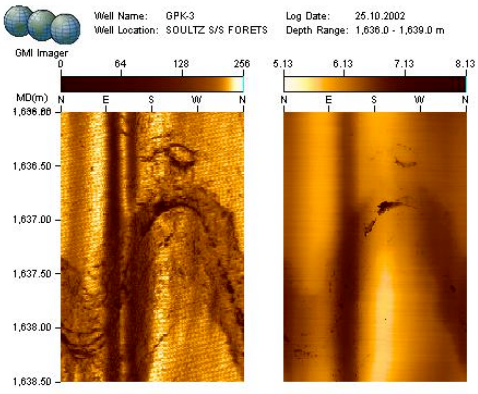

Figure 8 – Alteration zone on UBI in the GPK3 well.

Locally, it could be difficult to clearly identify natural fractures. The identification of the fracture zones is important because they correspond probably to the fluid pathway into the granite massive with a higher porosity (Genter *et al.*, 2002). The thickness of these zones is measured.

Complete sinusoidal trace

Fractures of this type show a sinusoidal trace complete or partially complete, but with more than 80% of the sinusoid (Figure 9). The traces are more or less wide and correspond to major fractures. Generally, the fracture aperture is not constant at the intersection between the well and the fracture plane. Thus, some parts of the fracture traces are wider such as the upper and lower parts of the sinusoid (Figure 9).

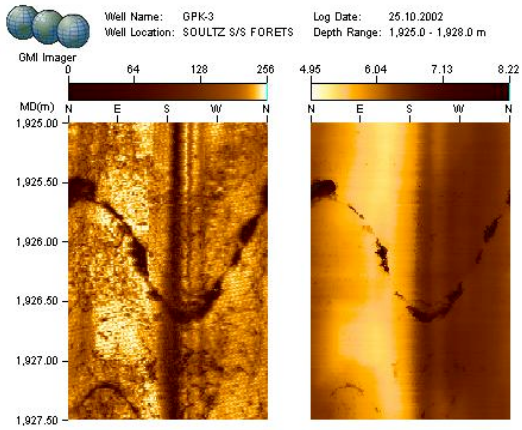

Figure 9 – Fracture showing 100% to 80% of the sinusoidal trace on the UBI in the GPK3 well.

More than 50% partial sinusoidal trace

For this type, the sinusoid is not continuous and only visible between 50% and 80% (Figure 10). In several sections of the wells, the images show non-geological features or artefacts, which hinder to clearly identify the fracture traces. In this case, sinusoidal traces present in this section are classified with this type but could be considered as complete trace. But generally, the fracture trace is less visible because the fractures are thinner. They probably have thickness variations but they correspond to small-scale fractures. Fractures of this partial type are as much important as the complete sinusoids.

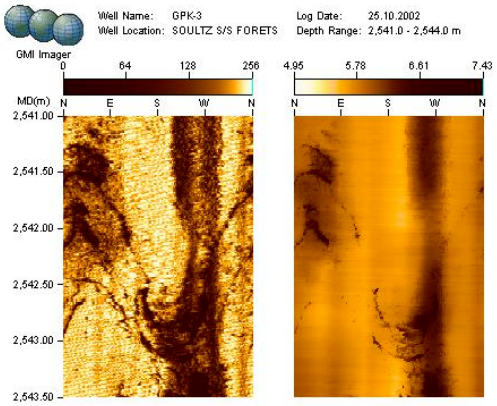

Figure 10 - Fracture showing 80% to 50% of the sinusoidal trace on the UBI in the GPK3 well.

Less than 50% partial sinusoidal traces

The trace is slightly visible with less than 50% of the sinusoid (Figure 11). Generally, only the upper part or the lower part of the sinusoid is clearly visible (Figure 11). This fracture type is a minor type because it corresponds to thinner fractures. However, as we know that the image tools detect about 20% of fractures only, these fractures must be taken into account in the structural analysis.

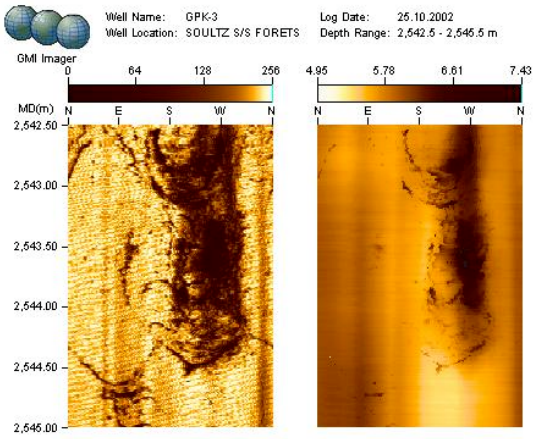

Figure 11 - Fracture showing less than 50% of the sinusoidal trace on the UBI in the GPK3 well.

Uncertain sinusoidal traces

Some fracture traces are difficult to characterise because they are too much discontinuous or are located within a section where there are too many significant image artefacts such as black-coloured vertical strings (Figure 12). These uncertain measurements could also be take into account in the fracture analysis if their whole orientation is consistent with the local tectonic framework.

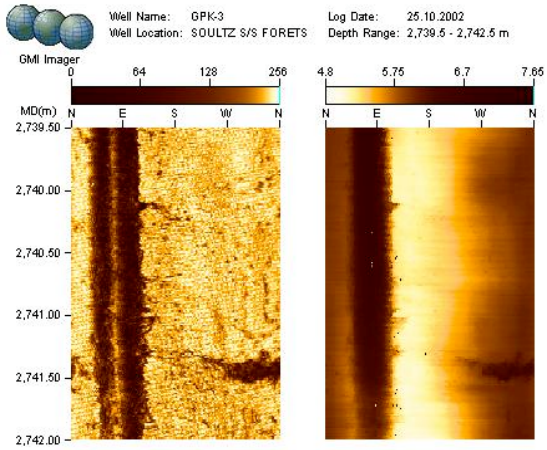

Figure 12 – Uncertain sinusoidal trace.

FRACTURE DENSITY

In the GPK3 and GPK4 wells, the cumulative density of fracture has been computed along the well trajectories respectively. Nine sections with variable density values alternate with depth (Figure 13).

In the GPK3 well, the high density value (0.8 fract./m) observed in the upper part of the granite is in agreement with

the previous studies done at Soultz (Genter *et al.*, 1997). From 1800m to about 2900m, the fracture density is quite constant with a low density (0.4 fract./m). These two sections correspond in terms of petrography to the standard pophyritic granite (Figure 13).

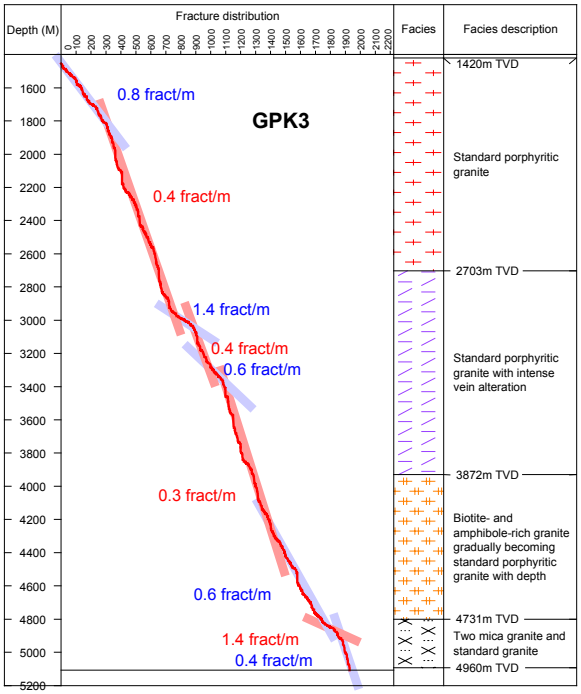

Figure 13 – Cumulative fracture density (all fracture types) derived from borehole image analysis in the GPK3 well. Depth in the left column corresponds to the measured depth along the borehole, from the drilling floor. The depth boudary of the granite facies in the right column correspond to the vertical depth, from the drilling floor.

In the intermediate part of the well, two high fracture density zones (1.4 fract./m and 0.6 fract/m) surround a low density zone (0.4 fract./m). These three zones correspond to the upper part (between 2900m and 3300m) of the highly fractured and altered standard granite facies (Figure 13).

Below these zones, there are two low and moderate fracture density zones, which are embedded into the biotite and amphibole rich granite (Figure 13).

In the lower part of the well (from 4800m), a very high fracture density zone occurs. This zone corresponds to the boundary between two granite facies: the standard porphyritic granite and the two-mica granite. In this deep fine-grained facies, the fracture density is very low and decreases significatly to 0.4 fract./m (Figure 13).

In the neighbouring GPK4 well, a high density value (0.8 fract./m) occurs of the upper part of the granite, as in the GPK3 well. Between about 1800m and 1900m, the fracture density increases to 1.25 fract./m. Below 1900m and to about 2700m, the fracture density is quite constant with a low density (0.55 fract./m). These three sections correspond in terms of petrography to the standard pophyritic granite (Figure 14).

In the intermediate part of the well, two very high fracture density zones (2.86 fract./m and 1.76 fract/m) alternate with two moderate density zones (0.71 fract./m). These four zones correspond to a highly fractured and altered standard granite facies, between 2900m and 3500m (Figure 14).

Below these zones, between 3500m and 4750m, the fracture density is very low and quite constant with a value of 0.23 fract/m (Figure 14).

In the lower part of the well (from 4750m to the bottom well), a high fracture density zone (0.89 fract./m) occurs in the lower part of the biotite and amphibole rich granite facies and the two mica-granite (Figure 14).

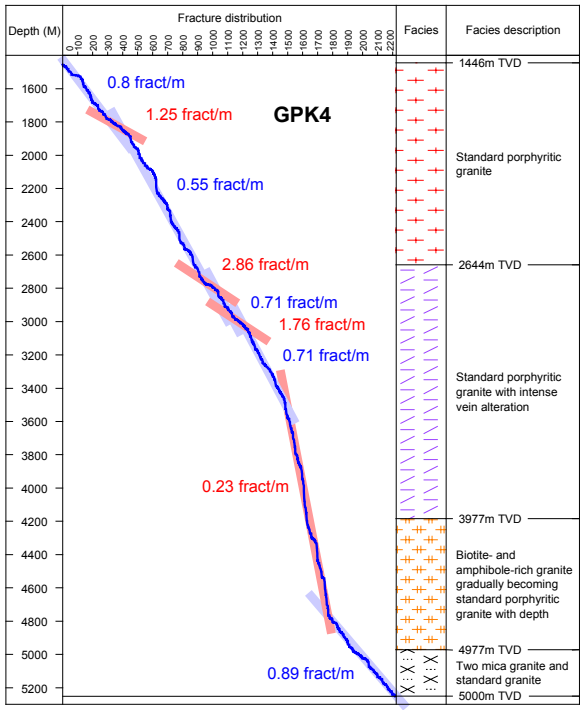

Figure 14 – Cumulative fracture density (all fracture types) derived from borehole image analysis in the GPK4 well. Depth in the left column corresponds to the measured depth along the borehole, from the drilling floor. The depth boudary of the granite facies in the right column correspond to the vertical depth, from the drilling floor.

FRACTURE ORIENTATION

In the granite, fracture orientations based on cores and image logs show good agreement between all the wells. The fracture network shows two conjugate fracture sets with a N-S principal direction and high dip values (Figure 15), consistent with both the tectonic setting of the graben (Dezayes *et al.*, 1995) and the present-day stress field (Klee and Rummel, 1993).

The EPS1 cores show a very high fracture density with about 3000 fractures measured on 810m of granite cores (i.e. 3.7 fract./m). All orientations are present but two major fracture sets appear: 1) a west-dipping major set that is more scattered with orientations of N175°E and N20°E and a 80° west dip (Figure 15); and 2) a second east-dipping set, oriented N170°E with a 70° east dip. In this well, located in the north-east quadrant of the Soultz site, it appears that west-dipping fractures are more dominant.

On the GPK1 BHTV logs, the fracture orientations are highly scattered (Figure 15), but two major fracture sets occur. These fracture sets are few scattered with a dominant N165°E trend. The fractures dip either 80° to the west or 75° to the east. The fracture set dipping to the west is dominating.

The fractures observed on UBI in the GPK2 well are gathered around two dominant sets oriented N170°E, which show rather the same proportion of nearly-vertical fractures dipping either to the west or to the east (Figure 15). This analysis is based on UBI log done in 1995, when the total depth of GPK2 was 3800m. In 1999, the well has been deepening to 5100m and a new UBI has been logged from 3200m. However, the UBI run has been stopped to 3875m, because of the occurrence of a well caving, which did not permit to run down this depth.

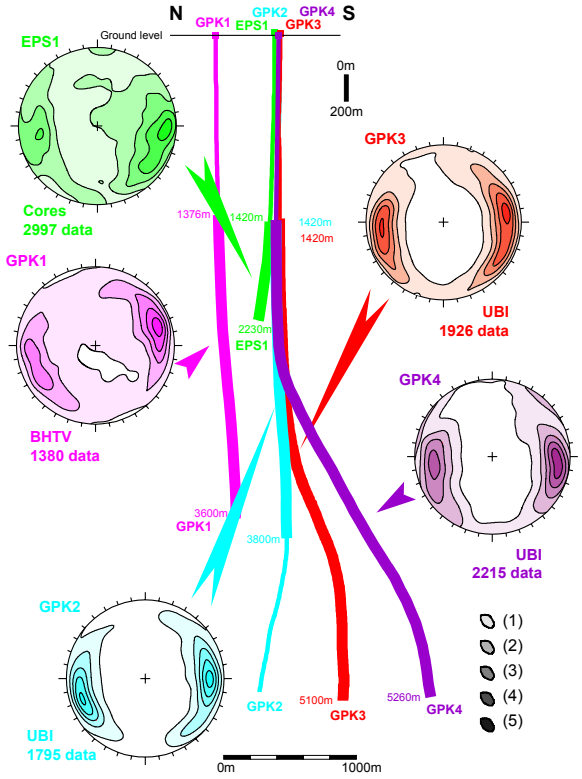

Figure 15 – Fracture network orientation in the Soultz wells based on cores and various borehole image logs. The thick lines represent the image log sections. The depths along the wells indicate the upper and the lower depth limits of the image logs (in measured depth along the well, from the drilling floor). Contour-density diagrams of all fracture types in Schmidt's projection, lower hemisphere: (1) 10%, (2) 30%, (3) 50%, (4) 70%, (5) 90% of the maximum frequency.

In the GPK3 and GPK4 wells, the whole granite section has been logged with an UBI tool, which permits to correlate the fracture network between the both wells (Valley *et al.*, 2005). In the GPK3 and GPK4 wells, the dominant fracture trend is about N170°E, with high dips either to the west or to the east (Figure 15). The major fracture sets dipping to west is rather consistent.

In GPK3, the fractures show different orientations and dips in the four main distinctive crystalline units. In the upper part, within the standard porphyritic granite between 1420m and 2702m depth, the major fracture set trends N5°E and dips 75° to the east. A second more scattered fracture set is oriented N30°E and dips to the west. In the highly fractured and altered granite section, between 2702m and 3930m, fracture orientations are more scattered (Figure 16). Two conjugate nearly vertical fracture sets are equally represented with a N170°E orientation. In the biotite and amphibole-rich granite, between 3930m and 4800m, orientations are also scattered (Figure 16). Two major fracture sets trend about N150°E with a more consistent dipping to the east. A third fracture set appears trending rather E-W with a high dip to the north (Figure 16). In the lower part, within the two-mica granite and standard granite section, the fractures are grouped around a major set oriented N5°E (Figure 16). This dominant set is dipping 70° to the west. A secondary fracture set dipping to the east occurs but is very less important. On the whole, the fractures are mainly oriented N-S and have high dips, but the dip direction is eastward in the upper part and westward in the lower part, and the two fracture sets are nearly equally represented in the intermediate part.

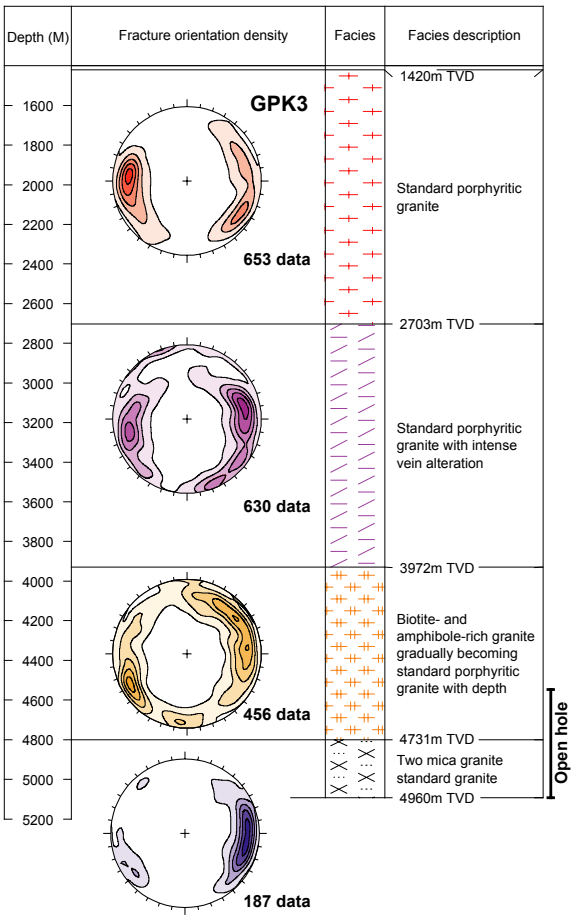

Figure 16 – Fracture orientation in relation to the major petrographical sections in the GPK3 well. Contour-density diagramms of all fracture types. Legend: see Figure 15. Depth in the left column corresponds to the measured depth along the borehole, from the drilling floor. The depth boudary of the granite facies in the right column correspond to the vertical depth, from the drilling floor.

In the GPK4 well, the fracture orientation distribution in relation with the major petrographical sections is rather identical with those observed in the GPK3 well. In the upper part of the porphyritic granite, between 1420m and 2658m, the two fracture sets trend N175°E with a more dominant dipping to the east (Figure 17). In the fractured and altered granite section, the fractures are very scattered with two sets trending N160°E. Both sets are nearly equally represented, but the est-dipping set is more vertical. In the biotite and amphibole-rich granite, fractures are also scattered but the trend is mainly N-S. The dominant set is dipping to the west

(Figure 17). As at the same depth section in GPK3, a minor E-W set occurs but it is very less important in the GPK4 well. In the lower part, in the two-mica granite and standard granite, the major set is grouped around the N280°E-80° orientation (N10°E trending).

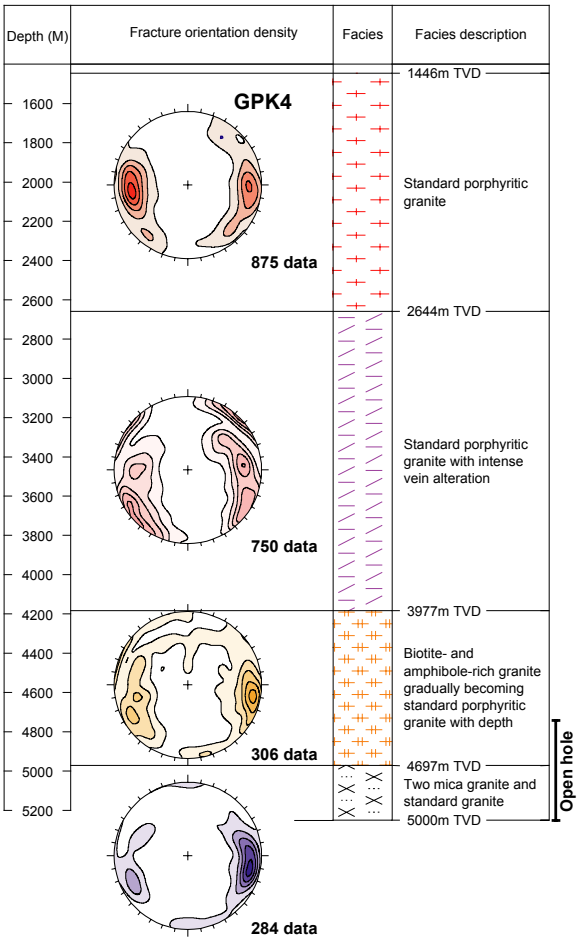

Figure 17 - Fracture orientation in relation to the major petrographical sections in the GPK4 well. Contour-density diagramms of all fracture types. Legend: see Figure 15. Depth in the left column corresponds to the measured depth along the borehole, from the drilling floor. The depth boudary of the granite facies in the right column correspond to the vertical depth, from the drilling floor.

Whatever the methods used for characterising the fracture system (cores or image logs), the fracture system observed in the Soultz wells is nearly vertical with a dominant orientation close to N-S. That geometry observed at great depth within the Rhine graben is consistent with the extensional regime, which occurred during Oligocene time (Dezayes *et al.*, 1995). However, a part of these fractures are inherited and was reactivated during the rifting.

FRACTURE NETWORK IN THE OPEN HOLE OF THE GPK3 AND GPK4 WELLS

In the open hole of the GPK3 and GPK4 wells, the fracture distribution with depth shows nearly the same characteristics (Figure 18, Figure 19). Three sections could be distinguished with depth showing two sections with low fracture density separated by a section with a high fracture density. The upper depth section shows nearly the same fracture density value, 0.67 fr./m to 4756m TVD (True Vertical Depth) in GPK3 (Figure 18) and 0.77 fract./m to 4668m TVD in GPK4 (Figure 19). This upper section corresponds in terms of lithofacies to the standard granite more or less enriched in biotite and amphibole. The highly fractured section corresponds to the upper part of the leucogranite pluton (Hooijkaas *et al.*, 2005; Dezayes *et al.*, 2005). In GPK3, this section (4825-4855m or 4756-4786m TVD, True Vertical Depth) has a thickness of 30m and the fracture density value is 1.97 fract./m (Figure 18). In GPK4, the highly fractured zone is thicker, 90m (4950-5040m or 4668-4764m TVD), with a fracture density value of 1.67 fract./m (Figure 19). In the lower part of the open holes, the fracture density decreases to 0.73 fract./m in GPK4 (Figure 19) and 0.43 fract./m in GPK3 (Figure 18), which is a low fracture density in the standard granite.

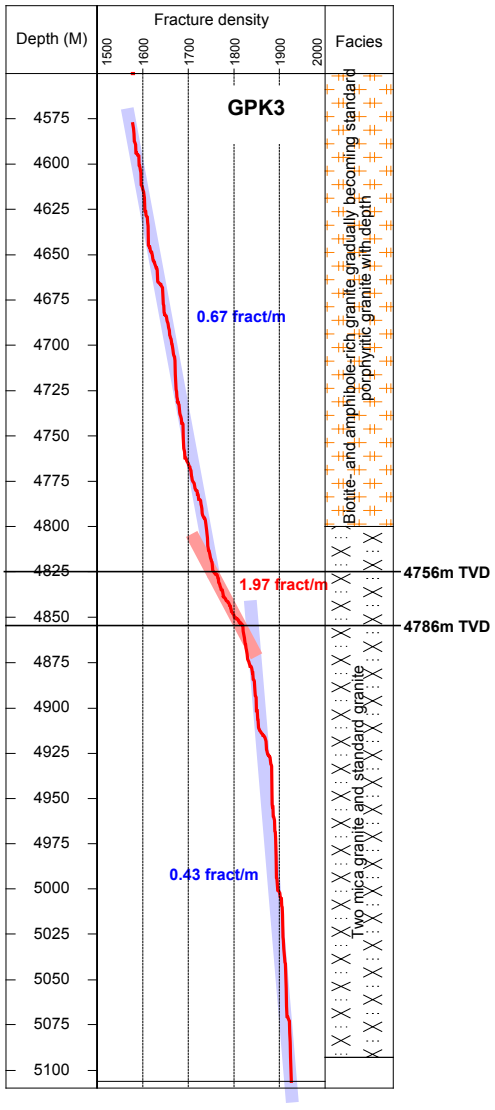

Figure 18 - Fracture density along the open hole section of the GPK3 well derived from UBI analysis. Column 1: depth measured along the borehole from the drilling floor. Column 2: fracture cumulative density along the well. Column 3: main lithofacies sections. At right, the depths are indicate in vertical dept from drilling floor.

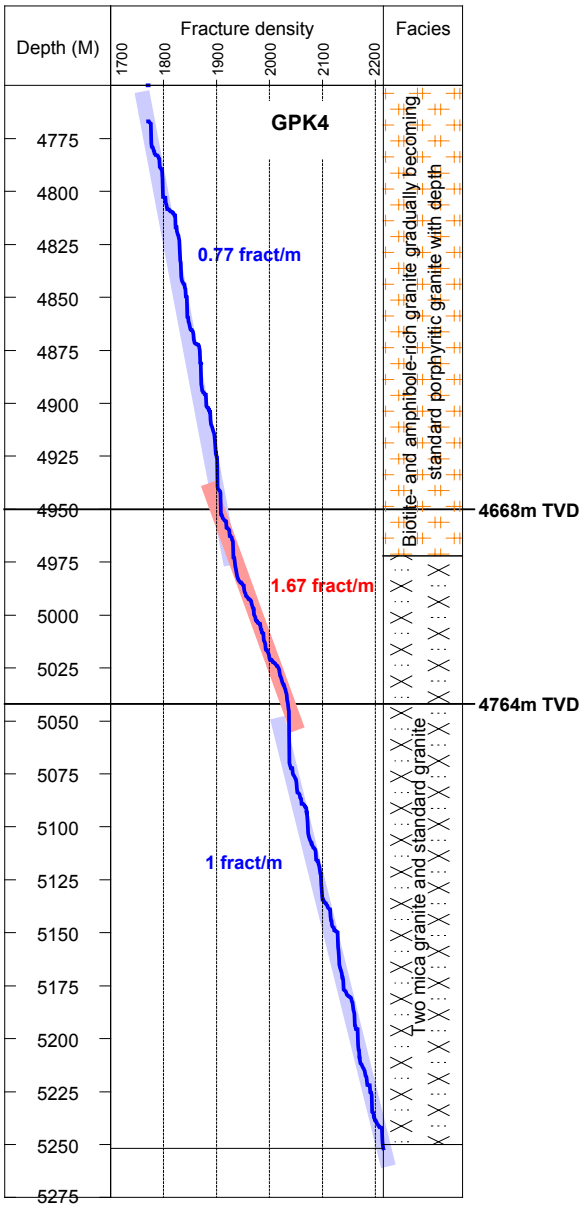

Figure 19 – Fracture density along the open hole section of the GPK4 well derived from UBI analysis. Legend: see Figure 18

In the open hole section of the GPK3 well, where tadpoles of fractures are plotted, the distribution of the open fracture type and closed fracture type versus depth is similar (Figure 20). In the upper part of the open hole section, the incomplete fracture types are dominant and very few complete fractures are present. In the other hand, in the deeper part, more complete fractures occur (Figure 20). At about 4775m, several complete fractures appear and some of them have a small dipping value (50° to the west). This zone corresponds to a large fracture zone, which forms a hydraulic pathway between GPK3 and GPK2 (Windler *et al.*, 2002; Dezayes *et al.*, 2004). In this highest fracture density zone, fracture types consist of closed and incomplete fractures mainly.

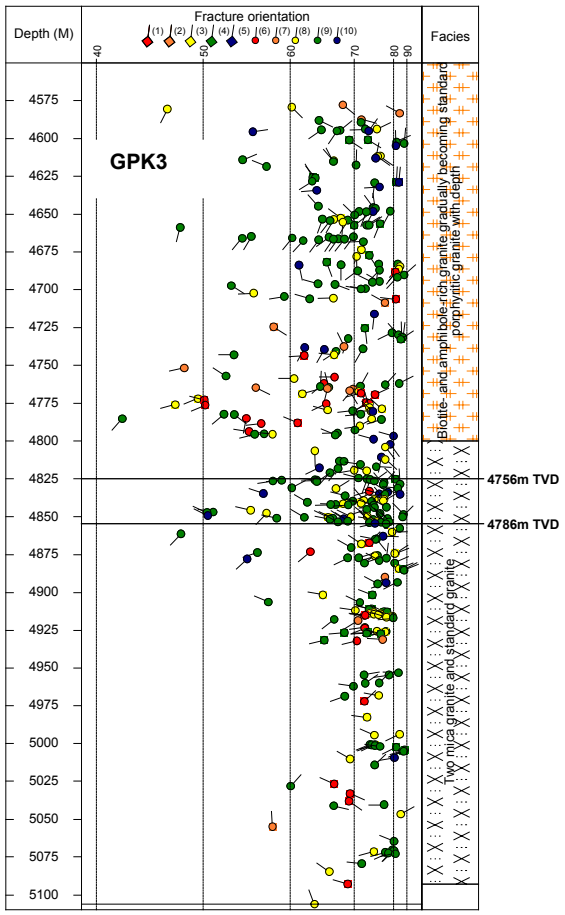

Figure 20 - Fracture orientations versus depth in the open hole section of the GPK3 well derived from UBI analysis. Column 1: depth measured along the borehole from the drilling floor. Column 2: orientation of fractures versus depth. The abscisse represents the dip value, the direction of the tadpole represents the dip direction of fractures (North to the top, East to the right). Colour of tadpole corresponds to the sinusoidal trace type of fracture on the UBI images: (1) open continue sinusoidal trace, (2) open alteration zone, (3) open more than 50% partial sinusoidal trace, (4) open less than 50% sinusoidal trace, (5) open uncertain sinusoidal trace, (6) closed continue sinusoidal trace, (7) closed alteration zone, (8) closed more than 50% partial sinusoidal trace, (9) closed less than 50% sinusoidal trace, (10) closed uncertain sinusoidal trace. Column 3: main lithofacies sections.

The different fracture types in the open hole of the GPK4 well have a similar distribution versus depth as those observed in the GPK3 well (Figure 21). In the upper part, there is no complete closed fracture, only incomplete closed fractures occur as well as complete open fractures. In the lower part, open and closed complete fractures are present. In the intermediate highly fractured part, numerous complete open fractures are present (Figure 21).

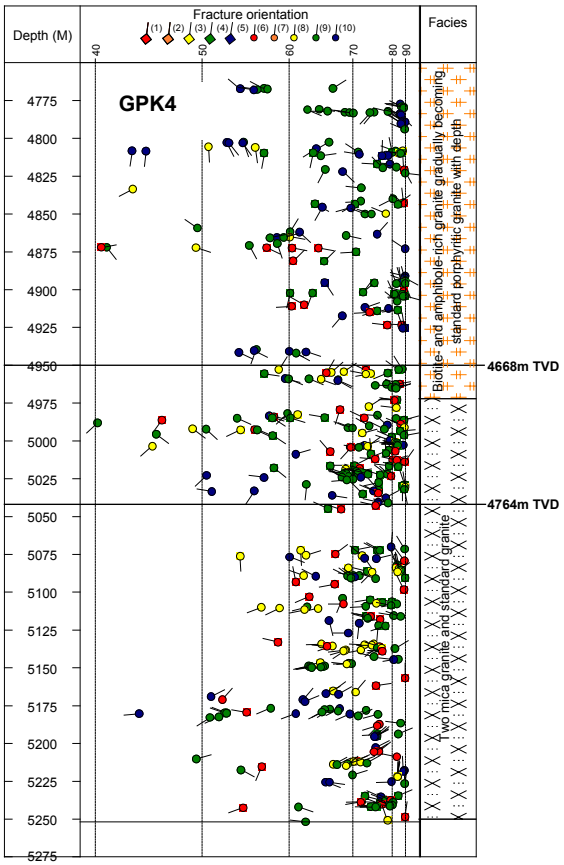

Figure 21 – Fracture orientations versus depth in the open hole section of the GPK4 well derived from UBI analysis. Legend: see Figure 20

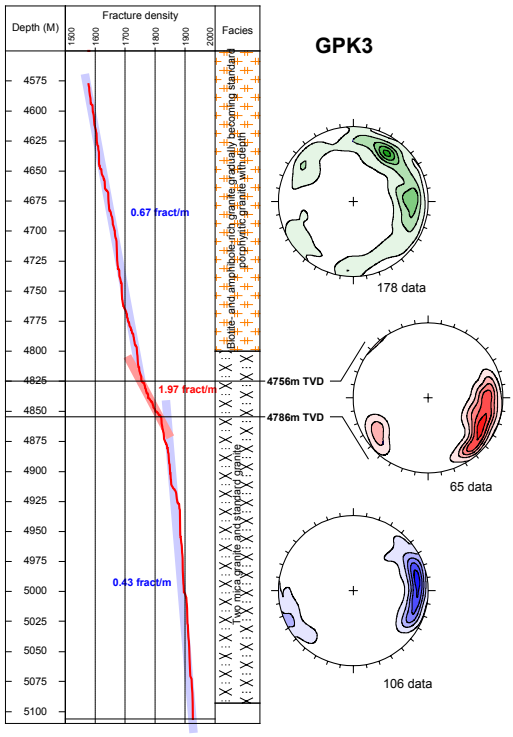

Figure 22 - Fracture orientations and density in the open hole section of the GPK3 well derived from UBI analysis. Fracture density legend, see Figure 18. Contour-density diagramms of all fracture types, legend see Figure 15.

In terms of orientation, the fractures in the open hole sections of GPK3 and GPK4 show a N10°E trend (Figure 22, Figure 23). One set is more consistent and dipping about 70° to the west. Following the different fracture density sections, the main fracture set orientation is variable. In the upper part of the open hole section of GPK3, the fracture orientations are scattered (Figure 22). A main fracture set appears with a N125°E trend and dipping 70° to the S. In the highly fractured zone, fractures are grouped in one nearly vertical set oriented around N30°E and dipping west. In the lower part, only one set is persistent, but with a N-S trending. Fractures dip also to the west.

In the open hole section of GPK4, fractures in the upper density section are scattered (Figure 23) around the N170°E trend and they dip westward mainly. In the intermediate part with in the high fracture density, only one fracture set, oriented N20°E and dipping west, occurs. This set is persistent in the lower part of the well with a rotate trend to nearly N-S (Figure 23).

The comparison of the fracture network in the both open hole sections shows the same organisation. In the upper part of the open hole sections, fractures are scattered with a low density. An intermediate section occurs with a higher fracture density at the boundary of the two different facies: standard porphyritic granite and two-mica granite. In this zone, only one fracture set occurs trending N20-30°E and dipping highly to the west. Below this zone, the fracture density is low again and only one west-dipping fracture set is persistent, with an orientation close to N-S.

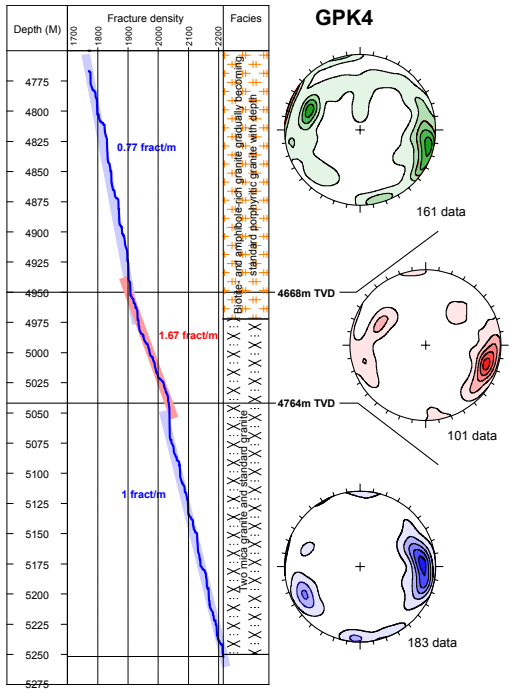

Figure 23 - Fracture orientations and density in the open hole section of the GPK4 well derived from UBI analysis. Legend : Figure 22.

DISCUSSION AND CONCLUDING REMARKS

The fracture network of the deep granite massif at Soultz-sous-Forêts has been investigated by five deep boreholes. Only one of them has been cored and 3000 fractures have been analysed on 810m of granitic cores (Genter *et al.*, 1997). The other wells have been drilled by destructive mode and partially or totally logged with borehole image tools. As a whole, about 14km of image logs were analysed and about 7300 natural fractures were measured and characterised within the crystalline basement.

This structural characterisation was supported by a fracture typology realised for the GPK3 and GPK4 image log analyses. This typology takes into account if the fracture trace is visible or not on the transit time image and the percentage of the visible fracture trace on the amplitude image. An added type takes into account the alteration zone associated with some fractures.

The fracture network analysis has been mainly based on the GPK3 and GPK4 wells, which are the most recent drilled borehole. The fracture density profiles show a high density in the upper part of the granite pluton. Below, the density is low to moderate. In the intermediate part of the wells, a high fracture density zone occurs in the upper part of the petrographical section characterised by the highly fractured and altered porphyritic granite. In the lower part of this petrographical section and in the biotite and amphibole-rich granite section, the fracture density is low to moderate. At the boundary with the two-mica granite pluton, the fracture density increases highly. Below, in the GPK3 well, the fracture density decreases highly, whereas in GPK4, the density stays also high.

The fracture orientation data derived from core analysis or image log analysis shows a good consistency between all the wells. The fractures are nearly vertical with a dominant orientation close to N-S. Two conjugate fracture sets are present dipping to the east and to the west. That geometry observed at great depth within the granite basement of the Rhine Graben is consistent with the extensional regime, which occurred during the rifting at Oligocene time (Dezayes *et al.*, 1995).

As the fracture geometry is very similar within the deep wells, there is no relationship between fracture geometry (trend, dip) and lithology (standard granite, two-mica granite, biotite rich-granite).

In the both GPK3 and GPK4 wells, within the upper part of the porphyritic MFK-rich granite, two conjugate main fracture sets occur with a more consistent dipping to the east. In the intermediate and lower part of the porphyritic granite pluton, corresponding to a zone with intense vein alteration and to the section richer in biotite and amphibole, fracture orientations are more scattered. The two main sets occur nearly equally, but the trend is slightly rotates to NNW-SSE. In the deeper part of the boreholes, a leucogranite appears which is fine-grained and contains muscovite, thus named two-mica granite. The fracture network in this deeper section shows a major set trending N10°E and highly dipping to the west, in the contrary with the upper part of the porphyritic granite. This tilting of the dip direction of the fractures in the granite massif could be in relation with the main regional structures close to the Soultz site, which constitute the boundary faults of the Rhine Graben. As the boreholes are located near the west border of the deep Soultz horst, we assume that the east-dipping fractures observed in the upperpart of the granite pluton could correspond to an antithetic relay fracture network related to the west-dipping border fault. Deeper, the main structure is dipping westward and could be related to the occurrence of a western major boundary fault of the Rhine graben (Figure 24).

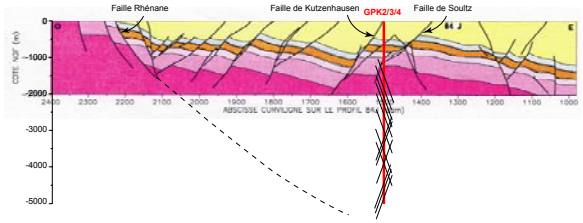

Figure 24 – Conceptual model of fracture tilting in the Soultz granite. Cross-section based on sismic line interpretation (Cautru, 1988).

In the open hole sections of the GPK3 and GPK4 wells, the fracture density is moderate with a highly density zone in the boundary of the porphyritic MFK-rich granite and the two-mica granite. In the upper part of the open hole sections, fracture orientation data are scattered, whereas in the deeper part, they are grouped into one N-S set dipping to the west. In the highly fractured intermediate part, one fracture set occurs trending about N20-30°E and highly dipping to the west. These open hole sections are the injection and production zones of the future heat exchanger. The fracture network intersected by these open hole sections is highly developed and may be favourably oriented in respect to the present-day stress field, if it is the same one than those determined in the upper part of the batholith (N170°E; Klee and Rummel, 1993). Such basic features of fracture system (orientation, density) could represent favourable conditions for creating a HFR heat exchanger at great depth.

ACKNOWLEDGEMENTS

This research was carried out in the framework of the European Hot Dry Rock Project funded by the Commission of the European Communities and the German Ministry of Research and Technology (BMBF). Geological investigations were supported in part by the BRGM (GEOTHER HFR Research Project). The authors are grateful to J. Baumgärtner, A. Gérard, T. Hettkamp, D. Teza (GEIE Soultz) and G. Homeier (SWBU) for their helpful assistance on site.

REFERENCES

Baumgärtner, J., Hettkamp T;, Teza D., Baria R; and Michelet S. (2004) – Building of a Hot Dry Rock scientific power plant at Soultz-sous-Forêts. *Geothermal Ressources Council Transactions*, Vol. 28, p. 201-206.

Cautru (1988) – Rapport annuel d'activités IMRG.

Dezayes C., Genter A., Chevremont P., Homeier G., Hooijkaas G., Tourlière B., Stein G., Degouy M. (2005) – Deep-seated geology of the Soultz basement besed on geological data of the GPK3 and GPK4 wells. Scientific Meeting Soultz, 17 and 18 March 2005.

Dezayes Ch., Genter A. and Gentier S. (2004) – Fracture network of the EGS Geothermal Reservoir at Soultz-sous-Forêts (Rhine Graben, France). *Geothermal Ressources Council Transactions*, Vol. 28, p. 213-218.

Dezayes, Ch., Villemin, Th., Genter, A., Traineau, H. and Angelier, J. (1995). "Analysis of fractures in boreholes of Hot Dry Rock project at Soultz-sous-Forêts (Rhine graben, France).", Scientific Drilling, V.5, p. 31-41.

Genter A., Dezayes C., Gentier S., Ledesert B. and Sausse J. (2002) – Conceptual fracture model at Soultz based on geological data. Geol. JB. Sonderhefte, SE1, 4th HDR forum, Strasbourg, 1998, p. 93-101.

Genter, A., Homeier, G., Chèvremont, Ph., Tenzer, H. (1999). "Deepening of GPK-2 HDR borehole, 3880-5090m (Soultz-sous-Forêts, France). Geological monitoring." BRGM report R 40685, 44 p.

Genter, A., Castaing, C., Dezayes, C., Tenzer, H., Traineau, H. and Villemin, T. (1997). « Comparative analysis of direct (core) and indirect (borehole imaging tools) collection of fracture data in the Hot Dry Rock Soultz reservoir (France).» Journal of Geophysical Research, Vol. 102, B7, p. 15419-15431.

Genter, A. & Traineau, H. (1996). "Analysis of mascroscopic fractures in granite in the HDR geothermal well EPS-1, Soultz-sous-Forêts, France." J. Volc. And Geoth. Res., V.72, p. 121-141.

Genter, A., Traineau, H., Dezayes, Ch., Elsass, Ph., Ledesert, B., Meunier, A. and Villemin, Th. (1995). "Fracture analysis and reservoir characterization of the granitic basement in the HDR Soultz project (France)". Geotherm. Sci. & Tech., V.4(3), p. 189-214.

Genter, A. & Traineau, H. (1992). "Borehole EPS-1, Alsace, France: preliminary geological results from granite core analyses for Hot Dry Rock research." Scientific Drilling, V. 3, p. 205-214.

Haenel, R., Legrand, R., Balling, N., Saxov, S., Bram, K., Gable, R., Meunier, J., Fanelli, M., Rossi, A., Salmone, M., Taffi, L., Prins, S., Burley, A.J., Edmunds, W.M., Oxburgh, E.R., Richardson, S.W., Wheildon, J. (1979). "Atlas of subsurface temperatures in the European Comminity.", Th. Schäfer Druckerei GmbH, Hannover, Germany, February 1980.

Hooijkaas G. R., Genter A. and Dezayes C. (2005) - Deep seated geology of the granite intrusions at the Soultz HFR site based on 5 km depth borehole data. *J. Volc. Geoth. Research*., in press.

Klee, G. and Rummel, F., 1993. "Hydrofrac stress data for the European HDR research test site Soultz-sous-Forêts" Int. J. Rock Mech. Sci. & Geomech. Abstr., V. 30, n°7, p. 973-976

Tenzer, H., Mastin, L. & Heinemann, B. (1991). Determination of planar discontinuities and borehole geometry in the crystalline rock of borehole GPK1 at Soultz-sous-Forêts. *Geotherm. Sci. & Tech.* **3**(1-4), 31-67.

Valley B., Dezayes A., Genter A., Maqua E. and Syren G. (2005) – Main fractured zones in GPK4 borehole and correlation with adjacent borehole. Scientific Meeting Soultz, 17 and 18 March 2005.

Weidler, R., Gérard, A., Baria, R., Baumgaertner, J., Jung, R. (2002). "Hydraulic and micro-seismic results of a massive stimulation test at 5km depth at the European Hot-Dry-Rock test site Soultz, France." Proceeding, 27th Workshop on Geothermal Reservoir Engineering. Stanford, California, January 28-30, 2002, p.95-100.

Ein Überblick über "Enhanced Geothermal Systems" (erweiterte geothermale Systeme) / Un aperçu des 'Enhanced Geothermal Systems' ('systèmes géothermiques stimulés')

Evans, K.F. and , Valley B.

ETH-Zurich, Engineering Geology, CH-8092 Zürich

Published in GEOforum ACTUEL, 4, 17-44, Akademie der Naturwissenschaften Schweiz.

Ein Überblick über «Enhanced Geothermal Systems» (Erweiterte Geothermale Systeme)

Un aperçu des systèmes géothermiques stimulés (Enhanced Geothermal Systems)

KEITH F. EVANS & BENOÎT VALLEY

«Enhanced Geothermal Systems» (EGS, Erweiterte Geothermale Systeme) versuchen, die grossen Vorkommen von Wärmeenergie zu erschliessen, welche unter den Kontinenten in Gesteinen geringer Porosität und in technisch bohrbaren Tiefen liegen. Das EGS-Konzept ist in Abbildung 1 dargestellt. Zwei oder mehr Bohrlöcher werden in Zonen abgeteuft, in denen die Gesteinstemperatur wirtschaftlich interessant ist. Diese Bohrungen bilden ein Zirkulationssystem für Fluide. Beim Durchfliessen des heissen Gesteins zwischen den beiden Bohrungen erwärmt sich das Fluid und die gespeicherte Wärmeenergie wird an der Oberfläche genutzt. Das Problem dieser einfachen Methode liegt in der meist zu geringen Permeabilität von tiefliegenden Kristallingesteinen. Um den erforderlichen Fluss zwischen den beiden Bohrungen zu generieren, muss deshalb die Gesteinspermeabilität erhöht werden.

Les «Enhanced Geothermal Systems» (EGS) visent à exploiter les vastes réserves de chaleur contenues dans les roches de faible porosité que l'on trouve dans d'importantes portions des masses continentales à une profondeur atteignable par des forages. Le concept des EGS est illustré en figure 1. La chaleur est extraite et amenée en surface grâce à une boucle de circulation d'eau établie entre deux ou plusieurs puits atteignant des roches dont la température est d'intérêt commercial. L'eau injectée s'échauffe en percolant dans les roches chaudes qu'elle traverse entre les forages, puis est remontée en surface. Le problème de ce simple schéma d'exploitation est que la perméabilité du socle cristallin est généralement trop faible pour laisser l'eau s'écouler au débit requis entre les deux puits. Cette perméabilité doit donc être stimulée. La création de cette connexion entre les puits constitue le principal

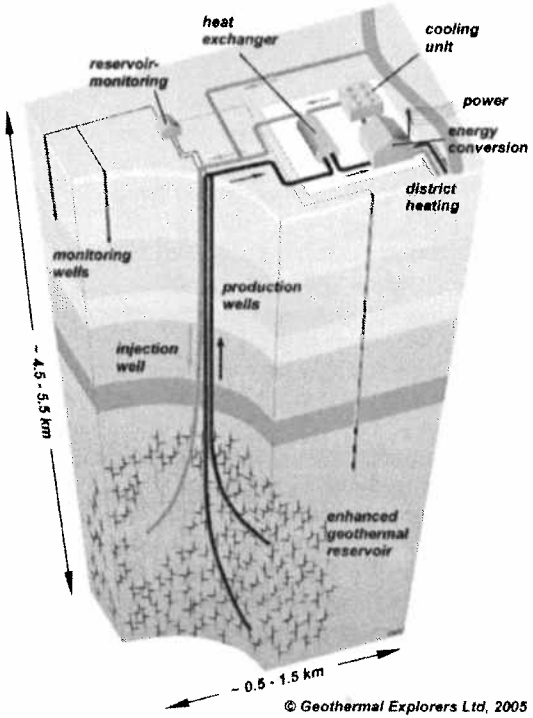

Abb. 1: Illustration eines EGS mit einer Injektionsbohrung und zwei Produktionsbohrungen. Die Überwachungsbohrungen sind für die mikroseismischen Sensoren. Figur mit freundlicher Genehmigung von M. Häring von Geothermal Explorers Ltd.

Fig. 1: Illustration d'un EGS incluant un puits d'injection et deux puits de production. Les forages d'observation (monitoring wells) sont équipés de séismographes. Figure mise à disposition par M. Häring, Geothermal Explorers Ltd.

Das künstliche Erzeugen einer permeablen Verbindung zwischen den Bohrungen stellt für die Entwicklung der EGS die grösste Herausforderung dar und ist das Hauptmerkmal, das sie von den natürlichen geothermalen Systemen unterscheidet.

Das EGS-Konzept wurde 1970 in den nationalen Laboratorien von Los Alamos in den USA entwickelt und wurde «Hot Dry Rock Systems» genannt. Ursprünglich wollte man die Hydrofrac-Technologie verwenden, welche durch die Erdöl- und Gas-Industrie entwickelt worden war, um Bohrlöcher mit künstlich erzeugten Kluftzonen zu verbinden. Hydro-Klüfte sind frische Dilatationsklüfte, welche durch das Injizieren grosser Mengen Fluid unter hohen Drucken entstanden sind. Erfahrungen aus den unzähligen Pilot-Projekten, welche bis dato durchgeführt wurden (siehe Tabelle 1), haben gezeigt, dass massive Fluid-Injektionen, auch Stimulations-Injektionen genannt, tatsächlich zur Erhöhung der Permeabilität des Umgebungsgesteins führen können. In den meisten Fällen jedoch beruht die bessere Durchlässigkeit nicht auf neuen Hydro-Klüften, denn diese scheinen sich in geklüfteten kristallinen Gesteinen nicht weit auszubreiten. Die bessere Durchlässigkeit ist eher eine Folge von Scherbrüchen in natürlichen Klüften, die während den Injektionen wegen den gesteigerten Drücken entstanden. Scherbewegung erhöht die Permeabilität, weil die rauhen Kluftflächen während der Scherung zu Dilatation neigen. Die Prozesse, welche zu einer Erhöhung der Permeabilität führen, sind im Detail sehr komplex und werden durch die Interaktion des generellen Spannungszustandes mit den natürlichen Klüften und Brüchen des

défi lors du développement d'EGS. C'est aussi ce qui distingue les EGS des systèmes géothermaux naturels.

Le premier concept d'EGS fut développé en 1970 à Los Alamos, aux Etats-Unis. Il était alors appelé «Hot Dry Rock Systems» (système des «roches chaudes et sèches»). L'idée première était d'utiliser les technologies d'hydrofracturation développées par l'industrie du pétrole et du gaz afin d'établir une connexion entre les forages par une série de fractures artificielles. Ces hydrofractures sont créées en tension (mode I) par l'injection de grandes quantités de fluide à pression et débit élevés. Les expériences menées jusqu'à ce jour dans le cadre de nombreux projets pilotes (voir table 1) ont montré que ces injections massives de fluides, également appelées stimulations, permettent effectivement d'améliorer la perméabilité des roches ciblées. Par contre, dans la plupart des cas, si ce n'est dans tous, l'augmentation de la perméabilité s'avère être due au cisaillement de fractures naturelles préexistantes et non à la création de nouvelles hydrofractures, ces dernières se propageant trop peu profondément dans le massif. L'accroissement de la pression interstitielle lors de l'injection provoque le cisaillement des fractures naturelles. L'augmentation de la perméabilité est alors due à ces mouvements cisaillants subis par les faces rugueuses des fractures naturelles impliquant une dilatation de ces dernières. Dans le détail, les mécanismes qui produisent cette augmentation de perméabilité sont très complexes. Ils résultent de l'interaction du champ de contrainte ambiant avec les fractures et les failles présentes dans le massif rocheux. Une source d'information permettant d'aborder ces mécanismes

Fenton Hill, New Mexico, USA	1972 – 1996	2.8 km / 3.6 km / 4.2 km	320°C
Rosemanowes, Cornwall UK	1978 – 1991	2.0 km / 2.2 km	85°C
Falkenberg, Bavaria, Germany	*1978 – 1985*	*0.25 km*	*13°C*
Higashi-Hachimantai, Japan	*1983 – 1988*	*0.4 km*	*60°C*
Le Mayet de Montagne, France	*1984 – 1994*	*~0.8 km*	*33°C*
Fjallbacka, Sweden	*1984 – 1989*	*0.5 km*	*15°C*
Hijiori, Japan	1985 – 2002	1.8 km/ 2.2 km	270°C
Soultz, France	1987 – present	3.3 km/ 5.0 km	200°C
Ogachi, Japan	1989 – 2001	0.7 km/ 1.0 km	250°C
Cooper Basin, Australia	2003 – present	4.2 km	240°C

Tab. 1: Liste der EGS-Projekte, die bis dato durchgeführt worden sind. Die Dauer der Aktivität am Teststandort und die Tiefen der entwickelten Reservoire und die Temperatur des tiefsten Reservoirs sind angegeben. Die Projekte in kursiv sind kleinskalige Forschungssysteme, um die massgeblichen Prozesse im Detail zu untersuchen.

Tab. 1: Liste des projets EGS menés jusqu'à ce jour. Sont indiquées, la période d'activité, les profondeurs des réservoirs développés ainsi que la température du réservoir le plus profond. Les projets en italiques sont des études détaillées menées à petite échelle et à relativement faible profondeur.

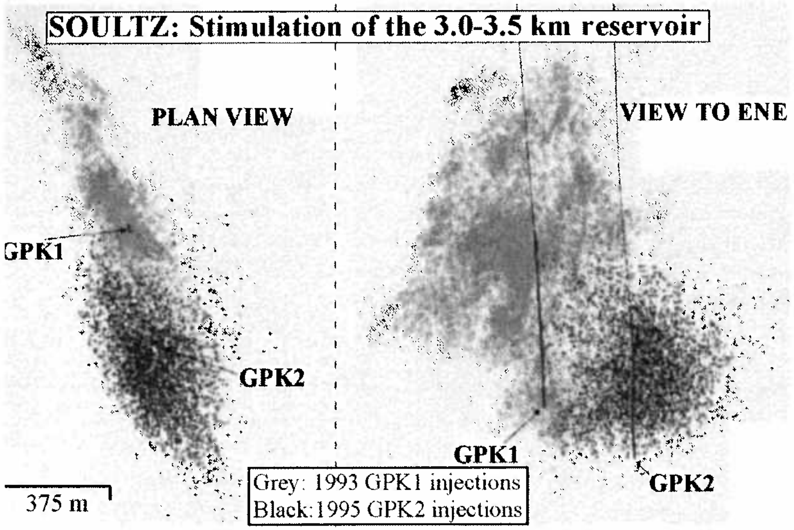

Abb. 2: Aufsicht und Seitenansicht von mikroseismischen Wolken, die während der Stimulation des 3.0 – 3.5 km Soultz Reservoirs generiert wurden. Bei unterschiedlichen Durchläufen wurde in jede Bohrung ca. 40 m^3 Wasser injiziert. Die offenen Intervalle der Bohrungen sind fett markiert.

Fig. 2: projection sur un plan horizontal et vertical des nuages microsismiques produits lors des stimulations du réservoir à 3.0 – 3.5 km de profondeur à Soultz. Approximativement 40 m^3 d'eau ont été injectés dans chaque puits lors des différentes stimulations. Les sections de forage non tubées sont représentées par un trait épais.

Umgebungsgesteins gesteuert. Glücklicherweise kann die Überwachung der mikroseismischen Aktivität, welche den Schermechanismus begleitet, einige Hinweise über die Mechanismen geben, die während solchen Injektionen auftreten. Durch die Lokalisierung der einzelnen Events kann eine 3D-Karte erstellt werden, welche die Entspannung des Gesteins und die begleitende Porositäts- und Permeabilitäts-Bildung darstellt. Ein Beispiel von überlagernden mikroseismischen Wolken, welche während Stimulations-Injektionen in das 3.0 bis 3.5 Kilometer tiefe Soultz Reservoir erzeugt wurden, ist in Abbildung 2 dargestellt. Die Kenntnis über die räumliche Verteilung der Permeabilitäts-Erhöhung ist essentiell für die Platzierung weiterer Bohrungen.

Wirtschaftlichkeit

Bis vor kurzem wurden EGS als elektrizitätsgewinnende Systeme betrachtet, die im Vergleich zu anderen Energiequellen auf dem Strommarkt nicht wettbewerbsfähig sind. Um Elektrizität effizient zu erzeugen, werden Wassertemperaturen von über 180°C benötigt.

complexes est l'étude de l'activité microsismique qui accompagne ces ruptures en cisaillement. Les zones du massif éprouvant un relâchement des contraintes et donc une augmentation de la porosité et de la perméabilité peuvent être mises en évidence par la détermination de la position du foyer de chaque événement microsismique. La figure 2 présente l'ensemble des événements microsismiques, aussi appelé nuage microsismique, mesurés à Soultz lors des stimulations d'un réservoir situé de 3 à 3.5 km de profondeur. Cette connaissance de la distribution spatiale du développement de la perméabilité est essentielle pour positionner les autres forages du système.

Considérations économiques

Jusqu'à récemment, les EGS étaient uniquement prévus pour la production d'électricité. Ils n'étaient, néanmoins, pas compétitifs par rapport aux autres sources énergétiques fournissant le marché de l'électricité. Pour produire du courant électrique avec un rendement acceptable, l'eau extraite doit avoir une température d'au moins

In den meisten Regionen Europas bedeutet dies, dass tiefe, teure Bohrlöcher erstellt werden müssten. Die steigenden Ölpreise, der Wille, gemäss Kyoto-Protokoll die CO_2-Emissionen zu reduzieren und die Anstrengungen einiger Länder, Alternativen für die Kernenergie zu finden, haben jedoch das Interesse an EGS wiederbelebt. Das generell akzeptierte Ziel für ein Bohrpaar ist die Produktionsrate von fünfzig Litern pro Sekunde bei einer Temperatur von 180°C. Für den Fall, dass das Zirkulationswasser bei einer Temperatur von 60° wieder in den Kreislauf gepumpt wird, ergibt sich eine thermische Leistung von fünfundzwanzig Megawatt, was bei der Umwandlung in elektrische Energie aber nur rund vier Megawatt einbringt. Die direkte Nutzung der Wärmeenergie, zum Beispiel zum Heizen, oder zumindest die Nutzung der Abwärme bei der Stromerzeugung (Wärme-Koppelung), bringt also grosse Vorteile. Die direkte Verwendung der Energie zum Heizen erfordert nicht so hohe Temperaturen und folglich weniger tiefe Bohrlöcher. Das Abteufen der Bohrungen bildet die kostenintensivste Einzelposition der EGS. Ein fünf Kilometer tiefes Bohrloch inklusive Ausbau kostet ca. 9 Millionen SFr.

Erfahrungen mit EGS-Forschungs-Prototypen

In Tabelle 1 sind die Forschungsanlagen aufgelistet, welche seit der Einführung des EGS-Konzepts vor 35 Jahren in Gebieten unterschiedlichster Geologie errichtet wurden. Viele dieser Versuchsanlagen erschliessen eher untiefe Gesteinsformationen, um die Prozesse zu untersuchen, die zur Reservoir-Bildung führen (kursiv in Tabelle 1). Sechs Anlagen jedoch sind grossskalige EGS-Prototypen, bei denen in verschie-

180°C. Pour la plupart des régions d'Europe, ceci nécessite des forages profonds et coûteux. Mais l'augmentation du prix du pétrole, les nouvelles contraintes sur les émissions de CO_2 établies par les accords de Kyoto, et, pour certains pays, la volonté de trouver des alternatives à l'énergie nucléaire, ont ravivé l'intérêt porté aux EGS. Actuellement, la production de 50 l/s d'eau à 180°C à l'aide de deux puits constitue une performance considérée comme acceptable. Dans ce cas, avec une réinjection de l'eau à 60°C, 25 MW thermiques sont alors produits. S'ils sont convertis en électricité, la production de 4 MW électriques est possible. Il est ainsi hautement favorable d'utiliser directement une partie de la chaleur produite, ou au moins la chaleur résiduelle après la production d'électricité, pour du chauffage par exemple (cogénération). Si uniquement une production d'énergie de chauffage est prévue, la température nécessaire est plus basse et donc les forages peuvent être moins profonds. Les frais de forage sont l'élément le plus coûteux d'un EGS. Le forage et l'équipement d'un puits de 5 km coûtent approximativement 9 millions de CHF.

Expérience acquise grâce aux projets pilotes

Lors de ces 35 dernières années, depuis que le concept d'EGS a été proposé, différents prototypes ont été développés sous diverses conditions géologiques. Ils sont listés dans le tableau 1, accompagnés de certaines de leurs caractéristiques. Une partie d'entre eux, mentionnée en italique, a été développée à faible profondeur dans le but d'étudier en détail les mécanismes de développement des réservoirs. Six autres sont par contre des implémentations «gran-

denen Tiefen Reservoire generiert wurden. Die Experimente haben viel zu unserem Wissen über die verschiedenen hydromechanischen Bedingungen und Prozesse beigetragen, welche in der oberen kontinentalen Kruste stattfinden. Nicht nur Klüfte sind allgegenwärtig, sondern auch hydraulisch verbundene Kluftzonen mit grossen Mengen an Fluid können vorhanden sein. Dies zeigt das Beispiel von Soultz – eine Entdeckung, die zum Begriff «Hot Wet Rock Geothermal Systems» führte. Die Scherkräfte im Umgebungsgestein sind grundsätzlich hoch und stützen die These, dass die Kruste der Erde «critically stressed» ist, d.h. Kräften nahe des mechanischen Versagens ausgesetzt ist. Scherung und Mikroseismizität als Folge von Fluid-Injektionen sind daher eher die Regel als die Ausnahme.

Der Erfolg der Versuche, eine befriedigende Verbindung zwischen den Bohrlöchern der Prototypen-EGS zu schaffen, kann durch Zirkulationstests beurteilt werden, welche nach der Stimulierung durchgeführt werden. Die folgenden Charakterisika sollen dabei angestrebt werden:

1. Der Fliesswiderstand zwischen den Bohrungen sollte so klein wie möglich sein, um den Energieverlust beim Pumpen zu minimieren. Ein Fliesswiderstand von 0.1 MPa/l/s ist allgemein als Wunschziel akzeptiert (eine Druckdifferenz von 5 MPa zwischen zwei Bohrungen würde beispielsweise einen Fluss von 50 l/s generieren).
2. Es sollte dabei ein möglichst grosses Gesteinsvolumen (grosse Benetzungsfläche) durchflossen werden, damit das System möglichst langlebig ist.

deur nature». Pour la plupart de ces projets, plusieurs réservoirs ont été développés à différentes profondeurs. Les expériences menées ont largement contribué au développement de nos connaissances des conditions et processus hydromécaniques prévalents dans la partie supérieure de la croûte continentale. Non seulement des fractures y sont omniprésentes, mais elles peuvent être largement connectées hydrauliquement, formant des zones pouvant contenir d'importants volumes de fluides. Tel est le cas au site EGS de Soultz. Cette découverte a engendré une évolution de la terminologie; ces systèmes ont alors été appelés «Hot Wet Rock Geothermal Systems» («systèmes géothermiques chauds et humides»). Le niveau des contraintes cisaillantes observé est toujours élevé. Ceci confirme l'hypothèse d'une croûte terrestre dans un état critique des contraintes, c'est-à-dire proche de la rupture. Ainsi les ruptures en cisaillement et la production de microséismicité lors de l'injection de fluide s'avèrent être les réactions normales du socle et non l'exception.

Lors du développement de réservoir, l'efficacité des stimulations menées et la qualité de la connexion créée entre les forages peuvent être évaluées par des essais de circulation. Les caractéristiques suivantes sont désirées :

1. La résistance à la circulation, appelée impédance hydraulique, doit être aussi faible que possible afin de minimiser l'énergie perdue pour le pompage. Une impédance de 0.1 MPa/l/s est généralement considérée comme acceptable. Une différence de pression de 5 MPa entre les deux puits permet alors de maintenir une circulation à un débit de 50 l/s.
2. Le fluide circulé doit percoler au travers d'une surface aussi grande que possible, permettant ainsi d'extraire la chaleur d'un grand volume de roche. Ceci garantira la longévité du système.
3. La perte de fluide lors de la circulation doit être maintenue à un niveau suffisamment bas, imposé par les caractéristiques spécifiques de chaque site.

3. Fluidverluste in das Umgebungsgestein sollten innerhalb der Grenzen liegen, welche durch den Standort vorgegeben sind.

Wie diverse Erfahrungen gezeigt haben, ist es oftmals schwierig, den Fliesswiderstand zwischen den Bohrungen auf das Wunschziel von 0.1 MPa/l/s zu reduzieren. Das Problem kann teilweise durch Reduktion der Distanz zwischen den Bohrungen gemildert werden. Bei Systemen mit Bohrungen, die näher als zweihundert Meter von einander abgeteuft wurden, kann es jedoch zu einem frühen Abfallen der Produktionstemperatur kommen, weil die Benetzungsfläche entlang des Fliessweges zwischen den Bohrungen zu klein ist, was das schnelle Vordringen der Kühlungsfront anzeigt. Im allgemeinen gibt es einen Kompromiss zwischen dem Design für einen geringen Fliesswiderstand (Bohrungen nahe beieinander) und der Langlebigkeit der Anlage (Bohrungen weit auseinander). 1997 wurde ein Meilenstein in der Entwicklung der EGS-Technologie erreicht, als mit dem 3.0 bis 3.5 km tiefen Soultz-System während vier Monaten bei 25 l/s ohne Anzeichen einer Abkühlung zirkuliert werden konnte. Die Distanz zwischen den Bohrungen betrug 450 m, und dennoch konnte der Fliesswiderstand mit Hilfe hydraulischer Stimulation der einzelnen Bohrungen erfolgreich auf das erklärte Ziel hinunter reduziert werden (Abbildung 2). Die Fluidverluste waren gleich null. Dieser Erfolg wurde möglicherweise durch wichtige, über 100 m lange sub-vertikale Kluftzonen im kristallinen Grundgebirge unterstützt. Das Gros der mikroseismischen Aktivität und implizit auch der Permeabilitätserhöhung trat innerhalb dieser Strukturen auf. Es ist wahr-

Les expériences acquises ont montré qu'il est souvent difficile d'obtenir le niveau d'impédance hydraulique de 0.1 MPa/l/s désiré. Une solution à ce problème serait de réduire la distance entre les puits. Mais les systèmes avec des puits séparés d'une distance inférieure à 200 m présentent une diminution prématurée de la température de production. Ceci reflète la progression rapide du front de refroidissement le long du chemin de circulation, due à une surface d'échange trop faible. Il s'agit donc de trouver une distance optimale entre les puits pour obtenir un compromis entre impédance (puits rapprochés) et longévité (puits éloignés). Malgré ces difficultés, un résultat remarquable a été obtenu en 1997 au site de Soultz, lorsqu'une circulation continue à 25 l/s a été maintenue à une profondeur de 3 à 3.5 km pendant quatre mois sans montrer aucun signe de refroidissement. La distance entre les puits était de 450 m et l'impédance a été réduite au niveau requis par la stimulation hydraulique des deux forages (figure 2). Aucune perte de fluide n'a été constatée. Ce succès est en partie dû au recoupement par les forages de zones de fractures subverticales longues de plus de 100m. La plupart de la microséismicité enregistrée, et par conséquent du développement

scheinlich, dass die Fliesswege, welche die Bohrungen verbinden, grösstenteils darin liegen. Dies illustriert, wie wichtig es ist, bei der Entwicklung der EGS die lokalen geologischen Verhältnisse zu berücksichtigen.

Ausblick

Der Erfolg mit dem untiefen Reservoir von Soultz lässt hoffen, dass unter gewissen geologischen Bedingungen die erklärten Leistungsziele der EGS bezüglich Elektrizitätsgewinnung erreicht werden können. Die bis heute gesammelten Erfahrungen zeigen jedoch, dass es nicht einfach ist, die erforderliche Durchlässigkeit zwischen den Bohrungen zu generieren. Unter Umständen kann der Erfolg gering sein, wenn auf Anlagen mit einer so hohen Leistung gezielt wird. Eine Herausforderung für die Zukunft wird die Entwicklung von Methoden sein, potentielle Reservoire realistisch und kostengünstig zu bewerten. Die Möglichkeit der EGS, signifikant zur Energienutzung beizutragen, wird deutlich erhöht, wenn sie ganz oder teilweise zum Heizen eingesetzt werden. Kommerziell genutzte EGS sind gegenwärtig im Bau bei Soultz (Frankreich), am Cooper Basin (Australien), Coso (USA), Basel (Schweiz) und diversen Standorten in Deutschland. Der Beginn der Arbeiten für das 5 km tiefe Bohrloch beim Projekt in Basel ist für den Frühling 2006 geplant.

Keith F. Evans & Benoît Valley
Ingenieurgeologie – Geologisches Institut
Eidgenössische Technische Hochschule
ETH Hönggerberg, 8093 Zürich

de la perméabilité, a pris place dans ces structures. Il est donc fortement probable que ces zones constituent la majorité des connexions empruntées par les fluides entre les forages. Ceci souligne la nécessité de «travailler avec la roche», c'est-à-dire de considérer les conditions du massif et sa pré-structuration lors du développement d'EGS.

Perspectives

Le succès obtenu à Soultz lors du développement d'un réservoir à 3.5 km permet d'entrevoir avec optimisme la création de systèmes aux performances adaptées à la production d'électricité lorsque les conditions géologiques sont favorables. Les expériences acquises montrent néanmoins que le développement du lien requis entre deux forages est une tâche ardue. Le taux de succès du processus d'augmentation des performances hydrauliques du système peut être faible dans certaines situations. Un défi pour l'avenir consiste alors à développer les méthodes permettant d'évaluer le potentiel d'un réservoir prospecté et ceci en maintenant les coûts à un niveau compétitif. Les EGS peuvent apporter d'autant mieux leur contribution aux besoins énergétiques de la société s'ils sont utilisés parallèlement ou complètement dans le cadre de réseaux de chauffage à distance. Des EGS commerciaux sont actuellement développés à Soultz (France), dans le Copper Basin (Australie), à Coso (USA), à Bâle (Suisse) et dans différents sites en Allemagne. A Bâle, un premier forage profond atteignant 5 km est prévu au printemps 2006.

Stress state at Soultz to 5km depth from wellbore failure and hydraulic observations

Benoît Valley* & Keith Evans*
**Engineering geology, ETH Zürich, Switzerland*

Presented at the Soultz Scientific Meeting at Soultz-sous-Forêts on 15-16 June 2006.

EC Contract SES6-CT-2003-502706

PARTICIPANT ORGANIZATION NAME: ETH Zürich

Synthetic 2nd year report

Related with Work Package: FP6-WP5

STRESS STATE AT SOULTZ TO 5KM DEPTH FROM WELLBORE FAILURE AND HYDRAULIC OBSERVATIONS.

Benoît Valley* & Keith F. Evans*
**Engineering Geology, ETH Zürich*
e-mail: valley@erdw.ethz.ch

ABSTRACT

Observations of breakouts and drilling-induced tension fractures (DITFs) in GPK3 and 4 have been combined with the analysis of pressure data from stimulation tests in all wells to obtained an improved description of the state of stress in the Soultz granite to 5 km depth. The orientation of the maximum horizontal stress, SHmax, is found to be N169°E±14°, in accord with previous results from the 3.5 km reservoir. Of the three existing characterisations of stress magnitudes based on data for the 3.5 km reservoir, the one proposed by Cornet and Bérard (2003) gives the best agreement with available data to 5 km. The wellbore failure observations allow refinement of this characterisation with regard to the magnitude of SHmax.
The proposed new characterisation for the Soultz site is given by:

SHmax orientation is N169°E±14°
Sv = 0.3 + 25.60 z[km]
Shmin=-1.11537+13.77z[km]
- 1.17 +22.95z[km] ≤ SHmax < -1.365 + 26.775z[km]

This characterisation more consistent with the collective data than the one in common use at Soultz which is usually (mistakenly) accredited to Klee and Rummel (1993).

INTRODUCTION

Knowledge of the state of stress is very important for the development of Enhanced Geothermal Systems (EGSs), not least because it is a primary factor influencing the reservoir response to the massive stimulation injections. Knowledge of the stress state in the 5 km deep reservoir at Soultz is largely based upon extrapolation of the characterisation defined for the shallower reservoir to 3.5 km depth. Although this has been extensively studied, some questions remain, principally with regard to the magnitude of the maximum horizontal principal stress, SHmax. This paper presents some new results that directly constrain the stress state in the deep reservoir, including the magnitude of SHmax. The constraints arise principally from analysis of breakouts and drilling-induced tension fractures (DITFs) on UBI images from two of the three wells that penetrate the deep reservoir. It is well established that these features constitute one of the best indicators of the orientation of the principal horizontal stresses. However, since they represent stress-induced failure of the wellbore, a careful analysis of the conditions of their formation allows constraints to be placed upon stress magnitudes. To obtain unique values for the two principal horizontal stress magnitudes requires that one be independently specified. Thus we analyse downhole pressure data from stimulation injections to estimate the magnitude of Shmin, and use this in the analysis of wellbore failure to constrain the magnitude of SHmax. The new characterisation of the stress state at Soultz proposed here is in-accord with the conclusions of the Seismo-hydraulics Working Group meeting held in January 2006 which sought to determine the current state of knowledge of the state of stress in the deep reservoir at Soultz.

BACKGROUND

Previous study on state of stress at Soultz

Constraints on stress orientation to 3.5 km:
Sv orientation: It is commonly assumed at Soultz and elsewhere that one principal stress is vertical. The presence of inclined DITFs along some vertical borehole section provides a fairly clear indication that this is not always the case, at least locally. Indeed, implied perturbations to vertical stress orientation are sometimes associated with major natural feature like faults. However, the balance of evidence shows that when averaged over scales greater than 100 m, one principal stress is vertical. This justifies the assumption that the magnitude of Sv is equal to the overburden.
SHmax orientation: The orientation of the horizontal principal stresses have been studied by several authors, mostly using breakouts and DITFs seen on the logs holes in the shallow reservoir down to about 3.5 km. Tenzer et al. (1992) identified axial tension fractures in ultrasonic televiewer records from GPK1 in the depth range 1450-2000 m and concluded that SHmax was oriented N169° ± 11°E. Nagel (1994) picked axial DITFs on an FMI logs run in GPK1 between 2000 and 3590 m and obtained a mean orientation of SHmax of 181°±22°. Brudy and Zoback (1999) extended Nagel's analysis to include en-echelon DITFs and found they indicated the same orientation as the axial DITFs. Bérard & Cornet (2003), identified compression-induced breakouts in GPK1 in the depth range 3050-3450 m that implied an SHmax orientation of N5°E±7°. Genter and Tenzer (1995) identified vertical DITFs in GPK2 in the depth range 1420 - 3880 m and found they indicated an orientation for SHmax of N175E±17°. These studies collectively provide an extraordinarily well-defined indication that the orientation of SHmax in the basement above 3800 m is essentially N-S. This is at odds with the SHmax orientation estimates obtained from inversion of focal mechanisms (Helm, 1996; Plenefisch and Bonjer, 1997; Cuenot et al., 2005) which suggest a more NW-SE orientation. Cornet and Bérard (2003) propose that the discrepancy reflects a systematic error in the inversion estimates that arises from the tendency for microseismic events to occur in place where stresses are locally perturbed.
Constraints on stress magnitudes to 3.5 km:
The magnitudes of principal stresses within rock masses are usually found to be reasonably represented by linear trends with depth. Estimates of Shmin at four depths between 2 and 3.5 km suggest that this is approximately the case in the Soultz shallow reservoir, at least for Shmin, although the details of the fit to the data are important. Three different

linear characterisations of stress magnitude have been proposed for the Soultz site based on observations in the shallow reservoir to 3.5 km. These are given in Table 1. The first characterisation, referred to here as the "standard stress characterisation", is the one most often reported in the literature (e.g. Baria et al., 1995), and is due to Heinemann (1994), although it is almost always mistakenly ascribed to Klee and Rummel (1993). The second is proposed by Cornet and Bérard (2003) and the third by Evans (2005). These will be described in more detail later. Almost all recent studies of the deeper reservoir assume that the standard stress characterisation can be extrapolated to 5 km depth. This characterisation predicts a switch in maximum stress orientation from vertical to horizontal at 3 km depth. Some support for such a transition comes from the focal mechanisms of seismic events that tend to become increasingly strike-slip with increasing depth, although rigorous inversion indicates that it occurs nearer 4.5 km (Cuenot, et al., 2005). The inversion results, however , must be treated with some caution as the shape factors obtained are inconsistent with the approximate equality of SHmax and Sv indicated by the transition. Furthermore, as described later, there are grounds to doubt the soundness of the SHmax estimates of the standard stress characterisation. Thus, it is important to constrain the stress state in the deeper reservoir directly through observation.

Sv magnitude: The magnitude of the vertical stress is taken as the integrated overburden as estimated from density logs or density measurements on core samples. Most published studies, including all three stress characterisations in Table 1, implicitly assume a density for the granite section of 2.6 gm/cc, which corresponds to the average density from a GPK1 log run between 1885 and 3564 m. Klee and Rummel (1999) propose an Sv profile based on a density of 2.66 gm/cc from core tests. The mean density from logs is slightly lower than this because it includes the effects

Table 1: Summary of stress magnitude estimates.

	Standard estimates	Cornet & Bérard (2003)	Evans (2005)
Sv [MPa]	-1.3+25.5 z[km]	-2.0655+25.5 z[km]	-1.3+25.5 z[km]
Shmin [MPa]	-5.9+14.9 z[km]	-1.11537+13.77 z[km] =(0.54 ± 0.02) Sv	-8.1+16.08 z[km]
SHmax [MPa]	-25.3 + 33.6 z[km]	-1.962225+24.225 z[km] =(0.95 ± 0.05) Sv	-1.3+25.5 z[km] (=1.0 Sv)
Pp [MPa]	0.9 + 9.8 z[km]		

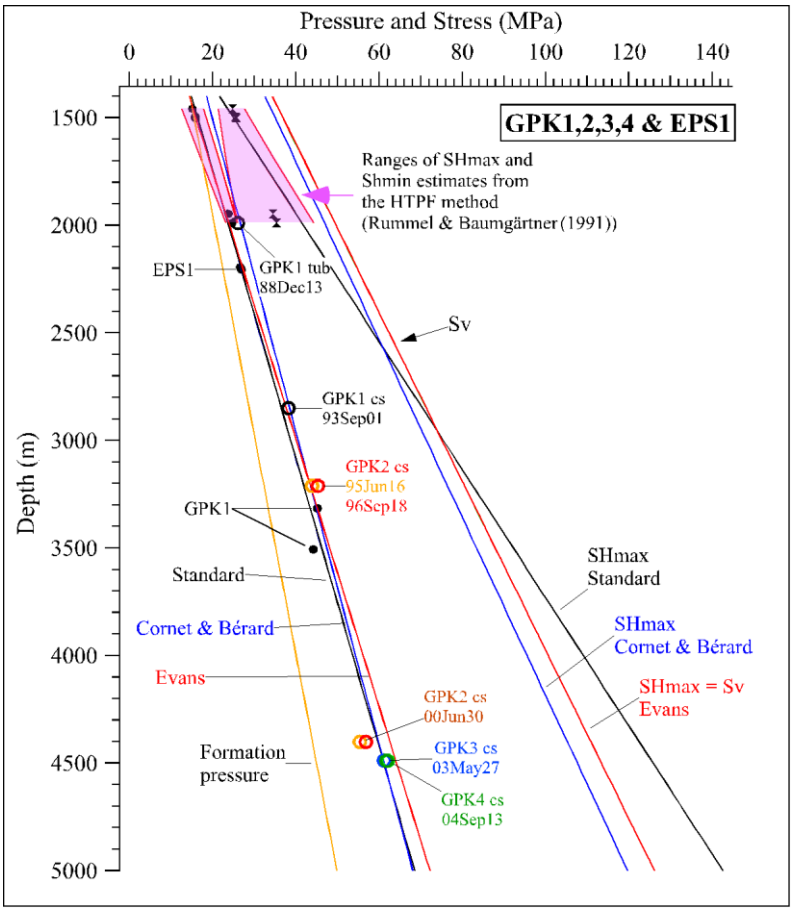

Figure 1: Stress magnitude datapoints from hydraulic tests, and linear profiles of the three stress characterisations proposed for the 3.5 km reservoir (Table 1). These have been extrapolated to 5 km. The Shmin datapoints with the subscript 'cs' represent the maximum pressures recorded at the casing shoe during the indicated stimulation injections and are plotted at the depth of the casing shoe. A listing of these data for the tests in the 5 km reservoir is given in Table 3.

of relatively low densities in altered zones. It is more representative of the net rock mass density and is thus preferred for Sv estimation. Comparison of the density of a core sample taken in GPK1 at 3524 m with the values registered on the density log in the vicinity showed good agreement, the log values being at most 0.015 gm/cc too low. Thus there are no grounds to doubt the validity of the density log. Unfortunately, there are no density logs below 3.5 km. Thus, it is assumed that the same average rock mass density prevails to 5 km as in the granite above 3.5 km. Another source of uncertainty in the estimates of Sv stems from the absence of density measurements in the uppermost 898 m of the sedimentary cover. Almost all published studies use an average density for the 1377 m thick sedimentary section of either 2.45 gm/cc after Rummel and Baumgärtner (1991), or 2.50 gm/cc after Heinemann-Glutsch (1994). A density log run over the lower part of the sediments below 898 m yielded a mean density and standard deviation of 2.54±0.11 gm/cc. However, the density of the overlying section is likely to be greater than this because of the prevalence of clay. To clarify the situation, a synthetic density profile was developed with judicious error margins based upon the probable mineralogy of the beds. The resulting mean density and standard deviation for the sedimentary section to 1377 m was 2.63±0.14 gm/cc. The implied value of Sv at the top of the granite (i.e. 1377 mTVD) is then equal to 35.5±1.9 MPa. This compares with 33.8 MPa for the 'Standard' and 'Evans' stress characterisations, and 33.0 for Cornet & Bérard's. Thus, all characterisations probably underestimate Sv by 2-3 MPa. In the analysis presented later we use the 'Standard' estimate, although this will be revised in future analyses.

Shmin magnitude: The magnitude of Shmin is constrained by five small-volume hydraulic tests on pre-existing fractures in the depth range 1450-1990 m (Rummel and Baumgärtner, 1991), and a further four tests on induced hydrofractures in the depth range 2190-3510 m (Klee and Rummel, 1993). These data were fitted by Heinemann-Glutsch (1994) to produce the Shmin profile of the standard stress state (Figure 1). The Evans (2005) profile is a best fit to the same data but without the lowermost point at 3508 m, which was almost certainly conducted in a zone of perturbed stress. Cornet & Bérard, (2003) discounted all small volume tests and claimed that a better Shmin estimate was given by the maximum pressures of large-volume, relatively high-rate injections where the jacking pressure is reached. In such cases they proposed that the maximum pressure at the top of the injection interval equals Shmin at that depth, an assumption that ignores near-wellbore pressure drops and poro-elastic perturbations of the ambient stress (Evans, 2005). They based their Shmin profile on two injection tests at 2000 and 2850 m, and state the uncertainty as ±3.5 MPa.

SHmax magnitude: The profile of SHmax in the standard stress characterisation is derived from the hydrofracture test data using the 're-opening method' (Klee and Rummel, 1993). Several authors have shown that this method yields invalid SHmax estimates (Ito, et al., 1999; Rutqvist, et al., 2000), particularly in deep holes, and hence both Cornet & Bérard (2003) and Evans (2005) discounted them. The best constraint on SHmax stems from the observation that focal mechanisms show a mix of normal and strike slip faulting, suggesting that SHmax is not greatly different from Sv. Both Cornet & Bérard (2003) and Evans (2005) adopt this equality as a working hypothesis. An extreme lower bound on SHmax is that it must be greater than Shmin by definition. An upper bound on SHmax is obtained by assuming that the strength of fractured rock masses is limited by the strength of optimally oriented fractures (Brace and Kohlstedt, 1980). The worldwide crustal stress dataset supports this view and indicates an upper limit on rock mass strength to be given by a Coulomb friction criterion with a friction coefficient of 1.0 and zero cohesion. Evans (2005) showed that this constraint imposes an upper limit on SHmax of 1.21Sv. The pore pressure estimate used in this calculation is based on brine density profiles given in Evans, et al. (1992).

Breakouts and drilling-induced tension fractures analysis

Breakouts or drilling-induced tension fractures occur when the local value of tangent compression or tension respectively at the borehole wall exceeds the rock strength. Breakouts are typically manifest as pairs of diametrically-opposite spall zones that extend along the borehole axis. In the simple case of a vertical borehole penetrating a rock mass in which one principal stress is vertical, breakouts, if they occur, indicate the orientation of the Shmin (Bell & Gough, 1979).

Drilling induced tension fractures (DITFs) form where cooling of the borehole wall by circulation of mud during drilling results in a net tangent stress distribution about the hole that is sufficiently tensile at some point to produce failure. The net tangent stress is the sum of a tensile cooling component, which is axially-symmetric, and the natural wellbore stress concentration arising from the 'far-field' stresses, which are not necessarily axially-symmetric and may be everywhere compressive. In the case of a vertical borehole penetrating a medium in which one principal stress is also vertical, the least compressive value of the circumferential stress variation about the borehole due to the far field stresses occurs in the direction of SHmax. Thus, it is in this direction that the greatest tension develops and a pair of diametrically-opposite DITFs form. Since the borehole axis is aligned with a principal stress, they will be axial, and denoted as A-DITFs. However, in the case where the borehole axis is not aligned with a principal axis, the criterion for tensile failure might still be met but then DITFs will tend to form as a stack of en-echelon, induced fractures, denoted E-DITFs. The relationship between the induced fracture geometry and the in-situ stress orientations and magnitudes in this case is not as simple as in the aligned case.

The theory for calculating the stress state acting around a borehole of arbitrary orientation with respect to the principal stresses of a general stress state is described in several papers (e.g. Hiramatsu and Oka, 1968; Mastin, 1988; Baumgärtner & al. 1989; Peška and Zoback, 1995). If the profile of the maximum cooling of the wellbore wall during drilling can be estimated, and the tensile and compressive strength of the rock are known, then the distribution of breakouts and DITFs, and the orientation of the latter can be predicted for arbitrary stress states. Thus, by a process of trial-and-error, stress states that are consistent with the observed style and geometry of wellbore failure can be identified. Unfortunately, in the Soultz case, the wellbores are inclined in the direction of SHmax, and it appears that the magnitudes of SHmax and Sv are similar. In this case, the 3-D orientation of the DITFs provide only limited information on the stress state, the primary constraint arising from the distribution of the breakouts and DITFs. In any case, it is advisable to combine the wellbore failure analysis with an independent estimate of Shmin derived from hydraulic data since this provides the strongest constraint on SHmax, which is generally the most difficult stress attribute to determine. In the following we apply this methodology to determine which of the proposed stress characterisations is most consistent with the observed breakout and DITF distributions to 5 km, and to tighten the constraints on the magnitude of SHmax.

DESCRIPTION OF THE DATASET

Wellbore failure observations

The primary data for this study are logs from the Schlumberger Ultrasonic Borehole Imager (UBI) sonde and the ancillary GPIT module that provides sonde positioning and orientation information. The latter also includes two on-board temperature sensors that provide a measure of borehole temperature at the time the logs were run, which

was shortly after the completion of drilling. Successful UBI logs were run in the granite section of both GPK3 and GPK4 to total depth (TD).

The GPK3 logs were acquired in two runs. The first run was acquired on 25th Oct. 2002 in the 12-1/4 inch section, some 5 days after the completion of drilling. This log extends throughout the 12-1/4 inch section from 1439 m MD (the casing shoe of a higher section) to 4532.6 m MD (MD denotes measured depth along hole from ground). The images of the lowermost 13.8 m are not oriented**.** The second log was run on 10th Nov. 2002, some 21 days after the hole had been extended as 8-1/2 inch diameter to TD at 5103 m MD. The log covers the 8-1/2 inch section from the 12-1/4 inch casing shoe at 4558.2 m MD to 5100.8 m MD, with the lowermost 2.6 m not oriented. The images are generally of good quality with few logging artefacts. 'Key seats' are visible along the entire inclined 12-1/4 section and some parts of the inclined 8-1/2 section, but they are easily identifiable and affect only a limited part of the borehole circumference.

The logs in the GPK4 borehole were also acquired in two runs that followed the drilling of the 12-1/4 inch and 8-1/2 inch sections. The log in the 12-1/4 inch was run on 15th Feb. 2004, some 15 hours after drilling, from 1421.3 to 4723.3 m MD. The log in the 8-1/2 inch section was run on 12th Apr. 2004, 18 hours after drilling operations ended, from 4730.3 to 5253.3 m MD. Images suitable for fracture geometry determination were obtained for 1445.3-4720.3 m MD and for 4757.3-5248.3 m MD. Outside these ranges, the logs are run in casing or suffer from acquisition problems.

STRESS ORIENTATION DOWN TO 5KM

As described in the introduction, analyses of wellbore failure in the shallow reservoir to 3.5 km depth indicate an approximately N-S direction for SHmax. The logs from GPK3 and GPK4 permit the analysis of SHmax-orientation to be extended to 5 km depth.

The analysis methodology was as follows. First, borehole intervals affected by either breakouts (BOs), axial drilling induced tension fractures (A-DITFs) and “en echelon” drilling induced tension fractures (E-DITFs) were identified. Then, for breakouts and A-DITFs the mean orientation of features were determined over successive 0.5 m depth windows. For E-DITFs the mean orientations (strike) of the best-fitting plane for each fracture pair were chosen. In all cases, the confidence of the identification was recorded by assigning an index ranging between 1 to 3, corresponding to low and high confidence respectively. The number of determinations and their confidence for each type of failure feature are summarized in Table 2 . Similar counts of features are obtained for both boreholes. About 10% of the logged borehole lengths are affected by breakouts, 10% for A-DITFs, and 7% for E-DITFs.

The orientation distribution with depth of the breakouts and A-DITFs in GPK3 are shown in the upper frame of Figure 2. The corresponding plot for GPK4 is given in Figure 3. The inclination of the boreholes are shown in the right frame of both figures. For the vertical borehole sections, the wellbore failure features provide a direct measure of the horizontal stress orientations: the breakouts denote the Shmin-orientation, and the DITFs the SHmax-orientation. For the purpose of the analysis we consider borehole sections that lie within 15° of vertical as being essentially vertical. For GPK3, this excludes from the analysis the section between 3257 m and 4037 m MD. Above 3257m MD, borehole failure is dominated by numerous A-DITFs**,** with only a few medium to low confidence identifications of breakouts. The high confidence A-DITFs show a preferred orientation in this section of 167.3° ± 12.1° (see histogram at right of Figure 2), a result that does not change by including medium- and low-confidence estimates. The orientation of the medium- and low-confidence breakouts is found to be 83.4° ± 17.3°, which is approximately 90° rotated from the mean A-DITF orientation, as would be expected if the identifications were correct. This indicates that some, albeit few, breakouts do indeed occur above 3257 m MD. In contrast, the lower sub-vertical section of the borehole, below 4037 m MD, is dominated by numerous breakouts with only a few low-confidence A-DITFs present. The high confidence breakouts have an orientation is 71.6° ± 20.3°. The A-DITFs have no clear preferred orientation. Since they are all of low confidence, it is probable that they are all erroneous identifications. A similar distribution of wellbore failure features is seen in GPK4, which is sub-vertical above 2490 m MD and below 4740 m MD. In the upper sub-vertical part, many A-DITFs are found whereas only one medium confidence breakout is present. High confidence A-DITFs for this upper section show a clear preferential orientation of 172.2° ± 11.8°. Below 4740 m MD, breakouts dominate with a few medium-to-low confidence A-DITFs. The high-quality breakouts have a strong preferred orientation of 83.8° ± 17° (see histogram in Figure 3). The medium-to-low confidence A-DITFs are oriented 173.9° ± 28.0°, and are thus 90° from the breakouts. This suggests that at least some of the identified A-DITFs are real.

The SHmax-orientation estimates obtained from the wellbore failure observations in all boreholes at the Soultz site are summarized in Figure 4. The high-quality estimates from A-DITFs in the upper sub-vertical sections of GPK3 (167°±12°) and GPK4 (172°±12°) are consistent with the results of previous analyses from the wells in the shallow reservoir (0°±20°). In the lower sub-vertical sections of GPK3 & 4, the high-quality breakout identifications indicate an SHmax-orientation for the deeper reservoir of 162°±20° and 174°±17° respectively, which is not significantly different from the SHmax-orientation in the shallow reservoir. Taking an average of all estimates from GPK3 and GPK4 by weighting each value by the length of borehole considered in the study yields a mean orientation for SHmax at the Soultz site from 1.4 km to 5 km depth of 169°±14°.

FAILURE OF BOREHOLE WALL

Borehole failure in the form of breakouts or DITFs is governed by the combination of the tangent stresses prevailing at borehole wall and the rock strength in compression and tension respectively. Since the fracture imaging logs from which the breakouts and DITFs were identified were run before any injections had been conducted, the failure must have occurred either during drilling or shortly afterwards. In general, the total stresses about a wellbore can be considered to result from the superposition of four components: 1) the stress concentration developed around an empty wellbore due to the far-field stresses applied to the medium with uniform pore pressure; 2) the stresses generated by the wellbore fluid pressure; 3) the stresses arising from a perturbation of pore pressure about the well, and 4) the stresses arising from a perturbation of temperature about the well. Components 1 and 2 are always present. The maximum and minimum tangent compression generated by these components as a function of depth in GPK3 are shown for the three stress characterisations in Figure 5. They represent the tangent stresses prevailing long after drilling, when the well has reached thermal and hydraulic equilibrium with the surroundings. In contrast, the conditions just after drilling (i.e. when the UBI logs were acquired) include the perturbing stress components 3 and 4 activated in tension by the cooling and overpressuring effects of the drilling mud. The latter is believed to be small for the holes in question since the annulus pressure was maintained at near-hydrostatic conditions. Hence it will be neglected. Thus, the analysis of borehole failure in tension reduces to estimating component 4, which in turn requires the estimation of the coolest temperature the borehole wall has seen at each

Table 2: Synthesis of borehole failure measurements. BOs=breakouts, A-DITFs=axial drilling induced tension fractures and E-DITFs='en échelon' drilling induced tension fractures.

	GPK3				GPK4			
Examined borehole length [m]	3619.8				3766			
confidence index	**all**	**1**	**2**	**3**	**all**	**1**	**2**	**3**
Number of BOs interval	56	11	16	29	81	6	16	59
Cumulated length of BOs [m]	294	29	79	186	355	14	53	288
Cumulated length of BOs [% of exanimate borehole length]	8.12	0.8	2.18	5.14	9.43	0.37	1.41	7.65
Number of orientation measurements	1026	88	282	656	1821	65	208	1548
Number of A-DITFs interval	48	17	7	24	54	9	11	34
Cumulated length of A-DITFs [m]	442	68	44	330	362	35	80	247
Cumulated length of A-DITFs [% of exanimate borehole length]	12.2	1.88	1.22	9.12	9.61	0.93	2.12	6.56
Number of orientation measurements	1520	230	136	1154	1334	153	322	859
Number of E-DITFs interval	43	9	8	26	66	28	3	35
Cumulated length of E-DITFs [m]	261	35	62	164	260	92	8	160
Cumulated length of E-DITFs [% of exanimate borehole length]	7.21	0.97	1.71	4.53	6.9	2.44	0.21	4.25

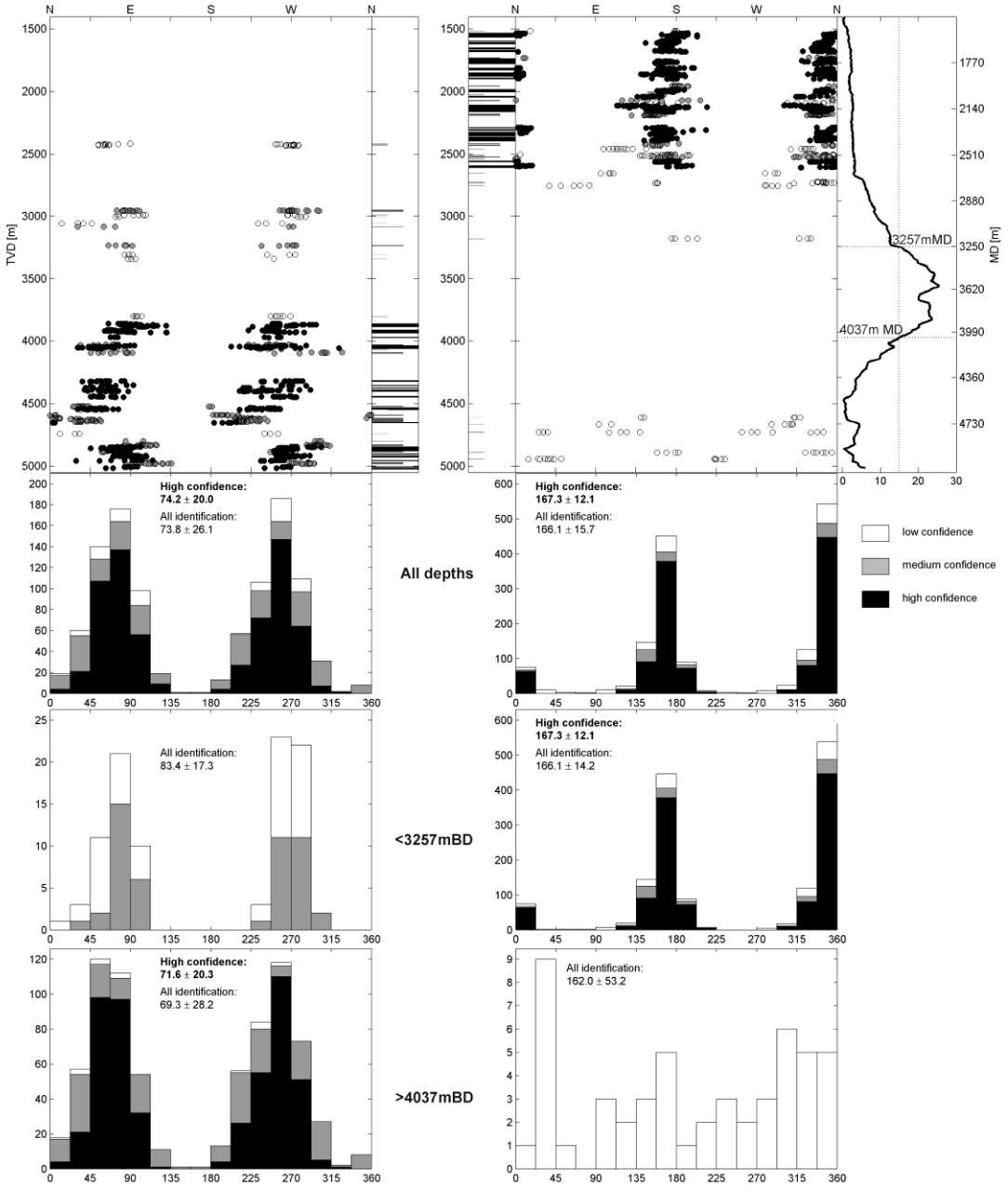

Figure 2: Orientation of breakouts and A-DITFs observed in GPK3.

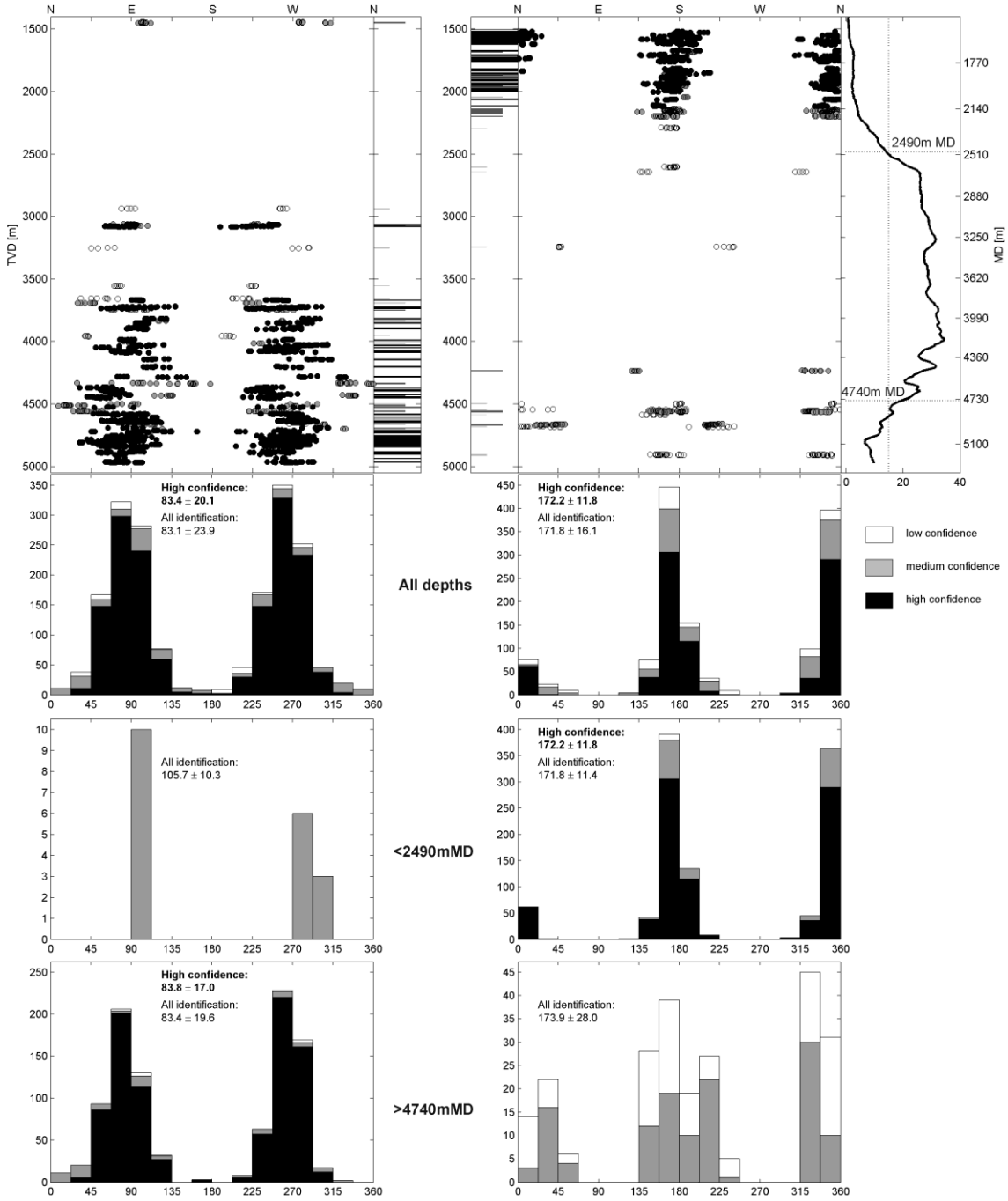

Figure 3: Orientation of breakouts and A-DITFs observed in GPK4.

depth. We will refer to this as the maximum-cooling profile, and describe its estimation in the next section.

Thermal perturbation and thermal stress

Cooling of the borehole wall by ΔT ($\Delta T < 0$) produces a hoop stress whose magnitude at the borehole wall, $S_{\theta\theta}^{therm}$ is given by Stephens and Voight (1982) as ,

$$S_{\theta\theta}^{therm} = \frac{\alpha E \Delta T}{1-\nu} \qquad (1)$$

Here, α is the coefficient of thermal expansion, E is the Young's modulus, and ν is the Poisson's ratio. The coefficient of thermal expansion was derived from the mineralogical composition of the rock and was found to be 8±2 x 10^{-6} K^{-1}. Young's Modulus will be taken equal to 54.0±2.0 GPa, the static value obtained from uniaxial compression tests (Evans & Valley, this issue). No reliable measurements of the static Poisson's ratio for the Soultz granite are available. Measured p- and s-wave velocities

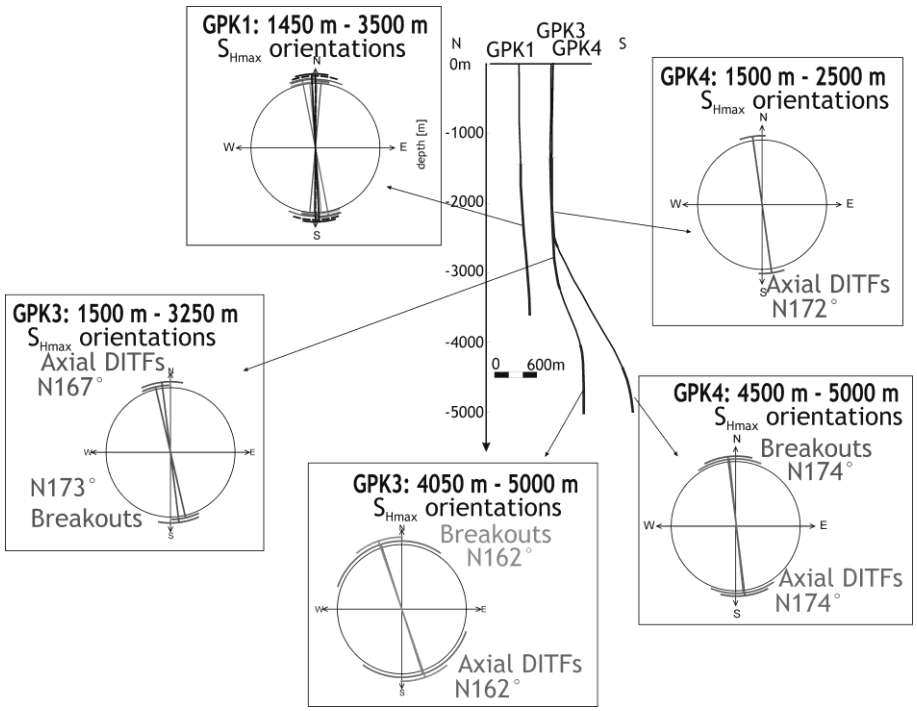

Figure 4: Summary of SHmax orientations obtained from various studies of breakouts and DITFs

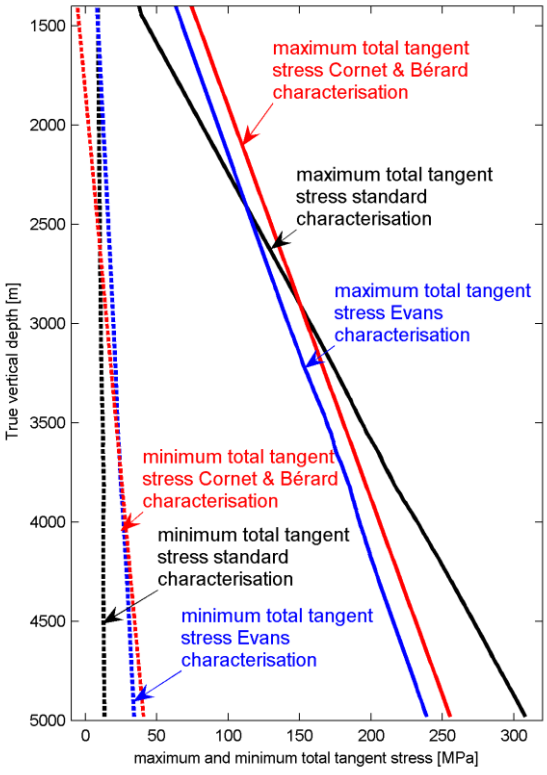

Figure 5: Profiles of maximum and minimum tangent total stress generated around GPK3 by the far-fields stresses of the three stress characterisations. The wellbore is also assumed to contain fluid at the formation pressure. The profiles for GPK4 are similar.

indicate a dynamic Poisson's ratio close to 0.25. However, static values are usually smaller than dynamic. Thus, we will consider Poisson's ratio values ranging between 0.2 and 0.25.

The key problem is to estimate the most negative value that ΔT ever reaches at each depth throughout the drilling operations. We shall assume that the borehole wall and mud are in thermal equilibrium. We will also assume that the depth of penetration of the cooling wave is unimportant for the initiation of DITFs, although it will control their depth of extent. The temperature profile along the borehole during drilling is very complicated owing primarily to heat transfer between the down-going fluid in the drill string, the up-going fluid in the annulus, and the surrounding rock mass. It is also complicated by the discontinuous nature of drilling operations, with periods of mud circulation during drilling interspersed with periods where the well is left to stand during bit changes, and perhaps periods of high-rate circulations designed to cool or clean-out the well. Neglecting the latter complications for the moment and assuming that the same mud flow rate is used throughout operations, then it is likely that the coolest mud temperature ever felt by the borehole walls at a given depth will occur just when the drilling bit reaches that depth. After this time, the mud flowing past the point will be warmer as it flows up the annulus and absorbs heat from the rock. Although the precise reconstruction of the profile of maximum cooling for the boreholes GPK3 and 4 is beyond the scope of this study, the available data are relatively good, particularly for GPK4, and place some relatively narrow bounds on this profile. The first bound is placed by bit temperature measurements of a 'measurement-while-drilling' (MWD) system that was intermittently operated during the drilling of the two wells. This system measures the temperature of the mud in the drilling string just before it emerges from the drill bit nozzle and thus constitutes a lower bound for the coolest temperature ever seen by the rock at the depth of the measurement. The second constraint is set by temperature profiles recorded by two sensors within the GPIT sondes of the logs run just after drilling. These data are not

'guaranteed' temperature measurements since they are the output of two sensors used in the temperature compensation of the magnetometers and accelerometers. Some doubts exist about their calibration in terms of absolute temperature. Different GPIT sondes were used to run the spectral-gamma and UBI sondes for both GPK3 and 4 (i.e. four GPIT sondes were used in all). For both wells, the two profiles from the UBI GPIT sonde were offset from each other by about 12°C degree, whereas those from the spectral-gamma GPIT sonde were mutually consistent, and moreover agreed with the mean value of the two traces from the UBI GPIT sonde. Schlumberger advised us that the GPIT sondes used with the spectral gamma logs in both wells were a newer version, and so the 'temperature' curves were more likely to be correct. Thus, we accept them as defining the temperature profile in the well shortly after drilling. The natural rock temperature profiles in both boreholes are obtained from temperature logs run several months after drilling completion during which time the boreholes have been left to equilibrate. The estimation of the maximum-cooling profile for GPK4 is presented first since the temperature information is more complete. The temperature data are shown in Figure 6a. The red solid line denotes the temperature profile recorded within the spectral-gamma GPIT sonde run 12hrs and 18 hrs after the end of drilling of the 12-1/4 inch and 8-1/2 inch sections respectively. Comparison with the natural temperature profile shows that the borehole remained cooled by 35-40°C in the 12-1/4 inch section and 25-30°C in the 8-1/2 inch section. The post-drilling log profile is an upper bound to the profile of maximum-cooling (note that even a log run immediately upon the termination of drilling would only be an upper bound for the latter, except near the hole bottom, because of warming of higher sections of the hole by up-flowing drill mud in the annulus). The spot measurements of temperature from the MWD system are indicated in Figure 6a by the blue crosses. Under normal circumstances, these constitute lower bounds on the maximum-cooling profile. Above 3 km in the 12-1/4 inch section and within the 8-1/2 inch section, the values lie below the post-drilling temperature profile, as expected. However, below 3 km in the 12-1/4 inch section, the MDW temperature estimates are about the same and occasionally exceed the post-drilling log profile. Whilst this is understandable near the hole bottom, it is perhaps surprising that it extends over 1 km. A possible explanation for this is that the lowermost kilometre of the 12-1/4 inch hole section was cooled below the lowest temperatures attained during drilling by a circulation conducted at the end of drilling operations in order to clean the hole. For this to have proven more effective in cooling the well than the circulation during drilling would require that the flow rate be greater than during drilling. Whether this is indeed the case is still under investigation. For the present, we take the lower bound on the maximum-cooling profile for the lowermost 1 km of the 12-1/4 inch section as given by the few MWD temperature measurements that are lower than the post drilling log. Although this leads to an uncertainty in the maximum cooling profile that appears unrealistically small in this section, the available evidence suggests that it is not greatly so. The bounding profiles of maximum-cooling are shown in Figure 6b. The amount of cooling in GPK4 is always more than 20°C, and may reach up to 65°C at some depths. The implied bounding profiles of hoop stress induced at the borehole wall are shown in Figure 6c. These were calculated from eqn (1) using the thermo-elastic parameter values and their uncertainties given earlier. The extreme estimates of thermally-induced hoop stress range from -8MPa to -48MPa. The mean value ranges from -17.1 MPa at 3160 m TVD to -31.3 MPa at 2235 m TVD.

The temperature data for GPK3 are shown in Figure 7a. The constraints placed on maximum-cooling are much less strong than for the GPK4 dataset. For the upper bound, the post-drilling temperature profiles were obtained from logs run significantly after the end of drilling operations (5 and 21 days for the 12-1/4 and 8-1/2 inch sections respectively) and thus there was time for the well to warm-up appreciably. For the lower bound, only 5 MWD measurements between 2.7 and 3.2 km MD are available. These MWD data suggest that the cooling is generally less pronounced than for GPK4. The analysis of the GPK3 data is still in progress. For the present, we take the data on face value and assume that the range of uncertainty in maximum-cooling within the 0.5 km section where there are MWD measurements applies at all depths. Under this assumption, cooling reaches about 25°C and is always greater than 5°C (Figure 7b). The thermally-induced hoop stress is shown in Figure 7c and ranges between -18MPa and -2 MPa. For the reasons discussed earlier, lower (i.e. more tensile) values are preferred as significant warming of the well almost certainly occurred before the logs were run. This work is on-going and so the results are provisional.

Failure criterion in tension

To determine whether the computed net minimum tangent stress at the borehole wall is sufficient to generate a DITF, a failure criterion in tension is required that includes an effective law. No laboratory measurements of the tensile strength of Soultz granite are available. A review of the literature suggests values for intact specimens will probably be of the order of a few tens of MPa. However, in-situ values will be less than this - perhaps as low as a few MPa. Indeed, many practitioners adopt a value of zero when considering similar borehole stability problems (e.g. Brudy and Zoback, 1993). In view of this, tensile strength will be considered to range between 0 and 5 MPa.

The effective stress law for tensile failure has the form:

$$\sigma_t = S_t - \beta_t P_p \qquad (2)$$

where σ_t is the effective tangent stress, S_t is the total tangent stress, P_p is the pore pressure, and β_t is the coefficient of effective stress for tensile failure. The value of β_t for low-porosity crystalline rocks has been subject to several laboratory studies, and all found a value of unity (Jaeger, 1963; Jaeger and Cooke, 1963; Schmitt and Zoback, 1992), except possibly when the loading rate is very high. This may be relevant for special problems like impacts or explosion but probably not for borehole failure. Thus, our starting hypotheses is that β_t is 1.0.

Failure criterion in compression

Compressive failure of the borehole wall that produces breakouts is driven by a triaxial stress state with a highly-compressive hoop stress, St, a relatively low normal stress equal to the mud pressure, Sn = Pw, and an axial stress whose magnitude at the borehole wall in the direction of SHmax is given for vertical holes by (e.g. Evans, et al., 1988):

$$S_v^{wall} = S_v + 2\nu(S_{H\max} - S_{h\min}) \qquad (3)$$

Evidently, direct measurement of rock strength under precise *in-situ* triaxial conditions requires *a-priori* knowledge of the stress state. To avoid this need, we ignore the vertical stress and use an approximate failure criterion based upon the uniaxial compressive strength (USC).

Whether failure conditions are met is evaluated using an effective stress law for compressive failure of the form:

$$\sigma_t = S_t - \beta_c P_p \qquad (4)$$

where σ_t is the effective tangent stress, S_t is the total tangent stress, P_p is the pore pressure, and β_c is the coefficient of effective stress for compressive failure. Brace and Martin, (1968) performed triaxial experiments on low-porosity crystalline rocks in the laboratory and found β_c = 1.0. Hence we use this value. If the borehole is in hydraulic equilibrium with the formation so that the wellbore pressure, Pw, is equal to the pore pressure, Pp, then the maximum effective tangent stress is given by, $\sigma_t = (S_t - P_w)$, and the effective

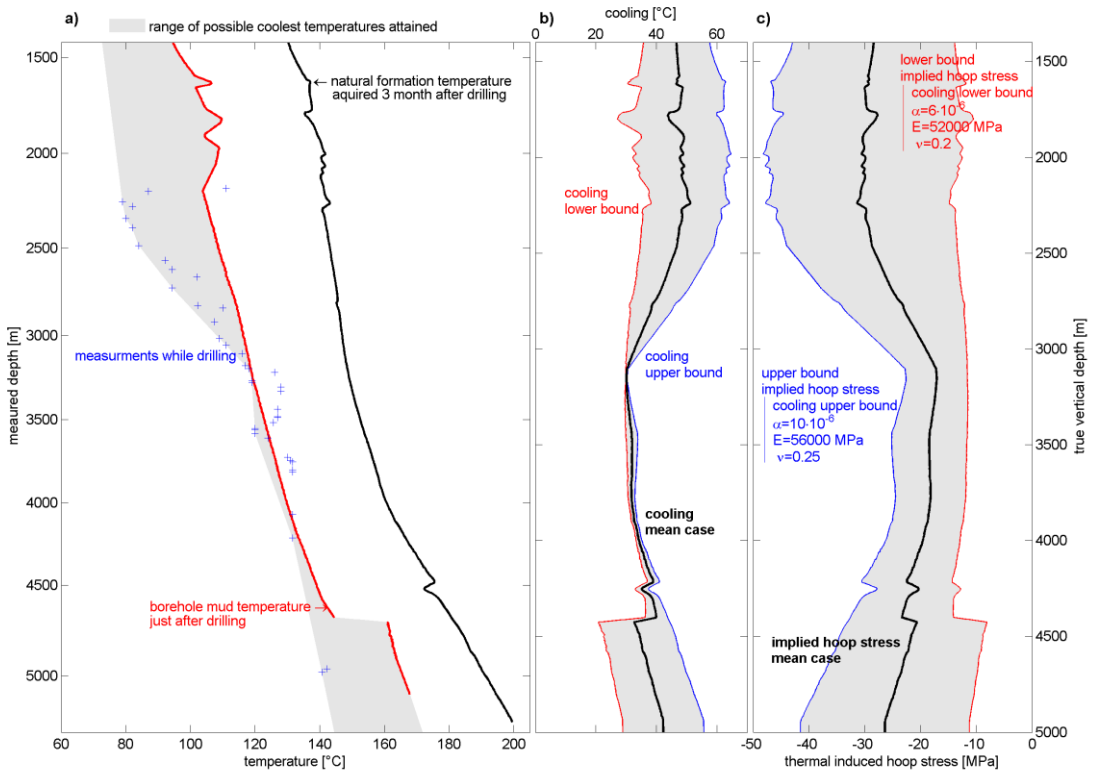

Figure 6: a) Estimates of the temperature profile in GPK4 shortly after drilling (red) and after 3 months (black). The blue crosses denote point-measurements of temperature of the mud within the bit during drilling obtained with a MWD system. The grey denotes the range of estimates of the coolest temperature that occurred during the drilling operations. b) Corresponding range of values of maximum-cooling of the borehole wall. c) Implied range of estimates for the thermally-induced hoop stress.

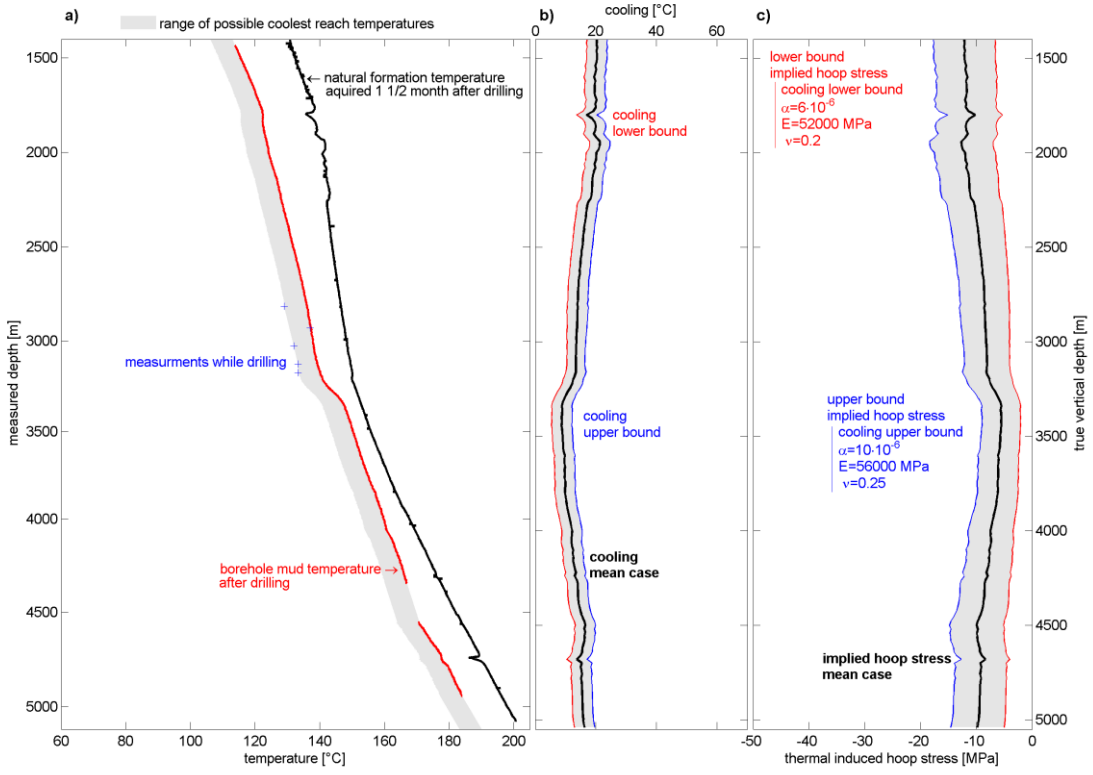

Figure 7: As Figure 6 but for GPK3

normal stress, $\sigma_n = (S_n - P_W) = 0$. Thus, if the axial (i.e. vertical) stress is neglected, the loading conditions become precisely uniaxial, and we can write the compressive failure criterion as:

$$\sigma_t = (S_t - P_W) > UCS \qquad (5)$$

Evans & Valley (this issue) measured the UCS of ten samples of unaltered granite and found values in the range 100-130 MPa. These values are less than would have been obtained had the test been conducted with one axis confined to simulate the non-zero effective vertical stress, although possibly not by much. However, there are other issues that should be born in mind when considering whether laboratory values of strength derived from tests on cores are representative of in-situ values.

Firstly, there is the question of microcracking induced by stress relief. Both cores and borehole wall have experienced complex stress paths when being drilled. Whilst these paths are not identical, both involve stress relief to some extent, and both will result in damage and strength reduction in comparison to that of *in-situ* rock remote from the wellbore (Diederichs, 2004; Martin, 1994). Thus, the reduction in strength of the core samples mimics that of the borehole wall to some degree. A second consideration is that stress corrosion cracking will serve to reduce the strength of the borehole wall on timescales which are long compared to the laboratory tests. This weakening of the wall rock will be promoted by the high in-situ temperature and the reactive nature of the pore fluid. In summary, although it is difficult to quantify the factors relating the laboratory-derived UCS estimates to the compressive strength of the rock at the borehole wall under *in-situ* conditions, it is considered probable that the latter is less than the former, particularly in the long term.

Stability of crust

A variety of data suggests that the strength of the crust is limited by the frictional strength of geological discontinuities that are pervasive in almost all rock masses (Brace and Kohlstedt, 1980; Zoback and Healy, 1984). It follows than an upper limit on the level of shear stress that a fractured rock mass can support is set by assigning it a Coulomb friction strength law with a friction coefficient, μ = 1.0. These considerations thus impose a further constraint on allowable magnitudes of the three principal stress components. We have evaluated whether the three proposed stress characterisations respect this constraint by computing the value of the shear stress, $\Delta\tau$, that must be added to the shear stress acting on optimally oriented fracture planes to bring them to failure for μ = 1.0. An acceptable stress state at a given depth will then be characterized by $\Delta\tau \geq 0$, and unacceptable ones by $\Delta\tau < 0$.

CONSTRAINTS ON MINIMUM HORIZONTAL STRESS MAGNITUDE FROM ANALYSIS OF HYDROTESTS

No hydrofracture of HTPF stress tests have been conducted below 3.5 km from which the magnitude of Shmin could be estimated. Thus, we follow Cornet and Bérard (2003) and assume that the maximum pressure attained during the stimulation injections provides a direct measure of Shmin at the depth of the casing shoe. This approach must be considered as tentative since it assumes the following conditions are met:

1. The maximum pressure attained during the test is controlled by jacking and not shearing.
2. Near-wellbore pressure drops (i.e. entrance losses) due to the focussing of flow are negligible.
3 The minimum stress prevailing at the time of maximum pressure reflects the ambient stress and is not elevated by poro-elastic effects.

As seen in Figure 1, these conditions appear to have been met for the large injections into the shallower reservoirs at 2.0 and 3.0 km, since the suggested Shmin profile of Cornet and Bérard (2003), which is based on maximum pressures during large volume injections, does not differ greatly from that determined from the small-volume injections. Violation of assumption 1 would result in underestimation of the ambient minimum stress, whereas 2 and 3 would result in overestimates. The data describing the maximum pressures inferred at the casing shoe during stimulation injections of the three wells of the 5 km reservoir are listed in Table 3 and are plotted in Figure 1. Only estimates derived from downhole pressure measurements are listed. It is evident that all data show pressure-limiting behaviour. The three datapoints from the 03May27 stimulation of GPK3 are from a sequence when the flow rate was stepped from 50 l/s to 70 l/s for 2 hrs and then back to 50 l/s. The small changes in pressure suggest that jacking was occurring, as required for the Shmin estimation procedure to be valid. Examination of Figure 1 shows that all datapoints lie close to the extrapolated Shmin trends of the 'Standard' and 'Cornet & Bérard' stress characterisations, whereas the curve of Evans is some 4 MPa higher than the Shmin estimates for GPK2.

RESULTS OF ANALYSIS

The results of the evaluation of the three proposed stress characterisations are summarised in Figures 8a-c and 9a-c for GPK3 and GPK4 respectively.

The leftmost two frames of each figure are concerned with breakouts. Frame 1 shows the distribution of observed breakouts in the two wells. In GPK3, a few breakouts appear below 3000 m TVD but their density increases markedly below 3850 m TVD. A similar distribution is found in GPK4, a few breakouts at 3000 m TVD giving way to an abundance below 3670m TVD. Frame 2 shows the computed profile of the maximum effective tangent stress for an effective stress law coefficient of 1.0. The failure line derived from the laboratory UCS tests is denoted by the vertical band.

For GPK3, the standard stress characterisation predicts that breakouts should occur below a threshold depth of 2657-3223 m TVD, which is in reasonable accord with the observations. The Cornet & Bérard stress characterisation predicts the onset at 2811 to 3668m TVD, whereas the Evans estimates predicts the onset at, 2506 to 3349m TVD, so these are in reasonable accord with the observations. For GPK4 the standard characterisation predicts an onset at 2760-3464m TVD, the Cornet and Bérard characterisation predicts 2942-4100m TVD and the Evans gives 2700-3728m TVD. Thus, the predicted onset of breakout failure for all three characterisations in both wells is in reasonable accord with the observations, although intense breakout development occurs some 500 m below the onset.

Table 3: Maximum pressures estimated at the casing shoe of the three wells penetrating the 5 km reservoir

Borehole	Injection test ID	Depth of casing shoe [m TVD from ground]	Max. pressure at casing shoe [MPa]	Flow rate at max. pressure [l/s]
GPK2	00JUN30	4402	55.4	31
GPK2	00JUN30	4402	56.9	50
GPK3	03May27	4488	60.8	50
GPK3	03May27	4488	61.5	70
GPK3	03May27	4488	61.2	50
GPK4	04SEP13	4489	62.1	30
GPK4	04SEP13	4489	61.7	40

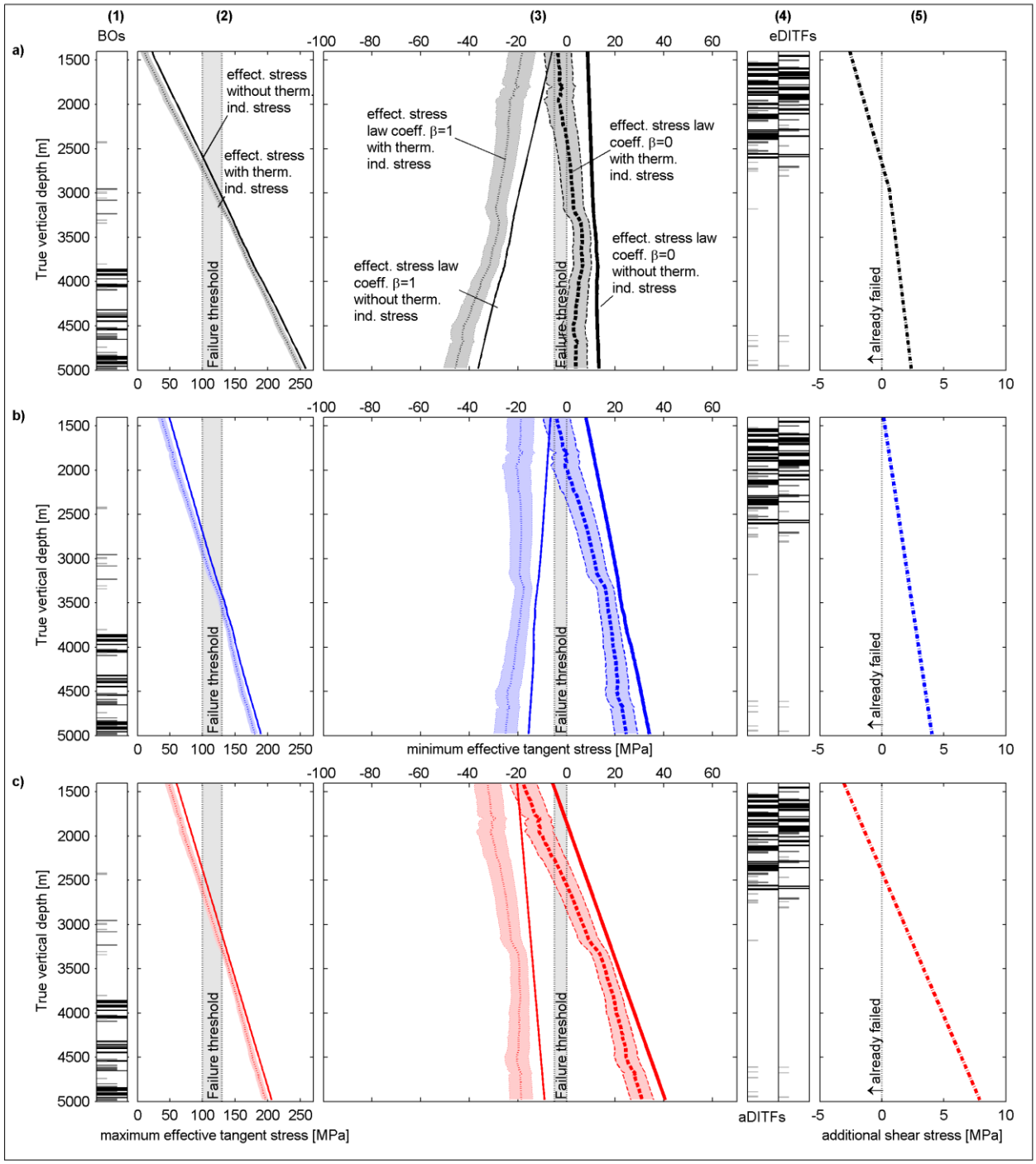

Figure 8: predicted stress magnitude at borehole wall for GPK3 assuming from top to bottom a) the standard stress characterisation, b) Cornet & Bérard characterisation and c) Evans characterisation. The frames from from left to right show: 1) Breakout locations. Black bars are for high confidence, gray bars for medium confidence and light gray bars for low confidence; 2) Maximum tangent effective stress for compressive failure. The vertical band denotes the compressive failure line; 3) Minimum tangent effective stress for tensile failure. The two solid lines are the effective stresses computed from the far field stress and wellbore pressure profiles of Figure 5 for effective stress law coefficients of 0.0 and 1.0, The two dashed curves are the same curves after adding the contribution for the thermal stress and its error range. 4) DITFs locations with same confidence rating that for the breakouts. 5) The 'Coulomb stress', which is the value of the shear stress that must be added to the stress resolved across optimally oriented planes to produce failure when the strength of the planes is described by a Coulomb friction criterion with a friction coeficient of 1.0. Negative values of the 'Coulomb stress' imply the shear stress is higher than can be supported by the rock mass with reasonable strength characteristics.

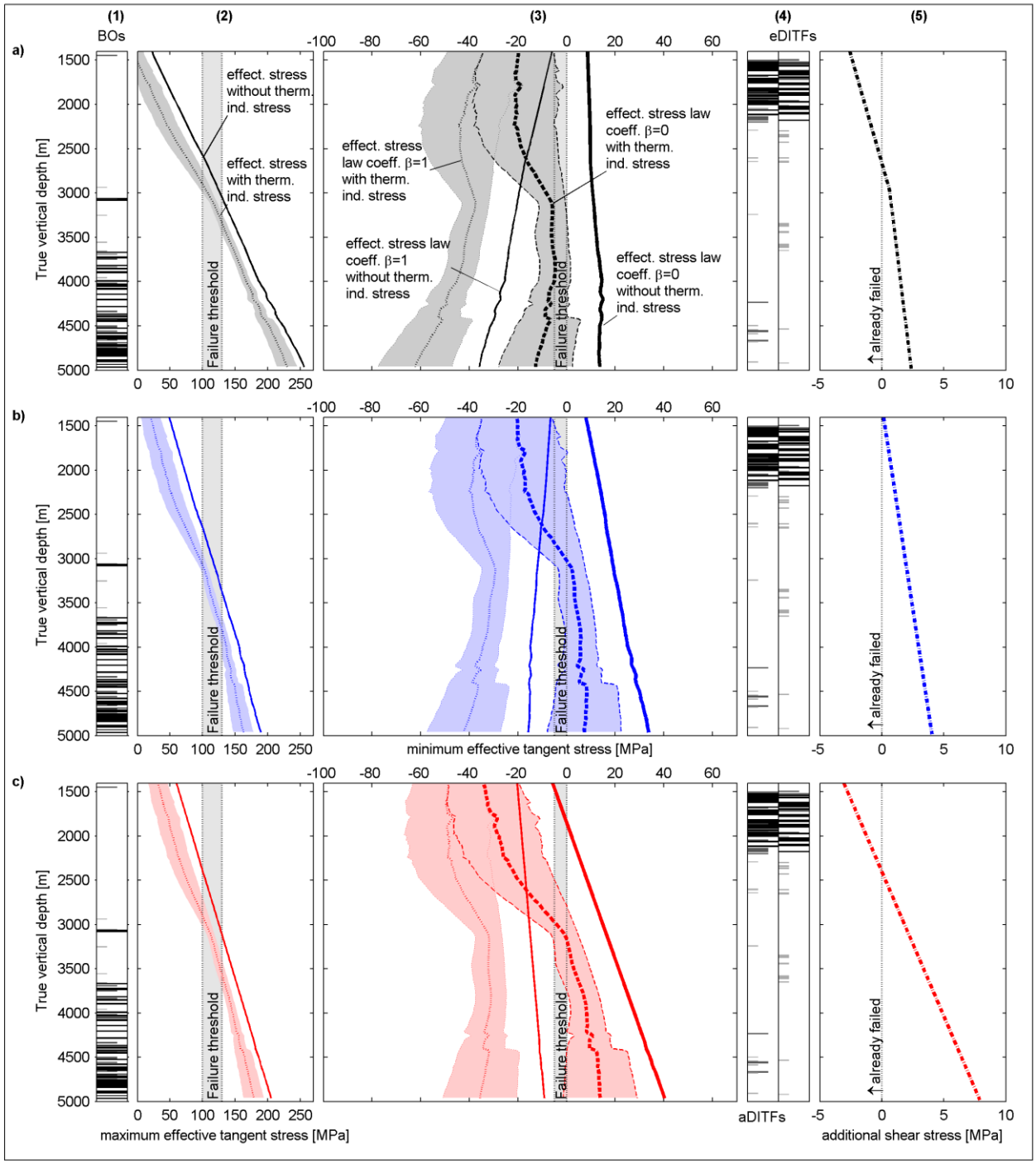

Figure 9: Same as Figure 8 but for GPK4

Frames 3 and 4 are concerned with tension failure. The distribution of observed DITFs are shown in Frame 4. GPK3 failed massively in tension down to 2610m TVD and GPK4 down to 2180m TVD. The predicted minimum effective tangent stress profiles are shown in Frame 3 for effective stress law coefficients of 1.0 and 0.0. The former leads to failure in tension of both boreholes along their entire depth regardless of which stress characterisation is considered, contrary to observation. The ubiquitous nature of the predicted tensile failure can be inhibited in two ways. The first is to reduce the magnitude of SHmax so that it is significantly less than Sv. However, this is not be in accord with the focal mechanisms solutions for microseismic events in the deep reservoir which suggest the two are not greatly different (e.g. Cuenot, 2005). The second and only remaining possibility is that the coefficient in the effective stress law for tensile failure be less than 1.0. The prediction for the case where the coefficient is reduced to 0.0 is shown in frame 4. For GPK3 with the standard stress characterisation, the band of minimum effective tangent stress now straddles the failure line, crossing it at the top and bottom of the well. Although this appears consistent with the presence of low-quality DITFs near the bottom of the well, the latter have no preferred orientation and are thus

unlikely to be real. In contrast, both the Cornet & Bérard and Evans stress characterisations predict tensile failure to be restricted to the top of the hole, the minimum tangent effective stress becoming increasingly compressive below 2350 m and 2850 m TVD respectively. In view of the possibility that cooling of this well was greater than shown, both estimates can be considered to fit equally well, and better than the profile from the standard characterisation. For GPK4, the stronger inferred cooling of this well, which is relatively well constrained by data, leads to the tensile failure criterion being met at all depths and for all stress characterisations, although for the Cornet & Bérard and Evans characterisations, the attainment is marginal below about 3000 m. This is precisely in accord with observations, where intense tensile failure of the upper part of the well gives rise to sporadic failure below, perhaps at points where stress heterogeneity produces a local pocket of more tensile stress. It should be noted that the DITFs near the bottom of GPK4 have a preferred orientation consistent with the SHmax orientation and are thus likely to be real.

Summarizing these observations, all stress characterisations correctly predict that breakouts will only appear in the lower parts of the wells. However, for the DITFs, the predictions of the Cornet & Bérard, and Evans stress characterisations fit the data from both wells better than the standard stress characterisation. Interestingly good agreement with the observations could be obtained only by setting the coefficient in the effective stress law for tensile failure to zero.

The borehole failure observations thus equally favour the Cornet & Bérard, and Evans stress characterisations over standard characterisation. However, consideration of the maximum shear stress that a fractured rock mass can support leads to the selection of the former as preferred. In frame 5 of Figures 8 and 9 are shown the profiles of additional shear stress required to bring the rock mass to the level considered an upper limit on fractured rock mass strength. Negative values imply that the shear stress already exceeds the upper limit and hence require the rock mass to be stronger than is considered reasonable. The profile for the Cornet & Bérard, stress characterisation remains positive at all depths, whereas that from the Evans characterisation becomes negative above 2500 m. Thus, this criterion favours the Cornet & Bérard, stress characterisation as the better of the three. As noted earlier, the extrapolated Shmin profile of Cornet & Bérard also fits the available Shmin estimates somewhat better than The Evans profile (Figure 1).

To complete the study, we used the wellbore failure observations and 'Coulomb' stress criterion to refine the bounds on SHmax. Figure 10 shows the effects on predicted borehole failure and the 'Coulomb' stress of varying the value of SHmax from 0.80Sv to 1.20Sv within the Cornet & Bérard characterisation. We consider only the well GPK4 where the induced thermal stress perturbation is the better constrained. In order to reproduce the marked reduction in incidences of tensile failure below 2100 m TVD, the value of SHmax must be limited to less than 1.05 (Figure 10-frames 3&4). On the other hand, SHmax must be greater then or equal to 0.9·Sv in order to reproduce the onset depth of breakouts. Thus, the wellbore failure observations constrain SHmax to lie between 0.9·Sv and 1.05·Sv.

CONCLUSION

Of the three proposed linear characterisations of stress at Soultz, the one of Cornet and Bérard is in best agreement with the observed depth distributions of breakouts and DITFs. This characterisation is also in accord with the estimates of Shmin obtained from the maximum pressure at the casing shoe of the stimulation injections into the 5 km reservoir, and is consistent with reasonable limits on the strength of fractured rock masses.

The standard stress characterisation is not in accord with wellbore failure observations and should no be used.

The wellbore failure observations allow a refinement of the uncertainty in SHmax of the Cornet and Bérard characterisation. Specifically, SHmax is found to be restricted to the range 0.9·Sv≤ SHmax <1.05·Sv.

Collectively, the diverse constraints suggest the following stress characterisation for Soultz that is valid between depths of 1.5-5.0 km (excluding the effects of local stress heterogeneity):

SHmax orientation is N169°E±14°
Sv = 0.3 + 25.60 z[km]
Shmin=-1.11537+13.77z[km]
- 1.17 +22.95z[km] ≤ SHmax < -1.365 + 26.775z[km]

The above estimate of the vertical stress includes the revised estimate of the density of the sediments of 2.63 gm/cc, and a granite density of 2.61 gm/cc consistent with density logs.

A further result of the analysis is that the coefficient of the effective stress law for tensile failure is close to zero.

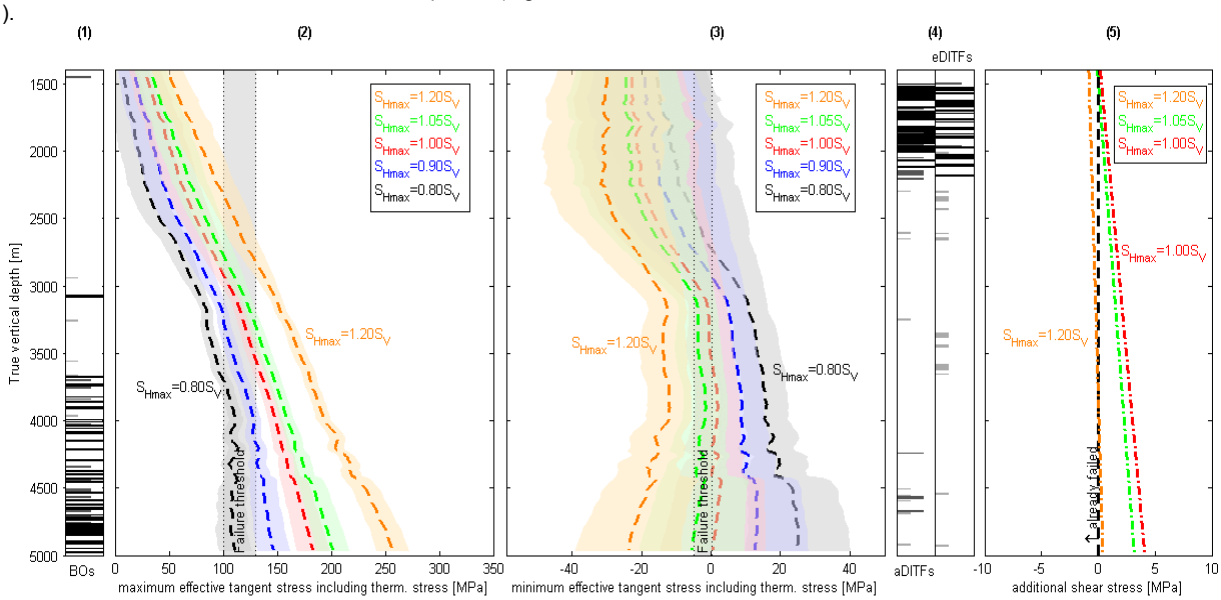

Figure 10: Parameter study of the effect of varying SHmax of the Cornet & Bérard stress characterisation on predicted wellbore failure and Coulomb stresses for GPK4. The figure layout is the same as Figure 8 and so the explanation will not be repeated.

REFERENCES

Baria, R., Garnish, J., Baumgärtner, J., Gérard, A. and Jung, R. (1995), Recent developments in the European HDR Research programme at Soultz-sous-Forêts (France). In: E. Barbier (Editor), World Geothermal Congress, Reykjavik, Iceland, pp. 2631-2637.

Baumgärtner, J., Carvalho, J. and McLennan, J. (1989), Fracturing deviated boreholes: an experimental laboratory approach, *ISRM-SPE international symposium.* Balkema (Rotterdam), Pau, pp. 929-937.

Bell, J.S. and Gough, D.I. (1979), Northeast-southwest compressive stress in Alberta: Evidence from oil wells. *Earth Planet. Sci. Lett.*, **45**: 475-482.

Bérard, T. and Cornet, F. (2003), Evidence of thermally induced borehole elongation: A case study at Soultz, France. *International Journal of Rock Mechanics and Mining Science*, **40**: 1121-1140.

Brace, W. F. and Kohlstedt D. L. (1980), Limits on lithospheric stress imposed by laboratory experiments, *Journal of Geophysical Research*, **85**, 6248-6252.

Brace, W.F. and Martin, R.J. (1968), A test of the law of effective stress for crystalline rock of low porosity. *International Journal of Rock Mechanics and Mining Science*, **5**(5): 415-426.

Brudy, M. and Zoback, M.D. (1993), Compressive and Tensile failure of boreholes arbitrarily-inclined to principal stress axes: application to the KTB boreholes, Germany. *International Journal of Rock Mechanics, Mining Science and Geomechanics Abstracts*, **30**(7): 1035-1038.

Brudy, M. and Zoback, M.D. (1999), Drilling-induced tensile wall-fractures: Implications for determination of in-situ stress orientation and magnitude. *International Journal of Rock Mechanics and Mining Science*, **36**: 191-215.

Cornet, F. H., and Bérard, T. (2003), A case example of integrated stress profile evaluation, paper presented at 3rd International Symposium on Rock stress, Balkema, Kumamoto

Cuenot, N., Charléty, J., Dorbath, L. and Haessler, H. (2005), Faulting mechanisms and stress tensor at the European HDR site of Soutz-sous-Forêts, paper presented at 30th Workshop on Geothermal Reservoir Engineering, Stanford University, Stanford, California.

Diederichs, M. S., Kaiser, P. K. and Eberhardt, E. (2004), Damage initiation and propagation in hard rock during tunnelling and influence of near-face stress rotation, *International Journal of Rock Mechanics and Mining Science*, **41**, 785-812.

Evans, K. F., Scholz, C. H. and Engelder T. (1988), An analysis of horizontal fracture initiation during hydrofrac stress measurements in granite at North Conway, New Hampshire, *Geophys. J.*, **93**, 251-264

Evans, K. F., Kohl, T., Hopkirk, R. J. and Rybach L. (1992), Modelling of energy production from Hot Dry Rock systems, Final Report to Swiss National Energy Research Fund (NEFF) under contract NEFF 359, Swiss Federal Institute of Technology/Polydynamics

Evans, K.F., (2005), Permeability creation and damage due to massive fluid injections into granite at 3.5 km at Soultz: 2. Critical stress and fracture strength. *Journal of Geophysical Research*, **110**(B4).

Evans, K.F. and Valley, B., (this issue), Strength and elastic properties of the Soultz granite. *EHDRA meeting june 2006*, Soultz-sous-Forêts.

Genter, A. and Tenzer, H., (1995), Geological monitoring of GPK2-HDR borehole, 1420-3880m (Soultz-sous-Forêts, France). *R-38-629, report BRGM*, Orléans, France.

Heinemann-Glutsch, B., (1994), Results of scientific investigations at the HDR test site, Soultz-sous-Forêts, Alsace, Socomine, BP 39, Route de Kutzenhausen, F-67250 Soultz sous Forets., France

Helm, J.A., (1996), The natural seismic hazard and induced seismicity of the European HDR (Hot Dry Rock) geothermal energy project at Soultz-sous-Forêts, France, *PhD thesis Univ. Louis-Pasteur*, Strasbourg, France.

Hiramatsu, Y. and Oka, Y., (1968), Determination of the stress in rock unaffected by boreholes or drifts, from measured strains or deformations. *International Journal of Rock Mechanics and Mining Science*, **5**: 337-353.

Ito, T., Evans, K., Kawai, K. and Hayashi, K. (1999), Hydraulic fracture reopening pressure and the estimation of maximum horizontal stress, *Int. J. Rock Mech. Min. Sci.*, **36**, 811-826.

Jaeger, J.C., (1963), Extension Failures in Rocks subject to fluid Pressure. *Journal of Geophysical Research*, **68**(21): 6066-6067.

Jaeger, J. C., and Cooke, N. G. W. (1963), Pinching-off and disking in rocks, *J. Geophys, Res.,*, **68**, 1759-1765

Klee, G. and Rummel, F., (1993), Hydrofrac stress data for the European HDR research project test site Soultz-sous-Forêts. *International Journal of Rock Mechanics, Mining Science and Geomechanics Abstracts*, **30**: 97, 3-976.

Klee, G., and Rummel, F. (1999), Stress regime in the Rhinegraben basement and in the surrounding tectonic units, paper presented at Proceedings of the European Geothermal Conference, Centre d'Hydrogéologie, Université de Neuchâtel, Basel, Switzerland, 28-30 Sept

Martin, C. D., and Stimpson, B. (1994), The effect of sample disturbance on laboratory properties of Lac du Bonnet granite, *Canadian Geotechnical Journal*, **31**, 692-702.

Mastin, L., (1988), Effect of borehole deviation on breakout orientations. *Journal of Geophysical Research*, **93**(B8): 9187-9195.

Nagel, R. (1994), Das Spannungsfeld in der Geothermiebohrung Soultz-sous-Forêts abgeleitet aus vertikalen Strukturen in eine Tiefe von 1.9 bis 3.6 km. PhD thesis, Univertsität Karlsruhe, Karlsruhe.

Peška, P. and Zoback, M.D., (1995), Compressive and tensile failure of inclined well bores and determination of in situ stress and rock strength. *Journal of Geophysical Research*, **100**(B7): 12791-12811.

Plenefisch, T. and Bonjer, K.-P., (1997), The stress field in the Rhine Graben area inferred from earthquake focal mechanisms and estimation of frictional parameters. *Tectonophysics*, **275**: 71-97.

Rummel, F. and Baumgärtner, J., (1991), Hydraulic fracturing stress meausrments in the GPK1 borehole, Soultz-sous-Forêts. *Geothermal Science and Technology*, **3**(1-4): 119-148.

Rutqvist, J., Tsang, C. F. and Stephansson, O. (2000), Uncertainty in the maximum principal stress estimated from hydraulic fracturing measurements due to the presence of the induced fracture, *Int. J. Rock Mech. Min. Sci.*, **37**, 107-120

Schmitt, D.R. and Zoback, M.D., (1992), Diminished pore pressure in low-porosity crystalline rock under tensional failure; apparent strengthening by dilatancy. *journal of Geophysical Research*, **97**(1): 273-288.

Stephens, G. and Voight, B., (1982), Hydraulic fracturing theory for conditions of thermal stress. *International Journal of Rock Mechanics, Mining Science and Geomechanics Abstracts*, **19**: 279-284.

Tenzer, H., Budeus, P. and Schnellschmidt, R., (1992), Fracture analyses in Hot Dry Rock drillholes at Soultz and Urach by Borehole Televiewer measurments. *Geothermal Resource Council Transactions*, **16**: 317-321.

Zoback, M. D., and Healy, J. H. (1984), Friction, faulting and "in situ" stress, *Annales Geophysicae*, **2**, 689-698.

Strength and elastic properties of the Soultz granite

Benoît Valley* & Keith Evans*
**Engineering geology, ETH Zürich, Switzerland*

Presented at the Soultz Scientific Meeting at Soultz-sous-Forêts on 15-16 June 2006.

EC Contract SES6-CT-2003-502706

PARTICIPANT ORGANIZATION NAME: ETH Zürich

Synthetic 2nd year report

Related with Work Package: FP6-WP5

STRENGTH AND ELASTIC PROPERTIES OF THE SOULTZ GRANITE

Benoît Valley* and Keith F. Evans*
**Engineering Geology, ETH Zürich*
e-mail: valley@erdw.ethz.ch

ABSTRACT

Twelve uniaxial tests were performed on Soultz granite in order to acquire its uniaxial compressive strength and static Young's modulus. Uniaxial compressive strength, a property never tested before on Soultz granite, ranges from 100 to 130 MPa for unaltered granite, and is unaffected by the strength of the pervasive alteration. One sample with significant vein alteration had a uniaxial compressive strength about 8MPa lower than the weaker unaltered sample. The Young's modulus of 'unaltered' Soultz granite is 54±2 GPa, regardless of the degree of pervasive alteration. However, two samples with vein alteration showed a significantly lower modulus of 39 GPa.

INTRODUCTION AND PREVIOUS WORKS

Twelve uniaxial compressive tests have been performed in order to determine some poorly known petrophysical properties of the Soultz granite: specifically, uniaxial compressive strength (UCS) and static Young's modulus. Although there are several determinations of Young's modulus reported in the literature, these are the first tests we are aware of that measure UCS.

Previous measurements of the Young's modulus on the Soultz granite are presented in Table 1. The only direct static measurements are from Schäfer (1990) from triaxial tests on 20 samples with 40 MPa confinement. Thirteen of them show no evidence of a type of hydrothermal alteration described later and referred to as 'vein alteration'. Such samples without vein alteration are usually called 'unaltered', although they invariable host a second type of alteration which will be referred to as 'pervasive alteration'. The mean E-modulus of samples without vein alteration was 49±4 GPa. Schäfer (1990) also tested four samples which showed vein alteration and found a lower Young's modulus of 30±14 GPa. Rummel, et al. (1989) derived static Young modulus from three points bending test on 62 mm and 30 mm diameter samples. Their summary makes no mention of the Young's modulus results of their tests on 60mm cores, but gives 83±4.7 GPa for their tests on 30 mm core. This appears to be in error as the highest value of Young's modulus listed in their results table is 80 GPa. Rummel (1991) later summarised the results of the 3-point bending tests and reports that the static Young's modulus of 29 tests was 38.0±8.5 MPa. This also appears to be in error as the smallest value in the dataset is 51 GPa. To clarify the situation, the mean and single standard deviation of the Young's modulus values listed in the results tables of Rummel, et al. (1989) were computed. For 28 tests on 62 mm granite samples without vein alteration, the static Young's modulus was 73±6 GPa, whereas for 16 tests of 30 mm granite samples without vein alteration, the value was 70±6 GPa. Rummel, et al. (1989) also conducted a few tests on samples with vein alteration. All tests yielded values lower than obtained for unaltered samples. One test on the 60 mm diameter samples yielded an value of 53 GPa, and seven on 30 mm samples gave values of 53±4 GPa.

The dynamic Young's modulus of the Soultz granite has been estimated from p- and s-wave velocity and density measurements derived either from laboratory tests or borehole logs. Schäfer (1990) performed measurements on 20 dry and 14 saturated cores in unconfined conditions and report values of 62±5 GPa and 88±4 GPa, respectively. Rummel & König (1991) made measurements on 335 granite cores taken from borehole EPS1 between the granite top to 2227 m and found an E-modulus of 64±8 GPa. Rummel & Schreiber (1993) measured p- and s-wave velocities in the axial and radial directions on granite core sample K21 taken from borehole GPK1 (3522.58-3525.88 m depth). These permit to highlight a slight anisotropy in the P- and S- wave velocities leading to lower axial E-modulus than radial E-modulus, i.e. 59±6 GPa and 65±10 GPa respectively. Dynamic elastic moduli have also been derived by combining precisely depth-matched sonic and density logs in well GPK1 over the depth interval 1949 to 3492 m. The average E-modulus between 1950 m and 3500 m was found to be 73±9 GPa with values dipping as low as 30 GPa within cataclastic shear zones where vein alteration is strongly present. The values in sections relatively free of vein alteration zones typically ranged between 73 GPa and 80 GPa. These values generally agree with the laboratory estimates of dynamic modulus if the stiffening effects of saturation are taken into consideration. They are also in agreement with the static E-modulus estimates derived from the 3-point bending tests, but not with the values from triaxial tests which are significantly lower. Generally speaking, static E-modulus values are usually substantially lower than the dynamic values, and so the results of the 3-point bending are somewhat surprising. Thus, the direct measurements of Young's modulus presented in this report are of some considerable interest.

SAMPLE DESCRIPTION AND PREPARATION

Twelve 78 mm diameter core pieces of the Soultz granite were tested under uniaxial compression. The samples were selected to represent various type and degrees of alterations. The details of the samples, including alteration type and degree, and the core identification numbers and depths of origin, are given in the six first columns of Table 2.

As noted earlier, the samples are affected by two different types of alteration called 'pervasive' and 'vein alteration' (Genter & Traineau, 1992). The pervasive alteration is a very early event that is probably related to reactions with magmatic fluids. It affects all of the granite so far explored at the Soultz site. This alteration is characterized by low grade alteration of biotite to chlorite and plagioclase to epidote (saussuritization). K-Feldspars are also affected and become reddish. Rock texture is not modified. The second type of alteration, vein alteration, is related to hydrothermal fluid

Table 1: Literature review of E-modulus determinations of Soultz granite

	Source	Type of measurement		Nb of data	E-mod [GPa] mean±std /min/max
Static modulus	Schäfer (1990)	Triaxial – 40MPa confinement	without vein alt.	13	49±4 / 43 / 56
			with vein alt.	4	30±14 / 14 / 48
	Rummel, et al. (1989)	Three point bending test on 62mm cores	without vein alt.	28	73±6 / 57 / 86
			with vein alt.	1	53
		Three point bending test on 30mm cores	without vein alt.	16	70±6 / 57 / 80
			with vein alt.	7	53±4 / 45 / 58
Dynamic modulus	Schäfer (1990)	Ultrasonic velocity measurement on dried cores		20	62±5 / 44 / 69
		Ultrasonic velocity measurement on saturated cores		14	88±4 / 86 / 94
	Rummel & König (1991)	Ultrasonic velocity measurement on cores		335	64±8 / 24 / 99
	Rummel, et al. (1992)	Ultrasonic velocity measurement on cores		4	71±5 / 63 / 76
	Rummel & Schreiber (1993)	Ultrasonic velocity measurement on cores	radial	8	65±10 / 46 / 84
			Axial	6	59±6 / 53 / 70
	Schlumberger sonic and density between 1949 and 3492 m in GPK1				73±9 / 26 / 106

circulation within fractures. It is characterized by the illitization of biotite and plagioclases, which usually imparts a yellowish color to the granite. Fractures which show vein alteration are sealed with quartz (occasionally geodic), calcite, illite, chlorite, sulfides, barite or hematite.

The degree to which the samples are affected by each of the two alteration types is indicated by four levels: 'none' (N), 'low' (L), 'medium' (M) or 'high' (H). The definition underlying this grading is given in Table 3, and the grades for each sample listed in Table 2.

The samples were prepared from the original 78 mm diameter cores by sawing them to length and grinding the ends to produce a right circular cylinder that was as close as possible to the ISRM norms (Bieniawski & Bernede, 1979). Two specifications of this norm were occasionally not quite attained: (1) the specification that the size of the largest grain in the rock should be related to the sample diameter with a ratio of at least 10:1. In the case of the Soultz granite with decametric K-Feldspath porphyroclasts this wasn't possible. (2) The specifications concerning the perpendicularity of the sample faces with the axis, and the mutual parallelism of the two faces could not quite be achieved for samples 2 and 4, although they was met for the other samples. This reflects the difficulty of machining heterogeneous materials like the Soultz granite. However, the deviation of samples 2 and 4 from the norms was not considered to be large enough to significantly influence the test results.

TESTS DESCRIPTION

The tests were performed at constant strain-rate of about 0.075mm/min and comprised three loading cycles (Figure 1). The first cycle extended to about 1/3 of the expected UCS, the second to about 2/3 of UCS; and the third continued until the sample failed. Each test took 30 to 40 minutes to perform. Unfortunately, samples 1 and 2 were tested with incorrect strain measurement settings and so it was not possible to estimate the Young's modulus of these samples. Moreover, the loading rate for sample 1 was to fast and so the UCS measurement is not considered valid.

All samples except sample 8 were tested on a loading frame were axial shortening was measured by displacement sensors on either side of the loading platens. For practical reasons, steel cylinders were placed between the loading frame platen and the sample (Figure 2). Thus, to determine the displacement across the sample it is necessary to remove the displacements across the steel cylinders and the interfaces. Once this was done, the sample strain was determined by dividing net sample length change by the sample length. Sample 8 was tested on another machine which allowed the sample axial strain to be directly measured with clip-on 'blade' strain gages. This permitted a comparison of results and a check calibration.

UCS was taken as being the highest stress value obtained during the testing of each samples. Three different Young Modulus estimates were determined from the slopes of the strain-stress curves. The one called E-average is taken as the slope of the linear part of the last loading cycle. E-min corresponds to the slope of the curve at the end of the last but one loading cycle. This is always slightly less than E-average. E-max is the slope of the curve at the beginning of the last unloading cycle. This is always slightly more than E-average. This procedure provides a realistic range for the Young's modulus value which includes all other candidate E-modulus estimators such as the secant modulus.

Table 2: properties of samples.

Sam-ple n°	Core n°	Core piece n°	Core piece btm depth [m]	Perv-asive alt.	Vein alt.	UCS	Eavg	Emin	Emax	Comments
1	K136	3270	1792.10	L	N	invalid test				
2	K136	3275	1794.72	L	N	131.14	invalid test			Failure not influenced by pre-existing cracks
3	K136	3279	1796.02	L	N	123.13	56.15	49.35	63.71	Failure not influenced by pre-existing cracks
4	K157	3794	1950.76	L	N	109.05	51.57	48.22	67.08	Failure not influenced by pre-existing cracks
5	K162	3914	1987.37	L	N	105.75	52.78	48.14	57.69	Failure not influenced by pre-existing cracks
6	K149	3634	1902.58	H	L	89.10	52.42	48.37	60.64	Failed along pre-existing cracks
7	K149	3628	1901.08	H	L	109.62	52.63	46.37	59.38	Failure not influenced by pre-existing cracks
8	K163	3933	1993.60	L-M	N	invalid test	55.88	50.00	61.88	Failure occurred in two load step with unloading in between. Then UCS is not reliable.
9	K107	2744	1626.00	M	L	101.52	54.98	45.70	59.07	Failed along pre-existing cracks
10	K113	2853	1657.63	M	M	98.28	39.24	34.19	48.87	Failure not influenced by pre-existing cracks
11	K101	2638	1598.78	M	N	129.66	58.35	47.39	61.35	Failure not influenced by pre-existing cracks
12	K113	2846	1656.57	H	H	65.47	39.81	33.24	47.38	Failed along pre-existing cracks

Table 3: classification of alteration.

Pervasive alteration	
None (N)	Unaltered biotite K-Feldspar and plagioclase. This case is never met.
Low (L)	Biotites are black showing only little alteration into chlorite, plagioclases are milky and K-feldspars are grey or pink.
Medium (M)	Biotites become greenish showing advanced alteration into chlorite, plagioclase show beginning of greenish coloring reflecting alteration in epidote and K-Feldspars are less pink and more reddish.
High (H)	Biotites are totally transformed into chlorite, plagioclases are dark green trough transformation in epidote and K-Feldspars are reddish to orange.
Vein alteration	
None (N)	No visible trace of vein alteration.
Low (L)	Small fractures present a yellowish halo of vein alteration which does not penetrate the whole sample.
Medium (M)	Former biotites and plagioclases are yellowish, reflecting alteration to illite. No major fractures cross the sample.
High (H)	The sample is traversed by fractures and biotites and plagioclases are totally altered to illite.

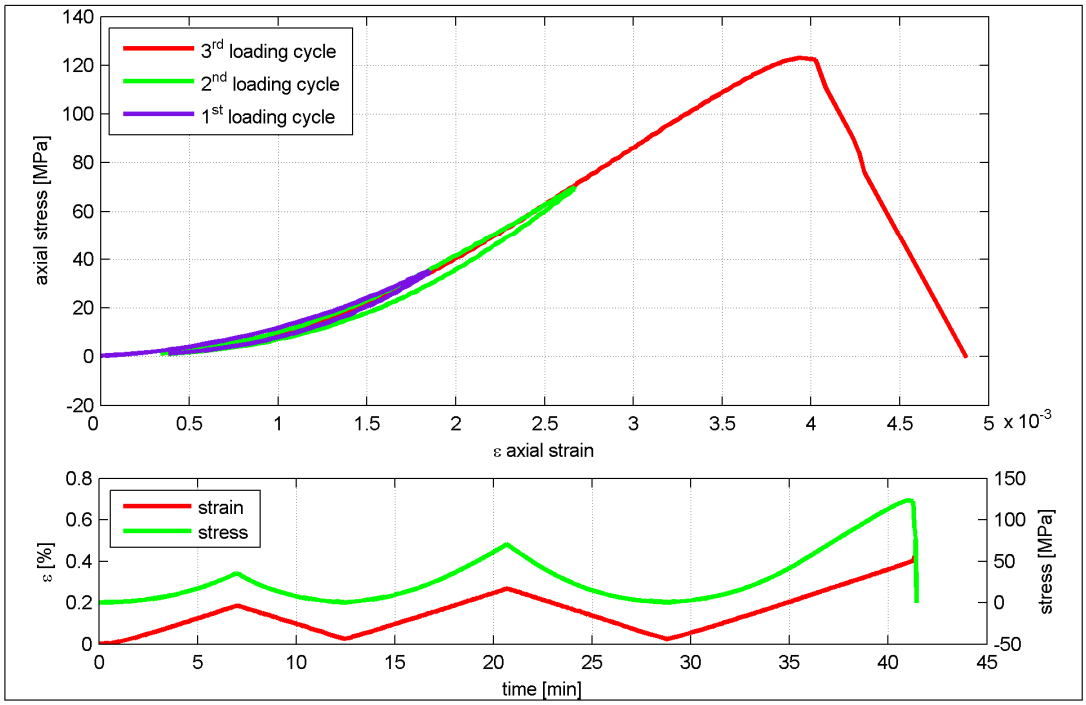

Figure 1: Example of a test record for sample 3. The upper frame shows axial stress vs axial strain for the 3 loading/unloading cycles performed during the test, each of which is shown with a different colour. The lower frame presents the history of stress (green) and strain (red) during the test. It is evident that the test is strain controlled as the strain curve has precisely linear segments, in contrast to the axial stress curve (in green).

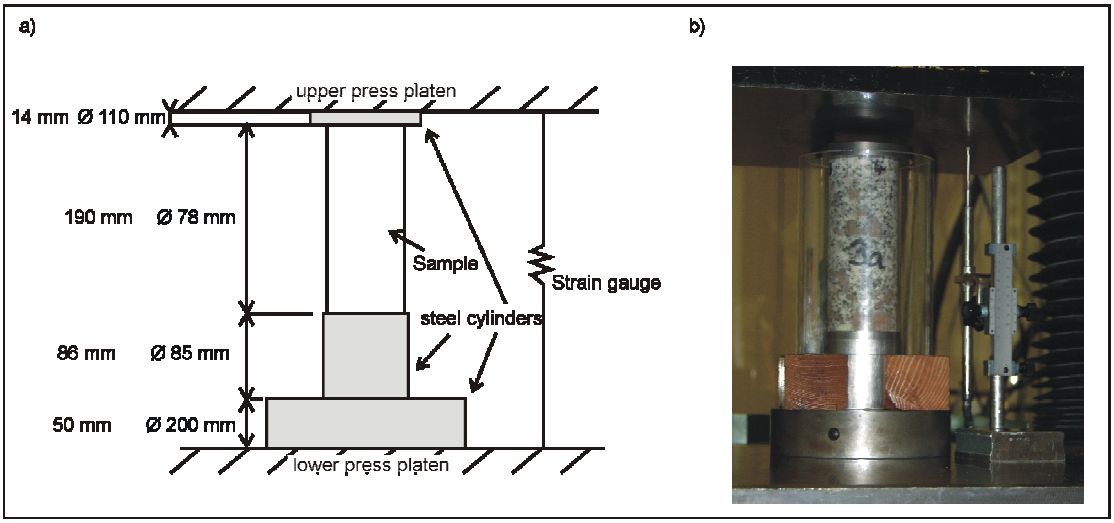

Figure 2: a) sketch of the test settings b) picture of sample 3 just before testing. The steel cylinder can be seen below the sample.

CALIBRATION AND CORRECTIONS OF E-MODULUS

As noted earlier, the estimation of axial sample strain from axial displacement of the platens requires the effect of steel cylinders at the end of the sample to be removed. This correction is not a trivial matter as the geometry of the cylinders is not precisely the same as the sample. Moreover, the compliance of the various interfaces in the load train also enters into the calculation but is unknown. To keep the analysis simple, we make the initial hypothesis that the effects of the interfaces are negligible, and that the diameters of the sample and cylinders are identical which is not the case as on can see on the sketch of figure 2a. The validity of these assumptions will be checked later. In the simplified case, the E-modulus of the complete stack can be expressed as a function of the E-module of each stack elements and their length by:

$$\frac{l_{tot}}{E_{tot}} = \frac{l_1}{E_1} + \frac{l_2}{E_2} + \frac{l_3}{E_3} + \ldots \qquad (1)$$

The E-modulus of the steel is precisely known as 210 GPa, and the lengths of the sample and steel cylinders are also known. Thus, the E-modulus of the sample can be estimated.

The validity of the assumptions made in obtaining the estimates was checked in two ways. First, the axial strain on

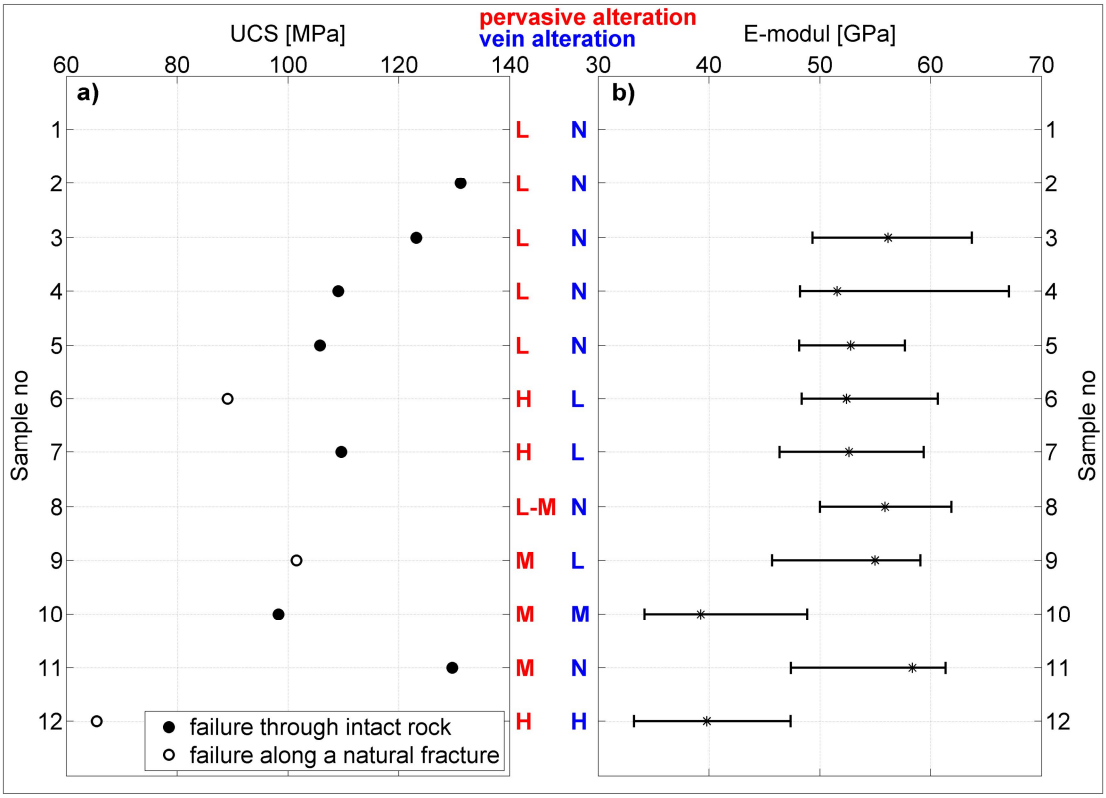

Figure 3: Illustration of the test results. a) Results for UCS . Failure of intact rock or activation of a natural fracture are denoted by close and open circles respectively. The letters in the middle of the figure denote the degree of pervasive and vein alteration. b) Results for E-modulus. The ranges extend from Emin to Emax and the stars denote Eavg.

sample 8 was measured relatively directly and so the concerns arising from the steel cylinder corrections do not apply. The E-modulus of this unaltered granite sample was in good agreement with the corrected E-modulus of the other unaltered granite samples. Second, and more definitively, a sample of fused quartz was tested in the load frame with the steel cylinders. The E-modulus of this sample was precisely known as 74 GPa (i.e. the E-modulus for crystal quartz). The estimate of E-modulus obtained from equation 1 for this sample was 73.7 GPa, which is within 1% of the true value. Thus, we conclude that the simplifying assumptions inherent in equation (1) do not have a significant effect of the resulting E-modulus estimates.

RESULTS AND DISCUSSION

Uniaxial compressive strength

The estimates of UCS obtained from the tests are listed in column 7 of Table 2 and are plotted in Figure 3a and 4a. In interpreting these values it is important to know whether sample failure involved the fracture of 'intact' rock or activation of a preexisting fracture. This information is given in column 11 of Table 2, and is included in Figure 3a an 4a by distinguishing points relating to activation of a pre-existing feature by open circles. Evidently, all but three tests involved the failure of intact rock. The UCS values obtained for these 'intact rock failure' samples ranged between 98.3 MPa and 131.1 MPa.

The relation between the UCS of samples which involved failure of intact rock and alteration grade is shown in Figure 4a. Samples with no vein alteration have relatively high UCS values ranging between 105.8 MPa and 131.1 MPa, regardless of whether the degree of pervasive alteration is high or low. Of the samples that involved intact rock failure, only sample 10 has a significantly high degree of vein alteration, and this has a UCS of 98.3 MPa, which is 8 MPa lower than the weakest sample without significant vein alteration. The result is consistent with the hypothesis that vein alteration tends to reduce the UCS, although more tests would be needed to establish this.

Three samples (6, 9 and 12) failed through the activation of a pre-existing fracture which was favourably-oriented for shear failure. In two of these cases (6 and 9), the pre-existing factures were sealed by quartz, and the UCS values of 89.1 and 101.5 MPa where relatively high. In contrast, the pre-existing fracture that failed in sample 12 had a black sealing, probably made of sulfide, and was much weaker, with a UCS of 65.47 MPa.

The UCS estimates obtained in this study cannot be compared with literature values as none exist. All that can be said is that the estimates lie in the lower range of values typical of granites, which may be due to the porphyric nature of the Soultz granite.

Young's modulus

The estimates of Young's modulus for all samples except 10 and 12 range between 50 and 60 GPa with a mean and single standard deviation of 54±2 GPa. Samples 10 and 12 are the only samples with significant vein alteration (i.e. medium or high grade), and their Young's modulus is 39 GPa, which is much lower.

The E-modulus estimates obtained in this study are in reasonable accord with the values obtained by Schäfer (1990) from triaxial tests with 40 MPa confining pressure (see Table 1). Our estimates (and those of Schäfer) are significantly lower that the values reported by Rummel, et al. (1989) from three-point bending tests. Given that our estimates and those of Schäfer constitute direct measurements of Young's modulus, whereas those of Rummel et al. (1989) are indirect, it would appear that the

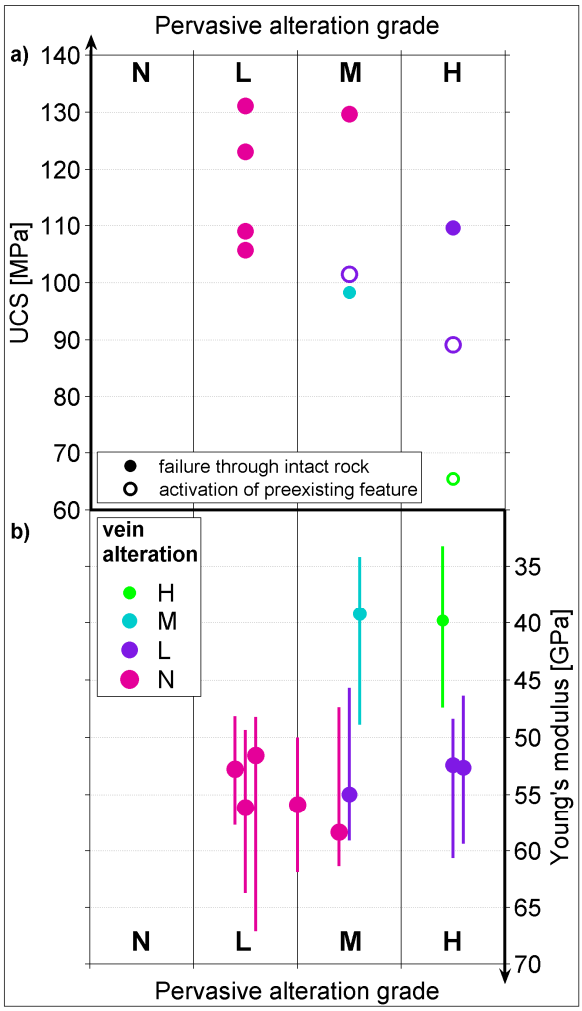

Figure 4: Illustration of the effect of the two types of alteration on the test results. The degree of pervasive alteration is indicated by the column, and the degree of vein alteration is denoted by both the colour and the size of the circles a) Results for UCS . Tests where sample failure occurred in intact rock are denoted as closed circles whereas those that involved activation of a natural fracture are indicated by open circles. b) Results for E-modulus. The ranges extend from Emin to Emax, and the circles denote Eavg.

latter are affected by some form of systematic error. A corollary of this is that the static E-modulus of the Soultz granite is of the order of 30% lower than the dynamic E-modulus, which is consistent with the literature (e.g. Eissa & Kazi,1988). Finally there can be no doubt that rock which has suffered from vein alteration has a lower Young's modulus. This has been found in all tests, regardless of whether they measure static and dynamic modulus.

CONCLUSIONS

The UCS of unaltered Soultz granite ranges between 100 and 130 MPa. Pervasive alteration does not appear to affect the strength of the granite. However, limited data suggests that the presence of vein alteration may reduce the strength slightly, although the data are too few to establish this firmly. The test also show that fractures with quartz sealing can be almost as strong as the intact rock. However, one sample that had a favorably oriented fracture filled with a dark material that was probably sulfide failed at about 65 MPa**.**
The static Young's Modulus of Soultz granite that has suffered little or no vein alteration is 54±2 GPa (average and single standard deviation of 8 samples). Two samples with significant vein alteration show substantially lower values of about 39 GPa. The static E-modulus of rock without vein alteration is about 75% of the estimates of dynamic E-modulus derived from both lab testing and wireline logs.

ACKNOWLEDGMENTS

Thanks are due to Erich Pimentel and Thomas Jaggi from IGT-ETH Zürich for the help in performing of the tests. We are grateful to Jean-François Mathier and Laurent Gastaldo from LMR-EPF Lausanne who helped with the sample preparation.

REFERENCES

Bieniawski, Z. T., and Bernede, M. J. (1979), Suggested methods for determining the uniaxial compressive strength and deformability of rock materials, *International Journal of Rock Mechanics and Mining Science & Geomechanics Abstracts*, **16**, p. 137-140.

Eissa, E. A., and Kazi, A. (1988), Relation between Static and dynamic Young's moduli of rocks, *International Journal of Rock Mechanics, Mining Science and Geomechanics Abstracts*, **25**, p. 479-482.

Genter, A., and Traineau, H. (1992), Borehole EPS-1, Alsace, France: preminilary geological results from granite core analyses for Hot Dry Rock research, *Scientific Drilling*, **3**, p. 205-214.

Rummel, F., te Kamp, L. and Schäfer, T. (1989), Fracture mechanic properties of granite cores from GPK1., 20 pp, Yellow report 7, Ruhr - Universität, Bochum, unpublished report.

Rummel, F. (1991), Physical properties of the rock in the granitic section of borehole GPK1, Soultz-sous-Forêts, *Geotherm. Sci. and Tech.*, **3**, p. 199-216.

Rummel, F., and König, E. (1991), Physical properties of Core samples, borehole EPS1, Soultz-sous-Forêts: Velocity, Density- and magnetic susceptibility- logs, depth interval 933-2227 m., 58 pp, Yellow report 6, Ruhr - Universität, Bochum, unpublished report.

Rummel, F., König, E. and Thieme, B. (1992), Fracture mechanics parameters of EPS1 Soultz granite cores., 44 pp, Yellow Report 10, Ruhr - Universität, Bochum, unpublished report.

Rummel, F., and Schreiber, D. (1993), Physical properties of the core K21, borehole GPK1, Soultz-sous-Forêts, depth interval 3522.58-3525.88 m., 11 pp, Yellow Report 12, Ruhr - Universtität, Bochum, unpublished report.

Schäfer, T. (1990), Ultraschallunguntersuchungen an Granitbohrkerne der Bohrung Soultz-sous-Forêts bezüglich einer Abschätzung von in-situ Spannungen anhand von Riessschliessungdrücken., Diploma thesis, 119 pp, Ruhr - Universität, Bochum.

Stress heterogeneity in the Soultz granite inferred from analysis of wellbore failure to 5 km depth

Benoît Valley* & Keith Evans*
**Engineering geology, ETH Zürich, Switzerland*

Presented at the Soultz Scientific Meeting at Soultz-sous-Forêts on 28-29 June 2007

EC Contract SES6-CT-2003-502706

PARTICIPANT ORGANIZATION NAME: Engineering Geology, ETH Zürich.

Related with Work Package FP6-WP5

Related with Working Group WG4, 'Hydraulics and induced seismicity'

STRESS HETEROGENEITY IN THE SOULTZ GRANITE INFERRED FROM ANALYSIS OF WELLBORE FAILURE TO 5 KM DEPTH

Benoît Valley and Keith F. Evans

Engineering Geology, Department of Earth Sciences, ETH Zürich, Switzerland

e-mail: valley@erdw.ethz.ch

ABSTRACT

Stress induced wellbore failure constitutes one of the best indicators of the orientation of the principal horizontal stresses. At Soultz-sous-Forêts, analysis of breakouts and drilling induced tension fractures (DITFs) between 1.4 km and 5 km depth in boreholes GPK3 and GPK4 indicated a mean orientation for the maximum horizontal principal stress of N169°±14°. However, significant variations in orientation about the mean are recognised, which reflect heterogeneity of the stress field. Such heterogeneity is thought to play an important role in determining the scale of failure in earthquakes, and may be a key factor governing the specific response of rock masses to stimulation injections. Despite its importance, insufficient is known about the magnitudes and spatial variations of stress variations in the crust, primarily because it is so difficult to characterise. Wellbore failure in the form of breakouts ad drilling-induced tension fractures (DITFs) constitute one the best direct methods of studying stress heterogeneity. In this paper we report results of an on-going study of variations in stress orientation along the trajectories of the two 5 km holes, GPK3 and GPK4, at Soultz. Significant variations are seen to occur at various scales, from relatively abrupt change over a couple of metres to much longer wavelength variations over several hundred metres. Deviations of the SHmax orientation of 45° occasionally occur. Scaling of the variations is found to be self-affine. Large wavelength variations (>50 m) are partially correlated in the upper part of the well (inter-well distance is about 20 m) and not correlated in the lower part of the well (inter-well distance is about 600 m), but they are in both case related with major structures, Short wave length variations can in most cases be directly associated with natural fractures intersecting the wells. The results suggest that the stress perturbations constitute remnant stresses arising from slip on the fractures in the past.

INTRODUCTION

Analysis of stress induced wellbore failure is a powerful tool to characterise the state of stress (e.g. Bell and Gough, 1979; Zoback et al., 2003). In rocks without strong strength anisotropy, the failure is controlled by the variation in tangent stress that develops around the wellbore circumference when the maximum stresses in the plane normal to the wellbore are not equal. Failure may be compressional where the tangent stresses are a maximum producing breakouts, or tensile where they are a minimum, giving rise to so-called drilling-induced tension fractures (hereafter referred to as DITFs). Wellbore failure occurs in the 5 km deep wells at Soultz-sous-Forêts, with DITFs dominating above 3 km and breakouts below 3.5 km. The data have been analysed by Valley and Evans (2007) to obtain the linear trends of the stress tensor variation with depth as needed for site stress characterisation. That study ignored the small and medium scale deviations from the large-scale trends. Such perturbations are commonly called stress heterogeneities, and they are believed to play a significant role in earthquake complexity (e.g. Shaw, 2004; Zöller et al., 2005), faulting mechanism (e.g. Faulkner et al., 2006), errors in the stress estimates obtained from inversion of seismic focal mechanism (Scotti and Cornet, 1994; Cornet and Jianmin, 1995; Cuenot et al, 2006) and reservoir stimulation (e.g. Cornet et al., 1992). Despite their perceived importance, stress heterogeneities are difficult to reliably identify, let alone quantify. Stress-induced wellbore failure in deep holes offers perhaps the best opportunity to the spatial variability of stress. In this paper we present results of an on-going analysis of variations in stress in the Soultz wells to 5 km as expressed through the breakouts and DITFs. A novel aspect of the data is that the two wells that serve as the data source are separated by 15-30 m over the depth range 1.5-2.5 km, allowing the lateral variation of the stress perturbations as well as the vertical to be examined. Possible stress perturbing mechanisms which may explain these variations are discussed.

BACKGROUND

The effect of gravity is such that stress magnitudes usually increase with depth. Commonly, the increase at a particular locality is seen to be reasonably well approximated by linear trends in stress magnitudes, a vertical principal stress that is equal to the integrated overburden, and a constant orientation for the horizontal principal stresses. This description is referred to as the stress characterisation of a site, and its estimation through measurement is an important task in developing EGSs (Engineered Geothermal Systems). Throughout this paper, stress variations or perturbations shall be taken to mean deviations in stress from this simple linear description. There is good reason to believe that stress variations should occur on all scales. At the largest scale, geodynamic processes give rise to changes at scales large compared to lithospheric thickness, the so-called first and second order patterns of lithospheric stress variation (M.L. Zoback, 1992). At smaller scale, the perturbation of stress around faults that slip in earthquakes is demonstrated by the success of the Coulomb stress concept in predicting aftershock distributions (Harris, 1998). This perturbation occurs on scales of the order of the length of slip, and so since earthquakes occur on all scales, perturbations of stress can be expected on all scales. However, the magnitude of the variations in stress that can build up as a consequence of the repeated action of stress-perturbing mechanisms is tempered by the limited strength of the fractured and faulted crust. For example, a stress perturbation generated by slip on a fault can be partly relaxed by post-seismic slip on secondary fractures and faults, of which aftershocks are a manifestation. Thus, the processes at work are complicated, and our understanding

of the degree of stress variability that typically prevails within the crust (if one can generalise), is poor. This is has important implications for EGSs, because it bears on the issue of whether the state of stress at a prospective EGS site will be essentially the same as a site ten kilometres distant where stress has been characterised. In this regard it is important to note that the E-W orientation of minimum horizontal principal stress at Soultz is significantly different to the regional orientation of NE-SW. It is thus relevant to quantify the deviations in the state of stress from the simple linear characterisation and understand their origin.

One of the most detailed analyses of variations of breakout orientation and their implications for stress heterogeneity comes from the Cajon Pass research borehole (Shamir, 1990). Heterogeneity was seen to be pervasive, occurring at various scales. No correlation with lithologic variations, borehole deviation and trend, drill bit penetration rate or changes in biotite content were found. However, in several cases perturbations occurred in the vicinity of local faults. Three ways in which stress perturbations can develop at faults have been proposed in the literature:

1) The stress perturbation is due to slip on faults that occurs before drilling and is thus pre-existing.

2) The stress perturbation is due to slip on faults that occurs during drilling. The slip may be initiated by the local modification of the stress field at the advancing bottom hole or around the wellbore, or through changes in pore pressure related to the circulation of drilling mud.

3) The stress perturbation is due to changes in elastic parameters within the damaged zone of a fault. Such changes are capable of producing significant stress rotations (Faulkner et al., 2006).

Stress perturbations can also arise from changes in lithology, such as between different intrusive units, or between sandstones and shales within sedimentary sequences (e.g. Evans et al., 1989).

For the Cajon Pass well, Shamir (1990) found that deviations in breakout orientation along sections of the hole where they were more-or-less continuous were self-similarly distributed between wavelengths of 10 cm and 10 m. Since natural fractures were also found to follow a similar distribution, he concluded that the fault-related stress perturbations were largely a consequence of mechanism (1) and hence were pre-existing.

Several authors have attempted to reproduce observed changes in breakout orientation on faults of know dip by calculating the stress field generated by prescribed slip on the fault and superposing this on the large-scale stress field (Shamir and Zoback, 1992; 1990; Barton and Zoback, 1994; Hickman et al. 2000). There are many degrees of freedom in the exercise with regard to specifying the geometry of slip (i.e. direction, magnitude distribution, and the boundaries). Only the simplest geometries were considered with slip occurring on a square dislocation surface centred on the wellbore, and the slip direction taken parallel to the maximum shear stress acting on the plane arising from the far-field stresses alone. Nested dislocation surfaces were used to simulate slip distributions of given constant stress drop, and the resulting stress field computed with dislocation theory codes (Dunbar, 1984; Erickson, 1987). Results show that key features of breakout patterns, such as the length scale and the magnitude of the perturbation in breakout orientation and their occasional disappearance in the fault vicinity can be reproduced with reasonable slip values. Barton and Zoback (1994) found that total stress drop was needed to explain the observed change in orientation of breakouts near a fault. The size of slip patches was similar to the wavelength of the perturbations.

DESCRIPTION OF THE DATASET

The data analysed in this study stem from two of the three deep boreholes drilled to 5km in granite at the Soultz-sous-Forêts geothermal project site where the granite top lies at 1400 m. The holes, called GPK3 and GPK4, penetrate granite at 1.4 km, and were drilled from the same pad. Both are vertical in the upper 2-3 km, which means their separation in the granite between 1.4 km and 2.4 km is less than 20 m (Figure 1b). Below 2.5 km, the wells deviate from vertical to build up separation before returning to sub-vertical in the lowermost 500 m (Figure 1a/2a). The upper and lower granite sections of the holes were drilled with two different bit sizes. A 12-1/4 inch bit size was used to 4583 m MD in GPK3 and 4757 m MD for GPK4, and 8-1/2 inch bits below. MD denotes measured depth along hole from ground level, which is at an altitude of 167.9 m (IGN69) for both holes. Schlumberger UBI (i.e. acoustic borehole televiewer) logs were run in each section days to weeks after drilling (Valley and Evans, 2006). The UBI logs provide a detailed images of borehole geometry in cross-section and acoustic reflectivity of the borehole wall. The UBI logs were run with the ancillary GPIT module which provides sonde positioning and orientation information. The same UBI sonde operating at the same frequency was used for both holes. The rotary sampling rate gave an angular resolution of 2°, and the logging speed was chosen to give a scan every 1 cm along hole. Details of the measurement principle are given in Luthi (2001). The UBI images are generally of good quality with few logging artefacts. 'Key seats' (see Lofts and Bourke, 1999) are visible along the entire inclined 12-1/4 section and some parts of the inclined 8-1/2 section of GPK4, but they are easily identifiable and affect only a limited part of the borehole circumference.

Wellbore failure was identified from both the borehole geometry and acoustic reflectivity. Breakouts are typically manifest as pairs of diametrically-opposite spall zones that extend along the borehole axis. They occur where the maximum tangent stress acting at the borehole wall exceeds the compressive strength of the rock. In the simple case of a vertical borehole penetrating a rock mass in which one principal stress is vertical, this maximum occurs in the direction of the minimum principle horizontal stress, *Shmin* (Bell and Gough, 1979).

DITFs are identified primarily on acoustic reflectivity images where they show as thin, often ragged fracture traces that may be either axial or en-echelon. DITFs seen on UBI images from GPK1 do not show on Azimuthal Resistivity Imager logs, indicating they do no penetrate deeply. They occur when the tangent stress at the borehole wall becomes sufficiently tensile to produce tensile failure. Although, in principle, the minimum tangent stress produced by far-field stresses can be tensile, it is usually the cooling stress component arising from the circulation of cool drilling fluids that is decisive in driving the minimum tangent stress to negative values and producing tensile fracturing. However, the cooling stress is symmetric, and so the location of the tensile fracture is governed by the far-field principal stress orientations. In the case of a vertical borehole penetrating a medium in which one principal stress is also vertical, the least compressive tangent stress at the borehole wall is horizontal and occurs in the direction of *SHmax*. This results in a pair of diametrically-opposite DITFs, which hereafter are denoted by A-DITFs. However, if the borehole axis is not aligned with a principal axis and the criterion for tensile failure is met, the least compressive tangent stress at the borehole wall will in general be inclined to the borehole circumference. In this case, tensile failure will occur as a stack of slightly-overlapping en-echelon tensile fractures, which hereafter are denoted by E-DITFs. The relationship between the induced fracture geometry and the in-situ stress orientations and magnitudes in this case is not as simple as in the aligned case (e.g. Peška and Zoback, 1995).

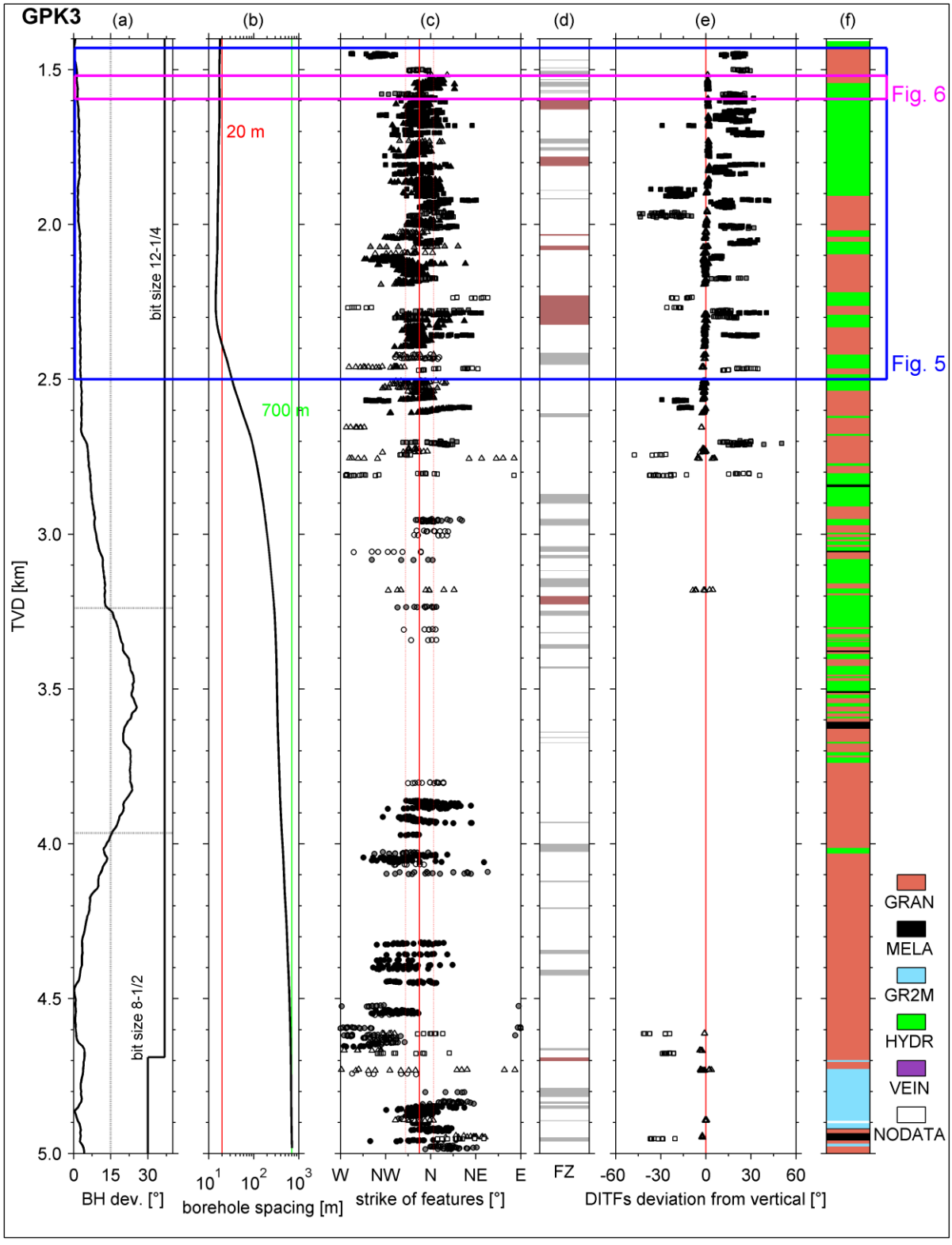

Figure 1: Stress induced wellbore failure data for the borehole GPK3: a) borehole deviation from vertical and bit size. b) horizontal separation of the boreholes plotted on a logarithmic scale. c) azimuth of high-quality DITF (squares) and breakout (circles) identifications with the latter rotated anticlockwise through 90°. The mean azimuth of the collective data is denoted by the vertical red line. d) location and thickness of fracture zones that intersect the well. Brown bands indicate the zones with evidence of permeability. e) deviation from vertical of high-quality en-echelon DITF identifications. Positive values denote dip to the east. f) simplified profile of lithology showing granite types GRAN: standard granite, MELA: biotite rich or xenolith-rich granite, GR2M: fine grained 2-mica granite, HYRD: hydrothermalised granite, VEIN: quartz vein (modified after Dezayes et al., 2003).

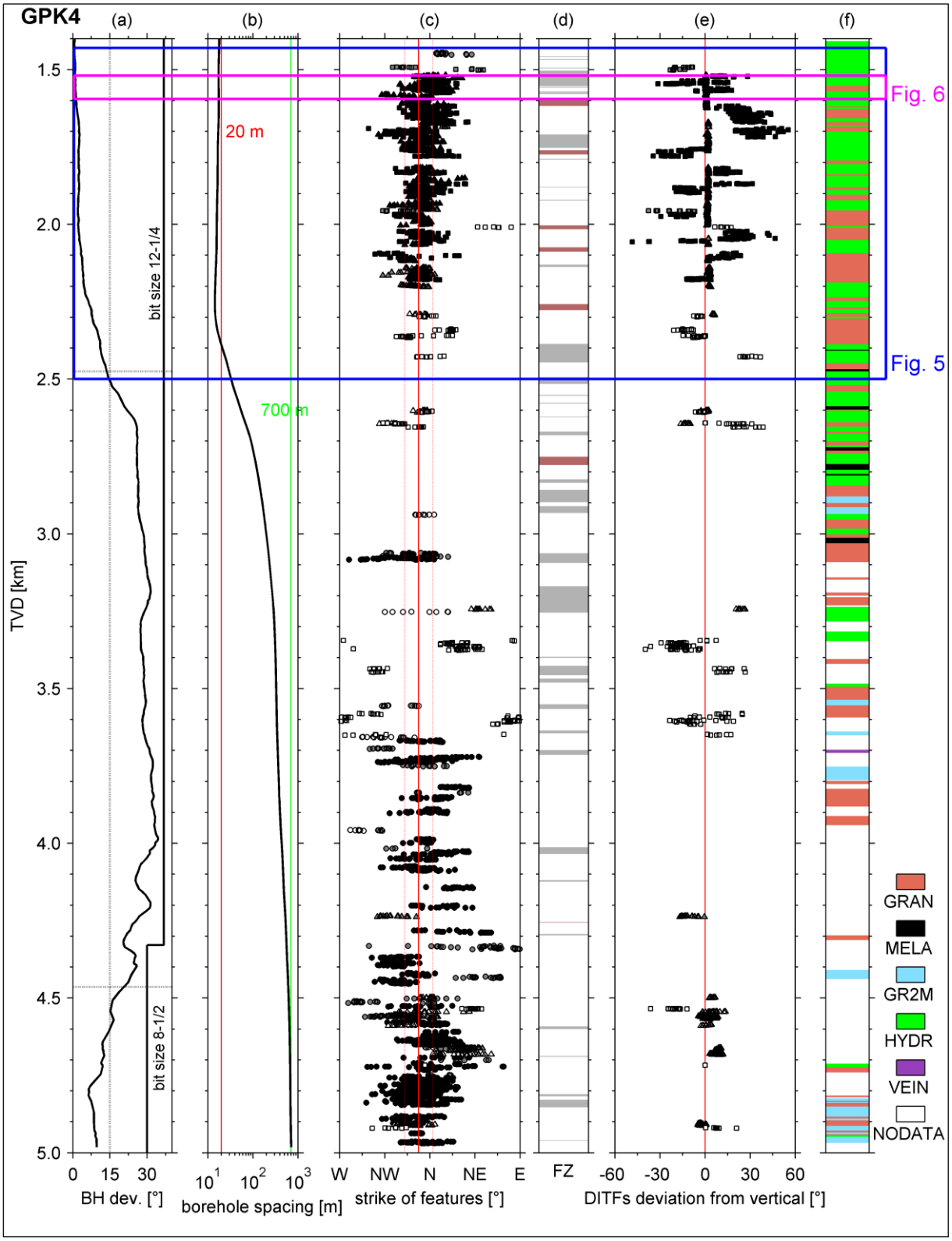

Figure 2: As Figure 1 but for GPK4. f) simplified lithology is modified after Dezayes et al. (2005).

The procedure employed in this study for describing the wellbore failure observations is as follows. First, intervals affected by either breakouts, A-DITFs or E-DITFs were identified. Then, for breakouts and A-DITFs, the mean azimuth of the two limbs of the features was determined for successive 0.5 m depth windows. For E-DITFs, the best-fitting plane to each fracture pair was found and the strike and dip of the plane noted. Typically, this led to one sample per 0.5 to 1 m. In all cases, the confidence of the identification was quantified by assigning an index ranging between 1 and 3, corresponding to low and high confidence respectively.

ANALYSIS OF VARIABILITY OF STRESS INDUCED FAILURE ORIENTATION

The orientation distributions of high-quality identifications of breakouts and DITFs in each borehole are shown in Figure 3. The stereographic plot of poles of the DITFs indicates a wide range of fracture strikes, although the rose diagram of Figure 3b makes clear that the vast majority of DITFs lie within 20° of the mean orientation with outliers being relatively few in number. A 5° discrepancy in mean orientation of the DITFs in the two boreholes is evident. A similar discrepancy is also seen for the breakout distributions of the two holes (Figure 3c). Given that the horizontal distance between boreholes is less than 35 m for the section where most of the DITFs occur (1400 m to 2500 m depth), so that essentially the same rock volume is sampled, the discrepancy must be due either to stress variations occurring over relatively short horizontal distances or to systematic error in the logging process. The former explanation seems most improbable, given that the observations span a depth range of 3.5 km. Different GPIT sondes were used in GPK3 and GPK4, the same sonde being used for both sections of each well. Thus, calibration error is possible.

The modal peaks of the breakout distributions, rotated through 90° in Figure 3c to permit direct comparison with the DITFs, are essentially identical to means of the DITF populations for the same hole. The distributions of the strikes of breakouts show greater scatter than the DITFs. This is at least partially due to the angular width that breakouts span which makes the determination of their representative orientation more uncertain than for DITFs. A slight asymmetry of the distribution is also visible for each borehole but particularly for GPK3 data: around the mode of the distribution which is about aligned with the DITFs strike directions, the breakouts orientation distribution is slightly overbalanced on the counter clockwise side. This may reflect a bimodal distribution with a main mode at 168° and a weak secondary mode at about 150°. Such a deviation may be related with the slight deviation of the hydro-thermally altered shear structures which shows a counter-clockwise bias comparing to the mean orientation of all fractures (Evans et al., 2005, Fig. 3).

A-DITFs and E-DTFs are clearly distinguished in Figure 3a, the former lying around the margin of the stereoplot, and the latter lying inside. E-DITFs with small deviation from axial are rare or absent, indicating that a critical deviation of the 'vertical' principal stress from alignment with the borehole axis is required before DITFs form in the en-echelon mode, as predicted from theory (Ito et al., 2001). With very few exceptions, deviations from verticality are less than 30°. Non-vertical DITFs dip preferentially to the east. In that respect, they mimic natural fractures which show a similar preference in the upper section of the wells (Valley et al., 2007).

The depth profile of variations of breakouts and DITF orientation are shown in Figure 1b and 2 b for GPK3 and GPK4 respectively. DITFs occur almost exclusively above 3.0 km, whereas only breakouts are confidently identified below 3.7 km. This partitioning of the different modes of failure reflects the depth trends of stress magnitude, as discussed by Valley and Evans (2007). Here we are interested only in the variation in the orientation of the horizontal principal stresses that the two indicators imply. Evidently, depth sections where the indicators have a stable orientation are rare: in most cases, the continuous sections of breakouts or DITFs show locally-progressive rotation in one direction or the other. The variations occur at all scales. This is demonstrated in Figure 4 where the power spectra of the deviation of the orientation from the mean for GPK4 is shown. The spectra were computed using the periodogram method on sections of relatively continuous data to avoid bias introduced by gap-filling (e.g. Stoica and Moses, 1997).

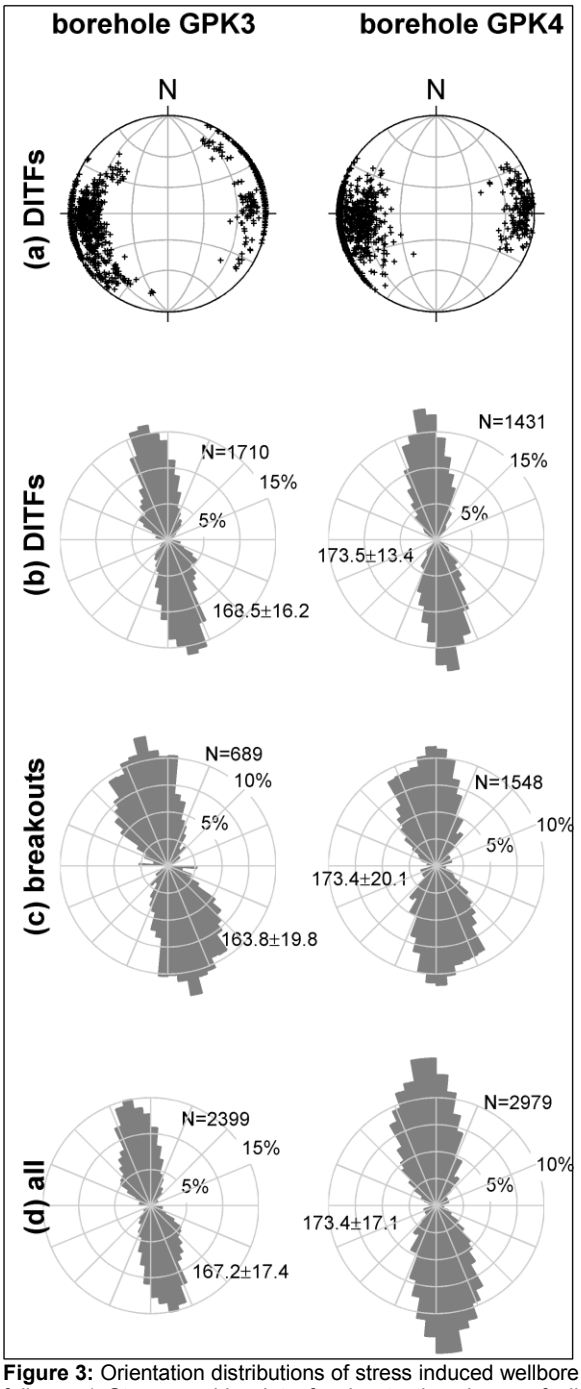

Figure 3: Orientation distributions of stress induced wellbore failure. a) Stereographic plot of poles to the planes of all high-quality DITF identifications (equal area, lower hemisphere). b) Polar plot of strikes of all high-quality DITFs. c) Polar plot of strikes of all high-quality breakout identifications rotated anticlockwise through 90° to permit direct comparison with the DITFs. d) Polar plot of strikes of all features together. Here also, 90° is added to breakouts direction. For all polar plots, *N* is the number of data point and the circular mean and single standard deviation is given.

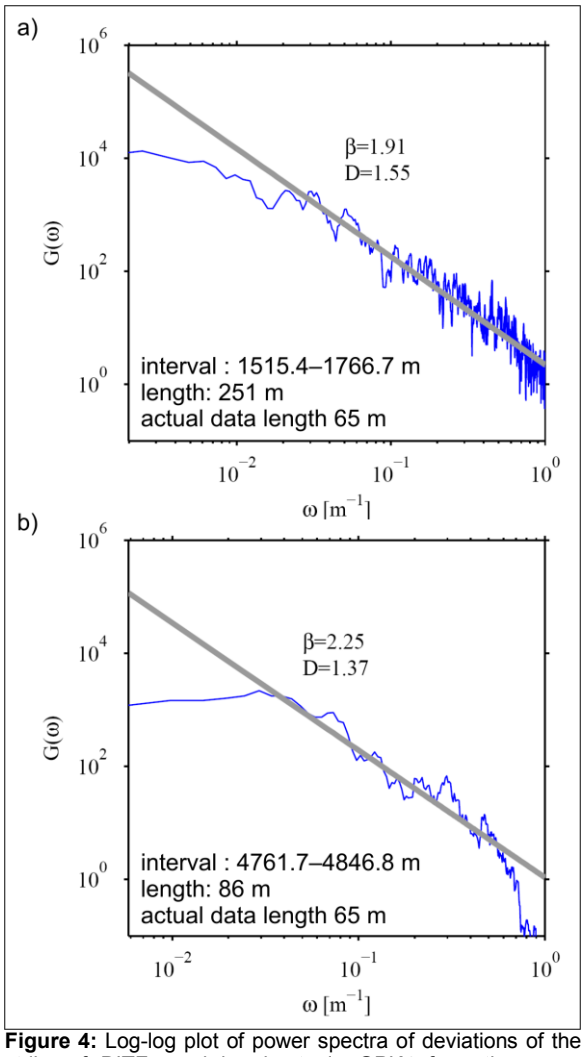

Figure 4: Log-log plot of power spectra of deviations of the strike of DITFs and breakouts in GPK4 from the mean orientations for the wells. a) The spectrum for a data section in the upper part of the well where DITFs occur more or less continuously. Small gaps were filled with straight lines before interpolating. No filter was applied. b) Same as a) but for a data section taken near the well bottom where breakouts occur. β denoted the slope of the roll-off towards higher spatial wavenumbers is indicated by the fitted line.

It is evident that at high spatial frequencies, the spectral decay conforms relatively closely with a linear trend indicating that the orientation variations follow a power law. The slopes, β, of the linear 'roll-offs' were determined by least-square fitting over the appropriate frequency band, ignoring deviation from linearity in the spectra extremities, and found to be close to -2.0. Power laws with slopes greater than -3.0 indicate a fractal process (Power and Tullis, 1991; Turcotte, 1989). A slope of -3.0 indicates self-similarity (i.e. scale invariance). Orientation variations that follow a power law with a slope of -3 would thus look identical at all scales (Power and Tullis, 1991). Slopes greater than -3 indicate self-affine behaviour, where variations look progressively rougher at smaller scales. The reduction of the magnitude of the variations with respect to wavelength with increasing wavelength implied by self-affine scaling is expected for directional data where the maximum deviation is limited to 90°. These power laws hold for wavelengths from 4 m up to 80 m, the longest wavelength that could be resolved from the short data spans. So it is clear that variations in horizontal principal stress orientation occur at various scales.

In the following, we will examine in more detail the variations that occur at long and short wavelengths. Long wavelength variations are taken to be those which are coherent at scales larger than 50 m. Since this is larger than the spacing between the wells between 1.5 and 2.5 km, where DITFs dominate, such variations seen in the vertical profiles of stress orientation should be relatively coherent between wells, assuming that their lateral extent is similar to their vertical. We will limit the study to changes in orientation of the horizontal stresses. The deviations from verticality of the 'vertical' principal stress as indicated by the E-DITFs will be examined in a later report.

Large scale stress variations

Long-wavelength variations in horizontal principal stress orientation can only be detected where wellbore failure occurs more or less continuously over large section of hole. This essentially restricts the study to the uppermost 1000 m of the granite where DITF failure occurs, and the lowermost 1.2 km where compressional failure is frequent. Long-wavelength variations in SHmax orientation can be seen in both sections in the plots of breakouts and DITFs azimuths in Figures 1c and 2c.

Considering the lower section first, significant deviations with wavelengths of several hundred metres can be seen near the bottom of both wells. The deviations amount to several tens of degrees, and are in the opposite direction in each well. Since the well bottoms are separated by some 600 m, there is no reason to expect that the two directions should be the same (i.e. that the stress perturbation is laterally coherent on scales of more than 600 m). To explain such large wavelength variations as due to the stress generated by slip on a fault would require slip to occur on a large scale, which implies a large fault. The probable explanation for the 400 m wavelength deviation in GPK3 is that it reflects the stress perturbation associated with a major fault that is penetrated at 4697 m TVD. This fault strikes approximately N160°E and dips at 50–60° to the west (Dezayes et al., 2004; Sausse et al., 2007), and is most certainly a structure that extends many hundreds of metres. If the structure dips at 60°, then it would lie within 100 m of the borehole over the ±200 m length of the stress orientation perturbation. A transition from breakouts to DITFs is seen to occur near the intersection of this structure with the well, indicating that stress magnitudes are also perturbed. Another potential contribution to the stress heterogeneity near the bottoms of the holes might arise from a lithological change from standard 'Soultz' porphyritic granite to a 'two-mica' granite that occurs near 4720 m TVD. The change is believed to reflect the interface between two separate intrusions. Stress perturbations might result from contrasts in elastic moduli. Since the elastic moduli of the two mica granite has currently not been measured, this possibility remains uncertain. In any case, the dominant factor is almost certainly the fault at 4697 m TVD in GPK3.

The large-wavelength perturbations in the upper section are particularly interesting because the two wells are less than 20 m apart and thus significant coherence between the variations in the wells might be expected. Figure 5 shows the DITF strike determinations for the upper section of the both wells. The data were interpolated to produce a continuous series, and a 100 m moving window (boxcar) applied to reveal the long-wavelength fluctuations. Some coherency between the two curves is evident, particularly between 2050-2250 m where the curves track each other well, and the gaps in wellbore failure, which are also manifestations of changing stress conditions, occur at the same point. However, the large 20° excursion in GPK3 of wavelength 300 m centred at 1950 m is not seen in GPK4. The partial coherence in the DITF-strikes between the two wells is illustrated in the cross-plot of Figure 5b. Linear

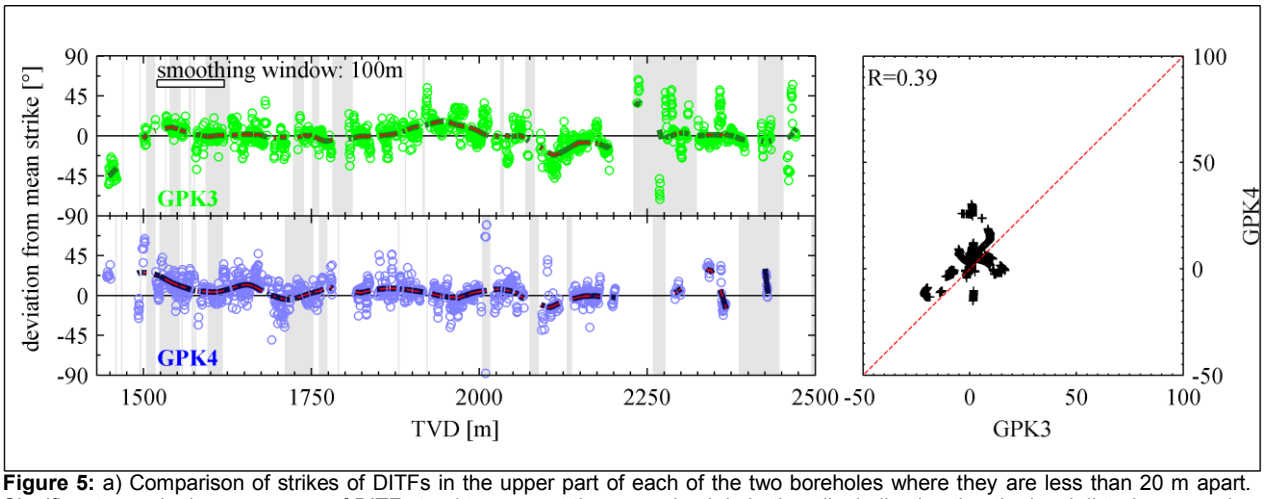

Figure 5: a) Comparison of strikes of DITFs in the upper part of each of the two boreholes where they are less than 20 m apart. Significant gaps in the occurrence of DITFs tend to occur at the same depth in both wells, indicating that the local disturbance to the stress field that inhibited failure is coherent between wells. The dark lines show the long-wavelength variations and were produced by smoothing the data with a 100 m boxcar filter. The location and width of fracture zones is indicated by the vertical grey bands. b) Cross-plot of long-wavelength deviations from the mean strike given by the smoothed curves.

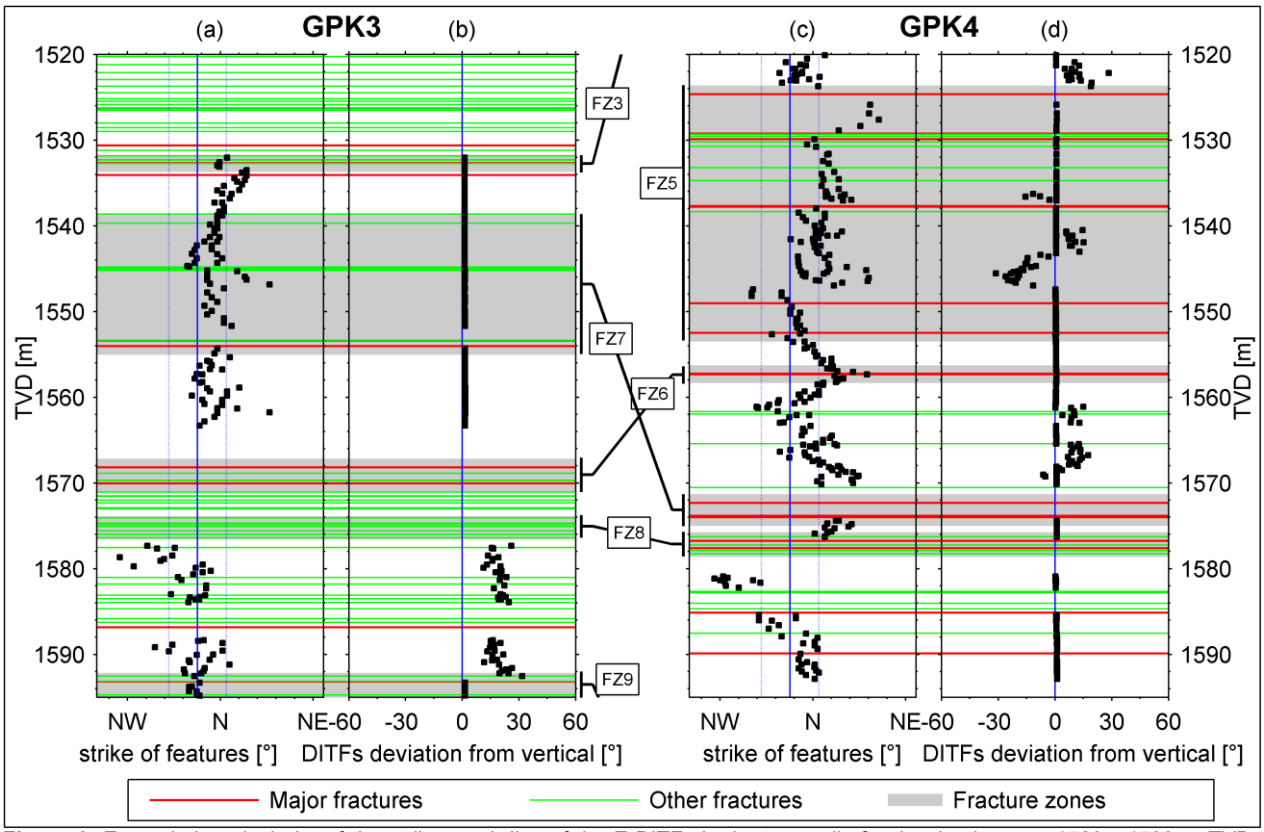

Figure 6: Expanded vertical plot of the strikes and dips of the E-DITFs in the two wells for the depth range 1520 - 1590 m TVD indicated by the box in Figures 1 and 2. The horizontal bands indicate to intersection of wells with fractures and fracture zones, some of which can be traced between boreholes (they intersect the wells at different depths owing to their dip). Progressive rotation of the DITF strikes over short intervals occurs frequently in GPK4, occasionally accompanied by changes in inclination. These short-wavelength variations in orientation, and the gaps in their occurrence, tend to be associated with fractures. The pattern of short-wavelength variation in the orientation of the DITFs in GPK3 is markedly different, although both indicate that on average the maximum principal horizontal stress in the 50 m section from 1520 to 1570 m is deviated from the mean orientation by 15-20° towards the east, indicating coherency at longer wavelengths.

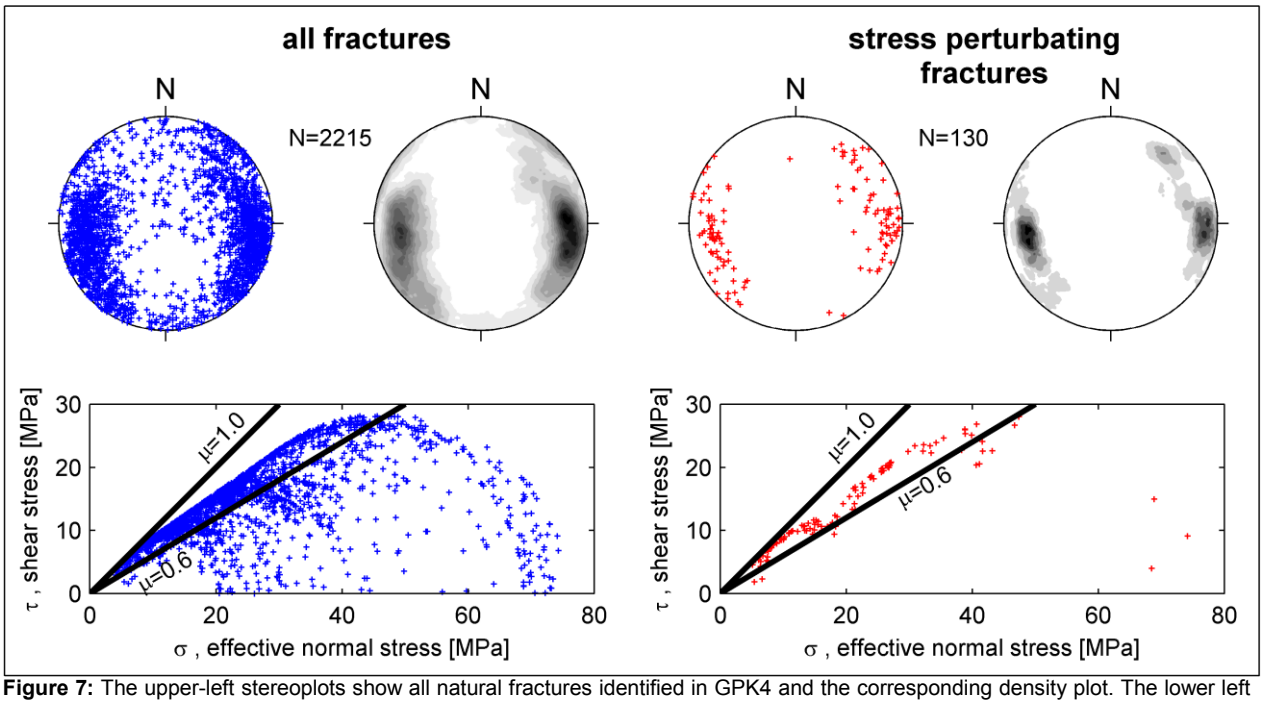

Figure 7: The upper-left stereoplots show all natural fractures identified in GPK4 and the corresponding density plot. The lower left figure shows the shear and normal stress resolved on these fractures assuming the linear stress characterisation given by Valley and Evans (2007). Failure lines appropriate for a coulomb strength criterion with coefficients 0.6 and 1.0 are shown. The right part of the figure shows the same as the left, but for fractures identified as 'stress perturbing'.

regression gives a regression coefficient between the two wells of 0.39. Given the closeness of the wells, it is difficult to understand how significant changes in stress orientation that occur vertically over scales of 100 m or more would not extend laterally only 20 m.

The origin of this discrepancy is uncertain, although a reasonable working hypothesis is that it is related to a major fracture zone that intersects the wells near this depth. This fracture zone is most certainly a major structure, perhaps of the same scale as the fault intersected at 4697 m TVD in GPK3 that was associated with the primary large-scale perturbation in the lower section of the reservoir. The zone was first intersected in GPK2 at 2110 m during the initial drilling of the well in 1995, and resulted in total loss of circulation fluid. No cuttings were obtained from the well during the subsequent drilling to 3876 m because they were swept into the fracture zone along with the drilling fluid. The zone was eventually plugged with 23 m^3 of cement during the extension of GPK2 to 5000 m in 1999. It is thus a zone of enormous capacity that has had a great deal of solid material injected into it. The structure dips at 74° to N95°E and crosses both wells at the bottom of the orientation discrepancy. The discrepancy might thus reflect a particularly strong lateral gradient in stress arising from the perturbation associated with this fracture zone.

Small scale stress variations

Small-scale variations have wavelengths less than 50 m. As noted earlier, it is rare for the strike of breakouts or DITFs to remain stable over tens of metres of borehole. More commonly, they rotate systematically in one direction of another for a short distance, giving rise to the seemingly horizontal streaks in Figures 1c and 2c. Deviations from the mean orientation of more than 45° occasionally occur. This behaviour is made clear in Figure 6 which shows vertically-expanded plots of DITF data from 1520-1595 m TVD. The variations in strike indicate that more often than not the azimuth of the principal horizontal stresses is rotating as one moves along the borehole. The trends are maintained for only a short distance before they reverse. The reversal points are almost always associated with the intersection of fractures and fracture zones with the boreholes, indicating that the rotations are related to stress perturbations localised at the fractures (Figure 6). Similarly, breakouts and DITFs tend to systematically stop or start at such features, or undergo abrupt changes in orientation. Gaps in otherwise continuous wellbore failure also commonly coincide with major fractures or fracture zones, again indicating a local change in stress state to one that does not produce wellbore failure (Figure 5). These observations are consistent with the conclusions of earlier workers that the rotations in the breakout and DITF orientations reflect the remnant stresses arising from slip on fractures that occurred some time in the past that predates the start of drilling. Just when the slip occurred is uncertain. Under the present-day stress field, 89% of the fractures that are associated with stress perturbations are critically-stressed, meaning that they require Coulomb friction strengths with coefficients of between 0.6 and 1.0 to remain stable (Figure 7). This compares with 70% for the entire fracture population. So the failure may reflect the on-going accommodation of crustal deformation (Zoback and Townend, 2001). However, it is also possible that failure and the generation of the stress perturbation predates the contemporary stress situation.

CONCLUSION

Variations in the orientation of breakouts and DITFs about their mean have been analyzed to investigate heterogeneity in the orientation of the horizontal principal stresses along the trajectory of the 5 km deep boreholes GPK3 and GPK4 at the Soultz site. The results to date suggest:

1) Variations in the wellbore failure orientation occur at various scales. Power spectral analysis of strike variations shows that the variations follow a power law with index close to -2, indicative of self-affine behaviour where variations look progressively rougher at smaller scales. The reduction in magnitude with respect to the wavelength with increasing wavelength implied by self-affine scaling is expected for directional data where the maximum deviation is limited to 90°.

2) Large scale variations in horizontal principal stress orientation with wave length greater than a hundred metres are also evident in the data. In the uppermost 1000 m of the granite, where the borehole separation is less than 20 m, the variations are partially correlated. The main variation in the uppermost borehole section is related to an observed major structure. Similarly another major variation observed in the lower section in GPK3 is also associated with a major structure described in that well. More generally, the large-scale variations are best explained as reflecting the stresses arising from slip on large-scale structures that may or may not intersect the wells.
3) The association of stress perturbations with natural fractures is evident in the analysis of short wavelength (<50 m) variations in stress orientation.
4) Almost all of the fractures which are associated with stress perturbations are critically stressed under the large-scale linear stress characterisation that prevails at the site. Thus, it is possible that they failed and generated the stress perturbations relatively recently, reflecting accommodation of on-going tectonic deformation of the crust. However, the data do not require this, and it is just as likely that the slip that generated the stress perturbations is much older.

ACKNOWLEDGMENTS

This work is supported by the Swiss State Secretariat for Education and Research under project number 03.04.60, and was performed as a contribution to the European Union's FP6 project 'Soultz EGS Pilot Plant' funded by ADEME, BMU, EC and EEIG 'Exploitation Minière de la Chaleur'.

REFERENCES

Barton, C. A., and M. D. Zoback (1994), Stress perturbations associated with active faults penetrated by boreholes: Possible evidence for near-complete stress drop and a new technique for stress magnitude measurements, *Journal of Geophysical Research*, 99 (B5), 9373–9390.

Bell, J. S., and D. I. Gough (1979), Northeast-southwest compressive stress in alberta: Evidence from oil wells, *Earth and Planetary Science Letters*, 45, 475–482.

Bérard, T. (2003), Estimation du champ de contrainte dans le massif granitique de Soultz-sous-forêts, implication sur la rhéologie de la croûte fragile, Ph.D. thesis, Institut de Physique du Globe.

Cornet, F. H., and Y. Jianmin (1995), Analysis of induced seismicity for stress field determination and pore pressure mapping, *Pure and Applied Geophysics*, 145 (3), 677–700, doi:10.1007/BF00879595.

Cornet, F. H., Y. Jianmin, and L. Martel (1992), Stress heterogeneities and flow paths in a granite rock mass, pre-workshop volume for the workshop on induced seismicity, in *33rd U.S. Symposium on Rock Mechanics 184*.

Cuenot, N., et al. (2006), Faulting mechanisms and stress regime at the European HDR site of Soultz-sous-Forets, France, *Geothermics*, *35*, 561-575.

Dezayes, C., A. Genter, G. Homeier, M. Degouy, and G. Stein (2003), Geological study of gpk3 hfr borehole (Soultz-sous-Forêts, france), Tech. Rep. RP-52311-FR, BRGM.

Dezayes, C., A. Genter, and S. Gentier (2004), Fracture network of the EGS geothermal reservoir at Soultz-sous-Forêts (Rhine graben, France), in Geothermal Research Council 2004.

Dezayes, C., P. Chevremont, B. Tourlière, G. Homeier, and A. Genter (2005), Geological study of the GPK4 HFR borehole and correlation with the GPK3 borehole (Soultz-sous-forêts, france), Tech. Rep. RP53697-FR, BRGM.

Dunbar, S. (1984), DIS3d a three dimensional fault modelling program. Stanford University.

Erickson, L. (1987), User's manual for dis3d: A three dimensional dislocation program with applications to faulting in the earth. Stanford University.

Evans, K. F., T. Engelder and R. A. Plumb (1989), Appalachian Stress Study 1. A Detailed Description of In Situ Stress Variations in Devonian Shales of the Appalachian Plateau, *journal of Geophysical Research*, *94*, 7129-7154.

Evans, K. F. (2005), Permeability creation and damage due to massive fluid injections into granite at 3.5 km at Soultz: 2. critical stress and fracture stength, *Journal of Geophysical Research*, 110 (B4).

Evans, K. F., A. Genter, and J. Sausse (2005), Permeability creation and damage due to massive fluid injections into granite at 3.5 km at Soultz: 1. borehole observation, *Journal of Geophysical Research*, 110 (B4).

Faulkner, D. R., T. M. Mitchell, D. Healy, and M. J. Heap (2006), Slip on 'weak' faults by the rotation of regional stress in the fracture damage zone, *Nature*, 444 (7121), 922–925, 0028-0836 doi:10.1038/nature05353

Genter, A., C. Castaing, C. Dezayes, H. Tenzer, H. Traineau, and T. Villemin (1997), Comparative analysis of direct (core) and indirect (borehole imaging tools) collection of fracture data in the hot dry rock Soultz reservoir (france)., *Journal of Geophysical Research*, 102 (B7), 15,419–15,431.

Harris, R. A. (1998), Introduction to special section: Stress triggers, stress shadows and implications for seismic hazard, *J. Geophys, Res.*, *103*, 24,347-324-358.

Hickman, S., M. D. Zoback, C. A. Barton, R. Benoit, J. Svitek, and R. Summers (2000), Stress and permeability heterogeneity within the dixie valley geothermal reservoir: recent results from well 82-5, in *25th Workshop on Geothermal Reservoir Engineering*, pp. 256–264, Stanford.

Ito, T., M. D. Zoback, and P. Peska (2001), Utilization of mud weights in excess of the least principal stress to stabilize wellbores: Theory and practical examples, *SPE Drilling and Completion*, *16*, 221-229.

Lofts, J. C., and L. T. Bourke (1999), The recognition of artefacts from acoustic and resistivity borehole image devices, in Borehole Imaging: applications and case histories, Special Publications, vol. 159, edited by M. A. Lovell, G. Williamson, and P. K. Harvey, pp. 59–76, Geological Society, London.

Luthi, S. M. (2001), Geological well logs : their use in reservoir modeling, Springer.

Peška, P., and M. D. Zoback (1995), Compressive and tensile failure of inlclined well bores and determination of in situ stress and rock strength, *Journal of Geophysical Research*, 100 (B7), 12,791–12,811.

Sausse, J., C. Dezayes, and A. Genter (2007), From geological interpretation and 3D modelling of the characterization of the deep seated EGS reservoir of Soultz (France), in EHDRA scientific conference, 28 - 29 June 2007, Soultz-sous-Forêts, France.

Scotti, O., and F. H. Cornet (1994), In-situ evidence for fluid-induced aseismic slip events along fault zones, *Int. J. Rock Mech. Min. Sci. & Geomech. Abst.*, *31*, 347-358.

Shamir, G. (1990), Crustal stress orientation profile to a depth of 3.5km near the san andreas fault at cajon pass, california, Ph.D. thesis, Stanford University.–Dept. of Applied Earth, Sciences, oCLC's Experimental Thesis Catalog [http://alcme.oclc.org/xtcat/servlet/OAIHandler] (United States) ER.

Shamir, G., and M. D. Zoback (1992), Stress orientation profile to 3.5 km depth near the san andreas fault at cajon pass, california., *Journal of Geophysical Research*, 97 (B4 Solid Earth and Planets), 5059–5080.

Shaw, B. E. (2004), Dynamic heterogeneities versus fixed heterogeneities in earthquake models, *Geophysical Journal International*, 156 (2), 275–286, doi:10.1111/j.1365-246X.2003.02134.x.

Stoica, P., and R. Moses (1997), Introduction to Spectral Analysis, Prentice-Hall.

Valley, B., and K. F. Evans (2006), Strength and elastic properties of the Soultz granite, paper presented at EHDRA Scientific meeting june 2006, Soultz-sous-Forêts.

Valley, B., and K. F. Evans (2007), Stress state at Soultz-sous-forêts to 5 km depth from wellbore failure and hydraulic observations, in *32nd workshop on geothermal reservoir engineering*, Stanford.

Valley, B., C. Dezayes, and A. Genter (2007), Multi-scale fracturing in the Soultz-sous-forêts basement from borehole images analyses, in EHDRA scientific meeting, 28 and 29 June 2007, Soultz-sous-Forêts.

Zoback, M. L. (1992), First- and second-order patterns of stress in the lithosphere: The World Stress Map project, *J. Geophys, Res.*, *97*, 11,703-711,728

Zoback, M. D., and J. Townend (2001), Implications of hydrostatic pore pressures and high crustal strength for the deformation of intraplate lithosphere, *Tectonophysics*, *336*, 19-30. Zoback, M. D., C. A. Barton, M. Brudy, D. A. Castillo, T. Finkbeiner, B. R. Grollimund, D. B. Moos, P. Peska, C. D. Ward, and D. J. Wiprut (2003), Determination of stress orientation and magnitude in deep wells, *International Journal of Rock Mechanics and Mining Sciences*, 40 (7-8), 1049–1076.

Power, W. L., and T. E. Tullis (1991), Euclidean and fractal models for the description of surface roughness, *Journal of Geophysical Research*, *96*, 415-424.

Zöller, G., M. Holschneider, and Y. Ben-Zion (2005), The role of heterogeneities as a tuning parameter of earthquake dynamics, *Pure and Applied Geophysics*, 162 (6), 1027–1049, doi:10.1007/s00024-004-2660-9.

Stress state at Soultz-sous-forêts to 5 km depth from wellbore failure and hydraulic observations.

Benoît Valley* & Keith Evans*
**Engineering geology, ETH Zürich, Switzerland*

Presented at the 32nd Workshop on Geothermal Reservoir Engineering, Stanford University, Stanford, California, January 22-24 2007

PROCEEDINGS, Thirty-Second Workshop on Geothermal Reservoir Engineering
Stanford University, Stanford, California, January 22-24, 2007
SGP-TR-183

STRESS STATE AT SOULTZ-SOUS-FORÊTS TO 5 KM DEPTH FROM WELLBORE FAILURE AND HYDRAULIC OBSERVATIONS.

Benoît Valley
Keith F. Evans

ETH Zürich – Engineering geology
ETH Hoenggerberg
Zürich, CH-8093, Switzerland
e-mail: valley@erdw.ethz.ch

ABSTRACT

Observations of breakouts and drilling-induced tension fractures (DITFs) in two 5 km deep boreholes of the European Enhanced Geothermal Project of Soultz-sous-Forêts, France have been combined with the analysis of pressure data from stimulation tests in all 3 deep wells to obtained a description of the state of stress in the granite down to 5 km depth. The orientation of the maximum horizontal stress, SHmax, in the 5 km deep reservoir is found to be N169°E±14°, in accord with previous results from the 3.5 km reservoir. Analysis of pressure at the casing shoe of the deep boreholes during stimulation permits the profile of Shmin magnitude to be extended down to 5 km depth. Finally, by combining all available information, bounds were set on the magnitude of SHmax. The result is a linear characterisation for the stress state at Soultz that is valid between depths of 1.5-5.0 km (excluding the effects of local stress heterogeneity).

INTRODUCTION

Knowledge of the state of stress is very important for the development of Enhanced Geothermal Systems (EGSs), not least because it is a primary factor influencing the reservoir response to the massive stimulation injections. Knowledge of the stress state in the 5 km deep reservoir at Soultz-sous-Forêts is largely based upon extrapolation of the characterisation defined for the shallower reservoir to 3.5 km depth. Although this has been extensively studied, some questions remain, principally with regard to the magnitude of the maximum horizontal principal stress, SHmax. This paper presents some new results that directly constrain the stress state in the deep reservoir, including the magnitude of SHmax. The constraints arise principally from analysis of breakouts and drilling-induced tension fractures (DITFs) on ultrasonic borehole wall images from two of the three wells that penetrate the deep reservoir. It is well established that these features constitute one of the best indicators of the orientation of the principal horizontal stresses. However, since they represent stress-induced failure of the wellbore, a careful analysis of the conditions of their formation allows constraints to be placed upon stress magnitudes. To obtain unique values for the two principal horizontal stress magnitudes requires that one be independently specified. Thus we analyse downhole pressure data from stimulation injections to estimate the magnitude of Shmin, and use this in the analysis of wellbore failure to constrain the magnitude of SHmax.

DESCRIPTION OF THE DATASET

The data analysed in this study stem from two of the three deep wells drilled to 5km at the Soultz-sous-Forêts geothermal project site, located in the Rhine Graben north of Strasbourg, France. The two wells, called GPK3 and GPK4, have both been drilled as deviated boreholes and reach a total true vertical depth of about 5km. GPK3 was drilled in 2002, while GPK4 was completed early in 2004. The geological section at Soultz consists of 1.4 km of Permian, Mesozoic and Cenozoic sediments underlain by a block-faulted, Hercynian age monzogranite basement. For more information about the project, refer to Dezayes (2005a).

Ultrasonic borehole images

The ultrasonic borehole televiewer images on which wellbore failure stress indicators were identified were obtained from Schlumberger Ultrasonic Borehole Imager (UBI) logs that were run with the ancillary GPIT module which provides sonde positioning and orientation information. The latter also includes two on-board temperature sensors that provide a measure of borehole temperature at the time the logs were run, which was shortly after the completion of drilling. Successful UBI logs were run in the granite section of both GPK3 and GPK4 to total depth (TD). The UBI tool provides detailed images of the ultrasonic reflectivity of the borehole wall together with borehole geometry sampled with an angular resolution of 2°. The logging speed is chosen that a

scan is made every 1 cm along hole. For detailed on measurement principle refer to Luthi (2001).

The GPK3 logs were acquired in two runs. The first run was acquired on 25th Oct. 2002 in the 12-1/4 inch section, some 5 days after the completion of drilling. This log extends throughout the 12-1/4 inch section from 1439 m MD (the casing shoe of a higher section) to 4532.6 m MD (MD denotes measured depth along hole from ground level). The images of the lowermost 13.8 m are not oriented**.** The second log was run on 10th Nov. 2002, some 21 days after the hole had been extended as 8-1/2 inch diameter to TD at 5103 m MD. The log covers the 8-1/2 inch section from the 12-1/4 inch casing shoe at 4558.2 m MD to 5100.8 m MD, with the lowermost 2.6 m not oriented. The images are generally of good quality with few logging artefacts. 'Key seats' (Lofts & Bourke, 1999) are visible along the entire inclined 12-1/4 section and some parts of the inclined 8-1/2 section, but they are easily identifiable and affect only a limited part of the borehole circumference.

The logs in the GPK4 borehole were also acquired in two runs that followed the drilling of the 12-1/4 inch and 8-1/2 inch sections. The log in the 12-1/4 inch was run on 15th Feb. 2004, some 15 hours after drilling, from 1421.3 to 4723.3 m MD. The log in the 8-1/2 inch section was run on 12th Apr. 2004, 18 hours after drilling operations ended, from 4730.3 to 5253.3 m MD. Images suitable for fracture geometry determination were obtained for 1445.3-4720.3 m MD and for 4757.3-5248.3 m MD. Outside these ranges, the logs are run in casing or suffer from acquisition problems.

Description of wellbore failure

Breakouts or drilling-induced tension fractures occur when the local value of tangent compression or tension respectively at the borehole wall exceeds the rock strength. Breakouts are typically manifest as pairs of diametrically-opposite spall zones that extend along the borehole axis. In the simple case of a vertical borehole penetrating a rock mass in which one principal stress is vertical, breakouts, if they occur, indicate the orientation of the Shmin (Bell & Gough, 1979).

Drilling induced tension fractures (DITFs) form where cooling of the borehole wall by circulation of mud during drilling results in a net tangent stress distribution about the hole that is sufficiently tensile at some point to produce failure. The net tangent stress is the sum of a tensile cooling component, which is axially-symmetric, and the natural wellbore stress concentration arising from the 'far-field' stresses, which are not necessarily axially-symmetric and may be everywhere compressive. In the case of a vertical borehole penetrating a medium in which one principal stress is also vertical, the least compressive value of the circumferential stress variation about the borehole due to the far field stresses occurs in the direction of SHmax. Thus, it is in this direction that the greatest tension develops and a pair of diametrically-opposite DITFs form. If the borehole axis is aligned with a principal stress, they will be axial, and denoted as A-DITFs. However, in the case where the borehole axis is not aligned with a principal axis, the criterion for tensile failure might still be met but then DITFs will tend to form as a stack of en-echelon induced fractures, denoted E-DITFs. The relationship between the induced fracture geometry and the in-situ stress orientations and magnitudes in this case is not as simple as in the aligned case.

The stress-controlled wellbore failure features were identified and described as follows. First, borehole intervals affected by either breakouts (BOs), axial drilling induced tension fractures (A-DITFs) or “en echelon” drilling induced tension fractures (E-DITFs) were identified. Then, for breakouts and A-DITFs the mean orientation of features was determined over successive 0.5 m depth windows. For E-DITFs the mean orientations (strike) of the best-fitting plane for each fracture pair were chosen. In all cases, the confidence of the identification was recorded by assigning an index ranging between 1 and 3, corresponding to low and high confidence respectively.

Similar counts of features were obtained for both boreholes. About 10% of the logged borehole lengths are affected by breakouts, 10% by A-DITFs, and 7% by E-DITFs. The orientation distributions with depth of the breakouts and DITFs in GPK3 are shown in Figure 1. The corresponding plot for GPK4 is given in Figure 2.

INTERPRETATION OF THE WELLBORE FAILURE TO CONSTRAIN STRESS STATE

Principal stress orientation

The inclination of the boreholes is shown in the left frames of Figures 1 and 2. The occurrence of A-DITFs along the vertical borehole sections suggests that one principal stress is locally vertical, whereas the presence of E-DITFs along such sections indicates a local deviation of the 'most vertical' principal stress from true verticality. Note that the E-DITFs are always fairly steep and deviate both to the east and to the west so that their mean orientation is about vertical. This suggests that one principal stress is, on average, vertical, with localised deviations from verticality indicating zones of stress heterogeneity. Thus, for the stress characterisation we take one principle stress as vertical and so only the

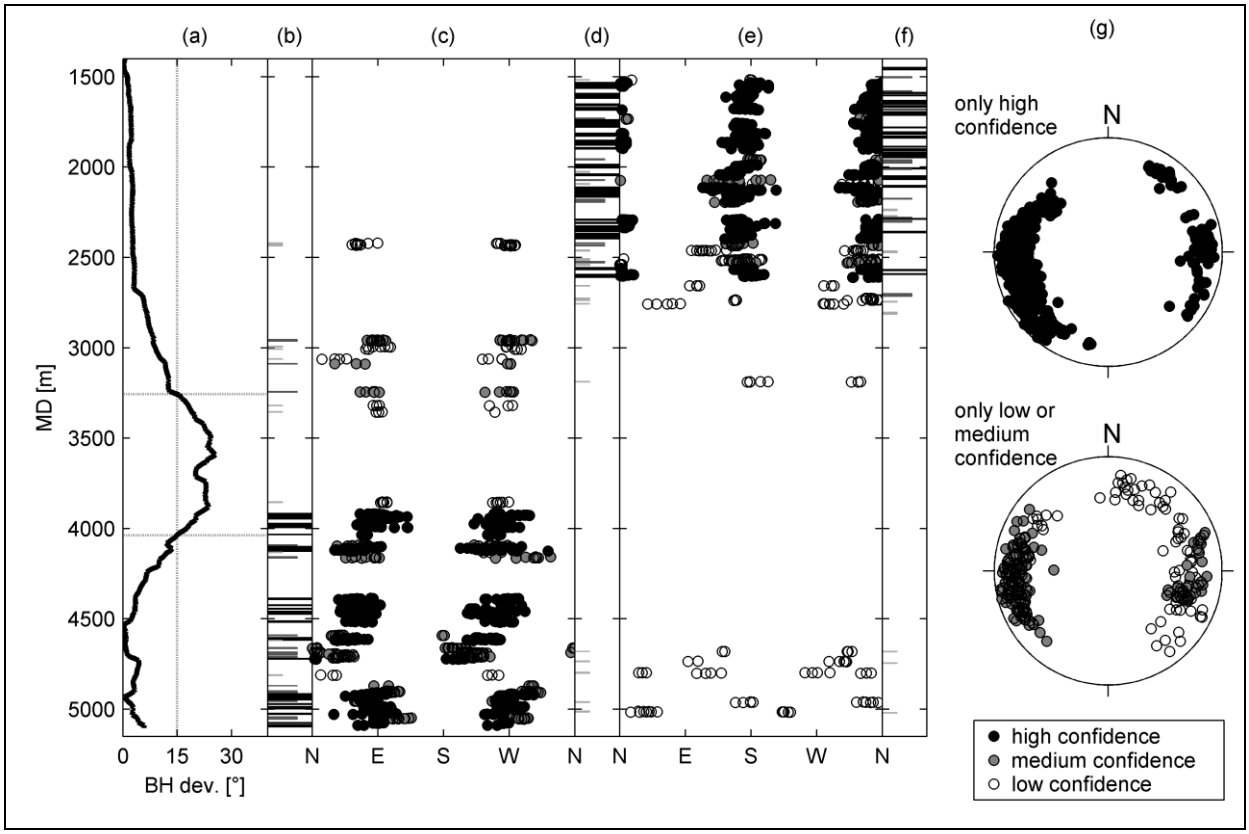

Figure 1: Summary of wellbore failure observations in the borehole GPK3. a) Borehole deviation from verticality. b) Breakout intervals. c) Breakout orientation. d) A-DITF intervals. e) A-DIFT strike directions. f) E-DITF intervals. g) Stereographic projections of poles to E-DITF planes (lower hemisphere, equal area).

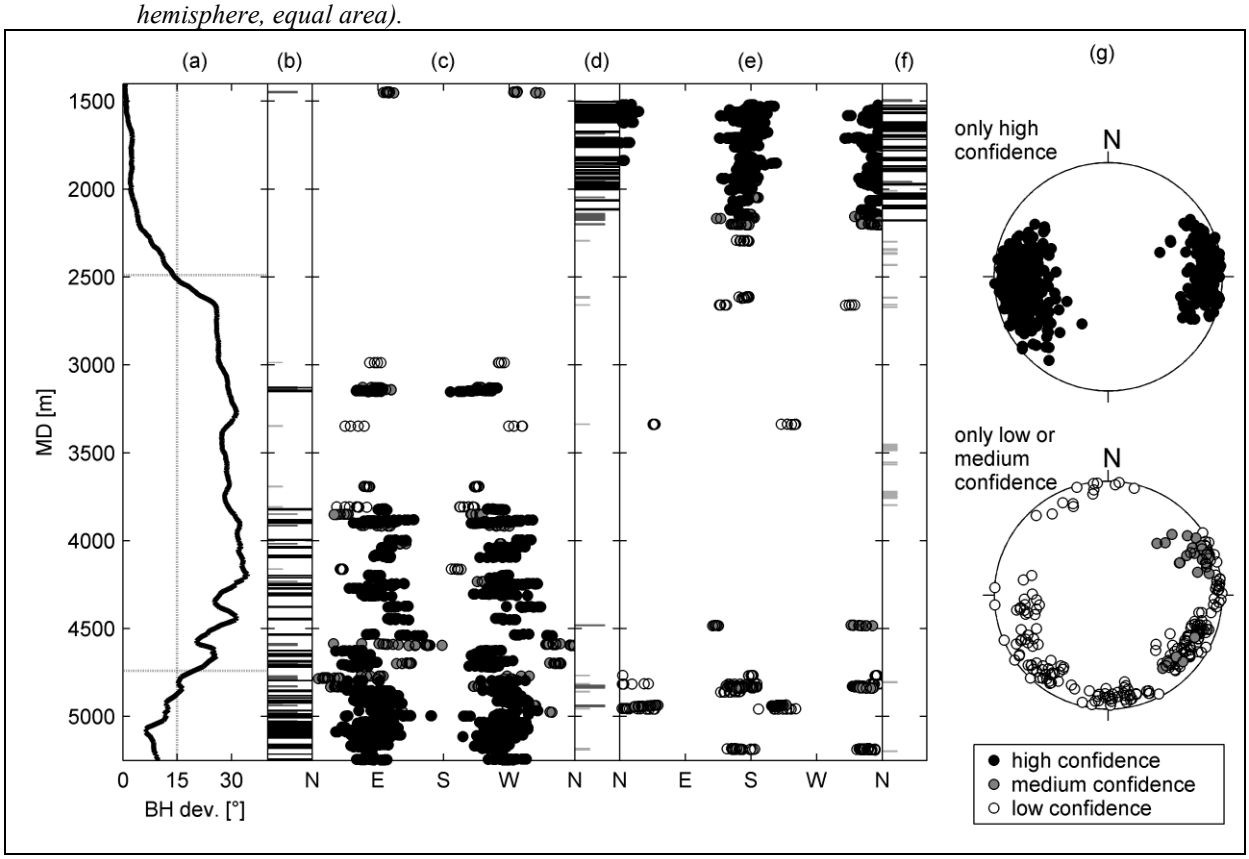

Figure 2: Summary of wellbore failure observations in the borehole GPK4. See Figure 1 caption for explanation.

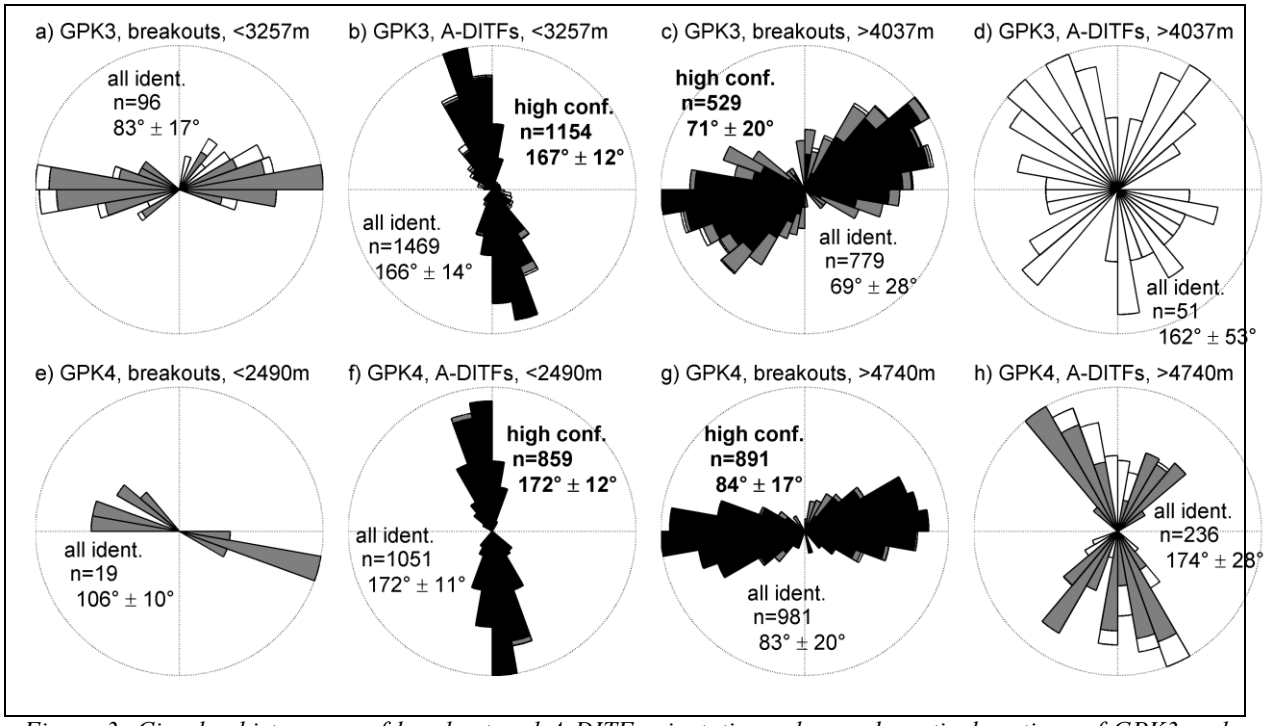

Figure 3: Circular histograms of breakout and A-DITF orientations along sub-vertical sections of GPK3 and GPK4. Unfilled denotes low confidence data; grey denotes medium confidence data, and black is for high confidence data. The circular mean direction and single standard deviation are given.

direction of the maximum horizontal stress has to be ascertained to fully characterise principal stress orientation.

For the vertical borehole sections, the wellbore failure features provide a direct measure of the horizontal stress orientations: the breakouts denote the Shmin-orientation, and the DITFs the SHmax-orientation. For the purpose of the analysis we consider borehole sections that lie within 15° of vertical as being essentially vertical. For GPK3, this excludes from the analysis the section between 3257 m and 4037 m MD. Above 3257m MD, borehole failure is dominated by numerous A-DITFs**,** with only a few medium- to low-confidence identifications of breakouts. The high-confidence A-DITFs show a preferred orientation in this section of 167.3° ± 12.1° (see histogram of Figure 3b), a result that does not significantly change by including medium- and low-confidence estimates. The orientation of the medium- and low-confidence breakouts is found to be 83.4° ± 17.3° (Figure 3a), which is approximately 90° rotated from the mean A-DITF orientation, as would be expected if the identifications were correct. This indicates that some, albeit few, breakouts do indeed occur above 3257 m MD. In contrast, the lower sub-vertical section of the borehole, below 4037 m MD, is dominated by numerous breakouts with only a few low-confidence A-DITFs present. The high confidence breakouts have an orientation of 71.3° ± 20.3°. The A-DITFs have no clear preferred orientation, and since they are all low-confidence, are possibly erroneous identifications.

A similar distribution of wellbore failure features is seen in GPK4, which is sub-vertical above 2490 m MD and below 4740 m MD. Many A-DITFs are found in the upper sub-vertical part, whereas only one medium confidence breakout is present. High confidence A-DITFs for this upper section show a clear preferential orientation of 172.2° ± 11.8°. Below 4740 m MD, breakouts dominate with a few medium-to-low confidence A-DITFs. The high-quality breakouts have a strong preferred orientation of 83.8° ± 17° (see histogram in Figure 3g). The medium-to-low confidence A-DITFs are oriented 173.9° ± 28.0°, and are thus 90° from the breakouts. This suggests that at least some of the identified A-DITFs are real.

SHmax-orientation estimates obtained from the mean direction of the high-quality A-DITFs in the upper sub-vertical sections of GPK3 (167°±12°) and GPK4 (172°±12°) are consistent with the results of previous analyses from the wells in the shallow reservoir (0°±20°). In the lower sub-vertical sections of GPK3 & 4, the high-quality breakout identifications indicate an SHmax-orientation for the deeper reservoir of 162°±20° and 174°±17° respectively, which is not significantly different from the SHmax-orientation in the shallow reservoir (see synthesis in Cornet et al., 2007). Taking an average of all estimates from GPK3 and GPK4 by weighting each value by the length of borehole considered in the study yields a mean orientation for SHmax at the Soultz site from 1.4 km to 5 km depth of 169°±14°.

Natural formation pressure

The natural formation pressure is required for computations that involve effective stresses. The value used here is based on brine density profiles given in Evans, et al. (1992) and is:

$$Pp = 0.9 + 9.8\ z[km] \quad (1)$$

Vertical stress magnitude

Since the evidence indicates that on average one principal stress is vertical, its magnitude can be taken as the integrated overburden as estimated from density determinations from either logs or tests on core samples. The density profile from 898 m to 3.6 km is reasonably well-constrained from density logs and tests of core samples. Klee and Rummel (1999) propose a Sv profile based on a density of 2.66 gm/cc from core tests. However, this is almost certainly an overestimate as it excludes the contribution of the relatively low densities found in alteration zones. Wireline density logs indicate a mean density for the granite to 3.6 km of 2.63 gm/cc. Moreover, comparison of the density of a core sample taken in GPK1 at 3524 m with the values registered on the density log in the vicinity showed excellent agreement, the log values being at most 0.015 gm/cc too low. Thus we regard the estimates from the density log as valid.

Above 898 m there is no density log from the Soultz site. A compilation by BRGM of density estimates from unspecified wireline logs run in unspecified boreholes in the Rhine Graben indicates values that show large scatter and differ significantly from the density log run in Soultz well GPK1 between 898 m and 1377 m. Thus, this compilation cannot be used to precisely estimate the density profile. However, a trend towards significantly lower densities in the upper 500 m is clearly defined in the compilation, presumably reflecting increasing porosity due to incomplete compaction and diagenesis. In view of these considerations, the density profile in the sedimentary section was estimated using the GPK1 density log between 1377 and 898 m, and the lithological composition of the sedimentary units above. A gradual upward reduction in density in the Cenozoic sediments above 594 m to a value of 2.0 gm/cc at surface was applied to simulate the effects of increasing porosity. The resulting mean density of the sedimentary section was found to be 2.50 gm/cc, in agreement with the value given by Heinemann-Glutsch (1994). Below 3.6 km, there is no published information on the density of the granite, and thus we use the value of 2.6 gm/cc that is valid for the granite above. This is somewhat questionable below about 4500 m TVD where petrological studies indicate a change in the composition of the granite (Dezayes, 2005b).

Drawing these considerations together, we conclude that the currently available data indicate that the vertical stress profile in the granite is given by:

$$Sv = -1.30 + 25.50\ z[km] \quad (2)$$

where we estimate the uncertainty level is approximately ±2 MPa.

Minimum horizontal stress magnitude

Down to 3.5km, the magnitude of Shmin is constrained by five small-volume hydraulic tests on pre-existing fractures in the depth range 1450-1990 m (Rummel and Baumgärtner, 1991), and a further four tests on induced hydrofractures in the depth range 2190-3510 m (Klee and Rummel, 1993). These data were fitted by Heinemann-Glutsch (1994) to constrain her Shmin profile (often mistakenly accredited to Klee and Rummel (1993) who actually propose a different profile in their paper based on tests above 2000 m). Evans (2005) best fits to the same data but without the lowermost point at 3508 m, which was almost certainly conducted in a zone of perturbed stress. Cornet & Bérard, (2003) discounted all small volume tests and claimed that a better Shmin estimate was given by the maximum pressures of large-volume, relatively high-rate injections where the jacking pressure is reached. In such cases they proposed that the maximum pressure at the top of the injection interval equals Shmin at that depth, an assumption that ignores near-wellbore pressure drops and poro-elastic perturbations of the ambient stress (Evans, 2005). They based their Shmin profile on two injection tests at 2000 and 2850 m, and state the uncertainty as ±3.5 MPa.

For the deep reservoir, no formal, hydraulic stress tests have been conducted below 3.5 km from which the magnitude of Shmin could be estimated. Thus, we follow Cornet and Bérard (2003) and assume that the maximum pressure attained during the stimulation injections provides a direct measure of Shmin at the depth of the casing shoe. This approach must be considered as tentative since it assumes the following conditions are met:

1. The maximum pressure attained during the test is controlled by jacking and not shearing.
2. Near-wellbore pressure drops (i.e. entrance losses) due to the focussing of flow are negligible.
3. The minimum stress prevailing at the time of maximum pressure reflects the ambient stress and is not elevated by poro-elastic effects.

These conditions appear to have been met for the large injections into the shallower reservoirs at 2.0 and 3.0 km, since the suggested Shmin profile of Cornet and Bérard (2003), which is based on maximum pressures during large volume injections, does not differ greatly from that

determined from the small-volume injections. Violation of assumption 1 would result in underestimation of the ambient minimum stress, whereas 2 and 3 would result in overestimates. The data describing the maximum pressures inferred at the casing shoe during stimulation injections of the three wells of the 5 km reservoir are listed in Table 1 and are plotted in Figure 4. Only estimates derived from downhole pressure measurements are listed. It is evident that all data show pressure-limiting behaviour. The three datapoints from the 03May27 stimulation of GPK3 are from a sequence when the flow rate was stepped from 50 l/s to 70 l/s for 2 hrs and then back to 50 l/s. The small, reversible changes in pressure that accompanied the flow rate steps indicates that jacking was occurring, as required for the Shmin estimation procedure to be valid.

The resulting estimates of Shmin are plotted as a function of depth in Figure 4, together with estimates from small-volume tests. In fitting the data with a linear trend we used only estimates obtained from large-volume injection tests because these are less sensitive to local stress heterogeneities. The Shmin estimates fall closely on a linear trend, with the exception of the data points for GPK2 which are too low by about 4 MPa. It is noteworthy that pressure was continuing to slowly increase at the end of this stimulation. This can be interpreted as indicating that the jacking pressure was not reached, although other explanations are possible. Because of this complexity, the GPK2 injection pressures were excluded from the fitting process. The resulting best-fit linear trend obtained from the casing-shoe injection pressures of the two GPK1 injections, the GPK3 and 4 injections is given by:

$$Shmin = -1.78 + 14.06\ z[km] \qquad (3)$$

Maximal horizontal stress magnitude

The commonly-used profile of SHmax for the Soultz site is derived from hydrofracture test data using the 're-opening method' (Klee and Rummel, 1993). Several authors have shown that this method yields invalid SHmax estimates (Ito, et al., 1999; Rutqvist, et al., 2000), particularly in deep holes, and this has led others to discount them (e.g. Cornet & Bérard, 2003; Evans, 2005). A semi-quantitative constraint on SHmax stems from the observation that focal mechanisms show a mix of normal and strike slip faulting, suggesting that SHmax is not greatly different from Sv. Both Cornet & Bérard (2003) and Evans (2005) adopt this equality as a working hypothesis. An extreme lower bound on SHmax is

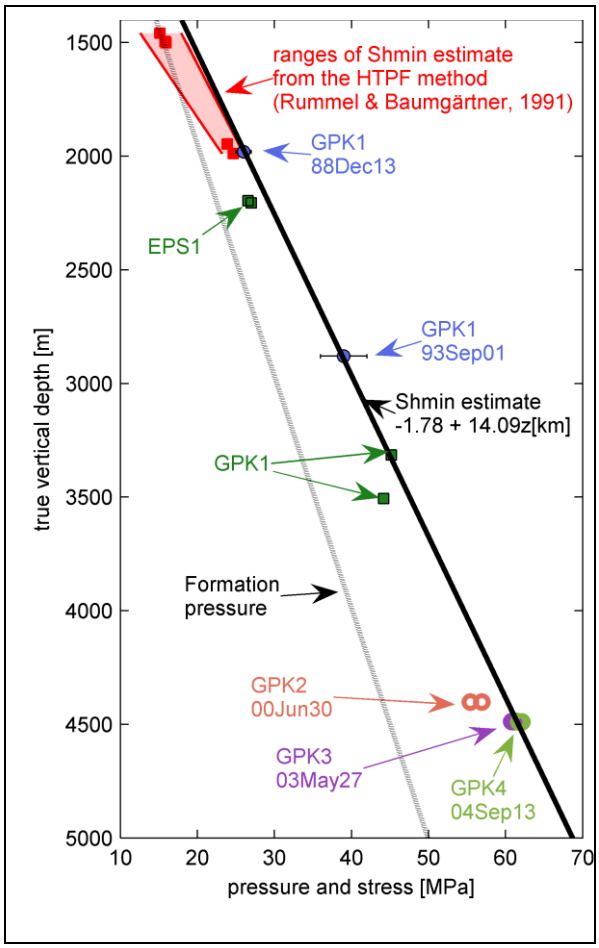

Figure 4: Estimates of the Shmin from small-volume injection tests (squares)and large-volume injection tests (circles). See text for details.

Table 1: Maximum pressures recorded at the casing shoe during the stimulation injections of the three deep wells. The data denote the pressures prevailing at the end of injection stages with different flowrates.

Borehole	Injection test ID	Depth of casing shoe [m TVD from ground]	Max. pressure at casing shoe [MPa]	Flow rate at max. pressure [l/s]
GPK2	00JUN30	4402	55.4	31
GPK2	00JUN30	4402	56.9	50
GPK3	03May27	4488	60.8	50
GPK3	03May27	4488	61.5	70
GPK3	03May27	4488	61.2	50
GPK4	04SEP13	4489	62.1	30
GPK4	04SEP13	4489	61.7	40

that it must be greater than Shmin by definition. An upper bound on SHmax is obtained by assuming that the strength of fractured rock masses is limited by thefrictional strength of optimally oriented fractures (Brace and Kohlstedt, 1980). The worldwide crustal stress dataset supports this view and indicates an upper limit on rock mass strength can be represented by a Coulomb friction criterion with a friction coefficient of 1.0 and zero cohesion. Evans (2005) showed that this constraint imposes an upper limit on SHmax of 1.21·Sv.

The observed partitioning of borehole failure mechanisms to different depth regimes in the deep Soultz boreholes allows a refinement of the SHmax profile. Specifically, tensile failure in the form of DITFs is seen to dominate at shallow depth, and compressive failure in the form of breakouts below. Since the UBI logs from which the breakouts and DITFs were identified were run before any injections had been conducted, the failure must have occurred either during drilling or shortly afterwards. In general, the total stresses about a wellbore can be considered to result from the superposition of four components: 1) the stress concentration developed around an empty wellbore due to the far-field stresses applied to the medium with uniform pore pressure; 2) the stresses generated by the wellbore fluid pressure; 3) the stresses arising from a perturbation of pore pressure about the well, and 4) the stresses arising from a perturbation of temperature about the well. Components 1 and 2 are always present. They represent the tangent stresses prevailing long after drilling, when the well has reached thermal and hydraulic equilibrium with the surroundings. In contrast, the conditions just after drilling (i.e. when the UBI logs were acquired) include the perturbing stress components 3 and 4 activated in tension by the cooling and overpressuring effects of the drilling mud. The latter is believed to be small for the holes in question since the annulus pressure was maintained at near-hydrostatic conditions. Hence it will be neglected. In this paper we consider components 1,2 and 4, and use data from hydraulic tests and temperature logs to constrain SHmax.

Analysis of the breakouts requires a compressive strength criterion. Uniaxial compressive tests were conducted on ten samples of unaltered Soultz granite, and yielded values of 100-130 MPa. Several authors (Wiebols and Cook, 1968; Haimson and Chang, 2005; Al-Ajmi and Zimmermann, 2006; Haimson, 2007) have proposed failure criteria that attempt to take into account the triaxial stress state at the borehole wall, although there is currently no consensus as to which is the most appropriate. We assume the appropriate strength is given directly by the UCS. Although it is true that higher strength estimates would have been obtained had the tests been conducted under the confining conditions that prevail at borehole wall, there are other issues that should be born in mind when considering whether laboratory values of strength derived from tests on cores are representative of in-situ values. Firstly, there is the question of microcracking induced by stress relief. Both cores and borehole wall have experienced complex stress paths when being drilled. Whilst these paths are not identical, both involve stress relief to some extent, and both will result in damage and strength reduction in comparison to that of *in-situ* rock remote from the wellbore (Diederichs, 2004; Martin, 1994). Thus, the reduction in strength of the core samples mimics that of the borehole wall to some degree. A second consideration is that stress corrosion cracking will serve to reduce the strength of the borehole wall on timescales which are long compared to the laboratory tests. This weakening of the wall rock will be promoted by the high in-situ temperature and the reactive nature of the pore fluid. In summary, there are competing effects that make it is difficult to decide whether UCS tests conducted in the laboratory are higher or lower than the strength of the rock at the borehole wall under *in-situ* conditions. The breakout analysis also includes an effective stress law for compressive failure with a coefficient of 1.0, as found by Brace and Martin (1968) to be valid even for very low-porosity crystalline rocks.

The results of the analysis for GPK4 are summarised in Figure 5. No high-confidence breakouts are identified above 3000 m (Figure 5a). Below 3000 m, breakouts are sparsely distributed until 3670 m TVD when the density increases markedly. Figure 5b shows the profile of maximum tangent effective stress obtained for a Shmin profile given by eqn 3, and a range of SHmax profiles. The profiles are primarily governed by stress-perturbing components 1 and 2 noted above. However, there is also potentially a component from thermal stress since the well had not warmed up to thermal equilibrium at the time the UBI log was run. Since the effect of the thermal stress is to generate a tensile stress it will serve to inhibit breakout formation. Thus, the analysis of whether conditions for breakout formation are met at a given depth requires knowledge of the hottest temperature the borehole has reached at that depth since its time of drilling up to the time of the UBI log. This is difficult to estimate because of the complicated circulation history of the well during drilling, and the cooling circulations performed before logging. Thus, we used an upper limit on the thermal stress from the temperature profile indicated by the GPIT sonde. This yields the lower bounds on the tangent stress shown in the dashed curves of Figure 5b. The dotted curve denotes the upper bound on tangent stress for the case SHmax = 1.2Sv, and is obtained by setting the thermal stress to zero. Evidently, the inclusion of thermal stress has little effect on the analysis. The grey band in Figure 5b

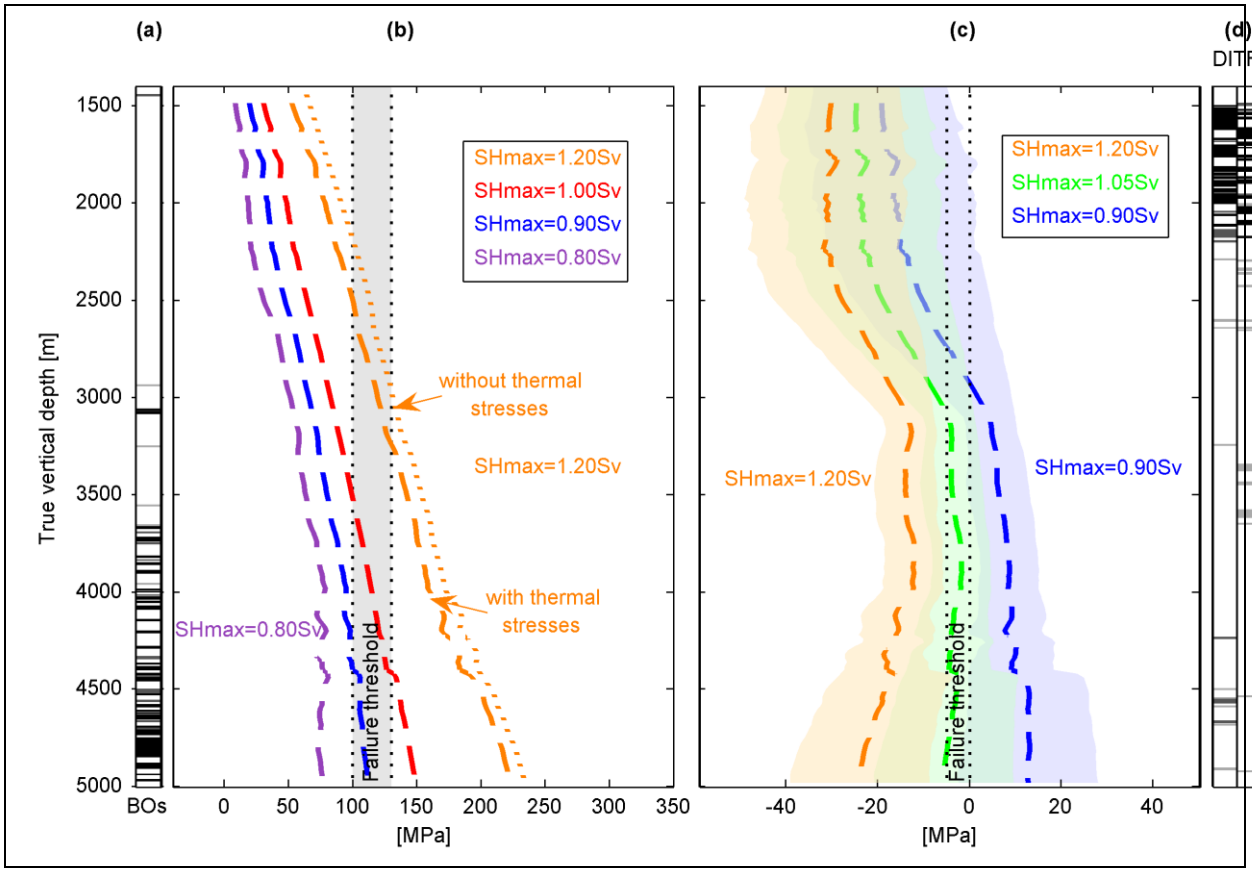

Figure 5: Constraints imposed on SHmax-magnitude by the observed wellbore failure in GPK4 . a) Breakout locations. Black bars are for high confidence, grey bars for medium confidence and light gray bars for low confidence. b) Maximum tangent effective stress for compressive failure. The coefficient in the effective stress law was taken as 1.0. The dashed profiles include a thermal hoop stress computed from the temperature profile at the time of the UBI logs, and the dotted profile is without a thermal hoop stress component. The vertical band denotes the compressive failure threshold derived from UCS measurements. c) Minimum tangent effective stress for tensile failure including an effective law with a coefficient of 0.0 and thermal hoop stress. Light coloured areas around the profiles represent uncertainty on the thermal hoop stress estimate. d) DITFs locations with same confidence rating that for the breakouts. See text for further discussion.

denotes the threshold tangent stress for compressive failure. The dashed curves indicate that SHmax must be greater than or equal to 0.9·Sv in order to reproduce the onset depth of breakouts at 3670 m.

The distribution of DITFs along GPK4 is shown in Figure 5d. Tensile failure of GPK4 is almost continuous down to 2180 m TVD, whereas below that depth it is sporadic and highly localised. To constrain SHmax from this distribution, profiles of minimum tangent stress were generated using the Shmin profile of eqn. 3 and a range of values of SHmax. Estimation of the component 4 (thermal stress) for the case of DITFs requires that the coolest temperature seen by the borehole wall be estimated at each depth. For this we used spot measurements of fluid temperature at the bit recorded by a 'measurement-while-drilling' system together with temperature measured within the GPIT tool during the UBI logs. These were run 12-15 hours after the end of drilling operations. The resulting profiles of minimum tangent stress are shown in Figure 5c. The coloured zones around each profile denote the potential error arising from the uncertainty in the true profile of 'coolest temperature' obtained from the data. The thermal stress component to the tangent stress profiles is found to range from -17.1 MPa at 3160 m TVD to -31.3 MPa at 2235 m TVD.

To determine whether the computed minimum tangent stress at the borehole wall is sufficient to generate a DITF, a failure criterion in tension is required that includes an effective law. No laboratory measurements of the tensile strength of Soultz granite are available. A review of the literature suggests values for intact specimens will probably be of the order of 10-20 MPa. However, in-situ values will be less than this – perhaps as low as a few MPa – owing to microcrack growth. Indeed, many practitioners adopt a value of zero when considering similar borehole stability problems (e.g. Brudy and Zoback, 1993). In view of this, tensile strength will be considered to range between 0 and 5 MPa. There is considerable uncertainty regarding the value of the coefficient in the effective stress law for tensile failure that is

appropriate for low-porosity crystalline rocks. Laboratory studies found a value of unity (Jaeger, 1963; Jaeger and Cooke, 1963; Schmitt and Zoback, 1992), except possibly when the loading rate is very high and fluid pressure equilibrium is not maintained. This may be relevant for special problems like impacts or explosion but probably not for borehole failure. Thus, our starting hypothesis is that this coefficient is equal to 1.0. However, it was found that taking a value of 1.0 led to tensile failure initiation along the entire length of the hole for all considered values of SHmax. Results that are in accord with observation can only be obtained by significantly reducing the coefficient. The minimum tangent stress curves in Figure 5c can be considered to be effective stresses for the extreme case where the coefficient is zero. These curves indicate that to prevent tensile failure in the lower half of the well it is necessary for SHmax to be at most 1.05·Sv. Thus, the breakouts and DITFs together constrain the profile of SHmax to be $0.90 \cdot Sv \leq SHmax \leq 1.05 \cdot Sv$.

Conclusions

A detailed description and analysis of stress-induced wellbore failure in the form of breakouts and drilling induced tension fractures was performed for two of the 5 km depth borehole of the European Enhanced Geothermal Project of Soultz-sous-Forêts. When combined with an estimate of Shmin magnitude from the maximum pressures developed at the casing shoes of the wells during major injections, the wellbore failure observations impose constraints on the magnitude of SHmax, as well as its direction. The collective analysis suggests the following stress characterisation for Soultz that is valid between depths of 1.5-5.0 km (excluding the effects of local stress heterogeneity):

SHmax orientation is N169°E±14°
Sv = -1.30 + 25.50 z[km]
Shmin= -1.78 + 14.06 z[km]
- 1.17+22.95z[km] ≤ SHmax < -1.37+26.78z[km]

A further result of the analysis is that the coefficient of the effective stress law for tensile failure is significantly less than unity.

ACKNOWLEDGEMENTS

This work is supported by the Swiss State Secretariat for Education and Research under project number 03.04.60, and was performed as a contribution to the European Union's FP6 project 'Soultz EGS Pilot Plant' funded by ADEME, BMU, EC and EEIG 'Exploitation Minière de la Chaleur'. We thank EEIG for access to the data. Special thanks to Marion Pfender and Dimi Teza for providing essential details.

REFERENCES

Al-Ajmi, A. M., and R. W. Zimmermann (2006), Stability of vertical boreholes using the Mogi-Coulomb failure criterion, *International Journal of Rock Mechanics and Mining Science*, **43**, p. 1200-1211.

Bell, J. S., and D. I. Gough (1979), Northeast-southwest compressive stress in Alberta: Evidence from oil wells, *Earth and Planetary Science Letters*, **45**, 2, p. 475-482.

Brace, W. F. and Kohlstedt D. L. (1980), Limits on lithospheric stress imposed by laboratory experiments, *Journal of Geophysical Research*, **85**, p. 6248-6252.

Brace, W. F., and R. J. Martin (1968), A test of the law of effective stress for crystalline rock of low porosity, *International Journal of Rock Mechanics and Mining Science*, **5**, p. 415-426.

Brudy, M., and M. D. Zoback (1993), Compressive and Tensile failure of boreholes arbitrarily-inclined to principal stress axes: application to the KTB boreholes, Germany, *International Journal of Rock Mechanics, Mining Science and Geomechanics Abstracts*, **30**, p. 1035-1038.

Cornet, F. H., and T. Bérard (2003), A case example of integrated stress profile evaluation, paper presented at 3rd International Symposium on Rock stress, Balkema, Kumamoto.

Cornet, F. H., Bérard, T. and S. Bourouis (2007), How close to failure is natural granite rock mass at 5 km depth ?, *International Journal of Rock Mechanics and Mining Science*, **44**, p. 47-66.

Dezayes, C., Gentier, S. and A. Genter (2005a), Deep Geothermal Energy in Western Europe: The Soultz Project, Public Report RP-54227-FR, 51 pp, BRGM, Orléans.

Dezayes, C., Chevremont, P., Tourlière, B., Homeier G. and A. Genter (2005b), Geological study of the GPK4 HFR borehole and correlation with the GPK3 borehole (Soultz-sous-Forêts, France), Public Report RP-53697-FR, 97 pp, BRGM, Orléans.

Diederichs, M. S., Kaiser, P. K. and E. Eberhardt (2004), Damage initiation and propagation in hard rock during tunnelling and influence of near-face stress rotation, *International Journal of Rock Mechanics and Mining Science*, **41**, p. 785-812.

Evans, K. F., Kohl, T., Hopkirk, R. J. and L. Rybach (1992), Modelling of energy production from Hot Dry Rock systems, Final Report, Bundesamt für Bildung und Wissenschaft.

Evans, K. F. (2005), Permeability creation and damage due to massive fluid injections into granite at 3.5 km at Soultz: 2. Critical stress and fracture strength, *Journal of Geophysical Research*, **110**,

Haimson, B., and C. Chang (2005), Brittle fracture in two crystalline rocks under true triaxial compressive stresses., in *Petrophysical properties of crystalline rocks.*, edited by P. K. Harvey, et al., pp. 47-59, Geological Society Special Publications, London.

Haimson, B. (2007), Micromechanisms of borehole instability leading to breakouts in rocks, *International Journal of Rock Mechanics and Mining Science*, **44**, p. 157-173.

Heinemann-Glutsch, B., (1994), Results of scientific investigations at the HDR test site, Soultz-sous-Forêts, Alsace, Socomine, BP 39, Route de Kutzenhausen, F-67250 Soultz sous Forets., France

Ito, T., Evans, K. F., Kawai, K. and K. Hayashi (1999), Hydraulic fracture reopening pressure and the estimation of maximum horizontal stress, *International Journal of Rock Mechanics and Mining Science*, **36**, p. 811-826.

Jaeger, J. C. (1963), Extension Failures in Rocks subject to fluid Pressure, *Journal of Geophysical Research*, **68**, p. 6066-6067.

Jaeger, J. C., and N. G. W. Cooke (1963), Pinching-off and disking in rocks, *Journal of Geophysical Research*, **68**, p. 1759-1765.

Lofts, J. C., and L. T. Bourke (1999), The recognition of artefacts from acoustic and resistivity borehole image devices, in *Borehole Imaging: applications and case histories*, edited by s

M. A. Lovell, et al., p. 59-76, Geological Society, London.

Klee, G., and F. Rummel (1993), Hydrofrac stress data for the European HDR research project test site Soultz-sous-Forêts, *International Journal of Rock Mechanics, Mining Science and Geomechanics Abstracts*, **30**, p. 973-976.

Luthi, S. M. (2001), Geological well logs : their use in reservoir modeling, 373 pp., Springer.

Martin, C. D., and B. Stimpson (1994), The effect of sample disturbance on laboratory properties of Lac du Bonnet granite, *Canadian Geotechnical Journal*, **31**, p. 692-702.

Rummel, F., and J. Baumgärtner (1991), Hydraulic fracturing stress meausrments in the GPK1 borehole, Soultz-sous-Forêts, *Geothermal Science and Technology*, **3**, 119-148.

Rutqvist, J., Tsang, C. F. and O. Stephansson (2000), Uncertainty in the maximum principal stress estimated from hydraulic fracturing measurements due to the presence of the induced fracture, *International Journal of Rock Mechanics and Mining Science*, **37**, p. 107-120.

Schmitt, D. R., and M. D. Zoback (1992), Diminished pore pressure in low-porosity crystalline rock under tensional failure; apparent strengthening by dilatancy., *journal of Geophysical Research*, **97**, p. 273-288.

Wiebols, G. A., and N. G. W. Cook (1968), An energy criterion for the strength of rock in polyaxial compression, *International Journal of Rock Mechanics and Mining Science*, **5**, 6, p. 529-549.

Multi-scale fracturing in the Soultz-sous-Forêts basement from borehole images analyses

Benoît Valley*, Chrystel Dezayes** and Albert Genter**

**Engineering Geology, ETH Zürich, Switzerland*
*** Geothermal Energy Division, BRGM, Orléans, France*

Presented at the Soultz Scientific Meeting at Soultz-sous-Forêts on 28-29 June 2007.

EC Contract SES6-CT-2003-502706

PARTICIPANT ORGANIZATION NAME: Engineering Geology, ETH Zürich.

Related with Work Package FP6-WP5

Related with Working Group WG7, 'Tectonics and borehole geophysics'

MULTI-SCALE FRACTURING IN THE SOULTZ-SOUS-FORÊTS BASEMENT FROM BOREHOLE IMAGES ANALYSES

Benoît Valley*, Chrystel Dezayes** and Albert Genter**
**Engineering Geology, ETH Zürich, Switzerland*
*** Geothermal Energy Division, BRGM, Orléans, France*
e-mail: valley@erdw.ethz.ch

ABSTRACT

When characterising fracturing for the development of an Enhanced Geothermal System (EGS), the scale relevant is related to the size of the targeted reservoir. At Soultz-sous-Forêts, it ranges from about 70 m to 2 km. Currently used investigation methods are restricted to smaller scale (borehole logging) or higher scale (regional tectonic studies). The present studies use information on natural fracturing at all available scale and particularly acoustic televiewer images from the 5 km deep boreholes of the Soultz geothermal site combined with statistical analysis, borehole correlation and genetic conceptual model in order to characterise the natural fracturing at the scale relevant for the reservoir development. The principal results are that the individual fractures observed at wellbore wall are smaller than our scale of interest, but they are clustered and form fractures zones with spacing in the order of magnitude of a couple of hundreds meters. The orientations of these fracture zones are probably similar to that observed at small and large scale, but a confirmation of this as well as constrains on the extend of these fracture zone, should be supplied by other geophysical data able to image structures remote from the boreholes (e.g. vertical seismic profile).

INTRODUCTION

The targeted size of an enhanced geothermal reservoir is in the order of magnitude of some km^3. At Soultz-sous-Forêts, extend of micro-seismicity events generated during stimulation permits to evaluate the size of the 5 km deep reservoir to be about 2 km (NNW-SSE) x 0.7 km (ENE-WSW) x 1.5 km (vertically), i.e. a total of about 2 km^3. This reservoir is taped by three deep boreholes with bottom hole horizontal distance of about 700 m. The size of the relevant structures which should be considered in the reservoir development, ranges then between a tenth of boreholes' spacing and the reservoir size, i.e. between about 70 m to 2 km. On the other hand, investigation methods like regional tectonic analysis, site geological mapping and geophysical investigations (surface seismic) catch only major faults and cannot resolve structures smaller than 2 km at the depth of the reservoir, i.e. about 5 km depth. A common investigation method in reservoir development is the monitoring of microseismicity during massive fluid injections, but the resolution of that method usually is too low to highlight fault zones and to resolve the details of their architecture. Special treatments of the micro-seismic dataset as e.g. collapsing (Jones and Steward, 1997, Evans et al., 2005a) or multiplet analysis Moriya et al., 2003) permit to get a better insight but never permit to exhaustively characterise fracture zones. At small scale, wellbore logging permits to obtain a very detailed picture of the fracturing at borehole wall but with an observation scale reduced to the borehole size, i.e. about 1 m in circumference.
In summary, in the current state of knowledge, there is a lack of information concerning the structures that drain fluids at the reservoir scale. In that context, the present study use the small scale fracturing imaged at wellbore wall combined with statistical analysis, boreholes correlation, structural analysis and genetic conceptual models in order to attempt to upscale the wellbore information to characterise the natural fracturing at the reservoir scale.

BACKGROUND

Soultz-sous-Forêts is located within the Upper Rhine Graben (URG), a cenozoic rift structure. The Soultz granite went through a complex multiphase tectonic history including hercynian and alpine orogeneses. This complex geological history is reflected by the orientations of the current structures forming the URG. A fault traces map of the URG area (see for example Illies, 1972; Illies and Greiner, 1979) permits to get an idea of the orientation of the major structures composing the graben and its vicinity. Three major directions are present. Firstly, a N0°-N20° direction, known as the Rhenish orientation, corresponds to the normal faults forming the URG. They were formed during the Oligocene opening of the Rhine Graben (Villemin and Bergerat, 1987, Schumacher, 2002), possibly reactivating an Hercynian structure called Mediterranean-Mjoesa-zone (Illies, 1962, 1972, 1975; Rotstein et al., 2006). A second prominent orientation, often called Erzgebirgian (Cloos, 1922; Edel and Weber, 1995; Edel et al., 2004), is the general Hercynian orientation to the NE to ENE. The major Variscan dislocation zones which delimited Hercynian tectonic realm strike in that direction. The third orientation corresponds to NW-SE structures. This orientation is rare in the Cenozoic sediments filling the URG and in mainly present in the border of the URG in pre-Cenozoic rocks. At a more local scale, the lineament analysis on SPOT images of Genter (1990) present the same dominant orientations with also some others, i.e. some NNW-SSE striking structures and a few others which are oriented WNW-ESE.
At the site scale, geological mapping, borehole logs from the Pechelbronn oil field and surface reflection seismic where used to characterise the major faults system (Menjoz et al., 1989). These data where included by Renard and Courrioux (1994) in the 3-D model presented on Figure 1a and c. In this model, all faults have a Rhenish (N–S) strike direction (Figure 1b) and are preferentially dipping to the West, i.e. antithetically to the Western Graben border fault. These major faults have a trace length on the regional geologic map of 2 to 20 km and occur with a spacing ranging from about 800 m to 3 km. The block diagram of figure 1c and the stereoplot of figure 3d make clear that basement top is generally horizontal, but at the top of the Soultz horst,

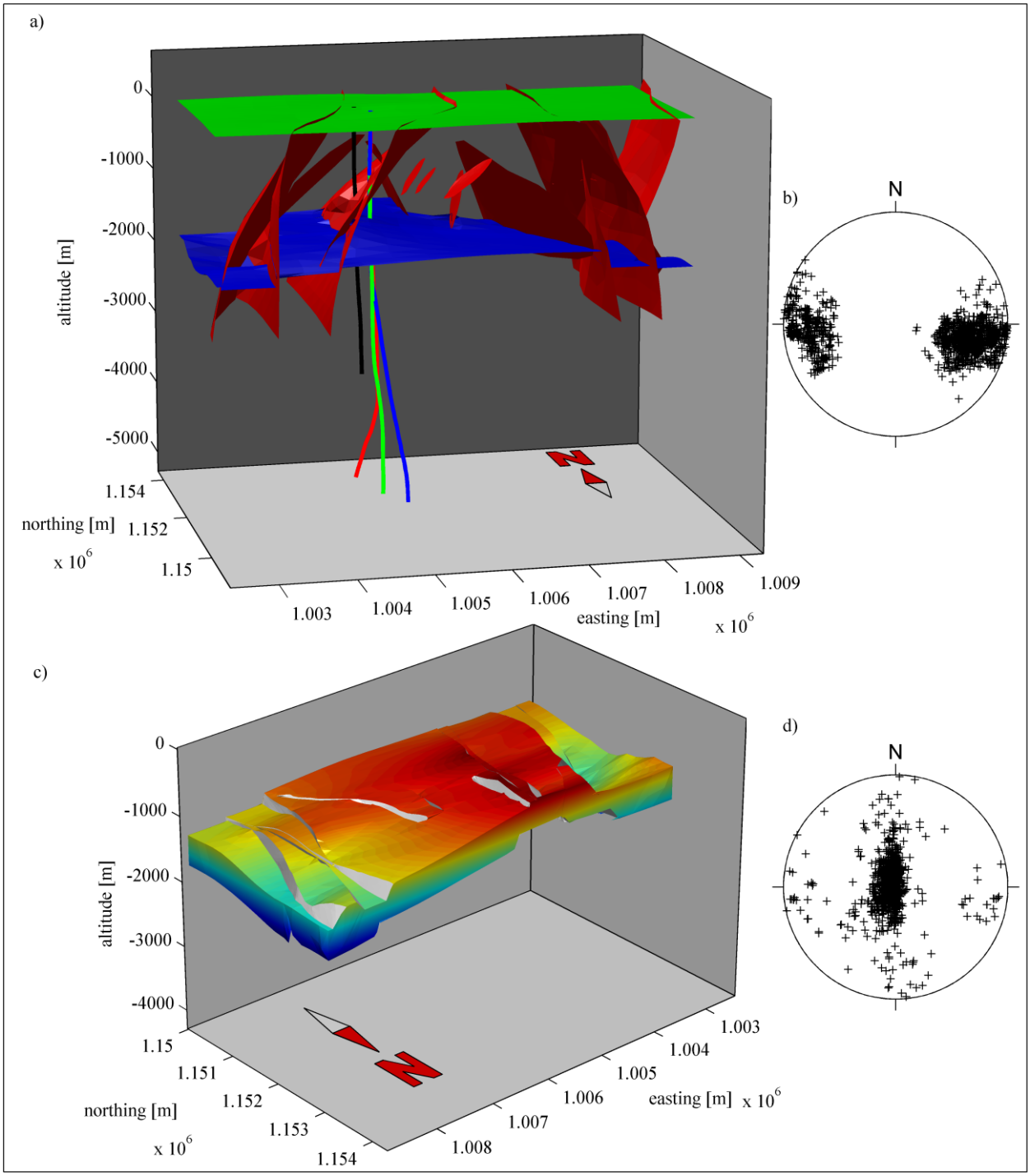

Figure 1: a) 3D model of the Soultz-sous-Forêts area. In green: topographical surface; in blue: basement top; in red: faults (after Renard, 1994). Boreholes trajectories are also displayed (GPK1:black, GPK2:red, GPK3:green and GPK4:blue) b) Poles of fault planes of the 3D model (lower hemisphere, equal area) c) View of the volume between top Buntsandstein and top basement in the form of a 3D block diagram. Point of view is from Northeast. d) Orientation of the top of the basement (lower hemisphere, equal area). Geographic coordinates are Lambert II coordinates. Altitudes are IGN69 altitudes.

basement dip slightly to SSE. Deviation of the basement top from horizontal occurs in a E–W direction where it express the delimitation of tilted blocks by the faults (half graben or roll-over) but also in the N–S direction possibility for strain transfer between relaying normal faults (relay ramp; for normal fault terminology, refer to Peacock et al. 2000). No connecting fault is present in that model in order to accommodate that lateral strain, but such fault may well be present outside the model or pre-existing ENE–WSW or NW–SE striking structures may be reactivated for that purpose.

DESCRIPTION OF THE DATASET

The data analysed in this study stem from the three deep wells GPK2, GPK3 and GPK4 drilled to 5 km at the Soultz-sous-Forêts geothermal site. In granite, boreholes GPK3 and GPK4 were drilled in two sections using two different bit sizes. A 12-1/4 inch bit was use down to 4582.8 m MD for GPK3 and down to 4757.3 m MD for GPK4. MD denotes measured depth along hole from ground level, which is at an altitude of 167.9 m for all three boreholes. GPK3 and GPK4 were then drilled to total depth with an 8-1/2 inch bit. GPK2 was drill down to 3880 in 1995 with a 8-1/2 inch drill bit. It was then deepened down 5093 m in 1999, down to 5057 with a 8-1/2 inch drill bit and down to 5093 m with a 6 inch core barrel.

Ultrasonic borehole images

The principal source of information arises from acoustic borehole televiewer logs. The ultrasonic borehole televiewer images were obtained by a Schlumberger Ultrasonic Borehole Imager (UBI) tool that was run with the ancillary GPIT module which provides sonde positioning and orientation information. Successful UBI logs were run in the entire granite section of both GPK3 and GPK4 to total depth and from granite top to 3800 m in GPK2. The UBI tool provides detailed images of the ultrasonic reflectivity of the borehole wall together with borehole geometry sampled with an angular resolution of 2°. The logging speed is chosen that a scan is made every 1 cm along hole. For details on measurement principle, refer to Luthi (2001).

The GPK3 logs were acquired in two runs. The first run was acquired on 25th Oct. 2002 in the 12-1/4 inch section, some 5 days after the completion of drilling. This log extends throughout the 12-1/4 inch section from 1439 m MD (the casing shoe of a higher section) to 4532.6 m MD. The images of the lowermost 13.8 m are not oriented. The second log was run on 10th Nov. 2002, some 21 days after the hole had been extended as 8-1/2 inch diameter to TD at 5103 m MD. The log covers the 8-1/2 inch section from the 12-1/4 inch casing shoe at 4558.2 m MD to 5100.8 m MD, with the lowermost 2.6 m not oriented. The images are generally of excellent quality with few logging artefacts. 'Key seats' (see Lofts and Bourke, 1999) are visible along the entire inclined 12-1/4 section and some parts of the inclined 8-1/2 section, but they are easily identifiable and affect only a limited part of the borehole circumference. The presence of borehole breakouts, particularly in the lower part of the wells also reduces the visibility of the natural fractures.

The logs in the GPK4 borehole were also acquired in two runs that followed the drilling of the 12-1/4 inch and 8-1/2 inch sections. The log in the 12-1/4 inch was run on 15th Feb. 2004, some 15 hours after drilling, from 1421.3 to 4723.3 m MD. The log in the 8-1/2 inch section was run on 12th Apr. 2004, 18 hours after drilling operations ended, from 4730.3 to 5253.3 m MD. Images suitable for fracture geometry determination were obtained for 1445.3-4720.3 m MD and for 4757.3-5248.3 m MD. Outside these ranges, the logs are run in casing or suffer from acquisition problems.

The logs in GPK2 were acquired on the 2nd of February 1995. Note that Logging conditions were significantly different, including different tools, crew and also a smaller borehole diameter than for GPK3 and GPK4 logs. In 1999, a UBI logging campaign was planned in the lower part of the GPK2 borehole, but due to technical problems, that attempt was unsuccessful. Finally, usable images were acquired between 1433.3 and 3793.3 m MD only.

Measurements of fracturing on wellbore images

Fractures have been measured on unwrapped borehole images by manually fitting sinusoid on them using the WellCad software package from ALT. The sensitivity of the method has been evaluated by Genter et al. (1997) by comparing fractures determined on cores and on ultrasonic boreholes images. Discrete fractures thinner than 1 mm are not properly detected. This is also the case for discrete fractures closer than 5 mm, which appear only as one single trace. In granite, only about 17% of the fractures detected on cores were seen on borehole images. The sensing of fractures is better in sane granite sections, where about 50% of the fractures seen on cores are capture by the BHTV than in altered granite section where only about 5% of the fracture were seen.

Natural fractures can be sometimes confounded with drilling induced tensile fractures. The latter form where cooling of the borehole wall by circulation of mud during drilling results in a net tangent stress distribution about the hole that is sufficiently tensile at some point to produce failure. The net tangent stress is the sum of a tensile cooling component, which is axially-symmetric, and the natural wellbore stress concentration arising from the 'far-field' stresses, which are not necessarily axially-symmetric and may be everywhere compressive. As indicated by their name, such fractures are not present before the borehole is drilled. Their repartition and orientation depend on the current stress conditions and on the drilling operations. In the present analysis, special care was taken to distinguish natural and drilling induced fractures. Only the natural fractures are analysed here, the analysis of drilling induced fractures being presented elsewhere (Valley and Evans, 2007).

The apparent dip and dip directions measured on borehole images have been transformed in true dip and dip directions using the borehole azimuth and deviation measurement provided by the ancillary GPIT tool. The accuracy of these measurements is sale by Schlumberger to be $\pm 2°$ in azimuth and in deviation. Evaluation of repeated logs permits to refine these values for the particular case of Soultz logging condition. Single standard deviations were found to be 1.0° on the azimuth measurement and 0.2° on borehole deviation measurements. On top of this the inaccuracy of the sinusoidal fitting process has to be considered. Natural fractures being barely perfectly planar, their unwrapped borehole trace is usually not a perfect sinusoid. The best fitting of the sinusoid trace is let to the expertise of the analyst and is then subjected to uncertainties. For steep fractures, as they are found in Soultz, that inaccuracy has been evaluated by repeated measurement of the same feature to be about $\pm 2.5°$ for the dip direction and $\pm 0.75°$ for the dip angle.

The importance of each fracture trace has been evaluated using an appropriate fracture typology. A two digit code is attributed to each fracture type. The first digit permits to distinguish between fractures which are visible on both reflectivity and transit time images (1) and those which are seen on reflectivity image only (2). The second digit estimates the 'physical importance' of the fractures at borehole wall by measuring their trace persistence. The visible length is compared with the full length of the fitted sinusoid and the second digit of the fracture code is attributed as following: 1 = 100-80%; 3 = 80-50%; 4 = 50-0% and 5 for low confidence determination. For example the code '23' will be attributed to a fracture visible only on the reflectivity image with its trace perceptible over more than 50% of the total trace length but less than 80%.

ANALYSIS OF THE GENERAL FRACTURING

In all, 1871 fractures were described on the GPK3 images and 2215 fractures on the GPK4 images. They are all dispatched in the classes defined in the typology presented here over. The repartition in the different classes is shown on Figure 2a. The repartition in both boreholes is globally the same, so the data from both boreholes are presented together within the same diagram. The dominant type is the type '24' which counts for 42% of the fractures, followed by the type '25' with about 17% of the fractures. The strong fractures of types '11' and '21' count together for only 12%.

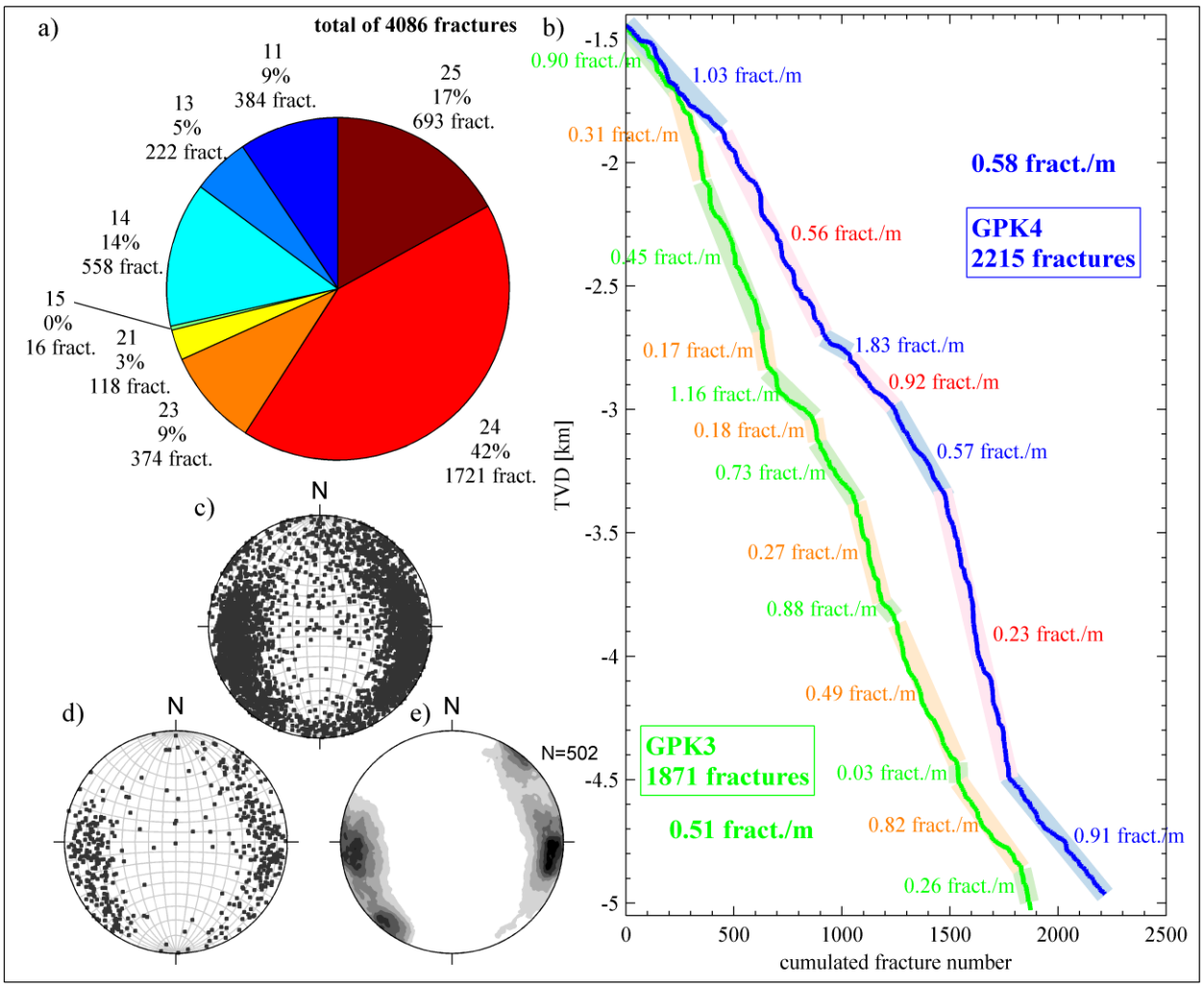

Figure 2: Presentation of the entire fracture data set from GPK3 and GPK4. a) Repartition of the fractures in the different types defined by the typology (see text for details). b) Cumulative number of fractures vs. depth. GPK3 is displayed in green and GPK4 in blue. Fractures frequencies are also displayed for various sections. c) Stereographic projection of the poles off all GPK3 and GPK4 fractures (lower hemisphere, equal area). d) poles of fractures type 11 and 21 of GPK3 and GPK4 (lower hemisphere, equal area). e) Weighted contouring of the fracture density of fracture data presented on d). Weighting is performed for a Terzaghi correction (e.g. Priest, 1993, p. 71).

Another aspect to look at is the repartition of fractures with depth. This is represented on Figure 2b by the mean of cumulated number of fracture vs. depth curves. Average fracture frequencies are 0.51 fractures per meter for GPK3 and 0.58 fracture per meter in GPK4. Frequencies are variable with depth ranging from a minimum of 0.17 fractures per meter to a maximum of 1.83. Evidently, very locally frequency may be even lower, e.g. no fractures for a few meters, or quite higher with one meter containing up to about ten fractures. Keep also in mind the results of Genter (1997) that only about 50% of the fractures are seen by a BHTV tool when the granite is unaltered and as few as 5% in altered zones. Altered zone may then well be largely under sampled and will not show up as steps on the cumulated number of fracture curves as we may expect if fractures were identified on cores. In a very simplified manner the cumulated number of fracture curves can be summarized in 5 sections:
A) a high frequency section, with about 0.9 to 1 fracture per meter, from granite top down to about 1800 mTVD.
B) a low frequency section, about 0.45 to 0.55 fractures per meter, from 1800 to 2800 mTVD.
C) a generally high frequency section with also some very low frequencies from 2800 to 3400 mTVD.
D) a generally very low frequency section, about 0.25 to 0.45 fracture per meter, from 3400 to 4500 mTVD
E) a high frequency section, about 0.8 to 0.9 fractures per meter, from 4500 mTVD to bottom hole.
In the detail there are significant discrepancies within this simplified scheme. Particularly, the very bottom section of GPK3 from 4850 mTVD has a low frequency of about 0.26 fractures per meter. Also the first high frequency section (A) lasts deeper in GPK4 than GPK3, and the first low frequency section (B) lasts deeper in GPK3 than GPK4. These two differences are responsible for the slightly higher average frequency in GPK4 than GPK3.
Figure 2c present the orientation of the poles of all GPK3 and GPK4 fractures on a stereographic projection, lower hemisphere and equal angle. The dominant orientation is N-S striking, with fractures dipping to the west or to the east. Dip angles are generally higher than 50°. These results are in agreement with previous study made on the dataset of the 'shallow reservoir' (Tenzer et al., 1991; Tenzer et al., 1992; Genter and Traineau, 1992, Dezayes, 1996). It has also to be emphasized that if they are dominating, steep N-S striking fractures are not the only direction in presence. Looking at all fracture simultaneously as in Figure 2c tends

to provide a blur image. Figure 2d and 2e presents plots of subset of data. This subset contains only the strongest features picked, i.e. fractures of type '11' and '21'. The fact that there is also the presence of totally other directions than N-S striking fractures is true again. This suggests that if these orientations are rather rare they nevertheless exist and cannot be attributed to uncertain picking. Figure 2e presents a contouring of data of Figure 2d applying a so called Terzaghi correction as described in Priest, 1993 (p. 71) in order to compensate the sampling bias arising from the sampling line orientation. On that plot, three maximum densities of fractures are visible. Two of them correspond to N-S striking fractures dipping steeply to the East or to the West. The third maximum corresponds to sub-vertical fractures striking NW-SE. Generally this plot gives the impression that the general description of dominantly N-S striking steep fracture is true but incomplete. For performing further analysis on the fracturing, the fracture orientations have to be clustered in order to sort the fractures in various sets.

Clustering of the fracture data to derive orientation sets

All the fractures data together couldn't be clustered in once over the entire borehole length, because the potential sets are overlapping and the major N-S striking sets are overprinting the other sets. In order to permit fracture set evaluations, the fractures have been treated borehole by borehole and using a 75 m long moving windows shifted by 25 m step along borehole depth. That way, two successive windows have a 50 m overlap which ensures coherent processing over the entire borehole length. For each window, a preliminary clustering was performed using the fully automatic algorithm described in Priest, 1993 (p. 76-87). That preliminary set repartition was then refined still by using the 75 moving windows and by coupling a semi-automatic k-means clustering algorithm adapted for spherical data with interactive manual control.

In all, seven sets have been isolated. The fourth first sets are the dominating sets. Set 1 and 2 strike N-S and dip to the West or to the East respectively (Figure 3). Together they contain more than 60% of the fractures. They orientations correspond to the Rhenish orientation already described at graben and site scale. Set 3 is sub-vertical, striking NW-SE an orientation also apparent a large scale. The set 4 is also sub-vertical and strike NE-SW, parallel to the Hercynian large scale structures. Together, the four first set includes 95% of all described fractures. They are actually the dominant sets, set 5 to 7 being more anecdotic fractures set. All sets contain more than 15% of indisputable fractures (type '11', '13', '21', or '23').

The study of the repartition with depth of the fractures within the different set shows that the four major sets 1 to 4 are present along the entire boreholes length, whereas sets 5 to 7 occur at specific locations. Set 5 which is sub-horizontal occurs mostly above 2.5 km and also between 3.2 and 3.8 km. Genter et al., 1991 and Genter and Traineau 1996, already described such sub-horizontal fractures on the GPK1 dataset and attributes them to exfoliation joints (Twidale,1973; Martel, 2006) which formed during the post-hercynian erosion. If that interpretation may hold for the fractures located close to the current basement top, it is unlikely to be true for fractures located at more than 2 km from the paleo-surface. The genesis of that deeply located sub-horizontal fractures is unknown. Set 6, a sub-vertical E-W striking fracture set, occurs mostly below 4 km depth as does also set 7, another E-W striking set, but dipping at about 45° to the South.

The repartitions of the four dominant set versus depth highlights that set 1 and 2 are globally well balanced except above 1835 m where set 2 (east dipping) is clearly dominating and below 4600 m where set 1 (west dipping) is more present. The reparation between set 3 and 4 is usually less well balanced, one set or the other is totally dominant or disappear totally for a given section.

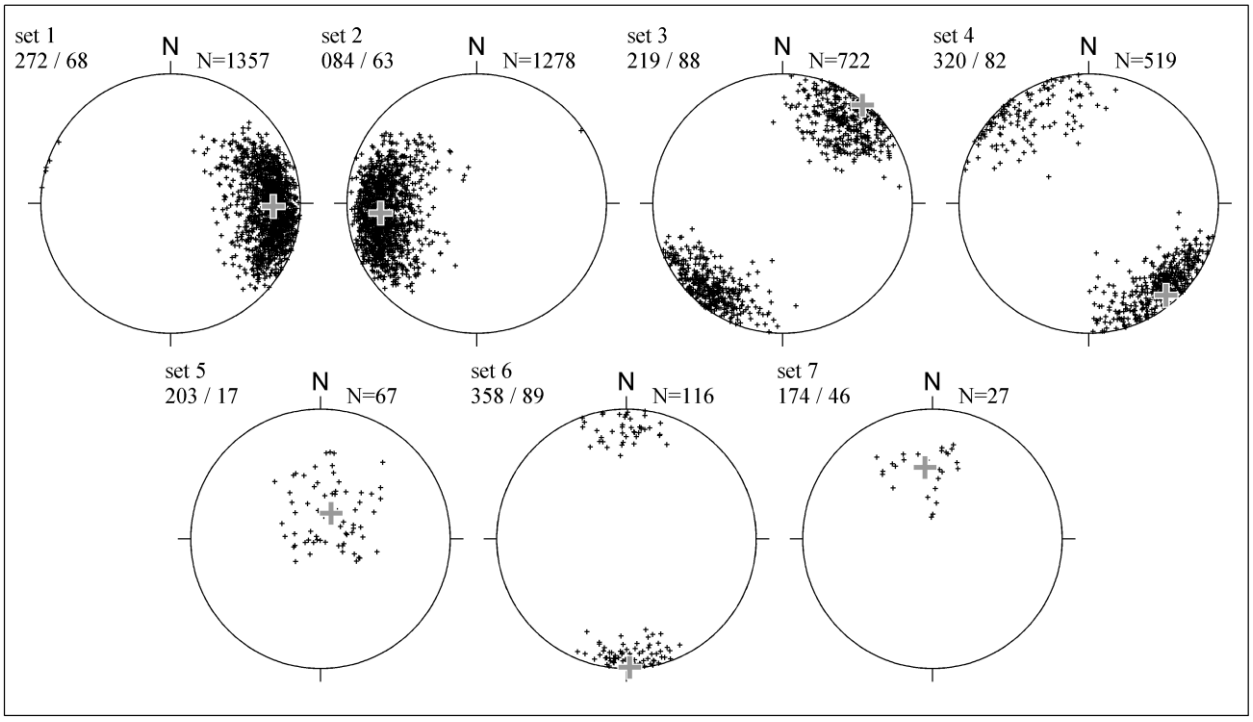

Figure 3: Result of the clustering process performed on the fracture data of Figure 2c. Poles of fracture for all seven isolated set are presented in stereographic projection (lower hemisphere, equal area). The mean orientation is display next to the set label and with a thick grey cross on the stereographic projection.

Abutting relations between the four main set have been studied by looking the singular case where the borehole cut two fractures at their intersection. In all, 124 such intersections implying the four major sets have been found along the entire granitic section of both boreholes. For each of these intersections, the abutting relations where described and a confidence index from 'high' to 'very low' was attributed to each characterisation.
Interactions between set 1 and set 2 show than in about two third of the case, set 1 is abutting on set 2. Interactions between set 1 and 3 shows in most of the case set 1 is abutting again set 3. Set 4 is most of the time abutting again set 1. Set 3 and 4 are abutting again set 2, and set 4 again set 3. So in summary, the less abutting or most persistent set is set 2, then set 3, then set 1 and finally set 4. Note that as the genesis mechanism of the fractures is not known, these abutting relations cannot be used as chronological markers. Indeed in the case of joints, i.e. mode I fractures, younger joints will stop on older ones. Contrarily, for faults, i.e. shear fractures, younger faults will displace older ones, and so older faults will be in abutting relation on younger faults.

Spacing distributions

For fracture set 1 to 4, true spacings have been computed. This was done by projecting the borehole length between two subsequent fractures in the mean normal direction of the fracture set.
Note that when considering true spacing that way, the effective total sampling length is then reduced comparing to the length measured along boreholes. The effective sampling length is like projecting the logged borehole section in on direction normal to the fracture planes. This can be also simply computed by summing all true spacing for a given set in a given borehole. These lengths are for set 1: 1398m (GPK3) and 1554m (GPK4), for set 2: 1493m (GPK3) and 1539m (GPK4), for set 3: 321m (GPK3) and 764m (GPK4) and for set 4: 908m (GPK3) and 1452m (GPK4). Remark that set 3, as it is unfavourably oriented relatively to the borehole trajectory has a quite short effective sampling length.
Statistical descriptive parameters and distributions for true spacing are presented in Table 1. Mean true spacing for set 1 is 2.30 m in GPK3 and 2.08 m in GPK4 with standard deviations of 4.21 m and 4.95 m respectively. Coefficient of variation ($CV = \sigma / \mu$) is 1.83 for GPK3 and 2.38 for GPK4. Mean spacing, standard deviation and CV for set 2 are slightly higher than for set 1. Set 3 has spacing of 1.04 m in GPK3 and 1.86 m in GPK4 which is the less spaced set. Keep in mind that this set is also the less favourably oriented relatively to the borehole trajectory to be efficiently sampled.

Table 1. Spacing statistics and distributions of the four major fracture sets.

	GPK3 set1	**GPK4 set1**	**GPK3 set2**	**GPK4 set2**
descriptive statistical parameters				
mean μ	2.3	2.08	2.62	2.18
standard deviation σ	4.21	4.95	6.66	5.31
maximum spacing	38.15	63.00	66.83	67.55
minimum spacing	0.00	0.00	0.00	0.00
coefficient of variation *CV*	1.83	2.38	2.54	2.44
best fit parameters				
log-normal ν, ρ *	-0.49, 1.78	-0.69, 1.70	-0.63, 1.73	-0.68, 1.72
exponential μ **	2.3	2.08	2.62	2.18
power law *D*, *i* ***	1.00, 376	1.03, 350	0.95, 468	1.06, 323

	GPK3 set3	**GPK4 set3**	**GPK3 set4**	**GPK4 set4**
descriptive statistical parameters				
mean μ	1.04	1.86	3.16	6.31
standard deviation σ	2.29	5.42	6.28	16.87
maximum spacing	16.46	64.61	37.28	115.41
minimum spacing	0.00	0.00	0.00	0.00
coefficient of variation *CV*	2.21	2.91	1.99	2.67
best fit parameters				
log-normal ν, ρ *	-1.79, 2.04	-1.90, 3.03	-0.35, 1.89	-0.21, 2.13
exponential μ **	1.04	1.86	3.16	6.31
power law *D*, *i* ***	0.63, 733	0.97, 205	0.75, 789	0.69, 1301

* log-normal law with parameters corresponding to the mean and standard deviation of the corresponding normal distribution and defined by: $y = f(x \mid \nu, \rho) = \frac{1}{x\rho\sqrt{2\pi}} \exp\left(\frac{-(\ln(x)-\nu)^2}{2\rho^2}\right)$

** exponential law is defined by : $y = f(x \mid \mu) = \frac{1}{\mu} \exp\left(\frac{x}{\mu}\right)$

*** power law is expressed by : $y = f(x \mid D) \propto x^{-D}$. *i* is the maximum theoretical spacing and it is computed by extrapolating the power law line to its intersection with the origin abscise.

CV for set 3 is 2.21 in GPK3 and significantly higher in GPK4, i.e. 2.91. Mean spacing of set 4 is significantly higher with respectively 3.16 m and 6.31 m. It is also accompanied with quite larger standard deviations, which implies then CV of 1.99 and 2.67.

Concerning the fitting of statistical distributions, negative exponential distributions are never in good agreement with the data set. Log-normal distributions agree usually quite well with the data, always with CV significantly higher than 1 ($\sigma>\mu$). This indicates a clustering of the fracture population (Gillespie et al., 2001). Comparisons between fractures identified on cores and fractures seen on BHTV images (Genter et al., 1997) show that if on BHTV spacing distribution usually agree well with a log-normal law, the spacing dataset from cores for the same borehole sections follows a power law over more than two decades. This is due to the selective sensing of the BHTV tool which does not see a significant portion of the fracture population. Indeed, small spacing will be neglected because some fractures are not seen on BHTV images, but also some large spacing will not be recorded due to the limited sampling length (Segall and Pollard, 1983; Einstein and Baecher, 1983; Bonnet et al., 2001). A power law has been adjusted on the segment of the spacing distribution between 1 and 5 m. This is not very reliable as the distributions don't follow power law over more than on decade. The obtained fractal number (*D*) is generally close to 1, in agreement with the one obtained on cores (Genter et al., 1997). Maximum theoretical spacing (*i*) can be computed by extrapolating the power law lines to their intersections with the origin abscise. In the case presented here, that maximum theoretical spacing ranges between 320 and 1300 m.

Variogram analysis on fracture spacing

Classical statistic and theoretical distribution fitting as presented here over are not sufficient to define joint spatial correlations. Geostatistics was introduced in fracture spacing analysis to deal with that particular aspect (e.g. Miller, 1979, Chilès, 1988, Villaescusa and Brown, 1990). Figure 4 presents variograms for the Soultz fracture spacing data with respect to distance as presented in Villaescusa (1990) and using the following equation to compute them:

$$\gamma(h) = \frac{1}{2n}\sum_{i=1}^{n}\left[z(x_i) - z(x_i + h)\right]^2 \qquad (1)$$

where *z* is the studied variable, *n* the number of observation couples, *h* the distance between two measurement, for example between $z(x_i)$ and $z(x_i + h)$ where x_i and $x_i + h$ is the spatial localisation of the measurements. γ is computed for successively increasing value of *h* in order to build the complete experimental variograms. Experimental variograms have been smooth using a moving average filter in order to highlights the trends (black lines on Figure 4).

For set 1, for both boreholes there is a nugget value of about a half of the entire sample variance, which indicate that there is some correlation in fracture spacing and it can be interpreted to reflect fracture clustering. Range is 90 m for GPK3 and 150 m for GPK4. This give an estimate of the distance of influence of the correlation and the cluster inter-distance should be then about twice the range, i.e. 180-300 m.

For the set 2, nugget value is again significantly lower than the entire sample variance which may be interpreted to be due to fracture clustering. Range is 110 m in GPK3 and 200 m in GPK4, so inter-cluster distance will be about 220-400 m. In GPK3, values clearly oscillate about the sill value with a wave length of 280m over two complete cycles. That particular experimental variogram may well be approximated by a modified hole-effect model (Miller, 1979) which indicated spatial periodicity for the occurrence of zones containing similar spacing. This also indicates an inter-cluster distance of about 280 m.

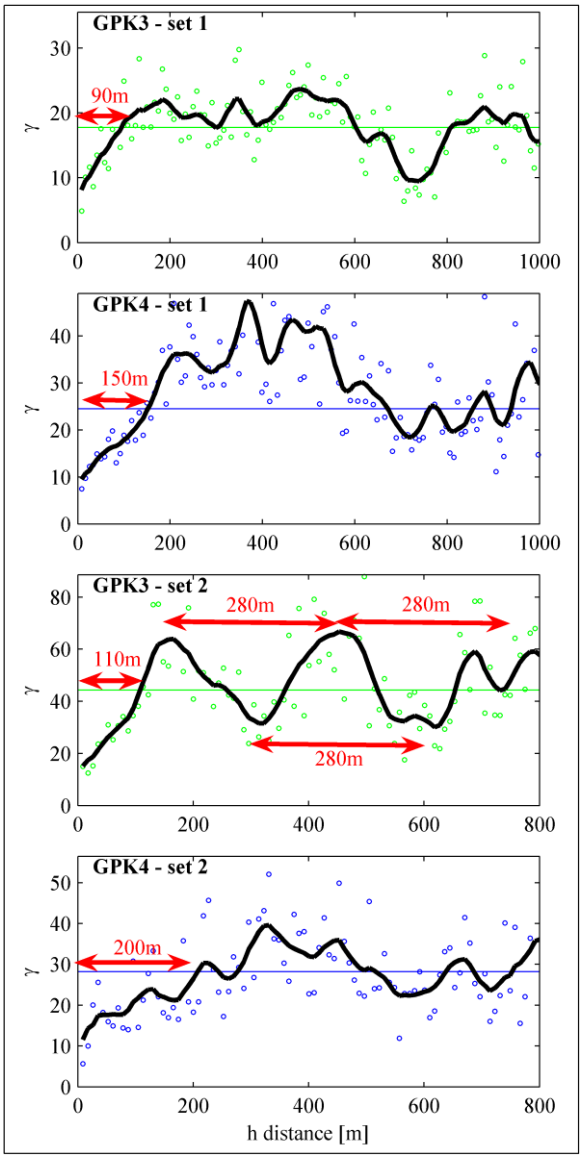

Figure 4: Variograms for fracture spacing with respect to distance for set 1 and set 2. Points correspond to the calculated experimental variogram. Black line smooth the experimental variogram with a moving average in order to highlights the data trends. The horizontal line in blue or in green correspond to the variance of the entire sample, i.e. the expected sill value.

Fracture correlation

Trajectories of the Soultz deep boreholes are very appropriate to try to perform fracture cross-hole correlation. Indeed, for the first kilometre of granite section, borehole GPK3 and GPK4 have a horizontal distance of less than 30m. At 1919 m TVD, horizontal distance reaches a minimum of 12.6 m. At the top of the granite, distance is about 15.2 m. From 1920 m that horizontal distance starts to increase and reaches 36.4 at 2500 m TVD and 705 m at bottom holes.

In the correlation process, each fracture was considered to be perfectly planar. The uncertainties on borehole

trajectories and fracture orientation, as described in the 'Description of dataset' section, were used in that process. For each fracture couple, i.e. two fractures, one belonging to GPK3 the other to GPK4, an index of the probability that the two fractures are actually perfectly co-planar was computed by a Monte Carlo simulation.

So combining the 1871 fractures of GPK3 with the 2215 fractures of GPK4 permits to test 4'144'265 fracture couples. Evidently most of the couples have a very low index of probability to be co-planar. Choosing an appropriate threshold for that index of probability permit isolate 280 couples of fractures most potentially correlated. In addition, as the correlation process do not warranty that each correlated is linked with a unique fracture on the other borehole, the 280 fractures couples have then to be sorted for uniqueness giving priority to couples with high index. This lead to 101 correlated fracture couples for which there is the warranty that each correlated fracture of GPK3 is linked with a single fracture on GPK4 and vice versa. The location of the correlated fracture couples along boreholes GPK3 and GPK4 is presented on Figure 5a.

Type and set of correlated fractures are presented on Figure 5 b) to i). In absolute number (a) and (b), the dominant type is the type 24. This was also true for all fractures together (see Figure 2a). More interesting is to look at relative number of correlated fracture for each type (c) and (d). In this view, excepting for 3 anecdotic correlated fractures of type 14 in GPK3, the dominant type is the type 21 where about than 30% of the fractures are correlated. In GPK4, the three best correlated types are also the strongly developed

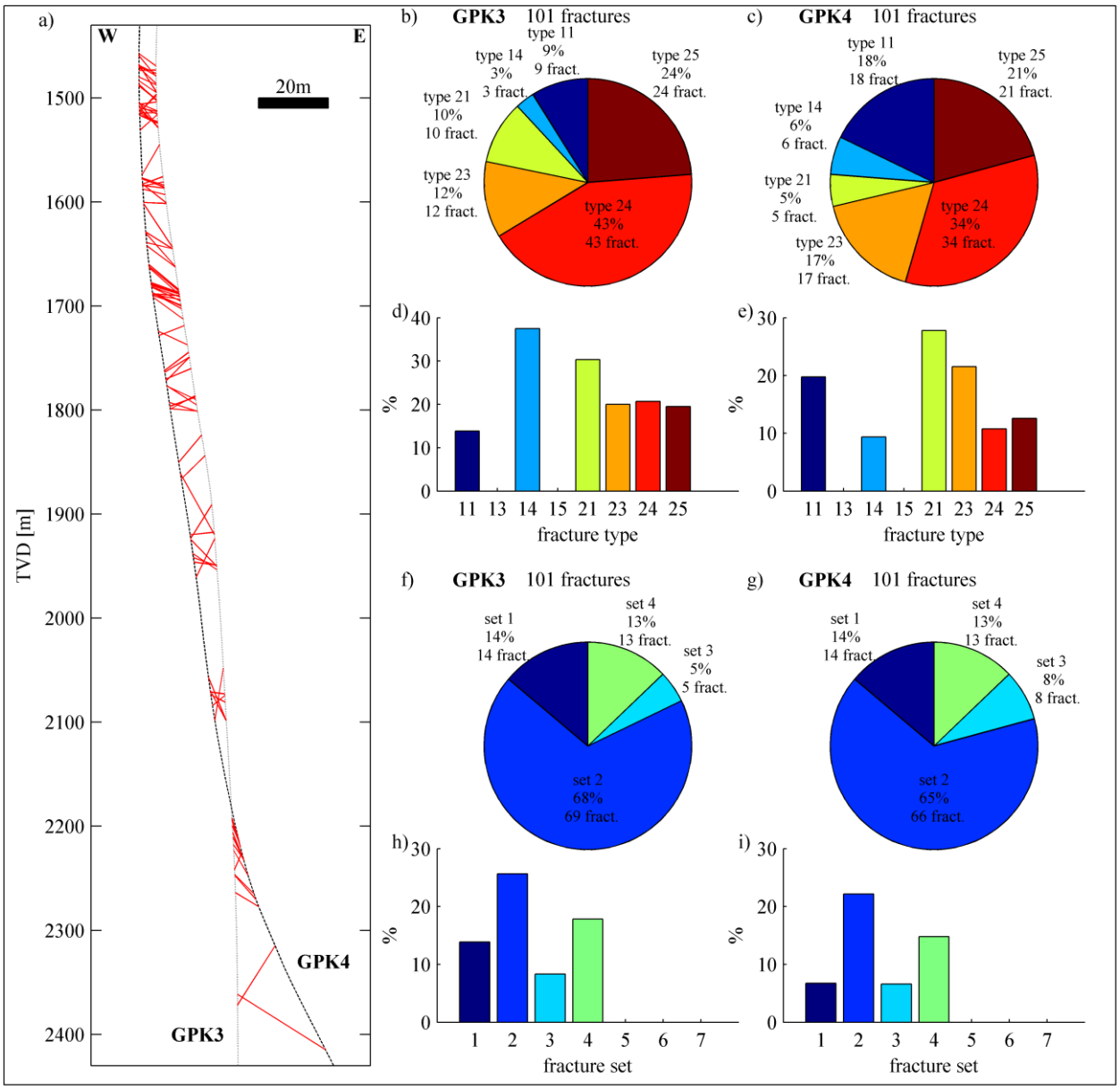

Figure 5. a) borehole projection in a W-E crosssection with link between the location of the 101 correlated fracture couples. Note that depth scale and horizontal scale are not identical. b) types of the correlated fractures in GPK3. c) types of the correlated fractures in GPK4. d) proportion of correlated fractures for each fracture type in GPK3. e) proportion of correlated fractures for each fracture type in GPK4. f) set of the correlated fractures in GPK3. g) set of the correlated fractures in GPK4. h) proportion of correlated fractures for each fracture set in GPK3. i) proportion of correlated fractures for each fracture set in GPK4.

features on borehole image (type 11, 21, 23). Other correlated types are types 14, 24 and 25 that are in general also the most present types. As these types are very common the probability to get by chance reasonably well aligned fractures that aren't the same geological structure is higher. So it cannot be excluded with this data set that some of the correlated fracture correspond to such occurrences. In GPK3, the types 14, 24 and 25 are as good correlated as the types 11 and 23.
Concerning the sets, the most correlated set is the set 2 (N-S striking, east dipping) both in absolute and relative number. About 25% of this set is correlated. The next best correlated set is set 4. Other correlated sets are sets 1 and 3 with less than 14% of correlated fractures or less than 7% if only GPK4 is considered. This is a good indicator that east dipping structures have a higher persistence than others, at least in the upper part of the granite, i.e. about from 1400 to 2400m.

Fracture size

The here over established dataset of correlated fractures permits to evaluate the size of the fractures. A first approach is purely deterministic: one can state that a correlated fracture is at least as big as the distance between boreholes in the correlated fracture plane. On the other hand, upper bound for fracture size cannot be set. Size of uncorrelated fractures cannot be estimate at all. Indeed, it cannot be exclude that a fracture that cross only one borehole has a very big extend, but in a direction opposite to the second borehole. One aspect related to fracture size is the fracture shape. From such punctual two borehole data set, this aspect cannot be solved at all. For seek of simplicity, we will consider penny shape fracture geometry. With this hypothesis, fracture size can simple be described by a single parameter, its radius *r*. This hypothesis is surely simplistic, particularly when a fracture begins to interact with other discontinuity, as for example in sedimentary rocks when fractures develop between two bank boundaries. Nevertheless in a nearly isotropic granite, penny shaped fracture geometry may well be an acceptable hypothesis. For the interpretation of the following results this undemonstrated initial hypothesis has to be kept in mind.
The inter-borehole half distances in the correlated fracture planes are presented on Figure 6. It corresponds to a lower bound for the radius of these fractures. The mean radius is about 10 m, maximum radius is 30.3 m and minimum radius is 6.4 m. Note that this minimum is not controlled by fracture size but by the borehole trajectories.
A probabilistic approach permits to give some more precise constrain on the fracture size. That approach consists of finding a relation between the fracture length distribution and

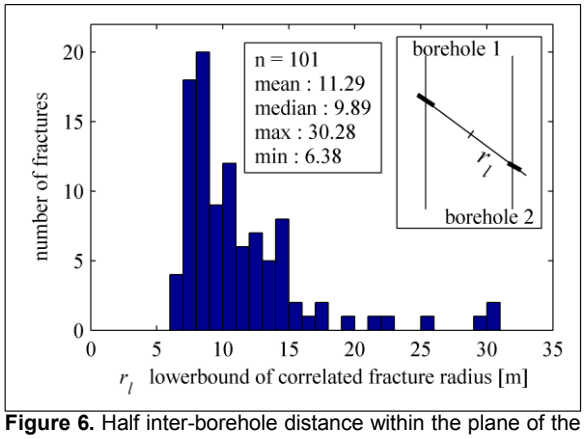

Figure 6. Half inter-borehole distance within the plane of the 101 correlated fractures couples, i.e. lower bound for the radius of these fractures.

the probability that a fracture will cross both boreholes. The actual probability that a fracture cross both boreholes is then approximated using the data by comparing the number of fracture which was actually found to cross both boreholes with the number of all other fractures which were not correlated between the boreholes.
In that computation, an a priori knowledge of the fracture length distribution is needed. The exponential negative distribution was chosen for seek of simplicity, such distribution being defined by a single parameter ($\mu=\sigma$), but we have no way to control what is the actual distribution of fracture length. The other main assumption in that computation is that the fractures are considered to be penny shaped.
The results of that computation permitted to determined that fracture radius ranges from 8 to 22 m with an average of 15 m.

ANALYSIS OF THE ZONE OF FRACTURE FROM WELLBORE IMAGES

The here over analysis of general fracturing suggests that fractures are clustered in order to form fracture zones. Such fracture zones are probably at the reservoir relevant scale and we believed that they play a salient role in the reservoir behaviour. For that reason, borehole sections crossed by fracture zones were tracked on the BHTV images. Such fracture zones may have various appearances at wellbore walls. Sometimes (type 1) fracture zone are characterized by clear alteration but without any strong fracture trace. Some fracture zones are characterized by virtually a single strong fracture without other indices on the images (type 2), but more often that single fracture is also accompanied by some trace of alteration (type 3). For these three first types it is sometimes difficult to decide if this single fracture or alteration zone has really to be considered as a major structure cutting through the granitic massif. Such doubts disappear when strong fractures occur in cluster as for type 4 (without clear alteration) or type 5 (with clear alteration). Sometimes, when the borehole intercepts a strong fracture zone, borehole wall spalling is so strong that it results in highly enlarged borehole sections. UBI tool do not perform well in such borehole section and usually individual fractures can hardly be isolated (type 6). But care must be taken in considering such section in the fracture zone determination process, as they may well be the major structure crossing the basement.
One key question concerning these fracture zones is to characterize their orientation from borehole images. The fracture zone architecture being unknown, it is not possible to use the fractures composing them to derive a priori a general orientation for the zone. Borehole cross-correlation of fracture zone permits to have some insight in to that problematic and to learn about the fracture zones intern architecture in the Soultz granite.
Between 1400 and 2200 m depth, 17 fracture zones were isolated and correlated between boreholes GPK2, GPK3 and GPK4. The intersection of a given fracture zone with all three boreholes forms three points in space from which the general orientation of the fracture zone can be computed. Comparing that general orientation with the fracture composing the fracture zone permits to better understand the fracture zone architecture.
Sometimes the components (i.e. the individual fractures) of the fracture zone have all the same orientation. The fracture zone itself in such case follow the same orientation than the components. When more than one orientation is present in the fracture zone's components, the general orientation of the fracture zone is found to be about the same than one present orientation corresponding usually to the strongest fracture. In such zones always significant variability in the fracture orientations composing the fracture zone are present. Also, the variability within one fracture zone from one borehole to the next is usually quite strong. Over the

couple of tens of meters between the intersections of a fracture zone with one borehole to the next, significant changes in thickness and architecture usually occur.
All this elements make us think that the adequate conceptual model for fracture zones is that they are built of anastomosed fractures networks with trough going strong fractures delimiting shear lenses. Such geometry correspond to the most developed stage of Riedel type shear zones, as presented e.g. in Naylor et al. (1986). Note that this formation model of shear zone is debated and other evolution model could produce similar final geometry (e.g. Martel, 1990). The analysis of the borehole image of Soultz-sous-Forêts does not provide a complete enough dataset to further develop that debate. The influence of tip damage zone as describe e.g. in Kim et al. 2004 or other more refined evolution models (e.g. Kim et al., 2003) cannot be distinguished with our data set.
The position and the general orientation of the 17 correlated fracture zones are displayed in black on the cross-section of Figure 7. Nine of the seventeen fracture zones are east dipping. They have orientation similar to the fracture of the set 2 described here over. A predominance of this orientation was already highlighted in the upper section in the analysis of the general fracturing. The other eight fracture zones have various orientations mostly about vertical NW–SE striking, comparable to the orientation of the fracture set 3 which was the second dominant set after the analysis of fracture abutting relations described here over. Only one zone is west dipping, an orientation comparable to the fracture set 1. There is no NE–SW striking fracture zone.

Below 2200m, fracture zones were also tracked in GPK3 and GPK4, but it wasn't possible to correlate them between boreholes. The general orientation were attributed to them following the here over described rule, i.e. the general orientation of the zone follow the orientation of its major fracture. At total number of 47 fracture zones are described in GPK3 (including the 17 one above 2200 m) and 45 fracture zones in GPK4 (also including the 17 first one above 2200 m).
Location and orientation of fracture zones are also presented on Figure 7, in green for GPK3 and in blue for GPK4. The predominance of East dipping fracture zones in the upper part of the granite was already highlighted. Below 2200 and down to 3 km West and East dipping fracture zones are better balanced. Between 3 km and 4 km there is the remarkable presence of less steep fracture zones. Below 4 km West dipping fracture zone are dominating.
The vertical distance between two subsequent fracture zones is in mean 80 m, with minimum and maximum ranging from 5 to about 300 m. Note that this distance is not a true spacing since the fractures zones have not the same orientation. If they were parallel and dipping at about 60° as they in the majority does, the mean true spacing would be about 70 m (80sin(60°)). Sorting fracture zone in set of fracture zone with similar orientation has not been considered, but considering similar sets and set distributions for the fracture zone than for the individual fractures, mean true spacing within one set of fracture zone should range

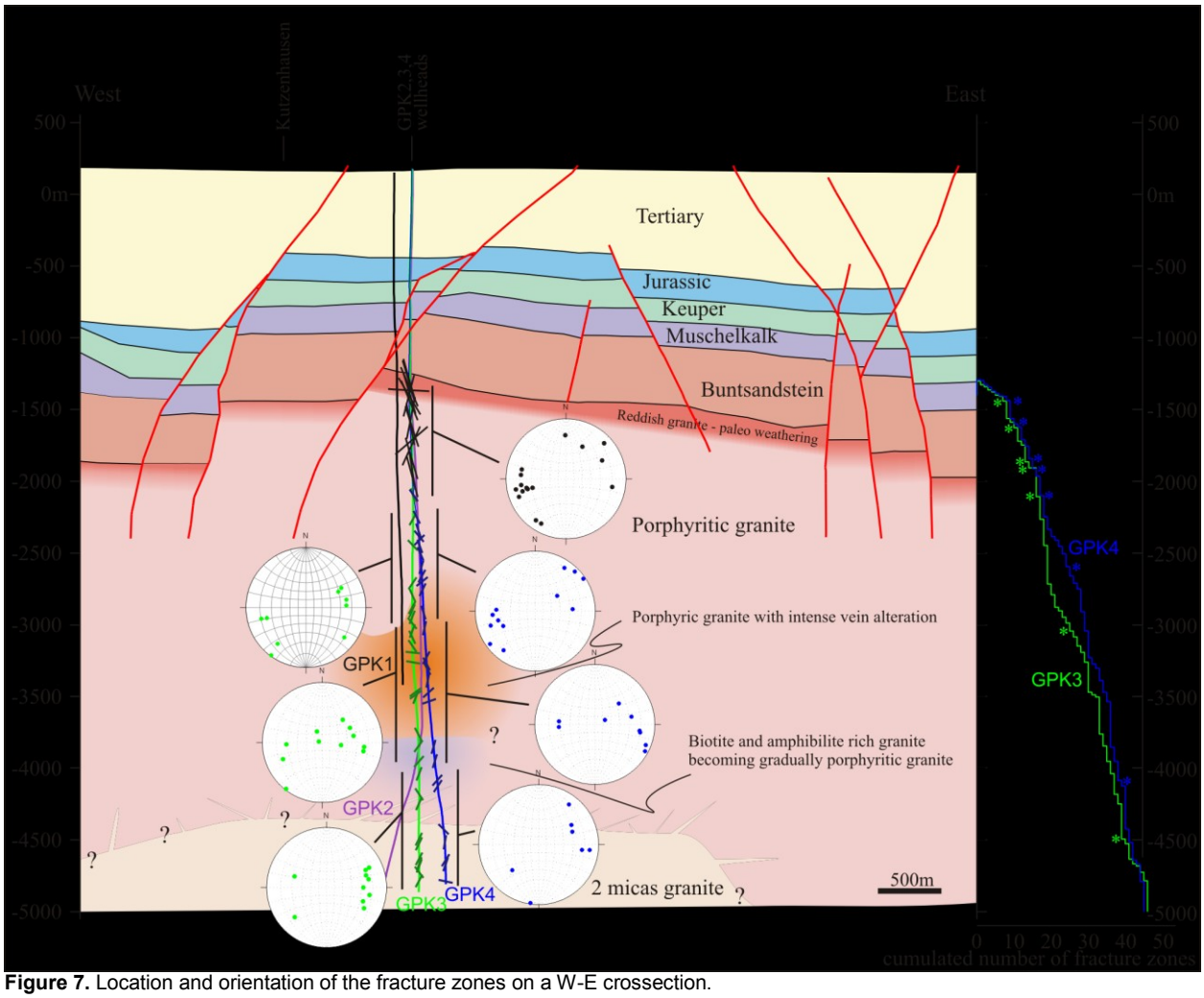

Figure 7. Location and orientation of the fracture zones on a W-E crossection.

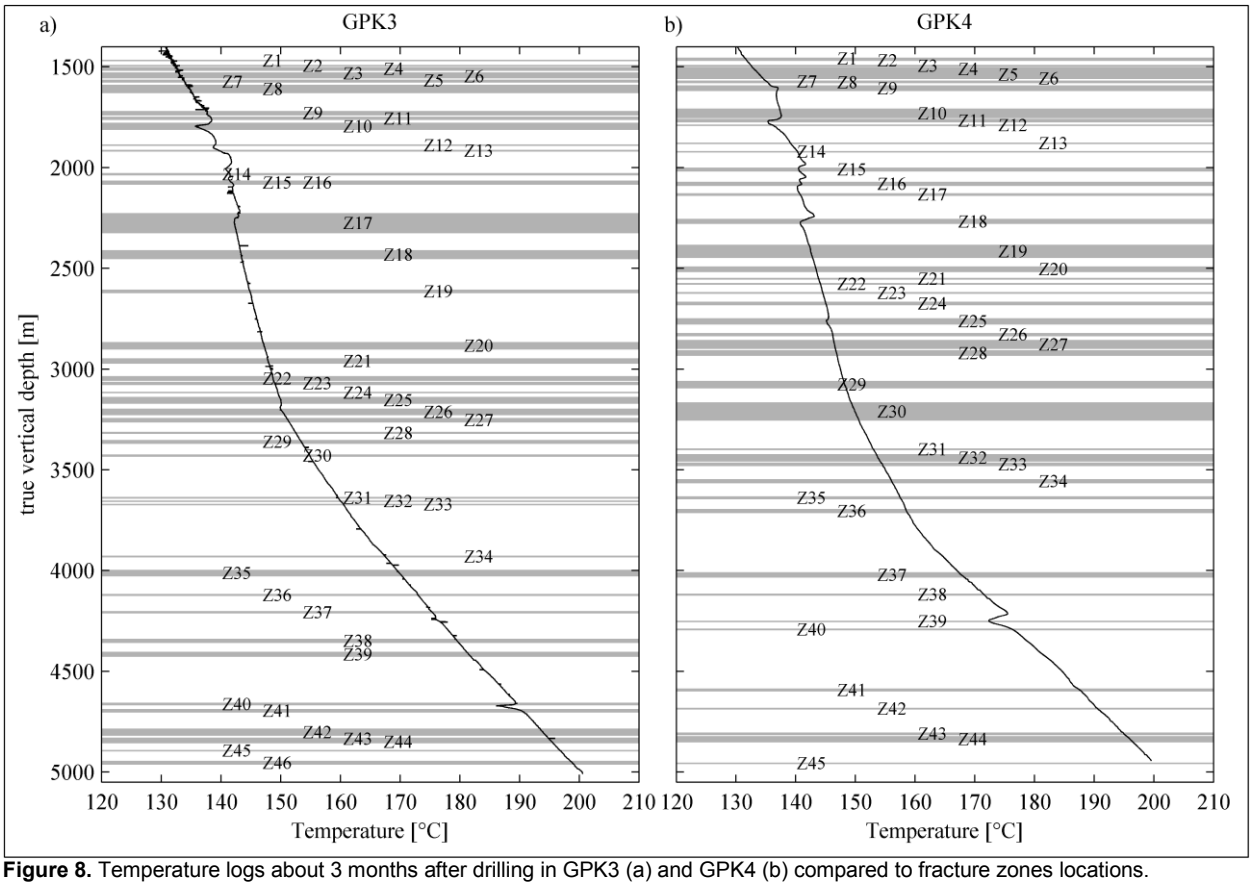

Figure 8. Temperature logs about 3 months after drilling in GPK3 (a) and GPK4 (b) compared to fracture zones locations.

between 200 and 400 m, in agreement with the indication from the variogram analysis presented here over.

One aspect that borehole wall images do not provide is the ability of the fracture zone to carry some flow. In order to get some insight in that aspect, location of fracture zones is displayed with temperature logs run about three after drilling completion on Figure 8. Permeable fracture zones will be more deeply cooled during drilling operations and present anomalies on the post drilling temperature profile. If run in adequate condition, temperature log can be very informative and permit to point out very precisely which fractures are flowing (see e.g. Evans et al., 2005b). In our case, month after drilling, the anomalies are smeared and we do not expect such precise indications as well as not an exhaustive listing of flowing fracture zones. Nevertheless, seven temperature anomalies were seen in each borehole, and all of them were clearly corresponding to a fracture zone determined on borehole images. Moreover, the four anomalies which were corresponding to correlated fracture zones (above 2200 m), were consistently indicating flows in the same fracture zone on both GPK3 and GPK4 boreholes.

Depth locations of flowing fracture zone are highlighted by asterisks on Figure 7. One the seven fracture zones which present temperature anomalies, five are situated in the upper part of the borehole. These five fracture zones are all East dipping. The other fractures zone located deeper in boreholes are all West dipping. As we are not sure to have a exhaustive listing of flowing fracture zones, that dataset cannot be used to estimate mean spacing between flowing fracture zones.

SYNTHESIS

The fracturing of the basement of the Upper Rhine Graben during its long tectonic history generated discontinuities at various scale. The here over presented analyses permitted to define these various structures and attempt to quantify their characteristic size. Figure 9 present these results in a synthetic manner.

On the upper end of the size scale, the Upper Rhine Graben, a major structure through central Europe, is 300 km long, 30 to 40 km wide and affects the entire thickness of the continental crust. It is itself a segment of the European Cenozoic Rift System which extends over a distance of some 1100 km (Dèzes et al., 2004). The border faults of that graben accommodate large strain with downthrow reaching about 4.5 km.

The inner architecture of the Upper Rhine Graben is made of tilted blocks delimited by major faults. These faults are brought in evidence by geological mapping and geophysical investigations. Their length range from about 2 km to 20 km. Example of such faults in the Soultz area are the Pechelbronn fault, the Surbourg-Kutzenhausen fault or the the Hermerswiller-Soultz fault. They built local little horst and graben systems with downthrow ranging from about 100 to 500 m. The spacing of such structures ranges from about 800 m to 3 km or even more.

Detailed analysis of the fracturing at borehole walls and appropriate statistical analyses and borehole cross-correlations permit to highlights structures at an intermediate scale that we call fracture zones. These fracture zones occur with a spacing ranging from about 80 to 400 m and sometimes less. Their extension cannot be reliably constrained with the available data, but we estimate that they are about 50 m to a maximum of maybe 500 m long.

Borehole wall images permit to describe thousand of fractures with mean spacing of 1 to 6 m. Spacing distribution follows log-normal low with coefficient of variation presenting clustering of the fractures which reflects the occurrence of the fracture zones mentioned here over. Due to sampling

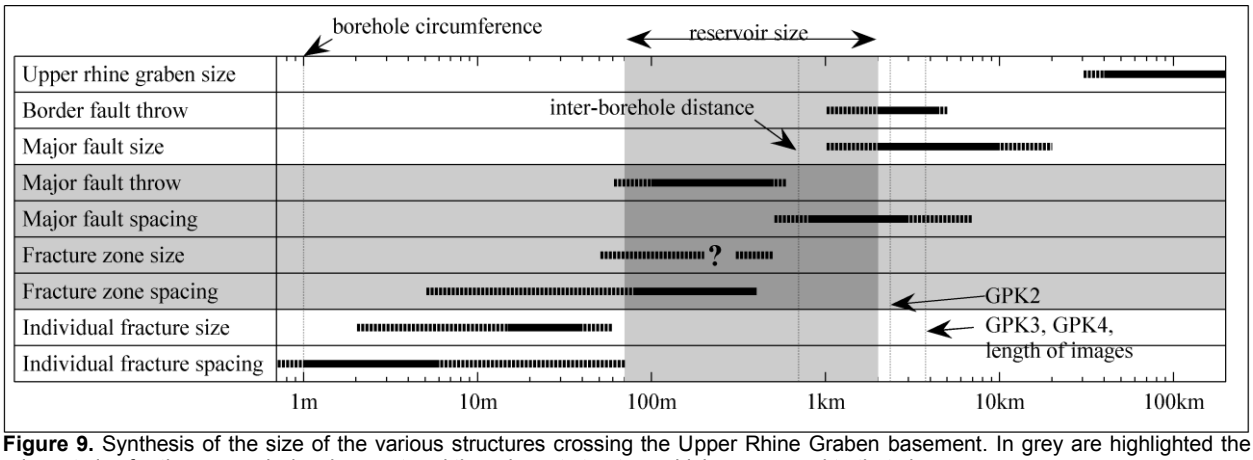

Figure 9. Synthesis of the size of the various structures crossing the Upper Rhine Graben basement. In grey are highlighted the relevant size for the reservoir development and the relevant structure which correspond to that size.

bias, power law distribution cannot be excluded and even maybe be most probable if considering previous studies on cores (Genter et al., 1997). The size of the fracture was evaluated considering them to be perfectly planar and penny shape by performing borehole cross-correlations. Mean fracture size was evaluated to be about 15 m to 40 m. With borehole data only, the fracture length distribution cannot be evaluated and an exponential negative distribution was used in the fracture length computation for easiness.

For the development of a geothermal reservoir, the relevant structures are clearly, due to their size and spacing, the fracture zones. Major faults may also play a role in the reservoir behaviour, but due to their spacing only one or two of these structures will cross a potential reservoir. They may be then dominant drain within the reservoir and produce short cuts which do not permit to build an efficient heat exchanger and so should possibly be avoided within a reservoir. At lower scale, single fractures may not have enough connectivity to carry significant flow rate, except within fracture zones.

The characterisation of fracture zone is then a key issue in the reservoir development. Unfortunately, major uncertainties remain concerning the exact geometry of these fracture zones. Their length is not constrained, but we believed that it is long enough to build connections between boreholes assuming the relay of a limited numbers of these structures. Spacings quantified here over are small enough to permit multiple flow paths between boreholes and so to efficiently exchange heat with the rock mass. The orientation of these fracture zones were estimated at borehole wall and seem to be similar to the orientation of the small scale fractures and large scale fault, i.e. N-S striking dipping at about 60° to the west or to the east, sub-vertical striking NW-SE or sub-vertical striking ENE-WSW. East dipping fracture zones dominate in the upper part of the basement while West dipping structures dominate at the level of the deep reservoir. Internal architecture of fracture zones seem to correspond to the conceptual model of anastomosed network of fractures delimiting shear lenses. But more important is the observed high heterogeneity of the architecture of fracture zones with major change in width and building over 10 to 20 m. Such heterogeneities may play a major role in the hydraulic behaviour of the fracture zones by channelling the flow in better developed fracture zone sections. This may explain the fact that only a limited number of fracture zones shows clear permeability at borehole, because indeed borehole can intercept a fracture zone but not necessary cross a present-day permeable channel of this fracture zone.

More effort should be done to characterise fracture zones, particularly their extension and geometry within the reservoir. This last aspect cannot be solved with borehole data only and other methods which permit to auscultate the volume between boreholes should be used. Presently, a VSP (Vertical Seismic Profile) survey is performed on the Soultz site which is expected to refine the results presented here.

CONCLUSIONS

Various structures with various size cross the basement under the geothermal site of Soultz-sous-Forêts. Detailed analysis of the fracturing permits to characterise and quantify the size of these structures. Results are following:

(1) Individual fractures have mean size ranging between 15 and 40 m and mean spacing between 1 to 6 m. Spacing distribution follow a log-normal law but this probably reflect sampling bias on a original power law distribution. Four major fracture orientation set were found. About 60% of the fractures strike N-S and dip about 60% to the East or to the West. East dipping fractures are dominant in the upper part of the basement while West dipping fractures dominate at reservoir depth, i.e. about 5 km depth. The two other major sets are sub-vertical, striking NW-SE and ENE-WSW.

(2) Individual fractures clustered to form fracture zones with spacing ranging from about 80 to 400 m. Their extension cannot be reliably constrained with the available data, but we estimate that they are about 50 m to a maximum of maybe 500 m long. Their orientations seem to include the major direction seen on general fracturing. Uncertainties subsist concerning their internal architecture, but it seems to correspond to the conceptual model of anastomosed network of fractures delimiting shear lenses. This includes also major variations in both building and width over distance of 10 to 20 m. These variations are suspected to play an important role in the hydraulic behaviour of the fracture zones by channelling the flow.

(3) Major faults have length of about 2 km to 20 km and spacing of about 800 m to 3 km or even more.

Due to their size and spacing, the most relevant structures on which a geothermal reservoir will developed are the fracture zones. The available data, i.e. principally the borehole images, have a scale of investigation limited to the borehole circumference which is about 1 m and do not permit to further characterise the extend and geometry of fracture zones within the reservoir volume. Alternative method like for example VSP will be used to refine the here presented results.

ACKNOLEDGMENTS

This work is supported by the Swiss State Secretariat for Education and Research under project number 03.04.60, and was performed as a contribution to the European Union's FP6 project 'Soultz EGS Pilot Plant' funded by ADEME, BMU, EC and EEIG 'Exploitation Minière de la Chaleur'.

REFERENCES

Bonnet, E., Bour, O., Odling, N.E., Davy, P., Main, I., Cowie, P.A., and Berkowitz, B., 2001, Scaling of fracture systems in geological media. *Reviews of Geophysics*, **39**, p. 347-383.

Chilès, J.P., 1988, Fractal and geostatistical methods for modeling of a fracture network. *Mathematical Geology*, **20**, p. 631-654.

Cloos, H., 1922, Über Ausbau und Anwendung der Granit-tektonischen Methode. *Abh. Preuss. Geol. Landesans.*, **89**, p. 1-18.

Dezayes, C., 1996, Caractérisation et interprétation d'un volume rocheux fracturé à partir de données de forages, les forages géothermiques de Soultz-sous-Forêts.*Thèse de doctorat de l'Université de Savoie thesis*, Université de Savoie.

Dèzes, P., Schimd, S.M., and Ziegler, P.A., 2004, Evolution of the European Cenozoic Rift System: interaction of the Alpine and Pyrenean orogens with their foreland lithosphere. *Tectonophysics*, **389**, p. 1-33.

Edel, J.B., and Weber, K., 1995, Cadomian terranes, wrench faulting and thrusting in central Europe Variscides : Geophysical and geological evidences. *Geologische Rundschau*, **84**, p. 412-432.

Edel, J.B., Schulmann, K., and Rotstein, Y., 2004, The Variscan tectonic inheritance of the Upper Rhine Graben: evidence of reactivations in the Lias, Late Eocene-Oligocene up to the recent. *International Journal of Earth Sciences*.

Einstein, H.H., and Baecher, G.B., 1983, Probabilistic and statistical methods in engineering geology. *Rock Mechanics and Rock Engineering*, **16**, p. 39-72.

Evans, K.F., Moriya, H., Niitsuma, H., Jones, R.H., Phillips, W.S., Genter, A., Sausse, J., Jung, R., and Baria, R., 2005a, Microseismicity and permeability enhancement of hydrogeologic structures during massive fluid injections into granite at 3km depth at the Soultz HDR site. *Geophysical Journal International*, **160**, p. 388-412.

Evans, K.F., Genter, A., and Sausse, J., 2005b, Permeability creation and damage due to massive fluid injections into granite at 3.5 km at Soultz: 1. Borehole observation. *Journal of Geophysical Research*, **110**.

Genter, A., 1990. Géothermie roches chaudes sèches: le granite de Soultz-sous-Forêts. (Bas-Rhin, France), Fracturation naturelle, altérations hydrothermales et interaction eau-roche. PhD Thesis, Orléans, 201 pp.

Genter, A., Martin, P., and Montaggioni, P., 1991, Application of FMS and BHTV tools for evalutation of natural fractures in the Soultz geothermal borehole GPK1. *Geothermal Science and Technology*, **3**, p. 69-82.

Genter, A., and Traineau, H., 1992, Borehole EPS-1, Alsace, France: preminilary geological results from granite core analyses for Hot Dry Rock research. *Scientific Drilling*, **3**, p. 205-214.

Genter, A., and Traineau, H., 1996, Analysis of macroscopic fractures in granite in the HDR geothermal well EPS-1, Soultz-sous-Forets, France. *Journal of Volcanology and Geothermal Research*, **72**, p. 121-141.

Genter, A., Castaing, C., Dezayes, C., Tenzer, H., Traineau, H., and Villemin, T., 1997, Comparative analysis of direct (core) and indirect (borehole imaging tools) collection of fracture data in the Hot Dry Rock Soultz reservoir (France). *Journal of Geophysical Research*, **102**, p. 15419-15431.

Gillespie, P.A., Walsh, J.J., Watterson, J., Bonson, C.G., and Manzocchi, T., 2001, Scaling relationships of joint and vein arrays from the Burren, Co. Clare, Ireland. Journal of Structural Geology, **23**, p. 183-201.

Illies, H., 1962, Oberrheinisches Grundgebirge und Rheingraben. *Geologische Rundschau*, **52**, p. 317--332.

Illies, H., 1972, The Rhine graben rift system - plate tectonic and transform faulting. *Geophysical Survey*, **1**, p. 27-60.

Illies, J.H., 1975, Recent and paleo-intraplate tectonics in stable Europe and the Rhinegraben rift system. *Tectonophysics*, **29**, p. 251-264.

Illies, H.J., and Greiner, G., 1979, Holocene movements and state of stress in the rhinegraben rift system. *Tectonophysics*, **52**, p. 349--359.

Jones, R. H., and R. C. Steward (1997), A method for determining significant structures in a cloud of earthquakes, *Journal of Geophysical Research*, **102**, p. 8245-8254.

Kim, Y.-S., Peacock, D.C.P., and Sanderson, D.J., 2003, Mesoscale strike-slip faults and damage zones at Marsalforn, Gozo Island, Malta. *Journal of Structural Geology*, **25**, p. 793-812.

Kim, Y.-S., Peacock, D.C.P. and Sanderson, D.J., 2004. Fault damage zones. *Journal of Structural Geology*, **26**(3). p. 503-517.

Lofts, J.C. and Bourke, L.T., 1999. The recognition of artefacts from acoustic and resistivity borehole image devices. In: M.A. Lovell, G. Williamson and P.K. Harvey (Editors), Borehole Imaging: applications and case histories. Special Publications. *Geological Society, London*, pp. 59-76.

Luthi, S.M., 2001, Geological well logs : their use in reservoir modeling, *Springer*, 373 p.

Martel, S.J., 1990, Formation of compound strike-slip fault zones, Mount Abbot quadrangle, California. *Journal of Structural Geology*, **12**, p. 869-877.

Martel, S.J., 2006, Effect of topographic curvature on near-surface stresses and application to sheeting joints. *Geophysical Research Letters*, **33**.

Menjoz, A., Cautru, J.P., Criaud, A., and Genter, A., 1989, Roches sèches chaudes. Caractérisation des réservoirs fracturées: Rapport annuel d'activités, *in* BRGM, ed., BRGM, p. 35-39.

Miller, S.M., 1979, Geostatistical analysis for evaluating spatial dependence in fracture set characteristics, 16th APCOM Symposium. Tucson, p. 537-545.

Moriya, H., Niitsuma, H., and Baria, R., 2003, Multiplet-Clustering Analysis Reveals Structural Details within the Seismic Cloud at the Soultz Geothermal Field, France. *Bulletin of the Seismological Society of America*, 93, p. 1606-1620.

Naylor, M.A., Mandl, G. and Supesteijn, C.H.K., 1986. Fault geometries in basement-induced wrench faulting under different initial stress states. *Journal of Structural Geology*, **8**(7). 737-752.

Peacock, D.C.P., Knipe, R.J., and Sanderson, D.J., 2000, Glossary of normal faults. *Journal of Structural Geology*, **22**, p. 291-305.

Priest, S.D., 1993, Discontinuity analyses for rock engineering, *Chapman and Hall*, 473 p.

Renard, P., and Courrioux, G., 1994, Three-dimensional geometric modeling of a faulted domain: The Soultz Horst example (Alsace, France). *Computers & Geosciences*, **20**, p. 1379-1390.

Rotstein, Y., Edel, J.B., Gabriel, G., Boulanger, D., Schaming, M., and Munschy, M., 2006, Insight into the structure of the Upper Rhine Graben and its basement from a new compilation of Bouguer Gravity. *Tectonophysics*, **425**, p. 55-70.

Schumacher, M., E., 2002, Upper Rhine Graben: Role of preexisting structures during rift evolution. *Tectonics*, **21**, p. 1006.

Segall, P., and Pollard, D.D., 1983, Joint formation in granitic rock of the Sierra Nevada. *Geological Society of America Bulletin*, **94**, p. 563-575.

Tenzer, H., Mastin, L., and Heinemann, B., 1991, Determination of planar discontinuities ans borehole geometry in crystalline rock of borehole GPK-1 at Soutz sous forets. *Geothermal Science and Technology*, **3**, p. 31-67.

Tenzer, H., Budeus, P., and Schnellschmidt, R., 1992, Fracture analyses in Hot Dry Rock drillholes at Soultz and Urach by Borehole Televiewer measurments. *Geothermal Resource Council Transactions*, **16**, p. 317-321.

Twidale, C.R., 1973, On the origin of sheet jointing. *Rock Mechanics and Rock Engineering*, **5**, p. 163-187.

Valley, B., and Evans, K.F., 2007, Stress state at Soultz-sous-Forêts to 5 km depth from wellbore failure and hydraulic observations, *32nd workshop on geothermal reservoir engineering*. Stanford.

Villaescusa, E., and Brown, E.T., 1990, Characterizing joint spatial correlation using geostatistical methods, *in* Barton, C.A., and Stephansson, O., eds., Rock Joints. *Rotterdam, Balkema*, p. 115-122.

Villemin, T., and Bergerat, F., 1987, L'évolution structurale du fossé rhénan au cours du Cénozoïque : un bilan de la déformation et des effets thermiques de l'extension. *Bulletin de la Société Géologique de France*, **3**, p. 245-255.

Milestone events & key observations in thermics, stress and hydraulics at Soultz (1987-2002)

Keith Evans[1], Bob Hopkirk[2], Reinhard Jung[3], Patrick Nam[i4], Marion Schindler[5], Dimitra Teza[6], Torsten Tischner[5]

1) Dept. of Earth Sciences, ETH-Zürich, Switzerland.
2) Polydynamics Engineering, Bahngasse 3, CH-8708 Männedorf, Switzerland.
5) Consultant,
4) Leibniz Institute for Applied Geosciences (GGA), Stilleweg 2, 30655 Hannover, Germany
5) Federal Institute for Geosciences and Natural Resources (BGR), Stilleweg 2, 30655 Hannover,

Presented at EHDRA Soultz scientific Meeting at Soultz on 24-25 September 2008.

EC Contract SES6-CT-2003-502706

PARTICIPANT ORGANIZATION NAME:.....

Related with Work Package 5 +

Related with Working Group 4

MILESTONE EVENTS & KEY OBSERVATIONS IN THERMICS, STRESS AND HYDRAULICS AT SOULTZ (1987-2002)

Keith Evans[1], Bob Hopkirk[2], Reinhard Jung[3], Patrick Nami[4], Marion Schindler[5], Dimitra Teza[6], Torsten Tischner[5]
1) Dept. of Earth Sciences, ETH-Zürich, Switzerland.
2) Polydynamics Engineering, Bahngasse 3, CH-8708 Männedorf, Switzerland.
5) Consultant,
4) Leibniz Institute for Applied Geosciences (GGA), Stilleweg 2, 30655 Hannover, Germany
5) Federal Institute for Geosciences and Natural Resources (BGR), Stilleweg 2, 30655 Hannover, Germany
6) BESTEC GmbH, Landauerstrasse 28, 76870 Kandel, Germany
e-mail: keith.evans@erdw.ethz.ch

ABSTRACT

In 2007 EHDRA decided that each Workgroup should produce a timeline-structured summary of key events and milestones in their area of expertise that have impacted the Soultz project since its inception. Here we present the current version of the summary of observations pertaining to thermics, stress and hydraulics prepared by Work Group 4 (Seismo-hydraulics). The work is still in progress: The task of expanding and writing commentary to the initial base-listing of events and observations has so far only reached 2003. Furthermore, Figures have yet to be included; and a thematic discussion section added. These elements will be developed during the next year.

EVENTS & MILESTONES

1987: GPK1 drilled to 2002 (582 m open hole) and stimulated

A surprise in drilling this first test hole into granite at the Soultz site was that the temperature at 2 km was only 140°C, instead of the 200°C that were expected from the thermal gradient in the first km (100°C/km). Although not recognised until later, this reflected active convection in the granite basement.
The ~600 m of open hole which extends almost to the granite top, was subjected to a comprehensive series of hydraulic tests using packers to isolate intervals. The program and results are reported in (Jung, 1991). Most facets of rock mass hydraulic behaviour seen in later, deeper project phases were manifest in the tests.
Difficulty was encountered with the use of inflation packers which tended to have short operational lifetimes owing to a combination of temperature and aggressive formation fluid (Rummel and Baumgärtner, 1991, Jung, 1991). This problem essentially prohibited the use of inflation packers in later phases of the project and led to the development of aluminium packer technology (Klee and Hegermann, 1995).
Pre-stimulation tests (e.g. 88MAY02) showed a reservoir production impedance of 1.7 MPa/l/s, with almost all production derived from a fracture zone at 1813 m. The remainder of the well had an impedance of less than 17 MPa/l/s, corresponding to an equivalent porous media (EPM) permeability of $< 3x10^{-17}m^2$. During testing, accidental overpressuring of the well led to a further zone near the bottom of the hole becoming active. Temperature logs suggest this zone consists of a 24 m long newly-induced axial fracture that intersects a natural fracture zone. The collective zone had an initial production impedance of 3.3 MPa/l/s (Jung, 1991?), and was subject to three focussed stimulation injections through a packer over a 2 year period, with progressively larger volumes and flow rates of 3 l/s (88DEC13), 7 l/s (91JUL11) and 15 l/s (91JUL18). In all three cases, the peak downhole overpressure was 6.0-6.5 MPa, indicating pressure-limiting behaviour. As a consequence of the injections, the production impedance of the zone was progressively increased to 0.24 MPa/l/s at 0.9 MPa drawdown, representing a tenfold increase.
Analysis of well test transients and the observation that pressure perturbations dissipated within a day indicated that the well was connected to a fault or fracture zone of large capacity that acted as a constant potential boundary. The well-test transients also showed that the impedance to both production and injection was non-Darcy, and had a turbulent-like component (Jung, 1992).
The shut-in pressure of injections suggested the minimum principal horizontal stress, Shmin is about 50% of the vertical stress (Rummel and Baumgärtner, 1991, Jung, 1991), which is typical of graben situations (Jamison and Cook, 1980). This implies a critical stress state where only small increases in pore pressure are required to produce shearing of optimally-oriented fractures (Barton et al., 1995, Evans, 2005). Breakouts and drilling-induced tension fractures indicated S_{Hmax} was oriented approximately N-S (Tenzer et al., 1992). Fault plane solutions to microearthquakes were a mix of strike-slip and normal, suggesting that $S_{Hmax} \approx S_V$.

1991 EPS1 drilled down to 2200 m depth and cased to 2007 m (193 m open hole)

The well was not tested until 1994 and was never stimulated. The initial reservoir impedance of the ~200 m open hole section to injection at 3 MPa was 15.4 MPa/l/s (94Apr08), but this decreased with higher pressure in later tests, particularly when downhole overpressure exceeded 4 MPa (Jung, field report?). This is close to the overpressure of 4.7 MPa required for jacking (Evans et al., 1996), as indicated by stress measurements. Four flow zones were identified in the well. Aluminium packers were successfully used for the first time to conduct hydraulic fracture stress tests at two locations near the hole bottom (Klee and Rummel, 1993). The results support the view that S_{hmin} is about 50% of the vertical stress.

1992 GPK1 extended to 3590 m (740 m open hole) and stimulated.

The temperature gradient continued to decline with depth averaging less than 10°/km between 2000 and 3000 m,

before increasing again in the lowermost few hundred metres. This essentially confirmed that convection was taking place within the granite (Le Carlier et al., 1994, Pribnow and Schellschmidt, 2000). The bottom-hole temperature at 3.6 km was 160°.

Practically all facets of hydraulic behaviour observed in the shallow tests to 2001 m also apply to this deeper interval. Prior to stimulation, evidence of natural permeability was seen at seven or so hydrothermally-altered fracture zones (HAFZ) that crossed the well every 50-100 m, although not all HAFZs were detectably permeable (Evans et al., 2005a). However, only the lowermost of these at 3480 m depth was hydraulically significant and accounted for almost all flow in well tests. The zone had large capacity and an injection impedance of ~1.4 MPa/l/s for flow rates up to 0.4 l/s (Jung et al., 1995b). At higher rates the impedance became turbulent-like and thus impedance increased with flow rate (Evans et al., 1996). The overlying 650 m section of hole that contained six flow points produced negligible flow and had an EPM permeability of ~10^{-17} m^2 (Evans et al., 2005a). Attempts to perform focussed stimulations using mechanical packers were hampered by packer flow-by (93AUG19, 93OCT01). Eventually, the well was sanded back to 3400 m, and the upper, low-permeability section was stimulated by injecting 20,000 m^3 of water at progressively higher flow rates from 0.15 l/s to 34 l/s (93SEP01). Pressure-limiting behaviour was observed, the maximum downhole overpressure of 9.0 MPa being attained by the 18 l/s stage. Well breakdown began almost immediately, and accelerated once the over pressure exceeded 6 MPa, the onset of detected microseismicity (Evans et al., 2005a, Baria et al., 1995). The breakdown during the early stages reflected progressive impedance reduction of individual flow zones throughout the depth range of the open hole, but this became focussed at the uppermost part of the hole once the limiting pressure was reached (Jones et al., 1995). At this time, jacking conditions were attained near the casing shoe and upward growth of microseismicity commenced. However, at greater depth, the wellbore pressure remained less than Shmin throughout the injection, suggesting shearing accounted for the impedance reduction in the lower section (Evans et al., 2005a). Systematic changes in the geometry of the microseismic cloud with depth are consistent with this (Cornet and Jones, 1994). A second stimulation was performed on the whole well by injecting 20,000 m^2 of water at 40 & 50 l/s (93Oct11). Initial injection pressure was ~1 MPa less than prevailed at the end of the earlier injection despite comparable flow rates at the flow zones, indicating some change had taken place during the 1 month shut-in.

Low-pressure step-rate injection and step-pressure production tests performed after the stimulations showed that the well impedance was the same for both production (94JUN15) and injection (94JUL04), and was governed by turbulent-like losses. Transient modelling demonstrated that the non-Darcy impedance was not just limited to the immediate vicinity of the wellbore, implying that flow paths within the rock mass had low divergence to maintain high flow velocities (Kohl et al., 1998). Modelling also demonstrated that the flow paths led to structures of large hydraulic capacity (i.e. constant potential features) (Jung et al., 1995b, Kohl et al., 1997). Spinner logs identified six flow zones, all of which showed turbulent-like impedance characteristics (Evans et al., 1996, Evans et al., 2005b). Some 50% of the flow occurred in a complex 80 m zone extending below the casing shoe, and the remainder was distributed between five discrete zones spaced every 100-150 m along the well. Importantly, the flow profile differed between injection and production tests, even though the wellhead impedance was the same, more flow entering the rock mass at a zone at 2950 m during injection at the expense of flow at a zone near 3225 m. This observation implies that a flow diversion between two zones 275 m apart was occurring which not change the net impedance. It follows that the two zones must be linked by a flow path of negligible impedance, possibly defined within a major microseismic structure that extends over 300 m near the zones, and that the impedance governing fluid exchange between these zones and the far-field must be common to both and lie beyond these zones, as shown in Figure 1 (Evans et al., 2005b).

The injection flow profile defined by this distribution did not change with injection pressure and was essentially the same as prevailed at the end of the simulation injections, suggesting that a relatively stable 'propped' network of flow paths had been created. The injectivity of the well increased 15 fold as a consequence of the injections, and 200 fold for the uppermost 650 m. The injectivity of the major HAFZ at 3480 m that was dominant prior to the stimulation increased by a factor of 2.

Five of the six major flow zones correspond to HAFZs that were determined to be permeable before stimulation. This suggests that the stimulated flow paths developed within existing, hydraulically-active structures. Repeat ultrasonic televiewer logs indicate that all major flowing fractures suffered dislocations of millimeters to centimetres, both in shear (Poitrenaud, 1994, Cornet et al., 1997), and opening mode (Evans, 2001, Evans et al., 2005a). The major flowing fractures tend to be accompanied by swarms of newly-permeable fractures that lie within the band of vein alteration about the major flowing fracture. These fractures support only minor flow, and show evidence of damage, most likely through shearing since they are critically-stressed (Evans et al., 2005a). There is little evidence for hydrofracture propagation from the well. Drilling-induced tension fractures occur more or less continuously from the casing shoe to 3250 m in the pre-stimulation fracture imaging logs (Bérard and Cornet, 2003). Despite this, almost all flow during stimulation enters the rock mass at the HAFZs.

Several wells sampling pore pressure near the top of the granite showed a reaction during the stimulation injections suggestive of communication through diffusion.

1995 GPK2 drilled to 3876 m (665 m open hole) some 450 m SSE of GPK1 and stimulated

During drilling, a HAFZ intersected at 2110 m proved so transmissive that mud laden with cuttings ascending the annulus flowed into the feature rather than to the surface. No cuttings or fluid were recovered from below 2110 m, demonstrating the enormous capacity that fracture zones within the granite can have.

The initial EPM permeability of the hole was determined before and after running the 7" casing when the open hole lengths were 2454 m and 665 m respectively. Prior to casing, a 15 l/s injection (95FEB02) was performed on the interval 1422 m - 3876 m. Temperature logs indicated more than 95% of the flow entered the rock mass at the fracture zone at 2110 m where the differential pressure was 0.53 MPa, implying a transmissivity of 3.7e-4 m^2/s (Jung, field report, 1995). The injection impedance of the entire 2454 m open-hole section of 0.03 MPa/l/s implies an EPM permeability of 5e-15 m^2. This compares with an EPM permeability for the 1766 m long section below the zone of less than 2e-16 m^2.

After casing the well to 3211 m, two 50 minute injections (95FEB10) were performed at 8.3 l/s to test the casing seal. Hydraulic data for these tests were not recorded, but it is reported that wellhead pressure rose to 8.0 and 8.6 MPa, and was probably still rising at shut-in (Socomine progress report, 1995). These data imply impedance of the 665 m open-hole section was at least 1 MPa/l/s. Spinner logs run during these tests indicated 14% of flow entered the formation at a double-fracture at 3245 m, 18% in a continuous zone extending 30 m below the fracture, ~13% at 3370 m, 12% between 3460 and 3480 m, and 13% below this point. Thus, relatively little flow entered in the lower half of the well. Several months later, a step-rate injection that attained steady-state was performed on the open hole at rates of 0.6 and 1.0 l/s and a maximum differential pressures of 1.55 and 2.75 MPa respectively (95JUN10), implying the reservoir impedance at these flow rates was Darcian and equal to 3 MPa/l/s, or an EPM permeability of 1.4e-16 m^2 (Jung et al., 1995a, Evans et al., 1996). This value is a lower limit of the natural impedance since it is possible that stimulation occurred

during the earlier, relatively high pressure injection. The flow profile

A novel stimulation technique that used a heavy brine to begin the injection was first tried on GPK2. The intention was to increase the hydrostatic gradient along the open-hole section thereby maximising the pressure attained at deeper intervals during the 'fracture initiation' phase. Thus a 'pre-pad' injection of 208 m^3 of heavy brine (ρ=1.18 gm/cc) was followed by 316 m^3 of formation brine (ρ=1.06 gm/cc) at 31 l/s (95JUN14). After a brief shut-in, injection resumed with 10,000 m^3 of formation fluid grading to 18,000 m^3 of fresh water injected at flow rate steps increasing from 13 l/s to 55 l/s (95JUN16). The well GPK1, which was shut-in, reacted almost immediately. Spinner logs in GPK2 indicate that at the end of the stimulation, flow entered the formation primarily at three zones: ~30% near the top of the open hole between 3215 and a prominent double fracture at 3237 m (25%), 30% across a broad zone with many flow points between 3300-3350 m; and 40% below 3448 m with 15% entering at a 2 m long vertical fracture that became progressively more active during the stimulation. Flow logs could not be run below 3470 m because of an obstruction. Identification of the nature of these extended zones of permeable fractures was hampered by the absence of cuttings.

A step-rate injection test conducted after stimulation (95JUL01) indicated the impedance to flow had been substantially reduced but was now turbulent-like (Kohl et al., 1996). Remarkably, the pressure-flow relation was very similar to that of GPK1, which had been stimulated with comparable volumes and maximum flow rates, although more flow entered in the lower part of the hole than was the case for GPK1. At 1.5 MPa downhole overpressure, the flow rate prior to stimulation was 0.6 l/s, and 12.5 l/s afterwards, indicating a 20-fold improvement in impedance.

The GPK1-GPK2 system was subjected to several trial circulations using GPK2 as the injection well and GPK1 as the production well. In the first test, GPK1 was produced under buoyancy drive through a choke at a flow rate of 15 l/s and GPK2 injected first for 6 days 15 l/s and then 9 days at 21 l/s (95JUL09). The test was terminated by a leak at the GPK2 wellhead assembly. The GPK1 production rate remained constant, in contrast to the decline observed in an earlier production tests without GPK2 injection (94JUN15). A downhole pump was then deployed at 380 m in GPK1 and a balanced circulation conducted for 9 days at the higher flow rate of 21 l/s (95AUG01). The circulation was terminated by the development of a leak at the GPK2 casing shoe. A stable drawdown in the pressure of GPK1 of ~2.5 MPa was reached after about 7 days.

GPK2 was subject to a further stimulation in 1996 with the injection of 27,000 m^3 of water at rates of 25, 46 and 78 l/s (96SEP18). Pressure at the casing shoe increased above the expected level of Shmin by 2-3 MPa. However, the excess is not large and essentially consistent with jacking with small entrance losses. Spinner logs, which could now be run to 3600 m because of the removal of an obstruction, showed that the flow profile remained largely unchanged from that prevailing at the end of the 1995 stimulation. Some 40% of the flow continued to enter below 3448 m, although the vertical fracture at 3448 m took a higher fraction of that flow (~25%). A step-rate test (96SEP29) following the stimulation showed the impedance remained turbulent-like, but had been reduced by a further 30% such that a 3.6 MPa downhole overpressure drove 25 l/s rather than 19 l/s following the 1995 stimulation, and 1.3 l/s using the initial Darcian impedance of 3 MPa/l/s.

1997 4 month circulation tests (97Jul12)

In summer 1997, the 3.0-3.5 km system was subject to a 4 month long, more-or-less continuous closed-loop, balanced circulation at ~ 24 l/s. Fluid was produced from GPK2 through a downhole pump that produced an estimated downhole drawdown of 3.0 MPa. Surface pressure was maintained at ~1.2 MPa to prevent scaling and CO2 outgassing before passing through the GPK1 reinjection pump.

Remarkably, reinjection pressure declined from 4.5 MPa at the start of the test to 2.0 MPa at the end, reflecting a decrease in injection impedance. Most of this decrease occurred in an episode lasting a few days in the middle of the test, although a gradual decline was evident throughout the test. The latter was primarily due to a gradual reduction in the impedance of a flow zone at 3250 m, possibly due to the effects of cooling stresses which could widen fracture apertures at the borehole and thus reduce entrance losses. However, the large, mid-test drop in injectivity is more complicated. The decline began shortly after the termination of the practice of adding an anti-scaling agent (Aquaprox) to the fluid prior to reinjection. A possible explanation of this coincidence is that the agent had somehow led to the build-up of deposits on the walls of the fracture entry points during the first part of the test, and this build-up precisely masked an increase in aperture resulting from the cooling stresses. Termination of the supply of Aquaprox led to the gradual depletion of the deposits, thereby eliminating the masking of the accrued effects of increased aperture on entrance losses. The impedance drop associated with the event occurred at both the flow zone at 3250 m that showed the gradual decline, and also a permeable fracture at 2860 m which is known to have suffered 2 cm of shear during the 1993 stimulation program (Evans et al., 1998). The impedance drops at these points resulted in increased focussing of flow and hence a change in the injection flow profile of the well, the first to have occurred since the 1993 stimulations. Although the impedance drops appear to indicate significant cooling-promoted reductions in pressure drops along flow paths leading from the well, it is unclear how far along the paths the implied aperture-increases extend.

The net impedance following the event produced a circulation impedance at the surface of 0.1 MPa/l/s, which the first time that this long-standing commercial target has been attained in any EGS system, and then for the largest well separation of 450 m ever attempted.

The production temperature increased throughout the circulation from 130°C to reach 142°C by the end. The increase probably reflects heating of the cooled rock volume around the well which had been cooled by the earlier stimulation injections. The productivity of GPK2 declined only slightly during the circulation, perhaps reflecting higher entrance losses due to thermo-elastic effects on the producing fractures. The usable thermal power produced assuming an injection temperature of 40°C attained ~11 MWt at the end of the test. The salinity of the production fluid increased during the test, reflecting a progressively larger fraction of formation water was present. This, together with the relatively small quantities of tracer recovered from tests indicates that production was accessing fluid stored in the 'far-field', probably in the network of major fracture zones and faults present in the rock mass. Nevertheless, the tracer results also showed a rapid response, indicating that at least some of the principal flow paths linking the wells were direct.

1999 GPK2 extended to 5024 m TVD (638 m open hole) and stimulated in 2000 (00JUN30)

Development of the 5 km deep system began in spring 1999 when the existing well GPK2 was extended from 3876 to 5084 m with open hole below 4431 m (all depths are measured along the hole from ground level). Prior to extension, the existing casing was removed and a downhole pump plus 150 m of tubing which had been lost in spring 1995 were fished. In addition, the major loss zone at 2110 m that had taken all cuttings during the initial drilling was plugged using a HMR (High Magnesium Resistant) cement which had been developed for the high temperature and high salinity conditions of Soultz. The success of the operation was demonstrated by the termination of the sensitivity of pressure in neighbouring well EPS1 to operations in GPK2. Leak-off into the stimulated fractures of the ‘upper reservoir’ between 3200

and 3600 m was not large enough to require remedial action. The hole was then reamed and extended to 5048 m with an 8-1/2 inch bit, and a 3 m core taken. A 33 m long 6-1/4 inch pilot bore was drilled at the hole bottom with the intention of conducting hydrofracture stress measurements. However, these were never conducted due to hole stability fears. Wireline logs including temperature, spectral gamma, ARI and UBI were run, the latter 3 only above 4650 m because of temperature limitations. The hole was sanded back and a 7 inch casing run with the shoe at 4431 m. The casing weight was supported by metal packers set above the casing shoe and ~260 m of cement. This was overlain by 460 m of fly-ash, the annulus being open above ~3740 m, just below the 'upper reservoir'. The sand was cleaned-out to 5069 m MD leaving 638 m of open hole.

A wireline gyro survey revealed that the hole becomes progressively deviated from vertical below 3870 m, the deviation reaching 26° at 4450 m before declining to 16° at TD. The deviation is consistently to the NW, suggesting it is controlled by a rock mass attribute. Severe spalling also occurred near the start of the deviation producing a cave between 3866 and 3891 m. A temperature log run six months after completion showed a bottom hole temperature of 202°C and a gradient in the lower kilometer of 30°C/km. Geological information from cuttings indicate major HAFZs at 4580-4600 and 4775 m, but no significant mud losses were noted at these depths (Genter et al., 1999). There are numerous other minor HAFZs defined by the presence of alteration minerals of illite and calcite, as in the upper reservoir.

Stress information from depths greater than the original bottom is sparse, because the UBI log was severely affected by stick-slip movement arising from the borehole irregularity.

Several hydraulic tests were performed without downhole pressure sensors prior to the stimulation in order to characterize the undisturbed formation and formation water: slug tests (99AUG02) yielded a near-field EPM permeability of 5-13e-17 m^2 (Weidler, 1999); a 5 week pump-assisted production test (99OCT25) conducted at 0.25 l/s attained steady-state and indicated a productivity index of 0.1 – 0.3 l/s/MPa, implying an EPM permeability of 4-12e-17 m^2 (Weidler and Jung, 2000); and a low rate injection test (00FEB25) conducted for 5 days at rates between 0.26 and 0.5 l/s attained quasi steady state conditions in several hours and indicated an injectivity index of 0.2 l/s/MPa, indicating an EPM permeability of 8e-17 m^2. Thus, all tests indicate the EPM permeability of the entire open hole section is of the same order as observed in the upper reservoir. The geochemical composition of the production fluid was also similar to that found in the upper reservoir, and the attainment of steady-state conditions in only a few hours indicates the existence of a large-capacity, hydraulic feature(s) close to the well - again a feature of the upper reservoir. It is of note that although wellhead pressure during the injection test did not exceed 2 MPa, irregularities in the pressure record were observed that suggest stimulation processes were being activated, possibly reflecting shearing on natural fractures. However, no evidence of microseismic emission was detected by a hydrophone in EPS1. None of the observation wells showed a pressure response to the injection which indicates the tightness of casing and the hydraulic isolation of the upper and lower reservoirs.

Attempts to identify flow points along the open hole during the low-rate injection were hampered by difficulty in running the P-T sonde past an enlarged zone at 4680 m. All that could be determined was that a flow entry point exists just below the casing shoe.

The entire open hole section was subjected to a major stimulation injection (00JUN30). Microseismicity was monitored by both an expanded surface network (Cuenot et al., 2008), and also an expanded and renovated downhole network (Dyer, 2001). A total volume of 23,400 m^3 of fluid was injected during 6 days in steps of 31, 41, and 51 l/s (Weidler, 2000). The main injection was preceded by a pad of 800 m^3 of heavy brine (1200 kg/m^3) injected abruptly at 32 l/s to reduce the pressure gradient along the open hole and thus maximise the pressure near hole bottom. The density of the brine was progressively reduced over a 6 hr period by mixing with stored formation water until fresh water injection commenced. All injected fluid was tagged by tracers. The 31 l/s and 41 l/s steps each lasted for ~1 day. Pressure at the casing show rose quickly and peaked at 12 MPa after 6 hrs during the brine-transition, before declining slightly. However, during the final stage, which lasted 4 days, differential pressure slowly but continually increased reaching 13.5 MPa at shut-in. This maximum pumping pressure is only slightly higher than required for stimulation of the upper reservoir and indicates both are critically-stressed (Hettkamp et al., 1998). The pressure decline upon shut-in was much longer than observed for the stimulations of the shallow reservoir, suggesting that either the reservoir has hydraulically-tighter boundaries, as also suggested by the pattern of microseismicity, or it has a larger storage capacity. As in the pre-stimulation tests, no hydraulic response was observed in the other wells, again suggesting hydraulic isolation of the upper and lower reservoirs (Weidler, 2000).

Only one spinner log was successfully performed to TD. This was run during the 30 l/s-step and indicated outlets near 4430 m (10 %), 4780 m (20 %), 4890 m (17 %) and below 4950 (52 % (Baria et al., 2002). However, the absence of a caliper profile below 4610 m, and the inference from logging that hole irregularity is significant severely degrades the confidence in these flow fractions. Nevertheless, the flow zone as 4780 m coincides with the HAFZ at ~4775 m inferred from drill cuttings, although the other major HAFZ at 4580-4600 m does not appear to have accepted significant flow.

Seismic activity was high throughout the injection with about 30,000-40,000 triggered events of which up to 14,000 were located (Dyer, 2001, Asanuma et al., 2001b). First events were located directly below the casing shoe, and around and below 4800 m, with predominantly downward migration. Seismic activity persisted after shut-in, even when the wellhead pressure approached its initial level. The primary microseismic structure defined by the events is a planar feature that strikes ~N155°E and dips 80° that intersects GPK2 at 4700 m (Asanuma et al., 2001a, Weidler, 2000).

The PTS sonde remained parked in the open hole at 4550 m for most of the stimulation. A flow/temperature log (TP20150) was run 6 days after shut-in on 12th July and the sonde re-parked at 4550 m. This was the last log run in the well. Shortly thereafter it was noticed that the sonde could not be moved upwards, and attempts to free it failed when the wireline snapped leaving 700 m of cable above the sonde. Camera inspection of the source of the problem in June 2002 showed that the casing had partially collapsed at 3904 m, leaving the sonde and cable trapped below. The collapse occurred near a cave zone, and it is thought to have been provoked when the casing was extending of the casing that was occurring due to warm-up after the stimulation, was blocked at the wellhead. However, it has also been suggested that the collapse was induced by shearing of a major structure that cuts the wellbore at the spall zone.

To characterise the improvement in reservoir productivity, an step-rate injection test (00JUL13) was performed one week after the stimulation, before the reservoir had returned to equilibrium. The test featured one-day stages of 15, 25 and 30 l/s, but was terminated midway through the 30 l/s stage due to the rising level of seismic activity. Steady-state conditions were not reached in any stage from which an injectivity could be estimated, although it was clearly higher than before the stimulation (Weidler, 2000).

In 2000 and 2001, a series of four production tests were conducted, two of which were long term with a cumulative volume of 4000 m^3. Steady-state conditions were not reached after 3 weeks. Chemical analyses of the produced fluid indicated that 40% was fresh water from the stimulation.

Two further production tests with volumes of 450 and 253 m^3 were performed mainly for geochemical investigations. At the end of the fourth production test, the freshwater

content was 19 % in contrast to the first production in 2000 where it was 46 %.
In June 2002, an investigation of the obstruction at 3904 m revealed that the casing had collapsed, trapping the sonde below, but that a 3 inch aperture to the hole below remained. A short injection test (2002JUN13) of 120 m^3 was performed at various flow rates to confirm the well was open, but the stages were too short to estimate the injectivity. This deficiency was addressed in a further injection test (03JAN23) conducted after GPK3 had been drilled and shut-in but not stimulated. GPK2 was injected with fresh water at 15 l/s for 7 days, with pressure monitored by a gauge 3500 m. (Tischner et al., 2007) analysed the shut-in pressure decline curve and estimated an injectivity of 0.35 l/s/bar. Wellhead pressure of GPK3 reacted immediately to the injection in GPK2 which indicates hydraulic coupling. Furthermore, the pressure in GPK1 also reacted, in contrast to earlier tests prior to the drilling of GPK3.
Examination of the core from the hole bottom indicated fractures filled with calcite, a mineral that is also known to be present in fractures both within and outside of HAFZs. To try to dissolve this mineral, an acidizing operation (03FEB12) was performed during a convention stimulation in which 5800 m^3 of fresh water was injected at a base flow rate of 15 l/s over 4 days. Four 6 hr pulses of 30 l/s were spaced over the 4 days. During the 2nd/3rd pulses 2/3 m^3 of HCl was added to 300/700 m^3 of water respectively (Hettkamp et al., 2004). A marked drop in injection pressure of 0.7 MPa occurred as soon as the first acid pulse reached the open hole, the second pulse having no clear effect. Comparison of the first and transient pressure histories for the fourth pulses showed that a reduction in the near-field impedance of the well had occurred.
(Tischner et al., 2006) summarize the hydraulic behaviour of GPK2 with a formation linear flow regime. A turbulent skin is observed as well as a high storage of 20 m^3/MPa and a high conductive fracture which is connected to the borehole. The productivity is 5.0 l/s/MPa after two days declining to 4 l/s/MPa after 4 days.

2003: Drill GPK3 to 5000 m TVD and stimulate (03May27) with simultaneous injection into GPK2

- One dominant fracture zone at 4760 m depth (total mud losses during drilling and flow log before stimulation show that production came only from this fracture).
- 03JAN23 15 l/s injection into GPK2 - GPK3 reacts almost immediately.
- 03Feb12 15/30 l/s inject into GPK2 with acidising. Reduces near-well impedance.
- Turbulent flow in GPK2 casing after collapse (possibly because of restriction in wellbore)
- 03May27 stimulation: Starting different than previous stimulation
- Characteristics of the pressure curve looks like normal hydraulic testing on a permeable feature at the beginning
- Downhole overpressure: 170 bars, high flow rate for 2 h: around 90 l/s
- No significant increase of injectivity after stimulation. (?)

- 03Jun24 15 l/s circulation between GPK2&3.
- It worked!
- Tracer return after 3 days suggest a relatively direct connection (probably along the fracture)
- Circulation on a distance of 600 m

2004 Drill GPK4 to 5000 m TVD and stimulate (04Sep13 & 05Feb04)
Acidization improvements in injectivity and communication with GPK3.

- Hydraulic stimulation with lower rates and lower volumes
- Initial injectivity very low: 0.01 l/s/bar, corresponding to an apparent porous media permeability of around 10-20 mD
- Maximum pressure higher in the second stimulation than in the first one
- HCl injection did not significantly improve the injectivity in the open-hole section (?)
- Flow log after RMA shows changes in the flow profile in the open-hole section and improvement of the injectivity (?)
- Improved connection to GPK3
- Casing leaks seen to develop (4360, 4712 MD). Possible explanation is that casings have been sheared by slip on a fracture zone (surprising USIT log did not see strong evidence of deformation)
- Image logs are recommended
- Real breakdown pressure with possibly a hydraulic axial fracture

REFERENCES

Asanuma, H., Ishimoto, M., Jones, R.H., Phillips, S. & Niitsuma, H., 2001a. A variation of the collapsing method to delineate structures inside a cloud. Bull. Seis. Soc. Am., 91**,** 154-160.

Asanuma, H., Mochizuki, S., Nakazato, K., Soma, N., Niitsuma, H. & Baria, R., 2001b. Data acquisition and analysis of microseismicity for simulation of deep reservoir by the MTC/Murphy International Collaborative Project. Geothermal Resources Council Transactions, 25**,** 161-165.

Baria, R., Garnish, J., Baumgärtner, J., Gérard, A. & Jung, R., Year. in World Geothermal Congress. Florence, Italy, pp. 2631-2637

Barton, C.A., Zoback, M.D. & Moos, D., Year. in Mechanics of Jointed and Faulted Rock. Vienna, pp. 381-387

Bérard, T. & Cornet, F., 2003. Evidence of thermally induced borehole elongation: a case study at Soultz, France. Int. J. Rock Mech. Min. Sci., 40**,** 1121-1140.

Cornet, F.H., Helm, J., Poitrenaud, H. & Etchecopar, A., 1997. Seismic and aseismic slip induced by large fluid injections. Pure Appl. Geophys., 150**,** 563-583.

Cornet, F.H. & Jones, R.H., Year. in 1st North American Rock Mechanics Symposium. Austin, Texas, pp. 61-69

Cuenot, N., Dorbath, C. & Dorbath, L., 2008. Analysis of microseismicity induced by fluid injections at the Hot Dry Rock site od Soultz-sous-Forêts (Alcace, France): Implications for the characterization of the geothermal reservoir. Pure and Applied Geophys., 165**,** 797-824.

Dyer, B.C., 2001. Soultz GPK2 stimulation (June/July 2000) seismic monitoring report., Report to Socomine, Semore Seismic, Falmouth, UK.

Evans, K.F., 2001. Determining the effect of stimulation injections on the rock mass around the well GPK1 from borehole data: analysis of the 1993 injections, Final report to the Swiss Department of Education and Science (BBW) under contract BBW 98.0008-1, Swiss Federal Institute of Technology.

Evans, K.F., 2005. Permeability creation and damage due to massive fluid injections into granite at 3.5 km at Soultz: Part 2 - Critical stress and fracture strength. Journal of Geophysical Research, 110**,** 14 pp.

Evans, K.F., Genter, A. & Sausse, J., 2005a. Permeability creation and damage due to massive fluid injections into granite at 3.5 km at Soultz: Part 1 - Borehole observations. Journal of Geophysical Research, 110**,** 19 pp.

Evans, K.F., Kohl, T., Hopkirk, R.J. & Rybach, L., 1996. Studies of the nature of non-linear impedance to flow within the fractured granitic reservoir at the European Hot Dry Rock Project site at Soultz-sous-Forêts, France, Final report to the Swiss Department of Education and Science (BBW) under contract BBW 93.0010, Swiss Federal Institute of Technology/Polydynamics Engineering.

Evans, K.F., Kohl, T. & Rybach, L., 1998. Analysis of the hydraulic behaviour of the 3.5 km deep reservoir

during the 1995-1997 test series, and other contributions to the European Hot Dry Rock Project, Soultz-sous-Forêts, France, Final Report to the Swiss Department of Education and Science (BBW) under contract number BBW 95.0673-2, Swiss Federal Institute of Technology.

Evans, K.F., Moriya, H., Niitsuma, H., Jones, R.H., Phillips, W.S., Genter, A., Sausse, J., Jung, R. & Baria, R., 2005b. Microseismicity and permeability enhancement of hydrogeologic structures during massive fluid injections into granite at 3 km depth at the Soultz HDR site. Geophys. J. Int., 160**,** 388-412.

Genter, A., Homeier, G., Chèvrement, P. & Tenzer, H., 1999. Deepening of GPK-2 HDR borehole, 3880-5090 m (Soultz-sous-Forêts, France): Geological Monitoring, Public report, BRGM.

Hettkamp, T., Baumgärtner, J., Baria, R., Gérard, A., Gandy, T., Michelet, S. & Teza, D., Year. in 29th Workshop on Geothermal Reservoir Engineering. Stanford University, Stanford, California, pp. 184-193

Hettkamp, T., Klee.G. & Rummel, F., Year. in Pre-conference proc. of 4th Int. Hot Dry Rock Forum. Strasbourg, France, pp.

Jamison, D.B. & Cook, N.G.W., 1980. Note on measured values for the state of stress in the Earth's crust. Journal of Geophysical Research, 85**,** 1833-1838.

Jones, R.H., Beauce, A., Jupe, A., Fabriol, H. & Dyer, B.C., Year. in World Geothermal Congress. Florence, Italy, pp. 2665-2669

Jung, R., 1991. Hydraulic fracturing and hydraulic testing in the granitic section of borehole GPK1, Soulz-sous-Forets. Geothermal Sci. and Tech., 3**,** 149-198.

Jung, R., 1992. Connecting a borehole to a nearby fault by means of hydraulic fracturing. Trans. Geotherm. Resources Council, 16**,** 433-437.

Jung, R., Reich, W., Engelking, U., Hettkamp, T. & Weidler, R., 1995a. Hydraulic tests in1995 at the HDR Project, Soultz-sous-Fôrets, France, Field Report, Bundesanstalt für Geowissenschaften und Rohstoffe (BGR), Hannover, Germany.

Jung, R., Willis-Richards, J., Nicholls, J., Bertozzi, A. & Heinemann, B., Year. in World Geothermal Congress. Florence, Italy, pp. 2671-2676

Klee, G. & Hegermann, P., Year. in World Geothermal Congress. Florence, Italy, pp. 2559-2561

Klee, G. & Rummel, F., 1993. Hydrofrac stress data for the European HDR research project test site Soultz-sous-Forêts. Int. J. Rock Mech. Min. Sci. & Geomech. Abst., 30**,** 973-976.

Kohl, T., Evans, K.F., Hopkirk, R.J., Jung, R. & Rybach, L., 1997. Observation and simulation of non-Darcian flow transients in fractured rock. Wat. Resourc. Res., 33**,** 407-418.

Kohl, T., Evans, K.F. & Rybach, L.R., Year. in Pre-conference proc. of the 4th Int. Hot Dry Rock Forum. Strasbourg, France, pp.

Kohl, T., Jung, R., Hopkirk, R.J. & Rybach, L., Year. in Proc. 3rd Int. Hot Dry Rock Forum. Santa Fe, New Mexico, pp. 85-87

Le Carlier, C., Royer, J.J. & Flores, E.L., 1994. Convective Heat Transfer at the Soultz-sous-Forêts geothermal Site: implication for oil potential. First Break, 12**,** 553-560.

Poitrenaud, H., 1994. Application des mesures par 'ultrasonic borehole imager' à la determination de glissements sur fractures preexistants, Masters Thesis (Rapport de DESS) in French, Institut de physique du globe de Paris.

Pribnow, D. & Schellschmidt, R., 2000. Thermal tracking of Upper Crustal flow in the Rhine Graben. Geophys. Res. Lett., 27**,** 1957-1960.

Rummel, F. & Baumgärtner, 1991. Hydraulic fracturing stress measurements in the GPK1 borehole, Soultz-sous-Forêts. Geotherm. Sci. and Tech., 3**,** 119-148.

Tenzer, H., Mastin, L. & Heinemann, B., 1992. Determination of planar discontinuities and borehole geometry in the crystalline rock of borehole GPK-1 at Soulz-sous-Forets. Geothermal Sci. and Tech., 3**,** 31-68.

Tischner, T., Pfender, M. & Teza, D., 2006. Hot Dry Rock Projekt Soultz: Erste Phase der Erstellung einer wissenschaftlichen Pilotanlage Final report to Bundesministerium für Umwelt, Naturschutz und Reaktorsicherheit for period: 1.04.2001-31.03.2005., Bundesanstalt für Geowissenschaften und Rohstoffe (BGR)

Tischner, T., Schindler, M., Jung, M. & Nami, P., Year. in Thirty-second Stanford Workshop on Geothermal Reservoir Engineering. Stanford University, pp. 322-328

Weidler, R., 1999. Slug test in the non-stimulated 5 km deep well GPK-2, Bundesanstalt für Geowissenschaften und Rohstoffe (BGR) Hannover.

Weidler, R., 2000. Hydraulic stimulation of the 5 km deep well GPK-2, Report to Socomine, Bundesanstalt für Geowissenschaften und Rohstoffe (BGR) Hannover.

Weidler, R. & Jung, R., 2000. Production test in the non-stimulated 5 km deep well GPK-2, Report to Socomine, Bundesanstalt für Geowissenschaften und Rohstoffe (BGR) Hannover.

Milestone Events & Key observations in Seismics at Soultz

Keith Evans[1], Stefan Baisch[2], Nicolas Cuenot[3], Louis Dorbath[4], Reinhard Jung[5]

1) Dept. of Earth Sciences, ETH-Zürich, Switzerland
2) Q-Con GmbH, Marktstr. 39, 76887 Bad Bergzabern, Germany
3) EEIG Heat Mining, Route de Kutzenhausen, Soultz-sous-Forêts, France
4) EOST/IPGS, 5, rue René Descartes, F-67084 Strasbourg
5) Consultant,

Presented at EHDRA Soultz scientific Meeting at Soultz on 24-25 September 2008.

EC Contract SES6-CT-2003-502706

PARTICIPANT ORGANIZATION NAME:……

Related with Work Package 5+

Related with Working Group 4

MILESTONE EVENTS & KEY OBSERVATIONS IN SEISMICS AT SOULTZ

Keith Evans[1], Stefan Baisch[2], Nicolas Cuenot[3], Louis Dorbath[4], Reinhard Jung[5]

1) Dept. of Earth Sciences, ETH-Zürich, Switzerland
2) Q-Con GmbH, Marktstr. 39, 76887 Bad Bergzabern, Germany
3) EEIG Heat Mining, Route de Kutzenhausen, Soultz-sous-Forêts, France
4) EOST/IPGS, 5, rue René Descartes, F-67084 Strasbourg
5) Consultant,
e-mail: keith.evans@erdw.ethz.ch

ABSTRACT

In 2007 EHDRA decided that the Workgroups should produce timeline-structured summaries of key events and milestones in their area of expertise that have impacted the Soultz project since its inception. This work remains in progress. Here we present the base-level listing of events and observations from which this document will be expanded.

EVENTS & MILESTONES

1988: GPK1 drilled to 2002 (582 m open hole) and stimulated

- 400 microseismic events observed that defined a cloud elongated in the NNW-SSE direction

1992 GPK1 extended to 3590 m and stimulated

- Methods of high-resolution location of events were developed and indicates the vast majority of events occur on and define planar or linear large-scale structures.
- Multiplets occurring within large structures indicate structural widths of tens of metres. The failure planes of the individual multiplets have dimensions of up to several tens of metres, and have orientations that scatter about that of the parent structure. This is consistent with failure on fractures within the damage zone of fracture zones.
- Stress derived from focal mechanism inversion is inconsistent with drilling-induced tension fractures observations.
- Dislocations of up to 2 cm seen on fractures in the well with relatively little nearby moment release suggest aseismic slip is occurring, as does changes in well injectivity during periods of negligible seismic activity.
- Cloud growing with time during stimulation
- Maximum magnitude was around 2
- Seismic event rate depends on the injected flow rate (moment versus volume, needs to be checked!!)
- Straight, sharp boundaries on the seismic cloud
- Development of downhole seismic sensors
- Soma's imaging method
- Distribution of events density versus distribution of moment density (needs to be checked!!)

1995 GPK2 extended to 3876 m (365 m open hole) and stimulated

- Use of the seismic cloud to target the new well
- Only a slight overlap with GPK1 cloud
- With GPK1 open, the seismic cloud did not move towards GPK1 but around. When the well was closed, the seismic cloud did approach GPK1.
- More spherical shape of the seismic cloud compared to GPK1 cloud. Might be related to the pumping schedule (GPK1 only well stimulated with step rates).
- Upward growth of the seismic cloud was more limited than for GPK1, perhaps because of the use of brine.

1997 4 month circulation tests (97Jul12)

- No significant seismic activity (?)
- Maximum magnitude below 1 (?)

2000 Extend GPK2 to 5000 m TVD and stimulate (00Jun30)

- Downward migration during injection, but upward migration during shut in
- Preferred growth to the North-West in the first phase of the stimulation, then sudden migration to the South (lower density)
- Maximum magnitude: 2.6, event occurred during the post-stimulation test
- Clear lower boundary for the upper stimulated volume and upper boundary for this stimulated area (gap in between)
- Released moment increased linearly with injected volume
- Average level of magnitude higher than for upper reservoir
- From downhole sensors, some events have high stress drop
- From surface sensors, events have normal stress drop, source size is bigger
- Focal mechanisms indicate mainly normal faulting, but also strike-slip and are consistent with the stress tensor.

2003 Drill GPK3 to 5000 m TVD and stimulate (03May27) with simultaneous injection into GPK2 for the latter part

- Onset of microseismicity started after 6h of injection (pressure 6 MPa higher than the downhole ambient pressure)
- Maximum magnitude observed during shut-in to date: 2.9
- General direction North-South (different from GPK2)
- Very large extension of the stimulated volume
- Large growth of seismic cloud during shut-in in comparison to GPK2
- Large upward growth
- Concentration of seismic events between the wells during dual injection
- Large magnitude events on the border of the cloud

2004 Drill GPK4 to 5000 m TVD and stimulate (04Sep13 & 05Feb04)

Acidization improvements in injectivity and communication with GPK3.

- Almost no overlapping with GPK3 seismic cloud
- General trend NNE-SSW
- Maximum magnitude: 2.3
- During the second stimulation, no seismicity until pressure reached the same pressure as during the first stimulation
- During the second stimulation, seismicity occurred after an injected volume only the half of the total volume injected during the first stimulation (not complete refilling of the previous stimulated volume)
- No overlapping between the September and the February seismicity
- Microseismicity clustered around top casing leak during post HCl step rate test in March 2005
- Microseismicity only around top casing leak during RMA test in May 2006
- No microseismicity during NTA test in October 2006
- Microseismicity around top casing leak during the OCA test in February 2007

2005 Circulation test (July to December 2005)

- No serious microseismicity
- Events were deep and below GPK4
- Maximum event size is (cf. Nicolas)
- Microseismicity increases with flow rate

Geological reconnaissance of deep fractured geothermal reservoirs: what we have learnt at Soultz in 20 years?

Genter A.*, Dezayes Ch.**, Ledesert B.,***, Sausse J.****, Valley B.*****

**GEIE EMC, Kutzenhausen, France*
***BRGM, Orléans, France*
****Cergy University, France*
*****Nancy University, France*
******ETH-Zurich, Engineering Geology, CH-8092 Zürich;*
now: MIRARCO/Laurentian University, 935 Ramsey Lake Road,
Sudbury, ON P3E 2C6, CANADA

Presented at EHDRA Soultz scientific Meeting at Soultz on 24-25 September 2008.

EC Contract SES6-CT-2003-502706

PARTICIPANT ORGANIZATION NAME: GEIE

Related with Work Package 5

Related with Working Groups 6/7

GEOLOGICAL RECONNAISSANCE OF DEEP FRACTURED GEOTHERMAL RESERVOIRS: WHAT WE HAVE LEARNT AT SOULTZ IN 20 YEARS?

Genter A.*, Dezayes Ch.**, Ledesert B.,***, Sausse J.****, Valley B.*****

**GEIE EMC, Kutzenhausen, France*

***BRGM, Orléans, France*

****Cergy University, France*

*****Nancy University, France*

******ETH-Zurich, Switzerland*

e-mail: genter@soultz.net

ABSTRACT

The Soultz geothermal project has been running for 20 years by taking into account both the nature and the structure of the deep crystalline basement penetrated by several deep exploration and geothermal wells. A lot of geological works have been done for exploring the crystalline rocks based on drilling data (cuttings, cores, well logging, borehole image logs) in the top basement (2km), in the upper reservoir (3,5km) and in the lower reservoir (5km). Fractures are nearly vertical and the major orientation in the granite is mainly NNW-SSE. Natural fractures and faults show a multi-scale organization in the deep granite from micro-cracks to large-scale normal faults. The geothermal target is a fractured granite reservoir characterized by hydrothermally altered and fractured zones showing low naturally permeability during drilling operations prior to any stimulations. The mineralogical composition of the fracture zones is made of some typical alteration mineral assemblages such as illite, secondary quartz, carbonates and locally sulfurs. This paper summarizes the main milestones and knowledge about Geology obtained in the Soultz wells over 20 years.

INTRODUCTION

The EGS technology has been under development over 20 years in the northern part of Alsace (France). This area was primarily selected due to the occurrence of one of highest large-scale geothermal anomaly well known from deep temperature measurements collected in a former petroleum field (Gérard et al., 1984). The geothermal area is located within the Upper Rhine graben which forms a part of the European Cenozoic rift system that extends in the foreland of the Alps from the Mediterranean to the North Sea coast (Dézes et Ziegler, 2001). The Moho which is the boundary between the Earth's crust and the mantle shows a topography of its depth thickness with a doming structure below the Rhine graben (Figure 1).

PRE-DRILLING PHASE

Previous data: the old Péchelbronn-oil field

At concessional scale, the Soultz area was well known before any geothermal drilling activity due to the large amount of geological data collected before the 70s' during the oil exploration of the Péchelbronn-Merkwiller oil field. More than 3000 oil wells were done giving a quite good overview of the geology within the post-Palaeozoic sediments. For example, in 1905, 1164 wells had been drilled representing a cumulative length of 290 km, the deeper well reached 600 m depth. In 1927, the first geophysical resistivity logging operation has been performed by the Schlumberger brothers. During oil exploration, numerous temperature measurements have been made in the Péchelbronn oil-bearing region (Haas et Hoffmann, 1929). Based on approximately 500 measurements, this old study shown that isotherms are influenced primarily by the tectonic structure of the Rhine graben (Figure 2). Indeed, there is a strong horizontal and vertical increase of temperature which is especially marked in the vicinity of fault zones. For example, the hottest zone at 400 m depth is located along the western part of the Soultz horst and is characterized by NE-SW elongation (Hass et Hoffmann, 1929). On the top of this area, the GPK1 well was drilled in 1987-1988 at 2000m.

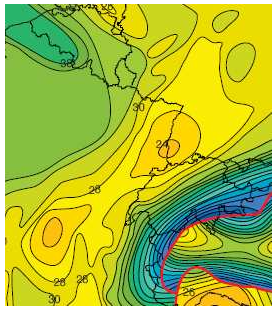

FIGURE 1. Map of the Moho depth expressed in km in Europe (Dézes et Ziegler, 2001). The Rhine graben is characterized by a minimum Moho depth of 24 km.

From a geological point of view, a structural compilation was done by Schnaebele et al. (1948) which illustrated the compartmenting of this area by normal faults inducing a horst and graben structure (Figure 3). In the 80s', several oil companies did seismic exploration in order to image the structure of the fault system inside the sedimentary cover of the Rhine graben. Therefore, before the GPK1 drilling, the top of the crystalline basement was known from both seismic reflection profiles and from a former oil well 4616 drilled to 1403m close to the site which reached the basement at 1380m. During oil exploration, a core was taken in this well and the petrography shown a typical granite rock composition. All these data were available and partly reinterpreted when the Soultz project started with the drilling of GPK1 (Figure 4).

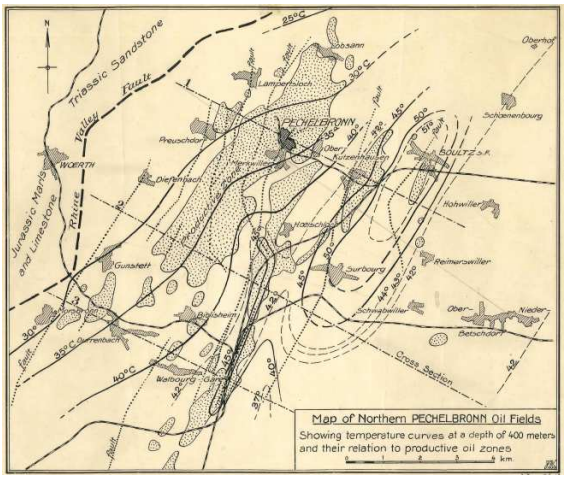

FIGURE 2. Temperature map done at 400 m depth based on data collected in oil wells between Merkwiller and Soultz (Haas et Hoffmann, 1929).

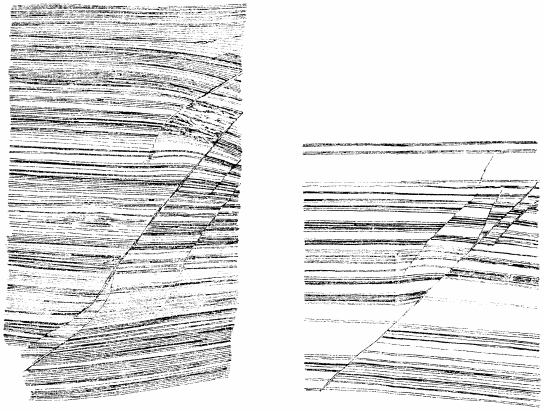

FIGURE 3. Example of normal faults observed at outcrop scale in the Péchelbronn oild field (Schnaebele et al., 1948).

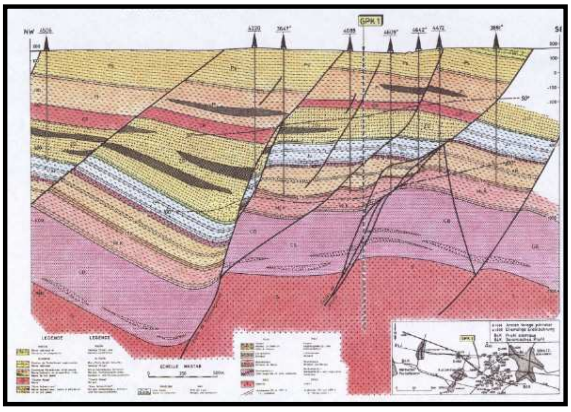

FIGURE 4. Geological W-E cross-section showing the Soultz Horst structure based on seismic line interpretation and old petroleum borehole data (Cautru, 1988).

Main geological studies before GPK1 drilling

Before any drilling operation, two different kinds of fracture studies were done by BRGM: a satellite image analysis and a structural study on relevant crystalline outcrops. At regional scale, a satellite image, called SPOT, was taken on November 1986 in order to investigate the large-scale fracture network visible on an area of 4500km². Large-scale fracture sets were outlined and are characterized by N-S, NE-SW, ENE-WSW and NW-SE orientations (Genter, 1989). On a field, a structural study was conducted in old quarries at Windstein located on the closest crystalline outcrops lying about 15 km westward of the geothermal site in the Vosges mountains. This structural analysis gave the first overview of the main nearly vertical pre-existing fracture sets which are oriented NW-SE, NNE-SSW and NE-SW (Genter and Martin, 1988).

EXPLORATION PHASE TO 2 KM DEPTH

After a pre-drilling phase leading to the site selection of the Péchelbronn-Soultz area (Gérard and Kappelmeyer, 1986), the first exploration vertical well GPK1 (Géothermie Puits Kutzenhausen 1) was drilled in 1987-1988 to 2 km depth by conventional drilling system (Herbrich, 1988). The bottom hole temperature was 140°C whereas 200°C was expect ed.
In 1987, the first exploration well, GPK1, reached 2 000 m, drilled in destructive mode. Originally, GPK1 was planned for a full coring of the basement (1400-2000m). Due to technical issues, the coring failed and only spot coring representing about a cumulative length of about 50 m of Triassic sediments and granitic cores was collected. Temperature at the bottom depth was 140°C. Based on well logging d ata, borehole image, cuttings analysis and spot coring calibrated on outcropping analogues, a first conceptual model of hydrothermally altered and fractured zone was defined at Soultz (Genter, 1989). The top of the basement was reached as expected at 1375 m. It corresponds to a Visean grey biotite-rich granite made of Feldspar megacrysts (Figure 5). This Visean granite is characterized by a heat production derived from radioactive logs of about 5 µW/m^3 (Rummel, 1991).

FIGURE 5. Granite core section from GPK1 well (3510m).

Surprisingly, a major permeable fracture zone having low natural permeability was evidenced at 1817m depth in GPK1 well based on total mud losses, gas and brines outflow (Vuataz et al., 1990) and specific hydrothermal alteration minerals such as clay mineral (Genter, 1989). The main secondary deposits related fracture zones are calcite, secondary quartz, illite and hematite mainly. Strong hydrothermal alteration halo was evidenced around this major permeable fault zone from cuttings, borehole image and well logging analysis (Genter et al., 1989, Traineau et al., 1991). The main hydrothermal alteration effect corresponds to the precipitation of illite (K-rich dioctaedric phyllosilicate) which results from the transformation of the primary biotite and Ca-plagioclase mainly (Figure 6b).

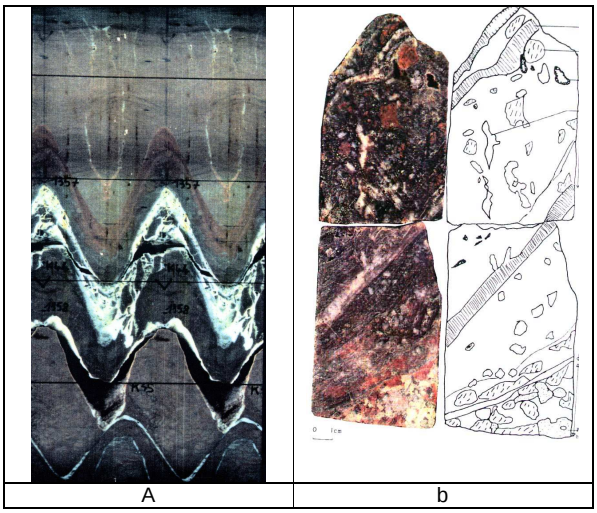

A | b

FIGURE 6. Examples of cores collected at Soultz. a) Fracture zone filled with barite and galena in the Triassic sandstone (EPS1, 1205 m, vertical scale 1m). b) Core K19 collected in a permeable fracture zone in GPK1 at 1809 m showing crushed granite and secondary quartz vein (vertical scale 30 cm).

Fracture geometry was deduced from electrical borehole imagery technique, called FMS (Formation MicroScanner) (Genter at al., 1991) and by acoustic borehole televiewer called BHTV (Figure 7, Tenzer et al., 1991). The main fracture orientation was N170°with high dipping va lues.

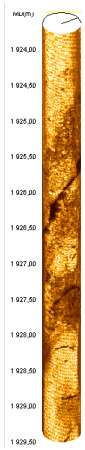

FIGURE 7. Example of 3D view of natural fractures visible on borehole image logs at Soultz.

In 1991, the reference well EPS1 which is an old oil well deepened to 2227 m, was deepened and fully cored with mining system to TD. Samples come from the lower Triassic sandstones formation (Buntsandstein) and from the same porphyritic granite penetrated previously by GPK1 (Genter and Traineau, 92). This well was originally planned to do the geological reconnaissance to 3,5km but from 2 km, as the deviation from horizontal was higher than 20°, the well was stopped. The high quality and the high recovery of the coring permit to characterize the granite petrography and its mineralogy, the hydrothermal alteration minerals as well as the fracture systems. A high quality structural and petrographic database was collected and used in various geological studies.

A major fractured zone filled with barite and sulphides was cross-cut at 1200 m in Triassic sandstones (Figure 6a). About 10 m thick of Permian clastic formations overlie the granite. The top of the basement was confirmed at 1417 m depth, i.e., deeper than in the northern well GPK1 confirming that this major interface is dipping southward with a low angle. The well penetrated the same granite massive (Stussi et al., 2002). A major permeable fracture zone was penetrated at 2160 m depth characterized by an outflow of geothermal brine (Figure 8). In this zone, organic matter is intimately associated with hydrothermal alteration like tosudite, a clay mineral bearing lithium (Ledesert et al., 1993). High mercury porosity values up to 25% were measured within this hydrothermally altered zone. Primary quartz was fully dissolved (Ledesert et al., 1999). The concept of HAFZ was refined based on core results by taking into account minerals dissolution and fracture organization (Genter et al., 1998, 2000). Pre-existing nearly-vertical fractures are mainly oriented N10°E and N170°E on core and BHTV (Genter et al., 1995; Genter et Traineau, 1996).

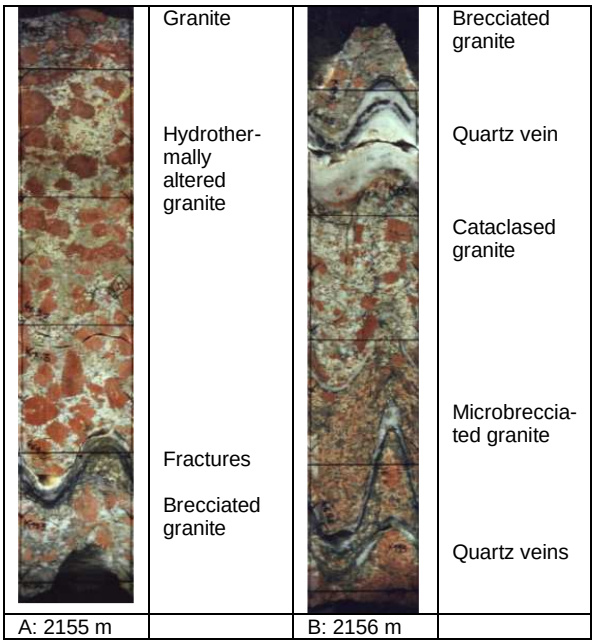

FIGURE 8. Example of Hydrothermally altered and fracture zone observed on core section in EPS1 well between 2155 and 2156 Measured Depth.

The fracture network was also investigated at very fine resolution scale with micro-crack studies done on cores in primary quartz crystals (Dezayes et al., 2000; Schild et al., 1998). In order to reconstruct the Tertiary palaeostress field and compare it with the structural Rhine graben evolution, palaeostress studies were carried out based of striated planes observed on cores (Dezayes et al., 1995) and on Vosges granite analogues (Dezayes, 1995). The cluster organization of fractures was validated based on core study by investigating fracture spacing, fracture thickness and fracture filling distribution with depth (Genter et al., 1997, Sausse et al., 1998).
Petrophysical characterization was mainly based on core samples taken in EPS1 (Rummel, 1991; Ledesert, 1993, Surma, 2003; Surma et Géraud, 2003, Sausse et al., 2006). Matrix porosity (Mercury, water) and thermal conductivities were evaluated. Altered samples show a large variation of porosity and thermal conductivity with an overall decrease of the thermal conductivity with the increase of porosity (Surma et Geraud, 2003).

Based on petro-structural studies on cores sample, the fabric of the granite was investigated. Sub-horizontal magmatic primary foliations were evidenced from petrofabric measurements (Schulmann et al., 1997). Sub-horizontal magnetic foliations indicate a magma emplacement in the centre of the batholith (Just et al., 2004). The dating of hydrothermal events on alteration minerals like illite give scattered ages between Permian, Jurassic and Cretaceous (Schleicher et al, 2006). Fluid inclusion studies showed that one of several fluid inclusion types has similar temperature to present thermal state (Dubois et al., 1996, Ledesert, 1993).

In the meantime, the reinterpretation of 5 seismic lines calibrated with oil well data permitted to build a 3D image of the Soultz Horst (Figure 9) in the sediments with the goCad geomodeller (Renard and Courrioux, 1994).

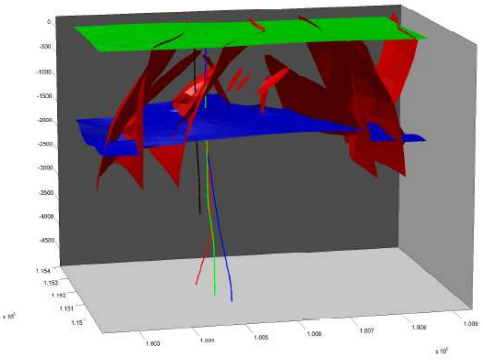

FIGURE 9. 3D model in the sediments derived from seismic line interpretation (goCad software).

EXPLORATION PHASE TO 3,5 KM DEPTH

The exploration phase to 3,5 km depth started by the deepening of GPK1 in destructive mode to 3,6km depth. The bottom hole temperature was 160°C. A core was taken at 3,510 m. The well penetrated the same granite massive (Genter et Traineau, 1991). The major permeable fracture zones characterized by outflow, mud losses, gas, and geodic quartz are located at 2815 m and 3490 m depth (Figure 10).

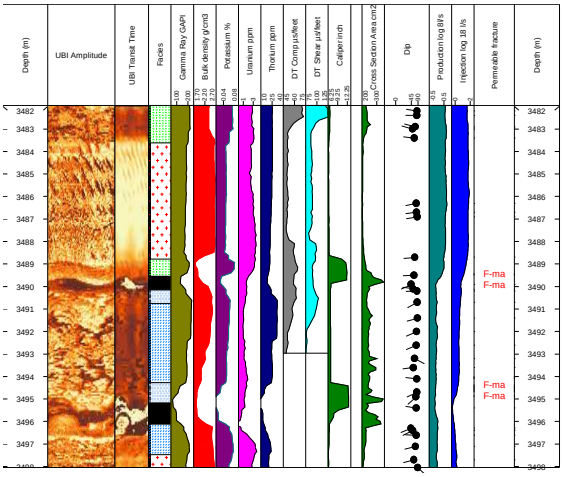

FIGURE 10. Relationship between permeable fracture, well logging data and flow log in a permeable fracture zone in GPK1 at 3,5 km.

The main nearly-vertical fracture orientation is N10°E, N20°E and N175°E. Fracture zone orientations are N140°E a nd N160°E in GPK1 and GPK2 (Genter et al., 1998). Frac ture apertures were evaluated from electrical borehole image ARI (Sausse et Genter, 2005). In GPK1, relationship between fracture zones and connected permeable paths were outlined (Evans et al., 2005).

The exploration of GPK2 showed a major permeable fracture zone penetrated at 2120 m provoking total mud and cutting losses from that depth to TD (Genter et Tenzer, 1995). Major faulted zones are located at 3240m and 3510 m and suspected at TD (3900 m). Fractures observed on UBI are nearly vertical and oriented N170°E±15° (Genter et al., 1997).

EXPLORATION PHASE TO 5 KM DEPTH

The deepening of GPK2 in 1999 to 5000 m showed the occurrence of a new fine grained two mica granite unit from 4860 m depth and confirmed by core examination (Genter et al., 1999). Rock dating of MFK rich granite and two mica fined grained granite gives 330 ±7 My and 327 ±3 My respectively (Alexandrov et al., 2001; Cocherie et al., 2004). Fractures are nearly vertical and oriented N170°E (Dezayes et al., 2004). Based on cuttings, fracture zones are located at 4580 m, 4780 and 4880 m (Genter et al., 1999). Calcimetry measurements in the cuttings samples showed some degree of matching of carbonate concentration and fracture zones (Grall et al., 2007). Compilation of geological data allows to propose a two granite body conceptual model (Dezayes et al., 2003; Hooijkaas et al., 2006).

The drilling of GPK3 and GPK4 gave similar geological results. A new fine grained two mica granite unit was evidenced from 4730 m depth in GPK3 (Dezayes et al., 2003). Fractures observed on UBI are nearly vertical and oriented N170°E (Dezayes et al., 2004; Valley, 2007). In GPK3, a natural large permeable fracture zone is located at 4770 m depth (Dezayes et al., 2003). There is not enough data for proposing a relevant fracture zone concept definition in the 2 mica granite. In the deepest part of GPK4, there is no natural large permeable fracture zone (Dezayes et al., 2005).

FRACTURE SCALES

The fracturing of the basement of the Upper Rhine Graben permitted to define structures at various scales and allowed to quantify their characteristic size (Valley, 2007; Figure 11).

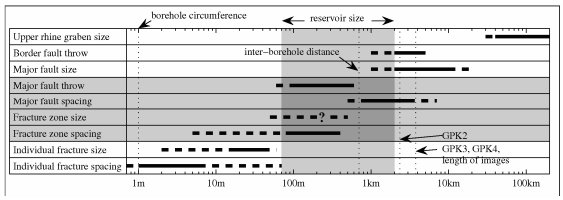

FIGURE 11. Synthesis of the size of the various structures crossing the Upper Rhine Graben basement. In grey are highlighted the relevant size for the reservoir development and the relevant structure which correspond to that size (Valley, 2007).

A general overview at fracture zone scale was done by Dezayes and Genter (2008). 39 fracture zones have been determined in the five deep wells of Soultz, GPK1, EPS1, GPK2, GPK3 and GPK4, and in the seismic monitoring well, named 4550. These zones have been plotted in 3D and compared with VSP and microseismicity results (Sausse et al., 2008)

CONCLUSIONS

As the Soultz geothermal target is a hidden granite batholith made of two superimposed granite units overlain by a thick post-Paleozoic sedimentary cover, the reconnaissance by drilling of this granitic body is much more difficult to explore than conventional high enthalpy fields. There are no surface hydrothermal manifestations of a deep resource such as fumaroles, hot springs, altered zone or geysers. The main indirect traces indicating a potential geothermal resource is the occurrence of high temperature at shallow depth (50°C at 400m depth) well-known from old-petroleum wells. Before drilling, a lot of sub-surface information was available in the sediments: seismic profiles, thousands of wells of various depth, and temperature measurements. The geothermal target is a Paleozoic altered and fractured granite overlain by a thick sedimentary cover made of Permian, Triassic, Jurassic and Tertiary sedimentary formations.

Based on 20 years of activities, geothermal exploration was mainly driven by high quality dataset acquisition, evaluation of rock composition of the pre-fractured crystalline rocks (petrography/mineralogy) and fracture network characterisation. Conceptual model of Hydrothermally Altered Fractured Zones (HAFZ) has been proposed at least for the MFK rich granite. 2 mains type of hydrothermal alterations were evidenced: pervasive and vein alterations. Occurrences of Hydrothermally Altered and Fractured Zones with illite, calcite and secondary quartz and low natural flow (brines) were found at various depths in the different Soultz wells. The fracture system is not homogenously distributed in space but some concentrations of fractures occur which alternate with poorly fractured sections. Highest fracture densities are mainly localized in the upper part of the geothermal site within 1400 and 2200 m depth. Fracture geometry is strongly influenced by the graben tectonics and shows nearly vertical fractures striking close to N170°E orientation.

CURRENT LIMITATIONS AND PERSPECTIVES

Despite of an exhaustive research work about geological characterisation, one must admit that there are still many open questions about deep-seated geology of the geothermal system. In sediments, there was not so many works. However, the vertical evolution of faults orientation with depth is debatable. Are faults striking with the same azimuth and dip with depth in sediment and in basement? Is there any variation in terms of orientation between N20°-N40°E fault geometry in sediments and N140°-N170° faults in the granite and in the Buntsandstein? Then, some new and innovative methods for imaging the top of the basement will be very helpful for evaluating the vertical persistence of faults as well as to check the occurrence of transverse faults oriented E-W. In granite, the HAFZ concept was proposed between core and well scales in the MKF-rich granite but no HAFZ model is available for the 2 mica granite. Fracture organisation and fracture extension beyond the borehole wall still remain open questions even VSP survey brings new inputs about large-scale fault zone. Fracture filling (composition, thickness) is always difficult to characterize based on cutting samples and well logging data.
Some research works for improving fracture zone concept based on various information (core, wells, analogues) are recommended. We need innovative geophysical tools/methods for better characterise the fault extension within the inter-well domain and in the reservoir and also 3D tool for taking into account the 3D complexity of fault geometry in hard rocks. Finally, relationships between channelling, permeability, hydrothermal alteration, and fault geometry have to be clarified.

REFERENCES

Alexandrov, P., Royer, J.J., Deloule, E., (2001). 331 ± 9 Ma emplacement age of the Soultz monzogranite (Rhine Graben basement) by U/Pb ion-probe zircon dating of samples from 5 km depth. *C.R.A.S.,* **332**, 747-754.

Cautru, J.P., (1988). Coupe géologique passant par le forage GPK1 calée sur la sismique réflexion, document BRGM IMRG, unpublished.

Chèvremont, Ph., Thiéblemont, D., Laforêt, C., Genter, A., Traineau, H., (1992). Etude pétrologique du massif granitique recoupé par le forage EPS-1 (Soultz-sous-Forêts, France). Rapport BRGM RCS 92 T15 SGN/IRG.

Cocherie, A., Guerrot, C., Fanning, C.M., Genter, A., (2004). Datation U-Pb des deux faciès du granite de Soultz (Fossé Rhénan, France). *Comptes Rendus Geoscience*, **336**, 775-787.

Dezayes Ch., Villemin Th., Pecher A., (2000). Microfracture pattern compared to core-scale fractures in the borehole of Soultz-sous-Forêts Granite, Rhine Graben, France, *Journal of Structural Geology*, vol. **22**, 723-733.

Dezayes, C., Genter, A., (2008). Large-scale fracture zone network based on Soultz borehole data. *Proceedings of the EHDRA scientific conference* 24-25 September 2008, Soultz-sous-Forêts, France.

Dezayes, Ch. (1995). Caractérisation et interprétation d'un volume rocheux fracturé à partir des données de forage. PhD thesis, Université de Savoie, France, 246 pp.

Dezayes, Ch., Chèvremont, Ph., Tourlière, B., Homeier, G., Genter, A., (2005). Geological study of the GPK4 HFR borehole and correlation with the GPK3 borehole (Soultz-sous-Forêts, France). Open file report BRGM/RP-53697-FR, 94 pp.

Dezayes, Ch., Genter, A. Gentier, S., (2004). Fracture network of the EGS Geothermal Reservoir at Soultz-sous-Forêts (Rhine Graben, France). Geothermal Resources Council Transactions, Palm Springs, California, USA, Vol. 28, 213-218.

Dezayes, Ch., Genter, A., Homeier, G., Degouy, M., Stein, G., (2003). Geological study of GPK3 HFR borehole (Soultz-sous-Forêts, France), Open file report BRGM/RP-52311-FR, 128 pp.

Dezayes, Ch., Villemin, Th., Genter A., Traineau, H., Angelier, J., (1995). Analysis of fractures in boreholes of the Hot Dry Rock project at Soultz-sous-Forêts (Rhine Graben, France), *Scientific Drilling*, vol. **5**, 31-41.

Dèzes, P., Ziegler, P. A., (2001). European Map of the Mohorovicic discontinuity. 2nd EUCOR-URGENT Workshop (Upper Rhine Graben Evolution and Neotectonics), Mt. St. Odile, France.

Dubois, M., Ayt Ougougdal, M., Meere, P., Royer, J.-J., Boiron, M.-Ch., Cathelineau, M., (1996). Temperature of paleo- to modern self-sealing within a continental rift basin: The fluid inclusion data (Soultz-sous-Forêts, Rhine Graben, France). *Eur. J. Mineral.*, vol. **8**, 1065-1080.

Evans, K.F., Genter, A., Sausse, J., (2005). Permeability creation and damage due to massive fluid injections into

granite at 3.5 km at Soultz: Part 1 - Borehole observations, *Journal of Geophysical Research*, **110**, B04203.

Genter, A., (1989). Géothermie Roches Chaudes Sèches : le granite de Soultz-sous-Forêts (Bas Rhin, France). Fracturation naturelle, altérations hydrothermales et interaction eau - roche. *PhD thesis*, **Université d'Orléans**, France, 201 pp.

Genter, A., Castaing, C., Dezayes, Ch., Tenzer, H., Traineau, H., & Villemin, T., (1997), Comparative analysis of direct (core) and indirect (borehole imaging tools) collection of fracture data in the Hot Dry Rock Soultz reservoir (France), *Journal of Geophysical Research*, **vol. 102**, B7, 15419-15431.

Genter, A., Cautru, J.-P., Montaggioni, P., Traineau, H., (1989), Geological interpretation of well logging data from the granitic section of the Soultz-sous-Forêts GPK1 well. *SPWLA*, 12th International Well Logging Symposium, SAID, **paper EE**, 25-27 Oct. 1989, Paris, 12 pp.

Genter, A., Dezayes, Ch., Gentier, S., Ledésert, B., Sausse, J., (1998). Conceptual fracture model at Soultz based on geological data. Geologisches Jahrbuch: Sondehefte: Reihe E. Geophysik ; H. SE 1, 4th International Hot Dry Rock (HDR) Forum, Strasbourg, France, Sept. 28-30 1998, 93-102.

Genter, A., Homeier, G., Chèvremont, Ph., Tenzer, H., (1999). Deepening of GPK-2 HDR borehole, 3880-5090 m (Soultz-sous-Forêts, France). Geological monitoring. Open file report BRGM/RR-40685-FR, 81 pp.

Genter, A., Martin, P., (1988). Analyse de la fracturation relevée sur les carottes de granite du forage GPK1 (Soultz-sous-Forêts, Bas-Rhin). *BRGM Open file report,* **RR-26086-FR**, 37 pp.

Genter, A., Martin, P., Montaggioni, P., (1991), Application of FMS and BHTV tools for evaluation of natural fractures in the Soultz geothermal borehole GPK1. *Geothermal Science & Technology*, **vol. 3**, 69-82.

Genter, A., Tenzer, H., (1995). Geological monitoring of GPK-2 HDR borehole, 1420-3880 m (Soultz-sous-Forêts, France). Soultz-sous-Forêts, Open file report BRGM/RR-38629-FR, 46 pp.

Genter, A., Traineau, H., (1991). Geological survey of the HDR borehole EPS1, Soultz-sous-Forêts, Bas-Rhin. Open file report BRGM/RR-32433-FR, SGN, IRG.

Genter, A., Traineau, H., (1996). Analysis of macroscopic fractures in granite in the HDR geothermal well EPS1, Soultz-sous-Forêts, France, *Journal of Volcanology and Geothermal Research*, **72**, 121-141.

Genter, A., Traineau, H., Bourgine, B., Ledésert, B., Gentier, S., (2000). Over 10 years of geological investigations within the European Soultz HDR project, France. Proceedings of the World Geothermal Congress 2000, Kyushu-Tohoku, Japan, May 28 - June 10, 2000, Editors E. Iglesias, D. Blackwell, T. Hunt, J. Lund, S. Tamanyu, 3707-3712.

Genter, A., Traineau, H., Dezayes, Ch., Elsass, P., Ledésert, B., Meunier, A., Villemin, T., (1995). Fracture analysis and reservoir characterization of the granitic basement in the HDR Soultz project (France). *Geothermal Science & Technology*, vol. **4** (3), 189-214.

Gérard, A., Kappelmeyer, O., (1986). The Soultz-sous-Forêts project and its specific characteristics with respect to the present state of experiments with Hot Dry Rocks, Proceedings EEC/US workshop on Hot Dry Rocks – Brussels, Belgium, 28-30 May 1986.

Gérard, A., Menjoz, A., Schwoerer, P., (1984), L'anomalie thermique de Soultz-sous-Forêts, *Géothermie Actualités*, **n°3** , 35-42.

Grall, C., Ledésert, B., Hébert, R., Genter, A., Bartier, D., Dezayes, Ch. Gérard, A., (2007). How calcimetry can help for a better knowledge of flow pathways in the Soultz-sous-Forêts Enhanced Geothermal System. Proceedings EHDRA Scientific Conference, 28 & 29 June 2007, Soultz-sous-Forêts, France, 6 p.

Haas, J.-O., Hoffmann, C.R., (1929), Temperature gradient in Pechelbronn ol bearing region, lower Alsace: its determination and relation to oil reserves. *Bull. Amer. Assoc. Petr. Geol.*, **XIII, n°10** , 1257-1273.

Herbrich, B., (1988), Le forage géothermique de Soultz-sous-Forêts (GPK1). Rapport de fin de sondage, *Rapport Compagnie Française de Géothermie*, 88 CFG 03, 118 pp.

Hooijkaas, G.R., Genter A., Dezayes C., (2006) Deep-seated geology of the granite intrusions at the Soultz EGS site based on data from 5 km-deep boreholes. *Geothermics*, **35**, n°5-6, p. 484-506.

Just, J., Kontny, A., de Wall, H., Hirt, A.M., Martín-Hernández, F., (2004). Development of magnetic fabrics during hydrothermal alteration in the Soultz-sous-Forêts granite from the EPS-1 borehole, Upper Rhine Graben. In: Martin-Hernandez F, Lüneburg CM, Aubourg C, Jackson M (eds), Magnetic fabric: Methods and applications, *Geological Society*, special publication **238**: 509-526.

Ledésert, B. (1993). Fracturation et paléocirculations hydrothermales. Application au granite de Soultz-sous-Forêts, PhD thesis, Université de Poitiers, France, 220 pp.

Ledésert, B., Berger, G., Meunier, A., Genter, A., Bouchet, A., (1999). Diagenetic-type reactions related to hydrothermal alteration in the Soultz-sous-Forêts granite, France, *Eur. J. Miner.*, vol. **11**, 731-741.

Ledésert, B., Joffre, J., Amblès, A., Sardini, P., Genter, A., Meunier, A., (1996). Organic matter in the Soultz HDR granitic thermal exchanger (France): natural tracer of fluid circulations between the basement and its sedimentary cover. *J. Volcan. & Geotherm. Research*, vol. **70**, 235-253.

Renard, Ph., Courrioux, G., (1994). Three-dimensional geometric modelling of faulted domain: The Soultz horst example (Alsace, France). *Computers & Geosciences*, **Vol. 20 (No. 9)**, 1379-1390.

Rummel, F., (1991). Physical properties of the rock in the granitic section of borehole GPK1, Soultz-sous-Forêts, *Geothermal Science & Technology*, **vol. 3**, 199-216.

Sausse J., (1998). Caractérisation et modélisation des écoulements fluides en milieu fissuré. Relation avec les altérations hydrothermales et quantification des paléocontraintes. PhD thesis, Université Henri Poincaré, Nancy I, France, 336 pp.

Sausse J., Fourar M., Genter A., (2006). Permeability and alteration within the Soultz granite inferred from geophysical and flow log analysis, *Geothermics*, Vol. **35**, No. 5-6, 544-560.

Sausse, J., Dezayes, Ch., Dorbath, L., Genter, A., Place, J., (2008). 3D fracture zone network at Soultz based on geological data, Image logs, microseismic events and VSP results, Proceedings of the EHDRA scientific conference 24-25 September 2008, Soultz-sous-Forêts, France.

Sausse, J., Genter, A., (2005). Types of permeable fractures in granite, P. K. Harvey, T.S. Brewer, P. A. Pezard & V. A. Petrov (eds)., Petrophysical Properties of Crystalline Rocks, *Geological Society of London*, special publication, **240**, 1-14.

Sausse, J., Genter, A., Leroy, J.L., Lespinasse, M., (1998). Altération filonienne et pervasive: Quantification des perméabilités fissurales dans le granite de Soultz sous Forêts (Bas-Rhin, France). *Bulletin de la Société Géologique de France*, **169** (5): 655-664.

Schild, M., Vollbrecht, A., Siegesmund, S., Reutel, Ch., (1998). Microcracks in granite cores frm EPS1 geothermal drill hole, Soultz-sous-Forêts (France): paleostress directions, paleofluids and crack-related Vp-anisotropies, *Geol Rundsch***, 86**, 775-785.

Schleicher, A.M., Warr, L.N., Kober, B., Laverret, E., Clauer, N., (2006). Episodic mineralization of hydrothermal illite in the Soultz-sous-Forêts granite (Upper Rhine Graben, France), *Contribution Mineralogy Petrology*, **152**, 349-364.

Schnaebele, R., Haas, J.-O., Hoffmann, C.R., (1948). Monographie géologique du champ pétrolifère de Pechelbronn. *Mémoire Service Carte Géologique Alsace*, **vol. 7**, Strasbourg, France, 254 pp.

Schulmann, K., Jezek, J., Venera, Z., (1997). Perpendicular linear fabrics in granite: Markers of combined simple shear and pure shear flows? In: Granite: From segregation of melt to emplacement fabrics (edited by Bouchez, J. L., Hutton, D. H. W. & Stephens, W. E.). Kluwer Acedemic Publishers, Dordrecht, 159-176.

Stussi, J.-M., Cheilletz, J.M., Royer, J.J., Chèvremont, P., Féraud, G., (2002). The hidden monzogranite of Soultz-sous-Forêts (Rhine Graben, France). Mineralogy, petrology and genesis, *Géologie de la France*, **1**, 45-64.

Surma, F., Géraud, Y., (2003). Porosity and thermal conductivity of the Soultz-sous-Forêts granite. Pure and *Applied Geophysics*, **160** (2003) 1125-1136.

Tenzer, H., Mastin, L., Heinemann, B., (1991). Determination of planar discontinuities and borehole geometry in the crystalline rock of borehole GPK1 at Soultz-sous-Forêts, *Geothermal Science & Technology*, **vol. 3**, 31-67.

Traineau, H., Genter, A., Cautru, J.-P., Fabriol, H., Chèvremont, Ph., (1991), Petrography of the granite massif from drill cutting analysis and well log interpretation in the geothermal HDR borehole GPK1 (Soultz, Alsace, France); European HDR Project at Soultz-sous-Forêts. *Geothermal Science & Technology*, **vol. 3**, 1-29.

Valley, B., (2007). The relation between natural fracturing and stress heterogeneities in deep-seated crystalline rocks at Soultz-sous-Forêts (France), PhD thesis, ETH-Zürich, Switzerland, 260 pp.

Vuataz, F.-D., Brach, M., Criaud, A., Fouillac, C., (1990). Geochemical monitoring of drilling fluids: a powerful tool to forecast and detect formation waters. *SPE*, Formation Evaluation, June 1990, 177-184.

The EGS Soultz project (France): from reservoir development to electricity production

A. Genter[1], K. Evans[2], N. Cuenot[1], F. Baticci[1,3], L. Dorbath[4], JJ. Graff[1], B. Sanjuan[5]

1 GEIE Exploitation Minière de la Chaleur, Kutzenhausen, France
2 ETH Zurich, Switzerland
3 Politecnico Milano, Italy
4 EOST, Strasbourg, France
5 BRGM, Département Géothermie, Orléans, France

Presented at Annual Meeting of the Geothermal Resources Council, Reno, Nevada, October 4-7 2009.

The EGS Soultz project (France): from reservoir development to electricity production

A. Genter[1], K. Evans[2], N. Cuenot[1], F. Baticci[1,3], L. Dorbath[4], JJ. Graff[1], B. Sanjuan[5]

1 GEIE Exploitation Minière de la Chaleur, Kutzenhausen, France
2 ETH Zurich, Switzerland
3 Politecnico Milano, Italy
4 EOST, Strasbourg, France
5 BRGM, Département Géothermie, Orléans, France

Contact: genter@soultz.net

Keywords
EGS, Reservoir, Granite, Fractures, ORC Power Plant, Soultz, France

ABSTRACT

Over two decades of research and development of the EGS Soultz reservoir carried out with French, German and Swiss governmental and European funding, a pilot geothermal power plant has been built by a French-German industrial consortium. The drilling of various exploration and geothermal boreholes at great depth, the deepest penetration into crystalline rock in France, has yielded fundamental insights into the geology, nature of fracturing, fluid geochemistry, temperature and hydraulic properties of deep crystalline rock masses. After the drilling operations, all the wells were hydraulically stimulated as well as chemically stimulated. Several circulation tests were done and showed encouraging results. The 3-well system was circulated in 2005 under buoyancy drive for 5 months with re-injection in the central well GPK-3 and production from the two outer wells, GPK-2 and GPK-4. This showed a good linkage between one duplet pair (GPK-3-GPK-2) but not the other (GPK-3-GPK-4). Further acidization operations on the low-productivity well, GPK-4, led to its productivity increasing to almost the same level than the other well. On surface, a binary power plant was designed and built based on an ORC technology (Organic Rankine Cycle). Surface equipments (turbine, heat exchanger, filtering system) and a corrosion loop as well as two different types of down-hole pumps (Line Shaft Pump-LSP, Electro Submersible Pump-ESP) were installed respectively on surface and in the production wells in 2008. The on-going Soultz project has been able to produce the first kWh of electricity in June 2008 but several components of the geothermal plant are still in their testing phase.

Introduction

Over two decades of research and development of the EGS Soultz reservoir carried out with French, German and Swiss governmental and European funding, a pilot geothermal power plant has been built by a French-German industrial consortium. The drilling of three boreholes to 5 km has yielded fundamental insights into the geology, nature of fracturing, fluid geochemistry, temperature and hydraulic properties of deep crystalline rock masses. However, the immediate focus of the various European teams involved in the project (Baumgaertner et al., 1998; Baria et al., 1999; Gerard et al., 2006) has been the development, testing and modeling of a geothermal fractured granite reservoir within the deep basement. A rich and diverse set of data has been collected, including geological, hydraulic, borehole logging, microseismic and active seismic, that provide insight into the hydro-thermo-mechanical and geochemical behavior of a deep crystalline basement subjected to forced fluid flow conditions (Genter et al., 2009). From 2007, a power plant has been designed, ordered and built with a net power capacity of 1,5 MWe. Different submersible pump technologies have been installed and tested in the different production wells (Fritsch et al., 2008). In the meantime, corrosion tests have been carried out with several steels coupons

(Baticci, 2009) immersed in a corrosion loop installed on surface at re-injection conditions (<70°C, 19 bars). This paper presents an overview of the project, and highlights the key results and milestones that mark the progress in this on-going project to date.

Phases of the Soultz project

Work at the Soultz site can be broken into three phases: a preparatory phase, a drilling, exploration and reservoir development phase that extended from 1987 to 2007, and a power plant construction and testing phase. The preparatory phase involved the compilation of existing literature and a site survey conducted using data from existing holes and the reinterpretation of old petroleum reservoir measurements. The drilling, exploration and reservoir development phase consists of three sequential campaigns (Figure 1). The first, conducted between 1987 and 1991, explored and tested the basement to 2.0 km depth with a single borehole.

1987 – 1991 **Exploration phase**	1991 – 1998 **Creation of the 2 wells system GPK1/GPK2 at - 3600 m**	1999 – 2007 **Creation of the 3 wells system GPK2/GPK3/GPK4 at - 5000 m**	2007 – 2009 **Construction of the first production unit**
• Drilling GPK1 at - 2000 m • Coring EPS1 at - 2227 m	• Deepening of GPK1 at - 3600 m and stimulation • Drilling of GPK2 at - 3880 m and stimulation • Circulation test between the 2 wells (4 months)	• Deepening of GPK2 at - 5080 m and stimulation • Drilling of GPK3 at - 5100 m and stimulation • Drilling of GPK4 at - 5270 m and stimulation • Circulation test between the 3 wells (5 months) • Complementary stimulations (chemical)	• Power plant construction • Installation of the LSP pump in GPK2 at 250 m • Inauguration of the power plant mid 2008 • Installation of the ESP pump in GPK4 at 500 m • Inter wells circulation tests

Figure 1. Main phases of the Soultz project between 1987 and 2009.

The second campaign, between 1991 and 1998, extended the exploration by coring a borehole to 2.2 km to provide geological information, and then drilling two boreholes to 3.6 and 3.9 km which were then linked to form a geothermal system that was subsequently hydraulically stimulated and circulated for 4 months (Figure 2). The third campaign, conducted between 1998 and 2007, explored still deeper by drilling three boreholes to 5.0 km and linking them to form a 3-well system. The third phase of surface power plant construction in preparation for the long-term circulation of the 5 km deep system began in 2007 and is on-going (Figure 1).

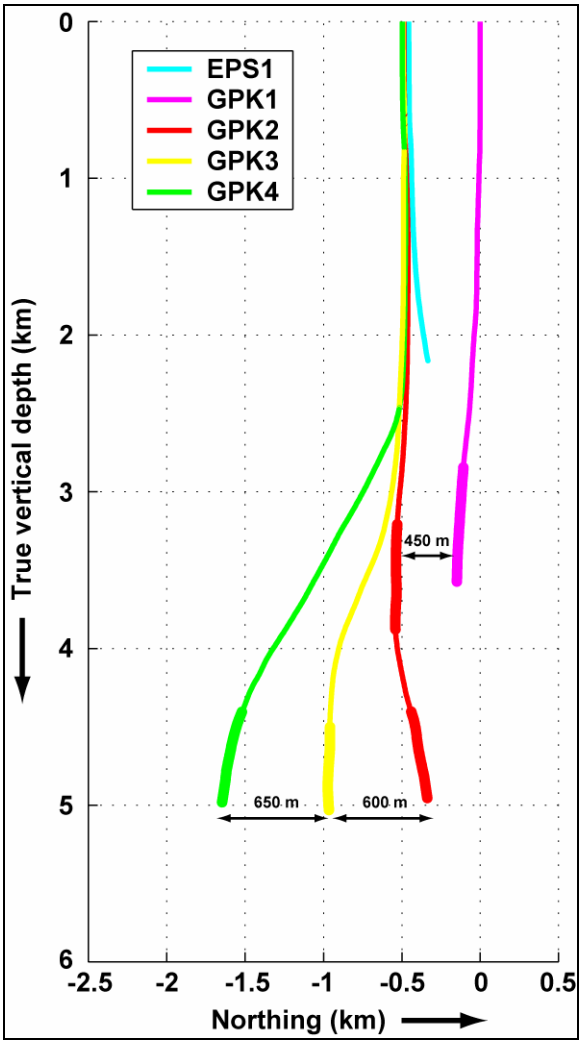

Figure 2. North-south vertical cross-section through the Soultz site showing the Soultz wells. The view shows the three 5 km deep geothermal wells (GPK-2, GPK-3, GPK-4) that are completed open-hole in the lower reservoir, and the wells GPK-1 and GPK-2 that form the upper reservoir. Also shown is the cored exploration well EPS-1. The thicker lines indicate the open-hole sections of the geothermal wells. Depths are expressed in True Vertical Depths (TVD).

The Soultz geothermal system from regional to concession scale

The Soultz geothermal area is located in the Upper Rhine graben, which is part of the European Cenozoic rift system that extends from the Mediterranean to the North Sea coast. The heat flow in the graben ranges between 100-120 $mW.m^{-2}$. The sediments of the Soultz area were well investigated in the past for oil exploration. Several thousands of oil wells were drilled prior to 1970, giving an excellent overview of stratigraphy and structures within the post-Palaeozoic sediments. Temperature measurements in these wells identified the exceptionally high temperature gradients that define the Soultz geothermal anomaly, and showed that the isotherms are primarily influenced by the tectonic structure of the Rhine graben (normal faults). From seismic reflection profiles done by oil companies, it was outlined that the hottest zone at shallow depth (<400 m) corresponds to a local horst structure, namely the Soultz horst, bounded by local normal faulted zones having a vertical off-set of several hundred meters (Figure 3). The first geothermal exploration well at Soultz, GPK-1, was drilled vertically into the top of the hottest area in 1987-1988. It reached the crystalline basement at 1376 m depth (Figure 3).

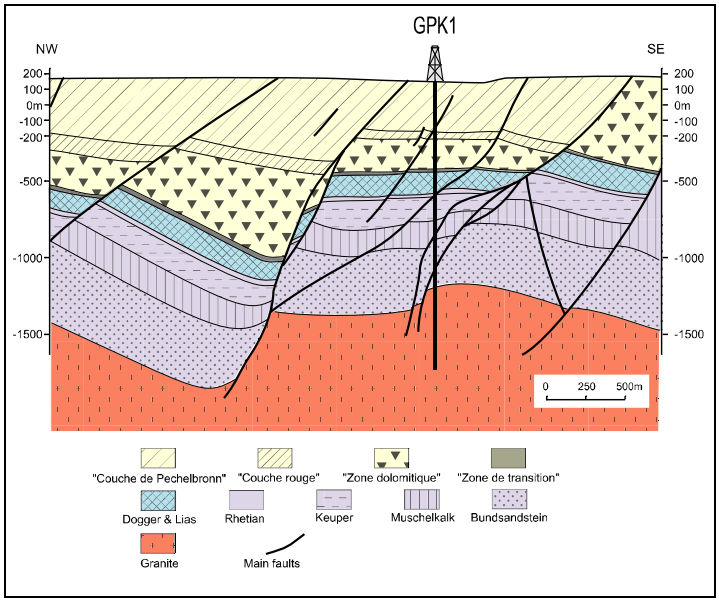

Figure 3. Local NW-SE geological cross-section of the Soultz site. GPK-1 well was drilled into the Soultz horst. Depths are expressed in m below the sea level.

Main scientific outcomes from exploration to reservoir development

Geology-Fluid Geochemistry

The deep basement was found to consist of Paleozoic granites that were highly fractured at all scales, from micro-crack at grain scale to fracture zones. Hydrothermal alteration is generally intimately associated with fracture zones. Some altered cataclastic shear zones showed a low natural permeability in channels characterized by the occurrence of brines (100 g/L) and were defined as Hydrothermally Altered and Fractured Zones (HAFZ) indicating both high fracture density and strong hydrothermal alteration (Genter et al., 2000). Natural fluid circulation in the fractures resulted in both a strong dissolution of the primary minerals such as biotite, plagioclase, and a significant deposition of some altered minerals such as clay minerals (illite), calcite and secondary quartz (Figure 4).

Samples of native formation fluid have similar chemical and isotopic compositions (NaCl brine with a pH value close to 5) and a high salinity (100 g/L), which suggest fluids at all depths to 5 km have a common sedimentary origin and have undergone identical fluid-rock interaction processes. Chemical and gas geothermometers suggest that the native geothermal brine and associated gases (predominant CO_2) are equilibrated with a mineralogical assemblage at temperatures close to 220-240°C. A tracer test conducted between 2000 and 2002 in the GPK-2 open hole section below 4.5 km indicated a natural flow rate of native geothermal brine of 1.0-1.2 m^3/h (Sanjuan et al., 2006).

Hydraulics

Hydraulic tests done on HAFZs have shown transmissibilities (i.e. the product of permeability and borehole length over which the permeability applies) from zero up to 10^{-11} m^3, whereas the transmissibility of the granite rock mass excluding the high-transmissibility zones is typically 10^{-16} to 10^{-17} m^3 (Evans et al., 2008). Hydraulic tests performed after hydraulic stimulation showed that the GPK-1 well had been connected to a fault or major fracture zone of large hydraulic capacity through flow paths that emerged into the well at the HAFZs (Evans et al., 2005). It is likely that the high-capacity fault that the well connects to via the stimulated flow paths is part of a connected system that allows fluids to move through the rock mass over significant distances.

Figure 4. Photograph of hydrothermally altered and fractured granite core taken at 1377 m depth in GPK-1 well. The horizontal scale is 3 cm.

Stimulation and microseismicity

Almost all wells at Soultz have been subjected to a hydraulic stimulation, and in all but one case the injectivity index (i.e. the injection flow rate per unit wellhead pressure under steady-state conditions) was significantly improved. For the three deep wells, each stimulated between 4.5 and 5.0 km TVD, the improvement for GPK-2 and GPK-4 was a factor of about 20, whereas that for GPK-3 was only a factor of ~1.5 (Nami et al., 2008). A variety of acid stimulations were conducted on all deep wells after the hydraulic stimulations, with limited success (Nami et al., 2008). The improvement in 3-day injectivity/productivity index by the acid treatments was a factor of about 1.25 for GPK-2, about 1.15 for GPK-3, and about 2.5 for GPK-4. It should be noted, however, that the large increase in productivity for GPK-4 was largely due to the development of leaks in the casing whose origin are currently uncertain. If only the open hole is considered, the improvement achieved by the acid treatments was a factor of 1.5-1.75.

Microseismic activity was monitored during all stimulations. Typically, several thousand of microseismic events would be recorded during single stimulation with a down-hole seismic network and somewhat fewer with a surface seismic network (Cuenot et al., 2006 and 2008; Dorbath et al., 2009). Comparison of the seismic responses to stimulation of the three deep wells showed that they are dependent to some degree on the nature of the HAFZs encountered in each of the wells (Dorbath et al., 2009). The open hole section of deep well GPK-2 is characterized by a dense network of medium scale fracture zones, and the seismic cloud is rather compact and includes ~700 events of magnitude higher than 1 (Figure 5). The initial injectivity/productivity index of this well was low, but was increased by a factor of 20 by the stimulation.

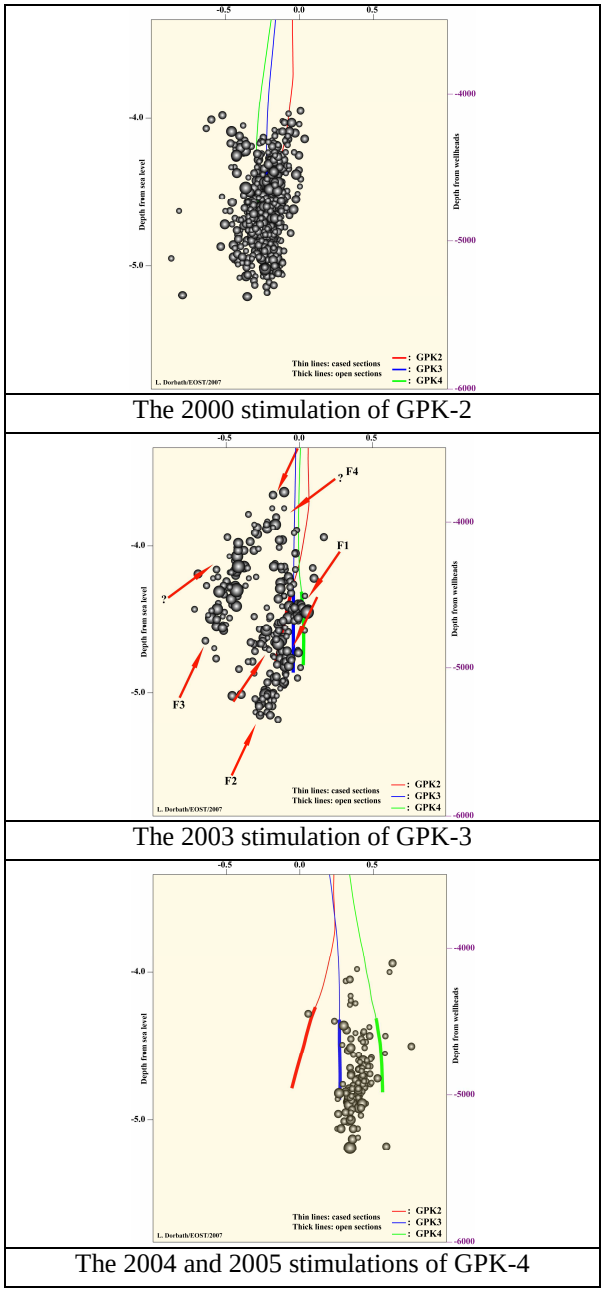

Figure 5. Hydraulic stimulations in the GPK-2, GPK-3 and GPK-4 Soultz wells. Seismic clouds of (M>1) events are plotted on nearly N-S cross-sections (from Dorbath et al., 2009).

The open hole section of well GPK-3 is hydraulically dominated by a very large HAFZ at 4.7 km MD (Measured Depth) that gave the well a high initial injectivity of 3 l/s/MPa. Stimulation produced 250 events larger than magnitude 1.0. But, the proportion of events with larger magnitudes (M>2) was greater for GPK-3 than for GPK-2. This observation could indicate that the characteristic of the seismicity around GPK-3 is influenced by the large-scale fracture zone (Figure 5). However, the increase in injectivity/productivity index after stimulation was small. For GPK-4, a limited number of events has a magnitude higher than 1. They are mainly clustered around an isolated large-scale fracture zone (Figure 5).

Thermics

Temperature profile to 5 km depth measured in well GPK-2 is presented in Figure 6. The profile is typical for all deep wells, with temperatures of 200°C being reached at 5 km depth. The localised disturbances at 2 km and 3.4 km reflect remnant cooling from stimulation

injections conducted at those depths. The profile can be divided into three sections with different geothermal gradients reflective of different heat transport processes. The upper section lies entirely in the sediments from the surface to 1 km and has a very high gradient of about 111°C/km indicating heat transport is predominantly conductive. The intermediate depth section from 1 km to about 3.3 km depth is characterised by a very low gradient of about 5°C/km, which suggests heat transport is dominated by convection, probably in the up-flowing limb of a convective system that is active in the granite and Triassic sandstones. This implies significant natural fluid movement is occurring within faults and fracture zones, at least between 1.0 and 3.3 km. Below 3.3 km, the geothermal gradient increases again to 30°C/km and becomes linear with depth, indicating a return to a conduction-dominated heat flow regime. This might be indicate that faults and fracture zones have insufficient connected permeability below 3.3 km depth to allow convection to develop.

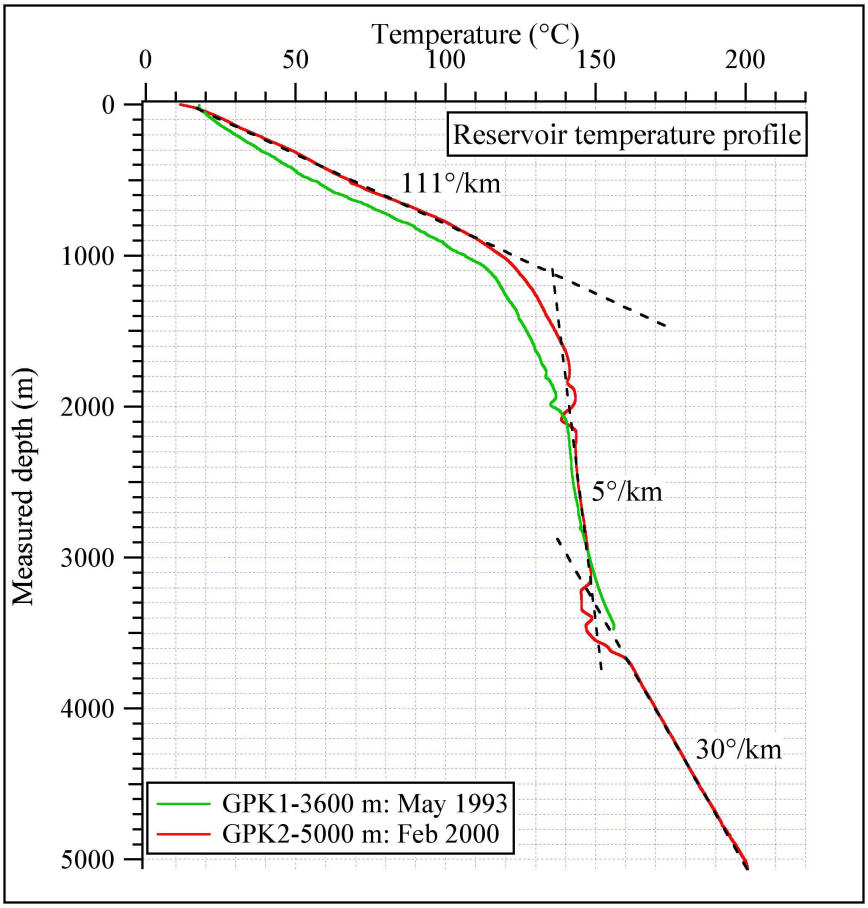

Figure 6. Equilibrium temperature profiles obtained in GPK-1 and GPK-2 several months after drilling operations finished. (Data from GGA-Hannover, Germany).

Performance of the 5 km depth system during circulation

Several limited-duration circulations have been performed in the lower reservoir to date: without downhole pumps in 2005, and with one downhole pump and power generation in 2008. The first circulation test of the triplet of wells penetrating the lower reservoir (4.5 - 5.0 km) took place for 5 months between July and December 2005 (Gerard et al., 2006). Tracer tests conducted during the circulation showed that ~25% of the injected tracer was recovered from GPK-2 but only 2% from GPK-4. This asymmetrical response reflects the complex organisation of fracture zones or faults describing different fluid circulation loops, the hydraulic connections between GPK-3 and GPK-2 being much more direct and faster than between GPK-3 and GPK-4 (Sanjuan et al., 2006). During this circulation, and all production

tests conducted at 5km depth, tracer tests and geochemical data invariably showed the presence of the native geothermal brine in the discharged fluids, even after large amounts of external fresh water had been injected into the wells (Sanjuan et al., 2006). This result points to the conclusion that the exchanger is connected to a deep natural reservoir. Some 600 microseismic events were recorded in the 6 months during and immediately following the circulation. Several exceeded magnitude 2.0, but none were felt.

The lower reservoir was again circulated in 2008, this time with a line-shaft production pump installed at 350 m depth in GPK-2, with GPK-4 remaining shut-in. Circulation began at the end of June 2008 and lasted until mid-August 2008. During this period, the pump-assisted production from GPK-2 was around 25 l/s at a temperature of 162°C. The production fluid pressure at the surface was maintained at 2 MPa in order to avoid scaling before passing through a pump for injection into GPK-3. Wellhead injection pressure began at 6 MPa and increased continuously albeit progressively more slowly to stabilize at 7 MPa for last week of the test. Approximately 190 microearthquakes were associated with the circulation, which gives an event rate comparable to that observed in the 2005 circulation (Figure 7a, b). They also occurred in much the same locations as the 2005 events, but the magnitude did not exceed 1.4, in contrast to the 2005 events, several of which exceeded 2.0. This may reflect several differences between the two tests: the duration (6 months in 2005, around 2 months in 2008); a larger volume of water circulated in 2005; and the use of a down-hole production pump in 2008 which induced higher production flow rates compared to artesian production with two production wells in 2005. Additionally, between 2005 and 2008, the wells were chemically stimulated. Moreover most of the larger magnitude earthquakes in 2005 occurred after a sudden increase of injection flow rate and pressure. This behaviour is quite similar to the tendency of large events to occur during the shut in phase of stimulation tests when injections are stopped and pressure decreases quickly, although the underlying mechanisms are not necessarily identical.

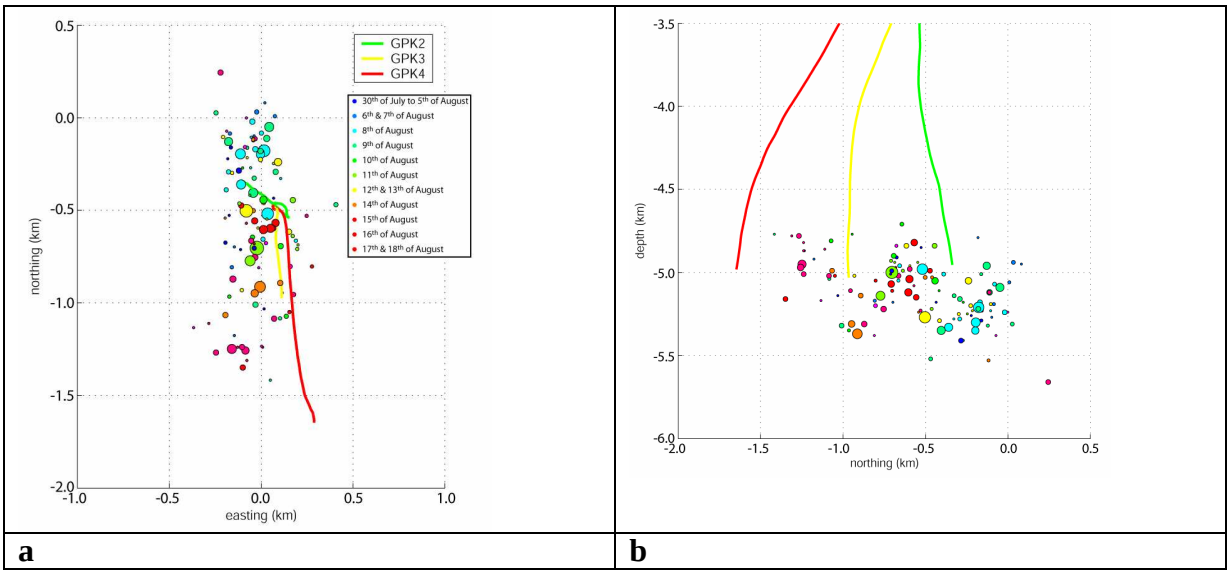

Figure 7. Location of the microseismic activity at Soultz during the 2008 summer circulation test. a) Plane view. b) North-South cross-section. The legend on figure 7a) is common for both pictures. Colours indicate the occurrence time of the seismic events and the diameter of the circle is proportional to the magnitude.

Main technological features of the Soultz power plant

An Organic Rankine Cycle (ORC) geothermal power plant has been built and a first 1,5 MWe unit has been ordered. The different components of the power plant have been installed

and power production of the first geothermal KWh was achieved on June 2008 (Figure 8). However, to reach a significant fluid production, it is necessary to install down-hole production pumps, because the artesian production is not sufficient. Thus, two types of production pumps were deployed and tested in the wells: a Line Shaft Pump (LSP) and an Electro-Submersible Pump (ESP). The LSP pump has been installed at 350 m depth into GPK2, which presents good verticality and is the best producer, and its motor has been put on the top of GPK-2 well-head. Due to hydraulic drawdown, the maximum expected flow rate with the LSP installed at 350 m is 35 l/s. During summer 2008, between 07th July and 17th August, after six weeks of geothermal production (25 l/s, 162°C), we observed some scaling problem within the lubrication part of the line shaft. The fresh water used for lubricating the shaft was too mineralized and some carbonate deposits precipitated. Then, a poor lubrication occurred and the first axis of the shaft broke. Between mid August and November 2008, both the shaft and the pump were fully dismantled, analyzed and a demineralization water system has been set up. The LSP pump has been re-installed at 250 m depth in GPK-2 and works properly.

With the ESP pump, both the pump and its motor are installed into the GPK-4 well at 500 m depth. The maximum expected flow rate from GPK-4 equipped with ESP is 25 l/s. A fiber optic cable has been deployed together with the EPS pump and allows monitoring the motor temperature and gives down-hole information about the geothermal drawdown in the well. In parallel to the re-installation of LSP in GPK-2 at 250m depth, the first production tests from GPK-4 with the ESP at an expected target of 25 l/s started on mid November 2008. After some days of production, GPK-4 production decreased to 12.5 l/s at 152°C and the geothermal water was re-injected in GPK-3 at 50°C. LSP was started again and GPK-2 flow-rate has been stabilized at 15 l/s for a temperature of around 160°C. Both flows coming from GPK-2 and GPK-4 have been re-injected under full automatism in GPK-3 at about 30 l/s. The ORC commissioning started with these geothermal conditions at around 155°C. GPK-3 well-head pressure must be maintained around 70-80 bars for re-injection. It was the first time that the triplet was operational for a while with the two producers equipped with production pumps.

Figure 8. The Soultz geothermal power plant: in the back, the ORC power unit; in the middle, the 3 geothermal wells; in the front, the cooled geothermal loop.

In order to investigate corrosion and scaling, an innovative corrosion pilot was set up on the geothermal loop in surface and tested for the first time between September 2008 and February 2009 (Baticci, 2009). Different kinds of steel (P110, N80, P265GH) are investigated for corrosion in the geothermal conditions of re-injection (19 bars, <70°C). Steel samples were introduced in the corrosion chambers, where the geothermal fluid circulates, and

remained there for different time intervals (Figure 9). A series of physico-chemical parameters, such as pH, Eh, conductivity and temperature, were measured in the meantime. After their extraction, samples were analyzed by various chemical techniques. The main results consist in a significant action of geothermal brine on all studied steels. Newly created deposits, mainly sulfates formed on the surface of samples were characterized by SEM analysis giving access to their structure. Corrosion occurred beneath the deposits and corresponds to pitting. Beneath the deposits layer, an interface region was identified, in which various chemical elements (As, Ca, Pb, Si, etc.) were identified. Corrosion products such as iron oxides (rust) were also found inside the deposits layer.

Figure 9. The Soultz corrosion pilot operating at re-injection part. The steel coupons are installed inside the 3 vertical cylinders.

Conclusions

Some 20 years of EGS research at the Soultz geothermal site has produced numerous scientific results and advancements relating to drilling, surface exploration methods, geology, geochemical and geophysical monitoring, tracer testing, hydraulic and chemical stimulations, and general EGS know-how.

Geochemical analyses and tracer tests revealed that a significant natural hydraulic reservoir exists in the rock mass, so that mixing of the injected fluid with the native formation water occurred, resulting in small return of injected tracer. The reservoir almost certainly resides in a connected network of permeable HAFZs which were seen at the wellbore on core and borehole images, and could be imaged remotely from the well from high-resolution images of the pattern of microseismicity. Good communication was observed between GPK-3 and GPK-2, most likely due to the presence of a major HAFZ that cuts both wells.

Exploration into the Soultz granite has shown that it does not correspond to the original, classical Hot Dry Rock (HDR) concept. The presence of the HAFZs, which together form a connected system of large hydraulic capacity (i.e. storage), means that the Soultz reservoirs share many facets of conventional geothermal reservoirs that benefit from re-injection.

A geothermal ORC power plant has been built with a net capacity of 1,5MWe and is still in its testing and commissioning phase. A negotiation with the French government is under discussion because the feed-in tariff in France is 12,5c€ per kWh. The target for the future should be to reach the tariff level in Germany which is 24c€ per kWh for power plants

producing a net power below 10MWe. This target would have been reached by September 2009 in France.

Acknowledgements

This work was performed within the framework of the European EGS Pilot Plant project which was supported mainly by the European Commission, BMU (Germany), ADEME (France), the Swiss Federal Offices of Education and Research (SER), and Energy (SFOE), and by a consortium of industrial members (EDF, EnBW, ES, Pfalzwerke, Evonik). The authors also thank the Soultz geothermal team and the Working Group members.

References

Baria R., J. Baumgaertner, A. Gerard, R. Jung, and J. Garnish, 1999. 'European HDR research programme at Soultz-sous-Forêts (France) 1987-1996", *Geothermics* 28, 4-5, p. 655-669.

Baticci F., 2009. "Material study on geothermal EGS (Enhanced Geothermal System) power plant: application to the Soultz-sous-Forêts site," Politecnico di Milano, Facoltà di Ingegneria Industriale, Corso di Laurea in Ingegneria Meccanica, Diploma thesis, Italy, 202 pp.

Baumgaertner J., A. Gerard, R. Baria, R. Jung, T. Tran-Viet, T. Gandy, L. Aquilina, and J. Garnish, 1998. "Circulating the HDR reservoir at Soultz: maintaining production and injection flow in complete balance: initial results of 1997 experiment", *Twenty-third Workshop on Geothermal Reservoir Engineering*, Stanford University Stanford California USA, p. 11-20.

Cuenot N., J. Charléty, L. Dorbath, and H. Haessler, 2006. "Faulting mechanisms and stress regime at the European HDR site of Soultz-sous-Forêts, France", *Geothermics*, vol. 35, 5-6, p. 561-575.

Cuenot N., C. Dorbath, and L. Dorbath, 2008. "Analysis of the microseismicity induced by fluid injections at the Hot Dry Rock site of Soultz-sous-Forêts (Alsace, France): Implications for the characterization of the geothermal reservoir properties", *Pure and Applied Geophysics*, 165, p. 797-828.

Dorbath L., N. Cuenot, A. Genter, and M. Frogneux, 2009. "Seismic response of the fractured and faulted granite to massive water injection at 5 km depth at Soultz-sous-Forêts (France)", *Geophysical Journal International*, doi: 10.1111/j.1365-246X.2009.04030.

Evans K.F., R. Hopkirk, R. Jung, P. Nami, M. Schindler, D. Teza, and T. Tischner, 2008. "Milestone events and key observations in Thermics, Stress and Hydraulics at Soultz (1987-2002)", *EHDRA scientific conference*, Soultz-sous-Forêts, France, 24-25 Sept. 2008, 6 pp.

Evans K.F., H. Moriya, H. Niitsuma, R.H. Jones, W.S. Phillips, A. Genter, J. Sausse, R. Jung, and R. Baria, 2005. "Microseismicity and permeability enhancement of hydrogeologic structures during massive fluid injections into granite at 3 km depth at the Soultz HDR site", *Geophysical Journal International*, 160, p. 388-412.

Fritsch D., J. Baumgaertner, N. Cuenot, J.J. Graff, and A. Genter, 2008. "The Soultz EGS pilot plant: energy heat and power from deep Enhanced Geothermal Systems", *EVER08*, March 27-30, 2008, Monte-Carlo (Monaco).

Genter A., H. Traineau, B. Bourgine, B. Ledésert, and S. Gentier, 2000. Over 10 years of geological investigations within the European Soultz HDR project, France. *World Geothermal Congress 2000*, Kyushu-Tohoku, Japan May 28 - June 10 2000, p. 3707-3712.

Genter A., D. Fritsch, N. Cuenot, J. Baumgaertner, and J.J. Graff, 2009. "Overview of the current activities of the European EGS Soultz project: from exploration to electricity production", 34th *Stanford Reservoir Engineering Geothermal Workshop* 2009, February 09-11 2009, San Francisco, California, USA, p. 163-169.

Gerard A., A. Genter, T. Kohl, Ph. Lutz, P. Rose, and F. Rummel, 2006. "The deep EGS (Enhanced Geothermal System) project at Soultz-sous-Forêts (Alsace, France)", *Geothermics*, vol. 35, 5-6, p. 473-483.

Nami P., R. Schellschmidt, M. Schindler, and T. Tischner, 2008. "Chemical Stimulation operations for reservoir development of the deep crystalline HDR/EGS system at Soultz-

sous-Forêts (France)". Proc. 33rd *Workshop on Geothermal Reservoir Engineering*, January 28-30, 2008, Stanford, California, USA, (2008).
Sanjuan B., J.-L. Pinault, P. Rose, A. Gérard, M. Brach, G. Braibant, C. Crouzet, J.-C. Foucher, A. Gautier, and S. Touzelet, 2006. "Tracer testing of the geothermal heat exchanger at Soultz-sous-Forêts (France) between 2000 and 2005", *Geothermics*, vol. 35, 5-6, p. 622-653.

The stress field at Soultz-sous-forêts from focal mechanisms of induced seismic events: cases of the wells GPK2 and GPK3

Louis Dorbath[1,2]*, Keith Evans[3], Nicolas Cuenot[4], Benoît Valley[3,5], Jean Charléty[6], Michel Frogneux[1]

1 EOST, Univ. Louis Pasteur, Strasbourg
2 LMTG, Univ. Paul Sabatier, Toulouse
3 Department of Earth Sciences, Swiss Federal Institute of Technology (ETH), Zürich
4 GEIE Exploitation minière de la chaleur, Kutzenhausen
5 MIRACO/Laurentian University, Sudbury, Canada
6 GeoscienceAzur, Sophia Antipolis

Submitted to Geoscience, 2009.

LE CHAMP DE CONTRAINTES A SOULTZ-SOUS-FORETS A PARTIR DES MECANISMES AU FOYER DES SEISMES INDUITS: CAS DES FORAGES GPK2 ET GPK3

THE STRESS FIELD AT SOULTZ-SOUS-FORÊTS FROM FOCAL MECHANISMS OF INDUCED SEISMIC EVENTS: CASES OF THE WELLS GPK2 AND GPK3

Louis Dorbath[1,2*]

Keith Evans[3]

Nicolas Cuenot[4]

Benoît Valley[3,5]

Jean Charléty[6]

Michel Frogneux[1]

1 EOST, Univ. Louis Pasteur, Strasbourg

2 LMTG, Univ. Paul Sabatier, Toulouse

3 Department of Earth Sciences, Swiss Federal Institute of Technology (ETH), Zürich (Suisse)

4 GEIE Exploitation minière de la chaleur, Kutzenhausen

5 MIRACO/Laurentian University, Sudbury, Canada

6 GeoscienceAzur, Sophia Antipolis

* Auteur correspondant:

adresse: EOST, 5, rue René Descartes, 67084, Strabourg cedex, France

tel.: 03 90 24 00 61

fax.: 03 90 24 01 25

mel.: louis.dorbath@eost.u-strasbg.fr

RESUME

Le champ de contraintes à Soultz-sous-Forêts où est installé le projet EGS de Géothermie a fait l'objet de nombreuses études étant donné son importance dans la réponse du réservoir aux stimulations hydrauliques. L'analyse des données de diagraphie dans les puits, principalement les fractures induites durant le forage, permettent de fixer la direction de SHmax entre 170° et 180° dans le granit.

Dans cet article, l'inversion des mécanismes au foyer (double-couple) des microséismes induits au cours des stimulations de GPK2 et GPK3 est réalisée à l'aide du S*lickenside Analysis Package* de Michael [15,16,17] afin de déterminer l'orientation et le facteur de forme du tenseur des contraintes. L'inversion montre que la direction de Shmin est bien établie dans GPK2 et GPK3. On observe une rotation horaire de 10° de cette direction de GPK2 à GPK3. Le tenseur définit une extension uniaxiale. Les résultats des deux méthodes, analyse des données de diagraphie et inversion des mécanismes au foyer, sont proches, les différences proviennent probablement du fait que le volume échantillonné par les mécanismes focaux est plus grand et inclut des hétérogénéités de contraintes.

Mots clefs: Soultz-sous-Forêts, Mécanismes au foyer, Contraintes

ABSTRACT

The stress field at the EGS geothermal site of Soultz-sous-Forêts has been the subject of many studies, because it largely controls the response of the reservoir to fluid injection. The analysis of borehole logging data, especially breakouts and drilling-induced tension fractures, in the four geothermal wells define an average SHmax orientation ranging between 170° and 180° down to 5 km depth. It also reveals strong heterogeneities in several depth intervals.

In this paper, the inversion of double-couple source mechanisms of seismic events induced during GPK2 and GPK3 stimulation tests is performed to retrieve the orientation and shape factor of the stress tensor, using the S*lickenside Analysis Package* of Michael [15,16,17]. The results indicate a well-determined orientation of Shmin in GPK2 and in GPK3; in GPK3 Shmin is clockwise rotated by about 10°. The stress tensor define an uniaxial extension. The results from both methods, analysis of borehole logging data and inversion of focal mechanisms, are only slightly different; the discrepancy may be due to the larger reservoir volume covered by the focal mechanisms, which can include strong stress heterogeneities.

Key words: Soultz-sous-Forêts, Focal mechanisms, stress field

INTRODUCTION

The study of the stress field at the geothermal site of Soultz-sous-Forêts (Alsace, France) is a story as long as the project itself. This fact underlines the importance of knowledge of the stress field for the development of deep geothermal projects. The stress field and the orientation of the pre-existing fractures and faults are two key parameters which together largely define the response of the medium to massive fluid injections. The stress field at Soultz has thus been the subject of many studies and there is a substantial literature on the subject. The first studies were carried out after the drilling of the first borehole GPK1 to 2000 m in 1987 [21,11], and continued with the extension of this well to about 3500 m depth. Until recently, the characterization of the stress field in the deeper reservoir at 5000 m depth was largely based on the extrapolation of the results from the shallow reservoir [12,4]. In the last few of years, however, the data from the deep reservoir have placed direct constraints on the stress state [25].

The orientation and magnitude of the principal stresses can be constrained through the study of breakouts and drilling-induced tension fractures (DITFs) that are seen in all deep wells, augmented by hydraulic data from large injections or small-volume dedicated stress tests. Another insight into the stress field can be obtained by examining the focal mechanisms of the seismic events induced by the injections. However, in this case, only the deviatoric part of the stress tensor can be determined, the absolute values of the principal stresses being strictly undetermined. Nevertheless, the stress magnitudes can be calculated if we assume that the vertical principal stress corresponds to the lithostatic load. Results obtained with this method differ sometimes from the direct observation of breakouts and DITFs. For instance, Helm [9] proposed a value of 124° +/- 20° for the orientation of the maximum horizontal principal stress[1], SHmax, from an analysis of microseismic events induced during the stimulation of the 3.0-3.5 km reservoir, whereas studies of breakouts and DITFs of boreholes

[1] Throughout this paper, SHmax represents the maximum horizontal principal stress, Shmin the minimum horizontal principal stress, and Sv the vertical stress.

in this reservoir provide an extraordinarily well-defined indication that SHmax above 3.8 km is on average oriented N175° +/- 10° [4]. The discrepancy can be partly explained by the uncertainty on the determination of the fault plane and the auxiliary plane of the focal mechanisms, which were not very well constrained, as recognized by Helm [9]. The recent studies of stress in the deeper reservoir by Valley & Evans [24], as well as a better determination of focal mechanisms of events induced during its the stimulation, due to the installation of numerous seismic stations during the stimulation of GPK2 and GPK3 [6], allows us to re-address the issue of the characterization of the deep stress field. This is the purpose of the present article.

STRESS ORIENTATION AND MAGNITUDE FROM BOREHOLE OBSERVATIONS

As early as 1988, Mastin & Heinemann [14] analysed the data from 4-arm caliper and ultrasonic televiewer (BHTV) logs in GPK1 and concluded that the direction of the maximum horizontal principal stress, SHmax was N169° +/- 21°. Rummel& Baumgärtner [21] applied the HTPF stress determination technique to just five hydraulic tests performed between 1458 and 1989 m depth in GPK1 and found SHmax was oriented N155° +/- 3°. However, given the few number of data, this cannot be considered a reliable estimate [4]. Tenzer et al. [22] analysed breakouts and DITFs for the same depth range in the same well and found an SHmax orientation of N169° +/- 11°. Nagel [18] analyzed vertical DITFs in GPK1 after its extension to 3600 m and found an SHmax orientation of 181° +/- 22°. Brudy & Zoback [3] extended Nagel's study by adding *en échelon* DITFs and found the same SHmax orientation. Hydrofracture stress tests performed in 1993 between 2195 and 3506 m as reported by Klee & Rummel [12] provide stress magnitude but no orientation information. Heinemann-Glutsch [8] analysed all stress data collected up to 1993 and proposed linear variations of stress magnitude with depth and an SHmax orientation of N170°E. Bérard & Cornet [2] identified breakouts in GPK1 between 2850 m and 3465 m and indicated an SHmax orientation of N5°E +/- 7°. Genter & Tenzer [7] identified vertical DITFs in GPK2 in the depth range 1420–3880 m and reported SHmax orientation of N175 ± 17°.

Stress orientation in the deeper reservoir as revealed by breakouts and DITFs in the two 5 km deep wells, GPK3 and GPK4, was studied by Valley and Evans [23,24]. DITFs dominate above 3 km whereas breakouts dominate below 3.5 km. Axial DITFs in GPK3

above 3257 m MD[2] depth indicate a mean SHmax direction of N167° +/- 12°. Below 3257 m MD in GPK3, the numerous breakouts indicate an SHmax orientation of N162° +/- 20°. The large standard deviation is partly due to the presence of a fault that cuts the borehole at 4770 m MD [10], and perturbs the stress orientation by up to 90° over several hundred meters [25]. In GPK4, the DITFs in the upper part of the well indicate an SHmax orientation of N172° ±12°. Below 3.7 km MD, the breakouts are numerous and show two large-scale systematic changes in orientation associated with fracture zones. They suggest that the mean SHmax orientation over the lowermost 1.5 km of hole is N174° +/-17°.

Maximum pressures at the casing shoes during the stimulation of the three deep wells appeared to be limited by jacking [24], and lay on the Shmin magnitude trend proposed by Cornet et al. [4]. The profiles of the presence or absence of breakouts and DITFs along the wells GPK3 and GPK4 suggest SHmax lies between 0.9 and 1.05 times the value of the vertical principal stress Sv [24], indicating a quasi uniaxial extensive stress regime .

STRESS ORIENTATION FROM FOCAL MECHANISMS

We used the seismological data recorded during the 2000 and 2003 hydraulic stimulations of the lower reservoir in GPK2 and GPK3 respectively to estimate the stress field about the lower sections of these holes. The study used 100 well-constrained focal mechanisms from the 6 days long injection stimulation of GPK2, from 30th June to 5th July 2000 [26], and 96 from the 10 days long injection stimulation of GPK3, from 27th May to 7th June 2003 [1,10]. The GPK2 events all occurred during the first 2 days of the injection, whereas the GPK3 events occurred throughout the injection. Consequently, hypocenters of the GPK2 events tend to be located near the injection whereas those from GPK3 spread over a larger volume. The seismological data recorded during the 2004 and 2005 stimulation injections of GPK4, the third 5 km deep well at Soultz, do not allow sufficiently well-constrained focal mechanisms to be derived. Thus we restrict the analysis to the GPK2 and GPK3 data. The focal mechanism solutions (FMSs) for GPK2 are constrained by at least 12 P-wave first-motion polarities recorded on both surface and downhole instruments, and the GPK3 events with at least 15. The FMSs are determined automatically with the code FPFIT [19] and fine-tuned by hand without any wrong polarity. The azimuthal coverage is usually good, so that there are always at least 3 covered quadrants (see [5], for more details on the seismic array deployed at Soutz-

[2] denotes measured depth along borehole and is not the same true vertical depth since GPK3 and GPK4 are inclined

sous-Forêts during the stimulation tests). The uncertainties on the azimuth and dip of the planes (or, at least, one of them) are around 10°.

We inverted the focal mechanism solutions for stress using the S*lickenside Analysis Package* of Michael [15,16,17]. Initially, for each injection, the full collection of FMSs were inverted with *a-priori* fixed fault planes. The results showed that the discrepancies between the 'observed' and predicted slip vectors in the fault plane, the misfit, for several mechanisms were unacceptably large, sometimes greater than 50°. Thus, for the next inversion run, the fault and auxiliary planes were switched for mechanisms that had a misfit greater than 30°. In many cases the misfit decreased significantly, and so the new planes were retained. However, in some cases the misfit remained large. These events were thus excluded from the calculation. The process was then repeated with the maximum misfit angle reduced by 5°, and so on until the maximum misfit angle reached 10°, which is comparable to the uncertainty in the 'observed' slip angle. At the end of this process, we obtained a stress tensor and a set of mechanisms which are compatible. We also checked that the misfit of the mechanisms which were excluded in the process remained large. For GPK2, 66 mechanisms out of 100 were found to have a misfit less than 10°, and 21 mechanisms showed a misfit higher than 15°. For GPK3, the numbers are 62 and 23 respectively. As suggested by Michael [16,17], we bootstrap resample the data set 1000 times flipping the selected fault and slip direction 10% of the time. As the fault planes were selected in the previous step, the resampling is only performed on the fault planes. We thus calculated 1000 stress tensors for each set of mechanisms. The principal directions of the tensors are presented in figures 1a (GPK2) and 2a (GPK3). On the same figures are shown the focal mechanisms used for the inversion (1b, 1c and 1d for GPK2 ; 2b, 2c and 2d for GPK3).

The principal directions of the stress tensor are reasonably well-determined for GPK2. σ_3, which is Shmin, is well constrained, and is near-horizontal with an orientation of N68° +/- 5°. Inverting the whole data set of 100 events yields an average Shmin direction of N68.3°, whereas for the 79 events with a misfit threshold less than 15°, the orientation is N69.9°. The vast majority of solutions for σ1 cluster near vertical, consistent with the predominant normal faulting component in the FMSs. The deviation of this axis from true verticality might be ascribed to local stress heterogeneity whose existence is demonstrated by the variations in orientation of breakouts and DITFs on scales of a hundred metres or more [25]. Alternatively, it might be due to near-equivalence of the magnitudes of σ1 and σ2, implying a uniaxial extensional stress state, which would also explain the scattering of a few inclined solutions across the plane normal to σ3. However, the shape factor F, defined as (σ2-σ3)/(σ1-σ3) is

~0.75, rather than the value of 1.0 that would define a uniaxial extensional regime. Normal faulting is dominant among the focal mechanism solutions. If we consider the west-dipping plane as the fault plane (even if it is actually not), then an azimuth for this plane of around 140°/150° would imply the shear component is dextral, while it would be senestral for azimuths of the order of 170°/180°. This is completely in agreement with the direction of extension. On figures 1c and 1d, we can notice strike-slip mechanisms with a normal component on N120° faults.

The distribution of principal axis orientations for the GPK3 data (Figure 2a) also shows that σ3 (i.e. Shmin) is well constrained to be horizontal, but is oriented at N77° +/- 4°. The solutions for the other two principal stress axes form a continuous band across the stereoplot, indicating the stress state has cylindrical symmetry consistent with a uniaxial extension regime. The shape factor value of ~0.9 estimated for the shape factor with the 62 events data set is reasonably consistent with uniaxial extension. The mechanisms (figures 2b-2d) are more or less very similar to those observed in GPK2. Nevertheless, close scrutiny reveals that the dextral strike-slip movements occur on planes whose strike is larger than in the GPK2 examples. This would be consistent with a slight rotation in the orientation of σ3. We also observe more mechanisms with a dominant strike-slip feature.

DISCUSSION

GPK2

As noted earlier, the state of stress in the shallow reservoir above 3.8 km is well established through studies of hydraulic tests and wellbore failure in wells GPK1 and GPK2. These have provided a very well-constrained estimate of the orientation of SHmax of N175°±10°. In the deeper reservoir, wellbore failure observations have been analysed in wells GPK3 and GPK4 to provide estimates of SHmax orientation. However, no reliable estimates are available for the deeper part of GPK2 owing to poor quality BHTV data. In the section of GPK2 above 3.8 km, Genter and Tenzer [7] found an orientation of N175° for SHmax based upon DITFs, which represents a difference of 15° with the SHmax orientation of N160° obtained from the inversion of focal mechanisms of events occurring in the rock mass about the lower section of the well. Valley & Evans [24] found an average SHmax orientation for GPK3 and GPK4 in the lower reservoir of N168° +/-19°, which is approximately midway between the two.

Cuenot et al. [5] inverted the first-motion polarities of subsets of events induced by the 2000 GPK2 stimulation in the deep reservoir using the inversion procedure of Rivera & Cisternas [20]. For the inversion of a subset of events that lay near the upper part of the reservoir, they obtained an undetermined result, where only σ1 was well-constrained and vertical. However, inversion of a subset that lay in the lower part of the reservoir yielded a well-determined Shmin-orientation of N244° (i.e. N64°) +/- 20°, with the other two principal axes forming an unconstrained band across the stereoplot. The Shmin-orientation is similar to the N70° obtained with the present inversion, but with much higher uncertainties. The higher error is due to the fact that Cuenot et al. [5] did not remove poorly-fitting events from the inversion, as was done in the present study.

GPK3

In comparison to the stress tensor calculated with GPK2 data, the tensor determined in GPK3 presents two significant changes. Firstly, there is an apparent anticlockwise rotation of σ3 of about 10°: from N68°+/-5° for GPK2 to N77° +/- 4° for GPK3. Secondly, a symmetry of rotation around σ3 is observed, indicating very similar values for σ1 and σ2.

In the lower part of GPK3, Valley & Evans [24] found an Shmin orientation of N71° +/- 20° from breakouts, which is consistent with the inversion results for both GPK2 and GPK3, the standard deviation being too large to discriminate. The large standard deviation is due in large part to a large-scale disturbance of the stress field extending along the GPK3 well between 4.5 and 4.8 km (true vertical depth) that is associated with a fault that dips at 50-60° towards N250° [25]. This perturbation results in changes in Shmin-orientation of up to 90°. The presence of such large perturbation is the principal justification for the process of removing focal mechanism solutions from the inversion that high large misfit since these are likely to be occurring within a stress perturbation. On figure 3, we show the location of the 23 seismic events for which the misfit between the observed and the calculated slip direction is higher than 15°. It can be seen that 11 of the 23 focal mechanisms are clustered within the cloud close to GPK3 (on this projection view) at depths between 4800 m and 5100 m.

CONCLUSION

In conclusion, direct observation of breakouts and DITFs in the boreholes appears to be the most accurate method to determine the linear-with-depth state of stress, and quantify the deviations from this (i.e. the heterogeneity). Nevertheless the inversion of focal

mechanisms can yield useful characteristics of the stress field, and has the advantage that is samples a much larger volume. The results obtained in the present study show that, for the well-constrained stresses, the discrepancy between the results of the focal mechanism and the wellbore failure observations is less than the uncertainty range. The approach of selecting compatible mechanisms produces simultaneously a set of rejected mechanisms, which can, in some favourable cases, highlight zones of strong stress heterogeneities.

Acknowledgements. Work at Soultz is funded and supported by the Europen Commission Directorate-General Research, contract SE6-CT-2003-502 706, EGS Pilot Plant, ADEME (contract ADEME-CNRS No. 05.05.C0076), the German Bundesministerium für Umwelt, Naturschutz und Reakorsicherheit, the Projektträger of the Forshungszentrtrum Jülich in Germany and the members of the GEIE "Exploitation Minière de la Chaleur" (EDF, EnBW, ES, Pfalzwerke, Evonik). The research was conducted with the financial support of ADEME. K. Evans and B. Valley acknowledge the support of the Swiss State Secretariat for Education and Science.

References

[1] R. Baria, S. Michelet, J. Baumgärtner, B. Dyer, A. Gérard, J. Nicholls, T. Hettkamp, D. Deza, N. Soma, H. Asanuma, J. Garnish T. Megel, Microseismic monitoring of the world's largest potential HDR reservoir, Proceedings 29th Workshop on Geothermal Reservoir Engineering, Standford University, Standford, California, 26/28th January (2004) 8pp.
[2] T. Bérard, FH. Cornet, Evidence of thermally induced borehole elongation: a case study at Soultz, France, Int. J. Rock Mech. Min. Sci. 40 (2003) 1121-1140.
[3] M. Brudy, M. D. Zoback (1999), Drilling-induced tensile wall-fractures: implications for determination of in-situ stress orientation and magnitude, Int. J. Rock Mech. Min. Sci., 36 (1999) 191-215.
[4] FH. Cornet, Th. Bérard, S. Bourouis, How close to failure is a granite rock mass at a 5 km depth?, Int. J. Rock. Mech. Min. Sci. 44 (2007) 47-66.
[5] N. Cuenot, J. Charléty L. Dorbath, H. Haessler, Faulting mechanisms and stress regime at the European HDR site of Soutz-sous-Forêts, France, Geothermics 35 (2006) 561-575.
[6] L. Dorbath, N. Cuenot, A. Genter, M. Frogneux, Seismic response of the fractured and faulted granite of Soultz-sous-Forêts (France) to 5 km deep massive water injections, Geophys. J. Int. (2008) in press
[7] A. Genter, H. Tenzer, Geological monitoring of GPK-2 HDR borehole, 1420-3880 m, BRGM, Orléans (1995)
[8] B. Heinemann-Glutsch, Results of scientific investigations at the HDR test site, Soultz-sous-Forêts, Alsace, Socomine, BP 38, route de Soultz, F-67250 Kutzenhausen, France (1994)

[9] J.A. Helm, The natural seismic hazard and induced seismicity of the European HDR (Hot Dry Rock) geothermal energy project at Soultz-sous-Forêts, France., Ph.D. thesis, Université Louis-Pasteur de Strasbourg (1996)
[10] T. Hettkamp, J. Baumgärtner, R. Baria, A. Gérard, T. Gandy, S. Michelet, D. Teza , Electricity production from Hot Rocks, Proceedings 29th Workshop on Geothermal Reservoir Engineering, Stanford University, Stanford, California, 26/28th January (2004) 10pp.
[11] R. Jung, Hydraulic fracturing and hydraulic testing in the granitic section of borehole GPK1, Soulz-sous-Forets, Geothermal Sci. and Tech. 3 (1991) 149-198.
[12] G. Klee, F. Rummel, Hydrofrac stress data for the European HDR research project test site Soultz-sous-Forêts, Int. J. Rock Mech. Min. Sci. & Geomech. Abst., 30 (1993) 973-976.
[13] G. Klee, F. Rummel (1999), Stress regime in the Rhinegraben basement and in the surrounding tectonic units, Proceedings of the European Geothermal Conference, 28/29/30th September, Bull. Hydrogéologie Special Issue, P. Lang ed., Bern, Switzerland, 135-142 (1999)
[14] L. Mastin, B. Heinemann, Evaluation of the caliper and televiewer data fromm the Soultz well between 1450 m and 2000 m depth, Karlsruhe University, Germany (1998)
[15] A.J. Michael, Determination of stress from slip data: faults and folds, J. Geophys. Res., 89 (1984) 11 517-11 526.
[16] A.J. Michael, A.J., 1987a, The use of focal mechanisms to determine stress: a control study, J. Geophys. Res., 92 (1987a) 357-368.
[17] A.J. Michael, Stress rotation during the Coalinga aftershock sequence, J. Geophys. Res., 92 (1987b) 7 963-7979.
[18] R. Nagel, Das Spannungsfeld in der Geothermiebohrung Soultz-sous-Forêts abgeleitet aus vertikalen Structuren in eine Tiefe von 1.9 bis 3.6 km, PhD thesis, Univ. Karlsruhe (1994)
[19] P.A. Reasenberg, D. Oppenheimer, FPFIT, FPPLOT and FPPAGE: Fortran computer programs for calculating and displaying earthquake fault-plane solutions, US Geological Survey (1985) 25pp.
[20] L. Rivera, A. Cisternas, Stress tensor and fault plane solutions for a population of earthquakes, Bull. Seis. Soc. Am. 80 (1990) 600-614.
[21] F. Rummel, J. Baumgärtner, Hydraulic fracturing stress measurements in the GPK1 borehole, Soultz-sous-Forêts, Geotherm. Sci. and Tech. 3 (1991) 119-148.
[22] H. Tenzer, L. Mastin, B. Heinemann (1992), Determination of planar discontinuities and borehole geometry in the crystalline rock of borehole GPK-1 at Soulz-sous-Forets, Geothermal Sci. and Tech. 3 (1992) 31-68.
[23] B. Valley, K.F. Evans (2005), Stress orientation estimates from analysis of breakouts and drilling-induced tension fractures in GPK3 and GPK4, Proceedings EHDRA Scientific Conference, Soultz-sous-Forêts, 17/18th March (2005)
[24] B. Valley, K.F. Evans, Stress state at Soultz-sous-Forêts to 5 km depth from wellbore failure and hydraulic observations, Proceedings 32nd Workshop on Geothermal Reservoir Engineering, Stanford University, Stanford, California, 22-24th January (2007a) 10pp.
[25] B. Valley, K.F. Evans, Stress heterogeneity in the Soultz granite inferred from analysis of wellbore failure to 5 km depth, Proceedings EHDRA Scientific Conference, Soultz-sous-Forêts. 28-29th June (2007b) 10pp.
[26] R. Weidler, Hydraulic stimulation of the 5 km deep well GPK-2, Report to Socomine, Bundesanstalt für Geowissenschaften und Rohstoffe (BGR) Hannover (2000)

Figure caption

Figure 1. GPK2: a: Principal stress directions, b,c and d: focal mechanisms used in the inversion of the stress tensor. Light grey: hypocenters of M>1 microearthquakes induced by

GPK2 stimulation (June/July 2000). Black: hypocenters of microearthquakes used in the inversion.
Figure 2. a, b, c, d: same as figure 1 for GPK3. Light grey: hypocenters of M>1 microearthquakes induced by GPK3 stimulation (May/June 2003). Black: hypocenters of microearthquakes used in the inversion.
Figure 3. Black: focal mechanisms with large (>15°) misfit. Light grey: hypocenters of M>1 microearthquakes induced by GPK3 stimulation (May/June 2003).

FIGURES

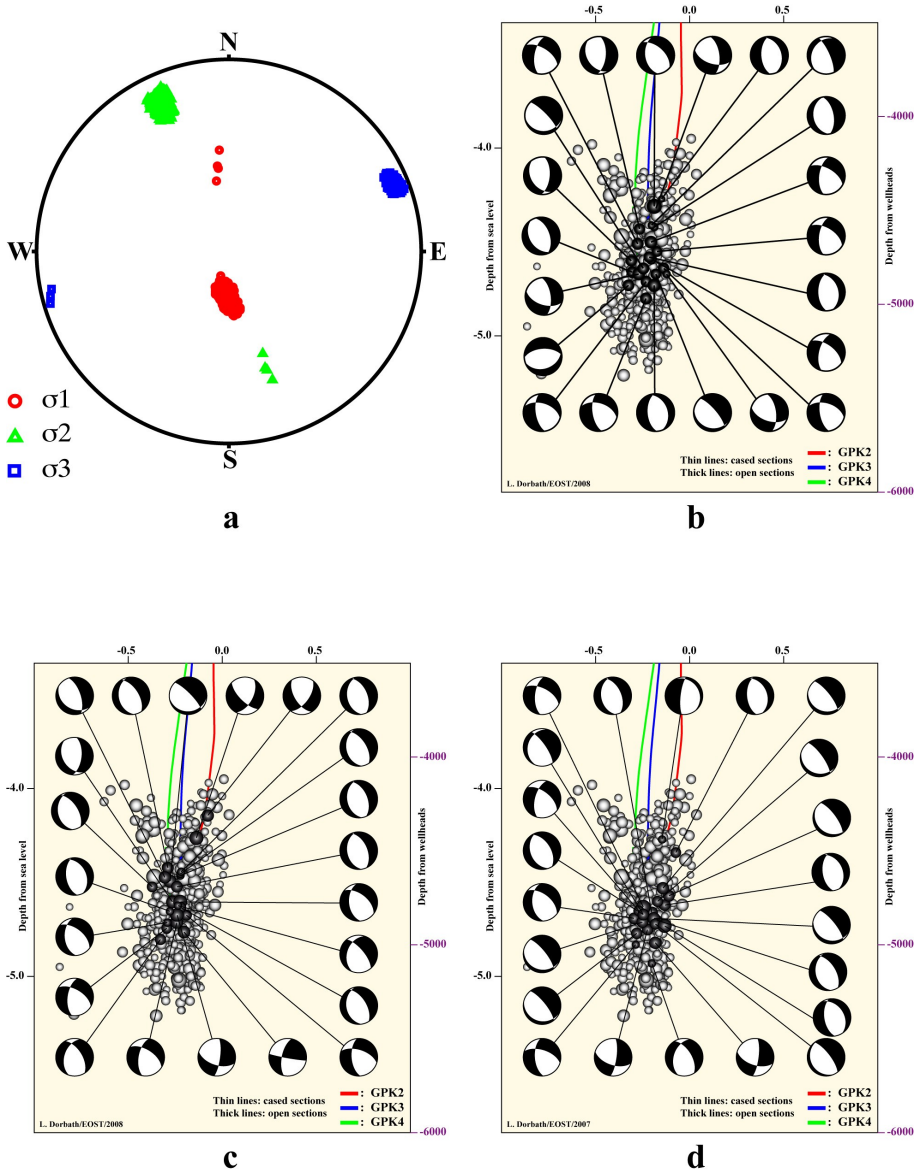

Figure 1

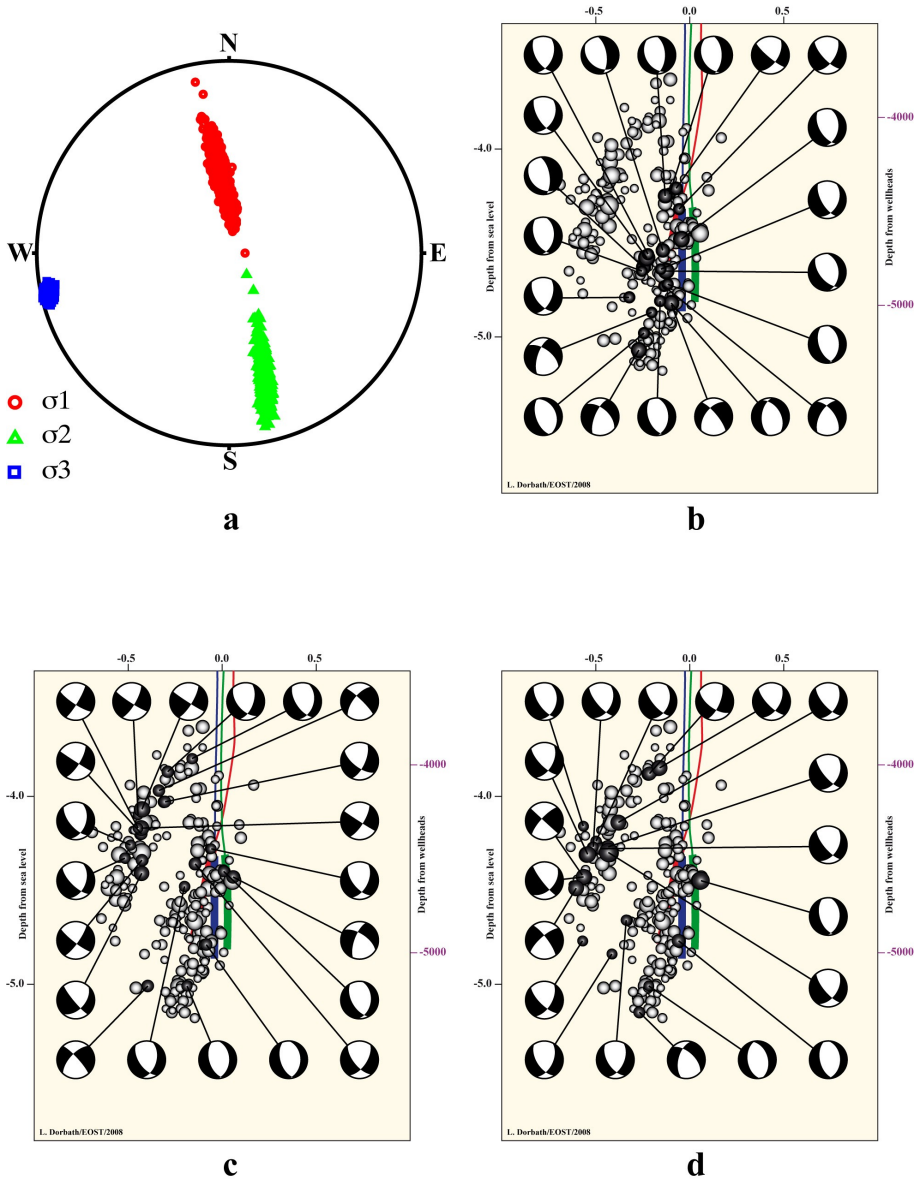
N
W
E
S
σ1
σ2
σ3
a
-0.5
0.0
0.5
-4.0
-5.0
Depth from sea level
-4000
-5000
Depth from wellheads
L. Dorbath/EOST/2008
b
c
d

Figure 2

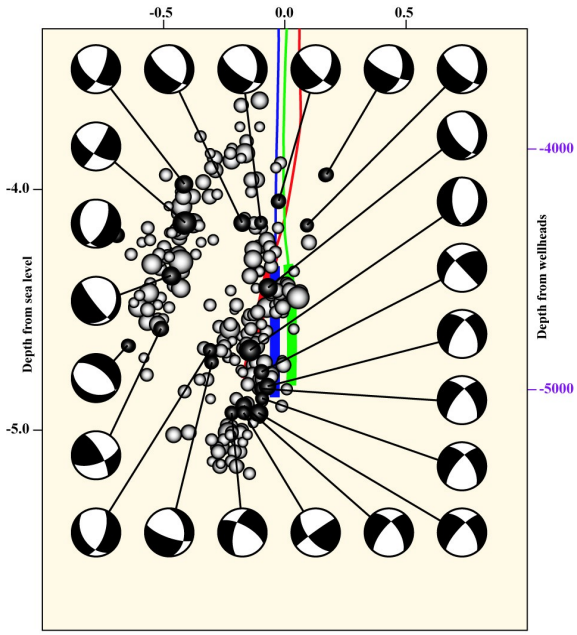
-0.5
0.0
0.5
-4.0
-5.0
Depth from sea level
-4000
-5000
Depth from wellheads

Figure 3

Structure of the low permeable naturally fractured geothermal reservoir at Soultz

Chrystel Dezayes*, Albert Genter**, Benoît Valley***

** BRGM, Geothermal Department, 3, avenue Cl. Guillemin, BP36009, F-45060 Orléans Cedex 2*
*** GEIE Exploitation Minière de la Chaleur, Route de Soultz, BP40038, F-67250 Kutzenhausen*
**** ETH Zürich, Engineering Geology, CH-8092 Zürich; now: MIRARCO/Laurentian University, 935 Ramsey Lake Road,*
Sudbury, ON P3E 2C6, CANADA

Submitted to Geoscience, 2009.

Elsevier Editorial System(tm) for Comptes rendus geoscience
Manuscript Draft

Manuscript Number: CRGEOSCIENCE-D-08-00001

Title: STRUCTURE OF THE LOW PERMEABLE NATURALLY FRACTURED GEOTHERMAL RESERVOIR AT SOULTZ

Article Type: Full Length Article / Article original

Section/Category: GEOPHYSIQUE INTERNE / INTERNAL GEOPHYSICS

Keywords: Rhine graben, Fractures, Fracture zones, Cores, Borehole images, Enhanced Geothermal System.
Fossé rhénan, Fractures, Zones de fractures, Carottes, Image de paroi, Système Géothermal Amélioré.

Corresponding Author: Mme Chrystel Dezayes,

Corresponding Author's Institution: BRGM - Geothermal departement

First Author: Chrystel Dezayes

Order of Authors: Chrystel Dezayes; Albert Genter; Benoît Valley

Manuscript Region of Origin:

Abstract: The structure of the granite geothermal reservoir of Soultz is constituted by both major fracture zones, connected to a dense network of small-scale fractures.
The small-scale fractures are nearly vertical and the major direction is about N0°E. This direction is locally different than the major direction of the Rhine graben, which is about N20°E. Fracture zones are about N160°E.
39 fracture zones have been characterized in six wells between 1400 and 5000 m depth. These fracture zones are spatially concentrated in three clusters. The upper cluster at 1800-2000m TVD is

highly permeable. At 3000-3400m TVD, the intermediate cluster constitutes a dense network developed in an altered matrix and constitutes the upper reservoir. In the lower part of the wells, the deeper cluster appears as a fractured reservoir developed within a low permeable matrix.

Suggested Reviewers:

Opposed Reviewers:

STRUCTURE OF THE LOW PERMEABLE NATURALLY FRACTURED GEOTHERMAL RESERVOIR AT SOULTZ

Chrystel Dezayes*, Albert Genter** & Benoît Valley ***

**BRGM, Geothermal Department, 3, avenue Cl. Guillemin, BP 6009, F-45060 Orléans Cedex 2*
*** GEIE Exploitation Minière de la Chaleur, Route de Soultz, BP38, F-67250 Kutzenhausen*
**** ETH Zürich, Engineering Geology, CH-8093 Zürich; now: MIRARCO/Laurentian University, 935 Ramsey Lake Road, Sudbury, ON P3E 2C6, CANADA*

Corresponding author e-mail: c.dezayes@brgm.fr

Abstract

The structure of the granite geothermal reservoir of Soultz is constituted by both major fracture zones, connected to a dense network of small-scale fractures.
The small-scale fractures are nearly vertical and the major direction is about N0°E. This direction is locally different than the major direction of the Rhine graben, which is about N20°E. Fracture zones are about N160°E.
39 fracture zones have been characterized in six wells between 1400 and 5000 m depth. These fracture zones are spatially concentrated in three clusters. The upper cluster at 1800-2000m TVD is highly permeable. At 3000-3400m TVD, the intermediate cluster constitutes a dense network developed in an altered matrix and constitutes the upper reservoir. In the lower part of the wells, the deeper cluster appears as a fractured reservoir developed within a low permeable matrix.

Résumé

Le réservoir géothermique de Soultz est constitué par des zones de fracture majeures connectées à un réseau dense de fractures secondaires.
Les méso-fractures sont pratiquement verticales et la direction majeure est à peu près N-S. Cette direction diffère de la direction régionale du fossé rhénan qui est localement à dominante N20°E.
39 zones de fracture ont été identifiées et caractérisées dans six puits entre 1400 et 5000 m de profondeur. Ces structures sont réparties en trois clusters suivant la profondeur. Le premier cluster à 1800-2000m TVD est très perméable. A 3000-3400m TVD, le cluster intermédiaire apparaît comme un réseau plus dense dans un milieu plus altéré et constitue le réservoir supérieur. Dans la partie inférieure des puits, le cluster profond apparaît comme un réservoir fracturé développé dans une matrice très peu perméable.
Key words: Rhine graben, fractures, fracture zones, cores, borehole images, Enhanced Geothermal System.
Mots-clés : Fossé rhénan, fractures, zones de fractures, carottes, image de paroi, Système Géothermal Amélioré.

1 Introduction

Since 1980 [24; 25], the EGS project at Soultz (France) goals to experiment and develop a new geothermal technology. After an initial Hot Dry Rock (HDR) concept of artificial fractures creation in a homogeneous rock by hydraulic fracturing, the concept at Soultz has progressively evolved to an Enhanced Geothermal System (EGS) where reservoir development proceed through the reactivation of the pre-existing fractures in the granite [13*;* 26]. Thus, a good knowledge and characterization of the rock mass and particularly of the fracture network are essential for many reasons, from the optimization of the borehole design to the understanding of the flow distribution at depth.

This fracture network is structured at different scales, from major fracture zones cross-cutting the granite batholith to intra-crystalline microfractures, which induce weakness in the rock mass [6].

The principle of the EGS technology consists to increase the low natural hydraulic performance of the geothermal reservoir by hydraulic or/and chemical stimulations. These stimulations allow having enough permeability to transport the geothermal brine. This permits to create a circulation between the wells by using the pre-existing fracture network for an efficient extraction of the geothermal fluid. The hydraulic stimulation consists in injecting water with high flow rate in order to increase the pore pressure within the rock mass which promotes the shearing of existing fractures, a mechanism accompanied by detectable induced microseismicity. When the injection is stopped, the shearing relaxation is irreversible and the reactivated fractures do not close totally, yielding to a new and/or enhanced permeability [23]. This mechanical effect of enhanced permeability occurs either in the well near-field or at some distance far away from the well. Chemical stimulation affects permeability essentially in the direct well vicinity and consists in injecting acids to dissolve the mineral fillings within the natural fractures, like calcite, secondary silica or clay minerals [36]. Both methods have to be associated to increase fluid pathways within the fracture network [34].

In this paper, we present our results concerning the intermediate scale, constituted by meso-scale fractures, and the large-scale, formed by fracture zones.

Several studies have shown that some fracture zones are water-bearing prior to stimulation [47; 16] and constitute the main flow channeling after stimulation and during circulation [13; 39]. These fracture zones are probably reactivated by shearing whilst the hydraulic stimulation. Moreover, other fracture zones not permeable prior stimulation have been reactivated during the stimulation and have been taking into account in this study. In the Soultz granite, the fracture zones have their own internal architecture with different constituents from the core center to external parts of the zone [16; 21]:

- secondary hydrothermal mineral deposit, as geodic quartz vein;
- microbrecciated to cataclased granite or highly fractured granite, due to intense shear-movement of the fault under tectonic stresses;
- hydrothermally altered granite, due to fluid circulation characterized by mineral dissolution and secondary clay mineral precipitation.

As these fracture zones present high alteration, they are named Hydrothermal Altered Fracture Zones (HAFZ).

Thus, fracture zones constitute the main fluid pathways connected to the dense network of meso-scale fractures to form the geothermal reservoir, which is about 1,125km^3 for the upper reservoir and 8 km^3 for the deeper reservoir, based on induced micro-seismicity study [4].

2 Geological and structural context

The Soultz site is located within the Upper Rhine Graben, which is a Cenozoic rift structure belonging to the West European Rift System (Fig. 1; 48). The filling sediments are constituted by marine and lacustrine limestones, marls and evaporites, including the petroleum layers of Pechelbronn, overlaying in unconformity the Jurassic limestones and the Germanic Trias (Fig. 1b). These Cenozoic and Mesozoic sediments have been deposited on the Paleozoic basement constituted by a porphyritic monzo granite and a two-mica granite [19; 41; 3; 28].

This granite unit is the target of the geothermal project and hosts the geothermal reservoir. This massif underwent a multiphase tectonic history including Hercynian and Alpine orogeneses. The Cenozoic tectonic history is reflected by the orientations of the current structures forming the Upper Rhine Graben (Fig. 1). The regional major border faults mapped on surface or derived from petroleum seismic reflection studies within the Upper Rhine Graben show a N0-30°E direction in relation to the three main directions of the graben (Fig. 1). In the southern part of the graben, the main direction is about N10°E. This direction rotates clockwise at the center of the graben to N30-25°E and becomes N0°E in its northern part. This Rhenish orientation was formed during the Oligocene opening of the Rhine graben [45], reactivating probably some Hercynian structures [29; 30; 38]. At the Soultz site, the Upper Rhine Graben rotates and the regional border faults are N45°E oriented. This direction is also present in the Triassic sediments in the west of the graben fault, in the Vosges area [33].

However, the granitic basement has been affected by ante-Cenozoic tectonics, in particularly the Hercynian orogen. The strike of the major dislocations delimiting the different Hercynian tectonic blocks is roughly N60°E (Fig. 1). At local scale, around the Soultz site, geological mapping, borehole data and interpretation of seismic profiles acquired during the exploration of the Pechelbronn oil field give lots of data to characterize the major fault system [14; 35]. These data were compiled to build a 3D geological model of the sedimentary cover [37; 2]. These studies show that in the sedimentary cover, the faults have a N20°E strike, i.e. a Rhenish direction (Fig. 1). On horizontal map, the faults have a trace length of about 2 to 20 km and occur with a spacing range of about 800m to 3km [44]. At depth, below the Soultz site, a horst structure is present and the top of the basement is at 1.4km depth (Fig. 1b). Within this horst structure, some local faults are detected on the seismic profiles, which are mainly dipping to the West (Fig. 1b).

3 Methodology

Unwrapped borehole image logs and cores studies allow to characterise the fracturing within the Soultz granite at various scales. On the cores, all the fractures are systematically sealed by hydrothermal filling but only 20% of them are visible on the borehole images [18]. However, only one borehole (EPS1) is fully

cored and some spot coring are available in other wells. But, the borehole images are suitable for detecting and measuring the orientation of the meso-scale fractures and fracture zones.

On the borehole images, fracture orientations are sometimes difficult to measure due to the fact that fractures are not perfectly planar as it is assumed for the dip calculation. Also, as mentioned above, fracture zones are complex and their orientation is difficult to define. Often, several individual fracture traces are visible on the log image within a given fracture zone, which is constitute by brecciated to microbrecciated zone. To determine the fracture zone overall orientation, we consider that the orientation of the border of the brecciated zone is representative of the overall orientation if this limit is well visible and defined and if it forms a well-marked planar structure. However, when several planar structures are present and roughly parallel, we assumed that the orientation of the fracture zone is well approximate with the 3D average orientation of the individual planes.

In order to better characterize low permeable fracture zones, we use the geological database based on petrographical description of cuttings, borehole image log and geophysical log analyses, as caliper, spectral gamma ray and drilling parameters (Fig. 2). The spectral gamma ray data, such as potassium, thorium and uranium contents, are used to detect radioactive element concentration due to the hydrothermal alteration of fracture zones.

However, we cannot determine if there are some evidences of natural permeability in a given fracture by interpreting geological data only. Then, in addition, temperature and flow logs analysis was used to determine the zone of fluid lost in the boreholes [11; 7].

In the framework of the Soultz geothermal project, several wells have been drilled for exploration and for the geothermal reservoir development and exploitation [8]. In these wells, different data have been acquired, but these data are not homogeneous in terms of characterization and resolution. Thus, fracture zone characterization will be not strictly equivalent for all wells.

4 Small-scale fractures

Many fracture data have been collected in the granite basement based on coring and especially borehole imaging [22]. The analyses of these fracture data show that the main strike is consistent between the different imagery logs and the different wells (Fig. 3; 15; 20, 7). In EPS1, the coring has begun at 830m in the lower Muschelkalk. The fractures present in the Buntsandstein formation have been measured and oriented as in the granite. In this sedimentary cover, the fracture network is limited scattering around N175°E. Two conjugate and symmetrical major poles are present, as well as it is more scattered and asymmetrical in the granite. In the granite, the major direction is varies from N160°E to N-S with steep dipping eastward and westward. However, the orientations of fractures observed on cores (EPS1) are rather scattered with various dipping values (Fig. 3). On these cores, some faults showing striations have been measured and the Oligocene paleostress states have been retrieved by inversion [5]. Among the fractures in granite, based on borehole image interpretation, seven sets have been isolated by statistical method [42]. 60% of fractures belong to two sets striking N-S and dipping to the west and to the east. This orientation corresponds to the Rhenish orientation described at graben and site scales. A sub-vertical set, striking NW-SE, appears also at large scale but outside of the Rhine graben in Vosges and Black Forest massif and in the Triassic sediments. Another subvertical perpendicular set, striking NE-SW,

is parallel to the Hercynian large scale faults, like the Lalaye-Lubine-Baden-Baden fault. These four sets include 95% of all fractures found in granite [42]. It appears clearly that the granite batholith has recorded a polyphased tectonic history. With depth, the strike of the main N-S sets remain roughly similar, however balance between the dominant dip orientation evolved (Fig. 3).In GPK3 and GPK4, between 1420m to 2700m TVD (True Vertical Depth), the main fracture set dips to the East. In the middle part of the borehole sections, between 2700m to about 4800m depth, the two conjugate sets are equally represented with fracture sets dipping westward and eastward. In the bottom part of the wells, below 4800m to 5000m depth, the westward set is dominant (Fig. 5). Studies of abutting relations and fracture size in GPK3 and GPK4 support also this repartition with depth [42].

5 Characterization of fracture zones

In the six wells of the Soultz site, we considered 39 fracture zones, which indicate some potential traces of fluid flow (Table 1, Fig. 4). This list of fracture zone is probably not extensive and could be completed later by further data acquisition or processing.

The fracture zones have been classified within three levels in attempting to reflect their relative scale and importance as fluid flow paths. The first level (1 in the table 1) concerns the major fracture zones, which have been detected during drilling operations with important mud losses and then are permeable prior to any stimulation operations. The fracture zones of the second level (2 in the table 1) show flow indication higher than 20% of water losses during stimulation and/or are characterized by the other available geological data to include at least one thick fracture accompanied with a significant halo of hydrothermal alteration. The last level (3 in the table 1) includes the fracture zones having a poorly developed alteration halo and a flow level below 20% of water losses during stimulation. This level indicates fracture zones of smaller size than those of the two other levels previously defined.

In the three wells EPS1, GPK1 and 4550, a major fault zone occurs in the Buntsandstein sediment at around 1200 m (Table 1). This zone has been cored by the EPS1 well and where it forms a large structure containing 3 sub-zones and presenting fractures with quartz, galena and barite fillings. In the GPK1 and 4550 wells, total drilling mud losses have been occurred when drilling through this zone [27; 46]. In the 4550 well, a BHTV log, is available and allows characterization the fracture zone. This presents a series of open steeply dipping fractures. However, the orientation value is not very precise due to the rather bad quality of the image log.

In the GPK1 well, another natural brine inflow occurred during the drilling at the depth of the large fracture zone at 1820m MD (Table 1, 27). At this depth, a very high Helium content anomaly was recorded [47] and other drilling anomalies were reported. This fracture zone contains geodic quartz veins, visible on a core taken at this depth as well as illite [15].

Also in the upper part of the granite, in GPK2 well, a fracture zone provoking total drilling mud losses has been intersected and no cuttings have been collected below [16]. The fracture zone at 2120m MD shows a high altered zone with several open fractures (Table 1). The hydraulic testing of an open hole interval including this fracture zone showed that 95% of the flow rate was absorbed by this zone [31]. This zone is also believed to be responsible for a large-scale stress perturbation, as highlighted by the analysis of borehole failure [42]

Deeper, no major fracture zone occurs except at the bottom of the GPK3 well, within the open hole, there is a major fracture zone located around 4770m MD (Table 1). This zone includes several individual fractures with a cumulative apparent thickness of around 15m along the well. The K content increases in the hanging wall of the zone and decrease in the center part indicating a high alteration halo. Flow rate show a 70% outflow matching this zone [7]. Analysis of borehole failure showed that this zone is inducing a major stress perturbation [42]. This is the major flow pathway in the geothermal reservoir at lower depth. GPK4 is the only well where there is no level 1 fracture zone (table 1). The description of the fracture zones is detailed in [9].

The orientation of these fracture zones is determined based on borehole images as described above (Fig. 4). Most of orientations of fracture zones have been determined according to the assumptions cited above. However, some of them are more difficult to estimate and are detailed in the following text. The orientation of the fracture zone in GPK3 at 3270m, which appears E-W striking (Fig. 4D, table 1), is very imprecise. The image log quality is locally poor and no correct measure has been done. Moreover, in GPK2, some orientation of fracture zones could no been measured at all. This well was drilled in two times, in 1995 and 1999, and some problems occurred at 3900m, where the first drilling stopped. At that depth, it appears a large cave based on the caliper log [19]. Some altered cuttings coming from this zone have been recovered at the end of the drilling operation in 1995. After the deepening in 1999, as this large cave occurs in a significantly deviated part of the well, the UBI tool stuck and no image log has been run below that depth. After that, the borehole has been cased and now, the presence of a casing restriction is suspected due a partial casing collapse induced by the fracture zone. Using 3D visualization [40], we suspect that this fracture zone is the same that the one cross-cutting the bottom of GPK3 well (GPK3-FZ4770 in table 1). Thus, we assumed that this zone has the same orientation (Table 1). However, due to this GPK2 borehole wall restriction at 3900m, no logging tools could be run below this depth now. Below 3900m, only temperature and flow logs are available. Then, we have located three zones with outflow which match with altered zones based on cutting observation. These zones occur at 4760m with 20% of flow, 4890m with 17% of flow and 50% of flow below 4960m which could correspond to a fracture zone occurring at 5060m, based on cutting observation. As there are no oriented image logs in this section, we have assumed a generic orientation, which is realistic but not proven, N250°E-65° (N160°E-65°W), the dominant orientation of fractures in the deeper part of the Soultz granite (Fig. 4C).

6 Discussion

Most of the fracture zones characterized in the framework of this study (Table 1) can be attributed to three main concentrations or clusters of fractures zones at about 1800-2000, 3000-3400 and around 4500-5000 m TVD (True Vertical Depth) (Fig. 5). In that regard, the borehole GPK4 is somehow untypical, presenting less clearly clustered, steeply dipping fracture (Fig. 5), while in the other wells, fracture zones more consistently correspond to these three fracture zone concentrations This result was already mentioned previously in the upper part of the granite body, before the deepening of GPK2 and the drilling of GPK3 and GPK4 [16; 17]. These three clusters of fracture zones are considered to reflect major fault, equivalent to the fault detected in the sedimentary cover based on seismic reflection [17]. If we assume

that these faults are steeply dipping structures with values higher than 60°, the raw spacing between to consecutive clusters of fracture zones is around 500 m, equivalent to the fault spacing in the sedimentary cover [44].

The upper cluster at 1800-2000m depth (Cluster I in Fig. 5) is located in the unaltered porphyritic granite. This cluster includes major fracture zones qualified as level 1 with permeable zones. The cluster II does not include major level 1 faults. It is located within the fractured and altered granite zone (Fig. 5). This granite facies is characterized by high pervasive alteration related to numerous small-scale fractures present in this zone [28]. This facies contains high proportion of clay and hydrothermal minerals. Possibly, the high fracturing of this facies leads to a generally weaker rock mass where the strain is distributed in small increments over a dense network of smaller fractures, instead of being concentrated by a few major faults. This location corresponds to the upper reservoir stimulated in the first phase of the project in 1997 [1]. In this reservoir, a two months circulation loop test has been performed with success. Then, it appears that there is a good fluid connection in this reservoir between GPK1 and GPK2. The lower cluster (Cluster III in the Fig. 5) is close to the interface between the 2 granite units at 4700 m depth TVD. The deep facies is characterized by massive granite characterized by a low pervasive alteration degree. The cluster III contains major fracture zone as the GPK3-FZ4770. Thus, it appears that the deformation in this facies tends to be localized along major isolated fracture zones. This last cluster is located in the lower reservoir, which has been stimulated previously, and is currently a part of the deep geothermal loop under testing for the electrical production test. Conceptually, this reservoir appears to behave as a fractured reservoir embedded in a low permeable matrix.

Based on this characterization of fracture zones at borehole scale, these major planes have been compared with other fracture information derived from other detection methods in order to build a 3D model [40]. These other methods are microseismicity data created within the reservoir during the stimulations of GPK2, GPK3 and GPK4 [10] and a VSP (Vertical Seismic Profiling) investigation [35]. Some of the fracture zones observed at the well scale match with microseismicity or VSP results. They correspond to fracture zones qualified by level 1 or 2 such as GPK1-FZ3490, GPK2-FZ3900 and GPK3-FZ4770, which match with microseismicity and VSP analysis. Moreover, the dip orientations of the fracture zones are very close and seem to define a large-scale fault intersecting the Soultz basement (Fig. 5). This orientation of the major fracture zone is about N230°E-70° (N140°E-70°W).

In GPK1, two fracture zones at 1820m and 2860m appear to match with the VSP analysis [35; 40].

In the lower part of the reservoir, two smaller fracture zones in GPK4 match geometrically with the microseismicity analysis at 4620m and 4970m [40]. These fracture zones are N10°E striking, steeply dipping to the west (Fig. 5).

The average strike direction of fracture zones characterised in the Buntsandstein sediments and the granite is N165°E±10° and N160°E±15° respectively (Fig. 6A1-6B1). A secondary fracture zone set in the Buntsandstein is N40°E striking. In the granite, two secondary sets are present with a N20°E±10° and N130°E±10° direction. The average dip is higher than 60° (Fig. 6 A1-6B1). These orientations are consistent through the granite and the Buntsandstein sedimentary cover. In both cases, fracture zones dominantly dip to the west. The orientation of meso-scale fractures measured in the Buntsandstein on the

EPS1 cores (Fig. 6A2) and in the granite on the borehole images shows a N0°E±20° and N175°E±30° direction respectively (Fig. 6B2). In the Buntsandstein, dips are equally-balanced between the west and the east, whereas in the granite, more fractures dip to the west. Then, it appears that there is no mechanical decoupling between this both geological brittle units.

If we compare the orientation of fracture zones with the meso-scale fractures, we can observe a clockwise rotation of 10-15° for both fractures in the Buntsandstein and in the granite (Fig. 6). However, in all the cases, the west dipping direction is dominating.

In previous studies, these fracture zone concentrations were interpreted as the occurrence of large-scale normal fault zones related to the Rhine graben tectonics. However, the direction of the fracture zone, as the direction of meso-scale fractures, is slightly different than the major fault orientation observed in the sedimentary cover, which have a Rhenish direction of N20°E and which corresponds to the graben opening at Oligocene. The granite contains numerous fracture orientations related to Hercynian and Alpine tectonics. It seems that the N160°E is an inherited direction, which has been reactivated during the graben tectonic. Thus, the main fracture zone orientation is rather different than those newly created in the sedimentary cover during Cenozoic. A remaining question is: what is the relationship between the major faults in the sedimentary cover and the fracture zone clusters? On-going work aims to tackle this question by developing a 3D large-scale geometrical model based on an exhaustive geological database [2; 35; 40].

Moreover, the average direction of the fracture zones is rather consistent with the present-day stress field with σ_H N169°E±14° [32; 43]. Some fracture zones which show flow anomalies or shearing indications appear as small fractures on the borehole image logs. This seems to indicate that critically oriented fractures relatively to the stress state orientation could shear during hydraulic stimulation [12].

7 Conclusions

Characterization of the main fracture zones likely to bear fluid flow prior or after stimulations was achieved along the Soultz wells based on direct (cores, cuttings) and indirect (borehole images, geophysical logs, flow logs) methods. We have compiled and matched these different data to highlight a set of 39 fracture zones intersecting the five boreholes of the geothermal site as well as a peripheral well. This list is not extensive and could be completed by further data acquisition or processing.

Fracture zones develop at multiple scales and this is reflected in our analysis by the categorization of the fracture zones within three levels according to their permeability prior to any stimulation, their size and their alteration degree.

The orientation of the fracture zones have been measured on borehole images and incertitude exits. But these orientations are compared with the meso-scale fractures and the orientations are 10-15° clockwise rotation. No difference appears between the Triassic sedimentary cover and the granite.

The fracture zones are rather homogeneously distributed along the GPK4 well. On contrary, on the other wells, the fracture zones are organized in cluster. Three clusters have been identified in the granite cross-cut by the boreholes. The upper cluster at 1800-2000m TVD is highly permeable. In the middle part of the wells, at 3000-3400m TVD, the intermediate cluster appears as a porous matrix-fractured zone and

constitutes the upper reservoir tested in 1997. In the lower part of the well, the third cluster appears as a fractured reservoir within a low permeable matrix tested in 2005.

The main direction of these fracture zones is around N160°E±10° with a dip angle higher than 60°. This orientation is consistent with the small-scale fractures embedded within the granite and is consistent with the present-day horizontal stress. It seems this direction is inherited and has been reactivated with the graben tectonic evolution.

These fracture zones could be compared with other data, which were acquired in the framework of the project as microseismicity or VSP [40]. It could be also used as a basis of numerous modeling approaches for a better understanding of the thermo-hydraulic mechanical behavior of this geothermal reservoir under stimulation or during its exploitation.

Acknowledgements

This work has been carried under financial support of ADEME, Europe and BRGM (EGS3D project). EHDRA working group 6 and 7 teams are kindly thank for their contributions and for fruitful discussion.

References

[1] Baumgärtner J., Jung R., Gérard A., Baria R., Garnish J., (1996). The European HDR project at Soultz-sous-Forêts: stimulation of the second deep well and first circulation experiments. Twenty-first Workshop Geothermal Reservoir Engineering, Stanford University, Stanford, California, USA, 267-274.

[2] Castera J., Dezayes Ch., Calcagno Ph., (2008). Large-scale 3D geological model around the Soultz site, Proceedings of the EHDRA scientific conference 24-25 September 2008, Soultz-sous-Forêts, France.

[3] Cocherie A., Guerrot C., Fanning C.M., Genter A., (2004). Datation U-Pb des deux faciès du granite de Soultz (Fossé Rhénan, France). Comptes Rendus Geoscience, 336, 775-787.

[4] Cuenot N., Charléty J., Dorbath L., Haessler H., (2006). Faulting mechanisms and stress regime at the European HDR site of Soultz-sous-Forêts, France, Geothermics, Vol. 35, No. 5-6, 561-575.

[5] Dezayes Ch., Villemin Th., Genter A., Traineau H., Angelier J., (1995). Analysis of fractures in boreholes of the Hot Dry Rock project at Soultz-sous-Forêts (Rhine Graben, France). Scientific Drilling, vol. 5, 31-41.

[6] Dezayes Ch., Villemin Th., Pêcher A., (2000). Microfracture pattern compared to core scale fractures in the borehole of Soultz-sous-Forêts granite, Rhine graben, France. Journal Of Structural Geology, 22, 723-733.

[7] Dezayes Ch., Genter A., Gentier S., (2004). Fracture network of the EGS Geothermal Reservoir at Soultz-sous-Forêts (Rhine Graben, France). Geothermal Resources Council Transactions, Palm Springs, California, USA, Vol. 28, 213-218.

[8] Dezayes Ch., Gentier S., Genter A., (2005). Deep Geothermal energy in Western Europe: the Soultz project. BRGM/RP-54227-FR, 48 pp.

[9] Dezayes Ch., Genter A., (2008). Large-scale fracture network based on Soultz borehole data. EHDRA Scientific Conference, Proceedings of the EHDRA scientific conference 24-25 September 2008, Soultz-sous-Forêts, France.

[10] Dorbath L., Cuenot N., Genter A., Frogneux M., (2009). Seismic response of the fractured and faulted granite to massive water injection at 5 km depth at Soultz-sous-Forêts (France), Accepted to Geophysical International Journal.

[11] Evans K.F., (2000). The effect of the 1993 stimulations of well GPK1 at Soultz on the surrounding rock mass: evidence for the existence of a connected network of permeable fractures. World Geothermal Congress 2000, Kyushu - Tohoku, Japan.

[12] Evans K.F., (2005). Permeability creation and damage due to massive fluid injections into granite at 3.5 km at Soultz: Part 2 - Critical stress and fracture strength, Journal of Geophysical Research, 110, B04204, 14 pp.

[13] Evans K.F., Genter A., Sausse J., (2005). Permeability creation and damage due to massive fluid injections into granite at 3.5 km at Soultz: Part 1 - Borehole observations, Journal of Geophysical Research, 110, B04203, 19 pp.

[14] Foehn J.P., (1985). Interprétation des campagnes sismiques 1981 et 1984, concession de Péchelbronn, permis de Haguenau. Total Exploration internal report, October 1985.

[15] Genter A., (1989). Géothermie Roches Chaudes Sèches : le granite de Soultz-sous-Forêts (Bas Rhin, France). Fracturation naturelle, altérations hydrothermales et interaction eau - roche. PhD thesis, Université d'Orléans, France, 201 pp.

[16] Genter A., Traineau H., Dezayes Ch., Elsass P., Ledésert B., Meunier A., Villemin Th., (1995). Fracture analysis and reservoir characterization of the granitic basement in the HDR Soultz project (France). Geothermal Science & Technology, vol. 4 (3), 189-214.

[17] Genter A., Castaing Ch., (1997). Effets d'échelle dans la fracturation des granites; Scale effects in the fracturing of granite. Comptes Rendus de l'Académie des Sciences, Serie II. Sciences de la Terre et des Planètes 325(6): 439-445.

[18] Genter A., Castaing C., Dezayes Ch., Tenzer H., Traineau H., Villemin Th., (1997). Comparative analysis of direct (core) and indirect (borehole imaging tools) collection of fracture data in the Hot Dry Rock Soultz reservoir (France), Journal of Geophysical Research, vol. 102, B7, 15419-15431.

[19] Genter A., Homeier G., Chèvremont Ph., Tenzer H., (1999). Deepening of GPK-2 HDR borehole, 3880-5090 m (Soultz-sous-Forêts, France). Geological monitoring. Open file report BRGM/RR-40685-FR, 81 pp.

[20] Genter A., Traineau H., Bourgine B., Ledésert B., Gentier S., (2000). Over 10 years of geological investigations within the European Soultz HDR project, France. Proceedings of the World Geothermal Congress 2000, Kyushu-Tohoku, Japan, May 28 - June 10, 2000, Full length paper on Cd-Rom, Editors E. Iglesias, D. Blackwell, T. Hunt, J. Lund, S. Tamanyu, 3707-3712.

[21] Genter A., Dezayes Ch., Gentier S., Ledésert B., Sausse J., (2002). Conceptual fracture model at Soultz based on geological data. Geologisches Jahrbuch: Sondehefte: Reihe E. Geophysik ; H. SE 1, 4th International Hot Dry Rock (HDR) Forum, Strasbourg, France, Sept. 28-30 1998, 93-102.

[22] Genter A., Cuenot N., Dezayes Ch., Sausse J., Valley B., Baumgartner J., Fritsch D., (2007). How a better characterization of a deep crystalline reservoir can contribute to improve EGS performance at Soultz, First European Geothermal Review, Geothermal Energy for Electric Power Production, October 29-31, 2007, Mainz, Rhineland Palatinate, Germany, Abstracts and Papers, 34-40.

[23] Gentier S., Hopkins D., Riss J., (2000). Role of fracture geometry in the evolution of flow paths under stress. In: Geophysical monograph 122: “Dynamics of fluids in fractured rocks”, 169-184.

[24] Gérard A., Menjoz A., Schwoerer P., (1984), L’anomalie thermique de Soultz-sous-Forêts, Géothermie Actualités, n°3, 35-42.

[25] Gérard A., Kappelmeyer O., (1987). The Soultz-sous-Forêts project: Proceedings of the first EEC/US workshop on geothermal Hot dry Rocks Technology, Geothermics, Special issue, 393-399.

[26] Gérard A., Genter A., Kohl T., Lutz Ph., Rose P., Rummel F., (2006). The deep EGS (Enhanced Geothermal System) project at Soultz-sous-Forêts (Alsace, France). Geothermics, Vol. 35, No. 5-6, 473-483.

[27] Herbrich B., (1988). Forage géothermiques de Soultz-sous-Forêts (GPK1). Rapport de fin de sondage. Rapport CFG n° 88 CFG 03, Janvier 1988.

[28] Hooijkaas G.R., Genter A., Dezayes Ch., (2006). Deep-seated geology of the granite intrusions at the Soultz EGS site based on data from 5 km-deep boreholes, Geothermics, Vol. 35, No. 5-6, 484-506.

[29] Illies H., (1972). The Rhine graben rift system - plate tectonic and transform faulting. Geophysical Survey, 1, 27-60.

[30] Illies J.H., (1975). Recent and paleo-intraplate tectonics in stable Europe and the Rhinegraben rift system. Tectonophysics, 29, 251-264.

[31] Jung R., Reich W., Engelking U., Hettkamp T., Weidler R., (1995). Hydraulic tests in1995 at the HDR Project, Soultz-sous-Fôrets, France, Field Report, Bundesanstalt für Geowissenschaften und Rohstoffe (BGR), Hannover, Germany.

[32] Klee G., Rummel F., (1993). Hydrofrac stress data for the European HDR research project test site Soultz-sous-Forêts. International Journal of Rock Mechanics and Mining Sciences & Geomechanics Abstracts 30(7): 973-976.

[33] Ménillet F. et al. (1989). Carte géologique de Lembach à 1/50 000. Feuille n°168, Edition du BRGM.

[34] Nami P., Schellschmidt R., Schindler M., Tischner T., (2008). Chemical stimulation operations for reservoir development of the deep crystalline HDR/EGS system at Soultz-sous-Forêts (France), Proceedings, Thirty-Third Workshop on Geothermal Reservoir Engineering Stanford University, Stanford, California, USA, January 28-30, 2008, SGP-TR-185.

[35] Place J., Diraison M., Naville Ch., Geraud Y., Schaming M., Dezayes Ch., (2008). Decoupling of deformation in the Upper Rhine Graben sediments seen by seismic reflection and coupled analysis of diffraction on 3-component Vertical Seismic Profiling (Soultz-sous-Forêts area). *Geosciences*, this issue, submitted.

[36] Portier S., Vuataz F.-D., Nami P., Sanjuan B., Gérard A., (2008). Chemical stimulation techniques for geothermal wells: experiments on the 3-well EGS system at Soultz-sous-Forêts. Submitted to Geothermics.

[37] Renard Ph., Courrioux G., (1994). Three-dimensional geometric modelling of faulted domain: The Soultz horst example (Alsace, France). Computers & Geosciences, Vol. 20 (No. 9), 1379-1390.

[38] Rotstein Y., Edel J. B., Gabriel G., Boulanger D., Schaming M., Munschy M., (2006). Insight into the structure of the Upper Rhine Graben and its basement from a new compilation of Bouguer Gravity, Tectonophysics, 425 (1-4), 55-70.

[39] Sanjuan B., Pinault J-L, Rose P., Gérard A., Brach M., Braibant G., Crouzet C., Foucher J-C, Gautier A., Touzelet S., (2006). Tracer testing of the geothermal heat exchanger at Soultz-sous-Forêts (France) between 2000 and 2005, Geothermics, Vol. 35, No. 5-6, 622-653.

[40] Sausse J., Dezayes Ch., Dorbath L., Genter A., Place J., (2008). 3D fracture zone network at Soultz based on geological data, Image logs, microseismic events and VSP results, *Geosciences*, this issue, submitted.

[41] Stussi J.-M., Cheilletz J.M., Royer J.J., Chèvremont P., Féraud G., (2002). The hidden monzogranite of Soultz-sous-Forêts (Rhine Graben, France). Mineralogy, petrology and genesis, Géologie de la France, 1, 45-64.

[42] Valley B., (2007). The relation between natural fracturing and stress heterogeneities in deep-seated crystalline rocks at Soultz-sous-Forêts (France), PhD thesis, ETH-Zürich, Switzerland, http://e-collection.ethbib.ethz.ch/view/eth:30407, 260 pp.

[43] Valley B., Evans K., (2007). Stress state at Soultz-sous-Forêts to 5 km depth from wellbore failure and hydraulic observations. Thirty-Second Workshop on Geothermal Reservoir Engineering Stanford University, Stanford, California, USA, January 28-30, 2008, SGP-TR-183, 329-338.

[44] Valley B., Dezayes Ch., Genter A., (2007). Multi-scale fracturing in the Soultz-sous-Forêts basement from borehole image analyses. Proceedings EHDRA Scientific Conference, 28 & 29 June 2007, Soultz-sous-Forêts, France, 14 pp.

[45] Villemin Th., Bergerat F., (1987). L'évolution structurale du fossé rhénan au cours du Cénozoïque : un bilan de la déformation et des effets thermiques de l'extension. Bull. Soc. Géol. France,, III, 2, 245-255

[46] Villeneuve B., Weber R., (1991). Forages pour observations sismiques de Soultz-sous-Forêts. Rapport de fin de forages. BRGM-CCE.

[47] Vuataz F.-D., Brach M., Criaud A., Fouillac Ch., (1990). Geochemical monitoring of drilling fluids: a powerful tool to forecast and detect formation waters. SPE, Formation Evaluation, June 1990, 177-184.

[48] Ziegler P., (1992). European Cenozoic rift system. Tectonophysics, 2008, 91-111.

Figure captions

Liste des figures

Figure 1 – Location of the EGS Soultz site and geology of the Upper Rhine Graben. I) Location of the Upper Rhine Graben with the West European Rift System. (1) Hercynian basement; (2) Tertiary basins; (3) Alpine molasse. II): W–E cross-section through the Rhine Graben border and the Soultz site. (a) Cenozoic; (b) Mesozoic; (c) Hercynian basement. III) Geological and structural map of the Rhine graben (1) Cenozoic sediments; (2) Cenozoic volcanics; (3) Jurassic; (4) Triassic; (5) Permo-Carbonifeous basins, (6) Hercynian basement; (7) boundary faults; (8) other faults; (9) overthrusts.

Figure 1 – Localisation du site de EGS de Soultz et géologie du Fossé rhénan supérieur. I) Localisation du Fossé rhénan supérieur dans le Systeme de Rift Ouest-Européen. (1) socle hercynien ; (2) bassins tertiaires ; (3) molasse alpine. II) Coupe E-W passant par la bordure du Fossé rhénan et le site de Soultz. (a) cénozoïque, (b) mésozoïque, (c) socle hercynien. III) Carte géologique et structurale du Fossé rhénan (1) remplissage cénozoïque, (2) édifices volcaniques cénozoïques, (3) Jurassique, (4) Trias, (5) bassins permo-carbonifères, (6) socle hercynien, (7) failles bordières, (8) autres failles, (9) chevauchements.

Figure 2 – Examples of composite logs for two fracture zones in GPK1 (A) and GPK3 (B). UBI: acoustic borehole image; HAC: Hierarchical Ascendant Classification; Legend of facies: red crosses: porphyritic granite, green crosses: two-mica granite; green hachure: altered granite; blue hachure: cataclased granite; blue crosses: brecciated granite; black: quartz vein.

Figure 2 – Examples de logs composites pour deux zones de fractures dans GPK1 (A) et GPK3 (B). UBI : images de paroi acoustiques ; HAC : Classification Ascendante Hiérarchique ; Légende des faciès : croix rouges : granite porphyritique, croix vertes : ganite à deux micas, hachures vertes : granite altéré, hachures bleues : granite cataclasé, croix bleues : granite bréchifié, noir : veine de quartz.

Figure 3 – Fracture orientation in the Soultz wells based on cores and various borehole image logs. For the GPK3 and GPK4 wells, data are grouped in relation with the major petrographical sections. The depths along the wells indicate the upper and the lower depth limits of the petrographical sections (in True Vertical Depth Sub Sea). Contour-density diagrams in Schmidt's projection, lower hemisphere: 10%, 30%, 50%, 70%, 90% of the maximum frequency. Geology: (1) Sedimentary cover, (2) Standard porphyritic granite, (3) Standard granite with intense vein alteration, (4) Biotite and amphibole rich granite gradually becoming standard granite with depth, (5) Two mica granite and biotite rich granite.

Figure 3 – Orientation des fractures dans les puits de Soultz à partir de l'analyse des carottes et des images de paroi. Pour les puits GPK3 et GPK4, les données sont regroupées par faciès pétrographiques

majeures. La profondeur le long des puits indique la limite supérieure et inférieure des sections pétrographiques (altitude à partir du niveau marin de l'IGN). Diagramme de densité en projection de Schmidt, hémisphère inférieure, courbes à %, 30%, 50%, 70%, 90% de la fréquence maximale. Géologie : (1) couverture sédimentaire, (2) porphyritique granite standard, (3) granite standard avec une altération de veine intensive, (4) granite riche en amphibole et en biotite redevenant progressivement un granite standard. (5) granite à deux micas et granite riche en biotite.

Figure 4 – Orientation of fracture zones in each Soultz well. Bold lines and black dots: cyclographic traces and poles of fracture zones of level 1; grey lines and grey dots: cyclographic traces and poles of fracture zones of level 2 (dotted grey line: supposed orientation); dotted line and white dot: cyclographic trace and pole of fracture zones of level 3 (Schmidt's projection, lower hemisphere).

Figure 4 – Orientation des zones de fracture dans les différents puits de Soultz. Lignes épaisses noires et points noirs : traces cyclographiques et poles des zones de fracture de niveau 1 ; lignes grises et points gris : traces cyclographiques et poles des zones de fracture de niveau 2 (ligne en pointillé gris : orientation hypothétique) ; lignes pointillées noires et points blancs : traces cyclographiques et poles des zones de fracture de niveau 3 ;

Table 1 – Characterization of all fracture zones determined in the Soultz wells. TVDss: True Vertical Depth Sub Sea. Depth: measured depth along the well. White rows: fracture zones in Buntsandstein, grey rows: fracture zones in the granite. Italic: supposed orientation.

Tableau 1 – Caractéristiques des zones de fractures déterminées dans les puits de Soultz. TDVss : altitude à partir du niveau de la mer IGN. Depth : profondeur mesurée le long du forage. Lignes blanches : zones de fracture dans le Buntsandstein, lignes grises : zones de fracture dans le granite. Italique : orientation hypothétique.

Figure 5 – N-S cross-section through the Soultz wells showing all fracture zones determined in this study. Sticks represent the apparent dip of fracture zones through the N-S cross-section. (a) fracture zones level 1, (b) fracture zones level 2, (c) fracture zones level 3, (d) supposed orientation. Pole and contouring diagram of the fracture zones in each cluster (Schmidt's projection, lower hemisphere, contouring diagram: 10%, 30%, 50%, 70%, 90% of the maximum frequency). Geology: (1) Sedimentary cover, (2) Standard porphyritic granite, (3) Standard granite with intense vein alteration, (4) Biotite and amphibole rich granite gradually becoming standard granite with depth, (5) Two mica granite and biotite rich granite.

Figure 5 – Coupe N-S à travers les puits de Soultz montrant les zones de fracture déterminées dans cette étude. Les bâtonnets représentent l'inclinaison apparente des zones de fracture le long de la coupe N-S.

(a) zones de fracture de niveau 1, (b) zones de fracture de niveau 2, (c) zones de fracture de niveau 3, (d) orientation hypothétique. Pôles et diagrammes de densité des zones de fractures pour chaques clusters (projection de Schmidt, hémisphère inférieur, courbes à %, 30%, 50%, 70%, 90% de la fréquence maximale). Géologie : (1) couverture sédimentaire, (2) porphyritique granite standard, (3) granite standard avec une altération de veine intensive, (4) granite riche en amphibole et en biotite redevenant progressivement un granite standard. (5) granite à deux micas et granite riche en biotite.

Figure 6 - Orientation of fracture zones and meso-scale fractures in the Buntsandstein sediments (A) and in the granite (B). (A1) Traces and poles of fracture zones in the Buntsandstein; (A2) strike rose diagram (10° class angle) of meso-scale fractures measured on EPS1 Buntsandstein cores; (B1) poles and strike rose diagram (10° class angle) of fracture zone in the granite; (B2) strike rose diagram (10° class angle) of meso-scale fractures measured on borehole images in the granite of all wells.

Figure 6 – Orientation des zones de fracture et des méso-fractures dans les sediments du Buntsandstein (A) et dans le granite (B). (A1) Traces et pôles des zones de fracture dans le Buntsandstein ; (A2) rosace de direction (classes de 10°) des méso-fractures mesurées sur les carottes de Buntsandstein du forage EPS1 ; (B1) pôles et rosace de direction (classes de 10°) des zones de fractures dans le granite ; (B2) rosace de direction (classes de 10°) des méso-fractures mesurées sur les images de paroi de tous les forages dans le granite.

Figure1

Click here to download high resolution image

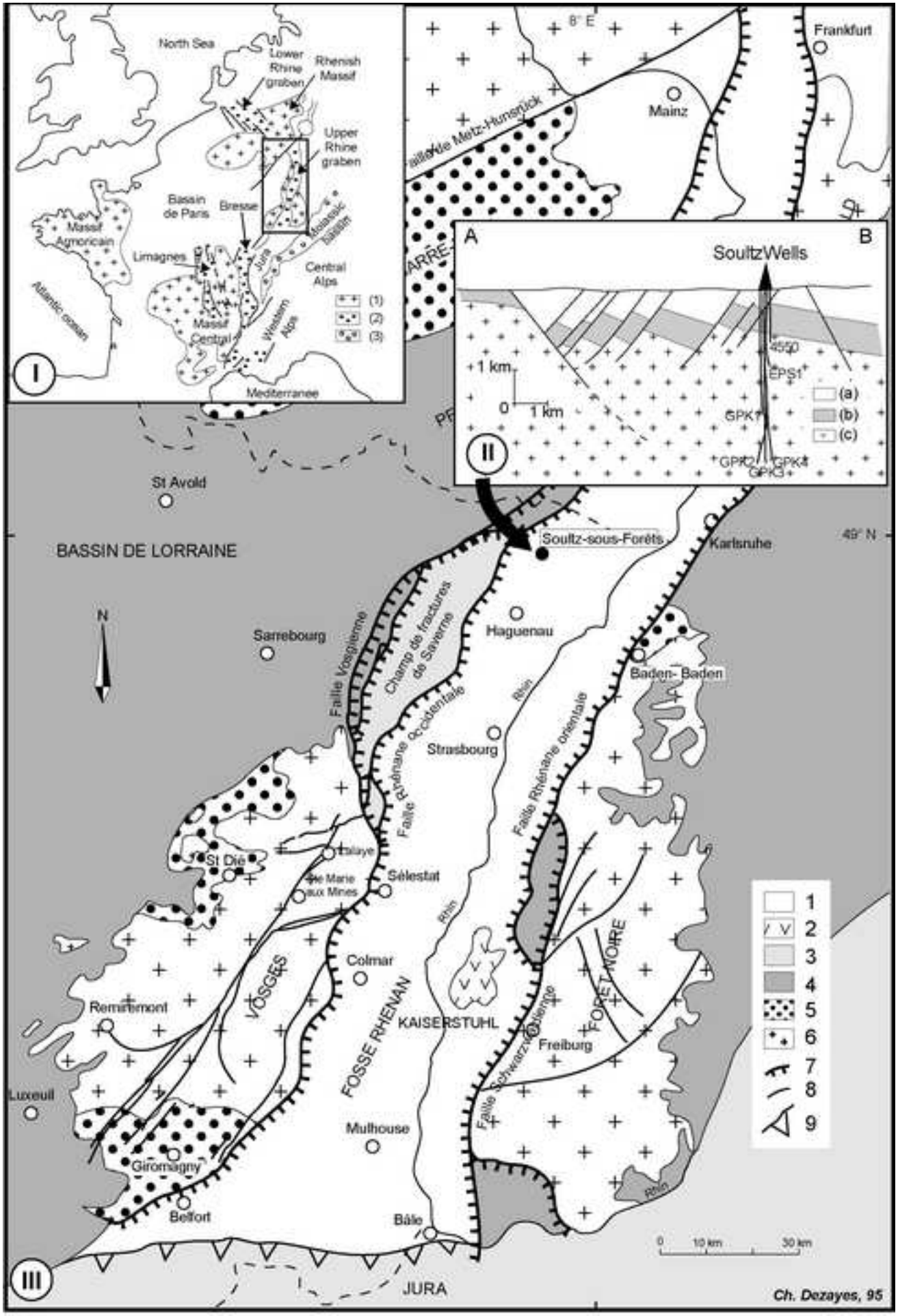

Figure2

Click here to download high resolution image

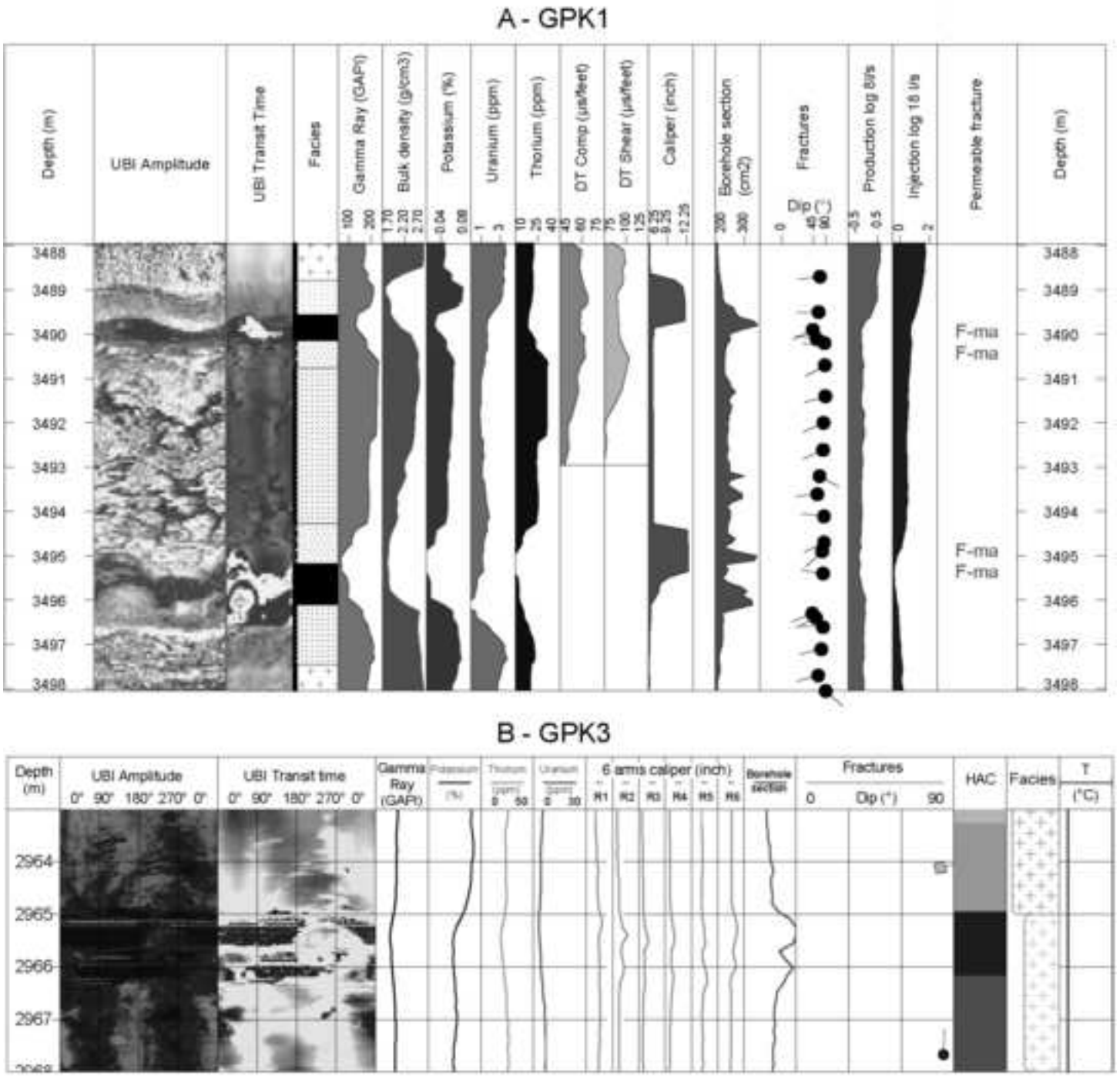

Figure3

Click here to download high resolution image

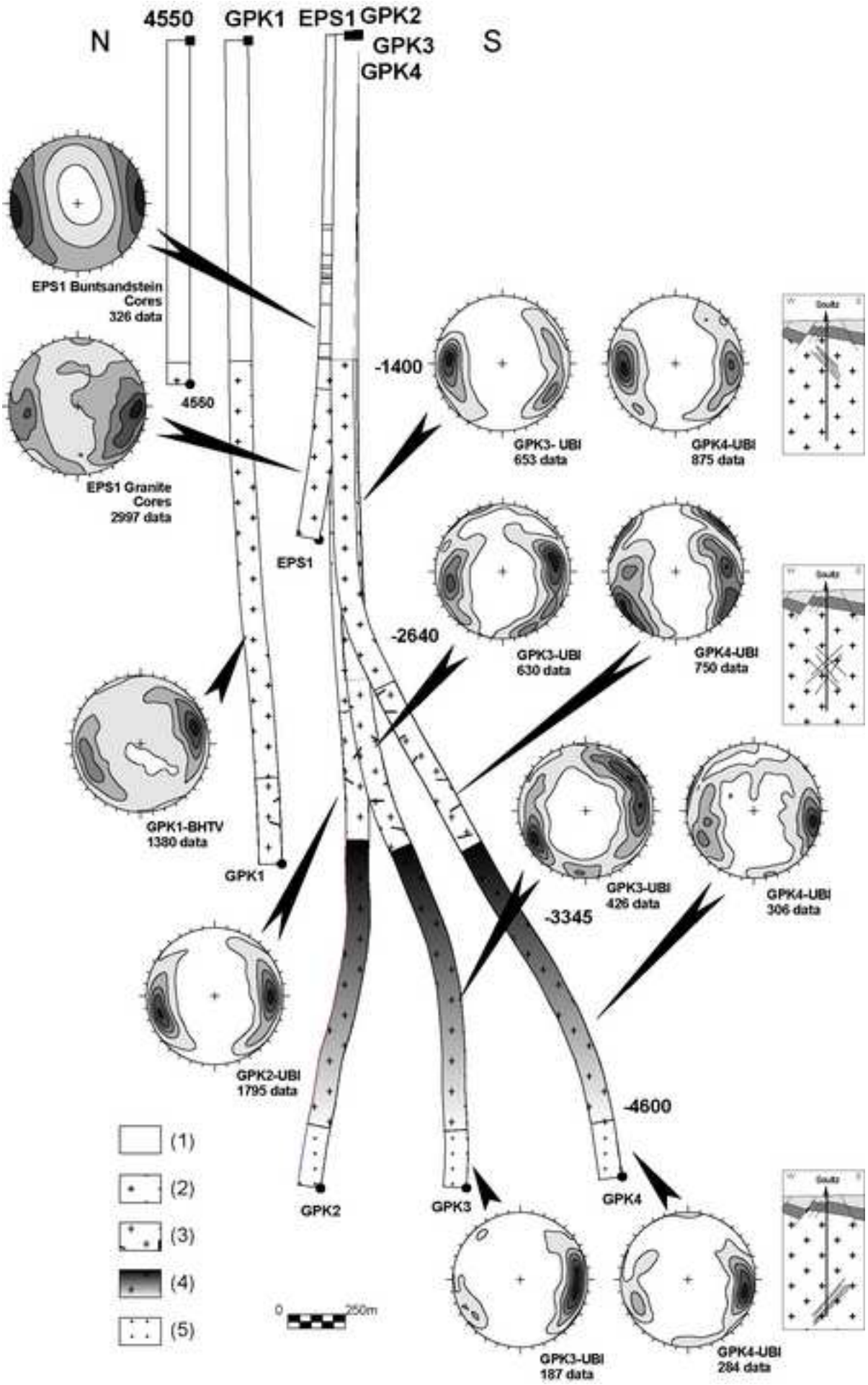

Figure4

Click here to download high resolution image

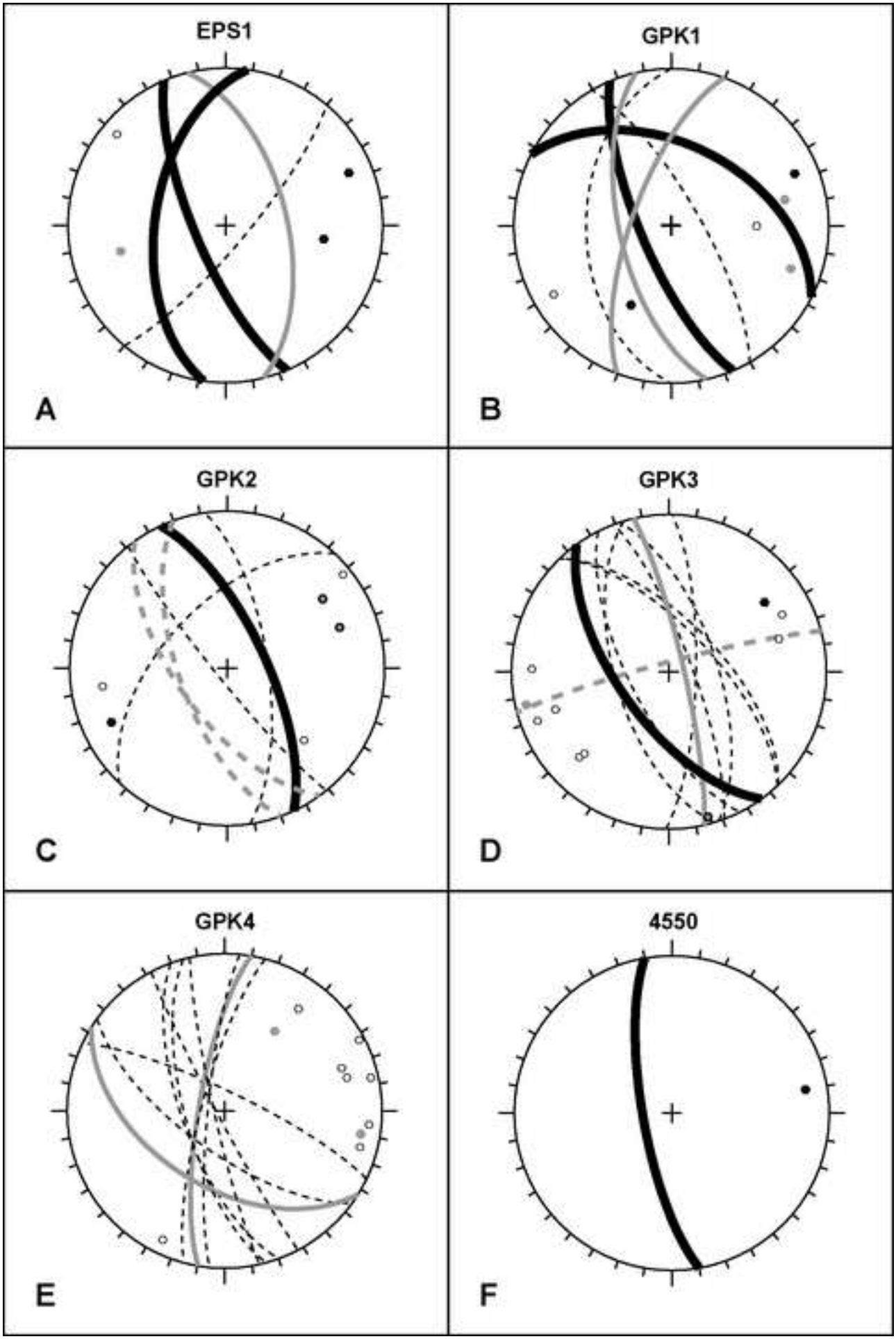

Figure5

Click here to download high resolution image

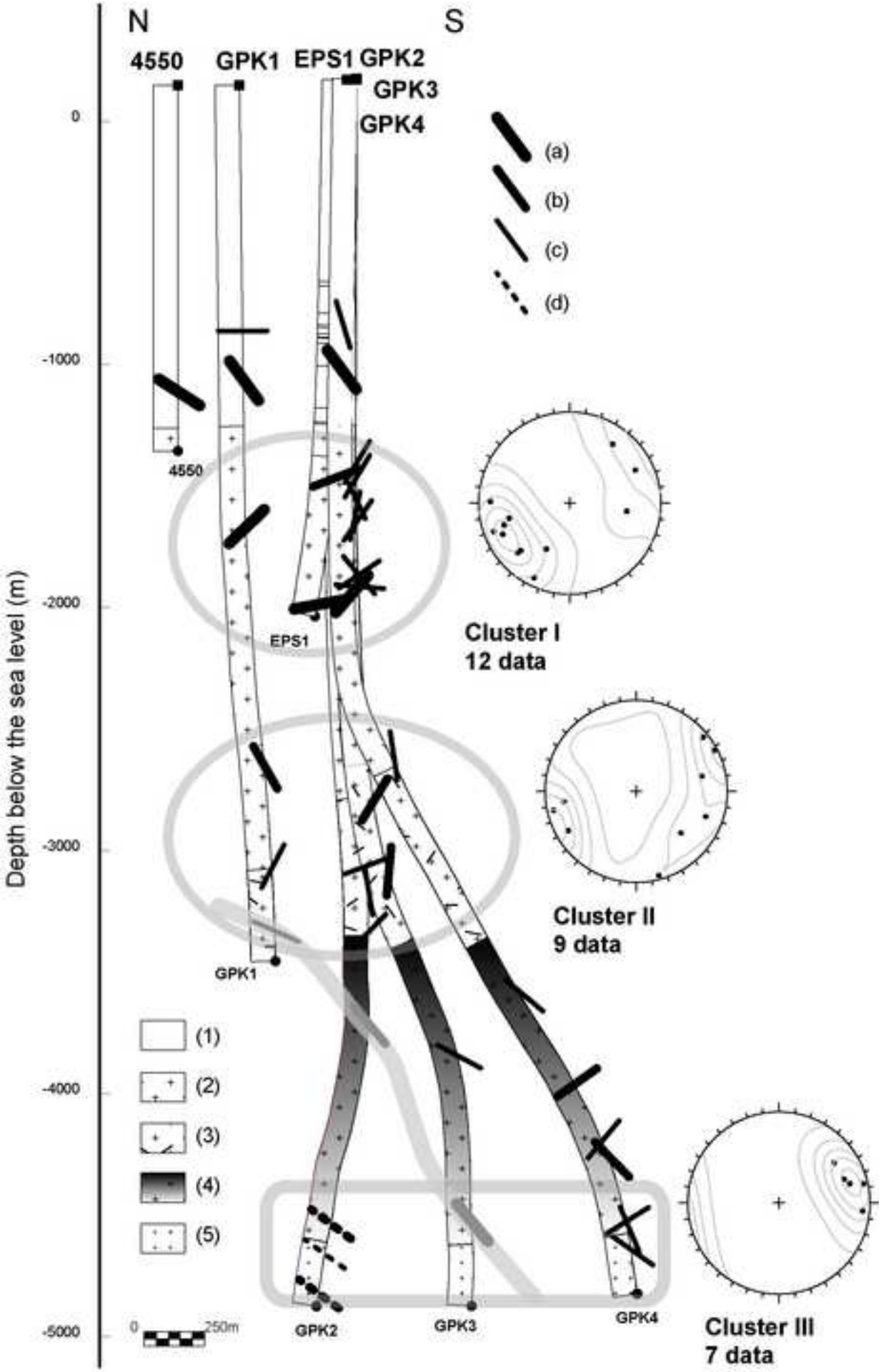

Figure6

Click here to download high resolution image

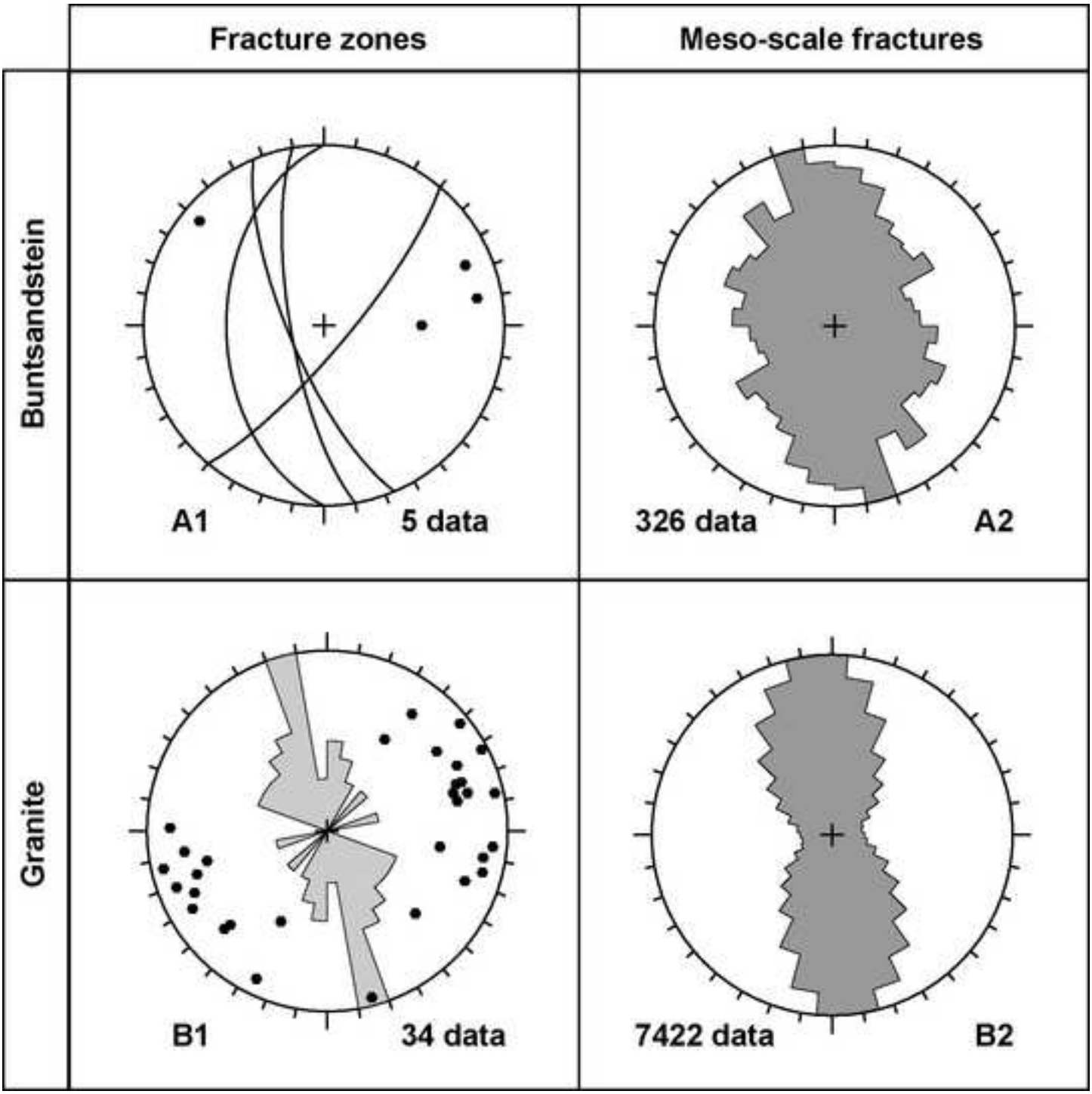

Table 1

Click here to download high resolution image

Well	Name	Depth	Level	TVDss	Dip_dir (°E)	Dip (°)	Thickness (m)
EPS1	EPS1-FZ1010	1012	3	836.637512	130	79	
EPS1	EPS1-FZ1200	1198	1	1021.84821	247	74	30
EPS1	EPS1-FZ1640	1643	2	1466.48914	76	58	25
EPS1	EPS1-FZ2180	2179	1	1988.09058	278	53	15
GPK1	GPK1-FZ1015	1015	3	862.00885	270	45	
GPK1	GPK1-FZ1220	1220	1	1066.59717	247	74	
GPK1	GPK1-FZ1820	1820	1	1666.24219	27	47	10
GPK1	GPK1-FZ2815	2815	2	2657.19238	230	70	8
GPK1	GPK1-FZ3220	3223	3	3064.05273	60	75	15
GPK1	GPK1-FZ3490	3492	2	3332.64502	257	63	8
GPK2	GPK2-FZ2120	2123	1	1953.37292	65	70	15
GPK2	GPK2-FZ3240	3242	3	3069.90625	82	69	0.5
GPK2	GPK2-FZ3350	3347	3	3174.62988	231	84	3
GPK2	GPK2-FZ3515	3514	3	3341.70801	313	56	12
GPK2	GPK2-FZ3900	3900	2	3726.61133	*234*	*64*	
GPK2	GPK2-FZ4760	4760	2	4544.82227	*250*	*65*	*No*
GPK2	GPK2-FZ4890	4890	3	4668.3252	*250*	*65*	*image*
GPK2	GPK2-FZ5060	5060	2	4831.29248	*250*	*65*	*logs*
GPK3	GPK3-FZ1580	1579	3	1410.36487	69	78	8
GPK3	GPK3-FZ1640	1637	3	1468.78821	46	68	8
GPK3	GPK3-FZ1820	1820	3	1651.01147	46	64	3-4
GPK3	GPK3-FZ2040	2042	3	1873.30823	72	65	8
GPK3	GPK3-FZ2045	2046	3	1876.76367	243	69	1
GPK3	GPK3-FZ2090	2092	3	1923.16223	91	76	6
GPK3	GPK3-FZ2970	2970	2	2798.43579	77	82	9
GPK3	GPK3-FZ3270	3271	2	3092.95361	*345*	*85*	15
GPK3	GPK3-FZ4090	4089	3	3856.2417	253	62	6
GPK3	GPK3-FZ4770	4775	1	4538.90137	234	64	15
GPK4	GPK4-FZ1720	1723	3	1554.30212	216	69	2
GPK4	GPK4-FZ1800	1801	3	1632.22925	26	80	12
GPK4	GPK4-FZ2820	2817	3	2762.20264	242	86	9
GPK4	GPK4-FZ3940	3940	3	3603.97852	250	68	60
GPK4	GPK4-FZ4360	4361	2	3963.29565	280	77	4
GPK4	GPK4-FZ4620	4620	3	4195.97852	285	78	40
GPK4	GPK4-FZ4710	4712	2	4279.59717	212	50	1
GPK4	GPK4-FZ4970	4973	3	4530.36914	276	81	2
GPK4	GPK4-FZ5050	5012	3	4568.51904	257	85	15
GPK4	GPK4-FZ5100	5100	3	4655.44922	255	69	10
4550	4550-FZ1265	1265	1	1107.95679	260	75	3

The Soultz geothermal adventure: 20 years of research and exploration of deep crystalline fractured rocks for EGS development

Albert Genter*, Keith Evans**, Nicolas Cuenot*, Daniel Fritsch*, Bernard Sanjuan***

**GEIE Exploitation Minière de la Chaleur, Route de Soultz, BP 38, F-67250 Kutzenhausen, France*
***ETH Zurich, Engineering Geology, Department of Earth Science, Swiss Federal Institute of Technology, CH-8092 Zürich, Switzerland*
****BRGM, Département Géothermie, 3, avenue C. Guillemin, BP 36009, F-45060 Orléans Cedex 2, France*

Submitted to Geoscience, 2009.

The Soultz geothermal adventure: 20 years of research and exploration of deep crystalline fractured rocks for EGS development

20 ans d'exploration par forages des réservoirs fracturés en milieu cristallin : le projet de géothermie de Soultz

Albert Genter*, Keith Evans, Nicolas Cuenot*, Daniel Fritsch*, Bernard Sanjuan*****

*GEIE Exploitation Minière de la Chaleur, Route de Soultz, BP 38, F-67250 Kutzenhausen, France

**ETH Zurich, Engineering Geology, Department of Earth Science, Swiss Federal Institute of Technology, CH-8092 Zürich, Switzerland

***BRGM, Département Géothermie, 3, avenue C. Guillemin, BP 36009, F-45060 Orléans Cedex 2, France

Submitted to *GEOSCIENCE*

Version: *23/02/2009*

Corresponding author:
Albert Genter
GEIE Exploitation Minière de la Chaleur
Route de Soultz
BP 38
F-67250 Kutzenhausen, France
Tel: 33 (0)3 88 80 99 13 Fax: 33 (0) 3 88 80 53 51
genter@soultz.net

Abstract

The Soultz experimental geothermal site in Alsace, France, has been explored and two reservoirs developed within granite at depths of 3.5 and 5 km over the past 20 years by the drilling of numerous boreholes, three of which extend to 5 km depth. Data on geology, fluid geochemistry, temperature, microseismicity, hydraulics and geomechanics have been collected and interpreted by the various teams from participating European countries and their international collaborators. The reservoir at 3.5 km was formed from two wells, 450 m apart, both of which were subjected to hydraulic stimulation injections. The system was circulated continuously for 4 months at 25 kg/s in 1997 using a downhole pump, and yielded results that were extremely encouraging. The impedance declined to 0.1 MPa/l/s, the first time this long-standing target had been attained. Construction of a deeper system began shortly afterwards with the drilling of 3 deviated wells to 5 km true vertical depth, where the temperature was 200°C. The wells were drilling in a line, 600 m apart, and all were hydraulically stimulated and subjected to acidization injections. The 3-well system was circulated under buoyancy drive for 5 months in 2005 with injection in the central well, GPK-3, and production from the two outer wells, GPK-2 and GPK-4. This showed good linkage between one duplet pair but not the other. Further acidization operations on the low-productivity well let to its productivity increasing to almost the same level at the other well. Construction of a power plant at the site was completed in 2008 and a trial circulation with a production pump in one well and the other shut-in was conducted with power production. Downhole pumps are now installed in both production wells in preparation for long-term circulation of the system. In this paper we present an overview of the principle accomplishments at Soultz over the past two decades, and highlight the main results, issues identified, and lessons learnt.

Key-Words:

Geothermal energy, Enhanced Geothermal Systems, Hot Dry Rock, Granite, Natural Fractures, Soultz-sous-Forêts, France.

Résumé:

Le site expérimental de Soultz-sous-Forêts en Alsace est le siège d'exploration géothermique par forages profonds depuis plus de 20 ans. Des travaux sur la géologie, la géochimie des fluides, les températures, la microsismicité et l'hydraulique du site ainsi que des calculs prédictifs via de la modélisation couplée ont été réalisés par de nombreuses équipes scientifiques en Europe. Le réservoir supérieur situé à 3.5 km de profondeur a été stimulé à partir de 2 forages distants de 450 m. Plusieurs tests de circulation de fluide en boucle (1997, 2005), réalisés entre les puits profonds, ont montré qu'au moins 30% du fluide injecté pouvait être récupéré dans les puits producteurs et que cette récupération limitée était, par ailleurs, toujours compensée par une contribution de saumure naturelle, caractérisant ainsi la présence de zones fracturées ouvertes en connexion directe avec un réservoir géothermique profond. En 1997, les 4 mois de circulation avec un débit massique de 25 kg/s ont conduit à des résultats très encourageants caractérisés par une chute de l'impédance hydraulique à 0.1MPa/l/s. La réalisation du dispositif souterrain constitué de trois puits déviés forés à 5 km de profondeur (deux producteurs, un injecteur) a permis d'atteindre une température de 200°C. Les 3 puits alignés et distants au fond de 600 m, ont fait l'objet de stimulations hydrauliques puis chimiques. En 2005, le test de circulation réalisé en production artésienne a mis en évidence une bonne connexion inter-puits mais sur une partie seulement du triplet. Des stimulations chimiques additionnelles ont été réalisées sur le puits le plus faiblement producteur. En 2008, la centrale géothermique a été construite, testée avec des moyens de production immergés et le premier kilowatt d'origine géothermique a été produit. Finalement, ce papier présente les principaux résultats scientifiques acquis à Soultz et les principales leçons déduites après plus de 20 années de recherches.

Mots-Clés:

Géothermie Profonde, Systèmes Géothermiques Stimulés, Granite, Fractures naturelles, Soultz-sous-Forêts, France

1 INTRODUCTION

The Soultz geothermal project was initiated by a French-German team in 1986 [33; 34] and has thus been running for more than 20 years. Early phases of the project were supported entirely by public funds from France, Germany, the European Union and a contribution from Switzerland, but since 1996 the work has been increasingly co-funded by the energy industry. The project has produced a substantial body of data that has proven relevant not only to geothermal but the geoscience community as a whole. The drilling of three boreholes to 5 km, the deepest penetration of crystalline rock in France, has yielded fundamental insights into the geology, nature of fracturing, fluid geochemistry, temperature and hydraulic properties of deep crystalline rock masses. However, the immediate focus of the various European teams involved in the project [7; 4; 32] has been the development, testing and modeling of two EGS reservoirs within the basement at 3.5 and 5 km depth. A rich and diverse set of data has been collected, including geologic, hydraulic, borehole logging, microseismic and active seismic, that provide insight into the hydro-thermo-mechanical and geochemical behavior of a deep crystalline basement subject to forced fluid flow conditions. These 20 years of scientific and technical activities have produced about 40 PhD theses and more than 200 publications in peer review journals. This paper presents an overview of the main phases of the project, and highlights the key results and milestones that mark the progress in this on-going project to date.

2 Phases of the Soultz project

Work at the Soultz site can be broken into three phase: a preparatory phase, a drilling, exploration and reservoir development phase that extended from 1987 to 2007, and a power plant construction phase. The preparatory phase involved the compilation of existing literature and a site survey conducted using data from existing holes and the reinterpretation of old petroleum reservoir measurements. The drilling, exploration and reservoir development phase consists of three sequential campaigns (Figure 1). The first, conducted between 1987 and 1991, explored and tested the basement to 2.0 km depth with a single borehole. The second campaign, between 1991 and 1998, extended the exploration by coring a borehole to 2.2 km to provide geological information, and then drilling two boreholes to 3.6 and 3.8 km which were then linked to form a system that was subsequently circulated for 4 months (Figure 2). The third campaign, conducted between 1998 and 2007, explored still deeper by drilling three boreholes to 5.0 km and linking them to form a 3-well

system. The third phase of surface power plant construction in preparation for the long-term circulation of the 5 km deep system began in 2007 and is on-going.

FIGURE 1

FIGURE 2

3 The Soultz geothermal system from regional to concession scale

The Soultz geothermal area is located in the Upper Rhine graben, which is part of the European Cenozoic rift system that extends from the Mediterranean to the North Sea coast [60]. The European Cenozoic rift system formed primarily through intraplate deformation produced by the Alpine orogeny. The present-day crustal geometry of the NW-Alpine foreland near the Rhine graben reflects the superposed effects of lithospheric thinning in the European Cenozoic rift system and long-wavelength lithospheric folding [9]. Crustal thickness within the Rhine graben ranges between 25 and 30 km, which is quite low. The heat flow in the graben ranges between 100-120m $W.m^{-2}$ [49]. Extensive borehole data show that the temperature within the graben at depths of 1 km is highly variable, with that at Soultz being particularly high, even though the crust is relatively thick at 30 km. The absence of a correlation between the temperature variations and crustal thickness, suggests that the variations are controlled by fluid flow.

The sediments of the Soultz area were well explored before the project began because they constitute the Péchelbronn-Merkwiller oil field. More than 5000 oil wells were drilled prior to 1970, giving an excellent overview of stratigraphy and structures within the post-Palaeozoic sediments. Temperature measurements in ~500 of these wells identified the exceptionally high temperature gradients that define the Soultz geothermal anomaly, and showed that the isotherms are primarily influenced by the tectonic structure of the Rhine graben [35]. As can be seen on Figure 3, there is a strong horizontal and vertical increase of temperature which is especially marked in the vicinity of the fault at Soultz-sous-Forêts where the hottest zone at 400 m depth is located along the western part of the Soultz horst and is characterized by a NE-SW elongation [34]. The first geothermal exploration well at Soultz, GPK-1 (Figure 2), was drilled into the top of this area in 1987-1988 [12; 33]. A structural evaluation of this locality was done by Schnaebele et al. [55] in 1948 for oil exploitation purposes. They noted that the area was compartmented by normal faults inducing a horst and graben structure (Figure 3). In the 80s', several oil companies conducted seismic exploration in order to image fault structures within the sedimentary section. Thus, prior to the drilling of GPK-1, the depth of the top of

the crystalline basement was known from both seismic reflection profiles and an old oil well drilled close to the site. This well, denoted as 4616, was drilled down to 1403 m and reached the basement at 1380 m. A core taken at the base of this well showed a typical granite rock composition. All these data were available and were partly reinterpreted during Phase 1 of the project, prior to the drilling of GPK-1.

FIGURE 3

4 Main scientific outcomes from exploration to reservoir development

Geology-Fluid Geochemistry

The sedimentary section at Soultz consists of sands, marls, clays and limestones to ~1 km depth, and Triassic and Permian fractured sandstones below. Basement was encountered at about 1.4 km depth, and found to consist of Paleozoic granites that were highly fractured at all scales, from micro-crack at grain scale to fracture or faulted zones. In the Soultz granite, two main natural fracture organizations are recognised: small-scale fractures corresponding to individual fractures of pluri-metric size that are pervasively distributed in the rock mass, and fracture zones which are larger-scale structures of highly clustered natural fractures that have thicknesses of up to 10-20 m. Hydrothermal alteration is generally intimately associated with fracture zones. The major fracture zones have extents of at least several hundred meters [27; 30]. Two petrographically-distinct granite units were encountered to 5 km: a grey porphyritic monzo-granite to about 4.5 km depth, and a grey fine-grained two-mica granite below [57; 14]. Some altered cataclastic shear zones showed a low natural permeability in channels characterized by the occurrence of brines (100 g/L, [59]) and were defined as Hydrothermally Altered and Fractured Zones (HAFZ) indicating both high fracture density and strong hydrothermal alteration [28]. Natural fluid circulation in the fractures resulted in both a strong dissolution of the primary minerals such as biotite, plagioclase, and a significant deposition of some altered minerals (Figure 4) such as clay minerals (illite, tosudite), calcite, secondary quartz and sulfides [29]. Organic matter was also observed in strongly altered granite in EPS1 well [41], indicating hydraulic communication between basement and sediments at some time in the past. Most of these geological results were known after the drilling of GPK-1 down to 2000 m and the coring of EPS1 to 2230 m. Subsequent drilling campaigns to 3.8 km and eventually to 5000 m depth largely confirmed the previous results, and revealed the two mica granite below 4.5 km.

The collection of a sample of native formation fluid that was free of contaminants such as drilling fluid proved difficult. The most relevant geochemical data on the nature, origin, circulation and deep

temperature of these fluids was obtained from GPK-1 and GPK-2 [45; 1; 52; 51]. Samples collected from the well-head and from depths ranging from 650 to 3470 m for GPK-2 have similar chemical and isotopic compositions (NaCl brine with a pH value close to 5) and a high salinity (total dissolved solids (TDS) of about 100 g/l), which suggest fluids at all depths to 5 km have a common sedimentary origin and have undergone identical fluid-rock interaction processes. Chemical and gas geothermometers, as well as geochemical modeling simulations, suggest that the native geothermal brine and associated gases (predominant CO_2) are equilibrated with a mineralogical assemblage at temperatures close to 220-240°C (> 202°C measured at the GPK-2 bottom-hole in [5]). Sodium/lithium geothermometers and isotopic lithium values suggest that these equilibrium reactions occurred in a sedimentary rather than a granite reservoir. These constraints collectively suggest that the brine at Soultz has migrated from a reservoir that is situated more towards the Graben centre, where the Triassic sedimentary formations are the deepest and temperatures of 220-240°C are found at 4 km depth [43]. Such migration could have occurred through a complex system of deep faults that is still poorly constrained. A tracer test conducted between 2000 and 2002 in the GPK-2 open hole section below 4.5 km indicated a natural flow rate of native geothermal brine of 1.0-1.2 m^3/h [52; 53], which is identical to that calculated from the fluid flow parallel to the Graben strike, based on a convection model and numerical 3D modeling [3].

FIGURE 4

Hydraulics

Hydraulic tests conducted on HAFZs have shown transmissibilities (i.e. the product of permeability and borehole length over which the permeability applies) from zero up to 1e-11 m^3, whereas the transmissibility of the granite rock mass excluding the high-transmissibility zones is typically 1e-16 to 1e-17 m^3 [25]. The highest transmissibility of 1.1e-11 m^3 was measured at a major HAFZ intersected at 2120 m depth in GPK-2 well which, once intersected, resulted in total mud and cuttings loss throughout the subsequent drilling operations. Pre-stimulation testing of the entire GPK-1 open-hole between 2.85 and 3.6 km showed a major transmissive HAFZ at 3.5 km and seven HAFZs of small but non-zero transmissibility spaced every 50-100 m along the well [24]. These zones were exclusively activated during the stimulation to become the principle transmissive features in the well. Hydraulic tests performed after hydraulic stimulation showed that the well had been connected to a fault or major fracture zone of large hydraulic capacity through flow paths that emerged into the well at the HAFZs. The hydraulic impedance (i.e. the resistance to flow) of these flow paths exhibited a

turbulent-like behaviour that was not limited to the near wellbore region [39; 22], suggesting the flow field was not strongly divergent. It is likely that the high-capacity fault that the well connects to via the stimulated flow paths is part of a connected system that allows fluids to move through the rock mass over significant distances. Such features are rarely intersected by vertical boreholes because they are high-angle. These considerations suggest a strategy for establishing a satisfactory hydraulic connection between two boreholes to form a duplet, and that is to link them individually to the connected system of major fracture zones and faults through stimulation operations.

Stimulation and microseismicity

Hydraulic stimulation is the principle reservoir development technique that has been used to increase the low natural permeability of the HAFZ penetrated by the different Soultz wells. The permeability increase is believed to be mainly governed by shearing mechanism occurring on pre-existing fractures, although the details of the geometry of the flow paths produced are uncertain [23; 27; 31]. For example, shearing of an offset fracture pair can produce a conduit that channels flow normal to the shearing direction [38; 27]. There is also evidence for localised, opening-mode (tensile) fracturing below the casing shoes of some boreholes, where wellbore pressure during stimulation tend to approach the local minimum principal stress level [15; 24; 37. 54]. However, vertical tensile fractures that are seen at the walls of most holes above 3 km are in most cases induced by cooling during drilling and, whilst good indicators of the directions of the principal horizontal stresses [58], are unlikely to extend significantly from the wellbores.

Almost all wells at Soultz have been subjected to a hydraulic stimulation, and in all but one case the injectivity index (i.e. the injection flow rate per unit wellhead pressure under steady-state conditions) was significantly improved. For the intermediate depth well GPK-1 stimulated between 2.8 and 3.6 km, the improvement was a factor of 15 [24]. For the three deep wells each stimulated between 4.5 and 5.0 km TVD, the improvement for GPK-2 and GPK-4 was a factor of about 20, whereas that for GPK-3 was only a factor of ~1.5 [44]. In all cases, the improvements reflect increased transmissibility of HAFZs, usually at the major altered fractures within the zone. In well GPK-1, these major fractures showed measurable dislocations of millimetres to centimetres [24]. Estimation of the post-stimulation injectivity/productivity indices of the three deep wells was complicated by the failure to reach steady-state conditions in the post-stimulation characterisation tests. Thus, 3-day, single-well injectivity/productivity indices were estimated based upon the wellhead pressure and flow prevailing 3 days after the start of the test, with the other wells shut-in [44]. The measured indices were 4.0 l/s/MPa for GPK-2, 3.5 l/s/MPa for GPK-3, and 2.0 l/s/MPa for GPK-4.

A variety of acid stimulations were conducted on all deep wells after the hydraulic stimulations, with limited success [44. 48]. The improvement in 3-day injectivity/productivity index by the acid treatments was a factor of about 1.25 for GPK-2, about 1.15 for GPK-3, and about 2.5 for GPK-4. It should be noted, however, that the large increase in productivity for GPK-4 was largely due to the development of leaks in the casing whose origin are currently uncertain. If only the open hole is considered, the improvement achieved by the acid treatments was a factor of 1.5-1.75. The net 3-day single-well injectivity/productivity indices after the acidizations were: 5.0 l/s/MPa for GPK-2, 4.0 l/s/MPa for GPK-3, and 5.0 l/s/MPa for GPK-4.

Microseismic activity was monitored during all stimulations to map the locations where shear failure was occurring [16; 36]. Typically, several thousand microseismic events would be recorded during single stimulation with a down-hole seismic network and somewhat fewer with a surface seismic network [6; 18; 13; 21]. High-precision mapping of the seismicity associated with the injection into GPK-1 illuminated the large scale geometry of HAFZs within the active volume and provided insights into their internal microstructure [27]. Comparison of the seismic responses to stimulation of the three deep wells showed that they are dependent to some degree on the nature of the HAFZs encountered in each of the wells [21]. The open hole section of deep well GPK-2 is characterized by a dense network of medium scale fracture zones, and the seismic cloud is rather compact and includes ~700 events of magnitude higher than 1. The initial injectivity/productivity index of this well was low, but was increased by a factor of 20 by the stimulations. The open hole section of well GPK-3 is hydraulically dominated by a very large HAFZ at 4.7 km MD that gave the well a high initial injectivity of 3 l/s/MPa. Stimulation produced 250 events larger than magnitude 1.0. Thus, the proportion of events with larger magnitudes was greater for GPK-3 than for GPK-2. This observation could indicate that the characteristics of the seismicity around GPK-3 is influenced by the large-scale fracture zone. However, the increase in injectivity/productivity index after stimulation was small.

Several earthquakes induced during stimulation tests attained a magnitude 2.0, the maximum being 2.9 during the injection into GPK-3, and were felt by the neighbouring population, provoking unwanted alarm. The highest magnitude events tended to occur shortly after the end of injection, during the shut in phase. Studies to better understand injection-induced microseismicity, particularly with regard to the generation of the larger events, are on-going. It is considered very important to identify ways to avoid disturbing populations that live close to geothermal projects that involve hydraulic stimulation operations.

Thermics

Temperature measurements were routinely performed in all wells at Soultz. The temperature profile to 5 km depth measured in well GPK-2 is presented in Figure 5. The profile is typical of all deep wells, with temperatures of 200°C being reached at 5 km depth. The localised disturbances at 2 km and 3.4 km reflect remnant cooling from stimulation injections conducted at those depths. The profile can be divided into three sections with different geothermal gradients reflective of different heat transport processes. The upper section lies entirely in the sediments from the surface to 1 km and has a very high gradient of about 110°/km indicating heat transport is predominantly conductive. The intermediate depth section from 1 km to about 3.3 km depth is characterised by a very low gradient of about 5°/km, which suggests heat transport is dominated by advection, probably in the up-flowing limb of a convective system that is active in the granite and Triassic sandstones [40]. This implies significant natural fluid movement is occurring within faults and fracture zones, at least between 1.0 and 3.3 km. Below 3.3 km, the geothermal gradient increases again to 30°/km and becomes linear with depth, indicating a return to a conduction-dominated heat flow regime. This might be explained as indicating that faults and fracture zones have insufficient connected permeability below 3.3 km depth to allow convection to develop [40; 49].

FIGURE 5

5 Performance of the upper and lower systems during circulation

The culmination of the 1991-1998 phase of Soultz was the 4 month continuous circulation of the upper-reservoir duplet system formed by the open hole sections of GPK-1 and GPK-2 which are 450 m apart [2; 5; 10]. Several limited-duration circulations have also been performed in the lower reservoir to date: without downhole pumps in 2005, and with one downhole pump and power generation in 2008 [17; 32; 52; 53]. The main results of the circulation tests are described in this section.

The upper reservoir between 3.0 and 3.6 km depth was the first truly engineered geothermal system to be constructed at Soultz (Figure 2). This reservoir was successfully circulated at 25 kg/s in closed-loop mode at fluid pressures far below the stimulation pressure levels for a four month period in 1997. A down-hole pump was installed at 430 m depth in the production well (GPK-2) to improve recovery by taking advantage of the natural far field permeability. Fluid mass balance (i.e. zero fluid loss) was maintained throughout the circulation with a minimum energy consumption. During this experiment, 244,000 tons of brine at temperatures up to 142°C were produced from GPK-2 and re-injected in GPK-1 with a centrifugal pump at a temperature of 40°. The GPK-1 wellhead injection pressure

declined from 4 MPa to 2 MPa during the test [2; 7]. The decline was slow and steady for the first half of the test, but then underwent a rapid drop after 60 days, an event that coincided with the termination of scaling inhibitor injection. Flow logs indicate the gradual change reflected declining impedance of a HAFZ at 3225 m [26], whereas the steep drop was largely due to an impedance drop at a HAFZ just below the casing shoe. Both have been ascribed to rock shrinkage due to cooling process [26, 10]. By the end of the circulation, the system circulation impedance was only 0.1 MPa/l/s. This was the first time that this long-standing commercial target had been attained in any EGS system worldwide, and then for the largest well separation of 450 m ever attempted [25]. The specific gravity of the production fluid increased during the test from 1.048g/cm^3 in July to 1.063g/cm^3 in November 1997 [50], reflecting a progressively larger fraction of formation water in the produced fluid. This, together with the relatively small quantities of tracer (i.e. 30%) recovered from tests, indicates that production was accessing fluid stored in the 'far-field', probably in the network of major fracture zones and faults present in the rock mass. Nevertheless, the tracer results also showed a rapid response, indicating that at least some of the principal flow paths linking the wells were direct. Application of a discrete fracture network model to the multi-scale fractured reservoir conditioned by the tracer response suggested that a 5% production temperature decrease could take place after 20 years of operating the doublet at a circulation rate of 25 l/s [10]. The usable thermal power produced for an injection temperature of 40°C attained ~11 MW thermal by the end of the 1997 test.

The first circulation test of the triplet of wells penetrating the lower reservoir (4.5 - 5.0 km) took place for 5 months between July and December 2005 (Figure 2). The wells had been hydraulically and chemically stimulated by that time, although some further acidization treatments of GPK-3 and GPK-4 were subsequently performed. A total of 209,000 m^3 of hot brine was produced by buoyancy drive at a flow rate of 15 l/s from the lateral boreholes GPK-2 (160°C) and GPK-4 without any downhole production pumps [32]. The produced fluid was re-injected into the central well GPK-3 at a wellhead pressure which increased from 4 to 7 MPa. Tracer tests conducted during the circulation showed that ~25% of the injected tracer was recovered from GPK-2 but only 2% from GPK-4 [52; 53]. This asymmetrical response reflects the complex organisation of fracture zones or faults describing different fluid circulation loops, the hydraulic connections between GPK-3 and GPK-2 being much more direct and faster than between GPK-3 and GPK-4 [52; 53]. During this circulation, and all production tests conducted in the lower reservoir, tracer tests and geochemical data invariably showed the presence of the native geothermal brine in the discharged fluids, even after large amounts of external water had been injected into the wells [52; 53]. This again points to the

conclusion that the exchanger is connected to a deep natural reservoir. Some 600 microseismic events were recorded in the 6 months during and immediately following the circulation. Several exceeded magnitude 2.0, but none were felt [19].

The lower reservoir was again circulated during the recent power-plant commissioning phase, this time with a line-shaft production pump installed at 350 m depth in GPK-2, with GPK-4 remaining shut-in (Figure 2). Since the earlier circulation in 2005, injection well GPK-3 had been subject to a further acid stimulation in 2007, which had little effect on injectivity [44], whilst well GPK-4 had been subject to three different types of acidization treatments with considerable success, as described earlier. Circulation began at the end of June 2008 and lasted until mid-August 2008. During this period, the pump-assisted production from GPK-2 was around 25 l/s at a temperature of 155°C. The production fluid pressure at the surface was maintained at 2 MPa before passing through a pump for injection into GPK-3. Wellhead injection pressure began at 6 MPa and increased continuously albeit progressively more slowly to stabilize at 7 MPa for last week of the test. Approximately 190 microearthquakes were associated with the circulation, which gives an event rate comparable to that observed in the 2005 circulation [19]. They also occurred in much the same locations as the earlier events, but the magnitude did not exceed 1.4, in contrast to the earlier events, several of which exceeded 2.0 [17]. This may reflect several differences between the two tests: the duration (6 months in 2005, around 2 months in 2008); a larger volume of water circulated in 2005; and the use of a down-hole production pump in July 2008 which induced higher production flow rates compared to artesian production with two production wells in 2005. Additionally, between 2005 and 2008, the wells were chemically stimulated [44]. Moreover most of the larger magnitude earthquakes in 2005 occurred after a sudden increase on injection flow rate and pressure. This behaviour is quite similar to the tendency of large events to occur during the shut in phase of stimulation tests [17], although the underlying mechanisms are not necessarily identical.

6 The Soultz reservoir: a channel network poorly connected through hydrothermally altered and fractured zones

By drilling into the Soultz granite to 5 km depth, several depth sections containing permeable fractures were observed [20]. This vertical zonation is organized in three main sections from top basement to TD. The main HAFZ are located (1) in a highly fractured and altered granite interval between 1.4 and 2.2 km (GPK-1, 1820 m; EPS-1, 2180 m; GPK-2, 2120 m), (2) in the upper reservoir between 3.5 and 3.9 km depth (GPK-1, 3490 m; GPK-2, 3900 m) and in the lower reservoir below 4.5 km depth (GPK-3, 4770 m). This vertical zonation does not reflect any geological “layering” but

corresponds to the geometrical intersection of nearly vertical drillholes with major nearly vertical fracture zones. As all the wells are roughly aligned along the N170°E striking direction and that those majors HAFZs range azimuthally between N150 and N170°E, they appear in cross-section in 3 main depth sections. The presence of additional fracture zones which don't intersect the wells is indicated from microseismic imaging [27; 42; 46] and VSP (Vertical Seismic Profiling) studies [47]. Moreover, there are several major fracture zones which are not hydraulically active. For example, the fracture zone in GPK-1 at 3.5 km is not the principal hydraulically active HAFZ in the well after stimulation, even though it was the principal hydro-geologic structure in the open hole section prior to stimulation [27].

The drilling of numerous wells at Soultz has provided a good description of structures present within the rock mass to 5 km depth. As noted earlier, these can be broadly viewed as falling into two categories: small-scale fractures (from grain-scale to meter-scale) that are widely distributed in the massive granite but are not hydraulically significant; and more localized, large-scale (i.e. > 100 m) hydrothermally-altered cataclastic fracture zone (HAFZ) structures created or reactivated by the Rhine graben tectonics. Both networks are steeply dipping and show a strong orientation anisotropy with similar strikes of N170°E ± 30°. Numerous HAFZs are intersected by the wells, and these are often found to be naturally permeable, although sometimes only slightly so. However, several of the HAFZs are clearly major structures in both a geological and hydrological sense. Structures recognised as major in both senses are listed in Table 1 of reference [20]. These major structures will be expected to have significant influence on the pattern of forced fluid flow within reservoirs developed in their vicinity, although they may not be dominant since other sub-vertical major HAFZ structures may be present that are not intersected by any well. High-resolution imaging of the microseismic cloud generated during the stimulation of the upper reservoir demonstrates that many HAFZ structures that do not intersect the wellbore are activated during stimulation [42, 46]. Most likely, almost all flow is confined to HAFZs, both before, during and after stimulation [27]. Within a given HAFZ, the natural permeability structure is probably channelized with a rather complex 3D organization [11].

Exploration at the Soultz granite has shown that it is not the classical Hot Dry Rock (HDR) of the original concept [56]. The presence of the HAFZs, which together form a connected system of large hydraulic capacity (i.e. storage), mean that the Soultz reservoirs share many facets of conventional geothermal reservoirs that benefit from reinjection. It is probable that the elements of the natural reservoir govern the flow field that develops under forced flow conditions within the reservoirs.

7 Future geothermal targets in the Rhine Graben

Exploration at the Soultz site has shown that the geothermal anomaly and the presence of oil in the Péchelbronn oil field are related, and that the heat distribution is mainly controlled by large-scale high-salinity fluid convection occurring within fractured formations (sandstones, granite). The granite near the top of the basement (1.4 to 2.2 km depth) is a promising geothermal target because it is more naturally fractured and more permeable than the upper and the lower reservoirs.

The nature of the deeper fractured basement at Soultz is well documented along the boreholes, but the inter-well domain is poorly constrained because all holes are near-vertical or steeply inclined. This borehole geometry was driven by the fact that the orientation of the main fracture system was aligned with the maximum horizontal principal stress [7]. Since it is difficult to image the fracture system in 3D prior to drilling, it might be more convenient for future geothermal projects in a similar geology/stress context to drill inclined holes perpendicular to the strike of the fracture system to maximise the likelihood of intersecting as many as possible. Such an approach has recently been successfully applied in a Soultz spin-off project near Landau, Rhineland Palatinate, Germany, some 40 km north of Soultz, where two shallow deviated wells were drilled into the lowermost sediments and the top of the basement [8].

8 Conclusions

Some 20 years of EGS research at the Soultz geothermal site has produced numerous scientific results and advancements relating to drilling, surface exploration methods, geology, geochemical and geophysical monitoring, tracer testing, hydraulic and chemical stimulations, and general EGS know-how.

An initial exploration well, GPK-1, was drilled to 2000 m depth and tested between 1987 and 1991. An important result of this early phase is that the nature of the rock mass and its response to hydraulic stimulations could be established, and that the results were found to be largely valid for the significantly deeper reservoirs. Increases in the injectivity of the well occurred through the enhancement of the transmissibility of hydrothermally-altered fracture zones (HAFZs) that cut the well. Almost all exchange of flow between the well and the rock mass occurred at these zones.

The upper reservoir duplet system was constructed between 3.0 and 3.6 km during the period 1992-1996, and circulated in closed-loop mode at 25 l/s/ for 4 months in 1997. The system impedance was only 0.1 MPa/l/s, the first time the long-established target for this parameter had been reached in any system developed world-wide, and then for the largest well separation of 450 m attempted up to that

time. Geochemical analyses and tracer tests revealed that a significant natural hydraulic reservoir existed in the rock mass, so that mixing of the injected fluid with the native formation water occurred, resulting in small return of injected tracer. The reservoir almost certainly resided in a connected network of permeable HAFZs which were seen at the wellbore on core and borehole images, and could be imaged remote from the well from high-resolution images of the pattern of microseismicity.

Construction of a triplet system in the lower reservoir between 4500 m and 5000 m TVD began in 1999 and was completed in 2005. The wells are arranged in a line that coincides with the maximum horizontal principal stress orientation, with the injection well, GPK-3, at the centre, and the two production wells, GPK-2 and GPK-4 a distance of 600 m away. Each well was hydraulically stimulated after completion. The maximum magnitudes of the seismic events induced by the injections were generally larger than for the stimulations in the upper reservoir, and were felt by the local population. Good communication was observed between GPK-3 and GPK-2, most likely due to the presence of a major HAFZ that cuts both wells. The connection between GPK-3 and GPK-4 was initially poor, tracer studies indicating that the flow between the wells was less direct. Following a series of acidizing stimulation operations on GPK-4, the productivity of GPK-4 was increased by a factor of 2.5. However, most of the improvement resulted from the appearance of casing leaks whose origin is currently uncertain. At present, the single-well injectivity/productivity indices of the three wells are: 5.0 l/s/MPa for GPK-2, 4.0 l/s/MPa for GPK-3, and 5.0 l/s/MPa for GPK-4.

The next phase of the project will involve the long-term circulation of the system with downhole pumps in both wells and electric power production from a recently-constructed power plant. This phase will begin shortly.

Acknowledgements

This work was performed within the framework of the European EGS Pilot Plant project which was supported mainly by the European Commission, BMU (Germany), ADEME (France), the Swiss Federal Offices of Education and Research (SER), and Energy (SFOE), and by a consortium of industrial members (EDF, EnBW, ES, Pfalzwerke, Evonik).

References

[1] L. Aquilina, H. Pauwels, A. Genter, C. Fouillac, Water-rock interaction processes in the Triassic sandstone and the granitic basement of the Rhine Graben: geochemical investigation of a geothermal reservoir, Geochimica and Cosmochimica Acta, vol 61 20 (1997) 4281-4295.

[2] L. Aquilina, P. Rose, L. Vaute, M. Brach, S. Gentier, E. Jacquot, P. Audigane, R. Jeannot, T. Tran-Viet, R. Jung, J. Baumgaertner, R. Baria, A. Gérard, A tracer test at the Soultz-sous-Forêts Hot Dry Rock geothermal site, Twenty-third Workshop on Geothermal Reservoir Engineering, Stanford University California USA (1998) 343-350.

[3] D. Bächler, Coupled thermal-hydraulic-chemical modelling at the Soultz-sous-Forêts HDR reservoir (France), Thesis Doctor of Natural Sciences, Swiss Federal Institute of Technology Zurich, 2003, 151 p.

[4] R. Baria, J. Baumgaertner, A. Gérard, R. Jung, J. Garnish, European HDR research programme at Soultz-sous-Forêts (France) 1987-1996, Geothermics 28 4-5 (1999) 655-669.

[5] R. Baria, J. Baumgaertner, A. Gérard, R. Weidler, R. Hopkirk *et al.*, European HDR geothermal research programme, 1998-2001, EU final report (2001), Contract n°JOR3-CT98-0313.

[6] R. Baria, S. Michelet, J. Baumgaertner, B. Dyer, A. Gérard, J. Nicholls, T. Hettkamp, D. Teza, N. Soma, H. Asanuma, J. Garnish, Th. Mégel, Microseismic monitoring of the world's largest potential HDR reservoir, 29th Workshop on Geothermal Reservoir Engineering, Stanford University California USA (2004) 194-201.

[7] J. Baumgaertner, A. Gérard, R. Baria, R. Jung, T. Tran-Viet, T. Gandy, L. Aquilina, J. Garnish, Circulating the HDR reservoir at Soultz: maintaining production and injection flow in complete balance: initial results of 1997 experiment, Twenty-third Workshop on Geothermal Reservoir Engineering, Stanford University Stanford California USA (1998) 11-20.

[8] J. Baumgaertner, H. Menzel, P. Hauffe, The geox GmbH Project in Landau - The first geothermal power plant project in Palatinate / Upper Rhine Valley, First European Geothermal Review, Geothermal Energy for Power Production, October 29 – 31, 2007, Mainz Germany (2007), 33.

[9] O. Bourgeois, M. Ford, M. Diraison, C. Le Carlier de Veslud, M. Gerbault, R. Pik, N. Ruby, S. Bonnet, Separation of rifting and lithospheric folding signatures in the NW-Alpine foreland, International Journal Earth Sciences 96 (2007) 1003-1031.

[10] D. Bruel D., Impact of induced thermal stress during circulation tests in an engineered fractured geothermal reservoir, Oil & Gas Science and Technology Revue IFP 57 no. 5 (2002) 459-470.

[11] J.S. Caine, J.P. Evans, C.B. Forster, Fault zone architecture and permeability structure. Geology 24 (1996) 1025-1028.

[12] J.P. Cautru, Coupe géologique passant par le forage GPK1 calée sur la sismique réflexion, document BRGM, Institut Mixte de Recherches Géothermiques Rapport interne (1988).

[13] J. Charléty, N. Cuenot, L. Dorbath, C. Dorbath, H. Haessler, M. Frogneux, Large earthquakes during hydraulic stimulations at the geothermal site of Soultz-sous-Forêts, International Journal of Rock Mechanics and Mining Sciences 44 (2007) 1091-1105.

[14] A. Cocherie, C. Guerrot, C.M. Fanning, A. Genter, Datation U-Pb des deux faciès du granite de Soultz (Fossé Rhénan, France), Comptes Rendus Geoscience 336 (2004) 775-787.

[15] F.H. Cornet, R. H. Jones, Field evidence on the orientation of forced water flow with respect to the regional principal stress directions, 1st North American Rock Mechanics Symposium, Balkema, Austin, Texas, USA, 1994.

[16] N. Cuenot, J. Charléty, L. Dorbath, C. Dorbath, A. Gérard, 2005 circulation experiments: views of the microseismic activity under production conditions, EHDRA Scientific meeting 2006, Soultz-sous-Forêts, June 2006.

[17] N. Cuenot, J. Charléty, L. Dorbath, H. Haessler, Faulting mechanisms and stress regime at the European HDR site of Soultz-sous-Forêts, France, Geothermics vol. 35 No. 5-6 (2006) 561-575.

[18] N. Cuenot, C. Dorbath, L. Dorbath, Analysis of the microseismicity induced by fluid injections at the Hot Dry Rock site of Soultz-sous-Forêts (Alsace, France): Implications for the characterization of the geothermal reservoir properties, Pure and Applied Geophysics 165 (2008) 797-828.

[19] N. Cuenot, L. Dorbath, M. Frogneux, H. Jund, Microseismic activity during circulation in summer 2008 and comparison with 2005 circulation test, EHDRA scientific conference, Soultz-sous-Forêts, France, 24-25 September 2008, (2008) 6 pp.

[20] Ch. Dezayes, A. Genter, Large-scale fracture zone network based on Soultz borehole data. Proceedings of the EHDRA scientific conference 24-25 September 2008, Soultz-sous-Forêts, France (2008).

[21] L. Dorbath, N. Cuenot, A. Genter, M. Frogneux, Seismic response of the fractured and faulted granite to massive water injection at 5 km depth at Soultz-sous-Forêts (France), Accepted to Geophysical Journal International (2009).

[22] K.F. Evans, The effect of the 1993 stimulations of well GPK1 at Soultz on the surrounding rock mass: evidence for the existence of a connected network of permeable fractures, World Geothermal Congress 2000, Kyushu - Tohoku Japan May 28 - June 10 2000 (2000) 3695-3700.

[23] K.F. Evans, Permeability creation and damage due to massive fluid injections into granite at 3.5 km at Soultz: Part 2 - Critical stress and fracture strength, Journal of Geophysical Research 110 B04204 (2005) 14 pp.

[24] K.F. Evans, A. Genter, J. Sausse, Permeability creation and damage due to massive fluid injections into granite at 3.5 km at Soultz: Part 1 - Borehole observations, Journal of Geophysical Research 110 B04203 (2005) 19 pp.

[25] K.F. Evans, R. Hopkirk, R. Jung, P. Nami, M. Schindler, D. Teza, T. Tischner, Milestone events and key observations in Thermics, Stress and Hydraulics at Soultz (1987-2002), EHDRA scientific conference, Soultz-sous-Forêts, France, 24-25 September 2008 (2008) 6 pp.

[26] K.F. Evans, Th. Kohl, L. Rybach, Analysis of the hydraulic behaviour of the 3.5 km deep reservoir during the 1995-1997 test series, and other contributions to the European Hot Dry Rock Project, Soultz-sous-Forêts, France, Report to Swiss Office of Education and Research under contract BBW 95.0673-2, 1998 Swiss Federal Institute of Technology.

[27] K.F. Evans, H. Moriya, H. Niitsuma, R.H. Jones, W.S. Phillips, A. Genter, J. Sausse, R. Jung, R. Baria, Microseismicity and permeability enhancement of hydrogeologic structures during massive fluid injections into granite at 3 km depth at the Soultz HDR site, Geophysical Journal International 160 (2005) 388-412.

[28] A. Genter, Géothermie Roches Chaudes Sèches : le granite de Soultz-sous-Forêts (Bas Rhin, France). Fracturation naturelle, altérations hydrothermales et interaction eau – roche, PhD thesis, Université d'Orléans, France, 1989, 201 p.

[29] A. Genter, H. Traineau, Borehole EPS-1, Alsace, France; preliminary geological results from granite core analyses for hot dry rock research, Scientific Drilling 3 (1992) 205-214.

[30] A. Genter, H. Traineau, B. Bourgine, B. Ledésert, S. Gentier, Over 10 years of geological investigations within the European Soultz HDR project, France. World Geothermal Congress 2000, Kyushu-Tohoku, Japan May 28 - June 10 2000 (2000) 3707-3712.

[31] S. Gentier, Les massifs rocheux fracturés : de la fracture à la géothermie, Mémoire d'habilitation à diriger des recherches (HDR), Université Bordeaux 1, 2004, France.

[32] A. Gérard, A. Genter, T. Kohl, Ph. Lutz, P. Rose, F. Rummel, The deep EGS (Enhanced Geothermal System) project at Soultz-sous-Forêts (Alsace, France), Geothermics vol. 35 No 5-6 (2006) 473-483.

[33] A. Gérard, O. Kappelmeyer, The Soultz-sous-Forêts project: Proceedings of the first EEC/US workshop on geothermal Hot dry Rocks technology, Geothermics (1987) 393-399.

[34] A. Gérard, A. Menjoz, P. Schwoerer, L'anomalie thermique de Soultz-sous-Forêts, Géothermie Actualités n°3 (1984) 35-42.

[35] J.-O. Haas, C.R. Hoffmann, Temperature gradient in Pechelbronn oil bearing region, lower Alsace: its determination and relation to oil reserves, American Association Petroleum Geologist Bulletin XIII n°10 (1929) 1257-1273.

[36] J. Horalek, Z. Jechumtalova, L. Dorbath, J. Sileny, Shear versus non-shear components in source mechanisms of micro-earthquakes induced in hydraulic fracturing experiment at the HDR site Soultz-sous-Forêts (Alsace) in 2003, EHDRA scientific conference, Soultz-sous-Forêts, France, 24-25 September 2008 (2008) 8 pp.

[37] R. Jung, T. Tischner, J. Baumgaertner, D. Teza, P. Nami, M. Schindler M., Review of hydraulic stimulation tests and hydraulic experiments at Soultz, EHDRA scientific conference, Soultz-sous-Forêts, France, 24-25 September 2008 (2008) 2 pp.

[38] R. Jung, R. Weidler, A conceptual model for the stimulation process of the HDR-system at Soultz, Geothermal Resources Council Transactions, Geothermal Resources Council, San Francisco, California, USA, 24-27 September, 2000.

[39] Th. Kohl, K.F. Evans, R.J. Hopkirk, R. Jung, L. Rybach, Observation and simulation of non-Darcian flow transients in fractured rock, Water Resources Research 33 3 (1997) 407-418.

[40] C. Le Carlier, J.-J. Royer, E.L. Flores, Convective heat transfer at the Soultz-sous-Forêts geothermal site: implication for oil potential, First Break 12 (1994) 553-560.

[41] B. Ledésert, J. Joffre, A. Amblès, P. Sardini, A. Genter, A. Meunier, Organic matter in the Soultz HDR granitic thermal exchanger (France): natural tracer of fluid circulations between the basement and its sedimentary cover, Journal Volcanology Geothermal Research vol. 70 (1996) 235-253.

[42] H. Moriya, K. Nakazato, H. Niitsuma, R. Baria, Detailed fracture system of the Soultz-sous-Forêts HDR field evaluated using microseismic multiplet analysis, Pure and Applied Geophysics 159 (2002) 517-541.

[43] F. Munck, F. Walgenwitz, P. Maget, K. Sauer, R. Tietze, Synthèse géothermique du Fossé rhénan Supérieur. Commission of the European Communities, BRGM Service Géologique Régional d'Alsace, Geologisches Landesamt Baden-Württemberg.

[44] P. Nami, R. Schellschmidt, M. Schindler, T. Tischner, Chemical Stimulation operations for reservoir development of the deep crystalline HDR/EGS system at Soultz-sous-Forêts (France). Proc.

32nd Workshop on Geothermal Reservoir Engineering, January 28-30, 2008, Stanford, California, USA, (2008).

[45] H. Pauwels, C. Fouillac, A.-M. Fouillac, Chemistry and isotopes of deep geothermal saline fluids in the Upper Rhine Graben: Origin of compounds and water-rock interactions, Geochimica and Cosmochimica Acta 57 (1993) 2737-2749.

[46] W. S. Phillips, Precise microearthquake locations and fluid flow in the geothermal reservoir at Soultz-sous-Forêts, France, Bull. Seis. Soc. Am. 90 1 (2000) 212-228.

[47] J. Place, C. Naville, A. Gérard, Test of VSP efficiency for the recognition of highly dipping faults in a deep granitic basement, (2007) unpublished GEIE report 27 pp.

[48] S. Portier, F-D. Vuataz, B. Sanjuan, P. Nami, A. Gérard, (2009). Chemical stimulation techniques for geothermal wells: experiments on the 3-well EGS system at Soultz-sous-Forêts, Geothermics (2009).

[49] D. Pribnow, R. Schellschmidt, Thermal tracking of Upper crustal fluid flow in the Rhine Graben, Geophysical Research Letters 27 13 (2000) 1957-1960.

[50] F. Rummel, T. Hettkamp T., U. Weber, Density measurements on fluid samples obtained during the HDR circulation test 97July12 (Part II), Yellow Report no. 18 (1997) Ruhr-University Bochum.

[51] B. Sanjuan, R. Millot, Ch. Dezayes, M. Brach, Main characteristics of the deep geothermal brine (5 km) at Soultz-sous-Forêts (France) determined using geochemical and tracer test data. Geoscience, this volume, (2009).

[52] B. Sanjuan, J.-L. Pinault, P. Rose, A. Gérard, M. Brach, G. Braibant, C. Crouzet, J.-C. Foucher, A. Gautier, S. Touzelet, Geochemical fluid characteristics and main achievements about tracer tests at Soultz-sous-Forêts (France). BRGM/RP-54776-FR final report, 2006a, 64 p.

[53] B. Sanjuan, J.-L. Pinault, P. Rose, A. Gérard, M. Brach, G. Braibant, C. Crouzet, J.-C. Foucher, A. Gautier, S. Touzelet, Tracer testing of the geothermal heat exchanger at Soultz-sous-Forêts (France) between 2000 and 2005, Geothermics vol. 35 No. 5-6 (2006b) 622-653.

[54] M. Schindler, P. Nami, R. Schellschmidt, D. Teza, T. Tischner, Correlation of hydraulic and seismic observations during stimulation experiments in the 5 km deep crystalline reservoir at Soultz, Annual EHDRA Scientific Conference of the Soultz Project, Soultz-sous-Forêts, France, 24-25 September 2008.

[55] R. Schnaebele, J.-O. Haas, C.R. Hoffmann, Monographie géologique du champ pétrolifère de Péchelbronn, Mémoire Service Carte Géologique Alsace, vol. 7, 1948, 254 p.

[56] M. Smith, A history of Hot Dry Rock geothermal systems, J. Volcan. Geotherm. Res., 15, (1983) 1-20.

[57] J.-M. Stussi, J.M. Cheilletz, J.-J. Royer, P. Chèvremont, G. Féraud, The hidden monzogranite of Soultz-sous-Forêts (Rhine Graben, France), Mineralogy, petrology and genesis, Géologie de la France 1 (2002) 45-64.

[58] B. Valley, The relation between natural fracturing and stress heterogeneities in deep-seated crystalline rocks at Soultz-sous-Forêts (France), PhD thesis, ETH-Zürich, Switzerland, 2007, 260 p.

[59] F.-D. Vuataz, M. Brach, A. Criaud, C. Fouillac, Geochemical monitoring of drilling fluids: a powerful tool to forecast and detect formation waters, SPE, Formation Evaluation (1990) 177-184.

[60] P. Ziegler, European Cenozoic rift system, Tectonophysics 2008 (1992) 91-111.

FIGURE AND TABLE CAPTIONS

Figure 1 - Main phases of the Soultz project between 1987 and 2009.

Figure 1 - Principales phases de développement du projet Soultz entre 1987 et 2009.

Figure 2 - North-south vertical cross-section through the Soultz site showing the location of the Upper and Lower Reservoirs. The view shows the three 5 km deep geothermal wells (GPK-2, GPK-3, GPK-4) that are completed open-hole in the lower reservoir, and the wells GPK-1 and GPK-2 that form the upper reservoir. Also shown is the cored exploration well EPS-1. Depths are expressed in True Vertical Depths (TVD).

Figure 2 - Coupe verticale S-N passant par les 3 puits géothermiques profonds (GPK-2, GPK-3, GPK-4) et par les puits d'exploration GPK-1 et EPS-1 montrant la localisation schématique des réservoirs supérieurs et inférieurs. Les profondeurs sont des profondeurs verticales corrigées.

Figure 3 - Temperature map at 400 m depth based on oil well measurements in the Péchelbronn-Soultz area from Haas and Hoffmann (1929).

Figure 3 - Carte des températures à 400 m de profondeur établie à partir de mesures réalisées dans des forages pétroliers dans le secteur de Péchelbronn-Soultz d'après Haas et Hoffmann (1929).

Figure 4 - Example of hydrothermally altered and fractured granite core taken at 1377 m depth in GPK-1 well showing a nearly vertical sheared fracture.

Figure 4 - Exemple de carotte de granite fracturé et altéré prélevé à Soultz dans le puits GPK-1 à 1377 m de profondeur. On notera la présence d'une fracture subverticale à jeu apparent cisaillant.

Figure 5 - Equilibrium temperature profiles obtained from logs run in GPK1 and GPK2 several months after drilling operations finished. (Data from GGA-Hannover, Germany).

Figure 5 - Profiles de température réalisés à l'équilibre plusieurs mois après la fin de la foration dans les forages GPK-1 et GPK-2 de Soultz (données collectées par GGA Hanovre, Allemagne).

Overview of the fracture network at different scales within the granite reservoir of the EGS Soultz site (Alsace, France)

Chrystel Dezayes*, Albert Genter**, Benoît Valley***

** BRGM, Geothermal Department, 3, avenue Cl. Guillemin, BP36009, F-45060 Orléans Cedex 2*
*** GEIE Exploitation Minière de la Chaleur, Route de Soultz, BP40038, F-67250 Kutzenhausen*
**** ETH Zürich, Engineering Geology, CH-8092 Zürich; now: MIRARCO/Laurentian University, 935 Ramsey Lake Road, Sudbury, ON P3E 2C6, CANADA*

Presented at the World Geothermal Conference at Bali on 25-29 April 2010.

Proceedings World Geothermal Congress 2010
Bali, Indonesia, 25-29 April 2010

Overview of the fracture network at different scales within the granite reservoir of the EGS Soultz site (Alsace, France)

Chrystel Dezayes*, Albert Genter**, Benoît Valley***

* BRGM, Geothermal Department, 3, avenue Cl. Guillemin, BP36009, F-45060 Orléans Cedex 2
** GEIE Exploitation Minière de la Chaleur, Route de Soultz, BP40038, F-67250 Kutzenhausen
*** ETH Zürich, Engineering Geology, CH-8093 Zürich; now: MIRARCO/Laurentian University, 935 Ramsey Lake Road, Sudbury, ON P3E 2C6, CANADA
c.dezayes@brgm.fr, genter@soultz.net, bvalley@mirarco.org

Keywords: Rhine graben, fractures, fracture zones, cores, borehole images, Enhanced Geothermal System.

ABSTRACT

In EGS-Soultz like concept, the knowledge of the fracture network is essential to understand the reservoir behavior and to plan further stimulations and long term hydraulic circulation. At Soultz, the targeted reservoir is located at 5km depth within the granite basement of the Upper Rhine Graben (France), nearby its western border. This granite underwent a complex tectonic history including Hercynian and Alpine orogeneses, leading to the currently observed fracturing. This fracturing is dominated by steeply dipping fracture sets which are distributed at various scales in the granite basement.

This structural work presents the characterization of the fracture network at different scales in order to understand and model the hydro-thermo-mechanical behavior of the granite geothermal reservoir through hydraulic stimulation and subsequent circulation tests. The small-scale fracture network has been characterized based on several kilometers of high resolution borehole image logs allowing characterizing different sets. We focused on large-scale fracture zones, which are the major fluid pathways. A total of 39 fracture zones have been described in detail based on borehole data. They have been compared to large-scale geophysical investigations, as Vertical Seismic Profile (VSP) and passive microseismicity, in order to build an extended fracture network in 3D. Hydraulically active fractures have been investigated in more detail in the different open-hole sections, based on image logs, flow logs and temperature logs. These near-well borehole fractures represent potential fluid pathway for connecting the borehole to the far-field geothermal reservoir.

In global view, the fracture network in the granite Soultz reservoir is constituted by large-scale fracture zones, which are connected to a dense network of small-scale fractures. However, fluid pathways are more complex with channelized structures, because only a limited number of fractures supports fluid flow.

1. INTRODUCTION

Since 1980 (Gérard *et al.*, 1984; Gérard and Kappelmeyer, 1987), the EGS project at Soultz (France) goals to experiment and develop a new geothermal technology. After an initial Hot Dry Rock (HDR) concept of artificial fractures creation in a homogeneous rock by hydraulic fracturing, the concept at Soultz has progressively evolved to an Enhanced Geothermal System (EGS) where reservoir development involved the reactivation of the pre-existing fractures in the granite (Evans *et al.*, 2005; Gérard *et al.*, 2006). Thus, a good knowledge and geometrical characterization of the rock mass and particularly of the fracture network are essential for many reasons, from the optimization of the borehole design to the understanding of the flow distribution at depth. At Soultz, this fracture network is structured at different scales, from major fracture zones cross-cutting the granite batholith to intra-crystalline microfractures, which induce weakness in the rock mass (Dezayes *et al.*, 2000).

Several studies have shown that some fracture zones are water-bearing prior to stimulation (Vuataz *et al.*, 1990; Genter *et al.*, 1995) and form the main flow channeling after stimulation and during circulation (Evans *et al.*, 2005; Sanjuan *et al.*, 2006). These fracture zones are probably reactivated by shearing whilst the hydraulic stimulation. Moreover, other fracture zones not permeable prior stimulation have been reactivated during the stimulation and have been taking into account in this study.

Thus, fracture zones form the main potential fluid pathways connected to the dense network of meso-scale fractures to form the geothermal reservoir, which is about 1,125km^3 for the upper reservoir and 8 km^3 for the deeper reservoir, based on induced micro-seismicity study (Cuenot *et al.*, 2006).

This paper presents a characterization of the intermediate scale to large-scale, formed by fracture zones, in order to make a geometrical update of the fracture data base likely to support conductive fluid flow. Small-scale fracture distribution and characterization have been extensively studies (Dezayes et al., 2000; Genter at al., 2000). The goal of this study is to define the geometry of the fracture network for a better understanding of the fluid circulation in a deep fractured granite reservoir dedicated to geothermal exploitation. These results are used for modeling the hydraulic stimulations and circulations of Soultz geothermal reservoir (Sausse *et al.*, 2009; Rachez et al., 2006; Rachez and Gentier 2008; Baujard and Bruel, 2005; Kohl and Megel, 2005) or geophysical interpretations or inversions (Place *et al.*, 2009; Schill and Geiermann, 2009).

2. GEOLOGICAL AND STRUCTURAL CONTEXT

The Soultz site is located within the Upper Rhine Graben, which is a Cenozoic rift structure belonging to the West European Rift System (Figure 1; Ziegler, 1992). The filling sediments are marine and lacustrine limestones, marls and evaporites, including the petroleum layers of Pechelbronn, overlaying in unconformity the Jurassic limestones and the Germanic Trias (Figure 1b). These Cenozoic and Mesozoic sediments have been deposited on the Paleozoic basement, which includes porphyritic monzo granite and two-mica granite (Genter *et al.*, 1999; Stussi *et al.*, 2002; Cocherie *et al.*, 2004; Hooijkaas *et al.*, 2006).

This granite unit is the target of the geothermal project and hosts the geothermal reservoir. This massif underwent a multiphase tectonic history including Hercynian and Alpine orogeneses. The Cenozoic tectonic history is reflected by the orientations of the current structures forming the Upper Rhine Graben (Figure 1). The regional major border faults mapped on surface or derived from petroleum seismic reflection studies within the Upper Rhine Graben show a N0-30°E direction in relation to the three main directions of the graben (Figure 1). In the southern part of the graben, the main direction is about N10°E. This direction rotates clockwise at the center of the graben to N30-25°E and becomes N0°E in its northern part. The Rhenish fracture orientation was formed during the Oligocene opening of the Rhine graben (Villemin and Bergerat, 1985), reactivating probably some Hercynian structures (Illies, 1972, Illies, 1975; Rotstein *et al.*, 2006). At the Soultz site, the Upper Rhine Graben rotates and the regional border faults are N45°E oriented. This direction is also present in the Triassic sediments in the west of the graben fault, in the Vosges area (Ménillet et al., 1989).

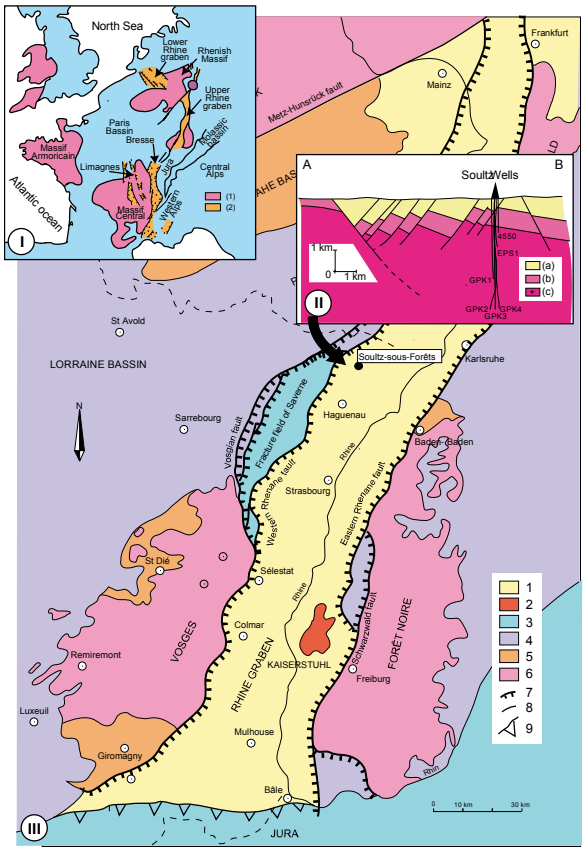

Figure 1 – Location of the EGS Soultz site and geology of the Upper Rhine Graben. I) Location of the Upper Rhine Graben with the West European Rift System. (1) Hercynian basement; (2) Tertiary basins; (3) Alpine molasse. II): W–E cross-section through the Rhine Graben border and the Soultz site. (a) Cenozoic; (b) Mesozoic; (c) Hercynian basement. III) Geological and structural map of the Rhine graben (1) Cenozoic sediments; (2) Cenozoic volcanics; (3) Jurassic; (4) Triassic; (5) Permo-Carbonifeous basins, (6) Hercynian basement; (7) boundary faults; (8) other faults; (9) overthrusts.

However, the granitic basement has been affected by ante-Cenozoic tectonics, in particularly the Hercynian orogen. The strike of the major dislocations delimiting the different Hercynian tectonic blocks is roughly N60°E (Figure 1). At local scale, around the Soultz site, geological mapping, borehole data and interpretation of seismic profiles acquired during the exploration of the Pechelbronn oil field give lots of data to characterize the major fault system (Foehn, 1985; Place *et al.*, 2009). These data were compiled to build a 3D geological model of the sedimentary cover (Renard and Courrioux, 1994; Castera *et al.*, 2008). These studies show that in the sedimentary cover, the faults have a N20°E strike, i.e. a Rhenish direction (Figure 1). In map view, the faults have a trace length of about 2 to 20 km and occur with a spacing range of about 800m to 3km (Valley *et al.*, 2007). At depth, below the Soultz site, a horst structure is present and the top of the basement is at 1.4km depth (Figure 1-II). Within this horst structure, some local faults are detected on the seismic profiles, which are mainly dipping to the west (Figure 1-II).

On the Soultz site, five boreholes have been drilled since 1987: two relatively shallow exploratory wells GPK1 and EPS1, fully cored, were drilled to 3600m and 2200m respectively, and three for reservoir development and heat exploitation (GPK2, GPK3 and GPK4). All of which were drilled to depths of approximately 5000m, where temperatures reach 200°C (Figure 2; Baumgärtner *et al.*, 2004). The exploitation triplet is formed by GPK2, GPK3 and GPK4, which were drilled from the same well pad and are slightly inclined with depth. The three wells are aligned at 5000 m depth in a N165°E direction and the horizontal distance between adjacent wells is about 700 m at depth (Figure 2).

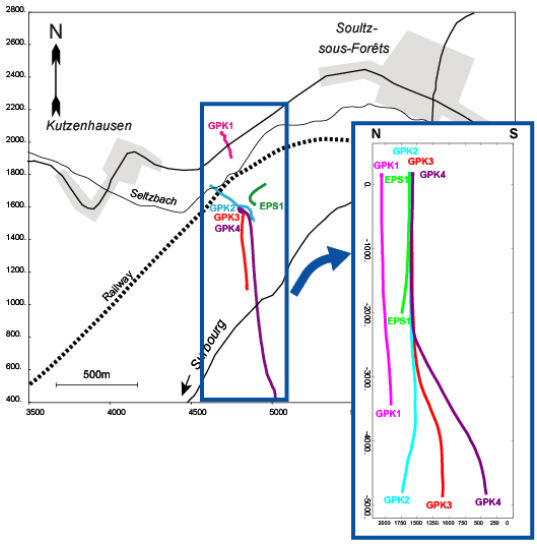

Figure 2 - Map view and N-S cross-section of the EGS well trajectories at Soultz.

METHODOLOGY

Orientation and classification of several thousand fractures were collected from oriented borehole images. High-resolution acoustic image logs such as BoreHole TeleViewer (BHTV) were acquired in GPK1 and EPS1, and Ultrasonic Borehole Imager (UBI) in GPK2, GPK3 and GPK4 (Figure 3). Various electrical image logs (FMS, FMI, ARI) have been run in the GPK1 and GPK2 wells and analysed in previous studies (Genter *et al.*, 1995; Dezayes *et al.*, 1995; Genter *et al.*, 1997).

In the cores, all the fractures are systematically sealed by hydrothermal filling but only 20% of them are visible on

the borehole images (Genter *et al.*, 1997). However, only one borehole, EPS1, is fully cored (Figure 3) and some spot coring are available in GPK1 and GPK2. But the borehole images are suitable for detecting and measuring the orientation of the meso-scale fractures and fracture zones.

For the analysis of the small-scale fractures, two main types of fractures have been defined along the wells based on their origin: the natural fractures, older than the drilling and in relation with the tectonic history of the granite massif, and the induced fractures, formed with the drilling and in relation with the present-day stress field. In this study, only the natural fractures have been taken into account. Induced fractures were studied in other papers like Tenzer *et al.* (1991), Genter *et al.* (1995), Dezayes *et al.* (1995), Valley and Evans (2005).

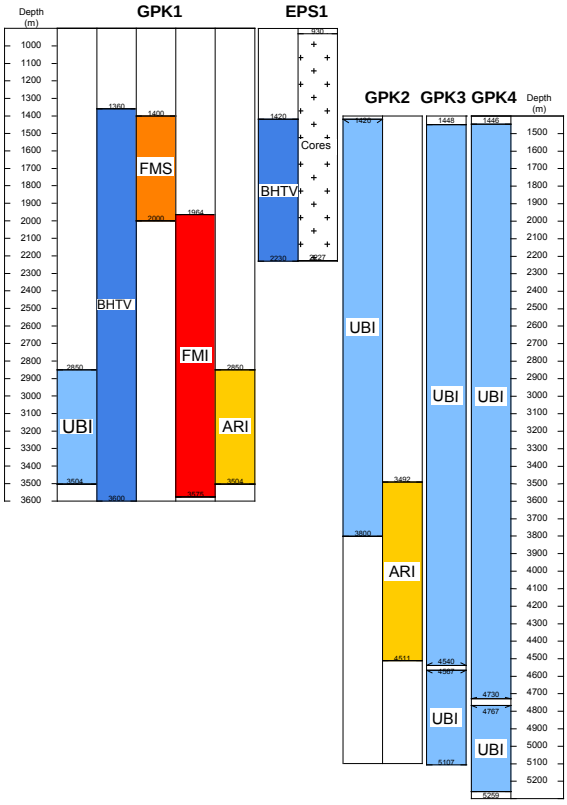

Figure 3 - Core and image data available in the Soultz wells. BHTV: BoreHole TeleViewer; UBI: Ultrasonic Borehole Imager; FMS: Formation Micro Scanner; FMI: Fullbore Micro Imager; ARI: Azimuthal Resistivity Imager. Depth: measured depth along the well (MD).

The natural fracture typology has been defined in order to get homogenous fracture datasets in the GPK3 and GPK4 wells (Dezayes *et al.*, 2005). This typology is based on two criteria mainly:

- the comparison between transit time and amplitude image logs permits to determine if the fracture is open (dark traces) or not (no trace).
- the continuity of the sinusoidal trace on the amplitude image to distinguish the scale of fractures (100% to 80% of the sinusoidal trace visible, between 80% and 50%, lower than 50% and uncertain sinusoidal fitting). The occurrence of an alteration halo surrounding the fracture is also taken into account.

In order to better characterize low permeable fracture zones, we use the geological database based on petrographical description of cuttings, borehole image log and geophysical log analyses, as caliper, spectral gamma ray and drilling parameters (Figure 4). The spectral gamma ray data, such as potassium, thorium and uranium contents, are used to detect radioactive element concentration due to the hydrothermal alteration related to fracture zones or some petrographical variations.

However, we cannot determine if there are some evidences of natural permeability in a given fracture by interpreting geological data only. Then, in addition, temperature and flow logs analysis was used to determine the zone of fluid lost in the boreholes (Evans, 2000; Dezayes *et al.*, 2004).

On the borehole images, fracture orientations are sometimes difficult to measure due to the fact that fractures are not perfectly planar as it is assumed for the dip calculation. Also, fracture zones are complex and their orientation is difficult to define. Often, several individual fracture traces are visible on the log image within a given fracture zone, which include brecciated to microbrecciated zone. To determine the fracture zone overall orientation, we consider that the orientation of the border of the brecciated zone is representative of the overall orientation if this limit is well visible and defined and if it forms a well-marked planar structure. However, when several planar structures are present and roughly parallel, we assumed that the orientation of the fracture zone is well approximate with the 3D average orientation of the individual parallel planes.

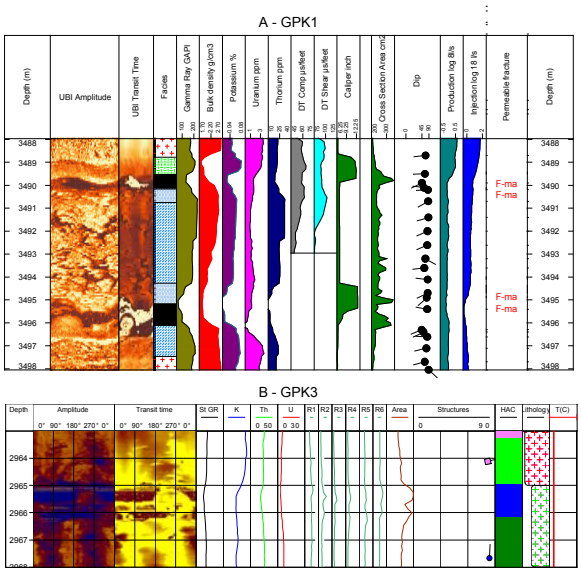

Figure 4 - Example of synthetic combined logs for two fracture zones in GPK1 (A) and GPK3 (B). Depth: measured depth along the well (MD).

In the open-hole sections of GPK3 and GPK4, several temperature and flow logs have been acquired during the stimulation of the granite reservoir. The detailed studie of these logs coupled with the borehole image logs allows to define the fluid exit zone, which connected the wells with the reservoir.

MESO-SCALE FRACTURES

Fracture orientation

Many fracture data have been collected in the granite basement based on coring and especially borehole imaging

(Genter *et al.*, 2007). The analyses of these fracture data show that the main strike is consistent between the different imagery logs and the different wells (Figure 5; Genter, 1989; Genter *et al.*, 2000; Dezayes *et al.*, 2004).

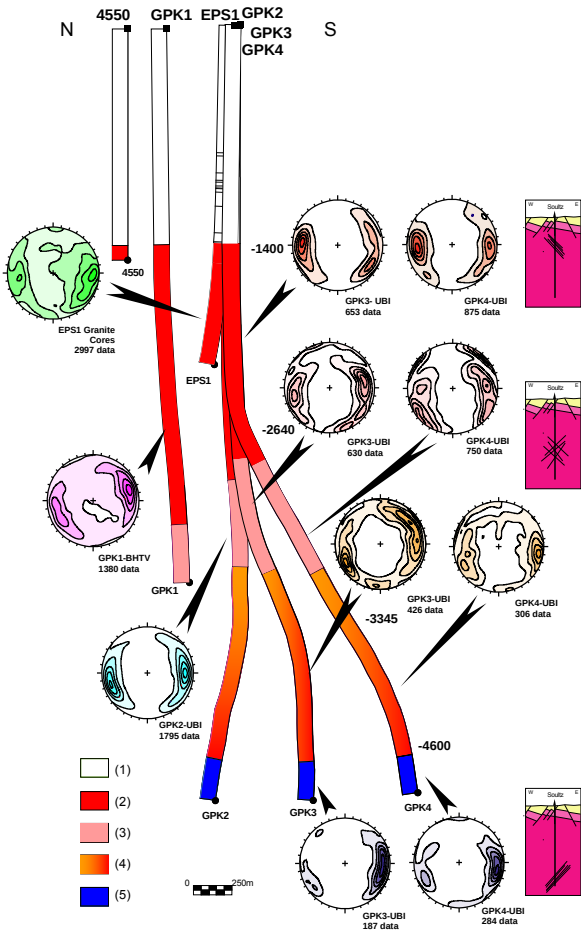

Figure 5 - Fracture orientation in relation with the major petrographical crystalline sections in GPK3 and GPK4. (1) Sedimentary cover, (2) standard porphyritic granite, (3) Standard granite with intense vein alteration, (4) Biotite and amphibole rich granite gradually becoming standard granite with depth, (5) Two mica granite and biotite rich granite. The depths along the wells indicate the upper and the lower depth limits of the petrographical sections (in True Vertical Depth, from the drilling floor). Contour-density diagrams of all fracture types in Schmidt's projection, lower hemisphere: 10%, 30%, 50%, 70%, and 90% of the maximum frequency.

In EPS1, the coring has begun at 920m in the lower Muschelkalk. In the granite, the major direction is varies from N160°E to N-S with steep dipping eastward and westward. However, the orientations of fractures observed in cores (EPS1) are rather scattered with various dipping values (Figure 5). In these cores, some faults showing striations have been measured and the Oligocene paleostress states have been retrieved by inversion (Dezayes *et al.*, 1995). Among the fractures in granite, based on borehole image interpretation, seven sets have been isolated by statistical method (Valley, 2007). 60% of fractures belong to two sets striking N-S and dipping to the west and to the east. This orientation corresponds to the Rhenish orientation described at graben and site scales. A sub-vertical set, striking NW-SE, appears also at large scale but outside of the Rhine graben in Vosges and Black Forest massif and in the Triassic sediments. Another subvertical perpendicular set, striking NE-SW, is parallel to the Hercynian large scale faults, like the Lalaye-Lubine-Baden-Baden fault. These four sets include 95% of all fractures found in granite (Valley, 2007). It appears clearly that the granite batholith has recorded a polyphased tectonic history. With depth, the strike of the main N-S sets remains roughly similar, however balance between the dominant dip orientation evolved (Figure 5). In GPK3 and GPK4, between 1420m to 2700m TVD (True Vertical Depth), the main fracture set dips to the east. In the middle part of the borehole sections, between 2700m to about 4800m TVD, the two conjugate sets are equally represented with fracture sets dipping westward and eastward. In the bottom part of the wells, below 4800m to 5000m TVD, the westward set is dominant (Figure 5).

Density

In the GPK3 and GPK4 wells, where we have a continuous fracture data set, the cumulative density of fracture has been computed along the well trajectories respectively. This density is a linear density along a subvertical sampling, whereas fractures are subvertical. The absolute values of density are then underestimated in relation with the real 3D density of fracture and are a minimum values. On the other hand, the relative values, and then the density variations, are significant. Nine sections with variable density values alternate with depth (Figure 6).

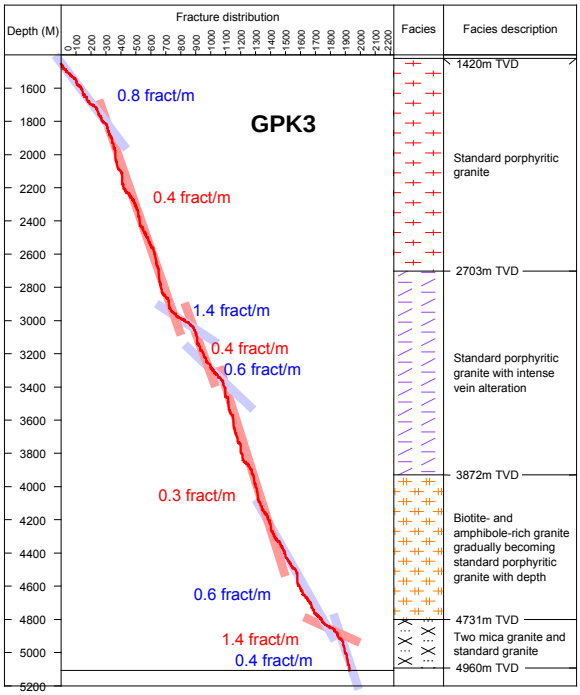

Figure 6 – Cumulative number of fracture with depth including all fracture types derived from borehole image analysis in the GPK3 well. Depth in the left column corresponds to the measured depth along the borehole, from the drilling floor. The depth boundary of the granite facies in the right column corresponds to the vertical depth, from the drilling floor.

In the GPK3 well, the high density value (0.8 fract./m) observed in the upper part of the granite is in agreement with the previous studies done at Soultz (Genter *et al.*,

1997). From 1800m to about 2900m, the fracture density is quite constant with a low density (0.4 fract./m). These two sections correspond in terms of petrography to the standard pophyritic granite (Hooijkaas *et al.*, 2006; Figure 6).

In the intermediate part of the well, two high fracture density zones (1.4 fract./m and 0.6 fract/m) surround a low density zone (0.4 fract./m). These three zones correspond to the upper part (between 2900m and 3300m MD) of the highly fractured and altered standard granite facies (Figure 6).

Below these zones, there are two low and moderate fracture density zones, which are embedded into the biotite and amphibole rich granite (Figure 6).

In the lower part of the well (from 4800m MD), a very high fracture density zone occurs. This zone corresponds to the boundary between two granite facies: the standard porphyritic granite and the two-mica granite. In this deep fine-grained facies, the fracture density is very low and decreases significantly to 0.4 fract./m (Figure 6).

In the neighbouring GPK4 well, a high density value (0.8 fract./m) occurs of the upper part of the granite, as in the GPK3 well. Between about 1800m and 1900m MD, the fracture density increases to 1.25 fract./m. Below 1900m and to about 2700m, the fracture density is quite constant with a low density (0.55 fract./m). These three sections correspond in terms of petrography to the standard porphyritic granite (Figure 7).

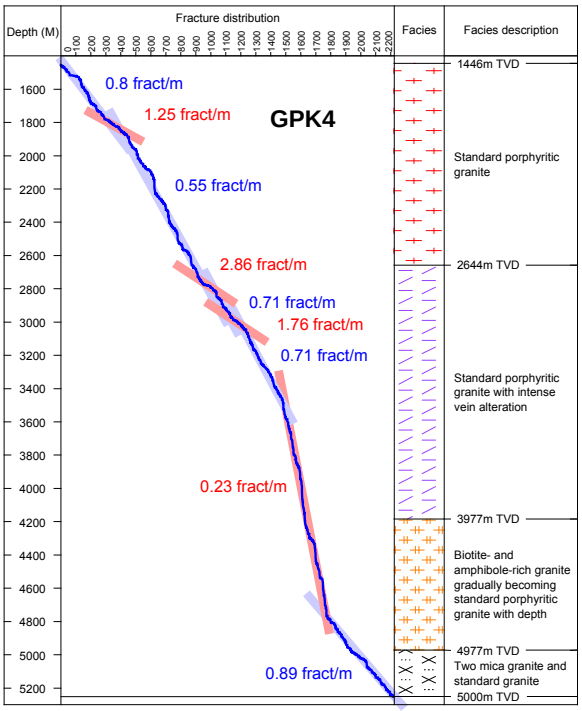

Figure 7 – Cumulative number of fracture with depth including all fracture types derived from borehole image analysis in the GPK4 well. Depth in the left column corresponds to the measured depth along the borehole, from the drilling floor. The depth boundary of the granite facies in the right column corresponds to the vertical depth, from the drilling floor.

In the intermediate part of the well, two very high fracture density zones (2.86 fract./m and 1.76 fract/m) alternate with two moderate density zones (0.71 fract./m). These four zones correspond to a highly fractured and altered standard porphyritic granite facies, between 2900m and 3500m MD (Figure 7).

Below these zones, between 3500m and 4750m MD, the fracture density is very low and quite constant with a value of 0.23 fract/m (Figure 7).

In the lower part of the well (from 4750m MD to the bottom well), a high fracture density zone (0.89 fract./m) occurs in the lower part of the biotite and amphibole rich granite facies and the two mica-granite (Figure 7).

FRACTURE ZONE NETWORK

Characterization of fracture zones

In the six wells of the Soultz site, we considered 39 fracture zones, which indicate some potential traces of fluid flow (Table 1, Figure 8). This list of fracture zone is probably not exhaustive and could be completed later by further data acquisition or processing.

Well	Name	Depth	Level	TVDss
EPS1	*EPS1-FZ1010*	*1012*	*3*	*836.637512*
EPS1	**EPS1-FZ1200**	**1198**	**1**	**1021.84821**
EPS1	EPS1-FZ1640	1643	2	1466.48914
EPS1	**EPS1-FZ2180**	**2179**	**1**	**1988.09058**
GPK1	*GPK1-FZ1015*	*1015*	*3*	*862.00885*
GPK1	**GPK1-FZ1220**	**1220**	**1**	**1066.59717**
GPK1	**GPK1-FZ1820**	**1820**	**1**	**1666.24219**
GPK1	GPK1-FZ2815	2815	2	2657.19238
GPK1	*GPK1-FZ3220*	*3223*	*3*	*3064.05273*
GPK1	GPK1-FZ3490	3492	2	3332.64502
GPK2	**GPK2-FZ2120**	**2123**	**1**	**1953.37292**
GPK2	*GPK2-FZ3240*	*3242*	*3*	*3069.90625*
GPK2	*GPK2-FZ3350*	*3347*	*3*	*3174.62988*
GPK2	*GPK2-FZ3515*	*3514*	*3*	*3341.70801*
GPK2	GPK2-FZ3900	3900	2	3726.61133
GPK2	GPK2-FZ4760	4760	2	4544.82227
GPK2	*GPK2-FZ4890*	*4890*	*3*	*4668.3252*
GPK2	GPK2-FZ5060	5060	2	4831.29248
GPK3	*GPK3-FZ1580*	*1579*	*3*	*1410.36487*
GPK3	*GPK3-FZ1640*	*1637*	*3*	*1468.78821*
GPK3	*GPK3-FZ1820*	*1820*	*3*	*1651.01147*
GPK3	*GPK3-FZ2040*	*2042*	*3*	*1873.30823*
GPK3	*GPK3-FZ2045*	*2046*	*3*	*1876.76367*
GPK3	*GPK3-FZ2090*	*2092*	*3*	*1923.16223*
GPK3	*GPK3-FZ2970*	*2970*	*2*	*2798.43579*
GPK3	GPK3-FZ3270	3271	2	3092.95361
GPK3	*GPK3-FZ4090*	*4089*	*3*	*3856.2417*
GPK3	**GPK3-FZ4770**	**4775**	**1**	**4538.90137**
GPK4	*GPK4-FZ1720*	*1723*	*3*	*1554.30212*
GPK4	*GPK4-FZ1800*	*1801*	*3*	*1632.22925*
GPK4	*GPK4-FZ2820*	*2817*	*3*	*2762.20264*
GPK4	*GPK4-FZ3940*	*3940*	*3*	*3603.97852*
GPK4	*GPK4-FZ4360*	*4361*	*2*	*3963.29565*
GPK4	*GPK4-FZ4620*	*4620*	*3*	*4195.97852*
GPK4	GPK4-FZ4710	4712	2	4279.59717
GPK4	*GPK4-FZ4970*	*4973*	*3*	*4530.36914*
GPK4	*GPK4-FZ5050*	*5012*	*3*	*4568.51904*
GPK4	*GPK4-FZ5100*	*5100*	*3*	*4655.44922*
4550	**4550-FZ1265**	**1265**	**1**	**1107.95679**

Table 1 - All fracture zones determined in this study. TVDss: True Vertical Depth Sub Sea. Depth: measured depth along the well. In bold, fracture zones of level 1; in normal, fracture zones in level 2; in italique, fracture zones in level 3.

The fracture zones have been classified within three levels in attempting to reflect their relative scale and importance as fluid flow paths. The first level (1 in the table 1) concerns the major fracture zones, which have been detected during drilling operations with important mud losses and then are permeable prior to any stimulation operations. The fracture zones of the second level (2 in the table 1) show flow indication higher than 20% of water losses during stimulation and/or are characterized by the other available geological data to include at least one thick

fracture accompanied with a significant halo of hydrothermal alteration. The last level (3 in the table 1) includes the fracture zones having a poorly developed alteration halo and a flow level below 20% of water losses during stimulation. This level indicates fracture zones of smaller size than those of the two other levels previously defined.

In the three wells EPS1, GPK1 and 4550 (a monitoring seismic well), a major fault zone intersects those wells within the Buntsandstein sediment at around 1200m (Table 1). This zone has been cored by the EPS1 well and where it forms a large structure containing 3 sub-zones and presenting fractures with quartz, galena and barite fillings. In the GPK1 and 4550 wells, total drilling mud losses have been occurred when drilling through this zone (Herbrich, 1988; Villeneuve and Weber, 1991). In the 4550 well, a BHTV log, is available and allows characterization the fracture zone. This presents a series of open steeply dipping fractures. However, the orientation value is not very precise due to the rather bad quality of the image log.

In the GPK1 well, another natural brine inflow occurred during the drilling at the depth of the large fracture zone at 1820m MD (Table 1; Herbrich, 1988). At this depth, a very high helium content anomaly was recorded (Vuataz *et al.*, 1990) and other drilling anomalies were reported. This fracture zone contains geodic quartz veins, visible in a core taken at this depth as well as illite (Genter, 1989).

Also in the upper part of the granite, in GPK2 well, a fracture zone provoking total drilling mud losses has been intersected and no cuttings have been collected below (Genter *et al.*, 1995). The fracture zone at 2120m MD shows a high altered zone with several open fractures (Table 1). The hydraulic testing of an open hole interval including this fracture zone showed that 95% of the flow rate was absorbed by this zone (Jung *et al.*, 1995). This zone is also believed to be responsible for a large-scale stress perturbation, as highlighted by the analysis of borehole failure (Valley, 2007).

At greater depths, there are no major fracture zones except at the bottom of the GPK3 well, within the open hole, there is a major fracture zone located around 4770m MD (Table 1). This zone includes several individual fractures with a cumulative apparent thickness of around 15m along the well. The K content increases in the hanging wall of the zone and decrease in the center part indicating a high alteration halo. Flow rate show a 70% outflow matching this zone (Dezayes *et al.*, 2004). Analysis of borehole failure showed that this zone is inducing a major stress perturbation (Valley, 2007). This is the major flow pathway in the geothermal reservoir at lower depth. GPK4 is the only well where there is no level 1 fracture zone (table 1). The description of the fracture zones is detailed in Dezayes and Genter, 2008).

The orientation of these fracture zones is based on borehole images as described above (Figure 8). Most of orientations of fracture zones have been determined according to the assumptions cited above. However, some of them are more difficult to estimate and are detailed in the following text. The orientation of the fracture zone in GPK3 at 3270m, which appears E-W striking (Figure 8D, table 1), is very imprecise. The image log quality is locally poor and no correct measure has been done. Moreover, in GPK2, some orientation of fracture zones could no been measured at all. This well was drilled in two times, in 1995 and 1999, and some problems occurred at 3900m, where the first drilling stopped. At that depth, it appears a large cave based on the caliper log (Genter *et al.*, 1999). Some altered cuttings coming from this zone have been recovered at the end of the drilling operation in 1995. After the deepening in 1999, as this large cave occurs in a significantly deviated part of the well, the UBI tool stuck and no image log has been run below that depth. Later, the borehole has been cased and now, the presence of a casing restriction is suspected due a partial casing collapse induced by the fracture zone. Using 3D visualization (Sausse *et al.*, 2009), we suspect that this fracture zone is the same that the one cross-cutting the bottom of GPK3 well (GPK3-FZ4770 in table 1). Thus, we assumed that this zone has the same orientation (Table 1). However, due to this GPK2 borehole wall restriction at 3900m, no logging tools could be run below this depth now. Below 3900m, only temperature and flow logs are available. Then, we have located three zones with outflow which match with altered zones based on cutting observation. These zones occur at 4760m with 20% of flow, 4890m with 17% of flow and 50% of flow below 4960m which could correspond to a fracture zone occurring at 5060m MD, based on cutting observation. As there are no oriented image logs in this section, we have assumed a generic orientation, which is realistic but not proven, N250°E-65° (N160°E-65°W), the dominant orientation of fractures in the deeper part of the Soultz granite (Figure 8C).

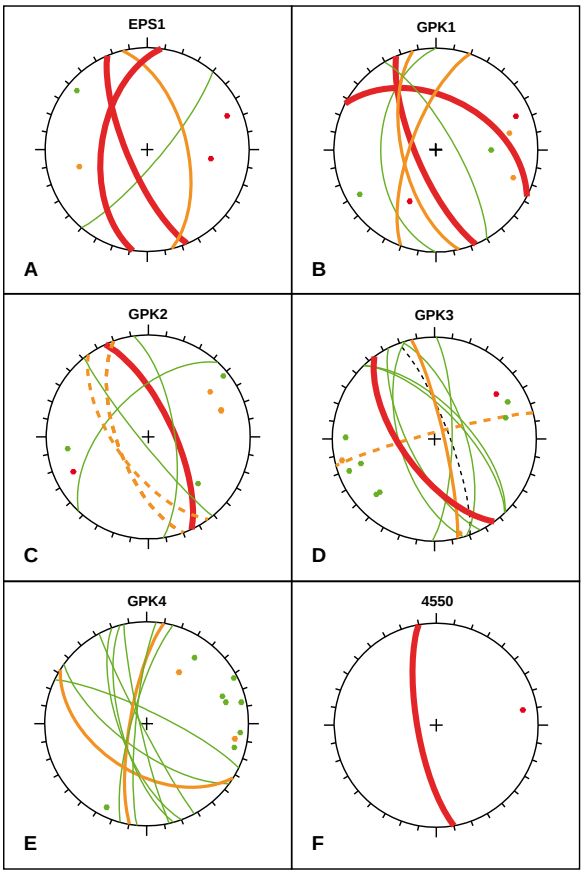

Figure 8 - Orientation of fracture zones in each Soultz well. Red lines and red dots: cyclographic traces and poles of fracture zones of level 1; orange lines and orange dots: cyclographic traces and poles of fracture zones of level 2 (dotted orange line: supposed orientation); green line and green dot: cyclographic trace and pole of fracture zones of level 3 (Schmidt's projection, lower hemisphere).

Organization of the fracture zones

Most of the fracture zones characterized in the framework of this study (Table 1) can be attributed to three main concentrations or clusters of fractures zones at about 1800-2000m, 3000-3400m and around 4500-5000m TVD (True Vertical Depth) (Figure 9). In that regard, the borehole GPK4 is somehow untypical, presenting less clearly clustered, steeply dipping fracture (Figure 9), while in the other wells, fracture zones more consistently correspond to these three fracture zone concentrations. This result was already mentioned previously in the upper part of the granite body, before the deepening of GPK2 and the drilling of GPK3 and GPK4 (Genter *et al.*, 1995; Genter and Castaing, 1997). These three clusters of fracture zones are considered to reflect major fault, equivalent to the fault detected in the sedimentary cover based on seismic reflection (Genter and Castaing, 1997). If we assume that these faults are steeply dipping structures with values higher than 60°, the raw spacing between to consecutive clusters of fracture zones is around 500 m, equivalent to the fault spacing in the sedimentary cover (Valley *et al.*, 2007).

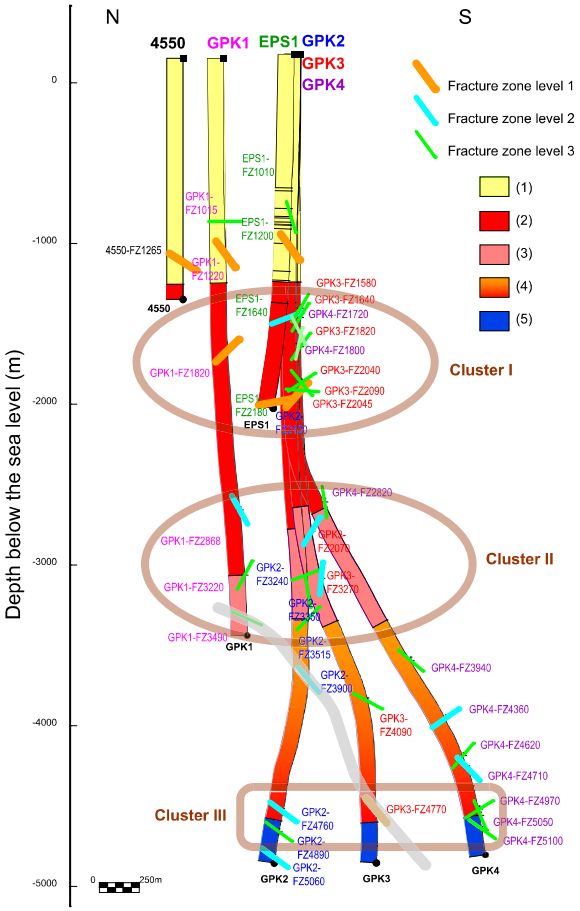

Figure 9 - Synthesis of the all fracture zones determined in this study along a N-S cross-section through the Soultz wells. (1) Sedimentary cover, (2) standard porphyritic granite, (3) Standard granite with intense vein alteration, (4) Biotite and amphibole rich granite gradually becoming standard granite with depth, (5) Two mica granite and biotite rich granite.

The upper cluster at 1800-2000m depth MD (Cluster I in Figure 9) is located in the unaltered porphyritic granite. This cluster includes major fracture zones qualified as level 1 with permeable zones. The cluster II does not include major level 1 faults. It is located within the fractured and altered granite zone (Figure 9). This granite facies is characterized by high pervasive alteration related to numerous meso-scale fractures present in this zone (Hooijkaas *et al.*, 2006). This facies contains high proportion of clay and hydrothermal minerals. Possibly, the high fracturing of this facies leads to a generally weaker rock mass where the strain is distributed in small increments over a dense network of smaller fractures, instead of being concentrated by a few major faults. This location corresponds to the upper reservoir stimulated in the first phase of the project in 1997 (Baumgärtner *et al.*, 1996). In this reservoir, a four months circulation loop test with tracer injection has been performed with success (Bruel, 2002). Then, it appears that there is a good fluid connection in this reservoir between GPK1 and GPK2. The lower cluster (Cluster III in the Figure 9) is close to the interface between the 2 granite units at 4700 m depth TVD. The deep facies is characterized by massive granite characterized by a low pervasive alteration degree. The cluster III contains major fracture zone as the GPK3-FZ4770. Thus, it appears that the deformation in this facies tends to be localized along major isolated fracture zones. This last cluster is located in the lower reservoir, which has been stimulated previously, and is currently a part of the deep geothermal loop under testing for the electrical production test. Conceptually, this reservoir appears to behave as a fractured reservoir embedded in a low permeable matrix.

Based on this characterization of fracture zones at borehole scale, these major planes have been compared with other fracture information derived from other detection methods in order to build a 3D model (Sausse *et al.*, 2009). These other methods are microseismicity data created within the reservoir during the stimulations of GPK2, GPK3 and GPK4 (Dorbath *et al.*, 2009) and a VSP (Vertical Seismic Profiling) investigation (Place *et al.*, 2009). Some of the fracture zones observed at the well scale match with microseismicity or VSP results. They correspond to fracture zones qualified by level 1 or 2 such as GPK1-FZ3490, GPK2-FZ3900 and GPK3-FZ4770, which match with microseismicity and VSP analysis. Moreover, the dip orientations of the fracture zones are very close and seem to define a large-scale fault intersecting the Soultz basement (Figure 9). This orientation of the major fracture zone is about N230°E-70° (N140°E-70°W).

In GPK1, two fracture zones at 1820m MD and 2860m MD appear to match with the VSP analysis (Place *et al.*, 2009; Sausse *et al.*, 2009).

In the lower part of the reservoir, two smaller fracture zones in GPK4 match geometrically with the microseismicity analysis at 4620m and 4970m MD (Sausse *et al.*, 2009). These fracture zones are N10°E striking, steeply dipping to the west (Figure 9).

FLOW PATTERN IN THE OPEN HOLE SECTIONS

Some of the fluid exit zones in the open holes correspond to fracture zones as the big ones in GPK3 at 4770m MD describe above. In this well, six other zones have been defined as fluid exit zone (Figure 10). They correspond to significant variations visible on the geophysical logs, but with lower amplitude. However, the occurrence of hydrothermal alteration associated with these fractures is not well constrained. Chemical fluid variations observed in the drilling mud do not always match with permeable zones (Figure 10). Moreover, the zone at 4670 m MD reveals the presence of tracers, but does not seem correspond to a fluid pathway during hydraulic testing (Sanjuan *et al.*, 2005).

Analysis of UBI data allows the determination of the orientation of open fractures located at the depth of the permeable zones observed from temperature and flow logs. The orientation and nature of the fracture zones vary in an important way. The most important zone at 4775 m MD, which takes 63% to 78% of fluid during the stimulation, is actually a cluster of fractures. The fractures within this cluster trend N160°E and most of them dip westward at an average angle of 52° (Figure 10).

The zone at 4875 m MD consists of four fractures, one of which appears thicker on the borehole images. The average orientation is N150°E-75°E. This zone takes 2% of the fluid during the stimulation tests. Chemical fluid variations and tracers observed from changes in the drilling mud indicate the presence of fractures bearing flow.

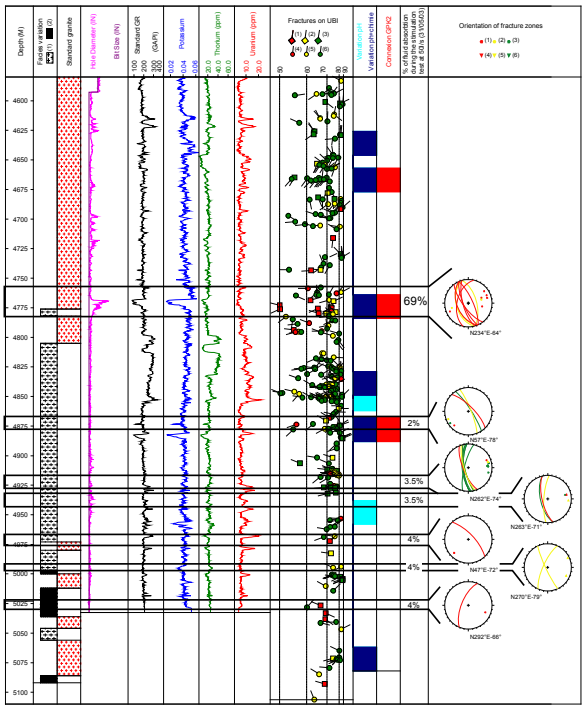

Figure 10 - Synthetic log of the open hole section of the GPK3 well showing characterization of the fluid exit fractures. Column 2: Facies variation log: (1) two mica granite, (2) biotite rich granite; Column 3: Standard granite: porphyritic MFK-rich granite; Column 9: Open fractures versus depth: grey density variation indicates the percentage of continuity of the fracture trace on UBI log: (1) 100%, (2) >50%, (3) <50%. The horizontal scale indicates the dip value of fractures. The direction of the tadpole indicated the dip direction of fractures (north is to the top, east to the right). Columns 10 and 11: Chemical fluid anomalies detected in the drilling mud flowing into and out of the drill hole.

The zone at 4920 m MD also consists of several fractures, with one being more prominent (Figure 10). This zone did not take any fluid during the last hydraulic test, which included injection at a rate of 50 l/s after two peaks at 90 l/s. The average orientation is N12°E-68°W (Figure 10). The zone at 4972 m MD shows a single open fracture without any alteration. The fracture is oriented N135°E-65°E and takes approximately 4% of the fluid during all of the hydraulic tests. A deeper zone at 5025 m MD also consists of a single fracture oriented N22°E-58°W (Figure 10). The fracture takes 10 to 15% of the total injection accepted by the wellbore during all the hydraulic tests.

Two zones, namely 4940 and 4990m MD, do not correspond to open fractures based on UBI image logs acquired shortly after the end of the drilling. However, these two zones appear to be hydraulically active under certain conditions. The zone at 4940 m MD accepted about 2-4% of the injected fluid at an injection rate of 25 and 30 l/s, but did not accept any fluid during injection at 50 l/s and after the 90 l/s period. The zone at 4990 m MD seems closed at the beginning of the stimulation (at an injection of 25 l/s), but later accepts 4% of the fluid flow. These zones may have initially been closed but later were re-opened during the hydraulic experiments.

In GPK4, as the flow logs have a bad quality, we based the determination of the fluid exit zones on the temperature analysis. We have located the temperature variation and characterize fractures matching depth on borehole images. Then, we have determined nine fluid exit zones Figure 11). As there are less data than in GPK3, the zones in GPK4 are less constrained and then we have attributed three degrees of fluid exit zones: certain, probable, and supposed (Figure 11). Three of them, ZA3, ZA5, and ZA7, have been included in the global fracture zone network.

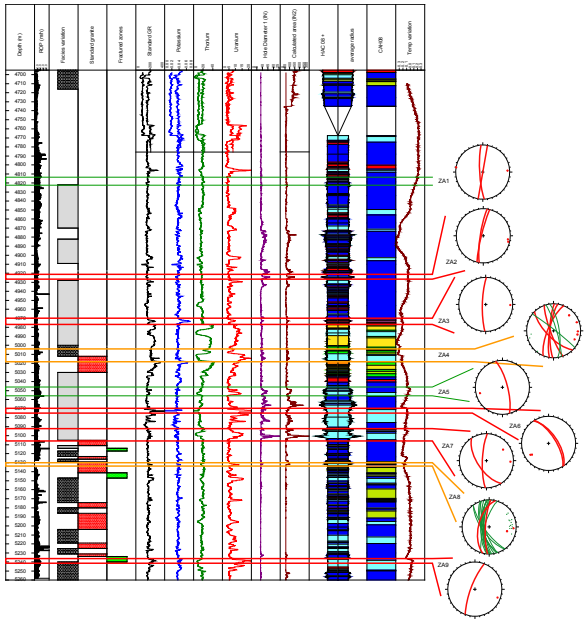

Figure 11 - Synthetic log of the open hole section of the GPK4 well showing characterization of the fluid exit fractures. Column 2: Rate of Penetration. Column 3: Facies variation log: (1) two mica granite, (2) biotite rich granite; Column 4: Standard granite: porphyritic MFK-rich granite; Column 5: Occurrence of minerals indicating fracture zones; Column 6: Standard Gamma ray; Column 7: Potassium content; Column 8: Thorium content; Column 9: Uranium content; Column 10: hole diameter; Column 11: hole area; Column 12-14: HAC; Column 15: temperature variation.

Five zones are described as “certainly” fluid exit zones at 4923m, 4973m, 5073m, 5100m and 5238m MD. At 4923m MD, two N-S high dipping fractures are associated with borehole cave and kind of breakout (Figure 11). A 4973m MD, one fracture, N-S with high dip too, is present with a 1m thick alteration halo in the both sides of the fracture.

This alteration is also indicated by a high potassium and uranium content (Figure 11). A series of NW-SE parallel fractures forms the zone at 5073m MD with a Gamma Ray anomaly. The potassium and thorium contents are very low whereas the uranium content is high (Figure 11). At 5100m MD, a brecciated zone is present with N-S and NNW-SSE borders. This zone is associated to a cave, observed on the calliper log, with low thorium content and high uranium content (Figure 11). The deeper zone at 5238m MD is a series of several NNE-SSW parallel fractures. This zone has been detected with the cuttings observation and presents a high uranium content (Figure 11).

The fluid exit zone "probable" qualified are located at 5010m and 5135m MD. The first one is a large zone 15m thick with lot of fractures. The average direction of these fractures is NNW-SSE with a high dip. This zone is characterized by a high uranium content (Figure 11). At 5135m MD, there are a series of fractures, but they are parallel with a NNW-SSE average direction (Figure 11).

Two other zones are qualified of "supposed". At 4822m MD, two N-S high dipping fractures are present but without Gamma Ray anomaly (Figure 11). A cave appears at 5050m MD associated with a high uranium content (Figure 11). At that depth, a N-S fracture exits associated with a kind of large breakout.

DISCUSSION

The average strike direction of fracture zones characterized in the granite is N160°E±15° (Figure 12). Two secondary sets are present with a N20°E±10° and N130°E±10° direction. The average dip is higher than 60° dominantly dip to the west (Figure 12). The orientation of meso-scale fractures measured in the granite on the borehole images and the cores shows a N175°E±30° direction with more fractures dip to the west (Figure 12).

If we compare the orientation of fracture zones with the meso-scale fractures, we can observe a clockwise rotation of 10-15° (Figure 12). However, in all the cases, the west dipping direction is dominating.

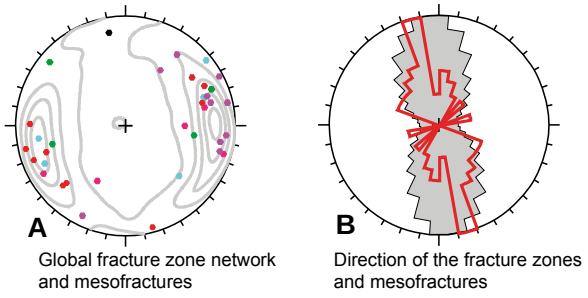

Figure 12 – Synthesis of the orientation of fracture at different scales in the Soultz granite. A- Poles of fracture zones from the different wells (Green: EPS1, pink: GPK1, blue: GPK2, red: GPK3, purple: GPK4, black: 4550) superimposed on frequency contouring diagram of the mesofractures observed in the all Soultz wells (in grey 7433 data). B- Rose diagram of the fracture zones in red (34 data) and mesofractures observed in the all Soultz wells in grey (7433 data). (Schmidt's projection, lower hemisphere, rose diagram: 10° class angle, contouring diagram: 10%, 30%, 50%, 70%, 90% of the maximum frequency).

The fluid exit zones determined in the open hole sections of GPK3 and GPK4 show nearly vertical fracture zones with a dominating N-S set dipping westward as well as a secondary NW-SE set dipping eastward (Figure 13) These orientations fit with a slightly clockwise rotation with the global orientation of the meso-fractures measured in the open hole sections (Figure 13). In this part of the granite, the main fracture set dips to the west.

In previous studies, these fracture zone concentrations were interpreted as the occurrence of large-scale normal fault zones related to the Rhine graben tectonics. However, the direction of the fracture zone, as the direction of meso-scale fractures, is slightly different than the major fault orientation observed in the sedimentary cover, which have a Rhenish direction of N20°E and which corresponds to the graben opening at Oligocene. The granite contains numerous fracture orientations related to Hercynian and Alpine tectonics. It seems that the N160°E is an inherited direction, which has been reactivated during the graben tectonic. Thus, the main fracture zone orientation is rather different than those newly created in the sedimentary cover during Cenozoic.

Moreover, the average direction of the fracture zones is rather consistent with the present-day stress field with σ_H N169°E±14° (Klee and Rummel, 1993; Valley and Evans, 2007). Some fracture zones which show flow anomalies or shearing indications appear as small fractures on the borehole image logs. This seems to indicate that critically oriented fractures relatively to the stress state orientation could shear during hydraulic stimulation (Evans, 2005).

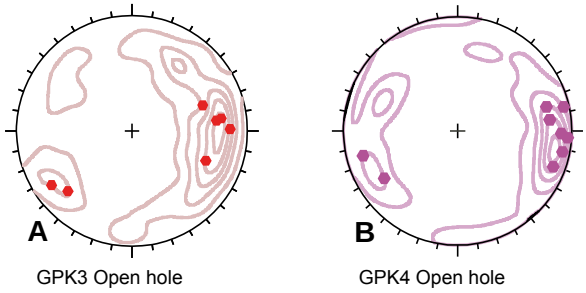

Figure 13 - A- Poles of the fluid exit zones superimposed on the frequency diagram of mesofractures (349 data) in the open hole of GPK3. B- Poles of the fluid exit zones superimposed on the frequency diagram of mesofractures (349 data) in the open hole of GPK4. (Schmidt's projection, lower hemisphere, rose diagram: 10° class angle, contouring diagram: 10%, 30%, 50%, 70%, 90% of the maximum frequency).

CONCLUSIONS

Characterization of the fracture at different scales was achieved along the Soultz wells based on direct (cores, cuttings) and indirect (borehole images, geophysical logs, flow logs, temperature logs) methods. Among the thousand of fractures detected and measured, we have highlighted a set of 39 fracture zones intersecting the five boreholes of the geothermal site as well as a peripheral well. This list is not extensive and could be completed by further data acquisition or processing. In the open hole sections of GPK3 and GPK4, 7 and 9 fluid exit zones respectively have been determined and characterized. In GPK2 some exit zones have been detected but no image logs are available for doing a geometrical characterization.

In previous study, these fracture zone concentrations were interpreted as the occurrence of large-scale normal fault zones related to the Rhine graben tectonics (Figure 14). However, the direction of the fracture zone is slightly different than the major fault orientation observed in the sedimentary cover, which have a Rhenish direction of N20°E and which corresponds to the graben formation at Oligocene. The granite contents numerous fracture directions related to Hercynian and Alpine tectonics. It seems that the N160°E is an inherited direction, which has been reactivated during the graben tectonic. Then, the main fracture zone orientation is rather different than those purely created in the sedimentary cover during Tertiary. Only a 3D large-scale geometrical model could be build to highlight the relationship between the major faults in the sedimentary cover and the fracture zone clusters. This is an on-going work based on exhaustive geological database (Castera *et al.*, 2008; Sausse *et al.*, 2008).

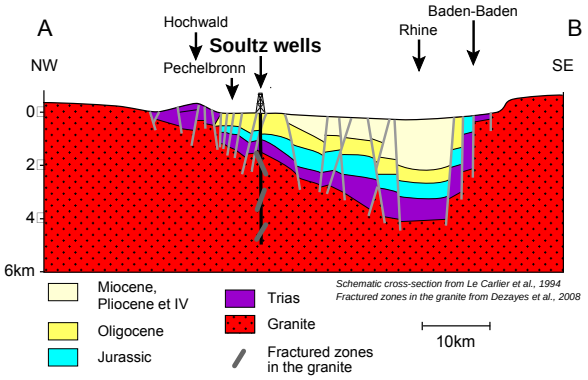

Figure 14 - Schematic NW-SE cross-section (from Le Carlier et al., 1994) and location of the three fracture zone clusters in the Soultz well, represented with an average orientation.

Knowledge and in situ characterization of fracture zone along the well have to be taken into account for a better understanding of the life time of the geothermal reservoir during early stages of hydraulic or chemical stimulations followed by long-term hydraulic circulations. Due to such hydraulic tests, different thermo-hydro-mechanical and chemical processes occur at depth in the reservoir and could modify fluid pathways. In the vicinity of the re-injection well GPK3, dominating mechanisms will be a general cooling of the fractured rock mass associated with forced fluid flow provoking thermo-mechanical stresses mainly. Temperature reduction could also generate some chemical effects inducing mineral dissolution or precipation and thus strongly modify the fluid pathway during circulation. Close to the production wells GPK2 and GPK4, the pumping due to submersible pumps could also induce some hydromechanical processes in the fractured rock mass. All these complex thermo-hydro-mechanical coupling will interact with the major fracture zone system and have to be seriously investigated by modeling for the reservoir life time (temperature drawdown, microseismicity risk, reservoir clogging). The fracture zone dataset studied in this paper could be used for modeling the thermo-hydraulic mechanical behavior of the deep geothermal granite reservoir submitted to hydraulic or chemical stimulations and hydraulic circulations (Rachez and Gentier, 2008).

ACKNOWLEDGEMENTS

This work has been carried under financial support of the ADEME, French Energy Agency, and the BRGM (EGS3D project). EHDRA working group 6 and 7 teams are kindly thank for their contributions and the fruitful discussion.

REFERENCES

Baujard C. and Bruel D. (2005). Recent results on the impact of fluid density on the pressure distribution and stimulated area in the reservoir using a finite volume numerical code. Proceedings of the EHDRA scientific conference 14-18 March 2005, Soultz-sous-Forêts, France.

Baumgärtner J., Jung R., Gérard A., Baria R., Garnish J., (1996). The European HDR project at Soultz-sous-Forêts: stimulation of the second deep well and first circulation experiments. Twenty-first Workshop Geothermal Reservoir Engineering, Stanford University, Stanford, California, USA, 267-274.

Baumgärtner, J., Hettkamp T; Teza D., Baria R; and Michelet S. (2004). Building of a Hot Dry Rock scientific power plant at Soultz-sous-Forêts. Geothermal Resources Council Transactions, Vol. 28, 201-206.

Bruel, D., (2002). Impact of induced thermal stress during circulation tests in an engineered fractured geothermal reservoir. Oil & Gas Science and Technology, Revue IFP, 57, no. 5, 459-470.

Castera J., Dezayes Ch., Calcagno Ph., (2008). Large-scale 3D geological model around the Soultz site, Proceedings of the EHDRA scientific conference 24-25 September 2008, Soultz-sous-Forêts, France.

Cocherie A., Guerrot C., Fanning C.M., Genter A., (2004). Datation U-Pb des deux faciès du granite de Soultz (Fossé Rhénan, France). Comptes Rendus Geoscience, 336, 775-787.

Cuenot N., Charléty J., Dorbath L., Haessler H., (2006). Faulting mechanisms and stress regime at the European HDR site of Soultz-sous-Forêts, France, Geothermics, Vol. 35, No. 5-6, 561-575.

Dezayes Ch., Villemin Th., Genter A., Traineau H., Angelier J., (1995). Analysis of fractures in boreholes of the Hot Dry Rock project at Soultz-sous-Forêts (Rhine Graben, France). Scientific Drilling, vol. 5, 31-41.

Dezayes Ch., Villemin Th., Pêcher A., (2000). Microfracture pattern compared to core scale fractures in the borehole of Soultz-sous-Forêts granite, Rhine graben, France. Journal of Structural Geology, 22, 723-733.

Dezayes Ch., Genter A., Gentier S., (2004). Fracture network of the EGS Geothermal Reservoir at Soultz-sous-Forêts (Rhine Graben, France). Geothermal Resources Council Transactions, Palm Springs, California, USA, Vol. 28, 213-218.

Dezayes Ch., Valley B., Maqua E., Syren G., Genter A., (2005). Natural fracture system of the Soultz granite based on UBI data in the GPK3 and GPK4 wells. EHDRA Scientific Conference, Proceedings of the EHDRA scientific conference 17-18 March 2005, Soultz-sous-Forêts, France.

Dezayes Ch., Genter A., (2008). Large-scale fracture network based on Soultz borehole data. EHDRA Scientific Conference, Proceedings of the EHDRA scientific conference 24-25 September 2008, Soultz-sous-Forêts, France.

Dorbath L., Cuenot N., Genter A., Frogneux M., (2009). Seismic response of the fractured and faulted granite to massive water injection at 5 km depth at Soultz-sous-Forêts (France), Geophysical International Journal, doi: 10.1111/j.1365-246X.2009.04030.x

Evans K.F., (2000). The effect of the 1993 stimulations of well GPK1 at Soultz on the surrounding rock mass: evidence for the existence of a connected network of permeable fractures. World Geothermal Congress 2000, Kyushu - Tohoku, Japan.

Evans K.F., (2005). Permeability creation and damage due to massive fluid injections into granite at 3.5 km at Soultz: Part 2 - Critical stress and fracture strength, Journal of Geophysical Research, 110, B04204, 14 pp.

Evans K.F., Genter A., Sausse J., (2005). Permeability creation and damage due to massive fluid injections into granite at 3.5 km at Soultz: Part 1 - Borehole observations, Journal of Geophysical Research, 110, B04203, 19 pp.

Foehn J.P., (1985). Interprétation des campagnes sismiques 1981 et 1984, concession de Péchelbronn, permis de Haguenau. Total Exploration internal report, October 1985.

Genter A., (1989). Géothermie Roches Chaudes Sèches : le granite de Soultz-sous-Forêts (Bas Rhin, France). Fracturation naturelle, altérations hydrothermales et interaction eau - roche. PhD thesis, Université d'Orléans, France, 201 pp.

Genter A., Traineau H., Dezayes Ch., Elsass P., Ledésert B., Meunier A., Villemin Th., (1995). Fracture analysis and reservoir characterization of the granitic basement in the HDR Soultz project (France). Geothermal Science & Technology, vol. 4 (3), 189-214.

Genter A., Castaing C., Dezayes Ch., Tenzer H., Traineau H., Villemin Th., (1997). Comparative analysis of direct (core) and indirect (borehole imaging tools) collection of fracture data in the Hot Dry Rock Soultz reservoir (France), Journal of Geophysical Research, vol. 102, B7, 15419-15431.

Genter A., Castaing Ch., (1997). Effets d'échelle dans la fracturation des granites; Scale effects in the fracturing of granite. Comptes Rendus de l'Académie des Sciences, Serie II. Sciences de la Terre et des Planètes 325(6): 439-445.

Genter A., Homeier G., Chèvremont Ph., Tenzer H., (1999). Deepening of GPK-2 HDR borehole, 3880-5090 m (Soultz-sous-Forêts, France). Geological monitoring. Open file report BRGM/RR-40685-FR, 81 pp.

Genter A., Traineau H., Bourgine B., Ledésert B., Gentier S., (2000). Over 10 years of geological investigations within the European Soultz HDR project, France. Proceedings of the World Geothermal Congress 2000, Kyushu-Tohoku, Japan, May 28 - June 10, 2000, Full length paper on Cd-Rom, Editors E. Iglesias, D. Blackwell, T. Hunt, J. Lund, S. Tamanyu, 3707-3712.

Genter A., Cuenot N., Dezayes Ch., Sausse J., Valley B., Baumgartner J., Fritsch D., (2007). How a better characterization of a deep crystalline reservoir can contribute to improve EGS performance at Soultz, First European Geothermal Review, Geothermal Energy for Electric Power Production, October 29-31, 2007, Mainz, Rhineland Palatinate, Germany, Abstracts and Papers, 34-40.

Gérard A., Menjoz A., Schwoerer P., (1984), L'anomalie thermique de Soultz-sous-Forêts, Géothermie Actualités, n°3, 35-42.

Gérard A., Kappelmeyer O., (1987). The Soultz-sous-Forêts project: Proceedings of the first EEC/US workshop on geothermal Hot dry Rocks Technology, Geothermics, Special issue, 393-399.

Gérard A., Genter A., Kohl T., Lutz Ph., Rose P., Rummel F., (2006). The deep EGS (Enhanced Geothermal System) project at Soultz-sous-Forêts (Alsace, France). Geothermics, Vol. 35, No. 5-6, 473-483.

Herbrich B., (1988). Forage géothermiques de Soultz-sous-Forêts (GPK1). Rapport de fin de sondage. Rapport CFG n° 88 CFG 03, Janvier 1988.

Hooijkaas G.R., Genter A., Dezayes Ch., (2006). Deep-seated geology of the granite intrusions at the Soultz EGS site based on data from 5 km-deep boreholes, Geothermics, Vol. 35, No. 5-6, 484-506.

Illies H., (1972). The Rhine graben rift system - plate tectonic and transform faulting. Geophysical Survey, 1, 27-60.

Illies J.H., (1975). Recent and paleo-intraplate tectonics in stable Europe and the Rhinegraben rift system. Tectonophysics, 29, 251-264.

Jung R., Reich W., Engelking U., Hettkamp T., Weidler R., (1995). Hydraulic tests in1995 at the HDR Project, Soultz-sous-Forêts, France, Field Report, Bundesanstalt für Geowissenschaften und Rohstoffe (BGR), Hannover, Germany.

Klee G., Rummel F., (1993). Hydrofrac stress data for the European HDR research project test site Soultz-sous-Forêts. International Journal of Rock Mechanics and Mining Sciences & Geomechanics Abstracts 30(7): 973-976.

Kohl T. and Megel T. (2005). Numerical modelling of hydraulic stimulations at Soultz-sous-Forêts. Proceedings of the EHDRA scientific conference 17-18 March 2005, Soultz-sous-Forêts, France.

Le Carlier C., Royer J. J., Flores E. L. (1994). Convective heat transfer at Soultz-sous-Forêts geothermal site: implications for oil potential. *First Break*, **12**, 11, 553-560.

Ménillet F. et al. (1989). Carte géologique de Lembach à 1/50 000. Feuille n°168, Edition du BRGM.

Place J., Diraison M., Naville Ch., Geraud Y., Schaming M., Dezayes Ch., (2009). Decoupling of deformation in the Upper Rhine Graben sediments seen by seismic reflection and coupled analysis of diffraction on 3-component Vertical Seismic Profiling (Soultz-sous-Forêts area). *Geosciences*, accepted.

Rachez X., Gentier S., Blaisonneau A. (2006). Hydro-mechanical behaviour of GPK3 and GPK4 during the hydraulic stimulation tests – Influence of the stress field. Proceedings of the EHDRA scientific conference, Soultz-sous-Forêts, France.

Rachez X. and Gentier S. (2008). BRGM modeling activities performed at the Soultz EGS reservoir. Proceedings of the EHDRA scientific conference 24-25 September 2008, Soultz-sous-Forêts, France.

Renard Ph., Courrioux G., (1994). Three-dimensional geometric modelling of faulted domain: The Soultz horst example (Alsace, France). Computers & Geosciences, Vol. 20 (No. 9), 1379-1390.

Rotstein Y., Edel J. B., Gabriel G., Boulanger D., Schaming M., Munschy M., (2006). Insight into the structure of the Upper Rhine Graben and its basement from a new compilation of Bouguer Gravity, Tectonophysics, 425 (1-4), 55-70.

Sanjuan B., Rose P., Gérard A., Brach M., Braibant G., Foucher J.-C., Gauthier A., Touzelet S. (2005). Tracer testing using Naphthalene disulfonate componds during the stimulation operations carried out in the GPK2, GPK3 and GPK4 wells between 2003 and 2004 at Soultz-sous-Forêts (France). Proceedings of the EHDRA scientific conference 17-18 March 2005, Soultz-sous-Forêts, France.

Sanjuan B., Pinault J-L, Rose P., Gérard A., Brach M., Braibant G., Crouzet C., Foucher J-C, Gautier A., Touzelet S., (2006). Tracer testing of the geothermal heat exchanger at Soultz-sous-Forêts (France) between 2000 and 2005, Geothermics, Vol. 35, No. 5-6, 622-653.

Sausse J., Dezayes Ch., Dorbath L., Genter A., Place J., (2009). 3D fracture zone network at Soultz based on geological data, Image logs, microseismic events and VSP results, *Geosciences*, accepted.

Schill E. and Geiermann J. (2009). Identification of EGS resources in the Upper Rhine valley by magnetotellruic methods. *Geosciences*. Soumis

Stussi J.-M., Cheilletz J.M., Royer J.J., Chèvremont P., Féraud G., (2002). The hidden monzogranite of Soultz-sous-Forêts (Rhine Graben, France). Mineralogy, petrology and genesis, Géologie de la France, 1, 45-64.

Tenzer, H., Mastin, L. & Heinemann, B. (1991). Determination of planar discontinuities and borehole geometry in the crystalline rock of borehole GPK1 at Soultz-sous-Forêts. Geotherm. Sci. & Tech. 3(1-4), 31-67.

Valley B., (2007). The relation between natural fracturing and stress heterogeneities in deep-seated crystalline rocks at Soultz-sous-Forêts (France), PhD thesis, ETH-Zürich, Switzerland, http://e-collection.ethbib.ethz.ch/view/eth:30407, 260 pp.

Valley B., Dezayes Ch., Genter A., (2007). Multi-scale fracturing in the Soultz-sous-Forêts basement from borehole image analyses. Proceedings EHDRA Scientific Conference, 28 & 29 June 2007, Soultz-sous-Forêts, France, 14 pp.

Valley B., Evans K.F., (2007). Stress state at Soultz-sous-Forêts to 5 km depth from wellbore failure and hydraulic observations. Thirty-Second Workshop on Geothermal Reservoir Engineering Stanford University, Stanford, California, USA, January 28-30, 2008, SGP-TR-183, 329-338.

Villemin Th., Bergerat F., (1987). L'évolution structurale du fossé rhénan au cours du Cénozoïque : un bilan de la déformation et des effets thermiques de l'extension. Bull. Soc. Géol. France,, III, 2, 245-255

Villeneuve B., Weber R., (1991). Forages pour observations sismiques de Soultz-sous-Forêts. Rapport de fin de forages. BRGM-CCE.

Vuataz F.-D., Brach M., Criaud A., Fouillac Ch., (1990). Geochemical monitoring of drilling fluids: a powerful tool to forecast and detect formation waters. SPE, Formation Evaluation, June 1990, 177-184.

Ziegler P., (1992). European Cenozoic rift system. Tectonophysics, 2008, 91-111.

Stress Heterogeneity in the Granite of the Soultz EGS Reservoir Inferred from Analysis of Wellbore Failure

Benoît Valley[1,2] & Keith Evans[1]

1) Engineering geology, ETH Zürich, Switzerland
2) MIRARCO/Laurentian University, 935 Ramsey Lake Road, Sudbury, ON P3E 2C6, CANADA

Submitted to the World Geothermal Conference at Bali on 25-29 April 2010.

Proceedings World Geothermal Congress 2010
Bali, Indonesia, 25-29 April 2010

Stress Heterogeneity in the Granite of the Soultz EGS Reservoir Inferred from Analysis of Wellbore Failure

Benoît Valley*,** and Keith F. Evans*

* Engineering Geology, Swiss Federal Institute of Technology (ETH), CH-8092 Zürich, Switzerland; **now: MIRARCO Mining Innovation/Laurentian University, 935 Ramsey Lake Road, Sudbury, ON P3E 2C6, CANADA
bvalley@mirarco.org, keith.evans@ethz.ch

Keywords: Borehole failure, Stress characterisation, Stress heterogeneities, Rhine Graben, Enhanced Geothermal System, Soultz-sous-Forêt

ABSTRACT

Stress heterogeneity is thought to play an important role in many aspects of crustal mechanics, including the influencing of the space-time distribution and scaling of earthquakes. As such, it is likely to have some influence on the reaction of rock masses to massive fluid injection such as at EGS sites. Unfortunately, too little is known about the magnitudes of spatial variations of stress in the crust, primarily because heterogeneity is so difficult to measure. In this paper we describe variations in stress orientation indicated by wellbore failure in two boreholes of the Soultz-sous-Forêts EGS site and attempt to explain them. A novel feature of these data is that the holes are separated by only 20 m between 1400 m and 2400 m where DITFs cover 55% of the borehole lengths, thus allowing the lateral coherence of the variations to be examined.

The variations are seen to occur at all scales, from relatively abrupt changes over a couple of metres, to gradual variations over scales of several hundred metres. Deviations in SHmax orientation from the mean in excess of 90° occasionally occur. The variations follow a power law scaling with an index close to -2.0, indicating self-affine behaviour where variations appear progressively "rougher" at shorter scales. Two large long-wavelength (>100 m) variations seen at 2.0 and 4.7 km correlate with the two most prominent fracture zones penetrated by the wells. The lowermost stress perturbation extends over several hundred metres and is characterised by SHmax rotations of up to 90° and changes in the mode of failure from compression (breakouts) to tension (DITFs). The uppermost stress perturbation occurs where the wells are separated by only 20 m, and is only partly correlated between wells, indicating high spatial gradients in stress about the perturbing fracture zone. Short wavelength variations in orientation occur more or less continuously and are usually associated with natural fractures. Little coherence is seen for short-wavelength variations between wells. Almost all fractures associated with stress perturbations are "critically stressed" under the linear stress characterisation of the site. E-DITFs are often seen to form parallel to natural fractures, which typically dip at 50 – 70°. The parallel geometry suggests partial relaxation of shear stress from near critical level on the associated natural fractures.

1. INTRODUCTION

Analysis of stress induced wellbore failure is a powerful tool to characterise the state of stress (e.g. Bell and Gough, 1979; Zoback et al., 2003). In rocks without strong strength anisotropy, the failure is controlled by the variation in tangent stress that develops around the wellbore circumference when the maximum stresses in the plane normal to the wellbore are not equal. Failure may be compressional where the tangent stresses reach a maximum, producing breakouts, or tensile where they reach a minimum, giving rise to so-called drilling-induced tension fractures (hereafter referred to as DITFs). Wellbore failure occurs in the 5 km deep wells at Soultz-sous-Forêts (see Figure 1 for location), with DITFs dominating above 3 km and breakouts below 3.5 km. The data have been analysed by Valley and Evans (2007) to obtain the linear depth trends of the attributes of the stress tensor at Soultz, as needed for site stress characterisation. That study ignored the small and medium scale deviations from the large-scale trends. Such perturbations are commonly called stress heterogeneities, and they are believed to play a significant role in earthquake complexity (e.g. Shaw, 2004; Zöller et al., 2005), faulting mechanism (e.g. Faulkner et al., 2006), errors in the stress estimates obtained from inversion of earthquake focal mechanism (e.g. Cornet and Jianmin, 1995; Cuenot et al., 2006; Scotti and Cornet, 1994) and reservoir stimulation (e.g. Cornet et al., 1992).

Despite their perceived importance, stress heterogeneities are difficult to reliably identify, let alone quantify. Stress-induced wellbore failure in deep holes offers perhaps the best opportunity to study the spatial variability of stress. In this paper we present results of an analysis of deviations for the linear stress trends in the Soultz wells to 5 km as expressed through the breakouts and DITFs. A novel aspect of the data is that the two wells that serve as the data source are separated by only 15–30 m over the depth range 1.5–2.5 km. Thus, the lateral variation of the stress perturbations as well as the vertical can be examined. Possible stress perturbing mechanisms which may explain these variations are discussed.

2. BACKGROUND

The effect of gravity is such that stress magnitudes usually increase with depth. Commonly, the increase at a particular locality is seen to be reasonably well approximated by linear trends for the magnitude of the two horizontal and the vertical principal stresses, the latter being equal to the integrated overburden, and a constant orientation for the horizontal principal stresses. This description is referred to as the linear stress characterisation of a site. Valley (2007) has presented a linear characterisation for the Soultz-sous-Forêts geothermal site. In this paper, stress variations or perturbations shall be taken to mean deviations in stress from this simple linear description.

There is good reason to believe that stress variations should occur on all scales The perturbation of stress around faults that slip in earthquakes is demonstrated by the success of the Coulomb stress concept in predicting aftershock distributions (Harris, 1998). This perturbation occurs on scales of the order of the length of slip, and so, since earthquakes occur on all scales, perturbations of stress can

be expected on all scales. However, the magnitude of the variations in stress that can build up as a consequence of the repeated action of stress-perturbing mechanisms is tempered by the limited strength of the fractured and faulted crust. For example, a stress perturbation generated by slip on a fault can be partly relaxed by post-seismic slip on secondary fractures and faults, of which aftershocks are a manifestation. Thus, the processes at work are complicated, and our understanding of the degree of stress variability that typically prevails within the crust (if one can generalise), is poor.

The limited state of knowledge has important implications for the development of EGS projects, because it bears on the issue of whether the state of stress at a prospective EGS site will be essentially the same as at a site say ten kilometres distant where stress has been characterised. In this regard it is important to note that the approximately N–S mean orientation of maximal horizontal principal stress at Soultz is significantly different to the regional orientation of NW–SE. It is thus relevant to quantify the deviations in the state of stress from the simple linear characterisation, and understand their origin. Another implication is related to the modelling and prediction of stimulation processes. Indeed, one basic input for most if not all numerical simulations of reservoirs is the initial state of stress. The uniform state of stress provided by the linear site characterisation reflects only partially the actual in-situ conditions. The introduction of stress heterogeneities into the initial stress conditions of the models would bring the simulations closer to reality and thus may give some improvement of the quality of the model predictions. This is particularly true for models that seek to simulate induced micro-earthquake frequency-moment distributions.

3. PRESENTATION OF THE DATA

The data analysed in this study stem from two of the three deep boreholes drilled to 5km in granite at the Soultz-sous-Forêts geothermal project site where the granite top lies at 1400 m (Figure 1). The main sources of information are UBI (ultrasonic borehole imager) images collected in these boreholes.

The UBI data were acquired in two holes GPK3 and GPK4 which were drilled from the same pad. Both are sub-vertical in the upper 2–3 km, and penetrate granite at 1.4 km, which means their separation in the uppermost kilometre of granite to 2.4 km is less than 20 m (Figure 2b). Below 2.5 km, the wells deviate from vertical to build up separation before returning to sub-vertical in the lowermost 500 m (Figure 2a). The granite sections in both wells were drilled with a 12-1/4 inch bit to 4514 m TVD (GPK3) and 4489 m TVD (GPK4), and then with 8-1/2 inch to total depth. The UBI logs in each well were run after completing each section, about a month apart. The wells were drilled one year apart. The same UBI sonde was used for both sections of each well but different sondes were used for each well.

Wellbore failure was identified from both the travel-time (i.e. borehole geometry) and acoustic reflectivity images. Breakouts are typically manifest as pairs of diametrically-opposite spall zones that extend along the borehole axis. They occur where the maximum tangent stress acting at the borehole wall exceeds the compressive strength of the rock. In the simple case of a vertical borehole penetrating a rock mass in which one principal stress is vertical, this maximum occurs in the direction of the minimum horizontal principal stress, Shmin (Bell and Gough, 1979).

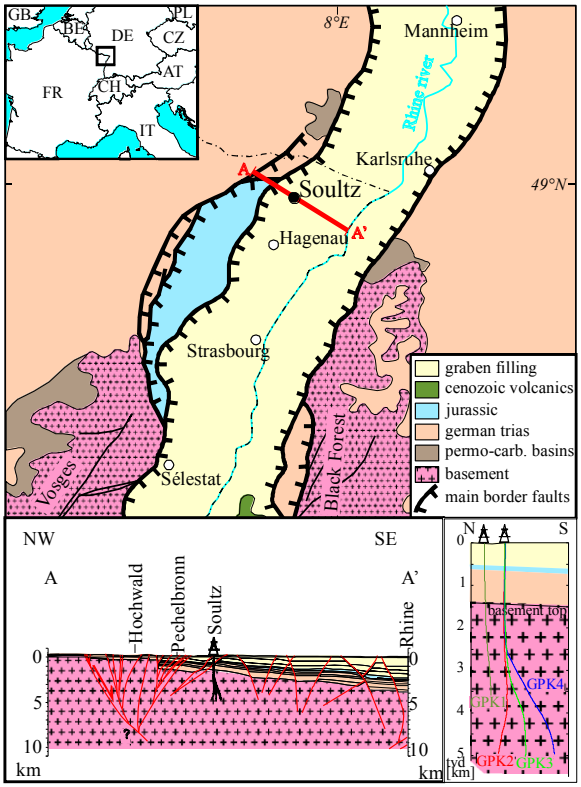

Figure 1: Soultz-sous-Forêts is located within the Upper Rhine Graben in north-eastern France. The Upper Rhine Graben is a Cenozoic structure part of the West European Rift System. The Soultz wells penetrate about 1.4 km of Cenozoic and Mesosoic sediments before entering the granitic basement rocks.

DITFs are identified primarily on acoustic reflectivity images where they show as thin, often ragged fracture traces that may be either axial or en-echelon. DITFs seen on UBI images from the 3.6 km deep well GPK1 do not show on Azimuthal Resistivity Imager (ARI) logs, indicating they do no penetrate deeply. DITFs occur when the tangent stress at the borehole wall becomes sufficiently tensile to produce tensile failure. Although, in principle, the minimum tangent stress produced by far-field stresses can be tensile, it is usually the cooling stress component arising from the circulation of cool drilling fluids that is decisive in driving the minimum tangent stress to negative values and producing tensile fracturing. However, the cooling stress is axi-symmetric, and so the location of the tensile fracture is governed by the far-field principal stress orientations. In the case of a vertical borehole penetrating a medium in which one principal stress is also vertical, the least compressive tangent stress at the borehole wall is horizontal and occurs in the direction of SHmax. This results in a pair of diametrically-opposite DITFs, which hereafter are denoted by A-DITFs. However, if the borehole axis is not aligned with a principal axis and the criterion for tensile failure is met, the least compressive tangent stress at the borehole wall will in general be inclined to the borehole circumference. In this case, tensile failure will occur as a stack of slightly-overlapping en-echelon tensile fractures, which hereafter are denoted by E-DITFs. The relationship between the induced fracture geometry and the in-situ stress attributes (i.e. orientations and magnitudes) in this case is not as simple as in the aligned case (e.g. Peška and Zoback, 1995).

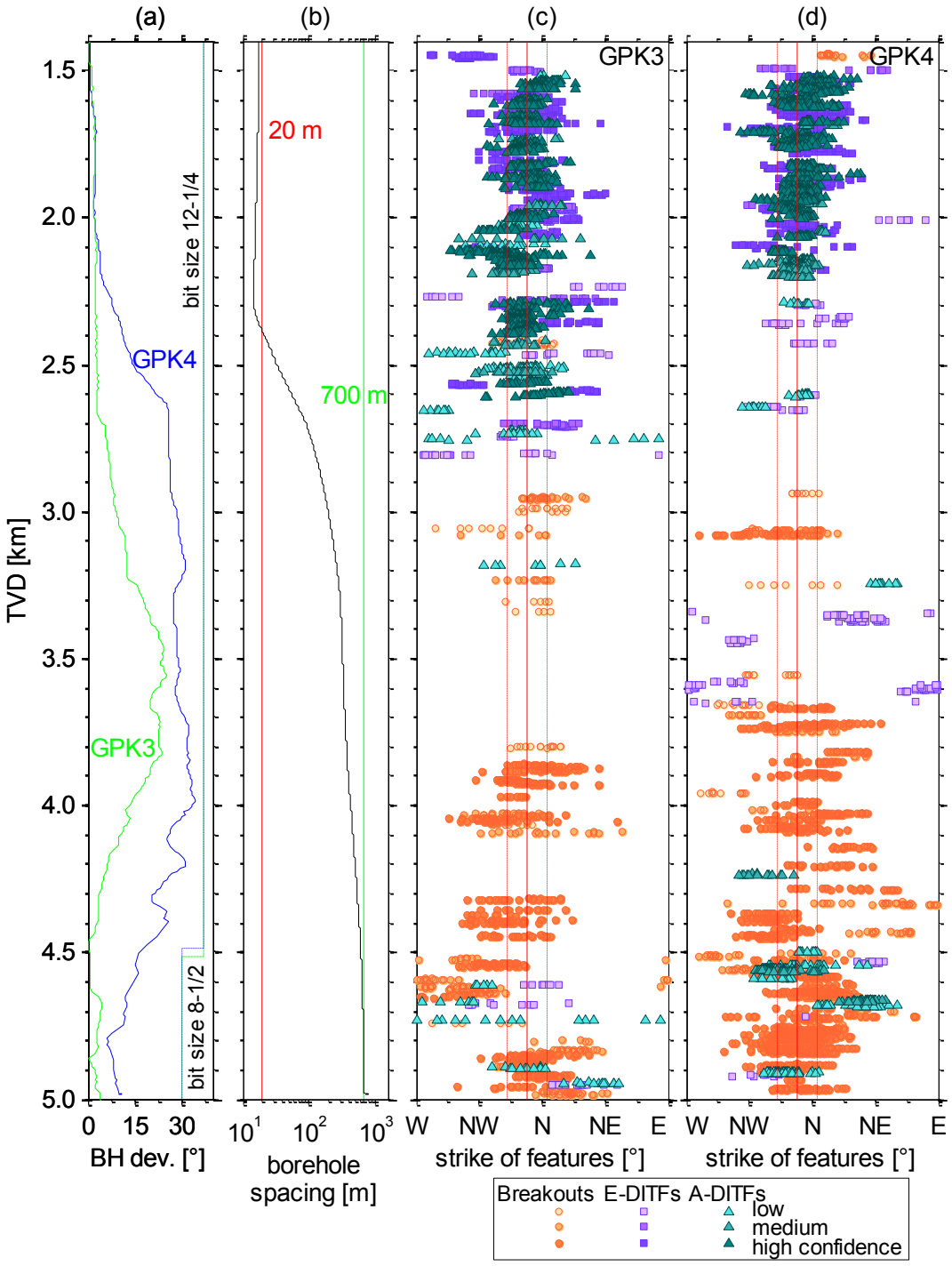

Figure 2: a) boreholes deviation from vertical and bit size (green GPK3 and blue GPK4). b) horizontal separation of the boreholes plotted on a logarithmic scale. c) and d) strike of A-DITFs (green triangles), E-DITFs(violet squares) and breakouts (orange circles) with the latter rotated anticlockwise through 90 for GPK3 and GPK4 respectively. The mean azimuth of SHmax and its standard deviation from all indicators in both GPK3 and GPK4 is denoted by the vertical redlines (N169°±14°).

The procedure employed in this study for describing the wellbore failure observations is as follows. First, intervals affected by breakouts, A-DITFs, or E-DITFs were identified. Then, for breakouts and A-DITFs, the mean azimuth of the two limbs of the features was determined for successive 0.5 m depth windows. For E-DITFs, the best-fitting plane to each member of each fracture pair was found and the strike and dip of the plane noted. Typically, this led to one sample every 0.5 to 1.0 m. In all cases, the confidence of the identification was quantified by assigning an index ranging between 1 and 3, corresponding to low and high confidence respectively.

4. VARIABILITY OF STRESS INDUCED FAILURE ORIENTATION

4.1 General variability in the orientation of stress indicators

The orientation distributions of high confidence breakouts and DITFs in each borehole are shown in Figure 3. The stereographic plot of poles of the true orientation, i.e.

corrected for borehole deviation, of DITFs indicates a wide range of fracture strikes, although the rose diagram of Figure 3b makes clear that the vast majority of DITFs lie within 20° of the mean orientation with outliers being relatively few in number. A 5° discrepancy in mean orientation of the DITFs in the two boreholes is evident, and a 10° discrepancy in the same sense for breakouts (Figure 3c). Given that the horizontal distance between boreholes is less than 35 m for the section where most of the DITFs occur (1400 m to 2500 m depth), so that essentially the same rock volume is sampled, the discrepancy must be due either to stress variations occurring over relatively short horizontal distances or to some systematic error in the logging process. The former explanation seems improbable, given that the observations span a depth range of 3.5 km. The UBI logs are oriented by coupling the sonde to a GPIT (General Purpose Inclinometer Tool) sonde. Different GPIT sondes were used in GPK3 and GPK4, but the same sonde was used for both sections of each well. Thus, calibration error is a possible explanation.

The modal peaks of the breakout distributions, which are shown in Figure 3c rotated through 90° to permit direct comparison with the DITFs, are essentially identical to the means of the DITF populations for the same hole. The distributions of the strikes of breakouts show greater scatter than the DITFs. This is at least partly due to the angular width that breakouts span which makes the determination of their representative orientation more uncertain than for DITFs. A slight asymmetry of the breakout distribution is also visible for each borehole but particularly for GPK3 data: the distribution is slightly overbalanced in an anti-clockwise sense about the mode of the distribution, which is approximately aligned with the DITFs strike directions. This may reflect a bimodal distribution with a main mode at 168° and a weak secondary mode at about 150°. Such a deviation may be associated with the reported counter-clockwise bias in the orientation distribution of hydro-thermally altered shear structures compared to the mean orientation of all fractures (Evans et al., 2005, Fig. 3). The same explanation was used by Bérard (2003) (see also Cornet et al., 2007, Fig. 5) to interpret a bimodal distribution seen in the orientation of wellbore failure in GPK2, although in that case the described features were 'thermal breakouts' — borehole elongation in the SHmax direction — a proposed new type of wellbore failure.

With very few exceptions, deviations from verticality of E-DITFs are less than 30° (Figure 3a). Some deviation from verticality of the DITFs are expected in inclined borehole sections even if one principal stress was always exactly vertical. The exact amount of deviation from verticality of the DITFs in such cases depends on the borehole deviation, the stress ratios and the Poisson ratio of the rock (e.g. Peška & Zoback, 1995). In the conditions encountered at Soultz, such deviations should not exceed about 10°. Thus, occasional deviation from verticality of a principal stress direction has to be assumed in order to explain the observed DITFs orientation pattern. Non-vertical DITFs dip preferentially to the east. In that respect, they mimic natural fractures which show similar preference in the upper section of the wells (Dezayes et al., 2010). A-DITFs and E-DITFs are clearly distinguished in Figure 3a, the former lying around the margin of the stereoplot, and the latter lying inside. E-DITFs with small deviation from axial are rare or absent, indicating that a critical deviation of the 'vertical' principal stress from alignment with the borehole axis is required before DITFs form in the en-echelon mode. This behaviour has been predicted theoretically (Ito et al., 2001). Neighbouring tensile fractures developing only a few degrees out of alignment with the borehole axis will tend to interact and link to form an axial fracture, albeit a ragged one. At some misalignment, the interaction will be insufficient for linkage to occur, resulting in en-echelon fractures.

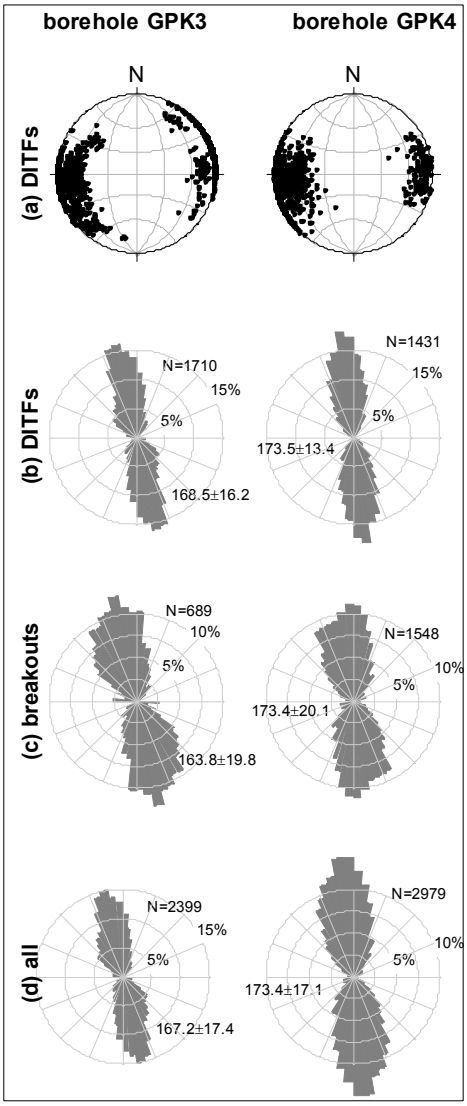

Figure 3: Orientation of high confidence stress induced wellbore failure in GPK3 and GPK4. Data from entire borehole length including both sub-vertical and inclined sections are shown. a) Stereographic plot of poles to DITF planes (equal area, lower hemisphere). b) Distribution of strikes of DITFs. c) Distribution of the orientation of borehole breakouts rotated through 90° to facilitate direct comparison with the DITFs. d) strike orientation of all features together. Here also, 90° has been added to the breakouts directions. For all circular histograms, N is the number of data point and the circular mean and single standard deviation are also displayed.

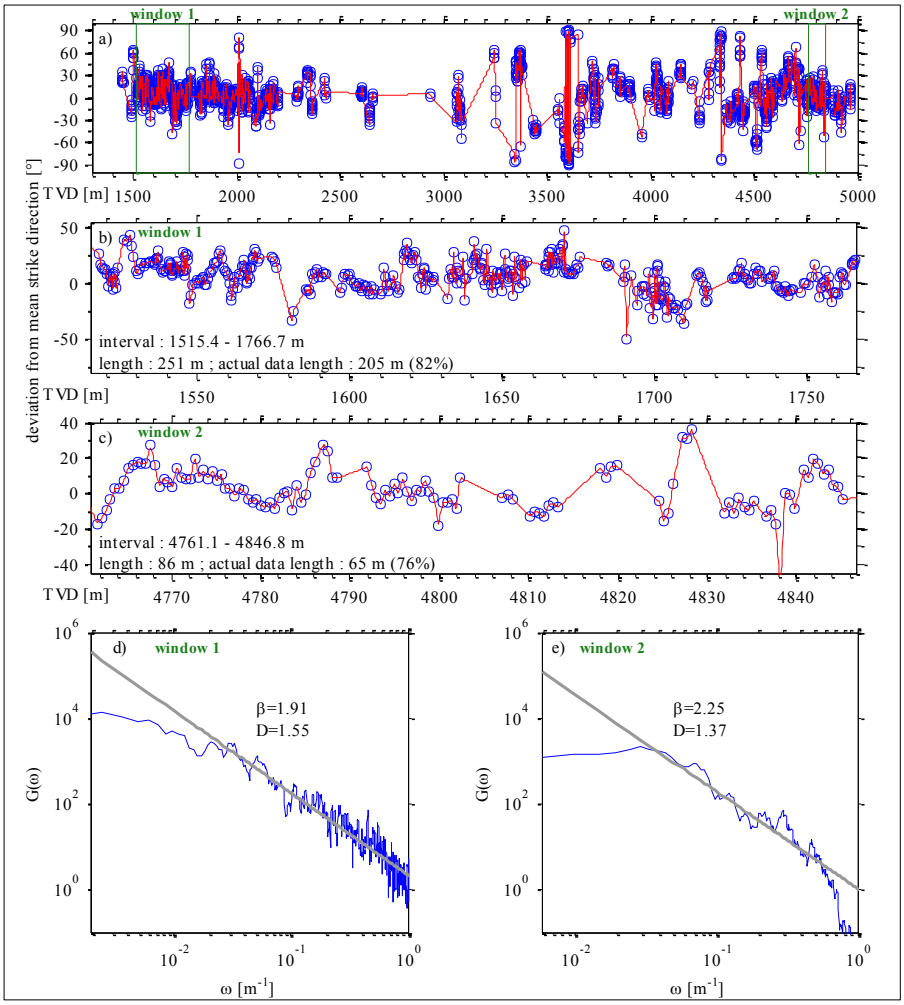

Figure 4: Power spectral analysis of the stress orientation variations in GPK4. a) Variation about the mean for the entire borehole. The blue circles denote data, and the red line is the linear interpolation of the data. The data sections used in the analysis are indicated. b) expanded view of the data window near the upper part of the borehole where DITFs occur. c) expanded view of the data window near the lower part of the borehole where breakouts occur. d) power spectrum of the data shown in b). The slope, β of the high-frequency roll-off and the fractal dimension, D, are indicated. e) power spectrum of the data shown in c).

4.2 Variability with depth of the stress orientation indicators

The depth profiles of the orientation of breakouts and DITFs are shown in Figure 2c and 2d for GPK3 and GPK4 respectively. DITFs occur almost exclusively above 3.0 km, whereas only breakouts are confidently identified below 3.7 km. This partitioning of the different modes of failure reflects the depth trends of stress magnitude, as discussed by Valley and Evans (2007). Here we are interested only in the variation in the orientation of the horizontal principal stresses that the two indicators imply. The variation of the orientations of the breakouts and DITFs about the mean for the site is shown in Figures 4a for GPK4. The nature of the variations is made clearer in the expanded views over selected depth windows in Figures 4b and 4c. Evidently, depth sections where the indicators have a stable orientation are rare: in most cases, the continuous sections of breakouts or DITFs show locally-progressive rotation in one direction or the other. These local rotations appear as streaks in the compressed-depth profiles in Figures 2c and 2d.

The variations occur at all scales. This is demonstrated in Figure 4d/e where the power spectral density, $G(\omega)$, of the variations in breakout- or DITF-orientation over the depth windows are shown. The windows were chosen to correspond to depth sections with relatively continuous data so as to reduce the bias introduced by gap-filling. The inevitable gaps were filled with linear interpolations and the series resampled with constant spacing. The spectra were computed using the periodogram method (e.g. Stoica and Moses, 1997) and the resulting spectra smoothed with a 5 point moving-average filter. Results are shown on log-log plots for the full range of spatial frequencies obtained from the analysis (i.e. from the highest, the Nyquist, down to the lowest, the reciprocal of the total window length).

It is evident that at high spatial frequencies, the spectral decay conforms relatively closely with a linear trend of slope, β, indicating that the orientation variations follow a power law of the type $G(\omega) \sim \omega^{-\beta}$. The slopes, β, of the linear 'roll-offs' were determined by least-square fitting over the appropriate frequency band, ignoring deviations from linearity in the spectra extremities, and found to be close to 2.0 for both GPK4 (Figure 4) and GPK3 (Valley, 2007). Power laws with slopes greater than -3.0 (e.g. -2.0) indicate a fractal process, the fractal dimension, D, being given by $D = (5-\beta)/2$ (Power and Tullis, 1991; Turcotte, 1989). A slope of -3.0 indicates self-similarity (i.e. scale invariance). Orientation variations that follow a power law with a slope of -3.0 would thus look identical at all scales

(Power and Tullis, 1991). Slopes greater than -3.0 indicate self-affine behaviour, where variations look progressively rougher at smaller scales. The proportionate reduction with increasing wavelength of the magnitude of the variations relative to wavelength as expressed by the self-affine scaling laws is expected for directional data where the maximum deviation is limited at 90°. These power laws hold for wavelengths from 4 m up to 80 m, the longest wavelength that could be resolved from the short data spans. So it is clear that variations in horizontal principal stress orientation occur at various scales.

In the following, the variations that occur at long and short wavelengths will be examined in more detail. Long wavelength variations are taken to be those that are coherent at scales larger than 50 m. Since this is larger than the spacing between the wells between 1.5 and 2.5 km, where DITFs dominate, such variations seen in the vertical profiles of stress orientation should be relatively coherent between wells, assuming that their lateral extent is similar to their vertical.

4.3 Large scale variations

Long-wavelength variations in horizontal principal stress orientation can only be detected where wellbore failure occurs more or less continuously over large sections of hole. This essentially restricts the study to the uppermost 1000 m of the granite, where DITF failure occurs, and the lowermost 1.2 km, where compressional failure is frequent. Long-wavelength variations in SHmax orientation can be seen in both sections in the plots of breakouts and DITFs azimuths in Figures 2c and 2d.

4.3.1 Large scale stress variations in the lower wells sections

Considering the lower sections first, significant variations in breakout orientation with wavelengths of several hundred metres and deviations from the mean of several tens of degrees can be seen near the bottom of both wells (Figure 2). In GPK3, a large excursion with a wavelength of about 400 m is centred at about 4650 m and has a maximum deviation from the mean of 50° to the west if the short-wavelength variations are smoothed-out. Another deviation to the west with an amplitude of 30° occurs at 4050 m, whilst at hole bottom, the deviation is 20° to the east, both having wavelengths of ~200 m. In GPK4, the only large scale excursion is centred at 4690 m. This has a deviation of about 50° to the east, and a wavelength of about 250 m.

The 400 m wavelength deviation centred at 4650 m in GPK3 almost certainly reflects the stress perturbation associated with a major fault that is penetrated at 4697 m TVD. This fault strikes approximately N160°E and dips at 50–60° to the west (Dezayes et al., 2004; Sausse et al., 2007, Dezayes et al., 2010), and is almost certainly a structure that extends many hundreds of meters if not kilometres. If the structure dips at 60°, then it would lie within 100 m of the borehole over the ±200 m length of the stress orientation perturbation. A transition from breakouts to DITFs is seen to occur near the intersection of this structure with the well, indicating that stress magnitudes are also perturbed. A major deviation in breakout orientation is also seen in GPK4 at a similar depth, but it occurs in the opposite direction. Since the well bottoms are separated by ~650 m, there is no compelling reason to expect that the two perturbations should be associated with the same fault, although that is possible. It is noteworthy that the difference in the orientations of the breakouts in GPK3 and 4 at 4650 m TVD, two points within the reservoir 650 m apart, amounts to 80°.

Another potential contribution to the stress heterogeneity near the bottoms of the holes might arise from a lithological change from standard 'Soultz' porphyritic granite to a 'two-mica' granite that occurs near 4720 m TVD. The change is believed to reflect the interface between two separate intrusions. Stress perturbations might result from contrasts in elastic moduli. Since the elastic moduli of the two mica granite have currently not been measured, this possibility remains uncertain. In any case, the dominant factor is almost certainly the fault at 4697 m TVD in GPK3.

The preferred explanation of the large-wavelength variations is that they reflect the stress generated by slip on faults. Based on the modeling results of Shamir (1990), perturbations with long wavelengths require slip on surfaces at least as large as the variations' wavelength, which, for the present data, implies structures that are at least 200 to 450 m in length. Such sizes correspond well with the expected lengths of fracture zones within the Soultz granite (Valley, 2007). There are many fracture zones intersected by the wells (see Dezayes et al., 2010), although none produce a perturbation as extensive as that associated with the fault in GPK3 at 4697 m TVD. In part, this may reflect the gaps in the definition of the stress field orientation in wellbore sections where there are neither breakouts nor DITFs. However, it is also probably an indication of the uncommonly large size of the 4697 m structure, which is manifest by its hydraulic (Tischner et al., 2007) and seismic (Dorbath and Charléty, 2007) properties, and its impact on drilling operations (Hettkamp et al., 2004).

4.3.2 Large scale variations in the upper wells sections

The long-wavelength perturbations in the upper section are particularly interesting because the two wells are less than 20 m apart and thus significant coherence between the variations in the wells might be expected. Figure 5 shows the large scale trend of the DITF strike determinations for the upper section of both wells. Large scale trends were extracted by applying interpolation and a moving window (boxcar) filter of 100 m to the raw data. Interpolation points filling the data gaps were given zero weighting in the averaging, and so the effective filter length is shorter near gaps. The resulting filtered series from both GPK3 and GPK4 are shown together in Figure 5 for comparison. For the depth range between 1535 m and 2200 m, which is relatively well sampled, three sections where the two series are reasonably correlated are found. These are denoted A (1535–1621 m), C (1783–1876 m), and E (2006–2200 m). However, the orientation variations between these sections are decidedly different. These are denoted as B (1621–1783 m) and D (1876–2006 m), and are marked by the light red bands in Figure 5. In section B, the two curves deviate from each other by only 9° over 60 m length scales, which is not a major inconsistency. However, the discrepancy for section D is much larger, amounting to 23° over a 130 m length scale. This is a surprising result, and it poses the question of how such a large change in stress orientation can occur vertically over a scale of 130 m yet not extend laterally only 20 m.

The origin of the discrepancy in section D is uncertain, although a reasonable working hypothesis is that it is related to a major fracture zone that intersects the wells near this depth (indicated by the black arrows in Figure 5). This fracture zone is most certainly a major structure, perhaps of

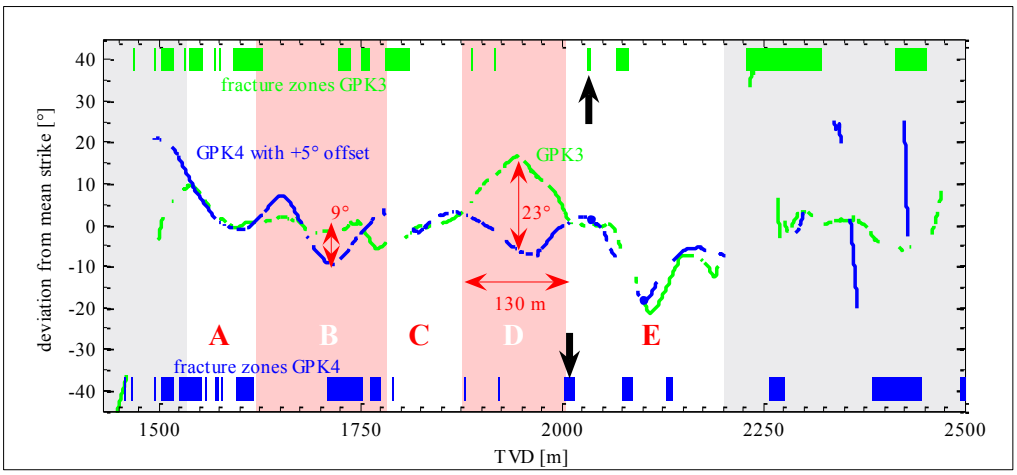

Figure 5: Superposition of the long wavelength components of the strike variations from GPK3 (green) and GPK4 (blue) extracted by interpolation in moving average filtering of the raw data. Note that the curve for GPK4 has been shifted by 5° to compensate for the apparent discrepancy in orientation measurement between the two holes. The two curves are essentially identical in zones A, C and E denoted by the white bands, but deviate significantly from each other in Zones B and D (light red bands). The distribution and width of fracture zones intersected in the two wells are shown at the top (GPK3) and bottom (GPK4) of the figure (from Valley, 2007). Black arrows point to the major fracture zone crossed by the boreholes at about 2100 m.

the same scale as the fault intersected at 4697 m TVD in GPK3 that was associated with the primary large-scale perturbation in the lower section of the reservoir. The zone was first intersected in GPK2 at 2110 m during the initial drilling of the well in 1995, and resulted in total loss of circulation fluid. No cuttings were obtained from the well during the subsequent drilling to 3876 m because they were swept into the fracture zone along with the drilling fluid. The zone was eventually plugged with 23 m^3 of cement during the extension of GPK2 to 5000 m in 1999. It is thus a zone of enormous capacity that has had a great deal of solid material injected into it. The structure dips at 74° to N95°E and crosses both wells at the bottom of the orientation discrepancy in section D (Figure 5). It is thus very close (<40 m) to the wells over the 130 m section of zone D. The discrepancy might thus reflect a particularly strong lateral gradient in stress arising from the perturbation associated with this fracture zone.

4.4 Small scale variations

Small-scale variations are considered to have wavelengths less than 50 m. As noted earlier, it is rare for the strike of breakouts or DITFs to remain stable over tens of metres of borehole. More commonly, they rotate systematically in one direction of another for a short distance, giving rise to the seemingly horizontal streaks in Figures 2c and 2d. An expanded view of DIFTs strike orientation in the upper section of GPK4 illustrates this case and is presented on Figure 6. Deviations from the local mean orientation of more than 45° occasionally occur (Figure 3). The variations in strike indicate that, more often than not, the azimuths of the principal horizontal stress axes are rotating as one moves along the borehole. The trends are maintained for only a short distance before they reverse. The reversal points are almost always associated with the intersection of fractures and fracture zones with the boreholes, indicating that the rotations are related to stress perturbations localised at the fractures. Also, many DITFs either terminate or change their form (e.g. A-DITF becomes E-DITF) at natural fractures. So, definitively, natural fractures have a large influence on the variability of stress induced failure.

4.4.1 Characteristics of DITF changes at natural fractures

At most intersections of DITFs with natural fractures, the DITF is unaffected and cuts through. However, in many cases, some change is seen. The types of terminations and transformations that DITFs generally undergo are shown in Figure 7 and their relative frequency of occurrence are shown in Figure 8a. About 70% of all observed DITFs either terminate or change from one form to the other (i.e. A-DITF to E-DITF) at natural fractures. Only 12–23% change from one form to the other remote from natural fractures. Of the remainder, 5–11% terminate remote from natural fractures, and a few stop near but not precisely at a natural fracture. In what follows we focus on the 70% that terminate or transform precisely at natural fractures since these suggest that the fractures are the source of the discontinuities in stress conditions at the borehole wall.

The types of change in DITFs that can occur at natural fractures are illustrated in Figure 7. Two types of E-DITFs are recognised according to whether they form in planes that are sub-parallel or oblique to the natural fracture. The relative frequency of occurrence of the various possible changes is shown in Figure 8b. Terminations of E-DITFs that are sub-parallel to the natural fractures are the most frequent in both wells, accounting for 41%, followed by termination of A-DITFs with 34–37%. Terminations of E-DITFs oblique to the natural fractures are rare. Of the transformations, only A-DITFs to E-DITFs that are sub-parallel to the fracture occur relatively frequently, the other two types being rare or non-existent. These changes for the

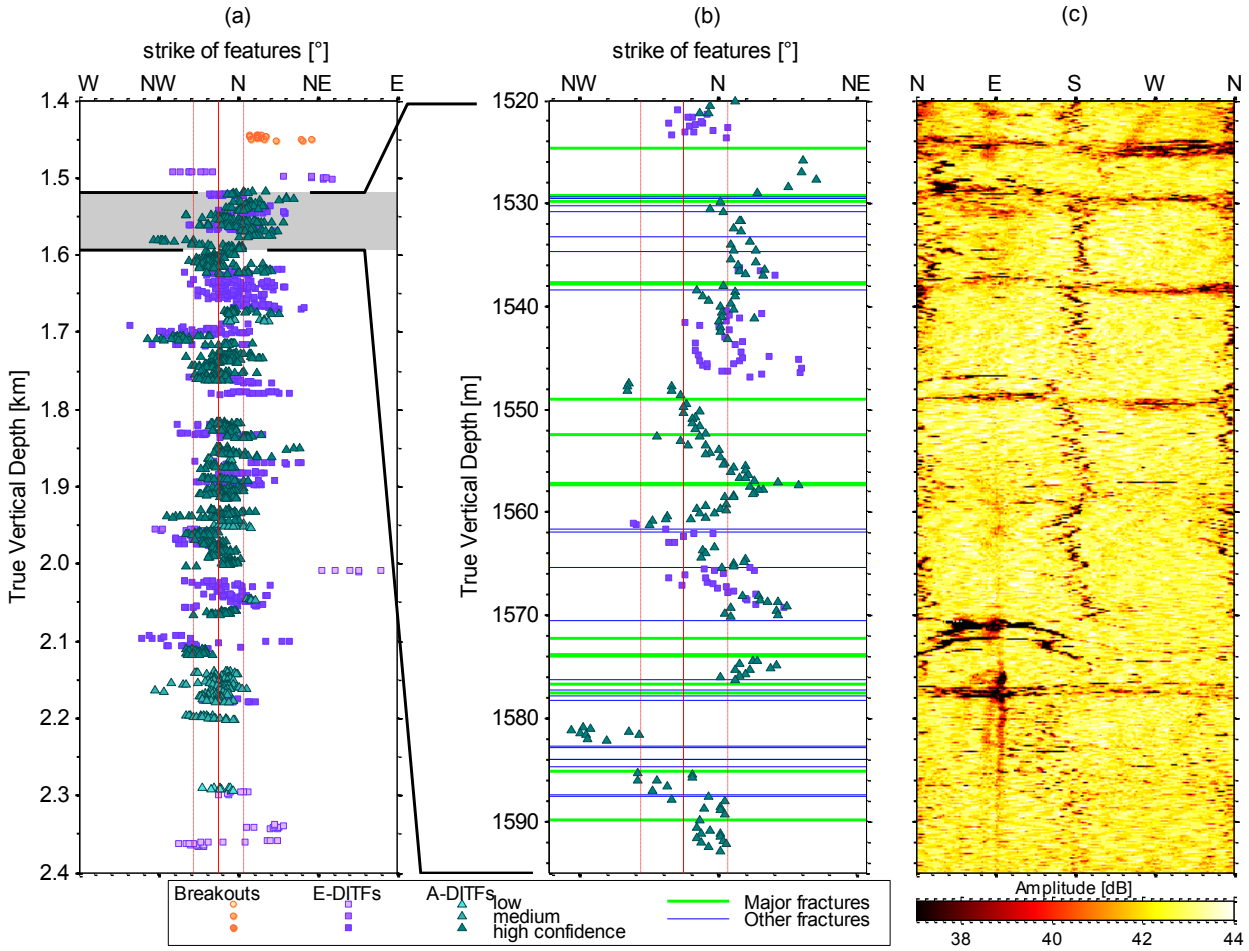

Figure 6: Expanded view (1520–1595 m TVD) of the variation of DITF strike in the upper granite sections of GPK4 illustrating the character of short wavelength (<50 m) variations. a) strike of A-DITFs (green triangles), E-DITFs(violet squares) and breakouts (orange circles) in the upper section of GPK4 with the latter rotated anticlockwise through 90° (see also figure 2). b) detailed view for the interval 1520 to 1595 m TVD including also location of natural fractures. c) Acoustic televiewer amplitude image for the same interval. The mean azimuth of SHmax and its standard deviation from all indicators in both GPK3 and GPK4 is denoted by the vertical redlines (N169°±14°) on a) and b).

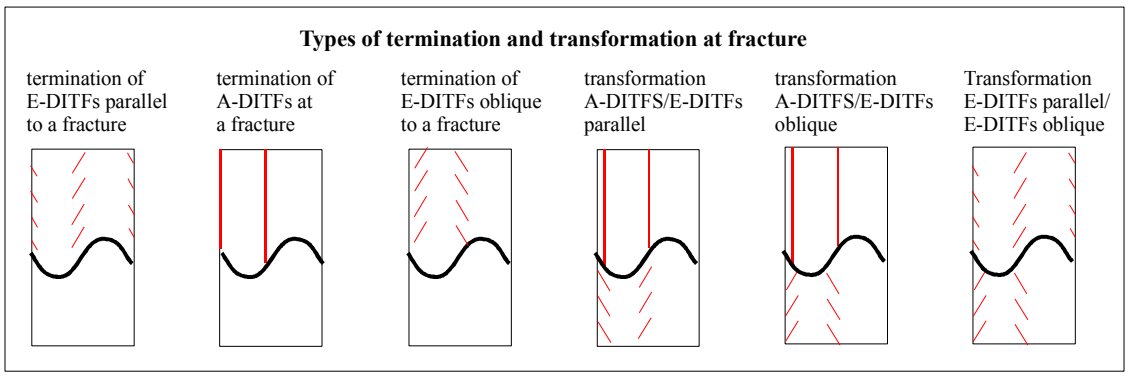

Figure 7: Types of terminations or transformation of DITF geometry that occur at natural fractures (see Figure 8b for relative frequency of occurrence).

most part indicate discontinuities in stress along the borehole wall that occur at natural fractures. Whilst the well-known tendency for natural fractures to arrest the propagation of tensile fractures might be a factor for some cases of termination, a change in either stress conditions or rock tensile strength on either side of the natural fracture must be present since otherwise DITFs would form on each side because of identical conditions.

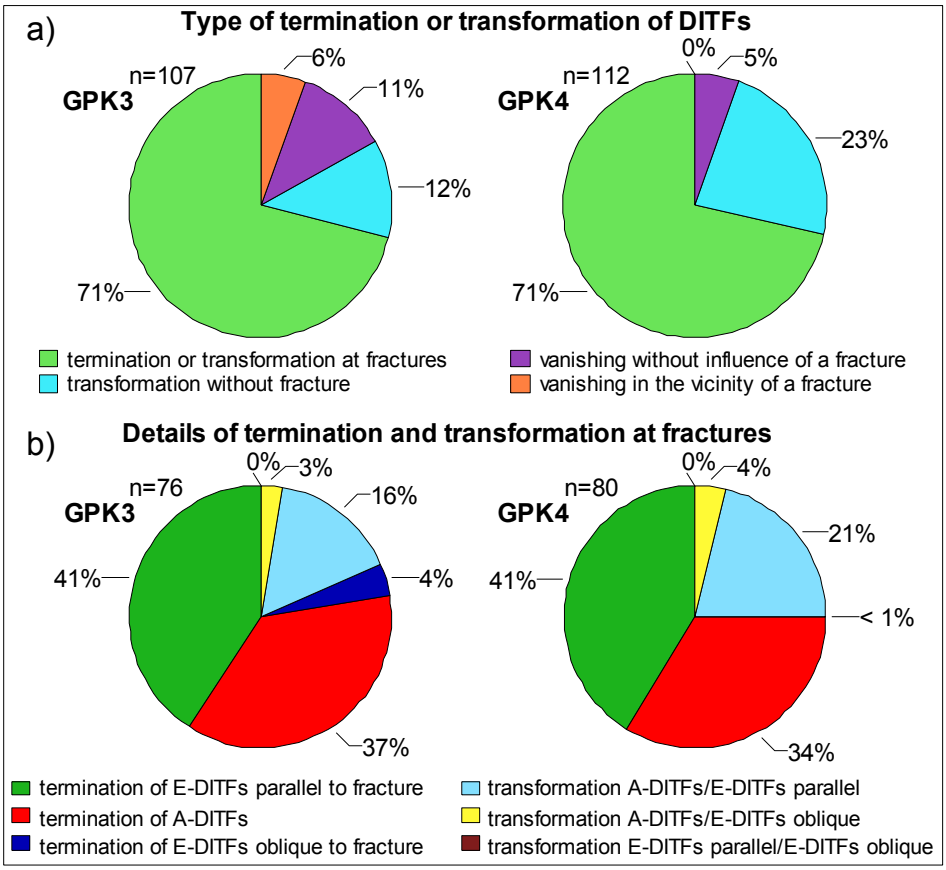

Figure 8: Terminations and transformations of DITFs. a) Relative frequency of types of termination or transformation of DITFs with regard to the proximity of natural fractures. b) Detail of the relative frequency of the types of terminations or transformation that occur at natural fractures (see Figure 7 for illustrations of the possible types).

4.4.2 Stress perturbing fractures

The preceding sections have served to establish the association of stress perturbations with natural fractures. In all, 144 fractures natural fractures in GPK4 could be unequivocally identified as associated with a stress perturbation through one of the following ways:

1. Orientation of induced failure (breakouts or DITFs) is modified in the vicinity of such fractures.

2. Induced failure stops on one side or the other of such fractures.

3. Induced failure changes form (i.e. A-DITFs to E-DITFs) in the vicinity of such fractures.

4. Induced failure is interrupted (i.e. no failure) in the vicinity of such fractures.

The 144 stress-perturbing fractures most surely underestimate the total number of stress-perturbing fractures since there are possibly many others that occur in regions of the borehole where conditions of wellbore failure were not met and thus there is no stress indicator generated in their vicinity. The distribution of the orientations of these fractures is shown in Figure 9a, together with the orientation distribution of all 2215 fractures identified in GPK4. The orientations of stress-perturbing fractures are more closely distributed than the latter, and fall into two major families (272/78 and 080/66), which are also the dominant orientations for the complete dataset.

The effective normal and shear stress resolved on the stress-perturbing and complete fracture datasets under the linear stress characterisation with ambient pore pressure are shown in the Mohr circle plots of Figure 9. All stresses have been normalised by the vertical stress, Sv. Evidently, almost all of the stress-perturbing fractures are critically-stressed in the sense that failure would occur of their strength were described by a Coulomb friction criterion with the coefficient of 0.6 (e.g. Barton et al., 1995; Evans, 2005; Ito and Zoback Mark, 2000; Zhang et al., 2002). As such, these fractures would be verging on failure under the simplified, linear representation of the prevailing stress field. The failure of these fractures will induce a stress perturbation, and thus the stress supported by these fractures will be modified from the values shown in Figure 9. The shear stress level supported by the fracture will be reduced, and this is particularly significant for fractures associated with sub-parallel E-DITFs. So it is possible that the perturbations in part reflect relatively recent failure associated with the on-going accommodation of crustal deformation (Zoback and Townend, 2001). However, it is also possible that they reflect failure that predates the contemporary stress situation.

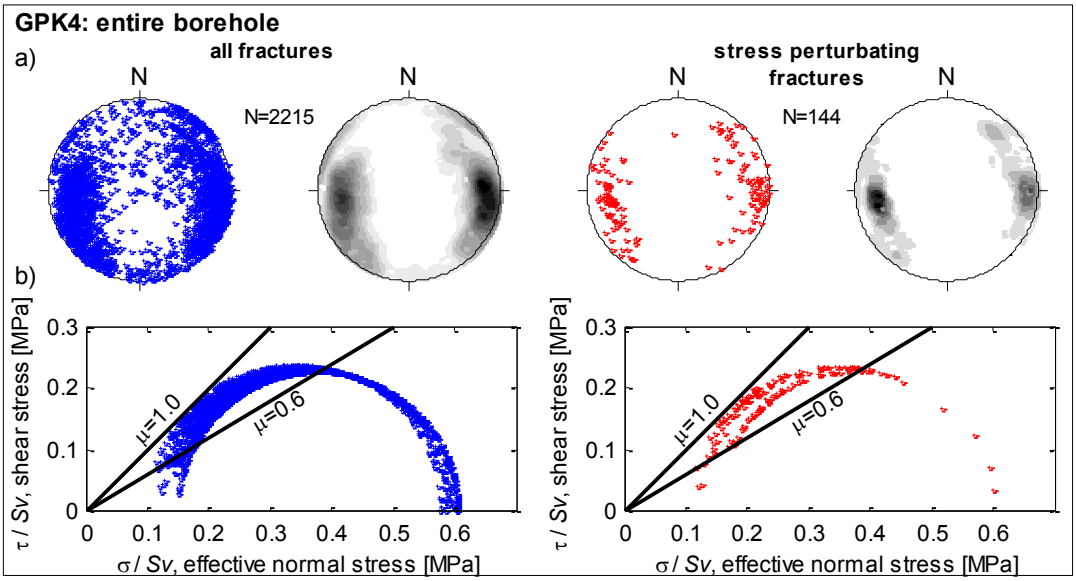

Figure 9: a) Stereographic plot of poles to all natural fractures identified in GPK4 (left) and the subset that were associated with stress perturbations (right). b) Mohr circle plots of the shear and effective normal stresses resolved on fracture sets in a). The stress was taken as given by the linear characterization for Soultz and the pore pressure as ambient.

5. CONCLUSIONS

Variations in the orientation of breakouts and DITFs about the mean orientations have been analyzed to investigate stress heterogeneity along the trajectory of the 5 km deep boreholes GPK3 and GPK4 at the Soultz site. The results suggest:

1) Variations in the stress orientation indicators occur at all scales amenable to analysis. Power spectra of the variations indicate power law behaviour between wavelengths 4 and 80 m, with slopes close to -2, indicative of self-affine behaviour. This indicates the relative amplitude of the variations with respect to wavelength decreases with larger scale.

2) The two most prominent large scale variations in horizontal principal stress orientation with wavelengths in excess of 100 m coincide with the two most significant fracture zones intersected by the wells. One of these occurs near 2000 m where the wells are only 20 m apart. Despite this lateral proximity, the large-scale variation is only partly correlated between wells, suggesting the presence of high lateral gradients in stress associated with the causal fracture zone.

3) Short-wavelength (<50m) variations in stress orientation with deviations from the mean of up to 90° occur frequently and are generally associated with natural fractures. Changes in stress across natural fractures are also indicated by coincident termination and transformation of DITFs from one form to another. Such variations are not usually correlated between wells in the section above 2000 m where the holes are 20 m apart

4) Almost all of the fractures which are associated with stress perturbations are critically stressed under the large-scale linear stress characterisation of the site. Thus, it is possible that they failed and generated the stress perturbations relatively recently, reflecting accommodation of on-going tectonic deformation of the crust. However, the data do not require this, and it is just as likely that the slip that generated the stress perturbations is much older.

6. AKNOWLEDGEMENTS

This work was supported by the Swiss State Secretariat for Education and Research under project number 03.04.60, and was performed as a contribution to the European Union's FP6 project 'Soultz EGS Pilot Plant' funded by ADEME, BMU, EC and EEIG 'Exploitation Minière de la Chaleur'. We thank EEIG for access to the data, and Albert Genter, Marion Pfender and Dimitra Teza for helpful information.

REFERENCES

Anders, M. H., and D. V. Wiltschko (1994), Microfracturing, paleostress and the growth of faults, *Journal of Structural Geology*, *16*, 795-815.

Barton, C. A., and M. D. Zoback (1994), Stress perturbations associated with active faults penetrated by boreholes: Possible evidence for near-complete stress drop and a new technique for stress magnitude measurements, *Journal of Geophysical Research*, *99*, 9373-9390.

Barton, C.A., Zoback, M.D. & Moos, D., 1995. Fluid flow along potentially active faults in crystalline rock, *Geology,* 23**,** 683-686.

Bell, J. S., and D. I. Gough (1979), Northeast-southwest compressive stress in Alberta: Evidence from oil wells, *Earth and Planetary Science Letters*, *45*, 475-482.

Bérard, T. (2003), Estimation du champ de contrainte dans le massif granitique de Soultz-sous-Forêts, implication sur la rhéologie de la croûte fragile, 264 pp, Institut de Physique du Globe de Paris, Paris.

Cornet, F. H., et al. (1992), Stress Heterogeneities and Flow Paths in a granite Rock Mass, Pre-Workshop Volume for the Workshop on Induced Seismicity, paper presented at 33rd U.S. Symposium on Rock Mechanics 184.

Cornet, F. H., and Y. Jianmin (1995), Analysis of induced seismicity for stress field determination and pore pressure mapping, *Pure and Applied Geophysics*, *145*, 677-700.

Cornet, F. H., et al. (2007), How close to failure is natural granite rock mass at 5 km depth ?, *International Journal of Rock Mechanics and Mining Sciences*, *44*, 47-66.

Cowie, P. A., and C. H. Scholz (1992), Physical explanation for the displacement-length relationship of faults using a post-yield fracture mechanics model, *Journal of Structural Geology*, *14*, 1133-1148.

Cuenot, N., et al. (2006), Faulting mechanisms and stress regime at the European HDR site of Soultz-sous-Forets, France, *Geothermics*, *35*, 561-575.

Dezayes, C., et al. (2004), Fracture network of the EGS geothermal reservoir at Soultz-sous-Forêts (Rhine graben, France), in *Geothermal Research Council 2004*, edited.

Dezayes, C., et al. (2010), Overview of the fracture network at different scales within the granite reservoir of the EGS Soultz site (Alsace, France). Proceedings World Geothermal Congress 2010 Bali, Indonesia, 25-29 April 2010

Dorbath, L., and J. Charléty (2007), What can we learn from large induced earthquakes at Soultz-sous-Forêts, paper presented at EHDRA scientific conference, 28 - 29 June 2007, Soultz-sous-Forêts, France, 28-29 June 2007.

Evans, K. F. (2005), Permeability creation and damage due to massive fluid injections into granite at 3.5 km at Soultz: 2. Critical stress and fracture strength, *Journal of Geophysical Research*, *110*.

Faulkner, D. R., et al. (2006), Slip on 'weak' faults by the rotation of regional stress in the fracture damage zone, *Nature*, *444*, 922-925.

Harris, R. A. (1998), Introduction to special section: Stress triggers, stress shadows, and implications for seismic hazard, *Journal of Geophysical Research*, *103*, 24347-24358.

Hettkamp, T., et al. (2004), Electricity production from hot rocks, paper presented at 29th workshop on geothermal reservoir engineering, Stanford, 26-28 January 2004.

Ito, T. & Zoback, M.D., 2000. Fracture permeability and in situ stress to 7 km depth in the KTB Scientific Drillhole, *Geophysical Research Letters,* 27**,** 1045-1048.

Ito, T., et al. (2001), Utilization of Mud Weights in Excess of the Least Principal Stress to Stabilize Wellbores: Theory and Practical Examples, *SPE Drilling and Completion*, *16*, 221-229.

Kastrup, U., et al. (2004), Stress field variations in the Swiss Alps and the northern Alpine foreland derived from inversion of fault plane solutions, *Journal of Geophysical Research*, *109*.

Mastin, L. (1988), Effect of borehole deviation on breakout orientations, *journal of Geophysical Research*, *93*, 9187-9195.

Peška, P., and M. D. Zoback (1995), Compressive and tensile failure of inlclined well bores and determination of in situ stress and rock strength, *Journal of Geophysical Research*, *100*, 12791-12811.

Power, W. L., and T. E. Tullis (1991), Euclidian and Fractal Models for the Description of Rock Surface Roughness, *Journal of Geophysical Research*, *61*, 415-424.

Rice, J. R. (1992), Fault stress states, pore pressure distributions, and the weakness of the San Andreas Fault., in *Fault mechanics and transport properties of rocks*, edited by B. Evans and T.-F. Wong, pp. 475-503, Academic Press, London.

Sausse, J., et al. (2007), From geological interpretation and 3D modelling of the characterization of the deep seated EGS reservoir of Soultz (France), paper presented at EHDRA scientific conference, 28 - 29 June 2007, Soultz-sous-Forêts, France, 28 and 29 June 2007.

Scotti, O., and F. H. Cornet (1994), In-situ stress fields and focal mechanism solutions in central France, *Geophysical Research Letters*, *21*, 2345-2348.

Shamir, G. (1990), Crustal stress orientation profile to a depth of 3.5 km near the San Andreas Fault at Cajon Pass, California Stanford University.--Dept. of Applied Earth, Sciences.

Shaw, B. E. (2004), Dynamic heterogeneities versus fixed heterogeneities in earthquake models, *Geophysical Journal International*, *156*, 275-286.

Stanchits, S., et al. (2006), Ultrasonic Velocities, Acoustic Emission Characteristics and Crack Damage of Basalt and Granite, *Pure and Applied Geophysics*, *163*, 975-994.

Stoica, P., and R. L. Moses (1997), *Introduction to Spectral Analysis*, 319 pp., Prentice-Hall.

Thompson, B., et al. (2006), Fracture in Westerly Granite under AE Feedback and Constant Strain Rate Loading: Nucleation, Quasi-static Propagation, and the Transition to Unstable Fracture Propagation, *Pure and Applied Geophysics*.

Tischner, T., et al. (2007), HDR project Soultz: hydraulic and seismic observations during stimulation of the 3 deep wells by massive water injections, in *32nd Workshop on Geothermal Reservoir Engineering*, edited, Stanford, California.

Turcotte, D. L. (1989), Fractals in geology and geophysics, *Pure and Applied Geophysics*, *131*, 171-196.

Valley, B., 2007. The relation between natural fracturing and stress heterogeneities in deep-seated crystalline rocks at Soultz-sous-Forêts (France), PhD, Eidgenössische Technische Hochschule ETH Zürich, Nr. 17385

Valley, B., and K. F. Evans (2007), Stress state at Soultz-sous-Forêts to 5 km depth from wellbore failure and hydraulic observations, paper presented at 32nd workshop on geothermal reservoir engineering, Stanford, 22-24 January 2007.

Vermilye, J. M., and C. H. Scholz (1998), The process zone: A microstructural view of fault growth, *Journal of Geophysical Research*, *103*, 12223-12238.

Wilson, J.E., Chester, J.S. & Chester, F.M., 2003. Microfracture analysis of fault growth and wear processes, Punchbowl Fault, San Andreas system, California, *Journal of Structural Geology,* 25**,** 1855-1873.

Zhang, X., Sanderson, D.J. & Barker, A.J., 2002. Stress control of hydraulic conductivity in fracture-saturated Swedish bedrock, *Geophysical Journal International,* 151**,** 452-468.

Zoback, M. D., et al. (1987), New Evidence on the State of Stress of the San Andreas Fault System, *Science*, *238*, 1105-1111.

Zoback, M.D. & Townend, J., 2001. Implications of hydrostatic pore pressures and high crustal strength for the deformation of intraplate lithosphere, *Tectonophysics,* 336**,** 19-30.

Zoback, M. D., et al. (2003), Determination of stress orientation and magnitude in deep wells, *International Journal of Rock Mechanics and Mining Sciences*, *40*, 1049-1076.

Zöller, G., et al. (2005), The Role of Heterogeneities as a Tuning Parameter of Earthquake Dynamics, *Pure and Applied Geophysics*, *162*, 1027-1049.